Non-equilibrium dynamics of artificial quantum matter

(Article begins on next page)

Thesis advisor   Author

Eugene Demler   **Mehrtash Babadi**

Non-equilibrium dynamics of artificial quantum matter

Abstract

The rapid progress of the field of ultracold atoms during the past two decades has set new mile-stones in our control over matter. By cooling dilute atomic gases and molecules to nano-Kelvin temperatures, novel quantum mechanical states of matter can be realized and studied on a table-top experimental setup while bulk matter can be tailored to faithfully simulate abstract theoretical models. Two of such models which have witnessed significant experimental and theoretical attention are (1) the two-component Fermi gas with resonant s-wave interactions, and (2) the single-component Fermi gas with dipole-dipole interactions. This thesis is devoted to studying the non-equilibrium collective dynamics of these systems using the general framework of quantum kinetic theory.

We present a concise review of the utilized mathematical methods in the first two chapters, including the Schwinger-Keldysh formalism of non-equilibrium quantum fields, two-particle irreducible (2PI) effective actions and the framework of quantum kinetic theory. We study the collective dynamics of the dipolar Fermi gas in a quasi-two-dimensional optical trap in chapter 3 and provide a detailed account of its dynamical crossover from the collisionless to the hydrodynamical regime. Chapter 4 is devoted to studying the dynamics of the attractive Fermi gas in the normal phase. Starting from the self-consistent T-matrix (pairing fluctuation) approximation, we systematically derive a set of quantum kinetic equations and show that they provide a globally valid description of the dynamics of the attractive Fermi gas, ranging from the weak-coupling Fermi liquid phase to the intermediate non-Fermi liquid pairing pseudogap regime and finally the strong-coupling Bose liquid phase. The shortcomings of the self-consistent T-matrix approximation in two spatial dimensions

are discussed along with a proposal to overcome its unphysical behaviors. The developed kinetic formalism is finally utilized to reproduce and interpret the findings of a recent experiment done on the collective dynamics of trapped two-dimensional ultracold gases.

Contents

Preface

6.5: For an answer which cannot be expressed, the question too cannot be expressed.

The "riddle" does not exist. If a question can be put at all, then it can also be answered.

– Ludwig Wittengstein, Tractatus Logico-Philosophicus

We understand matter by probing its properties using different scopes. Our first description of a phenomenon is based on its appearance in the bulk. We form coarse-grained concepts to refer to the recurring patterns, and deduce laws that govern the interplay between these concepts based on repeated observations. The traditional classification of the states of matter into gas, liquid and solid, the formation and clash of waves in the ocean and the propagation of mechanical waves and heat in piece of metal are examples of such coarse-grained descriptions. Thermodynamics and Newtonian mechanics are examples of the laws that govern such descriptions.

Our scopes improve over time, allowing us to observe the previously unobservable and giving us access to a finer description of the same phenomena: liquids and gases become a large collection of atoms and molecules gliding almost freely in space, and solids become a well-ordered collection of ions sitting on a lattice. Further observations reveal the laws that govern the interaction between the building blocks of matter. We immediately face the challenge of reconciling our coarse-grained concepts and laws with the new-found microscopic descriptions. Condensed-matter physics, by and large, is an endeavor to this end. This is done by *introducing as premises* hypotheses which permit us to omit all references to the macroscopic concepts (heat, wave, sound, etc) and to substitute only references to things which are a part of the subject-matter of the microscopic description. An exemplary instance of such a development is the groundbreaking kinetic theory of gases introduced by Ludwig Boltzmann in 1867: by construing *heat* as the mechanical motion of atoms, the laws of thermodynamics become deducible from those of Newtonian mechanics.[1]

---

[1] At the time Boltzmann posed the kinetic theory of gases, atoms and molecules were still considered to be fictitious concepts by the mainstream scientific and philosophical establishments. It takes the awe-inspiring insight of a brilliant mind and great courage to come up with such an accurate description of nature.

Building bridges between the microscopic and macroscopic realms is a truly worthwhile and indispensable effort: it is *only* by doing so that we may hope to understand and explain deep questions such as the universality of macroscopic laws, or the reason for their mere existence in the first place. The reason why ordinary matter manifests itself in three fundamental phases and not more, why matter has a tendency to reach thermal equilibrium, why good electrical conductors are shiny, and why certain materials suddenly become superconducting at low temperatures are among the typical questions addressed by the condensed-matter physics. It is ultimately through such understandings that we may gain control over nature, rearrange matter to suit our technological requirements, or even create new forms of matter artificially.

Condensed-matter physics proceeds by proposing approximate mathematical models to represent what is the case while neglecting what is irrelevant in the emergence of the bulk physics from the microscopic realm. It is by systematically tossing what is deemed as irrelevant details that a correspondence between the macroscopic concepts and laws, and the hypothesized microscopic correlates can be constructed. The first round of approximations starts by modeling the microscopic phenomenology in a tractable manner and often involves a certain degree of guesswork and neglect of details. The second round of approximations is in the mathematical analysis of the obtained microscopic model. The fabric of this process is made of experimental findings, analytical insights and numerical analyses.

For a long time, condensed-matter physics was devoted to the study of materials already existing in nature, whose microscopic laws were by large beyond our control. The microscopic phenomenology of some of the most promising materials, such as high-temperature superconducting compounds, is often so complicated that their tractable mathematical modeling inevitably involves a certain degree of oversimplification, such as neglecting lattice imperfections, neglecting the multiband structure of the energy levels, neglecting long-range interactions, etc. The resulting stripped-down models, while may still exhibit profound emergent properties, only approximately describe

the true phenomenology of any of the existing materials. The examples include lattice-spin systems, the Hubbard model and exactly solvable low-dimensional systems. The lack of relevant experimental data indeed hurdles the theoretical progress of the field.

The rapid advancement of the experimental techniques of trapping and cooling dilute atomic gases to nano-Kelvin temperatures in the late 90's and early 2000's presented a new perspective to the field and set a new milestone in our control over matter. The combination of atomic-molecular-optical (AMO) techniques such as laser cooling, evaporate cooling, optical lattices and Feshbach resonances allow *synthesizing* bulk matter in the quantum mechanical regime tailored to faithfully *simulate* some of the long-standing models of the condensed-matter physics. Some of the early developments include the realization of the Bose-Einstein condensate (BEC) of weakly-interacting atoms [1, 2], the Bose-Hubbard model [3], the Fermi-Hubbard model [4] and the strongly-interacting Fermi gas with resonant s-wave interactions [5]. Some of the more recent themes include engineering artificial gauge fields using Raman transitions [6] and engineering long-range interactions using Rydberg atoms [7] and polar molecules [8].

The experiments with ultracold atoms not only allow a clean realization of some of these central models, but also it provides us with powerful experimental probes such as time-of-flight imaging [9], in-situ imaging with single atom resolution [10], precision measurement of collective modes [11] and radio-frequency spectroscopy of spectral functions [12, 13]. The field of ultracold atoms has equipped us with an unprecedented degree of certitude both in our understanding of the fundamental laws of nature, and in the mathematical approximations involved in explaining emergent behavior from the microscopic models. One of the major themes in the condensed-matter physics is exploring the behavior of matter away from equilibrium, ranging from classical phenomena such as turbulence in fluid dynamics and pattern formation in complex networks to quantum phenomena such as charge transport in semiconducting devices, decoherence, dissipation, pre-thermalization, thermalization and more recent themes such as non-thermal steady states. The enormously larger mass of atoms

compared to electrons allows us to monitor the non-equilibrium evolution of degenerate quantum matter on a table-top experiment for the first time.

Two particularly important models which have been the subject of active experimental and theoretical research in the field of ultracold atoms are the (1) two-component attractive Fermi gas (AFG) with short-range interactions in two and three spatial dimensions and the associated physics of BCS to BEC crossover, and (2) fermions with dipole-dipole interactions. The AFG has previously served either as a toy model for explaining the emergence of superconductivity in electronic systems or in certain regimes for the quark-gluon plasma and the neutron stars. The advent of ultracold atoms has dramatically changed the status of this model by offering a genuine material realization for it on a table-top experiment. Dipolar quantum gases, on the other hand, are genuinely artificial matter with no analog in traditional condensed-matter systems. The anisotropic and long-range nature of dipole-dipole interactions is predicted to give rise to a wide range of novel phenomena and potential technological applications (e.g. see Ref. [14] and the references therein).

My central goal in this thesis is to describe the near-equilibrium dynamics of such artificial quantum many-body systems in the *kinetic* regime, i.e. when a large separation of scales exists between the microscopic time and length scales compared to the macroscopic scale of inhomogeneities. In fact, it is by imposing (or acknowledging) such a separation of scales that the concepts relevant to bulk matter (the *flow* velocity, energy and entropy *densities*, etc) can be construed as the collective behavior of a large aggregate of particles. Besides, the kinetic description is highly relevant to the analysis of typical experiments with ultracold quantum gases loaded in optical traps[2]. The central mathematical framework utilized in this thesis is the Schwinger-Keldysh formalism of non-equilibrium quantum fields, in conjunction with the formalism of two-particle irreducible effective

---

[2]In a typical experiment as such, the time scale of microscopic processes in set by the inverse of the Fermi energy and is of the order of $t_{micro} \sim 0.01$ ms, whereas the time scale of the bulk collective motion of atoms and molecules is set by the inverse trap frequency and is of the order of $t_{macro} \sim 1 \sim 10$ ms.
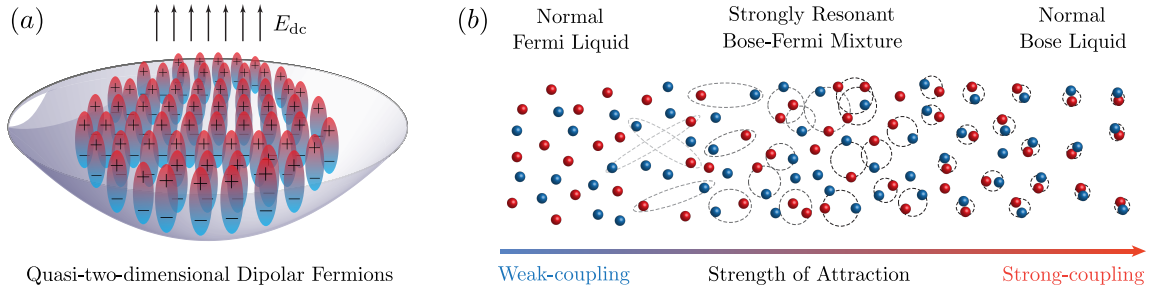
Figure 1: (a) A schematic illustration of dipolar fermions in a quasi-two-dimensional geometry with aligned dipole moments. The collective dynamics of this system is studied in chapter 3. (b) The crossover of the attractive Fermi gas from weak-coupling to strong-coupling. The dynamics of this system is studied in chapter 4 in two and three spatial dimensions.

actions (2PI-EA). The latter technique allows us to construct powerful non-perturbative approximations (the so-xcalled Φ-derivable approximations) that rigorously respect the symmetries of the microscopic action and give rise to exact conservation laws. This salient feature of the 2PI-EA formalism makes it an ideal tool for constructing approximate theories of non-equilibrium dynamics.

I have tried to make this thesis accessible to a broad audience, in particular, to researchers who wish to learn and utilize these techniques for the first time, by providing a concise, self-contained and critical review of the major conceptual tools in the introductory chapters. I have also tried to supplement the mathematical statements and derivations with intuitive ideas along the way. This thesis is organized as follows:

Chapter 1 provides a concise introduction to the Schwinger-Keldysh formulation of non-equilibrium quantum fields using the modern language of path integrals, followed by the formalism of 2PI effective actions and the related Φ-derivable approximations. I have dedicated some space to discuss a number of important but less-discussed issues such as the proper treatment of initial correlations, superconducting states and the 2PI Ward-Takahashi identities.

Chapter 2 provides a concise account of the derivation of quantum kinetic equations within the framework of 2PI-EA, along with extensive discussions on the validity domain of the kinetic description, the associated form of the conservation laws, the route to the Boltzmann equation, and

the linear response analysis within the kinetic description.

Chapter 3 is dedicated to studying the collective dynamics of trapped dipolar fermions in a quasi-two-dimensional geometry and is the first application of the formalisms introduced in the previous two chapters. The physical system is schematically illustrated in Fig. 1(a). Experimentally, this configuration may be realized by loading fermionic polar molecules (or atoms with permanent magnetic moments) onto a highly anisotropic optical trap as realized by combining a dipole trap and a one-dimensional optical lattice. The dipoles are aligned perpendicular to the confining plane by the application of an external field. In this setting, the dipole-dipole interaction gives rise to an effective long-range repulsion between the particles and produces a normal Fermi liquid state at low temperatures. This particular trapping configuration is also necessary in order to suppress inelastic dipolar collisions and also to reduce the rate of chemical reactions in experiments with reactive bi-alkali polar molecules [15, 16, 17]. The main question addressed in this chapter is the nature of bulk collective dynamics of the trapped particles (collisionless, hydrodynamical, or the dissipative crossover regime) at different temperatures, strengths of planar confinement and the strength of dipole-dipole interactions.

Chapter 4 is the longest part of this thesis and is dedicated to the study of two-component AFG with short-range interactions in two and three spatial dimensions– a long-standing model in condensed-matter physics with a rich descriptive power and application to several physical systems. Despite extensive theoretical work done on this model, a first-principle derivation of the quantum kinetic equations describing its bulk physics had not been achieved yet. We use the formalisms discussed in the first two chapters, in conconjuction with the widely used self-consistent T-matrix approximation (also known as the pairing fluctuation approximation) and develop such quantum kinetic equations in the normal (non-superfluid) state. The qualitative behavior of this model is schematically illustrated in Fig. 1(b). For small binding energies, the system is described as a weakly interacting Fermi liquid. Upon increasing the binding energy, pairing fluctuations prolifer-

ate and the system can be described as a resonant mixture of unpaired fermionic and paired bosonic molecules. The strong-coupling regime is described as a weakly interacting composite Bose liquid of the paired fermions. The kinetic equations to be derived manifestly exhibit such a crossover in the dynamics. We also find that the self-consistent T-matrix approximation leads to unphysical predictions in the strong-coupling regime in two dimensions, and propose a Φ-derivable approximation to overcome this defect. We will ultimately use the kinetic formalism to study the collective dynamics of ultracold atoms with s-wave resonant interactions in optical traps in order to reproduce and interpret the findings of a recent experiment done at the University of Cambridge [18].

Citations to Previously Published Work

The materials presented in this thesis is based on the research I have done during the last year of my graduate studies (May 2012 - June 2013). Chapter 3 is an extended version of the paper:

> M. Babadi and E. Demler, *Collective excitations of quasi-two-dimensional trapped dipolar fermions: transition from collisionless to hydrodynamic regime*, Phys. Rev. A **86**, 063638 (2012).

The results presented in chapter 4 are unpublished at the time this thesis was written.

In addition to the topics covered in this thesis, I have worked on other aspects of the physics of attractive Fermi gases and dipolar fermions during my graduate studies, including their quench dynamics and strong-coupling phase transitions. Many of these works were left out from this thesis with the hope of presenting a concise and coherent discussion of a single topic– the application of quantum kinetic equations to studying the dynamics of ultracold atoms and molecules. A brief summary of the omitted works is provided below for the record.

- Motivated by an experiment conducted at MIT and aimed at studying the ferromagnetic (Stoner) instability of repulsively interacting two-component fermions using ultracold atoms [19], we theoretically analyzed the competition between pairing and ferromagnetic instabilities in a two-component ultracold Fermi gas following a rapid quench to the repulsive side of the Feshbach resonance. In the paper,

    > D. Pekker, M. Babadi, R. Sensarma, N. Zinner, L. Pollet, M. W. Zwierlein and E. Demler, *Competition between Pairing and Ferromagnetic Instabilities in Ultracold Fermi Gases near Feshbach Resonances*, Phys. Rev. Lett. **106**, 050402 (2011),

    we showed that the pairing instability (i.e. formation of deeply bound molecules) is in fact the fastest instability channel in the dynamics following the quench, and that the pairing insta-

bility poses a fundamental limit on the possible formation and observation of ferromagnetic domains. The conclusions of this work was later confirmed experimentally in Ref. [20].

- We studied several aspects of the physics of quasi-two-dimensional dipolar fermions in the normal state, in particular, the effects of dipolar interactions on the band structure, the emergence of inter-band excitons and their experimental detection via modulation spectroscopy in:

> M. Babadi and E. Demler, *Collective phenomena in a quasi-two-dimensional system of fermionic polar molecules: Band renormalization and excitons*, Phys. Rev. A **84**, 033636 (2011).

- In a follow-up study, we investigated the strong-coupling instabilities of the normal state of a multi-band and multi-layer quasi-two-dimensional system of dipolar fermions to spin-density-wave-like (SDW) and charge-density-wave-like (CDW) states:

> M. Babadi and E. Demler, *Density ordering instabilities of quasi-two-dimensional fermionic polar molecules in single-layer and multilayer configurations: Exact treatment of exchange interactions*, Phys. Rev. B **84**, 235124 (2011),

where we showed that formation of CDW-like states (Wigner crystal) is the first strong-coupling instability of the normal state of quasi-two-dimensional dipolar fermions within the mean-field description.

- We continued the investigation of strongly-interacting dipolar fermions and the issue of Wigner crystallization by taking into account the effects of strong crystal correlations using a variational method. In the paper,

> M. Babadi, B. Skinner, M. M. Fogler and E. Demler, *Universal behavior of repulsive two-dimensional fermions in the vicinity of the quantum freezing point*,

Europhys. Lett. **103**, 16002 (2013),

we showed that the strongly-correlated liquid phase of repulsively interacting spinless fermions in two dimensions exhibits universal features near the freezing point, nearly independent of the microscopic interaction law. This finding allowed us to come up with accurate predictions for the thermodynamical quantities and Wigner crystal transition point of quasi-two-dimensional dipolar fermions by utilizing the wave functions of two dimensional electron gas as trial states.

Acknowledgments

Completing this doctoral work has been a wonderful journey, from its very first to its very last moments. Tough and challenging at times, yet extremely gratifying and truly worthwhile. This journey would have been impossible had it not been for the vibrant atmosphere of the Physics Department of Harvard University, and the incredible people with whom I had the opportunity to work. I would like to offer my special thanks to them here.

First of all, I express my deepest gratitude to my advisor, Eugene Demler. It has been a true privilege for me to have Eugene as my mentor for the past five years; I could not possibly ask for more. Eugene's enthusiasm for physics, his extraordinary style of thinking and his vast and intuitive knowledge of physics has never ceased to amaze me to this day. I have truly benefited from the invaluable discussions I had with Eugene over the years, often carried out in the form of scribblings on a piece of napkin at lunch. I wholeheartedly wish that the completion of this doctoral work only marks the beginning of a new era of productive collaboration and continued companionship with him.

Besides Eugene, I would like to express my gratitude to the faculty members of the Physics Department, in particular, my committee members Bertrand Halperin and Markus Greiner. Whenever I needed to get the most authoritative opinion on a physics issue, or just ask for some words of wisdom, Bert has been there and I can not thank him enough for that. Markus's groundbreaking contributions to the field of ultracold atoms has been instrumental in its establishment. It has always been a real peace of mind to feel that the scribblings on the blackboards of the forth floor of the Lyman laboratory are becoming part of the reality on the ground floor of the building. I would also like to thank Subir Sachdev and Arthur Jaffe, whose extraordinary physical and mathematical insights has always motivated me to try to think harder and better.

I have had the opportunity to collaborate and benefit from discussing with a number of brilliant post-doctoral researchers, visiting scholars and fellow graduate students over the years. In particular, I would like to thank Rajdeep Sensarma and David Pekker, the collaborators of my first ultracold

atoms project. I have benefited from the fruitful collaboration and illuminating discussions with Ville Pietilä and Takashi Oka on various aspects of non-equilibrium physics. I would also like to offer my special thanks to my other co-authors Brian Skinner and Michael M. Fogler. It is my pleasure to acknowledge short but fruitful discussions with Wolfgang Ketterle and Martin Zwierlein at MIT, and Michael Köhl on different occasions. Last but not the least, I wish to acknowledge the joyful companionship and insightful discussions I had with my friends and colleagues in the Physics Department, Mark W. Morales, Takuya Kitagawa, Kartiek Agarwal, Debanjan Chowdhury and Matthias Punk.

The vibrant and friendly environment of the Physics Department owes a lot to the wonderful administrative work of Carol Davis, Sheila Ferguson, Dayle Maynard and Lisa Cacciabaudo and I can not thank them enough for that.

Going further into the past, I would like to express my gratitude to my undergraduate advisor, Mohammad Reza Ejtehadi, who introduced me to the physics research early in college. My fascination and continued interest in fluid dynamics is indeed rooted in my early research projects with "Dr. Ejtehadi". Finally, I would like to offer my best to Nader Noori, the most inspiring and influential physics teacher I had, who showed me the beauty of physics and numerical analysis for the first time and left me no choice but to pursue physics as a career.

My life journey would have been unimaginably different had it not been for the constant presence of two extraordinary friends and lifelong companions, my brothers Behtash and Baktash. The most peaceful and joyful moments of my life, without doubt, has been the times I have played music together with Behtash for hours, or engaged in vigorous philosophical, social and economic discussions with Baktash in pretty much every imaginable occasion. Gentlemen, I tip my hat to you!

Above all, everything I have I owe to my parents and their unfathomable sacrifices since the very first moments of my life. How can I ever forget, or even understand, the unconditional love

of my mother for tirelessly taking me to various classes every single day, and the great sacrifices of my father, working from dawn to dusk and yet, always being there for us? I can not. This thesis is dedicated to them from the deepest of my heart.

Dedicated to my parents

1

Non-equilibrium quantum field theory and the 2PI effective action formalism

Non-equilibrium Green's function technique, initiated by Schwinger [21] and Kadanoff and Baym [22] is an indispensable method for investigating the quantum dynamics of many-particle systems which are neither in their ground-state nor in a thermal equilibrium. This formalism has been successfully used in various fields of physics including plasma, laser, chemical reactions, early universe, heavy ion collisions and ultracold quantum gases. It provides a rigorous mathematical

basis for exploring the quantum mechanical basis of thermalization and decoherence. Combined with self-consistent Φ-derivable approximations, the Schwinger-Keldysh formalism allows exploring previously uncharted territories such as far-from-equilibrium quantum dynamics with applications ranging from early universe physics to ultracold quantum gases.

The existing literature on the Schwinger-Keldysh formalism is vast and there exists several excellent review articles and textbooks on the subject [22, 23, 24, 25, 26, 27]. For the purpose of completeness, we provide a concise review of the mathematical foundations of the this formalism using the modern language of path integrals, and the functional method of 2-particle irreducible (2PI) effective actions in this chapter. The latter allows constructing powerful symmetry-preserving non-perturbative approximations for both the equilibrium and non-equilibrium description of strongly-interacting quantum many-body systems.

1.1 The Schwinger-Keldysh formalism and CTP Green's functions

1.1.1 The zoo of Green's functions

We consider a general non-relativistic field theory described by the following time-dependent Hamiltonian:

$$\hat{H}(t) = \sum_{ab} E_{ab}(t)\, \Psi_a^\dagger \Psi_b + \sum_{abcd} \lambda_{ab;cd}(t)\, \Psi_a^\dagger \Psi_c^\dagger \Psi_d \Psi_b. \tag{1.1}$$

The indices a, b, etc refer to the physical degrees of freedom such as space, spin, hyperfine state, etc. We restrict our analysis to fermionic fields in this thesis. The creation $\Psi_a^\dagger$ and annihilation Ψ_a field operators obey the usual fermionic anti-commutation relations:

$$\Psi_a \Psi_b^\dagger + \Psi_b^\dagger \Psi_a = \delta_{ab},$$

$$\Psi_a \Psi_b + \Psi_b \Psi_a = 0,$$

$$\Psi_a^\dagger \Psi_b^\dagger + \Psi_b^\dagger \Psi_a^\dagger = 0. \tag{1.2}$$

Here, δ_{ab} stands for the Kronecker δ for the discrete indices bundled in a and b, and the Dirac δ for continuous coordinates. The two-body interaction $\lambda_{ab;cd}$ can be taken as a real and fully anti-symmetric function, i.e. $\lambda_{ab;cd} = -\lambda_{cb;ad} = -\lambda_{ad;cb} = \lambda_{ba;cd}$. The Hamiltonian for a system of non-relativistic fermions moving in a continuous d-dimensional space and possibly with additional set of discrete indices σ is obtained via the following substitution rules:

$$a \to (\mathbf{x}_a, \sigma_a), \quad \delta_{ab} \to \delta_{\sigma_a \sigma_b} \delta^{(d)}(\mathbf{x}_a - \mathbf{x}_b), \quad \sum_a \to \sum_{\sigma_a} \int d^d \mathbf{x}_a,$$

$$E_{ab}(t) \to \left[-\frac{\nabla_{\mathbf{x}_a}^2}{2m} + U_{\sigma_a}(t_a, \mathbf{x}_a) \right] \delta_{\sigma_a \sigma_b} \delta(\mathbf{x}_a - \mathbf{x}_b),$$

$$\lambda_{ab;cd} \to \delta^{(d)}(\mathbf{x}_a - \mathbf{x}_b)\, \delta^{(d)}(\mathbf{x}_c - \mathbf{x}_d)\, v_{\sigma_a \sigma_b; \sigma_c \sigma_d}(\mathbf{x}_a - \mathbf{x}_c). \tag{1.3}$$

The Planck constant $\hbar$ will be set to unity throughout this thesis, unless it appears explicitly. The Einstein summation convention is assumed everywhere unless it is noted explicitly.

A central object in the field theoretic description of many-particle systems is the Green's function, which encodes the correlation between the field operators at different times. All of the thermodynamical quantities can be inferred from the Green's function for a system in equilibrium. In addition, the knowledge of the the variation of Green's functions with respect to the external (source) fields provides the answers to *all* of the questions that can be asked about the quantum system.

We assume that the state of the many-body system at $t = t_0$ is either specified explicitly via the density operator $\hat{\rho}_0$, or through a well-defined prescription for determining $\hat{\rho}_0$ (i.e. thermal equilibrium condition). A fermionic system in the normal state admits two independent Green's functions, $G^>$ and $G^<$, the so-called *greater* and *lesser* functions:

$$G^>(t_1 a_1; t_2 a_2) \equiv -i \left\langle \Psi_{a_1, H}(t_1)\, \Psi_{a_2, H}^\dagger(t_2) \right\rangle,$$

$$G^<(t_1 a_1; t_2 a_2) \equiv i \left\langle \Psi_{a_2, H}^\dagger(t_2)\, \Psi_{a_1, H}(t_1) \right\rangle. \tag{1.4}$$

The $\langle \ldots \rangle$ is a shorthand for $\mathrm{Tr}[\hat{\rho}_0 \ldots]$ and the H labels affixed to operators denote the Heisenberg

picture. We are concerned only with systems in their normal state in this thesis. Superconducting states and the associated anomalous Green's functions will be discussed briefly later for completeness. Besides the two fundamental Green's functions defined above, it is also useful to define a number of auxiliary Green's functions in terms of $G^>$ and $G^<$:

$$G^+(t_1a_1; t_2a_2) \equiv \theta(t_1 - t_2) \left[G^>(t_1a_1; t_2a_2) - G^<(t_1a_1; t_2a_2) \right],$$

$$G^-(t_1a_1; t_2a_2) \equiv -\theta(t_2 - t_1) \left[G^>(t_1a_1; t_2a_2) - G^<(t_1a_1; t_2a_2) \right],$$

$$G^c(t_1a_1; t_2a_2) \equiv \theta(t_1 - t_2) G^>(t_1a_1; t_2a_2) + \theta(t_2 - t_1) G^<(t_1a_1; t_2a_2),$$

$$G^a(t_1a_1; t_2a_2) \equiv \theta(t_1 - t_2) G^<(t_1a_1; t_2a_2) + \theta(t_2 - t_1) G^>(t_1a_1; t_2a_2),$$

$$G^K(t_1a_1; t_2a_2) \equiv G^<(t_1a_1; t_2a_2) + G^>(t_1a_1; t_2a_2). \tag{1.5}$$

These auxiliary functions are referred to as the retarded $(+)$, advanced $(-)$, chronological (c), anti-chronological (a) and Keldysh (K) Green's functions. The above definitions imply the following exact relations among the various Green's functions:

$$G^>(t_1a_1; t_2a_2) - G^<(t_1a_1; t_2a_2) = G^+(t_1a_1; t_2a_2) - G^-(t_1a_1; t_2a_2), \tag{1.6a}$$

$$G^c(t_1a_1; t_2a_2) + G^a(t_1a_1; t_2a_2) = G^K(t_1a_1; t_2a_2), \tag{1.6b}$$

$$G^>(t_1a_1; t_2a_2)^* = -G^>(t_2a_2; t_1a_1), \tag{1.6c}$$

$$G^<(t_1a_1; t_2a_2)^* = -G^<(t_2a_2; t_1a_1), \tag{1.6d}$$

$$G^c(t_1a_1; t_2a_2)^* = -G^a(t_2a_2; t_1a_1), \tag{1.6e}$$

$$\left[G^+(t_1a_1; t_2a_2) \right]^* = G^-(t_2a_2; t_1a_1). \tag{1.6f}$$

The equal-time commutation relation of the Heisenberg operators also trivially implies the following identity:

$$i \left[G^>(t, a; t, b) - G^<(t, a; t, b) \right] = \delta_{ab}. \tag{1.7}$$

1.1.2 The ground state formalism

It is useful for first consider the convectional ground-state formalism of quantum fields based on the adiabatic principle. In this case, $\hat{\rho}_0 = |\Psi\rangle\langle\Psi|$ where $|\Psi\rangle$ is ground state wavefunction of the interacting system. The Hamiltonian is assumed to be independent of time. We consider the expectation value of an operator with one time argument $\langle \hat{O}_H(t) \rangle$. The relation between $\hat{O}$ in the Heisenberg and interaction pictures is provided by:

$$\hat{O}_H(t) = \hat{U}(t_0, t)\,\hat{O}_I(t)\,\hat{U}(t, t_0),\tag{1.8}$$

where $\hat{O}_I(t)$ is the operator in the interaction picture and $\hat{U}$ is the evolution operator interaction picture. For $t > t_0$, U is given by:

$$\hat{U}(t, t_0) = T^c \left[\exp\left(-i \int_{t_0}^{t} \mathrm{d}t'\, \hat{H}_{\mathrm{int},I}(t') \right) \right],\tag{1.9}$$

where T^c is the shorthand notation for the chronological time-ordered product of the exponential and $\hat{H}_{\mathrm{int},I}(t')$ is the interaction part of the Hamiltonian. Likewise, for $t < t_0$ we have:

$$\hat{U}(t_0, t) = T^a \left[\exp\left(-i \int_{t}^{t_0} \mathrm{d}t'\, \hat{H}_{\mathrm{int},I}(t') \right) \right],\tag{1.10}$$

where T^a is the shorthand notation for the anti-chronological time-ordered product.

Conventionally, the interacting ground state $|\Psi\rangle$ is obtained by multiplying the interaction vertex $\lambda_{ab;cd}$ by a factor $\exp(-\epsilon|t|)$, which switches the interaction on and off at $t = \pm\infty$. The non-interacting ground state $|\Phi\rangle$ is assigned to the system at $t = -\infty$ and the interacting ground-state is obtained on the basis of the Gell-Mann and Low theorem: $|\Psi\rangle = \hat{U}(0, -\infty)|\Phi\rangle$ while taking the adiabatic limit $\epsilon \to 0$. We note that the usage of the Gell-Mann and Low procedure may not be always justified, in particular, in application to systems with gapless spectra or with spontaneously broken symmetries. In any event, it is important to note that a *necessary* condition for the validity

of the Gell-Mann and Low theorem is (1) the time-independence of the Hamiltonian, (2) $|\Phi\rangle$ being the non-interacting ground state, and (3) the non-degeneracy of the ground states. The expectation value of the operator $\hat{O}$ in the interacting ground state can be written as:

$$
\begin{aligned}
\langle\Psi|\hat{O}_H(t)|\Psi\rangle &= \langle\Phi|\hat{U}(-\infty,0)\,\hat{O}_H(t)\,\hat{U}(0,-\infty)|\Phi\rangle \\
&= \langle\Phi|\hat{U}(-\infty,0)\,\hat{U}(0,t)\,\hat{O}_I(t)\,\hat{U}(t,0)\,\hat{U}(0,-\infty)|\Phi\rangle \\
&= \langle\Phi|\hat{U}(-\infty,t)\,\hat{O}_I(t)\,\hat{U}(t,-\infty)|\Phi\rangle \\
&= \langle\Phi|\hat{U}(-\infty,\infty)\,\hat{U}(\infty,t)\,\hat{O}_I(t)\,\hat{U}(t,-\infty)|\Phi\rangle.
\end{aligned}
\tag{1.11}
$$

We have used the group property of $\hat{U}$, i.e. $\hat{U}(t_1,t_2)\,\hat{U}(t_2,t_3) = \hat{U}(t_1,t_3)$ to get the final result. Provided that the ground state of the interacting system is non-degenerate, the wave function $U(\infty,-\infty)|\Phi\rangle$ is proportional to $|\Phi\rangle$ up to a complex factor with unit modulus. This allows us make further progress as follows:

$$
\begin{aligned}
\langle\Psi|\hat{O}_H(t)|\Psi\rangle &= \langle\Phi|\hat{U}(-\infty,\infty)|\Phi\rangle\langle\Phi|\hat{U}(\infty,t)\,\hat{O}_I(t)\,\hat{U}(t,-\infty)|\Phi\rangle \\
&= \frac{\langle\Phi|\hat{U}(\infty,t)\,\hat{O}_I(t)\,\hat{U}(t,-\infty)|\Phi\rangle}{\langle\Phi|\hat{U}(\infty,-\infty)|\Phi\rangle} \\
&= \frac{\left\langle\Phi\left|T^c\left[\exp\left(-i\int_{-\infty}^{\infty}\mathrm{d}t'\,\hat{H}_{\mathrm{int},I}(t')\right)\hat{O}_I(t)\right]\right|\Phi\right\rangle}{\left\langle\Phi\left|T^c\left[\exp\left(-i\int_{-\infty}^{\infty}\mathrm{d}t'\,\hat{H}_{\mathrm{int},I}(t')\right)\right]\right|\Phi\right\rangle}.
\end{aligned}
\tag{1.12}
$$

To get the second line from the first line, we have used the identity $\langle\Phi|\hat{U}(\infty,-\infty)|\Phi\rangle = \langle\Phi|\hat{U}(-\infty,\infty)|\Phi\rangle^* = \left[\langle\Phi|\hat{U}(-\infty,\infty)|\Phi\rangle\right]^{-1}$. An identical analysis gives a similar result for the chronological Green's function in the ground state:

$$
\begin{aligned}
G^c(t_1 a_1; t_2 a_2) &\equiv -i\left\langle\Psi\left|T^c\left[\Psi_{a_1,H}(t_1)\Psi_{a_2,H}^{\dagger}(t_2)\right]\right|\Psi\right\rangle \\
&= \frac{-i\left\langle\Phi\left|T^c\left[\exp\left(-i\int_{-\infty}^{\infty}\mathrm{d}t'\,\hat{H}_{\mathrm{int},I}(t')\right)\Psi_{a_1,I}(t_1)\Psi_{a_2,I}^{\dagger}(t_2)\right]\right|\Phi\right\rangle}{\left\langle\Phi\left|T^c\left[\exp\left(-i\int_{-\infty}^{\infty}\mathrm{d}t'\,\hat{H}_{\mathrm{int},I}(t')\right)\right]\right|\Phi\right\rangle}.
\end{aligned}
\tag{1.13}
$$

The Feynman-Dyson perturbation expansion is obtained by expanding the time-ordered products in the powers of $\hat{H}_{\mathrm{int},I}$ and using the Wick's theorem to express the time-ordered product of field

operators in the interacting picture in terms of the non-interacting (bare) chronological Green's functions G_0^c. The disconnected diagrams are removed by the denominator at all orders in the perturbation expansion. We note that the perturbation series only involves the chronological Green's function.

1.1.3 Non-equilibrium formalism and the Schwinger-Keldysh contour

One of the convenient features of the ground state formalism is the uni-directional sense of the time integrations, each ranging from $-\infty$ to ∞. As discussed in the previous section, this is achieved using the Gell-Mann and Low theorem by making the substitution $\langle\Phi|\hat{U}(-\infty,0) = e^{i\phi}\langle\Phi|\hat{U}(+\infty,0)$ where $e^{i\phi}$ is a pure phase (cf. Eq. 1.11). In other words, the arrow of time can be switched in the anti-chronological propagations of the adjoint wave functions with the small cost of introducing a pure phase. This leads to a perturbation expansion of G^c in terms of G_0^c without the need to resort to other flavors of Green's functions.

The inapplicability of the Gell-Mann and Low theorem for general non-equilibrium states implies that the arrow of time may no longer be switched in anti-chronological propagations: the time evolutions inevitably involves separate forward and backward propagations and as a consequence, different types of Green's functions are needed perform the perturbation expansion. The bookkeeping, however, is simplified by introducing contour Green's functions which unify several Green's function in a concise notation. We will discuss this formalism in this section.

We start with the definition of the *lesser* and *greater* Green's functions. Making the unitary propagations of the Heisenberg operators explicit, we find:

$$G^>(t_1 a_1; t_2 a_2) = -i\mathrm{Tr}\left[\hat{\rho}_0\,\hat{U}(t_0,t_1)\,\Psi_{a_1}\hat{U}(t_1,t_2)\,\Psi_{a_2}^\dagger\,\hat{U}(t_2,t_0)\right], \qquad (1.14a)$$

$$G^<(t_1 a_1; t_2 a_2) = i\mathrm{Tr}\left[\hat{\rho}_0\,\hat{U}(t_0,t_2)\,\Psi_{a_2}^\dagger\,\hat{U}(t_2,t_1)\,\Psi_{a_1}\,\hat{U}(t_1,t_0)\right], \qquad (1.14b)$$

where the fields without time labels are in the Schrödinger picture at $t = t_0$. We have again used the group property of $\hat{U}$ to combined the middle two propagation operators into a single operator. Here, $\hat{U}$ denotes the propagation operator in the Schrödinger picture:

$$(t > t_0): \quad \hat{U}(t, t_0) = T^c \left[\exp\left(-i \int_{t_0}^{t} dt' \, \hat{H}(t') \right) \right],$$

$$(t < t_0): \quad \hat{U}(t_0, t) = T^a \left[\exp\left(-i \int_{t}^{t_0} dt' \, \hat{H}(t') \right) \right]. \tag{1.15}$$

Let us assume $t_1 > t_2$ for the moment. The above Green's function can be graphically represented as:

$$iG^>(t_1 a_1; t_2 a_2) = \text{Tr}\,\hat{\rho}_0 \quad \underset{t_0 \quad t_2 \quad t_1 \quad t_M}{\underbrace{\qquad\qquad\qquad}} \quad = \text{Tr}\,\hat{\rho}_0 \quad \underset{t_0 \quad t_2 \quad t_1 \quad t_M}{\underbrace{\qquad\qquad\qquad}},$$

$$-iG^<(t_1 a_1; t_2 a_2) = \text{Tr}\,\hat{\rho}_0 \quad \underset{t_0 \quad t_2 \quad t_1 \quad t_M}{\underbrace{\qquad\qquad\qquad}} \quad = \text{Tr}\,\hat{\rho}_0 \quad \underset{t_0 \quad t_2 \quad t_1 \quad t_M}{\underbrace{\qquad\qquad\qquad}}.$$

In the above diagrammatic notation, the lines corresponds to $\hat{U}$ and cross signs indicate field insertions. t_M is an arbitrary time greater than $\max\{t_1, t_2\}$. The equivalence of the two possible diagrams for each Green's function and the arbitrariness of t_M are all due to the group property of $\hat{U}$. For instance, increasing t_M to $t_M + \Delta t$ introduces two extra propagators $\hat{U}(t_M, t_M + \Delta t)$ and $\hat{U}(t_M + \Delta t, t_M)$ adjacent to each other so that their product reduces to the identity operator.

The above pictorial description suggests that both the *lesser* and *greater* Green's functions can be thought of as the special cases of a more general Green's function defined on the roundtrip contour going from t_0 to t_M (which can be taken as $+\infty$) and from t_M back to t_0. This technique was introduced by Schwinger [21], and four years later by Keldysh [28]. The roundtrip contour is referred to as the Schwinger-Keldysh contour. We refer to this contour as $\mathcal{C}$ symbolically and decompose it as $\mathcal{C} = \mathcal{C}^+ \cup \mathcal{C}^-$, where $\mathcal{C}^+$ is *forward branch* going from t_0 to ∞, and $\mathcal{C}^-$ is the

backward branch returning back from ∞ to t_0:
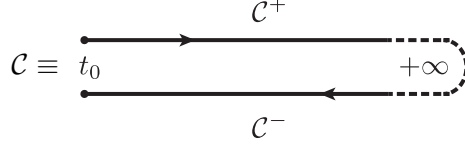
The bookkeeping is simplified upon introducing the *contour time* τ as the union of the physical time and the branch index:

$$\tau = (t, \sigma), \qquad \sigma = \begin{cases} + & \tau \in \mathcal{C}^+, \\ - & \tau \in \mathcal{C}^-. \end{cases} \tag{1.16}$$

$\mathcal{C}$ is a directed contour and is ordered via the natural binary operators $>_\mathcal{C}$ and $<_\mathcal{C}$. By definition, $\tau_1 >_\mathcal{C} \tau_2$ if and only if τ_1 lies ahead of τ_2 on $\mathcal{C}$ in the contour sense (the physical time t_1 may still be smaller than t_2). A useful auxiliary function is the contour Heaviside function $\theta_\mathcal{C}(\tau_1, \tau_2)$ defined as:

$$\theta_\mathcal{C}(\tau_1, \tau_2) \equiv \begin{cases} 1 & \tau_1 >_\mathcal{C} \tau_2, \\ 0 & \tau_1 <_\mathcal{C} \tau_2 \end{cases} \tag{1.17}$$

Differentiation and integration of the functions defined on $\mathcal{C}$ is defined in a natural way:

$$\int_\mathcal{C} \mathrm{d}\tau \, \mathcal{A}(\tau) \, \mathcal{B}(\tau) \equiv \int_{t_0}^\infty \mathcal{A}(t, +) \, \mathcal{B}(t, +) - \int_{t_0}^\infty \mathcal{A}(t, -) \, \mathcal{B}(t, -),$$
$$\frac{\mathrm{d}\mathcal{A}(\tau)}{\mathrm{d}\tau} \equiv \lim_{\epsilon \to 0} \frac{\mathcal{A}(\tau +_\mathcal{C} \epsilon) - \mathcal{A}(\tau)}{\epsilon}, \tag{1.18}$$

where $\tau_1 +_\mathcal{C} \delta t$ implies adding δt to τ_1 in the contour sense (i.e. adding δt if $\tau_1 \in \mathcal{C}^+$ and subtracting δt if $\tau_1 \in \mathcal{C}^-$). Finally, the contour Dirac δ function is defined either by differentiating $\theta_\mathcal{C}(\tau_1, \tau_2)$ with respect to τ_1 or through its measure-theoretic definition in integrals:

$$\delta_\mathcal{C}(\tau_1, \tau_2) \equiv \frac{\mathrm{d}\theta_\mathcal{C}(\tau_1, \tau_2)}{\mathrm{d}\tau_1}, \qquad \int_\mathcal{C} \mathrm{d}\tau' \, \delta_\mathcal{C}(\tau_1, \tau') \, \mathcal{A}(\tau') = \mathcal{A}(\tau_1). \tag{1.19}$$

An arbitrary function $\mathcal{A}(\tau_1, \ldots, \tau_n)$ defined on $\mathcal{C}$ is the union of 2^n independent functions of the n physical times, corresponding to the different placements of the time arguments on $\mathcal{C}^+$ and $\mathcal{C}^-$. We refer to these 2^n functions are the *explicit-time components* of $\mathcal{A}$. We generally reserve the

calligraphic roman letters to refer to the functions defined on $\mathcal{C}$ and refer to their explicit-time components with non-calligraphic letters. Furthermore, we refer to the contour times using the Greek letter τ and refer to the physical time using the Roman letter t.

Following this brief introduction to the Schwinger-Keldysh contour, the main object of this discourse, the contour Green's function $\mathcal{G}(\tau_1 a_1; \tau_2 a_2)$, also known as the closed-time-path (CTP) Green's function, is defined as:

$$\mathcal{G}(\tau_1 a_1; \tau_2 a_2) \equiv= -i \text{Tr} \left[\hat{\rho}_0 \, T_{\mathcal{C}} \left\{ \Psi_{a_1, H}(\tau_1) \, \Psi_{a_2, H}^{\dagger}(\tau_2) \right\} \right]. \tag{1.20}$$

The contour-ordering operator $T_{\mathcal{C}}$ orders the Heisenberg operators chronologically *in the contour sense*, with a factor of $(-1)^P$ where P is the number of permutation of the fermionic operators. The *lesser* and *greater* Green's functions can be obtained by investigating the explicit-time components of $\mathcal{G}$:

$$\mathcal{G}(\tau_1 a_1; \tau_1' a_1') \equiv \begin{bmatrix} G^c(t_1 a_1; a_1' t_1') & G^<(t_1 a_1; t_1' a_1') \\ G^>(t_1 a_1; t_1' a_1') & G^a(t_1 a_1; t_1' a_1') \end{bmatrix}. \tag{1.21}$$

In the above matrix notation, the matrix elements $(1, 1)$, $(1, 2)$, $(2, 1)$ and $(2, 2)$ correspond to the contour branch indices $(+, +)$, $(+, -)$, $(-, +)$ and $(-, -)$ respectively. Note that the four explicit-time components of the contour Green's function are not independent from each other: the diagonal elements can be expressed in terms of the off-diagonal elements using the exact relations given in Eq. 1.5. We use the relations that exist between the explicit-time elements of $\mathcal{G}$ as a template to define the *Keldysh functions*. It is easily shown that if $\mathcal{A}_1$ and $\mathcal{A}_2$ are two Keldysh functions, so is their convolution [23]:

$$\mathcal{A}_3(\tau_1 a_1; \tau_2 a_2) = \int_{\mathcal{C}} d\tau' \, \mathcal{A}_1(\tau_1 a_1; \tau' a') \, \mathcal{A}_2(\tau' a'; \tau_2 a_2), \tag{1.22}$$

where summation over a' is implied.

1.1.4   The path-integral on the Schwinger-Keldysh contour

The contour Green's function allows a unification of various Green's functions in a concise form. As we shall shortly see, the perturbation expansion of the contour Green's functions is formally identical to the expressions obtained in ground state formalism, with real times replaced by contour times and real time integrals with contour time integrals, $\int_{-\infty}^{\infty} \rightarrow \int_{\mathcal{C}}$. To this end, it is convenient to formulate Eq. (1.20) as a path-integral. Not only the path-integral formulation readily gives the Feynman-Dyson perturbation expansion, but also is an indispensable tool for transcending perturbation expansions and moving toward powerful non-perturbative functional approximations.

The construction of the path-integral representation of the contour Green's function is identical to that of the conventional Green's functions [29], with the only difference that the time integrations are done on the Schwinger-Keldysh contour instead of the real (or imaginary) lines. The path-integral representation of fermionic fields is done by introducing Grassmann numbers and fermionic coherent states. Here, we use the normalized coherent states that satisfy the completeness relation in the form:

$$\int \mathcal{D}\psi\mathcal{D}\bar{\psi}\,|\psi\rangle\langle\psi| = \mathbb{I}, \tag{1.23}$$

where $\mathbb{I}$ is the identity operator in the Fock space, $|\psi\rangle$ is a normalized fermionic coherent state with $\langle\psi|$ being its adjoint, and $\int \mathcal{D}\psi\mathcal{D}\bar{\psi}$ is the Berezin integral. As a first step, we use the trace formula to express the trace appearing in Eq. (1.20) as a Berezin integral over a fermionic coherent state $|\psi(t_0+)\rangle$ constructed from the field operators at $t = t_0$:

$$\mathcal{G}(\tau_1 a_1; \tau_2 a_2) = -i \int \mathcal{D}\psi(t_0+)\mathcal{D}\bar{\psi}(t_0+) \left\langle -\psi(t_0+) \left| \hat{\rho}_0 \, T_{\mathcal{C}} \left\{ \Psi_{a_1,H}(\tau_1)\, \Psi_{a_2,H}^{\dagger}(\tau_2) \right\} \right| \psi(t_0+) \right\rangle. \tag{1.24}$$

The minus sign in $\langle -\psi(t_0+)|$ is due to the anti-commutation of the Grassmann numbers. We further

plug in a resolution of identity between $\hat{\rho}_0$ and the field operator appearing above, so that:

$$\mathcal{G}(\tau_1 a_1; \tau_2 a_2) = -i \int \mathcal{D}\psi(t_0+)\mathcal{D}\bar{\psi}(t_0+)\mathcal{D}\psi(t_0-)\mathcal{D}\bar{\psi}(t_0-) \left\langle -\psi(t_0+) \left| \hat{\rho}_0 \right| \psi(t_0-) \right\rangle$$

$$\times \left\langle \psi(t_0-) \left| T_\mathcal{C} \left\{ \Psi_{a_1,H}(\tau_1) \Psi^\dagger_{a_2,H}(\tau_2) \right\} \right| \psi(t_0+) \right\rangle. \quad (1.25)$$

The reason for labeling these two coherent states as $|\psi(t_0+)\rangle$ and $|\psi(t_0-)\rangle$ will become clear shortly. As the next step, we break the forward and backward propagation of the Heisenberg operators into pieces of Δt apart, as graphically shown below:
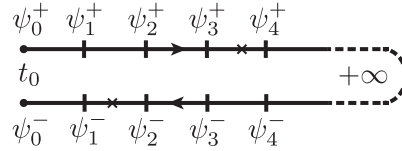
We insert the resolution of identity in terms of the coherent states, $\mathbb{I} = \int \mathcal{D}\psi^\pm(t\pm)|\psi_j^\pm\rangle\langle\psi_j^\pm|$, in place of each of the vertical lines. Taking the limit $\Delta t \to 0$, we obtain the real-time action, however, with the path integration running along the contour $\mathcal{C}$ instead of the real line:

$$\left\langle |\psi(t_0-)| T_\mathcal{C} \left\{ \Psi_{a_1,H}(\tau_1) \Psi^\dagger_{a_2,H}(\tau_2) \right\} \right| \psi(t_0+) \right\rangle = \int_{\psi(t_0+)}^{\psi(t_0-)} \mathcal{D}'[\psi,\bar{\psi}] \, \psi_{a_1}(\tau_1) \, \bar{\psi}_{a_2}(\tau_2) \, e^{iS[\psi,\bar{\psi}]},$$

$$(1.26)$$

where:

$$\int_{\psi(t_0+)}^{\psi(t_0-)} \mathcal{D}'[\psi,\bar{\psi}] \equiv \lim_{\Delta t \to 0} \int \mathcal{D}\psi(t_0+\Delta t,+)\mathcal{D}[\bar{\psi}(t_0+\Delta t,+)\mathcal{D}\psi(t_0+2\Delta t,+)\mathcal{D}[\bar{\psi}(t_0+2\Delta t,-)$$

$$\times \dots \times \mathcal{D}\psi(t_0+\Delta t,-)\mathcal{D}\bar{\psi}(t_0+\Delta t,-)\mathcal{D}\psi(t_0,-)\mathcal{D}\bar{\psi}(t_0,-), \quad (1.27)$$

and:

$$S[\psi,\bar{\psi}] = S_0[\psi,\bar{\psi}] + S_{\text{int}}[\psi,\bar{\psi}],$$

$$S_0[\psi,\bar{\psi}] = \int_\mathcal{C} \mathrm{d}\tau_1 \, \mathrm{d}\tau_2 \, \bar{\psi}_{a_1}(\tau_1) \, \mathcal{G}_0^{-1}(\tau_1 a_1; \tau_2 a_2) \, \psi_{a_2}(\tau_2),$$

$$S_{\text{int}}[\psi,\bar{\psi}] = -\int_\mathcal{C} \mathrm{d}\tau \, \lambda_{ab;cd}(t) \, \bar{\psi}_a(\tau) \, \bar{\psi}_c(\tau) \, \psi_d(\tau)\psi_b(\tau). \quad (1.28)$$

12

The bare inverse Green's function, $\mathcal{G}_0^{-1}$, is defined as:

$$\mathcal{G}_0^{-1}(\tau_1 a_1; \tau_2 a_2) \equiv [i\partial_{\tau_1}\delta_{a_1 a_2} - E_{a_1 a_2}(t_1)]\,\delta_{\mathcal{C}}(\tau_1, \tau_2). \tag{1.29}$$

The contour time derivative of the coherent state is defined as the limit given in Eq. (1.18). Putting together Eqs. (1.25) and (1.26), we finally find:

$$\mathcal{G}(\tau_1 a_1; \tau_2 a_2) = -i \int \mathcal{D}\psi(t_0+)\mathcal{D}\bar{\psi}(t_0+)\mathcal{D}\psi(t_0-)\mathcal{D}\bar{\psi}(t_0-)\,\langle -\psi(t_0+)\,|\hat{\rho}_0|\,\psi(t_0-)\rangle$$

$$\times \int_{\psi(t_0+)}^{\psi(t_0-)} \mathcal{D}'[\psi, \bar{\psi}]\,\psi_{a_1}(\tau_1)\,\bar{\psi}_{a_2}(\tau_2)\,e^{iS[\psi, \bar{\psi}]}. \tag{1.30}$$

The above expression has an interesting structure: the initial statistical fluctuations are represented by the matrix elements of $\hat{\rho}_0$ which weigh the paths based on their initial and final points $\psi(t_0+)$ and $\psi(t_0-)$. Quantum fluctuations are borne out of the multitude of paths. Further developments require the knowledge of the structure of the initial density matrix.

1.1.5 Initial correlations: the general theory

We derived the general expression for the contour Green's function in the previous section. While it is a useful result for formal developments, practical calculations is only made possible with further knowledge about the structure of the initial density matrix. It is useful to consider the general case first, where $\hat{\rho}_0$ is assumed to be via a general ansatz. Following Refs. [30, 31], we may parametrize the density matrix, without the loss of generality, via using following ansatz:

$$\langle -\psi(t_0+)|\hat{\rho}_0|\psi(t_0-)\rangle = \exp(iF[\psi, \bar{\psi}]),$$

$$F[\psi, \bar{\psi}] = \sum_{n=0}^{\infty} \frac{1}{n!} \int_{\mathcal{C}} \mathrm{d}\tau_1 \ldots \mathrm{d}\tau_n\,\alpha_n(\tau_1 a_1 c_1; \ldots \tau_n a_n c_n)\,\phi_{a_1, c_1}(\tau_1) \ldots \phi_{a_1, c_n}(\tau_n).$$

$$\tag{1.31}$$

The above compact notation is to be interpreted as follows:

(1) We have defined *charge implicit* Grassmann variables $\phi_{a,c}(\tau)$, where $c = +, -$. These Grassmann variables are related to the *charge explicit* variables, $\psi_a(\tau)$ and $\bar{\psi}_a(\tau)$ as $\phi_{a,+}(\tau) \equiv$

$\bar{\psi}_a(\tau)$ and $\phi_{a,-}(\tau) \equiv \psi_a(\tau)$. This convenient notation allows us to treat ψ and $\bar{\psi}$ on an equal footing.

(2) The initial density matrix only depends on the coherent states at the endpoints of $\mathcal{C}$, i.e. $|\psi(t_0+)\rangle$ and $|\psi(t_0-)\rangle$. Therefore, the α_n functions are only nonzero at the endpoints of the path. In other words, they carry contour Dirac δ functions that makes them non-vanishing only at $\tau = (t_0, \pm)$.

(3) We refer to α_n as the *initial correlation vertices* since they convey the initial correlations present in the system: α_0 sets the overall normalization of the density matrix according to the physical requirement $\text{Tr}[\hat{\rho}_0] = 1$, α_1 is zero for fermionic systems since $\langle \psi \rangle = \langle \psi^\dagger \rangle = 0$, and α_2 corresponds to the initial two-particle correlations (i.e. the number density, superconducting order parameter, etc), and so on. In a fermionic theory, the initial correlation vertices with an odd number of external legs vanish.

The above ansatz for the density matrix paves the way for the Feynman-Dyson diagrammatic expansion. To this end, we absorb α_2 into the Gaussian part of the original action S_0 and define the correlated bare inverse Green's function $\mathcal{G}_{0,\alpha_2}^{-1}$ as:
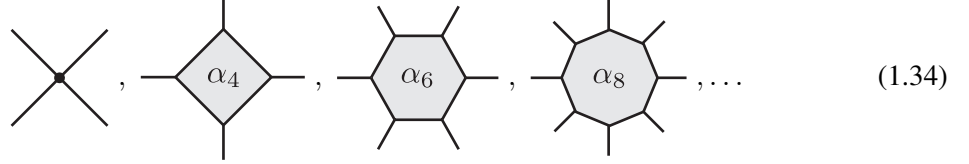
$$\mathcal{G}_{0,\alpha_2}^{-1}(\tau_1 a_1 c_1; \tau_2 a_2 c_2) \equiv \mathcal{G}_0^{-1}(\tau_1 \alpha_1; \tau_2 \alpha_2)\, \delta_{c_1,+} \delta_{c_2,-} + \frac{1}{2}\, \alpha_2(\tau_1 a_1 c_1; \tau_2 a_2 c_2). \qquad (1.32)$$

We further absorb the higher order correlation vertices in S_{int} and define $S_{\text{int},\alpha}[\phi]$ accordingly. The final result reads as:

$$\mathcal{G}(\tau_1 a_1; \tau_2 a_2) = -i \int_f \mathcal{D}[\psi, \bar{\psi}]\, \psi_{a_1}(\tau_1)\, \bar{\psi}_{a_2}(\tau_2)$$

$$\times \exp\left[i \underbrace{\int_{\mathcal{C}} d\tau_1\, d\tau_2\, \phi_{a_1, c_1}(\tau_1)\, \mathcal{G}_{0,\alpha_2}^{-1}(\tau_1 a_1 c_1; \tau_2 a_2 c_2)\, \phi_{a_2, c_2}(\tau_2)}_{S_{0,\alpha_2}[\psi,\bar{\psi}]} \right] \exp(i S_{\text{int},\alpha}[\phi]). \quad (1.33)$$

We remind that the only constraint on the paths is $\psi(t_0+) = -\psi(t_0-)$, as required by the fermionic trace formula. The f index affixed to the integral sign is a reminder for this constraint. We have also

absorbed the overall normalization constant $e^{i\alpha_0}$ into the integral measure $\mathcal{D}[\psi, \bar{\psi}]$. The vertices appearing in $S_{\text{int},\alpha}[\phi]$ can be graphically represented as follows:

$$\times \quad , \quad \diamondsuit{\alpha_4} \quad , \quad \hexagon{\alpha_6} \quad , \quad \octagon{\alpha_8} \quad , \ldots \tag{1.34}$$

there the dot vertex denotes the original interaction vertex $\lambda_{ab;cd}$ and the polygons are the initial correlation vertices (which only act at $\tau = t_0, \pm$).

Without the term $\exp(iS_{\text{int},\alpha}[\phi])$ in the kernel of Eq. (1.33), the path-integral reduces to a Gaussian integral and we find $\mathcal{G} = \mathcal{G}_0$, where $\mathcal{G}_0$ is the operator inverse of $\mathcal{G}_{0,\alpha_2}^{-1}$. In this formulation, the initial 2-particle correlations are explicitly contained in $\mathcal{G}_{0,\alpha_2}^{-1}$ through α_2. Taking higher order correlations and interactions into account, we may proceed by expanding $\exp(iS_{\text{int},\alpha}[\phi])$ in the powers of $S_{\text{int},\alpha}$. Since the path integral measure is a Gaussian, the Wick's theorem is applicable and we obtain a Feynman-Dyson's expansion of $\mathcal{G}$ in terms of $\mathcal{G}_{0,\alpha_2}$, λ and α_n ($n \geq 4$). We do not follow this development further and refer the reader to Ref. [31] for more details. In the next section, we consider the two special cases of (1) Gaussian initial correlations, and (2) thermal correlations.

1.1.6 Initial correlations: Gaussian and thermal correlations

Here, we consider two important and special cases where the calculations are considerably simpler, i.e. Gaussian initial correlations and thermal correlations.

Gaussian initial correlations:

Provided that $\hat{\rho}_0$ is expressible as the exponential of an arbitrary sum of one-body operators:

$$\hat{\rho}_0 = \exp \left[\mathscr{A}_{a_1,a_2} \Psi_{a_1}^\dagger(t_0) \Psi_{a_2}(t_0) \right], \tag{1.35}$$

the Wick's theorem hold [23] and as a result, only α_0 and α_2 will be non-zero. The explicit relation between the initial correlation vertices α_n and the initial correlations of the field operators at $t = t_0$

can be easily worked out (e.g. cf. Ref. [23, 32]). In the absence of higher order correlation vertices, the perturbation expansion only involves the interaction vertex $\lambda_{ab;cd}$. To first-order in $\lambda_{ab;cd}$, we find:

$$
\begin{aligned}
\mathcal{G}(\tau_1 a_1; \tau_2 a_2) = &-i \int \mathcal{D}[\psi, \bar{\psi}] e^{iS_{0,\alpha_2}[\psi, \bar{\psi}]} \, \psi_{a_1}(\tau_1) \bar{\psi}_{a_2}(\tau_2) \\
&\times \left[1 - i \int_{\mathcal{C}} d\tau' \lambda_{ab;cd}(t') \bar{\psi}_a(\tau') \bar{\psi}_c(\tau') \psi_d(\tau') \psi_b(\tau') + \dots \right] \\
= &\; \mathcal{G}_0(\tau_1 a_1; \tau_2 a_2) \left\langle 1 - i \int_{\mathcal{C}} d\tau' \lambda_{ab;cd}(t') \bar{\psi}_a(\tau') \bar{\psi}_c(\tau') \psi_d(\tau') \psi_b(\tau') + \dots \right\rangle_{S_{0,\alpha_2}} \\
&+ \int_{\mathcal{C}} d\tau' \, \mathcal{G}_0(\tau_1 a_1; \tau' a) \left[4i\lambda_{ab;cd}(t') \mathcal{G}_0(\tau' b; \tau' c) \right] \mathcal{G}_0(\tau' d; \tau_2 a_2) + \mathcal{O}(\lambda^2)
\end{aligned}
$$

$$
= \; \longleftarrow \left[1 + \bigcirc\!\!\bullet\!\!\bigcirc \right] + \;\raisebox{1ex}{$\bigcirc$}\!\!\!\!\!\!\longleftarrow\!\!\!\bullet\!\!\!\longleftarrow\; + \mathcal{O}(\lambda^2). \tag{1.36}
$$

We note that the appearance of the disconnected diagram in the series is only formal. A convenient feature of the contour formalism is that at any order in perturbation theory, the disconnected diagrams sum to zero. The reason is that the disconnected diagrams result from the perturbation expansion of $\langle \exp(iS_{\text{int}}) \rangle_{S_{0,\alpha_2}}$, i.e. the term in angled brackets appearing after the second equality sign above. This expression, however, is simply the path integral representation of the unitary propagation from t_0 to ∞ and back again to t_0, which is the identity operator. Therefore, $\langle \exp(iS_{\text{int}}) \rangle_{S_{0,\alpha_2}} \equiv \langle\, 1 \,\rangle_{S_{0,\alpha_2} + S_{\text{int}}} = \text{Tr}[\hat{\rho}_0] = 1$.

As promised, the non-equilibrium perturbation expansion is formally equivalent to the ground state formalism, however, with the time integrations done on $\mathcal{C}$ instead of the real line. We will discuss how the explicit-time components of $\mathcal{G}$ may be inferred from such contour expressions in Sec. 1.1.7.

Thermal initial correlations:

Another important scenario, which is often the case, corresponds to the systems which are in the thermal equilibrium at $t = t_0$, after which the equilibrium is disturbed due to the presence of time-dependent terms in the Hamiltonian. The density matrix at $t = t_0$ is given by:

$$\hat{\rho}_0 = \frac{e^{-\beta \hat{H}(t_0)}}{\text{Tr}[e^{-\beta \hat{H}(t_0)}]}. \tag{1.37}$$

Without the loss of generality, we may assume that the system has been in the thermal equilibrium with $\hat{H}(t_0)$ for all times prior to t_0 as well. We extend the the Hamiltonian to the times preceeding t_0 as follows:

$$\hat{H}(t < t_0) = \hat{H}(t_0) \equiv \hat{H}_{\text{eq.}} \tag{1.38}$$

The chemical potential μ is assumed to be absorbed to $\hat{H}$. The thermal correlations encoded in $\hat{\rho}_0$ can be accounted for using the technique of imaginary-time propagation, reminiscent of the Matsubara formalism [33]. This method obviates the need to calculate the correlation vertices α_n explicitly. As a first step, we express the matrix elements of $\hat{\rho}_0$ as a path integral along a directed vertical line $\mathcal{C}_\beta \equiv [0, -i\beta]$:

$$
\begin{aligned}
\langle -\psi(t_0+) | \hat{\rho}_0 | \psi(t_0-) \rangle &= \frac{\left\langle -\psi(t_0+) \left| e^{-\beta \hat{H}(t_0)} \right| \psi(t_0-) \right\rangle}{\text{Tr}[e^{-\beta \hat{H}(t_0)}]} \\
&= \frac{\displaystyle\int_{\psi(t_0-)}^{-\psi(t_0+)} \mathcal{D}[\psi, \bar{\psi}] \, e^{iS_\beta[\psi, \bar{\psi}]}}{\displaystyle\int_f \mathcal{D}[\psi, \bar{\psi}] \, e^{iS_\beta[\psi, \bar{\psi}]}},
\end{aligned} \tag{1.39}
$$

where $S_\beta[\psi, \bar{\psi}]$ is the same as in Eq. (1.28), however, with $\mathcal{C}_\beta$ in place of $\mathcal{C}$. We have also expressed the trace in the denominator of $\hat{\rho}_0$ as a fermionic path integral along $\mathcal{C}_\beta$. The above expression can be put into a more useful form by noting that the path integration in the denominator can be

deformed as follows:
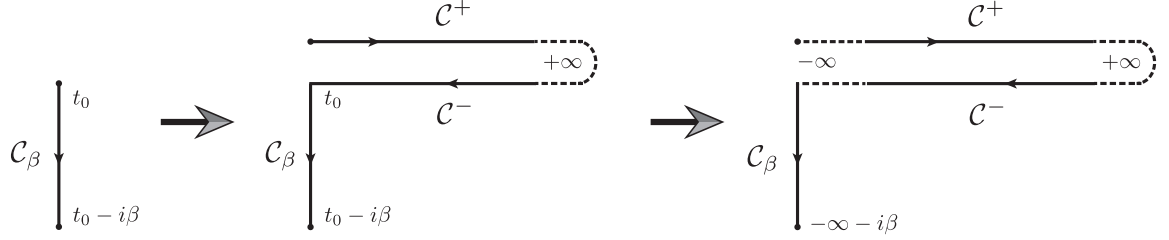
The successive deformations are allowed since the real time propagations along $\mathcal{C}^+$ and $\mathcal{C}^-$ are unitary and cancel each other (note that the path integrals are not interrupted by field operators in the denominator of Eq. 1.39). The analysis we present here is the path-integral adaptation of the Kadanoff and Baym's original approach [22] based on the analytical continuation procedure. We refer to the last contour $\mathcal{C}_{\mathrm{KB}} = \mathcal{C}^+ \cup \mathcal{C}^- \cup \mathcal{C}_\beta$ as the *Kadanoff-Baym contour*.

We proceed by plugging Eq. (1.39) in Eq. (1.30) and joining $\mathcal{C}_\beta$ to $\mathcal{C}^+ \cup \mathcal{C}^-$. Since $\tau_1, \tau_2 > t_0$, we may again deform the contour and send the starting time of the real-time branches to $-\infty$ (note that t_0 still refers to the time at which the time-dependent terms are switched on). This also allows us to calculate $\mathcal{G}$ for $\tau_1, \tau_2 < t_0$, which are simply the thermal Green's functions analytically continued to real times. To summarize, the final path-integral expression for $\mathcal{G}$ starting from an equilibrium state can be expressed as:

$$\mathcal{G}(\tau_1 a_1; \tau_2 a_2) = \frac{-i \int_f \mathcal{D}[\psi, \bar{\psi}] \, \psi_{a_1}(\tau_1) \, \bar{\psi}_{a_2}(\tau_2) \, e^{iS_{\mathcal{C}_{\mathrm{KB}}}[\psi, \bar{\psi}]}}{\int_f \mathcal{D}[\psi, \bar{\psi}] \, e^{iS_{\mathcal{C}_{\mathrm{KB}}}[\psi, \bar{\psi}]}}. \tag{1.40}$$

The above formula can be readily used to obtain the Feynman-Dyson perturbation expansion by separating the quadratic part of the action and expanding the interaction part. The ensuing expressions are identical to those shown in the previous section, however, the time integrations are performed along $\mathcal{C}_{\mathrm{KB}}$ instead of $\mathcal{C}$. Since the propagation is not unitary on $\mathcal{C}_{\mathrm{KB}}$ (due to the imaginary branch), the vacuum diagrams do not vanish in this case. However, they are removed by the denominator at all orders in the perturbation expansion.

Let us take a moment and examine the properties of the explicit-time equilibrium Green's function. These are found by placing τ_1, τ_2 on the real-time branches at physical times prior to t_0. The Hamiltonian is independent of time in this time regime and as a result, the Green's functions are only functions of the physical time difference $t \equiv t_1 - t_2$. Using Eq. (1.14a) and the cyclical property of the trace, we find:

$$G_{\text{eq.}}^>(t_1 a_1; t_2 a_2) = -iZ^{-1}\text{Tr}\left[\Psi_{a_1} e^{-it\hat{H}_{\text{eq.}}} \Psi_{a_2}^\dagger e^{-(\beta - it)\hat{H}_{\text{eq.}}}\right],$$

$$G_{\text{eq.}}^<(t_1 a_1; t_2 a_2) = iZ^{-1}\text{Tr}\left[\Psi_{a_1} e^{-(\beta + it)\hat{H}_{\text{eq.}}} \Psi_{a_2}^\dagger e^{it\hat{H}_{\text{eq.}}}\right], \tag{1.41}$$

where $Z \equiv \text{Tr}[\exp(-\beta\hat{H}_{\text{eq.}})]$ is the partition function. The above equations can be put in a more useful form by invoking the resolution of identity in terms of the complete spectrum of $\hat{H}_{\text{eq.}}$, i.e. in the Lehmann representation [33]:

$$G_{\text{eq.}}^>(a_1 t_1; a_2 t_2) = -iZ^{-1}\sum_{m,n}\langle\mathcal{E}_n|\Psi_{a_1}|\mathcal{E}_m\rangle\langle\mathcal{E}_m|\Psi_{a_2}^\dagger|\mathcal{E}_n\rangle\, e^{-\beta\mathcal{E}_n}e^{it(\mathcal{E}_n - \mathcal{E}_m)},$$

$$G_{\text{eq.}}^<(a_1 t_1; a_2 t_2) = iZ^{-1}\sum_{m,n}\langle\mathcal{E}_n|\Psi_{a_1}|\mathcal{E}_m\rangle\langle\mathcal{E}_m|\Psi_{a_2}^\dagger|\mathcal{E}_n\rangle\, e^{-\beta\mathcal{E}_m}e^{it(\mathcal{E}_n - \mathcal{E}_m)}, \tag{1.42}$$

where $\{\mathcal{E}_n\}$ correspond to the eigenvalues of $\hat{H}_{\text{eq.}}$ with eigenvectors $\{|\mathcal{E}_n\rangle\}$. Taking a Fourier transform of the above expressions in t, we find:

$$G_{\text{eq.}}^>(a_1, a_2; \omega) = -i\mathsf{A}_{\text{eq.}}(a_1, a_2; \omega)\left[1 - f_0(\omega)\right],$$

$$G_{\text{eq.}}^<(a_1, a_2; \omega) = i\mathsf{A}_{\text{eq.}}(a_1, a_2; \omega)f_0(\omega), \tag{1.43}$$

where $f_0(\omega) \equiv 1/[\exp(\beta\omega) + 1]$ is the Fermi-Dirac distribution function, and the *equilibrium spectral function* $\mathsf{A}_{\text{eq.}}(a_1, a_2; \omega)$ is defined as:

$$\mathsf{A}_{\text{eq.}}(a_1, a_2; \omega) \equiv Z^{-1}\sum_{m,n}(2\pi)\delta(\omega + \mathcal{E}_n - \mathcal{E}_m)\langle\mathcal{E}_n|\Psi_{a_1}|\mathcal{E}_m\rangle\langle\mathcal{E}_m|\Psi_{a_2}^\dagger|\mathcal{E}_n\rangle\left[e^{-\beta\mathcal{E}_m} + e^{-\beta\mathcal{E}_n}\right]. \tag{1.44}$$

Dividing the sides of Eq. (1.43) by each other, we find:

$$G_{\text{eq.}}^>(a_1, a_2; \omega) = -e^{\beta\omega}\, G_{\text{eq.}}^<(a_1, a_2; \omega). \tag{1.45}$$

This relation between $G_{\text{eq.}}^>$ and $G_{\text{eq.}}^<$ is called the *Kubo-Martin-Schwinger (KMS) condition*, also referred to as the *fluctuation-dissipation* relation.

In addition to the purely real-time Green's function, we also face the mixed-time Green's functions as found by placing τ_1 on either of the real-time branches and τ_2 on $\mathcal{C}_\beta$. An analysis similar what presented above yields the following expression for the mixed Green's functions:

$$G(a_1, t_1; a_2, T_0 - i\gamma) = i \int \frac{\mathrm{d}\omega}{2\pi} \, \mathsf{A}_{\text{eq.}}(a_1, a_2; \omega) f_0(\omega) \, e^{-i\omega(t_1 - T_0 + i\gamma)},$$

$$G(a_1, T_0 - i\gamma; a_2, t_2) = -i \int \frac{\mathrm{d}\omega}{2\pi} \, \mathsf{A}_{\text{eq.}}(a_1, a_2; \omega) \left[1 - f_0(\omega)\right] e^{-i\omega(T_0 - i\gamma - t_1)}. \tag{1.46}$$

In the above expressions, T_0 is the starting time of the real-time contours, $t_1, t_2 < t_0$ and $0 \leq \gamma \leq \beta$ is the imaginary time. Provided that the spectral function is a continuous function of ω, the Lebesgue-Riemann lemma implies:

$$\lim_{T_0 \to \infty} G(a_1, T_0 - i\gamma; a_2, t_2) = \lim_{T_0 \to \infty} G(a_1, t_1; a_2, T_0 - i\gamma) = 0, \tag{1.47}$$

owing to the presence of the rapidly oscillatory factors $e^{\pm i\omega T_0}$ in the frequency integrals appearing in Eq. (1.46). Therefore, the mixed Green's functions can be set to zero once the limit $T_0 \to -\infty$ is taken. This amounts to neglecting the imaginary branch of $\mathcal{C}_{\text{KB}}$ in the contour time integrals. While doing so, one must ensure:

$$\mathcal{G}(\tau_1 a_1; \tau_2 a_2)|_{t_1, t_2 < t_0} = \mathcal{G}_{\text{eq.}}(\tau_1 a_1; \tau_2 a_2). \tag{1.48}$$

This is conveniently implemented by imposing the KMS conditions as *boundary conditions* on the calculations, e.g. when solving the Kadanoff-Baym equations (cf. Sec. 1.2.5).

We finally remark that the above argument based on the Riemann-Lebesgue lemma is bound to the continuity of the spectral function (i.e. smearing of the energy levels) and may not hold in general. For instance, finite systems have a finite number of states and their spectral function consists of isolated δ peaks. Another counterexample is the non-interacting gas where the particles

strictly obey the mass-shell condition and the spectral function again consists of δ peaks. Here, we are concerned with interacting systems in the thermodynamical limit which have continuous spectral functions based on physical grounds. Therefore, we also adopt this usual practice hereafter and set the time contour $\mathcal{C}$ to the Schwinger-Keldysh roundtrip contour while sending T_0 to $-\infty$.

1.1.7 The Langreth rules

So far, we have handled the contour Green's functions and the expressions involving their convolution integral such as Eq. (1.36) on a formal level. In practice, however, we are interested in the explicit-time components of the Green's function. To this end, one requires a prescription to find the explicit-time components of convolution of two Keldysh functions. In the case where the time contour is the round-trip Schwinger-Keldysh contour, this prescription is given by the Langreth rules. We consider the following contour time convolution integral:

$$\mathcal{A}(\tau_1, \tau_2) = \int_{\mathcal{C}} \mathrm{d}\tau' \, \mathcal{B}(\tau_1, \tau') \, \mathcal{C}(\tau', \tau_2), \tag{1.49}$$

The *lesser* component of $\mathcal{A}$ can be found by placing τ_1 and τ_2 on $\mathcal{C}^+$ and $\mathcal{C}^-$ branches, respectively. In this case, Eq. (1.49) reads as:

$$
\begin{aligned}
A^<(t_1, t_2) &= \int_{-\infty}^{t_1} \mathrm{d}t' \, B^>(t_1, t') \, C^<(t', t_2) + \int_{t_1}^{\infty} \mathrm{d}t' \, B^<(t_1, t') \, C^<(t', t_2) \\
&\quad + \int_{\infty}^{t_2} \mathrm{d}t' \, B^<(t_1, t') \, C^<(t', t_2) + \int_{t_2}^{-\infty} \mathrm{d}t' \, B^<(t_1, t') \, C^>(t', t_2) \\
&= \int_{-\infty}^{t_1} \mathrm{d}t' \, \left[B^>(t_1, t') - B^<(t_1, t') \right] C^<(t', t_2) \\
&\qquad\qquad\qquad\qquad - \int_{-\infty}^{t_2} \mathrm{d}t' \, B^<(t_1, t') \left[C^>(t', t_2) - C^<(t', t_2) \right] \\
&= \int_{-\infty}^{\infty} \mathrm{d}t' \, \left[B^+(t_1, t') \, C^<(t', t_2) + B^<(t_1, t') \, C^-(t', t_2) \right].
\end{aligned}
\tag{1.50}
$$

The second equality is obtained by straightforward rearrangements and the last line follows from the definition of the retarded and advanced components. Likewise, the *greater* component is easily

found to be:

$$A^>(t_1, t_2) = \int_{-\infty}^{\infty} dt' \left[B^+(t_1, t') C^>(t', t_2) + B^>(t_1, t') C^-(t', t_2) \right]. \qquad (1.51)$$

The retarded and advanced components are found by subtracting the sides of Eqs. (1.51) and (1.50) from one another and multiplying by the θ function. We write the final results in a compact notation for future reference:

$$A^{\gtrless}(t_1, t_2) = \int_{-\infty}^{\infty} dt' \left[B^+(t_1, t') C^{\gtrless}(t', t_2) + B^{\gtrless}(t_1, t') C^-(t', t_2) \right],$$

$$A^{\pm}(t_1, t_2) = \int_{-\infty}^{\infty} dt' \, B^{\pm}(t_1, t') C^{\pm}(t', t_2). \qquad (1.52)$$

1.1.8 The Martin-Schwinger and BBGKY hierarchies

In the previous sections, we formulated the non-equilibrium Green's function as a path integral. Another useful approach toward calculating the Green's functions is the so-called equation of motion method, where a differential equation is found for $\mathcal{G}$. To this end, one starts from the time evolution of the field operators $\Psi^\dagger$ and Ψ in the Heisenberg picture, $i\partial_\tau \Psi_a^\dagger(\tau) = [\Psi_a^\dagger(\tau), H(t)]$, and $i\partial_\tau \Psi_a(\tau) = [\Psi_a, \mathcal{H}(\tau)]$. Expanding the commutators and using commutation relations, we find:

$$i\partial_{\tau_1} \Psi_{a_1}(\tau_1) = E_{a_1}(t_1)\Psi_{a_1}(\tau_1) + w_{a_1,b_1}(t_1)\Psi_{b_1}^\dagger(t_1)\Psi_{b_1}(t_1)\Psi_{a_1}(t_1), \qquad (1.53a)$$

$$i\partial_\tau \Psi_{a_2}^\dagger(\tau_2) = -E_{a_2}(t_2)\Psi_{a_2}^\dagger(\tau_2) - w_{a_2,b_2}(t_2)\,\Psi_{a_2}^\dagger(\tau_2)\Psi_{b_2}^\dagger(\tau_2)\Psi_{c_2}(\tau_2), \qquad (1.53b)$$

where we have specialized the generic Hamiltonian given in Eq. (1.1) by substituting $E_{ab}(t) = E_a(t)\delta_{ab}$ and $\lambda_{ab;cd}(t) = (1/2)\,w_{a,c}(t)\,\delta_{cd}\,\delta_{ab}$ for the clarity of discussion. The evolution equation for the contour Green's function $\mathcal{G}(\tau_1 a_1; \tau_2 a_2)$ in τ_1 is found by multiplying the sides of Eq. (1.53a) by $\Psi_{a_2}^\dagger(\tau_2)$ from the right and taking a trace with the initial density matrix. Likewise, the evolution equation in τ_2 is found by multiplying the sides of Eq. (1.53b) by $\Psi_{a_1}(\tau_1)$ from the left and taking

a the trace with the initial density matrix. The final result is:

$$[i\partial_{\tau_1} - E_{a_1}(t_1)]\,\mathcal{G}(\tau_1 a_1; \tau_2 a_2) = \delta_{a_1 a_2}\delta_{\mathcal{C}}(\tau_1, \tau_2) - iw_{a_1,b}(t_1)\,\mathcal{G}_2(\tau_1^- a_1, \tau_1 b; \tau_1^+ b, \tau_2 a_2),$$

$$\tag{1.54a}$$

$$[-i\partial_{\tau_2} - E_{a_2}(t_2)]\,\mathcal{G}(\tau_1 a_1; \tau_2 a_2) = \delta_{a_1 a_2}\delta_{\mathcal{C}}(\tau_1, \tau_2) - iw_{a_2,b}(t_2)\,\mathcal{G}_2(\tau_1 a_1, \tau_2 b; \tau_2^+ b, \tau_2^- a_2).$$

$$\tag{1.54b}$$

The δ functions appear due to equal-time commutation relations between the field operators and the time derivative of the contour-ordered operators. The $\mathcal{G}_2$ function is the 2-particle Green's function to be defined below. The $+$ $(-)$ sign on the contour times appearing in $\mathcal{G}_2$ implies addition (subtraction) of an infinitesimal time in the contour sense. Due to the presence of two-body interactions, this procedure does not yield a closed set of equations only in terms of $\mathcal{G}$ and the involvement of higher-order Green's functions (here, $\mathcal{G}_2$) is unavoidable. The n-particle contour Green's function $\mathcal{G}_n$ is generally defined as:

$$\mathcal{G}_n(\tau_1 a_1, \ldots \tau_n a_n; \tau_1' a_1', \ldots \tau_n' a_n') \equiv$$

$$(-i)^n \operatorname{Tr}\left[\hat{\rho}_0\, T_{\mathcal{C}}\left\{\Psi_{a_1}(\tau_1)\ldots\Psi_{a_n}(\tau_n); \Psi_{a_1'}^\dagger(\tau_1')\ldots\Psi_{a_n'}^\dagger(\tau_n')\right\}\right]. \tag{1.55}$$

We note that $\mathcal{G} \equiv \mathcal{G}_1$. Evolution equations for $\mathcal{G}_2, \mathcal{G}_3, \ldots$ can be obtained by multiplying Eqs. (1.53a) and (1.53b) with additional field operators and taking traces. The ensuing infinite hierarchy of equations is called the Martin-Schwinger (MS) hierarchy [34]. At the n'th level, the MS equation reads as:

$$[i\partial_{\tau_1} - E_{a_1}(\tau_1)]\,\mathcal{G}_n(1\,\ldots\,n; 1'\,\ldots\,n') =$$

$$\sum_{j'=1}^{n} \delta(1, j')(-1)^{n-j'}\mathcal{G}_{n-1}(2\,\ldots n; 1'\ldots j'-1, j'+1, \ldots n')$$

$$- iw_{a_1,b}(t_1)\,\mathcal{G}_{n+1}(1\,\ldots n, \tau_1 b; \tau_1^+ b, 1'\,\ldots\,n'). \tag{1.56}$$

We have used a shorthand notation and bundled (τ, a) pairs into integer variables, i.e. $j \equiv (\tau_j, a_j)$ and $j' \equiv (\tau_j', a_j')$. The equation of motion for the time derivatives acting on the rest of the time

variables can be worked out in a similar way. The MS hierarchy may also be derived directly using functional methods by invoking the so-called *Schwinger-Dyson equation* [35, 36]. Another related hierarchy equation is Bogoliubov-Born-Green-Kirkwood-Yvon (BBGKY) hierarchy [37]. Originally proposed in the context of the kinetic equation of classical gases, the BBGKY hierarchy relates the n-particle probability density function to the $(n+1)$-particle probability density function. The BBGKY hierarchy equations can be deduced from the MS hierarchy by restricting the latter to the equal-time Green's functions.

1.2 The 2PI effective action (2PI-EA) formalism

We briefly reviewed the Schwinger-Keldysh theory of non-equilibrium quantum fields in the previous section. Although the formalism shares many features with the conventional ground state and equilibrium approaches, practical non-equilibrium calculations involve additional complications which are not present in the usual equilibrium calculations. One of such complications is the appearance of *secular* terms in the Feynman-Dyson perturbation expansion of the non-equilibrium Green's functions. The secular terms grow with time and invalidate the perturbation expansion even for weakly coupled systems. Secularity persists even in the (conventional) non-perturbative technique such as the large-N expansion.

The second complication is the requirement of *universality*, i.e. the insensitivity of the late-time behavior to the details of the initial conditions. The the long-time fate a physical system is *uniquely* determined by the initial conserved charges (energy, particle number, momentum, etc). The emergence of an arrow of time and loss of information inevitably requires non-linear dynamical equations. Furthermore, the long-time persistence of conserved charges demands fulfillment of the conservation laws associated to the symmetries of the microscopic action at all times. Therefore, the above requirements impose stringent constraints on the many-body approximations to be

implemented within the non-equilibrium formalism.

It is useful to illustrate the pitfalls of the perturbation expansion in a simple problem. Consider a non-interacting two-component Fermi gas set in motion at $t = t_0$ starting from a thermal equilibrium state with inverse temperature β and chemical potential $\mu_\uparrow = \mu_\downarrow = \mu$. A short-range two-body interaction is immediately switched on at $t = t_0$:

$$\hat{H}(t) = \sum_{\sigma=\uparrow,\downarrow} \int d^d\mathbf{x} \, \Psi_{\sigma,\mathbf{x}}^\dagger \left(-\frac{\nabla^2}{2m} - \mu \right) \Psi_{\sigma,\mathbf{x}} + \theta(t - t_0) \lambda \int d^d\mathbf{x} \, \Psi_{\uparrow,\mathbf{x}}^\dagger \Psi_{\downarrow,\mathbf{x}}^\dagger \Psi_{\downarrow,\mathbf{x}} \Psi_{\uparrow,\mathbf{x}}. \quad (1.57)$$

The non-equilibrium Green's functions can be easily worked out similar to Eq. (1.36) order by order in λ. To first order in λ, we find:

$$G_\uparrow^<(t_1, t_2; \mathbf{k}) = i f_0(\xi_\mathbf{k}) e^{i\xi_\mathbf{k}(t_1-t_2)} + \lambda N_\downarrow f_0(\xi_\mathbf{k})(t_1 - t_2) e^{i\xi_\mathbf{k}(t_1-t_2)} + \mathcal{O}(\lambda^2),$$

$$G_\downarrow^<(t_1, t_2; \mathbf{k}) = i f_0(\xi_\mathbf{k}) e^{i\xi_\mathbf{k}(t_1-t_2)} + \lambda N_\uparrow f_0(\xi_\mathbf{k})(t_1 - t_2) e^{i\xi_\mathbf{k}(t_1-t_2)} + \mathcal{O}(\lambda^2), \quad (1.58)$$

where $\xi_\mathbf{k} = k^2/(2m) - \mu$ and $N_\uparrow = N_\downarrow = \int (d^d\mathbf{k})/(2\pi)^d \, f_0(\xi_\mathbf{k})$. The first-order corrections grow linearly in time and quickly invalidate the perturbation expansion. This is an example of secularity. It is easy to see that the n'th order term in the Dyson series (with the same self-energy) grows like $\sim t^n$. Therefore, finite-order perturbation expansion is of little practical use here. On a related note, the unbounded growth of the Green's function implies the violation of conservation of energy. We note that in this particular case, the secularity can be overcome by summing the same self-energy diagram to all orders. This results in an effective shift of the oscillation frequency of the Green's functions. This simple problem shows the necessity of infinite-order diagrammatic resummation in problems involving non-equilibrium evolutions. Although the secular terms could be removed by a simple resummation in this case, it is generally a non-trivial problem when the diagrammatic expansion involves different classes of diagrams.

Fortunately, functional methods provide a class of approximations which are free of such nuisances. Both of the mentioned requirements, i.e. non-secularity and universality, can be fulfilled using technique of *n-particle irreducible (nPI) effective actions* (*n*PI-EA). We shall motivate the *n*PI-EA formalism by asking the following question:

> *It is possible to express the n-particle Green's function $\mathcal{G}_n$ as exact functional of $\mathcal{G}$, $\mathcal{G}_2$,*
>
> *..., $\mathcal{G}_{n-1}$ (with possible dependence on the initial correlation vertices)? if the answer*
>
> *is positive, how can such a functional be constructed?*

The above question asks for a formalism similar to the density functional theory (DFT), where the ground state energy is given as a universal functional of the number density. Provided that the answer to the above question is positive, such a construction will be of utmost importance: the MS hierarchy can be closed at the level of $\mathcal{G}_{n-1}$ (cf. Eq. 1.56), and the exact dynamics of the many-body system can be determined by integrating the $n-1$ coupled MS equations forward in time.

The answer to the above questions is in fact *positive*, thanks for the *n*PI-EA formalism. Furthermore, provided that the system is initially in a thermal equilibrium state, $\mathcal{G}_n$ will be a *universal* functional, with no reference to the initial correlation vertices. The simplest and most useful method in this family is the 2PI-EA which gives $\mathcal{G}_2$ as a functional of $\mathcal{G}$ and subsequently yields a single self-consistent equation of motion for $\mathcal{G}$. This functional technique, introduced by Cornwall, Jakiw and Tomboulis [38], serves as a rigorous foundation for the Φ-derivable approximations proposed earlier by Baym and Kadanoff [39, 40]. We restrict our discussion to the 2PI-EA which is sufficient for the purpose of the forthcoming developments. Discussion regarding higher order effective actions can be found in Refs. [41, 42].

The 2PI-EA technique is non-perturbative by construction. Although the exact effective action can not be found analytically, its diagrammatic interpretation often allows controlled expansions which share many important features with the exact theory such as long-time universality, non-

secularity and rigorously conserved charges. We review this formalism in the next sections, with

emphasis on application to general superconducting states and the issue of conservation laws.

1.2.1 The generating functional of 2-connected $2n$-point correlators

A cornerstone of the functional techniques is the concept of generating functionals. In general,

a generating functional is obtained by coupling the field operators to one or more external fields,

called the *source fields*. The source fields can be thought of as our probes inside the quantum system.

The correlators are *probed* by varying the source fields. For our current purposes, we are interested

in a source field that couples to the fermion operators bilinearly. More explicitly, we define:

$$Z[K] \equiv \int_f \mathcal{D}[\psi, \bar{\psi}] \exp\left(iS[\psi, \bar{\psi}] + iS_2[\psi, \bar{\psi}, K]\right), \tag{1.59}$$

where K is a 2-particle source field on the time contour $\mathcal{C}$ that couples to the fermion operators as:

$$S_2[\psi, \bar{\psi}, K] \equiv$$

$$-\frac{1}{2} \int_{\mathcal{C}} d\tau_1 \, d\tau_2 \, \left(\psi_{a_1}(\tau_1) \ \bar{\psi}_{a_1}(\tau_1)\right) \begin{pmatrix} K_{--}(\tau_1 a_1, \tau_2, a_2) & K_{-+}(\tau_1 a_1, \tau_2, a_2) \\ K_{+-}(\tau_1 a_1, \tau_2, a_2) & K_{++}(\tau_1 a_1, \tau_2, a_2) \end{pmatrix} \begin{pmatrix} \psi_{a_2}(\tau_2) \\ \bar{\psi}_{a_2}(\tau_2) \end{pmatrix}.$$

$$\tag{1.60}$$

The microscopic action $S[\psi, \bar{\psi}]$ is given in Eq. (1.28). We have restricted our analysis to the systems

either with initial thermal correlations or Gaussian correlations, so that the initial density matrix can

be accounted for using the imaginary propagation or by absorbing the initial two-body correlations

α_2 in the path-integral measure (cf. 1.1.6). As mentioned earlier, arbitrary initial correlations can

be accounted using the Schwinger-Keldysh contour at the expense of introducing additional inter-

action vertices to S_{int}. In order to comply with the Fermi statistics, we require the source fields

to satisfy $K_{++}(\tau_1 a_1, \tau_2 a_2) = -K_{++}(\tau_2 a_2, \tau_1 a_1)$, $K_{--}(\tau_1 a_1, \tau_2 a_2) = -K_{--}(\tau_2 a_2, \tau_1 a_1)$, and

$K_{+-}(\tau_1 a_1, \tau_2 a_2) = -K_{-+}(\tau_2 a_2, \tau_1 a_1)$. We have considered the most general bilinear coupling

so that $Z[K]$ can also be used to calculate the anomalous Green's functions in the superconducting

states where the $U(1)$ gauge symmetry is spontaneously broken. The forthcoming discussion is much facilitated by introducing a uniform notation for the creation and annihilation fermion operators like before. To this end, we introduce a "charge" index, $c = \pm$ to the bundle of internal degrees of freedom a and define:

$$\phi_{\tilde{a}}(\tau) \equiv \begin{cases} \bar{\psi}_a(\tau), & c = +, \\ \psi_a(\tau), & c = -, \end{cases} \tag{1.61}$$

where $\tilde{a} = (a, c)$. We remember that the free part of the action is:

$$\begin{aligned} S_0[\psi, \bar{\psi}] &= \int_{\mathcal{C}} \mathrm{d}\tau \, \mathrm{d}\tau' \, \bar{\psi}_a(\tau) \, \mathcal{G}_0^{-1}(\tau a, \tau' b) \, \psi_b(\tau') \\ &= -\int_{\mathcal{C}} \mathrm{d}\tau \, \mathrm{d}\tau' \, \psi_a(\tau) \, \mathcal{G}_0^{*,-1}(\tau a, \tau' b) \, \bar{\psi}_b(\tau') - \left(\bar{\psi}_a^+ \psi_a^+ - \bar{\psi}_a^- \psi_a^- \right). \end{aligned} \tag{1.62}$$

where $\mathcal{G}_0^{-1}(\tau a, \tau' b) = [i\partial_\tau \delta_{ab} - E_{ab}(\tau)] \delta_{\mathcal{C}}(\tau, \tau')$. We have transferred the time derivative to $\bar{\psi}$ to get the second line. The boundary terms are only effective at $t = t_0$ and hence, only modify the initial conditions. We absorb them to the integral measure, $\mathcal{D}[\psi, \bar{\psi}]$. Using a vector notation $\phi_{\tilde{a}} = (\psi_a, \bar{\psi}_a)$, the free part of the action can be written as:

$$S_0[\phi] = \frac{1}{2} \int_{\mathcal{C}} \mathrm{d}\tau \, \mathrm{d}\tau' \, \phi_{\tilde{a}}^T(\tau) \underbrace{\begin{pmatrix} 0 & -\mathcal{G}_0^{-1}(\tau' b, \tau a) \\ \mathcal{G}_0^{-1}(\tau a, \tau' b) & 0 \end{pmatrix}}_{\equiv \tilde{\mathcal{G}}_0^{-1}(\tau\tilde{a}, \tau'\tilde{b})} \phi_{\tilde{b}}(\tau'). \tag{1.63}$$

It is easy to check that $\tilde{\mathcal{G}}_0^{-1}(\tau\tilde{a}, \tau'\tilde{b}) = -\tilde{\mathcal{G}}_0^{-1}(\tau'\tilde{b}, \tau\tilde{a})$. We also define a general n-particle CTP Green's function in the presence of the 2-particle source field K as:

$$\tilde{\mathcal{G}}_n(\tau_1 \tilde{a}_1 \dots \tau_{2n} \tilde{a}_{2n}; K) \equiv \frac{1}{i^n} \left\langle T_{\mathcal{C}} \left[\phi_{\tilde{a}_1}(\tau_1) \dots \phi_{\tilde{a}_{2n}}(\tau_{2n}) \right] \right\rangle_K, \tag{1.64}$$

where the average $\langle \dots \rangle_K$ implies the path integration with respect to the action $S + S_2$. By construction, permuting the arguments of $\tilde{\mathcal{G}}_n$ only results in a $(-1)^P$ factor, where P is the parity of the permutation. The usual Green's functions $\mathcal{G}$ and for superconducting states, $\mathcal{F}$ and $\bar{\mathcal{F}}$, can be easily

found from $\tilde{\mathcal{G}}$ by assigning appropriate charges to the external points. For instance:

$$\tilde{\mathcal{G}}(\tau_1 a_1 +, \tau_2 a_2 +) = -i \left\langle T_\mathcal{C} \left[\Psi_{a_1}^\dagger(\tau_1) \Psi_{a_2}^\dagger(\tau_2) \right] \right\rangle = \bar{\mathcal{F}}(\tau_1 a_1, \tau_2 a_2),$$

$$\tilde{\mathcal{G}}(\tau_1 a_1 +, \tau_2 a_2 -) = -i \left\langle T_\mathcal{C} \left[\Psi_{a_1}^\dagger(\tau_1) \Psi_{a_2}(\tau_2) \right] \right\rangle = \bar{\mathcal{G}}(\tau_1 a_1, \tau_2 a_2),$$

$$\tilde{\mathcal{G}}(\tau_1 a_1 -, \tau_2 a_2 +) = -i \left\langle T_\mathcal{C} \left[\Psi_{a_1}(\tau_1) \Psi_{a_2}^\dagger(\tau_2) \right] \right\rangle = \mathcal{G}(\tau_1 a_1, \tau_2 a_2),$$

$$\tilde{\mathcal{G}}(\tau_1 a_1 -, \tau_2 a_2 -) = -i \left\langle T_\mathcal{C} \left[\Psi_{a_1}(\tau_1) \Psi_{a_2}(\tau_2) \right] \right\rangle = \mathcal{F}(\tau_1 a_1, \tau_2 a_2), \qquad (1.65)$$

Also, by definition $\bar{\mathcal{G}}(\tau_1 a_1, \tau_2 a_2) = -\mathcal{G}(\tau_2 a_2, \tau_1 a_1)$. The matrix elements of K may also be bundled together by defining $K(\tau_1 \tilde{a}_1, \tau_1 \tilde{a}_2) \equiv K^{c_1 c_2}(\tau_1 a_1, \tau_2 a_2)$. Finally, we often find it useful to bundle a pair of fermion arguments into an effective "bosonic" argument and use a single symbol to refer to it, e.g. $\gamma \equiv (\tau_1 \tilde{a}_1, \tau_2 \tilde{a}_2)$. We also use a bar superscript to refer to the bosonic argument with exchanged fermion points, e.g. $\bar{\gamma} \equiv (\tau_2 \tilde{a}_2, \tau_1 \tilde{a}_1)$.

Before we start the analysis, we note that considerable care must be taken in calculating the functional derivatives with respect to K and $\tilde{\mathcal{G}}$. Since these quantities are antisymmetric, not all of their entries are independent variables. Another word of caution is in using the "chain-rule" for quantities that implicitly depend on $\tilde{\mathcal{G}}$ and K. One must make sure that only independent entries are varied in the chain-rule in order to avoid double counting.

By definition, $Z[K]$ is the generator of $2n$-point Green's functions. For instance, a direct calculation using Eq. (1.59) gives:

$$\frac{1}{Z[K]} \frac{\delta Z[K]}{\delta K(1,2)}\bigg|_{K=0} = -\frac{i}{2} \langle \phi(1)\phi(2) - \phi(2)\phi(1) \rangle = \tilde{\mathcal{G}}(1,2). \qquad (1.66)$$

Taking additional functional derivates with with respect to K produces higher order correlators.

This can be summarized by formally expanding $Z[K]$ about $K = 0$:

$$Z[K] = Z[0] + \int_{\mathcal{C}} \mathrm{d}\tau_1 \, \mathrm{d}\tau_1' \left. \frac{\delta Z[K]}{\delta K(\tau_1 \tilde{a}_1, \tau_1' \tilde{a}_1')} \right|_{K=0} K(\tau_1 \tilde{a}_1, \tau_1 \tilde{a}_1') + \dots$$

$$= Z[0] + \int_{\mathcal{C}} \mathrm{d}\tau_1 \, \mathrm{d}\tau_1' \, \tilde{\mathcal{G}}(\tau_1 \tilde{a}_1, \tau_1' \tilde{a}_1') \, K(\tau_1 \tilde{a}_1, \tau_1 \tilde{a}_1') + \dots$$

$$= Z[0] + \text{⬤} + \dots \tag{1.67}$$

K and $\tilde{\mathcal{G}}$ appear as a hatched circle and a line in the above diagram. Unless K appears explicitly in the argument of a Green's function (as in Eq. 1.64), we assume that the limit $K \to 0$ is implied. The n'th term in the expansion of the $Z[K]$ is:

$$\frac{1}{n!} \int_{\mathcal{C}} \prod_{j=1}^{n} \left(\mathrm{d}\tau_j \, \mathrm{d}\tau_j' \right) \tilde{\mathcal{G}}_n(\tau_1 \tilde{a}_1, \, \tau_1' \tilde{a}_1', \, \dots, \tau_n \tilde{a}_n, \, \tau_n' \tilde{a}_n')$$

$$\times K(\tau_1 \tilde{a}_1, \tau_1' \tilde{a}_1') \dots K(\tau_n \tilde{a}_n, \tau_n' \tilde{a}_n') \sim \text{⬤} \tag{1.68}$$

Consider a $n > 1$ term in the above series. The diagrams contributing to such a term are either fully *connected* to the n external bosonic vertices, or have *disconnected* parts. For example, consider the following decomposition:

$$\tilde{\mathcal{G}}_2(1, 2, 3, 4) = \tilde{\mathcal{G}}(1, 2) \, \tilde{\mathcal{G}}(3, 4) - \tilde{\mathcal{G}}(1, 3) \, \tilde{\mathcal{G}}(2, 4) + \tilde{\mathcal{G}}(1, 4) \, \tilde{\mathcal{G}}(2, 3) + \tilde{\mathcal{G}}_2^{(c)}(1, 2, 3, 4), \tag{1.69}$$

where the last term denotes the sum of all *fully connected* contributions. Plugging this expression into Eq. (1.68), we obtain the following contributions to $Z[K]$:

$$-\frac{1}{2} \left(\int_{\mathcal{C}} \mathrm{d}\tau_1 \, \mathrm{d}\tau_1' \, \tilde{\mathcal{G}}(1, 1') K(1, 1') \right) \left(\int_{\mathcal{C}} \mathrm{d}\tau_2 \, \mathrm{d}\tau_2' \, \tilde{\mathcal{G}}(2, 2') K(2, 2') \right)$$

$$-\frac{1}{2} \int_{\mathcal{C}} \mathrm{d}\tau_1 \mathrm{d}\tau_1' \mathrm{d}\tau_2 \mathrm{d}\tau_2' \left(-\tilde{\mathcal{G}}(1, 2)\tilde{\mathcal{G}}(1', 2') + \tilde{\mathcal{G}}(1, 2')\tilde{\mathcal{G}}(1', 2) + \tilde{\mathcal{G}}_2^{(c)}(1, 1', 2, 2') \right) K(1, 1') K(2, 2').$$

$$\tag{1.70}$$

The first contribution is explicitly the product of two disconnected diagrams, whereas the other three terms can not be disentangled. More generally, we define a 2-*connected diagram* in the

expansion of $Z[K]$ if it can not be decomposed into the product of two disconnected pieces. We use the prefix 2- in order to avoid confusion with the usual definition of connectedness, which requires connectedness at the level of 1-particle fields. The generator of the 2-connected $2n$-point Green's functions can be found from $Z[K]$ using the linked cluster theorem:

Theorem. *(linked cluster theorem for the generator of 2-connected $2n$-point Green's functions)*
If $Z[K]$ is the generator of $2n$-point Green's function, then $W[K] \equiv \ln Z[K]$ is the generator of the 2-connected $2n$-point Green's functions.

(proof) The easiest proof is by using the replica technique [29]. The basic idea of the replica method is to evaluate $Z[K]^n$ for integer n by replicating the system n times and expanding the result as follows:

$$Z[K]^n = e^{n \ln Z[K]} = 1 + n \ln Z[K] + \sum_{m=2}^{\infty} \frac{(n \ln Z[K])^m}{m!}. \qquad (1.71)$$

If we evaluate $Z[K]^n$ for integer n by perturbation theory, $\ln Z[K]$ is given by the coefficients of the terms proportional to n. A more general statement of the method is to calculate $Z[K]^n$ for integer n, continue the function to $n = 0$ (which is unique by Carlson theorem) and evaluate an appropriate expression involving the continued function to calculate the observable of interest. In the present case, we calculate:

$$\lim_{n \to 0} \frac{\mathrm{d}}{\mathrm{d}n} Z[K]^n = \lim_{n \to 0} \frac{\mathrm{d}}{\mathrm{d}n} \left(e^{n \ln Z[K]} \right) = \ln Z[K]. \qquad (1.72)$$

For integer n, we may write $Z[K]^n$ as a functional integral over n copies of fields, $\tilde{\psi}_a^{(\sigma)}$, where σ runs from 1 to n. Now, each propagator carries an index σ and all propagators entering or leaving a given vertex has the same index σ, and all σ's are summed from 1 to n. It is evident that each connected part of a diagram must carry a single single σ, hence, a factor of n, whereas a diagram with n_c connected pieces will have n_c free σ indices and therefore, is proportional to n^{n_c}.

Combining this fact with Eq. (1.71) gives the desired result.

We calculate the first few 2-connected Green's functions to explicitly demonstrate the theorem:

$$\tilde{\mathcal{G}}^{(2c)}(\gamma) \equiv \frac{\delta W[K]}{\delta K(\gamma)} = \tilde{\mathcal{G}}(\gamma), \tag{1.73a}$$

$$\tilde{\mathcal{G}}_2^{(2c)}(\gamma_1, \gamma_2) \equiv \frac{\delta^2 W[K]}{\delta K(\gamma_1)\,\delta K(\gamma_2)} = \tilde{\mathcal{G}}_2(\gamma_1, \gamma_2) - \tilde{\mathcal{G}}(\gamma_1)\,\tilde{\mathcal{G}}(\gamma_2), \tag{1.73b}$$

$$\tilde{\mathcal{G}}_3^{(2c)}(\gamma_1, \gamma_2, \gamma_3) \equiv \frac{\delta^3 W[K]}{\delta K(\gamma_1)\,\delta K(\gamma_2)\,\delta K(\gamma_3)} = \tilde{\mathcal{G}}_3(\gamma_1, \gamma_2, \gamma_3) - \tilde{\mathcal{G}}(\gamma_1)\,\tilde{\mathcal{G}}_2^{(2c)}(\gamma_2, \gamma_3)$$

$$- \tilde{\mathcal{G}}(\gamma_2)\,\tilde{\mathcal{G}}_2^{(2c)}(\gamma_1, \gamma_3) - \tilde{\mathcal{G}}(\gamma_3)\,\tilde{\mathcal{G}}_2^{(2c)}(\gamma_1, \gamma_2) - \tilde{\mathcal{G}}(\gamma_1)\,\tilde{\mathcal{G}}(\gamma_2)\,\tilde{\mathcal{G}}(\gamma_3). \tag{1.73c}$$

The above expressions at valid when $K \neq 0$ as well. We have used the "bosonic" index bundling defined earlier. The expressions on the right hand side of the above equation must be interpreted as follows: if $\gamma_i = (\tau_i \tilde{a}_i, \tau_i' \tilde{a}_i')$, then $\tilde{\mathcal{G}}(\gamma_1) \equiv \tilde{\mathcal{G}}(\tau_1 \tilde{a}_1, \tau_1' \tilde{a}_1')$, $\tilde{\mathcal{G}}_2(\gamma_1, \gamma_2) \equiv \tilde{\mathcal{G}}_2(\tau_1 \tilde{a}_1, \tau_1' \tilde{a}_1', \tau_2 \tilde{a}_2, \tau_2' \tilde{a}_2')$, etc. The bosonic indices can be freely permuted within in a Green's function without any sign changes. This is a consequence of time-ordering and the even parity of such permutations. Note that the term which is subtracted from $\tilde{\mathcal{G}}_2$ to give $\tilde{\mathcal{G}}_2^{(2c)}$ is exactly the term that produces the 2-disconnected graphs in Eq. (1.70).

1.2.2 The 2PI effective action and the Luttinger-Ward functional

The formalism we seek here has a strong resemblance to the least action principle in Lagrangian classical mechanics. In the latter, the dynamical equations are obtained by requiring the stationarity of the classical action, i.e. $\delta A[\{q_i\}] = 0$, where $\{q_i\}$ are the classical generalized coordinates. Here, we would like to find a functional $\Gamma[\tilde{\mathcal{G}}]$ such that it becomes stationary at the exact $\tilde{\mathcal{G}}$. In fact, using the results of the previous section, such a functional is easily within reach. Since the variations of $W[K]$ with respect to K gives $\tilde{\mathcal{G}}$, we can trade K with $\tilde{\mathcal{G}}$ via a Legendre transformation, i.e.

by defining[1] $\Gamma[\tilde{\mathcal{G}}] \equiv W[\tilde{\mathcal{G}}] - (1/2)\text{Tr}[K\tilde{\mathcal{G}}]$. The variation of $\Gamma[\tilde{\mathcal{G}}]$ with respect to $\tilde{\mathcal{G}}$ yields K. Since the physical Green's function is the one evaluated for vanishing source fields, we readily find $\delta\Gamma[\tilde{\mathcal{G}}(K=0)] = 0$. This is exactly our sought after functional, as first proposed by Cornwall, Jakiw and Tomboulis [38].

More explicitly, we define the 2PI-EA $\Gamma[\tilde{\mathcal{G}}]$ as:

$$\Gamma[\tilde{\mathcal{G}}] = W[K] - \frac{1}{2}\int \mathrm{d}\alpha \, \frac{\delta W[K]}{\delta K(\alpha)} \, K(\alpha)$$

$$= W[K] - \frac{1}{2}\int \mathrm{d}\alpha \, \tilde{\mathcal{G}}(\alpha) \, K(\alpha). \tag{1.74}$$

We have used a shorthand notation for summation over the bosonic argument bundle:

$$\int \mathrm{d}\alpha \, A(\alpha) \, B(\alpha) \equiv \int_{\mathcal{C}} \mathrm{d}\tau_1 \, \mathrm{d}\tau_1' \, A(\tau_1\tilde{a}_1, \tau_1'\tilde{a}_1') \, B(\tau_1\tilde{a}_1, \tau_1'\tilde{a}_1'). \tag{1.75}$$

The source field K in Eq. (1.74) must be thought of as a functional of $\tilde{\mathcal{G}}$ as implicitly defined by inverting Eq. (1.73a). Varying $\Gamma[\tilde{\mathcal{G}}]$ with respect to $\tilde{\mathcal{G}}$ gives:

$$\frac{\delta\Gamma[\tilde{\mathcal{G}}]}{\delta\tilde{\mathcal{G}}(\gamma)} = \frac{1}{2}\int \mathrm{d}\alpha \, \frac{\delta W[K]}{\delta K(\alpha)}\frac{\delta K(\alpha)}{\delta\tilde{\mathcal{G}}(\gamma)} - \frac{1}{2}\left(K(\gamma) - K(\bar{\gamma})\right) - \frac{1}{2}\int \mathrm{d}\alpha \, \tilde{\mathcal{G}}(\alpha) \, \frac{\delta K(\alpha)}{\delta\tilde{\mathcal{G}}(\gamma)} = -K(\gamma), \tag{1.76}$$

where we have used the antisymmetry of K and $\tilde{\mathcal{G}}$. The factor of $1/2$ in the appearing in the "chain rules" used for the first term is to cancel the double-counting. The cancellation of the first and the last term is due to Eq. (1.73a). By definition, the physical Green's function $\tilde{\mathcal{G}}_{\text{phys.}}$ is defined such that $K[\tilde{\mathcal{G}}_{\text{phys.}}] = 0$. Eq. (1.76) immediately implies:

$$\left.\frac{\delta\Gamma[\tilde{\mathcal{G}}]}{\delta\tilde{\mathcal{G}}(\gamma)}\right|_{\tilde{\mathcal{G}}=\tilde{\mathcal{G}}_{\text{phys.}}} = 0. \tag{1.77}$$

The above equation is the sought after *stationarity condition*.

---

[1] The factor $1/2$ is to compensate for double counting in summations in the trace (i.e. the product defined in Eq. 1.96). Note that $K(\gamma) = -K(\bar{\gamma})$ and $\tilde{\mathcal{G}}(\gamma) = -\tilde{\mathcal{G}}(\bar{\gamma})$.

Let us calculate Γ to 1-loop order. Using the standard Gaussian integration formula of Grassmann numbers, we easily find:

$$W^{1-\text{loop}}[K] = \frac{1}{2} \operatorname{Tr} \ln \left[-i(\tilde{\mathcal{G}}_0^{-1} - K) \right], \tag{1.78}$$

where the trace and logarithm function must be interpreted in a functional sense. Eq. (1.73a) gives the relation between K and $\tilde{\mathcal{G}}$ at the 1-loop order:

$$\tilde{\mathcal{G}}^{1-\text{loop}}(\gamma) = \frac{\delta W^{1-\text{loop}}[K]}{\delta K(\gamma)} = -\frac{1}{2} \left(\tilde{\mathcal{G}}_0^{-1} - K \right)^{-1} (\bar{\gamma}) + \frac{1}{2} \left(\tilde{\mathcal{G}}_0^{-1} - K \right)^{-1} (\gamma)$$

$$= \left(\tilde{\mathcal{G}}_0^{-1} - K \right)^{-1} (\gamma). \tag{1.79}$$

We have used the antisymmetry of K and $\tilde{\mathcal{G}}_0$ to get the second line. The above result can be written in the more familiar from of a Dyson's equation:

$$\tilde{\mathcal{G}}^{-1}(\gamma) = \tilde{\mathcal{G}}_0^{-1}(\gamma) - K(\gamma), \tag{1.80}$$

which is in fact the expected result in the 1-loop order. The inversion of K in terms of $\tilde{\mathcal{G}}$ is immediate and indeed requiring $K[\tilde{\mathcal{G}}_{\text{phys.}}] = 0$ gives $\tilde{\mathcal{G}} = \tilde{\mathcal{G}}_0$. The 1-loop 2PI effective action is readily found from its definition, Eq. (1.74):

$$\Gamma^{1-\text{loop}}[\tilde{\mathcal{G}}] = \frac{1}{2} \operatorname{Tr} \ln \tilde{\mathcal{G}}^{-1} + \frac{1}{2} \operatorname{Tr} \left(\tilde{\mathcal{G}}_0^{-1} \tilde{\mathcal{G}} \right) + \text{const.}, \tag{1.81}$$

where the constant is independent of $\tilde{\mathcal{G}}$. Beyond the 1-loop order, effective action will get corrections from interactions, which we may write as:

$$\Gamma[\tilde{\mathcal{G}}] = \frac{1}{2} \operatorname{Tr} \ln \tilde{\mathcal{G}}^{-1} + \frac{1}{2} \operatorname{Tr} \left(\tilde{\mathcal{G}}_0^{-1} \tilde{\mathcal{G}} \right) + \Phi[\tilde{\mathcal{G}}]. \tag{1.82}$$

The above equation defines $\Phi[\tilde{\mathcal{G}}]$. We will see shortly that $\Phi[\tilde{\mathcal{G}}]$ coincides with the *Luttinger-Ward functional* $Y'[\mathcal{G}]$ [43] for normal systems. The naming convention Φ become popular in the condensed-matter field theory literature after the important contributions of Baym and Kadanoff [39, 39] and the idea of "Φ-derivability" (to be discussed later). The Luttinger-Ward

functional is referred to a $\Gamma_2[\tilde{\mathcal{G}}]$ in the relativistic field theory literature, following Ref [38]. The Luttinger-Ward functional has the simple diagrammatic interpretation of being the *sum of all connected 2PI vacuum diagrams with full Green's functions in place of bare Green's functions*. Ref. [38] presents a rigorous proof of this fact by introducing an additional 1-particle source field J in order to remove the 1PI diagrams and replace the bare with full Green's functions. We refrain from this technical discussion. Instead, we investigate the interpretation of Φ using two simpler methods while deriving useful formulas along the way.

1.2.3 The self-consistent Dyson's equation

The stationarity condition of $\Gamma[\tilde{\mathcal{G}}]$ naturally yields the Dyson's equation for $\tilde{\mathcal{G}}$. This is easily noticed by combining Eqs. (1.76) and (1.82):

$$\frac{\delta\Gamma[\tilde{\mathcal{G}}]}{\delta\tilde{\mathcal{G}}(\gamma)} = \tilde{\mathcal{G}}^{-1}(\gamma) - \tilde{\mathcal{G}}_0^{-1}(\gamma) + \frac{\delta\Phi[\tilde{\mathcal{G}}]}{\delta\tilde{\mathcal{G}}(\gamma)} = -K(\gamma). \tag{1.83}$$

Requiring the source field to vanish, we find:

$$\tilde{\mathcal{G}}^{-1}(\gamma) = \tilde{\mathcal{G}}_0^{-1}(\gamma) - \tilde{\Sigma}(\gamma), \qquad \tilde{\Sigma}(\gamma) \equiv \frac{\delta\Phi[\tilde{\mathcal{G}}]}{\delta\tilde{\mathcal{G}}(\gamma)}. \tag{1.84}$$

The above equation is the Dyson's equation for the 1-particle Green's function in the differential form, with $\tilde{\Sigma}$ identified as the 1PI self-energy. The self-energy is obtained by taking a functional derivative of the Luttinger-Ward functional with respect to a Green's function, i.e. by breaking a line in the vacuum diagrams. Since $\tilde{\Sigma}$ is 1PI, the diagrammatic expansion of $\Phi[\tilde{\mathcal{G}}]$ may only contain 2PI diagrams. Therefore, we identify $\Phi[\tilde{\mathcal{G}}]$ as *the sum of 2PI connected vacuum diagrams with $\tilde{\mathcal{G}}$ in place of $\tilde{\mathcal{G}}_0$* as mentioned earlier. This result can be formally written as:

$$\Phi[\tilde{\mathcal{G}}] = \left[\ln \int \mathcal{D}[\psi, \bar{\psi}] \exp\left(iS_{\text{int}}[\psi, \bar{\psi}]\right)\right]_{\text{2PI}, \, \tilde{\mathcal{G}}_0 \to \tilde{\mathcal{G}}}, \tag{1.85}$$

where S_{int} is the interacting part of the action which is at least cubic in the field operators. The diagrammatic expansion rules for Φ is similar to that of the thermodynamical potential. Another

useful expression for Φ is the definition originally given by Luttinger and Ward [43] (generalized and adapted to our notation):

$$\Phi[\tilde{\mathcal{G}}] = \sum_{n,k} \frac{1}{2n} \int \mathrm{d}\gamma\, \tilde{\mathcal{G}}(\gamma)\, \tilde{\Sigma}_k^{(\mathrm{n})}(\gamma), \tag{1.86}$$

where $\tilde{\Sigma}_k^{(\mathrm{n})}$ denote 1PI self-energy diagrams with n interaction lines and k runs over the topologically distinct diagrams. For a theory with point-like two-body interactions, we obtain:

$$\Phi[\tilde{\mathcal{G}}] = \frac{1}{2}\;\; + \frac{1}{4}\;\; + \frac{1}{6}\;\; + \dots. \tag{1.87}$$

In application to normal systems, all lines are the usual $\mathcal{G}$ functions. Anomalous Green's functions must be included in application to superconducting states.

So far, we have treated the Green's functions and the self-energy as matrices in the operator charge space. While such a matrix notation is useful for derivations, it is more transparent to make the charge structure explicit in practice. The charge matrix structure can be made explicit by writing out the matrix elements of the Dyson's equation. Let us find the integral form of the Dyson's equation by multiplying Eq. (1.84) by $\tilde{\mathcal{G}}$ and $\tilde{\mathcal{G}}_0$ from left and right:

$$\tilde{\mathcal{G}}(1,1') = \tilde{\mathcal{G}}_0(1,1') + \int \mathrm{d}2\,\mathrm{d}2'\, \tilde{\mathcal{G}}_0(1,2)\, \tilde{\Sigma}(2,2')\, \tilde{\mathcal{G}}(2',1'). \tag{1.88}$$

The integrals imply summation over the internal degrees of freedom and the contour time. The Green's functions and self-energy are treated as matrices in the 2×2 operator charge space and a matrix product is implied everywhere. Writing the matrix products explicitly, we get:

$$
\begin{pmatrix} \mathcal{F}(1,1') & \mathcal{G}(1,1') \\ \bar{\mathcal{G}}(1,1') & \bar{\mathcal{F}}(1,1') \end{pmatrix}
=
\begin{pmatrix} 0 & \mathcal{G}_0(1,1') \\ \bar{\mathcal{G}}_0(1,1') & 0 \end{pmatrix}
$$
$$
+ \int \mathrm{d}2\,\mathrm{d}2'
\begin{pmatrix} 0 & \mathcal{G}_0(1,2) \\ \bar{\mathcal{G}}_0(1,2) & 0 \end{pmatrix}
\begin{pmatrix} \tilde{\Sigma}(2-,2'-) & \tilde{\Sigma}(2-,2'+) \\ \tilde{\Sigma}(2+,2'-) & \tilde{\Sigma}(2+,2'+) \end{pmatrix}
\begin{pmatrix} \mathcal{F}(2',1') & \mathcal{G}(2',1') \\ \bar{\mathcal{G}}(2',1') & \bar{\mathcal{F}}(2',1') \end{pmatrix}.
$$
$$\tag{1.89}$$

The relation between the usual normal and anomalous self-energies and the matrix elements of $\tilde{\Sigma}$ can be read out from the above equation:

$$\Sigma(1,2) \equiv \tilde{\Sigma}(1+,2-) = \frac{\delta\Phi[\tilde{\mathcal{G}}]}{\delta\bar{G}(1,2)} = -\frac{\delta\Phi[\tilde{\mathcal{G}}]}{\delta G(2,1)},$$

$$\bar{\Sigma}(1,2) \equiv \tilde{\Sigma}(1-,2+) = \frac{\delta\Phi[\tilde{\mathcal{G}}]}{\delta\mathcal{G}(1,2)} = -\frac{\delta\Phi[\tilde{\mathcal{G}}]}{\delta\bar{G}(2,1)},$$

$$\Sigma_F(1,2) \equiv \tilde{\Sigma}(1+,2+) = \frac{\delta\Phi[\tilde{\mathcal{G}}]}{\delta\bar{\mathcal{F}}(1,2)} = -\frac{\delta\Phi[\tilde{\mathcal{G}}]}{\delta\bar{\mathcal{F}}(2,1)},$$

$$\Sigma_{\bar{F}}(1,2) \equiv \tilde{\Sigma}(1-,2-) = \frac{\delta\Phi[\tilde{\mathcal{G}}]}{\delta\mathcal{F}(1,2)} = -\frac{\delta\Phi[\tilde{\mathcal{G}}]}{\delta\mathcal{F}(2,1)}. \tag{1.90}$$

Note that due to the antisymmetry of $\tilde{\Sigma}$ in the superfield notation, $\bar{\tilde{\Sigma}}(1,2) \equiv -\Sigma(2,1)$.

1.2.4 2PI vertices and the Bethe-Salpeter equation

In the last section, we inferred the diagrammatic interpretation of Φ using the Dyson's equation. The 2PI structure of Φ can be shown more directly by relating it to the generating functional of the 2-connected vacuum diagrams $W[K]$). To this end, we define the $2n$-point *2PI vertex* as:

$$\Phi^{(n)}(\gamma_1, \ \ldots, \ \gamma_n) \equiv \frac{\delta^n\Phi[\tilde{\mathcal{G}}]}{\delta\tilde{\mathcal{G}}(\gamma_1) \ldots \delta\tilde{\mathcal{G}}(\gamma_n)}. \tag{1.91}$$

This reason for this terminology will become clear shortly. Taking a second derivative with respect to $\tilde{\mathcal{G}}$ of Eq. (1.76) gives:

$$\frac{\delta^2\Gamma[\tilde{\mathcal{G}}]}{\delta\tilde{\mathcal{G}}(\gamma_1)\delta\tilde{\mathcal{G}}(\gamma_2)} = -\frac{\delta K(\gamma_1)}{\delta\tilde{\mathcal{G}}(\gamma_2)}. \tag{1.92}$$

Using Eq. (1.82), the left hand side of the above equation can be written as follows:

$$\frac{\delta^2\Gamma[\tilde{\mathcal{G}}]}{\delta\tilde{\mathcal{G}}(\gamma_1)\delta\tilde{\mathcal{G}}(\gamma_2)} = \Pi^{-1}(\gamma_1,\gamma_2) + \Phi^{(2)}(\gamma_1,\gamma_2), \tag{1.93}$$

where the inverse 2-particle propagator is given by:

$$\Pi^{-1}(\tau_1\tilde{a}_1, \tau_1'\tilde{a}_1'; \ \tau_2\tilde{a}_2, \tau_2'\tilde{a}_2') \equiv \tilde{\mathcal{G}}^{-1}(\tau_1\tilde{a}_1, \tau_2\tilde{a}_2)\,\tilde{\mathcal{G}}^{-1}(\tau_1'\tilde{a}_1', \tau_2'\tilde{a}_2')$$

$$- \tilde{\mathcal{G}}^{-1}(\tau_1\tilde{a}_1, \tau_2'\tilde{a}_2')\,\tilde{\mathcal{G}}^{-1}(\tau_1'\tilde{a}_1', \tau_2\tilde{a}_2). \tag{1.94}$$

On the other, the right hand side of Eq. (1.92) can be related to the inverse of the 2-connected 2-particle propagator by first noticing that:

$$\frac{\delta \tilde{\mathcal{G}}(\gamma_2)}{\delta K(\gamma_1)} = \frac{\delta}{\delta K(\gamma_1)} \left(\frac{\delta W[K]}{\delta K(\gamma_2)} \right) = \tilde{\mathcal{G}}_2^{(2c)}(\gamma_1, \gamma_2). \tag{1.95}$$

Defining a "bosonic" matrix product between two antisymmetric 4-point functions as:

$$(AB)(\gamma_1, \gamma_2) \equiv \frac{1}{2} \int \mathrm{d}\gamma_3 \, A(\gamma_1, \gamma_3) \, B(\gamma_3, \gamma_2), \tag{1.96}$$

and an antisymmetric bosonic 4-point identity operator $\mathbb{I}(\gamma_1, \gamma_2)$ in a natural way:

$$\mathbb{I}(\tau_1\tilde{a}_1, \tau_1'\tilde{a}_1'; \ \tau_2\tilde{a}_2, \tau_2'\tilde{a}_2') \equiv \delta_{\mathcal{C}}(\tau_1, \tau_2) \, \delta_{\mathcal{C}}(\tau_1', \tau_2') \, \delta_{\tilde{a}_1, \tilde{a}_2} \, \delta_{\tilde{a}_1', \tilde{a}_2'} - \delta_{\mathcal{C}}(\tau_1, \tau_2') \, \delta_{\mathcal{C}}(\tau_1', \tau_2) \, \delta_{\tilde{a}_1, \tilde{a}_2'} \, \delta_{\tilde{a}_1', \tilde{a}_2},$$

$$\tag{1.97}$$

the right hand side of Eq. (1.92) is simply the matrix inverse of $\tilde{\mathcal{G}}_2^{(2c)}(\gamma_1, \gamma_2)$ save for a minus sign. Combining the above results, we find:

$$\Pi^{-1}(\gamma_1, \gamma_2) + \Phi^{(2)}(\gamma_1, \gamma_2) = -\tilde{\mathcal{G}}_2^{(2c),-1}(\gamma_1, \gamma_2). \tag{1.98}$$

The above equation implies that $\Phi^{(2)}$ is sum of all diagrams connected to γ_1 and γ_2, with the 2-particle reducible graphs removed. This justifies the terminology *2PI vertex* for $\Phi^{(2)}$. The same methods can be utilized to show that all $\Phi^{(n)}$ is the sum of all 2PI diagrams pinned to n bosonic external points. Let us elaborate on Eq. (1.98) further by converting it into an integral equation for $\tilde{\mathcal{G}}_2^{(2c)}$:

$$\tilde{\mathcal{G}}_2^{(2c)} = -\left(\Pi^{-1} + \Phi^{(2)} \right)^{-1} = -\Pi - \Pi \, \Phi^{(2)} \, \tilde{\mathcal{G}}_2^{(2c)}, \tag{1.99}$$

We have dropped the shared (γ_1, γ_2) arguments for brevity. Π is the inverse of Π^{-1}, which has the interpretation of the bare 2-particle propagator:

$$\Pi(\tau_1\tilde{a}_1, \tau_1'\tilde{a}_1'; \ \tau_2\tilde{a}_2, \tau_2'\tilde{a}_2') \equiv \tilde{\mathcal{G}}(\tau_1\tilde{a}_1, \tau_2\tilde{a}_2) \, \tilde{\mathcal{G}}(\tau_1'\tilde{a}_1', \tau_2'\tilde{a}_2') - \tilde{\mathcal{G}}(\tau_1\tilde{a}_1, \tau_2'\tilde{a}_2') \, \tilde{\mathcal{G}}(\tau_1'\tilde{a}_1', \tau_2\tilde{a}_2). \tag{1.100}$$

Eq. (1.99) a *Bethe-Salpeter* equation for $\tilde{\mathcal{G}}_2^{(2c)}$ with the following diagrammatic representation:

$$- \left(\tilde{\mathcal{G}}_2^{(2c)} \right) = \underline{\quad\quad} + \underline{\quad} \left(\Phi^{(2)} \right) \left(\tilde{\mathcal{G}}_2^{(2c)} \right) - (\text{exchange leftmost vertices}). \tag{1.101}$$

The dashed lines imply the product defined in Eq. (1.96).

The Bethe-Salpeter equation for $\tilde{\mathcal{G}}_2^{(2c)}$ provides yet another way to interpret the diagrammatic expansion of the Luttinger-Ward functional. By definition, $\tilde{\mathcal{G}}_2^{(2c)}$ is the sum of connected diagrams pinned to two external bosonic points. The 1PI diagrams can be removed by replacing $\tilde{\mathcal{G}}_0$ with $\tilde{\mathcal{G}}$ in the perturbation expansion of $\tilde{\mathcal{G}}_2^{(2c)}$. The Bethe-Salpeter equation further removes the 2PI diagrams, so that $\Phi^{(2)}$ is the sum of all 2PI diagrams pinned to two bosonic vertices. Remembering that $\Phi^{(2)}$ is obtained from Φ by breaking two fermion lines and converting them into bosonic vertices, we again find that Φ is the sum of all 2PI vacuum diagrams (see Eq. 1.85).

The various linear response functions can be calculated directly from $\tilde{\mathcal{G}}_2^{(2c)}$. We consider the retarded density-density response function for concreteness, defined as:

$$\chi_{\text{dd}}^+(t_1 a_1, t_2 a_2) \equiv \frac{\delta n(t_1 a_1; U)}{\delta U(t_2 a_2)}, \tag{1.102}$$
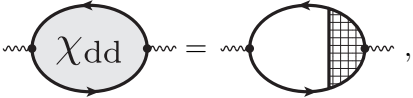
where $n(t_1 a_1) \equiv -iG^<(t_1 a_1, t_1^+ a_1) = -i\tilde{G}^<(t_1 a_1 -, t_1^+ a_1 +)$ is the density, δn is its linear change due to the presence a scalar field $U(t_2 a_2)$ that produces a term $-\int_{\mathcal{C}} d\tau \, \bar{\psi}(\tau a) \, U(ta) \, \psi(\tau a)$ in the action. Since U is a physical field, it assumes the same values on both $\mathcal{C}^+$ and $\mathcal{C}^-$ at a given time. We may express the change in the density as:

$$\delta n(t_1 a_1) = -i \int_{\mathcal{C}} d\tau_2 \, \frac{\delta \tilde{\mathcal{G}}(\tau_1 a_1 -, \tau_1^+ a_1 +; K)}{\delta K_{+-}(\tau_2^+ a_2, \tau_2 a_2)} \, U(t_2 a_2). \tag{1.103}$$
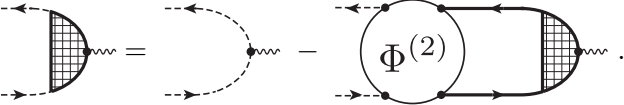
The functional derivative is expressible in terms of $\tilde{\mathcal{G}}_2^{(2c)}$. Here, τ_1 can be placed on either of the contour branches and the result must be the same. Taking a derivative with respect to U results in two contributions from both forward and the backward branch integrations. The result is:

$$\chi_{\text{dd}}^+(t_1 a_1, t_2 a_2) = -i \Bigg[\mathcal{G}_2^{(2c)}(\tau_1 a_1, \tau_1^+ a_1; \tau_2^+ a_2, \tau_2 a_2) \Big|_{\tau_2 \in \mathcal{C}^+}$$
$$- \mathcal{G}_2^{(2c)}(\tau_1 a_1, \tau_1^+ a_1; \tau_2^+ a_2, \tau_2 a_2) \Big|_{\tau_2 \in \mathcal{C}^-} \Bigg], \tag{1.104}$$

where $\mathcal{G}_2^{(c)}(1,2;3,4) \equiv \tilde{\mathcal{G}}_2^{(2c)}(1-,2+;3-,4+)$ in terms of the super Green's functions. The above result is applicable to linear response in both equilibrium and non-equilibrium states. One may write an integral equation for χ_{dd} using the Bethe-Salpether equation of $\mathcal{G}_2^{(2c)}$. Here, we give the result for normal systems:

$$i\chi_{dd}(1,2) = \int d3\, d4\, \mathcal{G}(1,3)\, \mathcal{G}(4,1)\, \Gamma(3,4;2),$$

$$(1.105)$$

where Γ is the scalar vertex function[2] and satisfies the following integral equation:

$$\Gamma(1,2;3) = \delta_{\mathcal{C}}(1,3)\, \delta_{\mathcal{C}}(2,3) - \int d4\, d5\, \frac{\delta^2 \Phi[\mathcal{G}]}{\delta\mathcal{G}(2,1)\, \delta\mathcal{G}(4,5)}\, \mathcal{G}(4,7)\, \mathcal{G}(8,5)\, \Gamma(7,8;3).$$

$$(1.106)$$

1.2.5 The Kadanoff-Baym equations

The Kadanoff-Baym (KB) equations are the exact evolution equation for the 1-particle Green's function. As mentioned earlier in the introductory remarks, the KB equation is just the MS equation for $\tilde{\mathcal{G}}$ (Eq. 1.54) supplemented with $\tilde{\mathcal{G}}_2$ as a functional of $\tilde{\mathcal{G}}$. In the current formulation, the KB equations are obtained by operating the Dyson equation (Eq. 1.83) on $\tilde{\mathcal{G}}$ from the left and integrating over the intermediate contour times and field indices. The result in terms of the normal $\mathcal{G}$ and anomalous $\mathcal{F}$ Green's functions and their related self-energies reads as:

$$[i\partial_{t_1}\delta_{ac} - E_{ac}(t_1)]\, \mathcal{G}(\tau_1 c; \tau_2 b) = \delta_{\mathcal{C}}(\tau_1, \tau_2)\, \delta_{ab} + \int_{\mathcal{C}} d\tau' \, [\Sigma(\tau_1 a; \tau' c) + K_{+-}(\tau_1 a; \tau' c)]$$

$$\times \mathcal{G}(\tau' c; \tau_2 b) + \int_{\mathcal{C}} d\tau' \, [\Sigma_{\mathcal{F}}(\tau_1 a; \tau' c) + K_{++}(\tau_1 a; \tau' c)]\, \bar{\mathcal{F}}(\tau' c; \tau_2 b),$$

$$(1.107a)$$

---

[2]The scalar vertex function is not to be confused with the 2PI-EA.

$$[-i\partial_{t_2}\delta_{cb} - E_{cb}(t_2)]\,\mathcal{G}(\tau_1 a; \tau_2 c) = \delta_{\mathcal{C}}(\tau_1, \tau_2)\,\delta_{ab} + \int_{\mathcal{C}} d\tau'\,\mathcal{G}(\tau_1 a; \tau' c)\,[\Sigma(\tau' c; \tau_2 b)$$

$$+ K_{+-}(\tau' c; \tau_2 b)] + \int_{\mathcal{C}} d\tau'\,\mathcal{F}(\tau_1 a; \tau' c)\,[\Sigma_{\bar{\mathcal{F}}}(\tau' c; \tau_2 b) + K_{--}(\tau' c; \tau_2 b)]\,,$$

$$(1.107\text{b})$$

$$[i\partial_{t_1}\delta_{ac} - E_{ac}(t_1)]\,\mathcal{F}(\tau_1 c; \tau_2 b) = \int_{\mathcal{C}} d\tau'\,[\Sigma(\tau_1 a; \tau' c) + K_{+-}(\tau_1 a; \tau' c)]\,\mathcal{F}(\tau' c; \tau_2 b)$$

$$+ \int_{\mathcal{C}} d\tau'\,[\Sigma_{\mathcal{F}}(\tau_1 a; \tau' c) + K_{++}(\tau_1 a; \tau' c)]\,\bar{\mathcal{G}}(\tau' c; \tau_2 b),$$

$$(1.107\text{c})$$

$$[-i\partial_{t_2}\delta_{cb} - E_{cb}(t_2)]\,\bar{\mathcal{F}}(\tau_1 a; \tau_2 c) = \int_{\mathcal{C}} d\tau'\,\bar{\mathcal{F}}(\tau_1 a; \tau' c)\,[\Sigma(\tau' c; \tau_2 b) + K_{+-}(\tau' c; \tau_2 b)]$$

$$+ \int_{\mathcal{C}} d\tau'\,\bar{\mathcal{G}}(\tau_1 a; \tau' c)\,[\Sigma_{\bar{\mathcal{F}}}(\tau' c; \tau_2 b) + K_{--}(\tau' c; \tau_2 b)]\,.$$

$$(1.107\text{d})$$

We have kept the source fields K in place for future use. Turning off the source fields K, the above equations constitute a complete set of evolution equations for the Green's functions. The time convolution integrals over the Schwinger-Keldysh time contour can be decomposed into physical time integrations using the Langreth rules (cf. Sec. 1.1.7).

The above KB equations are written in the most general form. Here, we consider a system of identical non-relativistic fermions with mass m in a continuum with d spatial dimensions. We further restrict it to the normal state in which $\mathcal{F}$, $\bar{\mathcal{F}}$, $\Sigma_{\mathcal{F}}$ and $\Sigma_{\bar{\mathcal{F}}}$ are identically zero. The field indices a, b, etc denote the space variable $\mathbf{x}$ in this case and E_{ab} is given in Eq. (1.3). The KB equations read as:

$$\left[i\partial_{t_1} - \frac{\nabla_1^2}{2m} - U(t_1, \mathbf{x}_1)\right]\mathcal{G}(\tau_1 \mathbf{x}_1; \tau_2 \mathbf{x}_2) = \delta_{\mathcal{C}}(\tau_1, \tau_2)\,\delta^d(\mathbf{x}_1 - \mathbf{x}_2)$$

$$+ \int_{\mathcal{C}} d\tau' \int d^d \mathbf{x}'\,[\Sigma(\tau_1 \mathbf{x}_1; \tau' \mathbf{x}') + K_{+-}(\tau_1 \mathbf{x}_1; \tau' \mathbf{x}')]\,\mathcal{G}(\tau' \mathbf{x}'; \tau_2 \mathbf{x}_2), \quad (1.108\text{a})$$

$$\left[-i\partial_{t_2} - \frac{\nabla_2^2}{2m} - U(t_2, \mathbf{x}_2)\right] \mathcal{G}(\tau_1\mathbf{x}_1; \tau_2\mathbf{x}_2) = \delta_{\mathcal{C}}(\tau_1, \tau_2)\,\delta^d(\mathbf{x}_1 - \mathbf{x}_2)$$

$$+ \int_{\mathcal{C}} \mathrm{d}\tau' \int \mathrm{d}^d\mathbf{x}'\, \mathcal{G}(\tau_1\mathbf{x}_1; \tau'\mathbf{x}') \left[\Sigma(\tau'\mathbf{x}'; \tau_2\mathbf{x}_2) + K_{+-}(\tau'\mathbf{x}'; \tau_2\mathbf{x}_2)\right]. \quad (1.108b)$$

The equations for the explicit-time components (*lesser*, *greater*, retarded and advanced) can be determined from Eq. (1.52):

$$\left[i\partial_{t_1} - \frac{\nabla_1^2}{2m} - U(t_1, \mathbf{x}_1)\right] G^{\gtrless}(t_1\mathbf{x}_1; t_2\mathbf{x}_2) =$$

$$\int_{-\infty}^{\infty} \mathrm{d}t' \int \mathrm{d}^d\mathbf{x}' \left[\Sigma^+(t_1\mathbf{x}_1; t'\mathbf{x}') + K_{+-}^+(t_1\mathbf{x}_1; t'\mathbf{x}')\right] G^<(t'\mathbf{x}'; t_2\mathbf{x}_2)$$

$$\int_{-\infty}^{\infty} \mathrm{d}t' \int \mathrm{d}^d\mathbf{x}' \left[\Sigma^{\gtrless}(t_1\mathbf{x}_1; t'\mathbf{x}') + K_{+-}^{\gtrless}(t_1\mathbf{x}_1; t'\mathbf{x}')\right] G^-(t'\mathbf{x}'; t_2\mathbf{x}_2), \quad (1.109a)$$

$$\left[-i\partial_{t_2} - \frac{\nabla_1^2}{2m} - U(t_1, \mathbf{x}_1)\right] G^{\gtrless}(t_1\mathbf{x}_1; t_2\mathbf{x}_2) =$$

$$\int_{-\infty}^{\infty} \mathrm{d}t' \int \mathrm{d}^d\mathbf{x}'\, G^+(t_1\mathbf{x}_1; t', \mathbf{x}') \left[\Sigma^{\gtrless}(t'\mathbf{x}'; t_2\mathbf{x}_2) + K_{+-}^{\gtrless}(t'\mathbf{x}'; t_2\mathbf{x}_2)\right]$$

$$\int_{-\infty}^{\infty} \mathrm{d}t' \int \mathrm{d}^d\mathbf{x}'\, G^{\gtrless}(t_1\mathbf{x}_1; t', \mathbf{x}') \left[\Sigma^-(t'\mathbf{x}'; t_2\mathbf{x}_2) + K_{+-}^-(t'\mathbf{x}'; t_2\mathbf{x}_2)\right], \quad (1.109b)$$

$$\left[i\partial_{t_1} - \frac{\nabla_1^2}{2m} - U(t_1, \mathbf{x}_1)\right] G^\pm(t_1\mathbf{x}_1; t_2\mathbf{x}_2) = \delta(t_1 - t_2)\,\delta^d(\mathbf{x}_1 - \mathbf{x}_2)$$

$$\int_{-\infty}^{\infty} \mathrm{d}t' \int \mathrm{d}^d\mathbf{x}' \left[\Sigma^\pm(t_1\mathbf{x}_1; t'\mathbf{x}') + K_{+-}^\pm(t_1\mathbf{x}_1; t'\mathbf{x}')\right] G^\pm(t'\mathbf{x}'; t_2\mathbf{x}_2), \quad (1.109c)$$

$$\left[-i\partial_{t_2} - \frac{\nabla_1^2}{2m} - U(t_1, \mathbf{x}_1)\right] G^\pm(t_1\mathbf{x}_1; t_2\mathbf{x}_2) = \delta(t_1 - t_2)\,\delta^d(\mathbf{x}_1 - \mathbf{x}_2)$$

$$\int_{-\infty}^{\infty} \mathrm{d}t' \int \mathrm{d}^d\mathbf{x}'\, G^\pm(t_1\mathbf{x}_1; t', \mathbf{x}') \left[\Sigma^\pm(t'\mathbf{x}'; t_2\mathbf{x}_2) + K_{+-}^\pm(t'\mathbf{x}'; t_2\mathbf{x}_2)\right]. \quad (1.109d)$$

We would like to emphasize on an earlier remark that the terms involving the mixed imaginary/real time Green's functions have been neglected after taking the limit $T_0 \to -\infty$. The initial thermal correlations are put back in by requiring the KMS boundary condition, Eq. (1.48). The KB equations constitute a convenient starting point for deriving quantum kinetic equation, a problem

which we discuss in the next chapter.

An important aspect of the KB equations is their non-Markovian structure, which is evident from the convolution integrals appearing on the right hand side of the above equations. The appearance of non-Markovian terms are referred to as *memory effects*. We would like to compare the KB equations to the Schrödinger's equation of the many-body wave function, the MS hierarchy and the BBGKY hierarchy, all three of of which have a Markovian structure, albeit in an extremely large state space[3] The emergence of memory effects in a natural consequence of any (exact) reduction of the state space. Let us explain this using a simple toy model. Consider a two state system with the state vector $\Psi = (\psi_1, \psi_2)$ with a simple linear Markovian evolution:

$$i\partial_t \psi_1(t) = a_{11}(t)\psi_1(t) + a_{12}(t)\psi_2(t),$$

$$i\partial_t \psi_2(t) = a_{21}(t)\psi_1(t) + a_{22}(t)\psi_2(t). \tag{1.110}$$

Solving ψ_2 in terms of ψ_1, we find the following evolution equation for ψ_1:

$$i\partial_{t_1} \psi_1(t) = a_{11}(t)\psi_1(t) + a_{12}(t) \left(\psi_2(t_0) e^{-iA_{22}(t)} - i \int_{t_0}^{t} dt' \, e^{-i[A_{22}(t) - A_{22}(t')]} a_{21}(t')\psi_1(t') \right),$$

$$\tag{1.111}$$

where $A_{22}(t) = \int_{t_0}^{t} dt' \, a_{22}(t')$. The last equation shows that by reducing the state space, i.e. $(\psi_1, \psi_2) \rightarrow \psi_1$, the exact evolution equation for ψ_1 will depend on the full history of the reduced state vector (here, ψ_1). In other words, it is only by knowing the full history of the reduced state vector that we can reproduce the effects of the lost degrees of freedom. This simple toy model provides a useful analogy between the KB equation and the MS hierarchy: reducing the infinite dimensional state vector of the MS hierarchy $(\mathcal{G}, \mathcal{G}_2, \mathcal{G}_3, \ldots)$ to $\mathcal{G}$, the emergence of memory effects is quite natural. In other words, it is only by referring to the complete history of the 2-point correlations that

---

[3]The state state of the many-body Schrödinger's equation is the Fock space $\mathcal{F}$. The state space of the MS and BBGKY hierarchy is the infinite dimensional bundle of all Green's functions and partial traces of the density matrix, respectively. The time evolution of these bundles only depends on the instantaneous Hamiltonian (cf. 1.1.8).

the effects of higher-order correlations can be reconstructed. In fact, the Bethe-Salpeter equation discussed in the previous section (Eq. 1.101) provides an explicit expression for $\mathcal{G}_2$ in terms of $\mathcal{G}$ and $\Phi^{(2)}[\mathcal{G}]$ in the form of an integral equation. The reconstruction of higher order Green's functions $\mathcal{G}_3$, $\mathcal{G}_4$, etc is achieved by taking additional derivatives of the effective action and following the same steps. *Nothing is lost.*

The history of the 2PI-EA formalism:

The 2PI-EA formalism is a modern development and terminology. The first and the most important developments along this line is the seminal contribution of Baym and Kadanoff [39, 40], which was an attempt to construct symmetry conserving linear response functions. In Ref. [39], Baym and Kadanoff pointed out the sufficient conditions on approximate expressions for G_2 such that the evolution equations respect the conservation laws. In Ref. [40], Baym introduced a large class of many-body approximation, the so-called "Φ-derivable" approximations, which satisfy the criteria Baym and Kadanoff had proposed earlier. More explicitly, Baym shows that if $\Phi[G]$ is *any* functional of G that is invariant under symmetry transformations of G, and that the self-energy is obtained from $\Phi[G]$ by a functional differentiation, then the ensuing 1-particle evolution equations respect the conserved charges. It was also shown that $\Phi[G]$ is simply the sum of 2-particle-irreducible (2PI) vacuum diagrams one obtains from the perturbation expansion of the thermodynamic potential, with full Green's functions G in place of bare Green's functions G_0. Historically, Luttinger and Ward's $Y'[G]$ functional [43], introduced in an attempt to organize and sum large class of Feynman diagrams, coincides with Baym's $\Phi[G]$. For this reason, Φ is often referred to as the Luttinger-Ward functional. A closely related formulation was also proposed by De Dominicis and Martin [44].

Baym and Kadanoff's original idea was developed further, mostly in the particle physics community, and using functional methods. Cornwall, Jakiw and Tomboulis [38] generalized the existing technique of 1PI-EA for bosonic fields to composite operators, and introduced the 2PI-EA formal-

ism. This idea was later generalized to higher order composite operators [41, 42], resulting in the notion of nPI-EA.

1.3 General approximation schemes of the Luttinger-Ward functional

The Luttinger-Ward functional Φ is formally defined as the sum of the quantum corrections to the effective action beyond the 1-loop order (cf. Eq. 1.82). In general, no universally applicable method exists for approximating Φ in a controlled way with bounded error. An important and often challenging step in using the 2PI-EA formalism is choosing the right approximation scheme for Φ. Approximate Luttinger-Ward functionals can be constructed using the diagrammatic interpretation of Φ, Eq. (1.85), by keeping only a certain class of vacuum diagrams. Such approximations are referred to as Φ-*derivable approximations* following Baym [40].

The most salient feature of Φ-derivable approximations is that regardless of the choice of vacuum diagrams, conservation laws associated to the symmetries of the action will be rigorously respected. Arguably, respecting conservation laws is the most basic requirement from a microscopic theory. We will discuss this in the next section. We remark that regardless of one's choice for Φ, the resulting Dyson's equation is non-perturbative by construction and corresponds to an infinite-order expansion in the interaction coupling. This is due to the fact that the Φ-derived self-energy $\Sigma[\mathcal{G}] = \delta\Phi[\mathcal{G}]/\delta\mathcal{G}$ is a functional of the *full* Green's function. It is exactly such self-consistencies that result in the emergence of conservation laws, non-secularity and for powerful enough truncations (beyond the 2-loop level), long-time universality.

A simple and controlled expansion of Φ for weakly interacting systems is the *loop expansion*, where the vacuum diagrams are characterized based on the number of interaction vertices. A vacuum diagram with n interaction vertex insertions has n momentum loop integrals and is proportional to λ^n, where λ is the coupling constant. The 2-loop and 3-loop corrections give rise to the Hartree-

Fock and Born self-energy diagrams (discussed in next section).

If the system in question has a large number of field operators N, such as the $O(N)$-symmetric ϕ^4 field theory [38], the $SU(N)$-symmetric quantum gas with N hyperfine states [45], and the $Sp(N)$-symmetric attractive Hubbard and t-J models [46, 47], the vacuum diagrams can be classified in terms of the small parameter $1/N$. The resulting scheme is referred to as the $1/N$-*expansion*, also known as the *large-N expansion*. At the leading order in $1/N$, one recovers the mean-field theory which becomes exact in the limit $N \to \infty$. The inclusion of next to leading order corrections in $1/N$ adds in the effects of quantum fluctuations order by order. The large-N expansion is often utilized heuristically by artificially enlarging the symmetry group of the physical system, i.e. $O(2) \to O(N)$, so that a systematic categorization of the vacuum diagrams is made feasible.

A third scheme is the low-density expansion for systems with repulsive interactions with a range r_0 much smaller than the inter-particle separation $n^{-1/d}$. The diagrams with the same number of cycles contribute to the same order in $n^{1/d}r_0$. We discuss the loop expansion, and the large-N expansion for the $Sp(N)$-symmetric Fermi gas in the next sections.

1.3.1 Loop expansion

We consider the microscopic action given in Eq. (1.121). For concreteness, we consider a single-component system in the normal state with $\lambda(1, 2)$ representing a instantaneous and possibly long-range interaction, i.e. $\lambda(1, 2) \to V(\mathbf{x}_1 - \mathbf{x}_2)\,\delta_{\mathcal{C}}(\tau_1, \tau_2)$. The 2PI vacuum diagrams and their accompanying symmetry factors can be evaluated directly from Eq. (1.85). Expanding $\Phi[\mathcal{G}]$ to the 3-loop order (up to two interaction vertices), we find:

$$\Phi[\mathcal{G}] = \underbrace{\frac{1}{2}\,\bigcirc\!\!\cdots\!\!\bigcirc + \frac{1}{2}\,\bigcirc}_{\Phi_{\mathrm{HF}}[\mathcal{G}]} + \underbrace{\frac{1}{4}\,\bigcirc\bigcirc + \frac{1}{4}\,\boxtimes}_{\Phi_{\mathrm{B}}[\mathcal{G}]} + \mathcal{O}(V^3). \qquad (1.112)$$

The pre-factors accompanying each vacuum diagram can be determined by a direct investigation. A simple heuristic method is to consider the resulting self-energy diagrams. Since the self-energy

diagrams have no symmetry factors, the pre-factor of a given vacuum diagram is simply given by $n_\Sigma/n_\mathcal{G}$, where n_Σ is the number of topologically distinct self-energy diagrams that results from the vacuum diagram upon breaking a Green's function line, and $n_\mathcal{G}$ is the number of Green's function lines in the vacuum diagram.

The first two diagrams are known as the *Hatree-Fock* (HF) contributions and give the self-energy:

$$\Sigma_{\mathrm{HF}}(1,1') = -\frac{\delta\Phi_{\mathrm{HF}}[\mathcal{G}]}{\delta\mathcal{G}(1',1)} = \delta_\mathcal{C}(\tau_1,\tau_1')\left[\delta(\mathbf{x}_1-\mathbf{x}_1')\int \mathrm{d}^d\mathbf{x}_2\, V(\mathbf{x}_1-\mathbf{x}_2)\,(-i)G^<(t_1,\mathbf{x}_2;t_1,\mathbf{x}_2)\right.$$
$$\left. + V(\mathbf{x}_1-\mathbf{x}_1')\,iG^<(t_1,\mathbf{x}_1;t_1,\mathbf{x}_1')\right]. \quad (1.113)$$

The HF approximation is a mean-field description. Going back to the MS hierarchy equations and forgetting the heavy machinery of 2PI-EA for a moment, we notice that the HF approximation can be obtained by neglecting 2-particle correlations. It is indeed straightforward to see that plugging Σ_{HF} into the KBE yields the same equation of motion as the one obtained from truncating the MS hierarchy using the prescription $G_2(1,2,3,4) \rightarrow G(1,4)G(2,3) - G(1,3)G(2,4)$. The HF self-energy is instantaneous and $\Sigma_{\mathrm{HF}}^\gtrless = 0$. Without $\Sigma^\gtrless$, the KB equations are Markovian (memoryless) and do not describe important phenomena such as collisional damping and thermalization. The last two diagrams, known as the *Born diagrams*, describe the simplest processes that introduce memory effects. The self-energy corresponding to the Born diagram is given by:

$$\Sigma_{\mathrm{B}}^\gtrless(1,1') = -\frac{\delta\Phi_{\mathrm{B}}[\mathcal{G}]}{\delta\mathcal{G}(1',1)} = \int \mathrm{d}^d\mathbf{x}_2\,\mathrm{d}^d\mathbf{x}_2'\, V(\mathbf{x}_1-\mathbf{x}_2)\,V(\mathbf{x}_2'-\mathbf{x}_1')\left[G^\gtrless(t_1,\mathbf{x}_1;t_1',\mathbf{x}_1')\right.$$

$$\times G^\gtrless(t_1,\mathbf{x}_2;t_1',\mathbf{x}_2')\,G^\lessgtr(t_1',\mathbf{x}_2';t_1,\mathbf{x}_2) - G^\gtrless(t_1,\mathbf{x}_1;t_1',\mathbf{x}_2')\,G^\gtrless(t_1,\mathbf{x}_2;t_1',\mathbf{x}_1')\,G^\lessgtr(t_1',\mathbf{x}_2';t_1,\mathbf{x}_2)\Big].$$
$$(1.114)$$

The self-energy at the 3-loop level is simply the sum of the above two self-energies:

$$\Sigma_{3-\mathrm{loop}}[\mathcal{G}] = \Sigma_{\mathrm{HF}}[\mathcal{G}] + \Sigma_{\mathrm{B}}[\mathcal{G}]. \quad (1.115)$$

We will refer to the 3-loop self-energy as the Born approximation for brevity. Higher order vacuum diagrams in the loop expansion of Φ can be treated in the similar fashion.

1.3.2 $1/N$ **expansion**

The $1/N$-expansion is a useful scheme for a systematic classification of the vacuum diagrams. It has been successfully utilized to study the far-from-equilibrium dynamics of quantum fields in the context of early universe and inflation [48, 49, 50, 51] and ultracold Fermi gases [52]. Keeping the leading-order (LO) and the next-to-leading-order (NLO) terms is sufficient for describing collisions and memory effects in a systematic way, leading to pre-thermalization [32] and thermalization [51] phenomena.

As an illustration of the large-N expansion for a model which will be studied in chapter 4, we consider a fictitious system with $2N$ field operators, $\psi_{\sigma j}$ and their conjugates. Here, the *spin* index assumes two values, $\sigma = \uparrow, \downarrow$, while the *flavor* index j ranges from 1 to N. We consider the action studied in Refs. [46, 47]:

$$
S_0[\psi, \bar{\psi}] = \int d1 \bar{\psi}_{\sigma j}(1) \left(i\partial_{t_1} + \mu + \frac{\nabla_1^2}{2m} \right) \psi_{\sigma j}(1),
$$

$$
S_{\text{int}}[\psi, \bar{\psi}] = -\frac{\lambda}{4N} \int d1 \left(\mathscr{I}_{\sigma_1 j_1; \sigma_2 j_2} \, \bar{\psi}_{\sigma_1 j_1}(1) \, \bar{\psi}_{\sigma_2, j_2}(1) \right) \left(\mathscr{I}_{\sigma_1' j_1'; \sigma_2' j_2'} \psi_{\sigma_2' j_2'}(1) \, \psi_{\sigma_1' j_1'}(1) \right),
$$

$$
\tag{1.116}
$$

where $\mathscr{I}_{\sigma_1 j_1; \sigma_1 j_1}$ is the standard $2N \times 2N$ skew-symmetric matrix defining the $Sp(N)$ Lie algebra:

$$
\mathscr{I}_{\sigma_1 j_1; \sigma_1 j_1} = \begin{pmatrix} \boxed{\begin{matrix} 0 & 1 \\ -1 & 0 \end{matrix}} & & \\ {}_{j_1, j_2 = 1} & \boxed{\begin{matrix} 0 & 1 \\ -1 & 0 \end{matrix}} & \\ & {}_{j_1, j_2 = 2} & \ddots \end{pmatrix}.
\tag{1.117}
$$

The above action is the $Sp(N)$-symmetric extension of the two-component attractive Fermi gas with contact interactions. Note that the numerical factors in the action is chosen such that both S_0 and S_{int} scale like N. Let us consider in passing the vacuum diagrams at the 2-loop order in a

(possibly) superconducting state:

$$\Phi^{2-\text{loop}} = \underbrace{\text{(diagram)}}_{\text{LO} \sim \mathcal{O}(N)} + \underbrace{\text{(diagram)}}_{\text{NLO} \sim \mathcal{O}(1)} . \qquad (1.118)$$

The first diagram is the Bogoliubov diagram built from two anomalous propagators. Each anomalous propagation has a N flavor degeneracy and the flavor indices of the $\mathcal{F}$ and $\bar{\mathcal{F}}$ lines are independent. This diagram scales like $\mathcal{O}(N \times N \times 1/N) = \mathcal{O}(N)$ and is the only LO diagram. The next diagram is the usual mean-field Hartree. In this case, the flavor indices of the two normal Green's functions are not independently summed and the diagram is $\mathcal{O}(N \times 1/N) = \mathcal{O}(1)$, i.e. it is a NLO diagram. In the limit $N \to \infty$, the Luttinger-Ward functional is dominated by the Bogoliubov diagram and the BCS theory becomes exact (independent of the number of spatial dimensions).

We only consider the normal state hereafter. In the absence of the anomalous propagators, the leading diagrams are at least $\mathcal{O}(1)$ (NLO) and in the large-N limit, the system is described as the free Fermi gas. A guiding principle for classifying the vacuum diagrams of the above theory is that a sub-diagram with parallel fermion lines introduce a factor of N. Therefore, the leading order diagrams must include the maximum number of particle-particle bubbles. The smallest NLO diagram is the Hartree diagram shown above. It is straightforward to see that the rest of the NLO diagrams are given as the sum of ring diagrams constructed from particle-particle bubbles:

$$\Phi^{\text{NLO}}[\mathcal{G}] = \text{(diagram)} + \frac{1}{2}\text{(diagram)} + \frac{1}{3}\text{(diagram)} + \frac{1}{4}\text{(diagram)} + \dots \quad (1.119)$$

A ring diagram with l links gets a factor of N^l and a factor of $1/N^l$ from the interaction vertices, amounting to $\mathcal{O}(1) \equiv \text{NLO}$. The symmetry factors $1/l$ is due to the $\mathbb{Z}_l$ rotation symmetry of the vertices on the ring. We recognize the above expansion as the self-consistent T-matrix approximation.

The self-energy functional is readily obtained by opening a fermion line:

$$\Sigma^{\text{NLO}}[\mathcal{G}] = \ldots + \qquad\qquad\qquad + \ldots \qquad (1.120)$$

The shown diagram is obtained from a vacuum diagram with 5 rings. We remind that all of the Green's functions appearing in the self-energy are the fully dressed Green's functions. The self-energy diagrams in terms of the bare Green's function $\mathcal{G}_0$ includes all of the possible ring-type decorations. We will use this Φ-derivable approximation in chapter 4 to study the non-equilibrium dynamics of attractive two-component fermions in the normal state.

1.4 Symmetries, conservation laws and the 2PI Ward-Takahashi hierarchy

In the classical field theory, the relation between symmetries and conserved quantities is provided by the Noether's theorem, the statement and proof of which in provided in Sec. A.1. The Noether's theorem can be generalized to quantum fields in light of the Ehrenfest's theorem, and one finds that the Noether currents are conversed at the level of expectation values. Since the many-particle Hilbert space in which the quantum fields reside is a much larger space than the classical space-time, the Noether's theorem imposes a more stringent constraint on classical fields than on quantum fields. It is therefore expectable that the dynamics of quantum fields would be constrained by additional conservation laws not described by the Noether's theorem. Indeed, for each symmetry there exists an infinite hierarchy of identities that impose constraints on the relation between various correlation functions of the quantum fields, known as the Ward-Takahashi hierarchy (WTH). The conserved Noether's currents lie at the bottom of this hierarchy.

In this section, we briefly discuss the WTH associated to the $U(1)$ gauge symmetry, and the Galilean symmetry of non-relativistic quantum fields for the exact theory and the Φ-derivable approximations. For concretenees, we consider a N-component fermionic field described with the action $S[\psi, \bar{\psi}] = S_0[\psi, \bar{\psi}] + S_{\text{int}}[\psi, \bar{\psi}]$, where:

$$S_0[\psi, \bar{\psi}] = \int \mathrm{d}1\, \mathrm{d}2\, \bar{\psi}_\alpha(1)\, \mathcal{G}_{0,\alpha\beta}^{-1}(1,2)\, \psi_\beta(2),$$

$$S_{\text{int}}[\psi, \bar{\psi}] = -\frac{1}{2N} \int \mathrm{d}1\, \mathrm{d}2\, \lambda(1,2)\, \bar{\psi}_\alpha(1)\, \psi_\alpha(1)\, \bar{\psi}_\beta(2)\, \psi_\beta(2). \tag{1.121}$$

Here, the integer arguments refer to the space and time, i.e. $j \equiv (\tau_j, \mathbf{x}_j)$, and $\int \mathrm{d}j \equiv \int_{\mathcal{C}} \mathrm{d}\tau_j \int_{\mathbb{R}^d} \mathrm{d}^d\mathbf{x}_j$, and the Greek letter indices ranging from 1 to N denote the discrete field component index. The bare Green's function $\mathcal{G}_{0,\alpha\beta}^{-1}(1,2)$ is defined as:

$$\mathcal{G}_{0,\alpha\beta}^{-1}(1,2) \equiv \left[i\partial_{\tau_1} + \frac{\nabla_{\mathbf{x}_1}^2}{2m_\alpha} + \mu_\alpha - U_\alpha(t_1, \mathbf{x}_1) \right] \delta_{\alpha\beta}\, \delta^d(\mathbf{x}_1 - \mathbf{x}_2)\, \delta_{\mathcal{C}}(\tau_1 - \tau_2). \tag{1.122}$$

The interaction potential is given by $\lambda(1,2) \equiv \delta_{\mathcal{C}}(\tau_1, \tau_2)\, v(\mathbf{x}_1 - \mathbf{x}_2)$. The following symmetries can be identified in the above action:

▷ *Global U(1) gauge invariance for each component:* for each component α, the action is invariant under the simultaneous transformation $\psi_\alpha(1) \to e^{i\theta}\psi_\alpha(1)$, $\bar{\psi}_\alpha(1) \to e^{-i\theta}\bar{\psi}_\alpha(1)$. The associated Noether's current is the current density of α's component. The conserved charge is the total number of α particles.

▷ *Galilean invariance:* In the absence of the external field U_α, the action is invariant under space and time translations. The associated Noether's current is the energy-momentum tensor. The conserved charge is total energy and momentum.

Differential forms of the conservation laws can be obtained by considering *local* $U(1)$ gauge and Galilean transformations.

1.4.1 Global $U(1)$ symmetry

We first show that the exact quantum theory with a global $U(1)$ symmetry implies the continuity equation for the expectation value of the local currents, reminiscent of the Ehrenfest's theorem. We start with the generating functional $Z[K]$ in the superfield notation. In this section, the integer labels to refer to the bundle of time, internal degrees of freedom and the operator charge index. The path integral measure is invariant under a translation $\phi(1) \to \phi(1) + \delta\phi(1)$. Therefore, we find:

$$0 = \int \mathcal{D}[\psi, \bar{\psi}] \left(\int \mathrm{d}1 \, \frac{S[\phi]}{\delta\phi(1)} \, \delta\phi(1) \right) e^{iS[\phi]}, \qquad (1.123)$$

where $S = S_0 + S_{\mathrm{int}} + S_K$. Consider a $\delta\phi$ corresponding to a local $U(1)$ gauge transformation, $\delta\phi(1) = -i\Lambda(1)\phi(1)$, where $\Lambda(\tau, a, c) \equiv c\,\Lambda(\tau, a)$. $\Lambda(\tau, a)$ is an arbitrary field on the time contour and $c = \pm$ is the operator charge. Here, a refers to the bundle of component index and spatial coordinate $\mathbf{x}$. The interaction term in the action involves a balanced number of operators with positive and negative charges and is invariant to linear order in Λ. Therefore, only $S_0 + S_K$ contribute to the curly parentheses in the above equation and we get:

$$0 = \int \mathcal{D}[\psi, \bar{\psi}] \, e^{iS[\phi]} \int \mathrm{d}1 \, \mathrm{d}2 \, \bigg(\left[\tilde{\mathcal{G}}_0(1,2)^{-1} - K(1,2) \right] \left[-i\phi(2)\,\phi(1)\,\Lambda(1) \right]$$
$$+ \left[\tilde{\mathcal{G}}_0(1,2)^{-1} - K(1,2) \right] \left[-i\Lambda(2)\,\phi(2)\,\phi(1) \right] \bigg). \quad (1.124)$$

The above equation is readily written in terms of the super Green's function:

$$\int \mathrm{d}1 \, \mathrm{d}2 \, \bigg(\left[\tilde{\mathcal{G}}_0(1,2)^{-1} - K(1,2) \right] \left[\tilde{\mathcal{G}}(2,1;K)\Lambda(1) \right]$$
$$+ \left[\tilde{\mathcal{G}}_0(1,2)^{-1} - K(1,2) \right] \left[\Lambda(2)\,\tilde{\mathcal{G}}(2,1;K) \right] \bigg) = 0. \quad (1.125)$$

The above equation can be put in a more useful form by laying bare its structure in the operator charge space. The inverse bare Green's function can be explicitly written as:

$$\tilde{\mathcal{G}}_0^{-1}(\tau_1 a_1 c_1, \tau_2 a_2 c_2) =$$

$$\begin{pmatrix} 0 & i\partial_{t_1} - \frac{\nabla_1^2}{2m} - \mu_{a_1} + U(\tau_1, a_1) \\ i\partial_{t_1} + \frac{\nabla_1^2}{2m} + \mu_{a_1} - U(\tau_1, a_1) & 0 \end{pmatrix} \delta_{a_1 a_2} \delta_{\mathcal{C}}(\tau_1, \tau_2), \quad (1.126)$$

where the $(1, 1)$, $(1, 2)$, $(2, 1)$ and $(2, 2)$ matrix elements refer to $--$, $-+$, $+-$ and $++$ charges.

Likewise, the source field and full Green's function can be written in a matrix form as:

$$\tilde{\mathcal{G}}(\tau_1 a_1 c_1, \tau_2 a_2 c_2; K) = \begin{pmatrix} \mathcal{F}(\tau_1 a_1, \tau_2 a_2; K) & \mathcal{G}(\tau_1 a_1, \tau_2 a_2; K) \\ \bar{\mathcal{G}}(\tau_1 a_1, \tau_2 a_2; K) & \bar{\mathcal{F}}(\tau_1 a_1, \tau_2 a_2; K) \end{pmatrix},$$

$$K(\tau_1 a_1 c_1, \tau_2 a_2 c_2) = \begin{pmatrix} K_{--}(\tau_1 a_1, \tau_2 a_2) & K_{-+}(\tau_1 a_1, \tau_2 a_2) \\ K_{+-}(\tau_1 a_1, \tau_2 a_2) & K_{++}(\tau_1 a_1, \tau_2 a_2) \end{pmatrix}. \quad (1.127)$$

A straightforward calculation yields the following explicit form for Eq. (1.125):

$$\int d1\, d2\, \Lambda(\tau_1 a_1) \left\{ \left[\partial_{t_1} n(\tau_1 a_1; K) + \nabla_1 \cdot \mathbf{j}(\tau_1 a_1; K) \right] \delta_{\mathcal{C}}(\tau_1, \tau_2)\, \delta_{a_1 a_2} \right.$$

$$+ \left(K^{+-}(\tau_1 a_1, \tau_2 a_2)\, \mathcal{G}(\tau_2 a_2, \tau_1 a_1; K) - K^{+-}(\tau_2 a_2, \tau_1 a_1)\, \mathcal{G}(\tau_1 a_1, \tau_2 a_2; K) \right)$$

$$\left. - K^{--}(\tau_1 a_1, \tau_2 a_2)\mathcal{F}(\tau_2 a_2, \tau_1 a_1; K) + K^{++}(\tau_1 a_1, \tau_2 a_2)\bar{\mathcal{F}}(\tau_2 a_2, \tau_1 a_1; K) \right\} = 0, \quad (1.128)$$

where we have defined the number density $n(\tau_1 a_1; K)$ and current $\mathbf{j}(\tau_1 a_1; K)$ as:

$$n(\tau_1 a_1) \equiv -i\mathcal{G}(\tau_1 a_1, \tau_2 a_2; K)\Big|_{a_2 = a_1, \tau_2 = \tau_1^+} = \left\langle \bar{\psi}_a(\tau_1 a_1)\, \psi_a(\tau_1 a_1) \right\rangle_K,$$

$$\mathbf{j}(\tau_1 a_1) \equiv \frac{\nabla_1 - \nabla_2}{2m} \mathcal{G}(\tau_1 a_1, \tau_2 a_2; K)\Big|_{a_2 = a_1, \tau_2 = \tau_1^+}$$

$$= \frac{i}{2m} \left\langle \nabla_1 \bar{\psi}(\tau_1 a_1)\, \psi(\tau_1 a_1) - \bar{\psi}(\tau_1 a_1)\, \nabla_1 \psi(\tau_1 a_1) \right\rangle_K. \quad (1.129)$$

Since Eq. (1.130) is valid for all Λ, the term in the square bracket must vanish, bringing us to the final result:

$$\partial_{t_1} n(\tau_1 a_1; K) + \nabla_1 \cdot \mathbf{j}(\tau_1 a_1; K) + \int d2\, \mathrm{Tr}_c \left[\frac{\delta\Gamma[\tilde{\mathcal{G}}]}{\delta\tilde{\mathcal{G}}(\tau_1 a_1, \tau_2 a_2)} \tilde{\mathcal{G}}[K](\tau_2 a_2, \tau_1 a_1)\, \hat{\tau}_z \right] = 0, \quad (1.130)$$

where Tr_c implies the trace in the 2×2 charge space according to to the matrix notation of Eq. (1.127), and $\hat{\tau}_z$ is the third Pauli matrix. In the last term, a_1 is a free variable and is not summed over. We have also used Eq. (1.76) to trade the source field K with the derivative of Γ with respect to the Green's function.

Turning off the source fields, the last term in Eq. (1.130) vanishes while the n and $\mathbf{j}$ become the *physical* number density and particle current, respectively. In this limit, the above identity becomes the statement of the conservation of the Noether's current at the level of the expectation value. This result, however, is just the simplest consequences of Eq. (1.130). The full content Eq. (1.130) can be extracted by taking additional derivatives with respect to K before sending it to zero. The K-derivatives of $n(K)$ and $\mathbf{j}(K)$ can be expressed in terms of the scalar and vector vertex function. The ensuing infinite hierarchy of relations between the vertex functions is known as the *generalized 2PI Ward-Takahashi identities* (2PI-WTIs) and constitute the complete statement of conservation laws associated to the global $U(1)$ gauge invariance. We refer to the hierarchy of generalized 2PI Ward-Takahashi identities as the 2PI Ward-Takahashi hierarchy (2PI-WTH), with Eq. (1.130) as the generator of the 2PI-WTH.

So far, we have shown that the global $U(1)$ gauge invariance implies conservation laws in the form of the 2PI-WTH. It remains to be investigated whether the same conclusion holds for Φ-derivable approximations. The pioneering work was done by Baym and Kadanoff in Ref. [39, 40] in which they have shown that the expectation value of the Noether's currents are conserved quantities for Φ-derivable approximations. The status of higher order 2PI-WTIs require further considerations. It has been shown in Ref. [53] that indeed Φ-derivable approximations for bosonic field theories that spontaneously break the $U(1)$ gauge symmetry (i.e. $\langle \phi \rangle \neq 0$) violate the 2PI-WTH. This defect, however, can be remedied by introducing the *2PI-resummed* effective action [53, 54]. Fortunately, one does not face these complications for fermionic field theories where the symmetry breaking

does not occur at the level of single field operator expectation values. In fact, it has been shown in Ref. [54] that the 2PI-WTH is satisfied in Φ-derivable approximations of quantum electrodynamics.

We establish the satisfaction of 2PI-WTH for the simpler theory of non-relativistic fermions by showing that the generator of 2PI-WTH, Eq. (1.130) also follows from Φ-derivable approximations. The only requirement is that approximate Φ must be constructed from legitimate 2PI vacuum diagrams. To this end, we note that the following linear 2nd rank transformation of $\tilde{\mathcal{G}}$ leaves each vacuum diagram invariant:

$$\tilde{\mathcal{G}}(1,2) \to \tilde{\mathcal{G}}'(1,2) = \tilde{\mathcal{G}}(1,2) - i\left[c(1)\Lambda(1) + c(2)\Lambda(2)\right]\tilde{\mathcal{G}}(1,2), \quad (1.131)$$

where $c(i) = \pm 1$ is the operator charge. This statement is a direct consequence of the conservation of the total operator charge on each interaction vertex. Expanding the sides of $\Phi[\tilde{\mathcal{G}}] = \Phi[\tilde{\mathcal{G}}']$ for first order in Λ and recalling the definition $\tilde{\Sigma} = \delta\Phi[\tilde{\mathcal{G}}]/\delta\tilde{\mathcal{G}}$, we find:

$$\int d1\,d2\,c_1\,\Lambda(1)\,\tilde{\Sigma}(1,2)\,\tilde{\mathcal{G}}(1,2) = 0, \quad (1.132)$$

Since the above equation is valid for all $\Lambda(1)$, we find:

$$\sum_{c_1=\pm 1}\int d2\,c_1\,\tilde{\Sigma}(1,2)\,\tilde{\mathcal{G}}(1,2) = 0. \quad (1.133)$$

In the above equation, the space, time and the discrete indices in 1 are free, but c_1 is summed over. The validity of this identity is only bound to the symmetry properties of Φ and holds with or without the source field K. The above equation yields the following identity in terms of the usual Green's functions:

$$\int d2\left[\Sigma(1,2)\,\mathcal{G}(2,1) - \mathcal{G}(1,2)\,\Sigma(2,1) + \Sigma_{\mathcal{F}}(1,2)\,\bar{\mathcal{F}}(2,1) - \mathcal{F}(1,2)\Sigma_{\bar{\mathcal{F}}}(2,1)\right] = 0. \quad (1.134)$$

Subtracting the sides of the KB equations for $\mathcal{G}$ and its adjoint (Eqs. 1.107a and Eqs. 1.107b) from

one another, we find:

$$\left[i\partial_{t_1} + i\partial_{t_1'} + \frac{\nabla_1^2 - \nabla_{1'}^2}{2m} \right] \mathcal{G}(\tau_1 a_1; \tau_1' a_1')$$

$$- \int d2 \left[\Sigma(1,2)\,\mathcal{G}(2,1') - \mathcal{G}(1,2)\,\Sigma(2,1') + \Sigma_{\mathcal{F}}(1,2)\,\bar{\mathcal{F}}(2,1') - \mathcal{F}(1,2)\Sigma_{\bar{\mathcal{F}}}(2,1') \right]$$

$$- \int d2 \left[K_{+-}(1,2)\,\mathcal{G}(2,1') - \mathcal{G}(1,2)\,K_{+-}(2,1') \right.$$

$$\left. + K_{++}(1,2)\,\bar{\mathcal{F}}(2,1') - \mathcal{F}(1,2)K_{--}(2,1') \right] = 0. \tag{1.135}$$

Setting $a_1 = a_2$ and taking the limit $\tau_1' \searrow \tau_1$ (in the contour sense), the terms involving the self-energy vanish in the virtue of Eq. (1.134) and we recover Eq. (1.130), the generator of the 2PI-WTH, as promised.

We conclude this section by deriving the Ward-Takahashi identity that relates the scalar and vector vertex functions. This identity lies at the second level of the hierarchy and is derived by taking the first derivative of Eq. (1.130) with respect to $K_{+-}(2,2')$ before setting the source fields to zero. The result is:

$$\partial_{t_2}\Lambda(1,1';2) + \nabla_2 \cdot \boldsymbol{\Lambda}(1,1';2) = i \left[\delta_{\mathcal{C}}(1,2) - \delta_{\mathcal{C}}(1',2) \right] \mathcal{G}(1,1'), \tag{1.136}$$

where we have defined:

$$\Lambda(1,1';2) \equiv \left. \frac{\delta\mathcal{G}(2,2';K)}{\delta K_{+-}(1,1')} \right|_{\tau_2 \searrow \tau_2', a_2 = a_2'}^{K=0} = -\left\langle T_{\mathcal{C}} \left[\psi(1)\,\bar{\psi}(1')\,\hat{n}(2) \right] \right\rangle_{\text{connected}},$$

$$\boldsymbol{\Lambda}(1,1';2) \equiv \frac{i(\nabla_2 - \nabla_{2'})}{2m} \left. \frac{\delta\mathcal{G}(2,2';K)}{\delta K_{+-}(1,1')} \right|_{\tau_2 \searrow \tau_2', a_2 = a_2'}^{K=0} = -\left\langle T_{\mathcal{C}} \left[\psi(1)\,\bar{\psi}(1')\,\hat{\mathbf{j}}(2) \right] \right\rangle_{\text{connected}}.$$

$$\tag{1.137}$$

The number density and current operators $\hat{n}$ and $\hat{\mathbf{j}}$ are defined as:

$$\hat{n}(1) = \bar{\psi}(1)\,\psi(1),$$

$$\hat{\mathbf{j}}(1) = \frac{i}{2m} \left(\nabla_1\bar{\psi}(1)\,\psi(1) - \bar{\psi}(1)\,\nabla_1\psi(1) \right). \tag{1.138}$$

Eq. (1.136) can be expressed in a more familiar form by introducing the scalar and vector vertex functions, Λ and $\boldsymbol{\Lambda}$, as obtained by removing removing the Green's functions legs attached to 1 and $1'$ external points of $\Lambda(1, 1'; 2)$ and $\boldsymbol{\Lambda}(1, 1'; 2)$:

$$\Gamma(1, 1'; 2) = -\int \mathrm{d}3\, \mathrm{d}3'\, \mathcal{G}^{-1}(1, 3)\, \mathcal{G}^{-1}(1', 3')\, \Lambda(3, 3'; 2),$$

$$\boldsymbol{\Gamma}(1, 1'; 2) = -\int \mathrm{d}3\, \mathrm{d}3'\, \mathcal{G}^{-1}(1, 3)\, \mathcal{G}^{-1}(1', 3')\, \boldsymbol{\Lambda}(3, 3'; 2). \tag{1.139}$$

The WTI Eq. (1.136) in terms of Γ and $\boldsymbol{\Gamma}$ read as:

$$\partial_{t_2}\Gamma(1, 1'; 2) + \nabla_2 \cdot \boldsymbol{\Gamma}(1, 1'; 2) = -i\left[\delta_{\mathcal{C}}(1', 2) - \delta_{\mathcal{C}}(1, 2)\right]\mathcal{G}^{-1}(1, 1'), \tag{1.140}$$

The above equation is known as the generalized Ward identity in the literature of electron-phonon systems [55] and relate the self-energy (which appears in $\mathcal{G}^{-1}$) to the scalar and vector vertex functions. With some simple rearrangements, Eq. (1.136) gives the longitudinal f-sum rule for the retarded density-density response function at equilibrium χ_{dd}^+ [39]:

$$\int_{-\infty}^{\infty} \mathrm{d}\omega\, \omega\, \chi_{\mathrm{dd}}^+(\mathbf{x}_1, \mathbf{x}_2; \omega) = -i\pi\, \nabla_1 \cdot \nabla_2 \left[n_0(\mathbf{x}_2)\delta^d(\mathbf{x}_1 - \mathbf{x}_2)\right], \tag{1.141}$$

where $\chi_{\mathrm{dd}}^+(\mathbf{x}_1, \mathbf{x}_2; \omega)$ is the Fourier transform of $\chi_{\mathrm{dd}}^+(t_1\mathbf{x}_1; t_2\mathbf{x}_2)$ in $t_1 - t_2$.

1.4.2 The Galilean symmetry

In this section, we derive the conservation laws associated to the Galilean symmetry. In a classical field theory, the associated Noether's current is the energy-momentum tensor (cf. A.1). Similar to the analysis of the global $U(1)$ gauge symmetry presented in the previous section, we find that the energy-momentum tensor also emerges as a conserved quantity for the quantum fields. We only consider normal systems here and loosely follow Baym and Kadanoff's original analysis [39] and that of Ref. [26]. In addition to the conservation laws at the level of expectation values, we also obtain the generating equations for the 2PI-WTH associated to the Galilean symmetry. The

generalization to superconducting states is straightforward.

We consider the following transformation of the Green's functions:

$$\mathcal{G}(\mathbf{x}_1\tau_1; \mathbf{x}_2\tau_2) \rightarrow$$

$$\left[1 + \frac{1}{4}\partial_{\tau_1}\theta(\tau_1) + \frac{1}{4}\partial_{\tau_2}\theta(\tau_2)\right]\mathcal{G}\left(\mathbf{x}_1 + \mathbf{R}(\tau_1), \tau_1 + \theta(\tau_1); \mathbf{x}_2 + \mathbf{R}(\tau_2), \tau_2 + \theta(\tau_2)\right). \quad (1.142)$$

Here, $\theta(\tau)$ and $\mathbf{R}(\tau)$ are arbitrary functions on the time contour. It is easy to see that the vacuum diagrams of a theory with Galilean invariant interaction terms is invariant to linear order in θ and $\mathbf{R}$ upon replacing all Green's functions with the above transformed version. This is easily seen by observing that (1) a change of variables from $\mathbf{x}$ to $\mathbf{x} + \mathbf{R}$ leaves the interaction potentials invariant, and (2) a change of variables from τ to $\tau + \theta$ introduces Jacobians which are compensated to linear order by the factors affixed to the Green's functions. To linear order, the change introduced to the Green's function is:

$$\delta\mathcal{G}(1, 2) = \left[\frac{1}{4}\left(\partial_{\tau_1}\theta(1) + \partial_{\tau_2}\theta(2)\right) + \mathbf{R}(1) \cdot \nabla_1 + \theta(1)\,\partial_{\tau_1} + \mathbf{R}(2) \cdot \nabla_2 + \theta(2)\,\partial_{\tau_2}\right]\mathcal{G}(1, 2).$$
$$(1.143)$$

The invariance of $\Phi[\mathcal{G}]$ with respect to the above transformation implies $\int \mathrm{d}1\,\mathrm{d}2\,\delta\Phi/\delta\mathcal{G}(1, 2)\,\delta\mathcal{G}(1, 2) = 0$. Setting $\theta = 0$ and using the arbitrariness of $\mathbf{R}$, we find:

$$\int \mathrm{d}^d\mathbf{x}_1\,\mathbf{Q}(\tau_1, \mathbf{x}_1) = 0, \quad (1.144)$$

where:

$$\mathbf{Q}(\tau_1, \mathbf{x}_1) = \frac{i}{2}\left(\nabla_1 - \nabla_{1'}\right)\int \mathrm{d}2\,\left[\Sigma(1, 2)\mathcal{G}(2, 1') - \mathcal{G}(1, 2)\Sigma(2, 1')\right]_{1'=1}. \quad (1.145)$$

Likewise, the arbitrariness of θ implies:

$$\frac{\mathrm{d}\mathcal{E}_{\text{int}}(\tau_1)}{\mathrm{d}\tau_1} + \int \mathrm{d}^d\mathbf{x}\,Q_{\mathcal{E}}(\tau_1, \mathbf{x}_1) = 0, \quad (1.146)$$

where:

$$\mathcal{E}_{\text{int}}(\tau_1) = -\langle S_{\text{int}}\rangle_{\tau_1} = -\frac{i}{4}\int d^d\mathbf{x}_1\, d2\,[\mathcal{G}(1,2)\Sigma(2,1) + \Sigma(1,2)\mathcal{G}(2,1)],$$

$$Q_{\mathcal{E}}(\tau_1,\mathbf{x}_1) = i\,\partial_{\tau_1}\int d^d d2\,[\mathcal{G}(1,2)\Sigma(2,1') + \Sigma(1,2)\mathcal{G}(2,1')]_{1'=1}. \tag{1.147}$$

The differential form of the momentum conservation law is found by operating the sides of the KB equation and its adjoint (Eqs. 1.108a and 1.108b) by $i(\nabla_1 - \nabla_2)/(2m)$ and subtracting the latter from the former. The final result is:

$$\partial_{t_1}\mathbf{j}(1) + \frac{1}{m}\nabla_1\cdot\Theta_K(1) + \frac{n(1)}{m}\nabla_1 U(1) - \frac{1}{m}\mathbf{Q}(1)$$
$$= \frac{i}{2m}(\nabla_1 - \nabla_{1'})\int d2\,[K_{+-}(1,2)\mathcal{G}(2,1') - \mathcal{G}(1,2)K_{+-}(2,1')]_{1'=1}, \tag{1.148}$$

where:

$$[\Theta_K]_{ij} \equiv \frac{i}{4m}(\nabla_{1,i} - \nabla_{2,i})(\nabla_{1,j} - \nabla_{2,j})\,\mathcal{G}(1,2)\Big|_{\tau_2\searrow\tau_1,\mathbf{x}_2=\mathbf{x}_1}, \tag{1.149}$$

is the kinetic part of the pressure tensor. In the absence of the source field K_{+-}, the above equation is the space-like component of the divergence of the energy-momentum tensor. Here, $\mathbf{Q}$ is identified as the gradient of the pressure. The integral form of the conservation of momentum is obtained by integrating over $\mathbf{x}_1$ space and using Eq. (1.144):

$$\partial_{t_1}\int d^d\mathbf{x}_1\,\mathbf{j}(1) = -\int d^d\mathbf{x}_1\,\frac{n(1)}{m}\nabla_1 U(1). \tag{1.150}$$

In the presence of the source field K_{+-}, Eq. (1.148) serves as the generator of the 2PI-WTH associated to the conservation of momentum.

The differential conservation law of energy is obtained by operating the sides of the KB equation and its adjoint (Eqs. 1.108a and 1.108b) by $i\partial_{t_2}$ and $i\partial_{t_1}$, respectively, and summing the sides of two resulting equations:

$$\partial_{t_1} \mathcal{E}_K(1) + \nabla_1 \cdot \mathbf{j}_K(1) + U(1) \, \partial_{t_1} n(1) - Q_{\mathcal{E}}(1) =$$

$$\int d2 \left[i\partial_{t_1'} K_{+-}(1,2)\mathcal{G}(2,1') + i\partial_{t_1} \mathcal{G}(1,2)K_{+-}(2,1') \right]_{\tau_1' \searrow \tau_1, \mathbf{x}_1 = \mathbf{x}_1'}, \quad (1.151)$$

where the kinetic energy density $\mathcal{E}_K$ and current $\mathbf{j}_K$ are defined as:

$$\mathcal{E}_K(1) = -\frac{i}{2m} \, \nabla_1 \cdot \nabla_2 \, \mathcal{G}(1,2)\Big|_{\tau_2 \searrow \tau_1, \mathbf{x}_1 = \mathbf{x}_2},$$

$$\mathbf{j}_K(1) = \frac{i}{2m} \, (\partial_{t_1} \nabla_2 + \partial_{t_2} \nabla_1) \, \mathcal{G}(1,2)\Big|_{\tau_2 \searrow \tau_1, \mathbf{x}_1 = \mathbf{x}_2}. \quad (1.152)$$

Turning off the source field K_{+-} and integrating the sides of Eq. (1.151) over $\mathbf{x}_1$, we obtain:

$$\frac{d}{dt_1} \int d\mathbf{x}_1 \left[\mathcal{E}_K(1) + \mathcal{E}_{\text{int}}(1) \right] = -\int d^d\mathbf{x}_1 \, \mathbf{j}(1) \cdot \nabla_1 U(1). \quad (1.153)$$

We have used Eq. (1.146) and the continuity equation for the particle current to get the last result.

Finally, we note that Eq. (1.151) serves as the generating equation for the 2PI-WTH associated to

the conservation of energy.

2

Quantum kinetic theory

We reviewed the foundations of non-equilibrium quantum field theory in the previous section and discussed the method of 2PI effective action which allows constructing conserving approximations in a systematic way. The final product of the non-equilibrium theory is the Kadanoff-Baym equation which describes the evolution of the non-equilibrium Green's function. The Kadanoff-Baym equation is a non-linear integro-differential equation and its solution can be challenging even for the simplest Φ-derivable approximations. It is therefore desirable to exploit the symmetries and scale separations specific to the problem under investigation in order to simplify the evolution

equations before attempting to solve them.

A large class of physical systems possess a well-defined separation of length and time scales between the microscopic and macroscopic processes. Let us consider the electrons in a metallic specimen or a semiconducting device subject to a time-varying gate voltage. The microscopic processes in such a system is governed by time and length scales $t_{\text{micro}} \sim \hbar/\epsilon_F \sim 10^{-16}\,s$ and a length scale $l_{\text{micro}} \sim 1/k_F \sim 10^{-10}\,m$, where $\epsilon_F \sim 1\,eV$ and $k_F = \sqrt{2mE_F}/\hbar$ denote the Fermi energy and wavelength, respectively. For a specimen with a linear dimension of $l_{\text{macro}} \sim 1\,mm$ and an alternating gate voltage in the gHz regime $t_{\text{macro}} \sim 10^{-9}\,s$, we find 7 orders of magnitude difference between the micro and macro time scales. Therefore, the electrons at any given point in the specimen can be thought as being part of a large homogeneous system which is subject to a weakly inhomogeneous external field. A similar scale separation governs experiments with ultra cold fermionic gases, where the Fermi energy is in the $10\,\hbar\,$kHz range while the trap frequency that sets the scale of inhomogeneities is in the $10 \sim 100\,\hbar\,$Hz range.

The existence of such dramatic separation of scales allows us to simplify the dynamical equations to a great extent. Let us consider an arbitrary 2-point function $\mathcal{A}(t_1 \mathbf{x}_1, t_2 \mathbf{x}_2)$, such as the non-equilibrium Green's function or the self-energy. We define the *microscopic* and *macroscopic* coordinates as:

$$t \equiv t_1 - t_2, \quad \mathbf{x} \equiv \mathbf{x}_1 - \mathbf{x}_2, \quad x \equiv (t, \mathbf{x}) \qquad \text{(microscopic)},$$

$$T \equiv (t_1 + t_2)/2, \quad \mathbf{R} \equiv (\mathbf{x}_1 + \mathbf{x}_2)/2, \quad X \equiv (T, \mathbf{R}) \qquad \text{(macroscopic)} \qquad (2.1)$$

Any such function can be parametrized using $(t, \mathbf{x}; T, \mathbf{R})$ with no loss of generality. We refer to the reparametrized function using the same function name. For weakly inhomogeneous systems as

described above, we expect:

$$|\partial_{\mathbf{R}}\mathcal{A}|/|\partial_{\mathbf{x}}\mathcal{A}| \sim l_{\text{macro}}^{-1}/l_{\text{micro}}^{-1} \ll 1,$$

$$|\partial_T \mathcal{A}|/|\partial_t \mathcal{A}| \sim t_{\text{macro}}^{-1}/t_{\text{micro}}^{-1} \ll 1. \tag{2.2}$$

We take the above conditions as the definition of a *weakly inhomogeneous system*. We define $f(T, \mathbf{R})$ to be a weakly inhomogeneous function with respect to a certain physical system with microscopic scales $(t_{\text{micro}}, l_{\text{micro}})$ if $|\partial_T f|/f \ll t_{\text{micro}}^{-1}$ and $|\partial_{\mathbf{R}} f|/f \ll l_{\text{micro}}^{-1}$. In light of such separation of scales, we can expand the Kadanoff-Baym equations to first order in the derivatives with respect to X to an excellent approximation, while taking a Fourier transform in x to exploit the existence of the well-resolved microscopic energy and momentum. This is achieved using Wigner transformations and Groenewold-Moyal product formula. The resulting evolution equations, as will shortly see, assume a very simple form reminiscent of the classical Boltzmann equation and serve as an excellent starting point for studying the dynamics of weakly inhomogeneous systems. Derived first by Kadanoff and Baym [22], the resulting quantum mechanical Boltzmann equation is referred to as the *Kadanoff-Baym kinetic equation*.

In this chapter, we will briefly review the derivation of Kadanoff-Baym kinetic equation and discuss practical numerical methods for solving them for systems subject to a weakly inhomogeneous external fields.

2.1 Preliminaries

The convenience of representing the correlation functions in the Fourier space is a well-known fact when dealing with space-time translation invariant systems. The kinetic energy part of the Hamiltonian is readily diagonalized in the Fourier space, and the convolution integrals appearing in various places such as perturbation series, Dyson's equations, Bethe-Salpeter equations, etc., turn

into simple algebraic products, owing to the conservation of energy and momentum at the interaction vertices.

As long as the high energy (short time) and large momentum (short wavelength) processes are concerned, the large scale inhomogeneities are not resolved and a weakly inhomogeneous system is locally identical to a homogeneous system. Therefore, we might as well expect to be able to partially benefit from the convenience of Fourier transforms when dealing with such systems. The representation tailored for this purpose is known as the *Wigner representation*. The Wigner representation was introduced by Wigner in 1932 as part of a program to include quantum corrections to classical statistical mechanics [56, 57]. The representation enables us to extend the concept of "phase space" in classical statistical mechanics to quantum statistical mechanics. Another useful concept is the *statistical/spectral decomposition* of the 2-point functions in the Wigner representation, which illuminates the structure of the non-equilibrium functions. We will explore these preliminary conceptual tools in this the following subsections.

2.1.1 Wigner representation

The Wigner transform of a general 2-point function is defined as:

$$\mathfrak{W}[A](\omega, \mathbf{p}; T, \mathbf{R}) \equiv \int_{-\infty}^{\infty} \mathrm{d}t \, e^{i\omega t} \int_{\mathbb{R}^d} \mathrm{d}^d\mathbf{x} \, e^{-i\mathbf{p}\cdot\mathbf{x}} \, A(T + t/2, \mathbf{R} + \mathbf{x}/2; T - t/2, \mathbf{R} - \mathbf{x}/2). \quad (2.3)$$

The microscopic coordinates $(t, \mathbf{x})$ are Fourier transformed while the macroscopic coordinates are left intact. The conditions for the existence of the Wigner transforms is similar to those for Fourier transforms. Similar to the case of Fourier transforms, we often encounter functions with ill-defined Wigner transform due to undamped oscillations. In such cases, we formally define the Wigner transform by (1) promoting ω (and/or $\mathbf{p}$) to a complex variable by adding to subtracting a small imaginary number, and (2) taking the proper limit back to the real line. Two important cases are the Wigner transform of retarded and advanced Green's functions. Let A^+ (A^-) be an arbitrary

retarded (advanced) function. We define its Wigner transform as:

$$\mathfrak{W}[A^{\pm}](\omega, \mathbf{p}; T, \mathbf{R}) \equiv \lim_{\epsilon \to 0^{\pm}} \mathfrak{W}[A^{\pm}](\omega + i\epsilon, \mathbf{p}; T, \mathbf{R}). \tag{2.4}$$

The limit exists as long as $\mathcal{A}^{\pm}$ is exponentially bounded. We often use the shorthand $\mathfrak{W}[\mathcal{A}^{\pm}](\omega^{\pm}, \mathbf{p}; T, \mathbf{R})$ to refer to such a limiting procedure. Whenenver the notation is not ambiguous, we use the same function name for the Wigner transformed functions.

We remark that the Wigner transformed functions have a complicated transformation law under gauge transformations. Let us consider the $U(1)$ gauge field of electromagnetism. The action is given by:

$$S[\psi, \bar{\psi}] = \int d1\, \bar{\psi}(1) \left(i\partial_{t_1} - \frac{1}{2m} \left[-i\nabla_{\mathbf{x}_1} - (e/c)\mathbf{A}(1) \right]^2 - e\,\phi(1) \right) \psi(1) + S_{\text{int}}[\psi, \bar{\psi}], \tag{2.5}$$

where $\mathbf{A}$ and ϕ are the vector and scalar gauge potentials. Under a gauge transformation $\mathbf{A}(1) \to \mathbf{A}(1) + \nabla_{\mathbf{x}_1} \Lambda(1)$, $\phi(1) \to \phi(1) - (1/c)\,\partial_{t_1} \Lambda(1)$, the Green's function (and the self-energy) transform as:

$$\mathcal{G}(1, 1') \to \mathcal{G}_{\Lambda}(1, 1') \equiv e^{i(e/c)[\Lambda(1) - \Lambda(2)]} \mathcal{G}(1, 1'). \tag{2.6}$$

It is easily seen that $\mathfrak{W}[\mathcal{G}_{\Lambda}(1, 1')]$ is not trivially related to $\mathfrak{W}[\mathcal{G}(1, 1')]$ due to the mixing of the microscopic and macroscopic coordinates by the gauge transformation. A workaround was proposed by Stratonovich in 1956 [58]. The idea is to use a manifestly gauge-invariant Wigner transform as follows:

$$\mathfrak{W}_{\text{I}}[A](\omega, \mathbf{p}; T, \mathbf{R}) \equiv$$
$$\int_{-\infty}^{\infty} dt\, e^{i\omega t} \int_{\mathbb{R}^d} d^d\mathbf{x}\, e^{-i\mathbf{p}\cdot\mathbf{x}}\, e^{-iI(t,\mathbf{x};T,\mathbf{R})}\, A(T + t/2, \mathbf{R} + \mathbf{x}/2; T - t/2, \mathbf{R} - \mathbf{x}/2). \tag{2.7}$$

where:

$$I(t, \mathbf{x}; T, \mathbf{R}) \equiv \frac{e}{c} \int_{(T-t/2, \mathbf{R}-\mathbf{x}/2)}^{(T+t/2, \mathbf{R}+\mathbf{x}/2)} A_{\mu}(s)\, ds^{\mu}, \tag{2.8}$$

where the integration is along the straight line connecting the two space-time points, $A_\mu = (-c\phi, \mathbf{A})$ and $\mathrm{d}s^\mu = (\mathrm{d}t, \mathrm{d}\mathbf{r})$. Now, under a gauge transformation, e^{iI} transforms like $\mathcal{G}$ and $\mathfrak{W}_\mathrm{I}[\mathcal{G}]$ is manifestly gauge-invariant. In this thesis, we are dealing only with scalar potentials and the global $U(1)$ symmetries are not gauged. Therefore, we will use the original definition of the Wigner's function.

2.1.2 Properties of Wigner transformed Keldysh functions

The exact relations that exist between the matrix components of Keldysh functions transform into analogous relations between the Wigner transformed functions. These relations take a particularly concise form if the Keldysh function in question is diagonal in its discrete indices, i.e. if $\mathcal{A}_{\sigma_1\sigma_1'}(\tau_1, \mathbf{x}_1; \tau_1', \mathbf{x}_1') = \delta_{\sigma_1\sigma_1'}\mathcal{A}_{\sigma_1}(\tau_1, \mathbf{x}_1; \tau_1', \mathbf{x}_1')$. In this case, Eq. (1.6f) implies:

$$A_\sigma^+(\omega, \mathbf{p}; T, \mathbf{R})^* = A_\sigma^-(\omega, \mathbf{p}; T, \mathbf{R}). \tag{2.9}$$

Combining the above identity with Eq. (1.6a), we find:

$$\Im[A_\sigma^+](\omega, \mathbf{p}; T, \mathbf{R}) = \frac{1}{2i}\left[A_\sigma^>(\omega, \mathbf{p}; T, \mathbf{R}) - A_\sigma^<(\omega, \mathbf{p}; T, \mathbf{R})\right]. \tag{2.10}$$

Since A_σ^+ is a retarded function, it is analytic in the upper half complex ω-plane. Therefore, the real part of A_σ^+ can be found using the Kramers-Kroning transform:

$$\Re[A_\sigma^+](\omega, \mathbf{p}; T, \mathbf{R}) = \mathrm{P.V.}\int_{-\infty}^\infty \frac{\mathrm{d}\omega'}{\pi}\frac{\Im[A_\sigma^+](\omega', \mathbf{p}; T, \mathbf{R})}{\omega' - \omega}. \tag{2.11}$$

Here, P.V. denotes the principal value integration.

2.1.3 Groenewold-Moyal product and gradient expansion

The KB equations for the Green's function involve convolution integrals of the self-energy and the Green's function. The Φ-derivable self-energy functionals may also involve convolution integrals of the Green's functions. A necessary tool for transforming the KB equations into a form

suitable for studying weakly inhomogeneous systems is a prescription for dealing with such convolution integrals.

In case of the convolution integrals of translationally invariant two-point functions, the prescription is given by the Fourier convolution theorem. Generalized to the case of Wigner transforms, the convolution theorem remains formally the same, however, the algebraic product will be replaced with the more complicated Gorenewold-Moyal (GM) product [59, 60]:

$$\mathfrak{W}[\mathcal{A} \star \mathcal{B}] = \mathfrak{W}[\mathcal{A}] \star_{\mathrm{GM}} [\mathcal{B}] \equiv \exp\left[\frac{i}{2}\left(\partial_\omega^\mathcal{A}\partial_T^\mathcal{B} - \partial_\mathbf{p}^\mathcal{A} \cdot \partial_\mathbf{R}^\mathcal{B}\right) - \frac{i}{2}\left(\partial_\omega^\mathcal{B}\partial_T^\mathcal{A} - \partial_\mathbf{p}^\mathcal{B} \cdot \partial_\mathbf{R}^\mathcal{A}\right)\right]\mathfrak{W}[\mathcal{A}]\,\mathfrak{W}[\mathcal{B}].$$

(2.12)

The $\star$ operator denotes the convolution integral. The above definition must be interpreted order-by-order by expanding the exponential function as a formal power series. The GM product is also sometimes called the Weyl-Groenewold product.

The GM product is a non-commutative, associative binary operator. For translationally invariant $\mathcal{A}$ and $\mathcal{B}$, $\partial_T = \partial_\mathbf{R} = 0$, so that the operator in the square brackets vanishes and the GM product becomes the algebraic product. In application to weakly inhomogeneous system, we are often interested only in the leading order corrections in ∂_X. Expanding to GM product to first order, we find:

$$\mathfrak{W}[\mathcal{A} \star \mathcal{B}] = \mathfrak{W}[\mathcal{A}]\,\mathfrak{W}[\mathcal{B}] + \frac{i}{2}\{\mathfrak{W}[\mathcal{A}], \mathfrak{W}[\mathcal{B}]\} + \mathcal{O}(\partial_X^2),$$

(2.13)

where $\{A, B\}$ is a generalized *Poisson bracket* defined as [22]:

$$\{A, B\} \equiv \partial_\omega A\, \partial_T B - \partial_T A\, \partial_\omega B - \partial_\mathbf{p} A\, \partial_\mathbf{R} B + \partial_\mathbf{R} A\, \partial_\mathbf{p} B.$$

(2.14)

Note that the generalized Poisson bracket coincides with the usual Poisson bracket of classical Hamiltonian mechanics when applied to functions with no ω-dependence. The Poisson bracket is anti-symmetric, i.e. $\{A, B\} = -\{B, A\}$, and associative, i.e. $\{A, BC\} = \{A, B\}C + B\{A, C\}$. These elementary properties show that:

$$\{A, f(A)\} = 0,$$

(2.15)

provided that $f(\cdot)$ is an analytic function. This identity can be proved order-by-order by expanding $f(A)$ as a power series.

2.1.4 Decomposition into spectral and statistical functions

A useful representation of Wigner transformed Keldysh functions is obtained by separating the parts that encode the spectral and statistical properties. Given such a Keldysh function $\mathcal{D}$, we define the *spectral* function A and the statistical function ϕ through the following equation:

$$\mathcal{D}^> - \mathcal{D}^< = -i\mathsf{A},$$

$$\mathcal{D}^> + \mathcal{D}^< = -i\mathsf{A}(1 \pm 2\phi), \tag{2.16}$$

where $+$ and $-$ signs corresponds to bosonic and fermionic parametrizations, respectively. While the choice of sign of ϕ in defining the spectral/statistical parametrization is arbitrary, it is natural to choose $+$ $(-)$ for functions that satisfy the bosonic (fermionic) KMS condition at equilibrium. An equivalent definition for the spectral function can be obtained using Eq. (2.10):

$$\mathsf{A} = -2\Im[\mathcal{D}^+]. \tag{2.17}$$

The nomenclature for A and ϕ stems from the forms they assume in the thermal equilibrium (cf. Eq. 1.43). The spectral part of Green's function encodes the information about the (local) distribution of single particle states. The statistical function ϕ, on the other hand, assumes the form of Bose-Einstein or Fermi-Dirac distributions in equilibrium. Using Eq. (2.16), we find:

$$\mathcal{D}^< = \pm\mathsf{A}\phi,$$

$$\mathcal{D}^> = -i\mathsf{A}(1 \mp \phi). \tag{2.18}$$

2.2 Kadanoff-Baym quantum kinetic equation

In this section, we apply the concepts introduced earlier to derive the Kadanoff-Baym quantum kinetic equation. A significant part of the required theoretical steps was taken by Wigner in

1932 [56]. However, it was only after the introduction of Φ-derivable approximations by Baym and Kadanoff in 1961-1962 [39, 40, 22] that the conceptual framework of quantum kinetic equations became most appealing. As mentioned earlier, Φ-derivable approximations provide an ingenious "conserving" closure to the BBGKY hierarchy. We will see in this section that once the machinery of Wigner transformation is applied to the Φ-derivable approximations, a Boltzmann-like transport equation follows very naturally.

The idea is express the KB equations in the Wigner representation and to disentangle the convolution integrals via a first-order expansion of the GM product. We restrict our analysis to cases where the external fields and the Green's functions are diagonal in the space of discrete indices. This class of systems, for instance, excludes spin$-1/2$ particles in a magnetic field with a direction that varies in space or time. The resulting quantum kinetic equation for these systems is somewhat more complex and is beyond the scope of our current applications in this thesis.

Our starting point is the KB equation for the greater/lesser and the retarded/advanced components of the non-equilibrium Green's functions, Eqs. (1.109a)-(1.109b) and Eqs. (1.109c)-(1.109d), respectively. The Wigner transforms of the right hand sides are trivial. The left hand sides, however, involve differential operators and must be handled with some care. A straightforward calculation shows that the following result holds:

$$\mathfrak{W}\left[G_{0,\sigma}^{-1} \star G_{\sigma}^{\gtrless}\right] = \mathfrak{W}\left[G_{0,\sigma}^{-1}\right] \star_{\text{GM}} \mathfrak{W}\left[G_{\sigma}^{\gtrless}\right], \tag{2.19}$$

with the following expression for $\mathfrak{W}\left[G_{0,\sigma}^{-1}\right]$:

$$\mathfrak{W}\left[G_{0,\sigma_1}^{-1}\right] \equiv \omega + \mu_\sigma - \frac{|\mathbf{p}|^2}{2m_\sigma} - U_\sigma(T, \mathbf{R}). \tag{2.20}$$

Likewise, the Wigner transform of the left hand side of Eq. (1.109b) can be written as:

$$\mathfrak{W}\left[G_{\sigma}^{\gtrless} \star \overleftarrow{G}_{0,\sigma}^{-1}\right] = \mathfrak{W}\left[G_{\sigma}^{\gtrless}\right] \star_{\text{GM}} \mathfrak{W}\left[\overleftarrow{G}_{0,\sigma}^{-1}\right], \tag{2.21}$$

with $\mathfrak{W}\left[\overleftarrow{G}_{0,\sigma}^{-1}\right]$ given by the same equation (Eq. 2.20). The Wigner transform of left hand sides of the KB equation for the retarded and advanced components has an identical structure. The final

result is:

$$\mathfrak{W}\left[G_{0,\sigma}^{-1}\right] \star_{\text{GM}} \mathfrak{W}\left[G_\sigma^\gtrless\right] = \mathfrak{W}\left[\Sigma_\sigma^+\right] \star_{\text{GM}} \mathfrak{W}\left[G_\sigma^\gtrless\right] + \mathfrak{W}\left[\Sigma_\sigma^\gtrless\right] \star_{\text{GM}} \mathfrak{W}\left[G_\sigma^-\right],$$

$$\mathfrak{W}\left[G_\sigma^\gtrless\right] \star_{\text{GM}} \mathfrak{W}\left[G_{0,\sigma}^{-1}\right] = \mathfrak{W}\left[G_\sigma^+\right] \star_{\text{GM}} \mathfrak{W}\left[\Sigma_\sigma^\gtrless\right] + \mathfrak{W}\left[G_\sigma^\gtrless\right] \star_{\text{GM}} \mathfrak{W}\left[\Sigma_\sigma^-\right], \qquad (2.22)$$

and for the retarded/advanced components:

$$\mathfrak{W}\left[G_{0,\sigma}^{-1}\right] \star_{\text{GM}} \mathfrak{W}\left[G_\sigma^\pm\right] = 1 + \mathfrak{W}\left[\Sigma_\sigma^\pm\right] \star_{\text{GM}} \mathfrak{W}\left[G_\sigma^\pm\right],$$

$$\mathfrak{W}\left[G_\sigma^\pm\right] \star_{\text{GM}} \mathfrak{W}\left[G_{0,\sigma}^{-1}\right] = 1 + \mathfrak{W}\left[G_\sigma^\pm\right] \star_{\text{GM}} \mathfrak{W}\left[\Sigma_\sigma^\pm\right]. \qquad (2.23)$$

At this point, we drop the Wigner transform symbol for brevity. All of the Keldysh functions appearing hereafter are assumed to be in the Wigner representation unless it is explicitly noted.

So far, we have not made any approximations and Eqs. (2.22) and (2.23) are identical to Eqs. (1.109a)-(1.109b) and Eqs. (1.109c)-(1.109d) in context. Following procedure outlined in the introduction, we now expand the GM products appearing in the above expressions of the KB equations to first order in derivatives with respect to the macroscopic coordinates. For the lesser/greater parts we find:

$$G_{0,\sigma}^{-1}G_\sigma^\gtrless + \frac{i}{2}\{G_{0,\sigma}^{-1}, G_\sigma^\gtrless\} = \Sigma_\sigma^+ G_\sigma^\gtrless + \frac{i}{2}\{\Sigma_\sigma^+, G_\sigma^\gtrless\} + \Sigma_\sigma^\gtrless G_\sigma^- + \frac{i}{2}\{\Sigma_\sigma^\gtrless, G_\sigma^-\} + \mathcal{O}(\partial_X^2), \quad (2.24a)$$

$$G_\sigma^\gtrless G_{0,\sigma}^{-1} + \frac{i}{2}\{G_\sigma^\gtrless, G_{0,\sigma}^{-1}\} = G_\sigma^+ \Sigma_\sigma^\gtrless + \frac{i}{2}\{G_\sigma^+, \Sigma_\sigma^\gtrless\} + G_\sigma^\gtrless \Sigma_\sigma^- + \frac{i}{2}\{G_\sigma^\gtrless, \Sigma_\sigma^-\} + \mathcal{O}(\partial_X^2), \quad (2.24b)$$

and for the retarded/advanced parts we get:

$$G_{0,\sigma}^{-1}G_\sigma^\pm + \frac{i}{2}\{G_{0,\sigma}^{-1}, G_\sigma^\pm\} = 1 + \Sigma_\sigma^\pm G_\sigma^\pm + \frac{i}{2}\{\Sigma_\sigma^\pm, G_\sigma^\pm\} + \mathcal{O}(\partial_X^2), \qquad (2.25a)$$

$$G_\sigma^\pm G_{0,\sigma}^{-1} + \frac{i}{2}\{G_\sigma^\pm, G_{0,\sigma}^{-1}\} = 1 + G_\sigma^\pm \Sigma_\sigma^\pm + \frac{i}{2}\{G_\sigma^\pm, \Sigma_\sigma^\pm\} + \mathcal{O}(\partial_X^2). \qquad (2.25b)$$

It is useful to investigate these equations order by order in ∂_X. In the static limit, as obtained by neglecting the Poisson brackets, Eqs. (2.24) read as:

$$(G_{0,\sigma}^{-1} - \Sigma_\sigma^+)G_\sigma^\gtrless = \Sigma_\sigma^\gtrless G_\sigma^- + \mathcal{O}(\partial_X), \qquad (2.26a)$$

$$G_\sigma^{\gtrless}(G_{0,\sigma}^{-1} - \Sigma_\sigma^-) = G_\sigma^+ \Sigma_\sigma^{\gtrless} + \mathcal{O}(\partial_X). \tag{2.26b}$$

Likewise, collecting the local terms of Eqs. (2.25), we find:

$$(G_{0,\sigma}^{-1} - \Sigma_\sigma^\pm)G_\sigma^\pm = 1 + \mathcal{O}(\partial_X). \tag{2.27}$$

The last three equations immediately give:

$$G_\sigma^\pm = \frac{1}{G_{0,\sigma}^{-1} - \Sigma_\sigma^\pm} + \mathcal{O}(\partial_X),$$

$$G_\sigma^{\gtrless} = G_\sigma^+ \Sigma_\sigma^{\gtrless} G_\sigma^- + \mathcal{O}(\partial_X) = |G_\sigma^+|^2 \, \Sigma_\sigma^{\gtrless} + \mathcal{O}(\partial_X), \tag{2.28}$$

where we have used the property $G^- = (G^+)^*$ in the last equality.

The first order (gradient) corrections can be found from the same set of equations, Eqs. (2.24) and (2.25). This can be done in various ways. The usual method is to subtract Eq. (2.24b) from Eq. (2.24b). Since the zeroth order terms are common between the two equations, we end up with a purely first order equation:

$$\frac{i}{2}\{G_{0,\sigma}^{-1}, G_\sigma^{\gtrless}\} - \frac{i}{2}\{G_\sigma^{\gtrless}, G_{0,\sigma}^{-1}\} = \frac{i}{2}\{\Sigma_\sigma^+, G_\sigma^{\gtrless}\} - \frac{i}{2}\{G_\sigma^+, \Sigma_\sigma^{\gtrless}\} + \frac{i}{2}\{\Sigma_\sigma^{\gtrless}, G_\sigma^-\} - \frac{i}{2}\{G_\sigma^{\gtrless}, \Sigma_\sigma^-\}$$

$$+ (\Sigma_\sigma^+ - \Sigma_\sigma^-)G_\sigma^{\gtrless} - (G_\sigma^+ - G_\sigma^-)\Sigma_\sigma^{\gtrless} + \mathcal{O}(\partial_X^2). \tag{2.29}$$

The above equation can be put in a more useful form using the exact relations between the explicit-time components of the Keldysh functions (cf. Eqs. 1.6a and 1.6f):

$$\{G_{0,\sigma}^{-1} - \Re[\Sigma_\sigma^+], iG_\sigma^{\gtrless}\} + \{\Re[G_\sigma^+], i\Sigma_\sigma^{\gtrless}\} = \Sigma_\sigma^> G_\sigma^< - G_\sigma^> \Sigma_\sigma^< + \mathcal{O}(\partial_X^2). \tag{2.30}$$

The above equation is the celebrated *Kadanoff-Baym (KB) quantum kinetic equation.*

We note that the KB kinetic equation for $G^>$ and $G^<$ have different physical contents and are both important part of the full physical picture. The content of the the equations can be laid bare with some elementary rearrangements. Subtracting the sides of two equations for $G^>$ and $G^<$ from

one another, or alternatively summing the sides of Eqs. (2.25a) and (2.25a), we obtain:

$$G_\sigma^\pm = \frac{1}{G_{0,\sigma}^{-1} - \Sigma_\sigma^\pm} + \mathcal{O}(\partial_X^2) \tag{2.31}$$

It is crucial to note that the exactness of the above equation to $\mathcal{O}(\partial_X)$ is bound to using $\Sigma^\pm$ which is also exact to $\mathcal{O}(\partial_X)$. The above result can be put in a more useful form by switching to the spectral/statistical representation. To this end, we introduce:

$$\begin{aligned}
G_\sigma^< &\equiv i\mathsf{A}_\sigma f_\sigma, & \Sigma_\sigma^< &\equiv i\Gamma_\sigma c_\sigma, \\
G_\sigma^> &\equiv -i\mathsf{A}_\sigma(1 - f_\sigma), & \Sigma_\sigma^> &\equiv -i\Gamma_\sigma(1 - c_\sigma).
\end{aligned} \tag{2.32}$$

Note that the above definitions and the exact relations between the components of the Keldysh functions imply $\Gamma_\sigma = -2\Im[\Sigma_\sigma^+]$ and $\mathsf{A}_\sigma = -2\Im[G_\sigma^+]$. The above definitions combined with Eq. (2.31) yield:

$$\mathsf{A}_\sigma = \frac{\Gamma_\sigma}{\mathsf{M}_\sigma^2 + \Gamma_\sigma^2/4} + \mathcal{O}(\partial_X^2), \qquad \Re[G_\sigma^+] = \frac{\mathsf{M}_\sigma}{\mathsf{M}_\sigma^2 + \Gamma_\sigma^2/4} + \mathcal{O}(\partial_X^2), \tag{2.33}$$

where we have defined the *mass-shell function* M_σ as:

$$\mathsf{M}_\sigma \equiv G_{0,\sigma}^{-1} - \Re[\Sigma_\sigma^+] = \omega + \mu_\sigma - \frac{|\mathbf{p}|^2}{2m_\sigma} - U_\sigma(T, \mathbf{R}) - \Re[\Sigma_\sigma^+]. \tag{2.34}$$

Plugging the spectral/statistical representation into the KB kinetic equation for either of $G^>$ or $G^<$ and using Eq. (2.31), we find the second result:

$$\{\mathsf{M}_\sigma, \mathsf{A}_\sigma f_\sigma\} + \left\{\frac{\mathsf{M}_\sigma}{\mathsf{M}_\sigma^2 + \Gamma_\sigma^2/4}, \Gamma_\sigma c_\sigma\right\} = -\Gamma_\sigma \mathsf{A}_\sigma(f_\sigma - c_\sigma) + \mathcal{O}(\partial_X^2). \tag{2.35}$$

Eqs. (2.33) and (2.35) constitute an exact rewriting of the original KB kinetic equations for $G^>$ and $G^<$. The right hand side of the KB kinetic equation is referred to as the *collision integral*:

$$\mathsf{C}_\sigma \equiv G_\sigma^> \Sigma_\sigma^< - \Sigma_\sigma^> G_\sigma^< = -\Gamma_\sigma \mathsf{A}_\sigma(f_\sigma - c_\sigma). \tag{2.36}$$

The collision integral accounts for the change in the phase space density due to retardation effects. The two Poisson brackets appearing on left hand side of the quantum kinetic equation are referred to

as the *streaming terms*. The first Poisson bracket is the generalized kinetic drift in the $(\omega, \mathbf{p})$ phase space, including corrections from the self-consistent field $\Re[\Sigma^+]$ (i.e. the *drag flow*). The second Poisson bracket has no classical counterpart (cf. Sec. 2.2.2) and is associated to the finite damping width of the particles Γ_σ. It can be decomposed into terms representing the many-body back-flow and the off-mass-shell response [61].

We note that the quantities appearing in the expression for the collision integral must be expanded consistently within the first order gradient expansion. In principle, $\mathsf{A}_\sigma(\omega, \mathbf{p}; T, \mathbf{R})$, $\Gamma_\sigma(\omega, \mathbf{p}; T, \mathbf{R})$ and $c_\sigma(\omega, \mathbf{p}; T, \mathbf{R})$ can be decomposed into the sum of a part with only local dependence on the quantities at $(T, \mathbf{R})$, and a non-local part (memory terms). It is useful to make a distinction between local and memory terms in the collision integral:

$$
\begin{aligned}
\mathsf{C}_\sigma &= G_\sigma^> \Sigma_\sigma^< - G_\sigma^< \Sigma_\sigma^> \\
&= \left(G_\sigma^>\right)^{\text{loc.}} \left(\Sigma_\sigma^<\right)^{\text{loc.}} - \left(G_\sigma^<\right)^{\text{loc.}} \left(\Sigma_\sigma^>\right)^{\text{loc.}} + \delta \mathsf{C}_\sigma^{\text{mem.}} . \\
&= -\Gamma_\sigma^{\text{loc.}} \mathsf{A}_\sigma^{\text{loc.}} \left(f_\sigma - c_\sigma^{\text{loc.}}\right) + \delta \mathsf{C}_\sigma^{\text{mem.}} .
\end{aligned}
\tag{2.37}
$$

The quantities with a *loc.* label are evaluated in the local approximation (by neglecting the gradient corrections), and $\delta \mathsf{C}_\sigma^{\text{mem.}}$ denotes the correction to C_σ due to gradient terms. A systematic analysis of the structure of the vacuum diagrams shows that the local part of the collision term has the

following general structure [61]:

$$
\mathsf{C}_\sigma^{\text{loc.}}(\omega, \mathbf{p}; T, \mathbf{R}) = \frac{1}{2} \sum_{m,m'} \int \frac{\mathrm{d}\omega_1}{2\pi} \frac{\mathrm{d}^d \mathbf{p}_1}{(2\pi)^d} \cdots \frac{\mathrm{d}\omega_m}{2\pi} \frac{\mathrm{d}^d \mathbf{p}_m}{(2\pi)^d} \frac{\mathrm{d}\omega_1'}{2\pi} \frac{\mathrm{d}^d \mathbf{p}_1'}{(2\pi)^d} \cdots \frac{\mathrm{d}\omega_{m'}'}{2\pi} \frac{\mathrm{d}^d \mathbf{p}_{m'}'}{(2\pi)^d}
$$

$$
\times \, R_{m,m'}(\omega_1, \mathbf{p}_1, \ldots, \omega_m, \mathbf{p}_m; \omega_1', \mathbf{p}_1', \ldots, \omega_{m'}', \mathbf{p}_{m'}'; T, \mathbf{R})
$$

$$
\times \, \mathsf{A}_1 \ldots \mathsf{A}_m \, \mathsf{A}_1' \ldots \mathsf{A}_{m'}'
$$

$$
\times \, \left([1 - f_1] \ldots [1 - f_m] f_1' \ldots f_{m'}' - f_1 \ldots f_m [1 - f_1'] \ldots [1 - f_{m'}'] \right)
$$

$$
\times \, \left[\sum_{j=1}^{m} \delta_{\sigma \sigma_j} (2\pi)^{d+1} \delta(\omega_j - \omega) \delta^d(\mathbf{p}_j - \mathbf{p}) - \sum_{j=1}^{m'} \delta_{\sigma \sigma_j} (2\pi)^{d+1} \delta(\omega_j' - \omega) \delta^d(\mathbf{p}_j' - \mathbf{p}) \right]
$$

$$
\times \, (2\pi)^{d+1} \delta \left(\sum_{j=1}^{m} \omega_j - \sum_{j=1}^{m'} \omega_j' \right) \delta^d \left(\sum_{j=1}^{m} \mathbf{p}_j - \sum_{j=1}^{m'} \mathbf{p}_j' \right), \tag{2.38}
$$

where $f_j \equiv f_{\sigma_j}(\omega_j, \mathbf{p}_j; T, \mathbf{R})$, $f_j' \equiv f_{\sigma_j'}(\omega_j', \mathbf{p}_j'; T, \mathbf{R})$ and $R_{m,m'}$ is a transition rate independent of the state of the system. The structure of the memory part, $\delta \mathsf{C}_\sigma^{\text{mem.}}$, depends on the details of the used approximate Luttinger-Ward functional.

The KB kinetic equations can be put in a slightly simpler form by noting that one may use local approximation for all of the quantities appearing in the Poisson brackets within the validity domain of the first-order gradient expansion. One such simplification, as suggested first by Botermans and Malfliet [24], is to replace the statistical part of the self-energies c_σ appearing in the second Poisson bracket by its zeroth-order approximation. The justification comes either from Eq. (2.28) or by simply observing that the left hand side of Eq. (2.35) is $\mathcal{O}(\partial_X)$, so that:

$$
c_\sigma = f_\sigma + \mathcal{O}(\partial_X). \tag{2.39}
$$

Replacing c_σ with f_σ in the second Poisson bracket, we find:

$$
\{\mathsf{M}_\sigma, \mathsf{A}_\sigma f_\sigma\} + \left\{ \frac{\mathsf{M}_\sigma}{\mathsf{M}_\sigma^2 + \Gamma_\sigma^2/4}, \Gamma_\sigma f_\sigma \right\} = -\Gamma_\sigma \mathsf{A}_\sigma (f_\sigma - c_\sigma) + \mathcal{O}(\partial_X^2), \tag{2.40}
$$

which can be written in the following form with some straightforward manipulations:

$$\frac{\mathsf{A}_\sigma^2 \Gamma_\sigma}{2} \left[\{\mathsf{M}_\sigma, f_\sigma\} - \frac{\mathsf{M}_\sigma}{\Gamma_\sigma}\{\Gamma_\sigma, f_\sigma\} \right] = -\Gamma_\sigma \mathsf{A}_\sigma (f_\sigma - c_\sigma) + \mathcal{O}(\partial_X^2). \tag{2.41}$$

We refer to the last equation as the kinetic equation in the Botermans-Malfliet (BM) form. We drop $\mathcal{O}(\partial_X^2)$ in the kinetic equations hereafter. It has been shown in Ref. [62] that the KB quantum kinetic equations respect the conservation laws, reminiscent of the original KB equations, provided that all quantities are consistently expanded to first order in ∂_X. In particular, the memory part of the collision integral $\delta\mathsf{C}^{\mathrm{mem.}}$ shall not be neglected.

The physical content of KB kinetic equations and memory effects:

Since Eq. (2.33) does not have a differential structure, it may seem that A_σ can be readily solved for f_σ, effectively reducing the two kinetic equations for $G^>$ and $G^<$ to a single equation for f_σ. While possible in principle, this task is not always trivial. Provided that the Luttinger-Ward functional contains vacuum diagrams with three interaction vertices or more, the self-energy functional will have a *non-local* dependence on the Green's functions [61]. This implies that upon gradient expansion, Σ will depend on both G and $\partial_X G$. As a result, the mass-shell function and the spectral broadening appearing in Eq. (2.33) will also be non-local functionals of A_σ and f_σ. Therefore, the self-consistent solution of Eq. (2.33) for A_σ can be a non-trivial task despite its deceptive algebraic structure. The non-locality of the self-energy implies the emergence of memory effects in A_σ.

The memory effects can be physically inconsequential in certain systems, such as dilute Fermi for Bose gases with short-range repulsive interactions. In this case, the particles only meet during the short period of collisions and propagate as essentially free particles otherwise. The history of past collisions does not play a consequential role in the dynamics. On the other hand, had the interactions been strongly attractive, the particles could form long-lived bound pairs, propagate with their partners for a long time, and undergo several collisions before possibly breaking up. In

this case, the memory can persist for a long time and will have an important role in the dynamics. Therefore, the non-Markovian structure of kinetic equations can be an important effect in systems with bound states and neglecting the memory effects can lead to wrong results. Paying attention to this subtlety is of utmost importance in a proper derivation of the kinetic equations for the attractive Fermi gas, a problem which will be discussed in chapter 4. In fact, we find that the transport of the attractive Fermi gas in the strong-coupling regime is essentially encoded in the spatio-temporal fluctuations of the spectral function A_σ while the statistical function f_σ is virtually void of physical content!

2.2.1 The Born approximation

So far, we have discussed the quantum kinetic formalism in full generality and without reference to any particular Φ-derivable approximation. In this section, we give explicit expressions for the retarded self-energy and the collision integral by expanding the Luttinger-Ward function to the 3-loop order. The loop expansion is controlled for weakly interacting systems. We consider a single-component system for simplicity. The 3-loop expansion of the self-energy of such a system was discussed earlier in Sec. 1.3.1. This approximation is often referred to as the Born approximation. Let us consider the HF self-energy (Eq. 2.42). Expressing Σ_{HF} in the Wigner representation, we find:

$$\Sigma_{\mathrm{HF}}^+(\mathbf{p};T,\mathbf{R}) = \underbrace{\int \mathrm{d}^d\mathbf{R}'\, V(\mathbf{R}-\mathbf{R}')\, n(T,\mathbf{R}')}_{\text{Direct (Hartree)}} + \underbrace{\int \mathrm{d}^d\mathbf{p}_1\, \mathcal{V}(\mathbf{p}-\mathbf{p}_1) \int \frac{\mathrm{d}\omega_1}{2\pi}\, iG^<(\omega_1,\mathbf{p}_1;T,\mathbf{R})}_{\text{Exchange (Fock)}},$$

(2.42)

where:

$$n(T,\mathbf{R}) \equiv \int \frac{\mathrm{d}\omega}{2\pi}\, \frac{\mathrm{d}^d\mathbf{p}}{(2\pi)^d}\, (-i)G^<(\omega,\mathbf{p};T,\mathbf{R}),$$

(2.43)

is the local particle density. We notice that if the effective range of the interactions is comparable to l_{macro}, the Hartree contribution will break locality in the macroscopic coordinate $\mathbf{R}$. The HF con-

tributions are instantaneous and $\Sigma_{\mathrm{HF}}^{\gtrless} = 0$. Note that Σ_{HF}^{+} has no ω-dependence. The greater/lesser part of the Born self-energy is:

$$
\Sigma_{\mathrm{B}}^{\gtrless}(\omega, \mathbf{p}; T, \mathbf{R}) = \int \frac{\mathrm{d}\omega_1}{2\pi} \frac{\mathrm{d}^d \mathbf{p}_1}{(2\pi)^d} \frac{\mathrm{d}\omega'}{2\pi} \frac{\mathrm{d}^d \mathbf{p}'}{(2\pi)^d} \frac{\mathrm{d}\omega'_1}{2\pi} \frac{\mathrm{d}^d \mathbf{p}'_1}{(2\pi)^d} (2\pi)^{d+1} \delta^d(\mathbf{p} + \mathbf{p}_1 - \mathbf{p}' - \mathbf{p}'_1)
$$

$$
\times \delta(\omega + \omega_1 - \omega' - \omega'_1) \left[\mathcal{V}(\mathbf{p} - \mathbf{p}')^2 - \mathcal{V}(\mathbf{p} - \mathbf{p}') \mathcal{V}(\mathbf{p} - \mathbf{p}'_1) \right]
$$

$$
\times G^{\lessgtr}(\omega_1, \mathbf{p}_1; T, \mathbf{R}) \, G^{\gtrless}(\omega', \mathbf{p}'; T, \mathbf{R}) \, G^{\gtrless}(\omega'_1, \mathbf{p}'_1; T, \mathbf{R}). \quad (2.44)
$$

Using the spectral/statistical representation of the Green's functions, we find:

$$
\Sigma_{\mathrm{B}}^{\gtrless}(\omega, \mathbf{p}; T, \mathbf{R}) = \int \mathcal{D}_{\omega, \mathbf{p}}^{(3)} \, W \, P^{\gtrless}, \quad (2.45)
$$

where:

$$
\mathcal{D}_{\omega, \mathbf{p}}^{(3)} \equiv \frac{\mathrm{d}\omega_1}{2\pi} \frac{\mathrm{d}^d \mathbf{p}_1}{(2\pi)^d} \frac{\mathrm{d}\omega'}{2\pi} \frac{\mathrm{d}^d \mathbf{p}'}{(2\pi)^d} \frac{\mathrm{d}\omega'_1}{2\pi} \frac{\mathrm{d}^d \mathbf{p}'_1}{(2\pi)^d} (2\pi)^{d+1} \delta^d(\mathbf{p} + \mathbf{p}_1 - \mathbf{p}' - \mathbf{p}'_1) \delta(\omega + \omega_1 - \omega' - \omega'_1),
$$

$$
(2.46a)
$$

$$
W \equiv \frac{1}{2} \left| \mathcal{V}(\mathbf{p} - \mathbf{p}') - \mathcal{V}(\mathbf{p} - \mathbf{p}'_1) \right|^2 = \frac{1}{2} \left| \begin{array}{c} \mathbf{p}' \quad \mathbf{p}'_1 \\ \diagdown \cdots \diagup \\ \diagup \quad \diagdown \\ \mathbf{p} \quad \mathbf{p}_1 \end{array} - \begin{array}{c} \mathbf{p}' \quad \mathbf{p}'_1 \\ \times \\ \mathbf{p} \quad \mathbf{p}_1 \end{array} \right|^2 \quad (2.46b)
$$

$$
P^{>} \equiv -i \, \mathsf{A}(\omega_1, \mathbf{p}_1) \, \mathsf{A}(\omega', \mathbf{p}') \, \mathsf{A}(\omega'_1, \mathbf{p}'_1) \, f(\omega_1, \mathbf{p}_1) \left[1 - f(\omega', \mathbf{p}') \right] \left[1 - f(\omega'_1, \mathbf{p}'_1) \right], \quad (2.46c)
$$

$$
P^{<} \equiv i \, \mathsf{A}(\omega_1, \mathbf{p}_1) \, \mathsf{A}(\omega', \mathbf{p}') \, \mathsf{A}(\omega'_1, \mathbf{p}'_1) \left[1 - f(\omega_1, \mathbf{p}_1) \right] f(\omega', \mathbf{p}') \, f(\omega'_1, \mathbf{p}'_1). \quad (2.46d)
$$

We have dropped the common argument $(T, \mathbf{R})$ in the quantities appearing in the definition of $P^{\gtrless}$ for brevity. The auxiliary quantities such as Γ, $\Re[\Sigma^{+}]$, and C are easily found according to their definitions:

$$
\Gamma(\omega, \mathbf{p}; T, \mathbf{R}) = \int \mathcal{D}_{\omega, \mathbf{p}}^{(3)} \, \mathsf{A}(\omega_1, \mathbf{p}_1) \, \mathsf{A}(\omega', \mathbf{p}') \, \mathsf{A}(\omega'_1, \mathbf{p}'_1) \, W \left\{ f(\omega_1, \mathbf{p}_1) \left[1 - f(\omega', \mathbf{p}') \right] \right.
$$

$$
\left. \times \left[1 - f(\omega'_1, \mathbf{p}'_1) \right] + \left[1 - f(\omega_1, \mathbf{p}_1) \right] f(\omega', \mathbf{p}') \, f(\omega'_1, \mathbf{p}'_1) \right\}, \quad (2.47a)
$$

$$
\Re[\Sigma^{+}](\omega, \mathbf{p}; T, \mathbf{R}) = \Sigma_{\mathrm{HF}}^{+}(\mathbf{p}; T, \mathbf{R}) - \frac{1}{2} \mathfrak{K}\mathfrak{K}[\Gamma](\omega, \mathbf{p}; T, \mathbf{R}), \quad (2.47b)
$$

$$\mathsf{C}(\omega, \mathbf{p}; T, \mathbf{R}) = \int \mathcal{D}^{(3)}_{\omega, \mathbf{p}} \, \mathsf{A}(\omega, \mathbf{p}) \, \mathsf{A}(\omega_1, \mathbf{p}_1) \, \mathsf{A}(\omega', \mathbf{p}') \, \mathsf{A}(\omega'_1, \mathbf{p}'_1) \, W \left\{ [1 - f(\omega, \mathbf{p})] \right.$$

$$\times \left. [1 - f(\omega_1, \mathbf{p}_1)] \, f(\omega', \mathbf{p}') \, f(\omega'_1, \mathbf{p}'_1) - f(\omega, \mathbf{p}) \, f(\omega_1, \mathbf{p}_1) \left[1 - f(\omega', \mathbf{p}') \right] \left[1 - f(\omega'_1, \mathbf{p}'_1) \right] \right\}$$

$$= \int \mathcal{D}^{(3)}_{\omega, \mathbf{p}} \left[\begin{array}{cc} & \\ W & - & W \\ & \end{array} \right]. \tag{2.47c}$$

2.2.2   The route to the Boltzmann equation

The passage from quantum kinetic equation to the Boltzmann equation has been discussed in Ref. [22]. The conditions for the validity of this procedure have been discussed at length by [23]. Here, we provide a brief account of the Boltzmann limit and its applicability criteria. The Boltzmann equation describes the evolution of single-particle probability distribution function of an ensemble of classical particles, $n(\mathbf{p}; T, \mathbf{R})$[1]. By definition, $n(\mathbf{p}; T, \mathbf{R}) \, \mathrm{d}^d\mathbf{p} \, \mathrm{d}^d\mathbf{R}$ indicates the number of particles having momentum $\mathbf{p}$ at position $\mathbf{R}$ at time T. In the absence of inter-particle interactions, the trajectory of each classical particle is given by Hamilton equations and the evolution of f is governed by the classical Liouville equation, which is the statement of conservation of phase space volume. In its simplest form, the Boltzmann equation reads as:

$$\partial_T n + \frac{\mathbf{p}}{m} \cdot \partial_{\mathbf{R}} \, n + \mathbf{F}(T, \mathbf{R}) \cdot \partial_{\mathbf{p}} n = \left(\frac{\partial n}{\partial T} \right)_{\text{coll.}}, \tag{2.48}$$

where $\mathbf{F}(T, \mathbf{R})$ is the net external force experienced by a single particle. The right hand side is a non-Liouvillian correction due to collisions and denotes the net rate of particles entering the phase space point. Conservation of particle number, momentum and energy requires:

$$\int \mathrm{d}^d\mathbf{p} \, \mathrm{d}^d\mathbf{R} \left(\frac{\partial n}{\partial T} \right)_{\text{coll.}} = \int \mathrm{d}^d\mathbf{p} \, \mathrm{d}^d\mathbf{R} \, \mathbf{p} \left(\frac{\partial n}{\partial T} \right)_{\text{coll.}} = \int \mathrm{d}^d\mathbf{p} \, \mathrm{d}^d\mathbf{R} \, \frac{|\mathbf{p}|^2}{2m} \left(\frac{\partial n}{\partial T} \right)_{\text{coll.}} = 0. \tag{2.49}$$

In case of long-range interactions, one must also add the net force produced by the other particles to $\mathbf{F}$ as well, so that $\mathbf{F}$ becomes a functional of n. Except for the trivial case of free particles, the

---

[1]The single-particle probability distribution function is often called $f(\mathbf{p}; T, \mathbf{R})$. Following Ref. [23], we use the notation $n(\mathbf{p}; T, \mathbf{R})$ in order to avoid any confusion with the Wigner's statistical function $f(\omega, \mathbf{p}; T, \mathbf{R})$ defines earlier.

validity of the Boltzmann equation requires the possibility of having a well-defined single-particle distribution function. Treating n like a random variable, this requires the many-body limit where $\sqrt{\text{Var}[n]} \ll \langle n \rangle$. The condition of weakly inhomogeneous disturbances further guarantees this condition at all times.

The passage from quantum kinetic equations to a Boltzmann-like description evidently requires the notion of particles, a sufficient condition for which is the system being in the classical regime where the thermal de-Broglie wavelength $\lambda_T \equiv h/\sqrt{2\pi m k_B T}$ is much smaller than the inter-particle separation $\ell \equiv n^{-1/d}$ and quantum effects are immaterial. For fermions, this implies $T \gg T_F$, where $T_F = \epsilon_F/k_B$ is the Fermi temperature. Well-defined quasiparticles may exist in the quantum regime as well. For repulsively interacting quantum degenerate fermions in $d > 1$, the particles near the Fermi surface have a long lifetime proportional to $(T_F/T)^2$ due to Pauli exclusion. This is the cornerstone of Landau Fermi liquid theory.

Provided that the lifetime of (quasi-)particles is large compared to the microscopic time scales, we can take the limit $\Gamma/\epsilon_F \to 0$ and only retain the terms that are leading order in Γ in the kinetic equation. In the Fermi liquid regime, taking this limit is only warranted for $|\mathbf{p}| \sim p_F$, where p_F is the Fermi momentum, However, since the states corresponding to $|\mathbf{p}| < p_F$ are Pauli blocked and the excitation of $|\mathbf{p}| \gg p_F$ quasiparticles is thermally suppressed, we do not need to single-out the Fermi momentum in this procedure. Following Ref. [23], we take the limit $\Gamma \to 0$ in the Poisson brackets appearing on the streaming side of the kinetic equation as a first step. This is admissible to leading order in Γ since the neglected corrections are $\mathcal{O}(\Gamma \partial_X)$, whereas the collision integral is $\mathcal{O}(\partial_X)$. In the same approximation, we can neglect the second Poisson bracket altogether since it is $\mathcal{O}(\Gamma \partial_X)$. This brings us to:

$$\{\mathsf{M}_\sigma, \mathsf{A}_\sigma f_\sigma\} = \mathsf{C}_\sigma + \mathcal{O}(\partial_X^2, \Gamma \partial_X). \tag{2.50}$$

In the quasiparticle limit, the fermion spectral function assumes the form:

$$A_\sigma^{(qp)} \equiv \lim_{\Gamma_\sigma \to 0} A_\sigma = \lim_{\Gamma_\sigma \to 0} \frac{\Gamma_\sigma}{M_\sigma^2 + \Gamma_\sigma^2/4} = 2\pi\,\delta(M_\sigma), \tag{2.51}$$

justifying the nomenclature *mass-shell* for M_σ. Using the explicit expression for M_σ, one finds:

$$A_\sigma^{(qp)}(\omega, \mathbf{p}; T, \mathbf{R}) = 2\pi\,\delta\left(\omega - \mu_\sigma - |\mathbf{p}|^2/(2m_\sigma) - U_\sigma(T, \mathbf{R}) - \Re[\Sigma_\sigma^+(\omega, \mathbf{p}; T, \mathbf{R})]\right)$$

$$= 2\pi Z_\sigma(\mathbf{p}; T, \mathbf{R})\,\delta(\omega - E_\sigma(\mathbf{p}; T, \mathbf{R})), \tag{2.52}$$

where the *quasiparticle energy dispersion* E_σ and the *quasiparticle residue* Z_σ are defined as:

$$E_\sigma(\mathbf{p}; T, \mathbf{R}) - \mu_\sigma - |\mathbf{p}|^2/(2m_\sigma) - U_\sigma(T, \mathbf{R}) - \Re[\Sigma_\sigma^+(\omega, \mathbf{p}; T, \mathbf{R})]\Big|_{\omega = E_\sigma(\mathbf{p}; T, \mathbf{R})} = 0,$$

$$Z_\sigma(\mathbf{p}; T, \mathbf{R}) \equiv (\partial_\omega M_\sigma)^{-1}\Big|_{\omega = E_\sigma(\mathbf{p}; T, \mathbf{R})} = \left(1 - \partial_\omega \Re[\Sigma_\sigma^+(\omega, \mathbf{p}; T, \mathbf{R})]\right)^{-1}\Big|_{\omega = E_\sigma(\mathbf{p}; T, \mathbf{R})}. \tag{2.53}$$

Note that Γ/ϵ_F can be much smaller than unity for the Landau quasiparticles, yet, Z can be considerably smaller than unity since it depends on the off-shell processes. For the same reason, while $\Sigma^\gtrless/\epsilon_F \sim \Gamma/\epsilon_F$ can be small for the on-shell quasiparticles, $\Re[\Sigma^+]/\epsilon_F$ can be large and have a significant ω-dependence.

The equation for the quasiparticle energy dispersion is an implicit equation and must be solved self-consistently. Since the quasiparticles are on-shell, the ω-dependence of the kinetic equation is redundant and can be removed by integrating both sides of Eq. (2.50) over ω. Using the fact that $\{M_\sigma, 2\pi\,\delta(M_\sigma)\,f_\sigma\} = 2\pi\,\delta(M_\sigma)\,\{M_\sigma, f_\sigma\}$, we find:

$$\int \frac{d\omega}{2\pi}\,\{M_\sigma, 2\pi\,\delta(M_\sigma)f_\sigma\} = \int d\omega\,\delta(M_\sigma)\,\{M_\sigma, f_\sigma\}$$

$$= \int d\omega\,\delta(M_\sigma)\,(\partial_\omega M_\sigma\,\partial_T f_\sigma - \partial_\mathbf{p} M_\sigma \cdot \partial_\mathbf{R} f_\sigma - \partial_T M_\sigma\,\partial_\omega f_\sigma + \partial_\mathbf{R} M_\sigma \cdot \partial_\mathbf{p} f_\sigma)$$

$$= Z_\sigma^{-1}\left[\partial_T + \left(\frac{\mathbf{p}}{m_\sigma} + \partial_\mathbf{p}\Re\left[\Sigma_\sigma^+(E_\sigma, \mathbf{p}; T, \mathbf{R})\right]\right) \cdot \partial_\mathbf{R}\right.$$

$$\left. - \left(\partial_\mathbf{R} U_\sigma(T, \mathbf{R}) + \partial_\mathbf{R}\Re\left[\Sigma_\sigma^+(E_\sigma, \mathbf{p}; T, \mathbf{R})\right]\right) \cdot \partial_\mathbf{p}\right] n_\sigma(\mathbf{p}; T, \mathbf{R}), \tag{2.54}$$

where the *quasiparticle distribution function* $n_\sigma(\mathbf{p}; T, \mathbf{R})$ is defined as the on-shell fermionic statistical function:

$$n_\sigma(\mathbf{p}; T, \mathbf{R}) \equiv f_\sigma(E_\sigma, \mathbf{p}; T, \mathbf{R}). \tag{2.55}$$

Combining Eqs. (2.50) and (2.54) gives the final result:

$$\begin{aligned}
\left[\partial_T + \left(\frac{\mathbf{p}}{m_\sigma} + \partial_\mathbf{p} \Re \left[\Sigma_\sigma^+(E_\sigma, \mathbf{p}; T, \mathbf{R}) \right] \right) \cdot \partial_\mathbf{R} \right. \\
\left. - \left(\partial_\mathbf{R} U_\sigma(T, \mathbf{R}) + \partial_\mathbf{R} \Re \left[\Sigma_\sigma^+(E_\sigma, \mathbf{p}; T, \mathbf{R}) \right] \right) \cdot \partial_\mathbf{p} \right] n_\sigma(\mathbf{p}; T, \mathbf{R}) = \left(\frac{\partial n_\sigma}{\partial T} \right)_\text{coll.},
\end{aligned} \tag{2.56}$$

where:

$$\left(\frac{\partial n_\sigma}{\partial T} \right)_\text{coll.} \equiv I_\sigma[n] \equiv Z_\sigma(\mathbf{p}; T, \mathbf{R}) \int \frac{\mathrm{d}\omega}{2\pi} \, \mathsf{C}_\sigma[f]. \tag{2.57}$$

The collision integral can be calculated in the local approximation within the validity domain of the quasiparticle approximation. If the Luttinger-Ward functional includes no more than two fermion loops (as in the Born and T-matrix approximations), the general structure of the collision integral can be read from Eq. (2.38):

$$\begin{aligned}
I_\sigma[n] = Z_\sigma(\mathbf{p}; T, \mathbf{R}) \sum_{\sigma_1, \sigma', \sigma_1'} \int \frac{\mathrm{d}^d\mathbf{p}_1}{(2\pi)^d} \frac{\mathrm{d}^d\mathbf{p}'}{(2\pi)^d} \frac{\mathrm{d}^d\mathbf{p}_1'}{(2\pi)^d} (2\pi)^{d+1} \delta^d(\mathbf{p} + \mathbf{p}_1 - \mathbf{p}' - \mathbf{p}_1') \\
\times \delta \left(E_{\mathbf{p},\sigma} + E_{\mathbf{p}_1,\sigma_1} - E_{\mathbf{p}',\sigma'} - E_{\mathbf{p}_1',\sigma_1'} \right) W(\mathbf{p}, \sigma; \mathbf{p}_1, \sigma_1 \to \mathbf{p}', \sigma'; \mathbf{p}_1', \sigma_1') \\
\times \left\{ \left[1 - n_\sigma(\mathbf{p}) \right] \left[1 - n_{\sigma_1}(\mathbf{p}_1) \right] n_{\sigma'}(\mathbf{p}') n_{\sigma_1'}(\mathbf{p}_1') \right. \\
\left. - n_\sigma(\mathbf{p}) \, n_{\sigma_1}(\mathbf{p}_1) \left[1 - n_{\sigma'}(\mathbf{p}') \right] \left[1 - n_{\sigma_1'}(\mathbf{p}_1') \right] \right\},
\end{aligned} \tag{2.58}$$

where W is the transition amplitude. In the Born approximation, $W \equiv |\mathcal{M}|^2/2$ (cf. Eqs. 2.47c and 2.46b). Eq. (2.56) may also written in the following concise form:

$$\partial_T n_\sigma + \{n_\sigma, E_\sigma\} = I_\sigma[n], \tag{2.59}$$

which is reminiscent of the Liouville equation of classical Hamiltonian systems, save for two important differences: (1) E_σ is a *functional* of n_σ and is found from the self-consistent solution of

Eq. (2.53), and (2) the presence of the collision integral $I_c[n]$ describing the change in the phase-space density due to collisions. If we neglect the self-energy corrections on the left hand side of Eq. (2.46b), which is admissible either if the interactions are weak, or if $T \gg T_F$, the above equation reduces to the classical Boltzmann equation, Eq. (2.48).

The various limits of the quasiparticle kinetic equation have appeared in the literature by different authors. In the zero-temperature limit, the low-energy excitations are infinitely long-lived quasiparticles on the Fermi surface $|\mathbf{p}| = p_F$ and the collision integral vanishes identically. Neglecting long-range interactions, the ensuing equation is known as the *Landau kinetic equation* and constitutes an exact kinetic description of ultracold neutral fermionic matter such as ^{3}He, as long as $Z > 0^2$. Including long-range Coulomb interactions in case of charged fermions, the ensuing equation is often called the *Landau-Silin kinetic equation*. Finally, neglecting collisions and self-energy corrections beyond Hartree-Fock level but taking into account long-range forces and external electromagnetic fields, the *Vlasov equation* is obtained. We refer to Eq. (2.56) in its most general form as the *collisional Boltzmann-Vlasov* (CBV) equation.

2.3 Global and local equilibrium states

The first step toward investigating the nature of slow varying collective excitations of a system about its equilibrium state is to first establish its properties in the equilibrium state. This can be done most easily done by taking a step back and remembering that at the thermal equilibrium, the Green's function are constrained by the KMS boundary condition. The equilibrium Green's functions, $\mathcal{G}_{\sigma,\mathrm{eq}}(\tau_1, \mathbf{x}_1; \tau_1', \mathbf{x}_1')$, may only be functions of the difference of the two time arguments, i.e. they do not depend on the macroscopic time $T = (t_1 + t_1')/2$. Fourier transforming the time

---

^{2}The exact description, of course, requires the knowledge of the exact self-energy functional or equivalently, the Landau quasiparticle interaction function $f(\mathbf{p}, \mathbf{p}') \equiv (2\pi)^d \, \delta E(\mathbf{p})/\delta n(\mathbf{p}')$ [63, 64, 65, 22].

difference to the frequency domain, the KMS boundary condition implies (see Eq. 1.45):

$$G^>_{\sigma,\mathrm{eq}}(\omega; \mathbf{x}_1, \mathbf{x}'_1) = -e^{\beta\omega} G^<_{\sigma,\mathrm{eq}}(\omega; \mathbf{x}_1, \mathbf{x}'_1). \tag{2.60}$$

The above equation in the Wigner representation reads:

$$G^>_{\sigma,\mathrm{eq}}(\omega, \mathbf{p}; \mathbf{R}) = -e^{\beta\omega} G^<_{\sigma,\mathrm{eq}}(\omega, \mathbf{p}; \mathbf{R}). \tag{2.61}$$

The above equation sets the statistical part of $\mathcal{G}_{\sigma,\mathrm{eq}}$ to the Fermi-Dirac distribution function $f_0(\omega)$:

$$f_{\sigma,\mathrm{eq}}(\omega, \mathbf{p}; \mathbf{R}) = f_0(\omega) \equiv \frac{1}{e^{\beta\omega} + 1}. \tag{2.62}$$

Note that the chemical potential has been absorbed to the Hamiltonian. It is easy to show that the self-energy at equilibrium, Σ_{eq}, also obeys the KMS boundary condition. This can be most easily inferred from the Dyson's equation:

$$\mathcal{G}_\sigma(1, 1') = \mathcal{G}_{\sigma,0}(1, 1') + \int d2 \, d2' \, \mathcal{G}_{\sigma,0}(1, 2) \, \Sigma_\sigma(2, 2') \, \mathcal{G}_\sigma(2', 1'). \tag{2.63}$$

Using the Langreth rules and remembering that $\mathcal{G}^{\gtrless}_{\sigma,0} = 0$, we find:

$$\mathcal{G}^\pm_\sigma(1, 1') = \mathcal{G}^\pm_{\sigma,0}(1, 1') + \int d2 \, d2' \, \mathcal{G}^\pm_{0,\sigma}(1, 2) \, \Sigma^\pm_\sigma(2, 2') \, \mathcal{G}^\pm_\sigma(2', 1'),$$

$$\mathcal{G}^{\gtrless}_\sigma(1, 1') = \int d2 \, d2' \, \mathcal{G}^+_{0,\sigma}(1, 2) \left[\Sigma^+_\sigma(2, 2') \, \mathcal{G}^{\gtrless}_\sigma(2', 1') + \Sigma^{\gtrless}_\sigma(2, 2') \, \mathcal{G}^-_\sigma(2', 1') \right], \tag{2.64}$$

which in combination give:

$$\mathcal{G}^{\gtrless}_\sigma(1, 1') = \int d2 \, d2' \, \mathcal{G}^+_\sigma(1, 2) \, \Sigma^{\gtrless}_\sigma(2, 2') \, \mathcal{G}^-(2', 1'). \tag{2.65}$$

Assuming thermal equilibrium and taking a Fourier transform in the time difference, the above equation yields:

$$\mathcal{G}^{\gtrless}(\omega; \mathbf{x}_1, \mathbf{x}'_1) = \int d\mathbf{x}_2 \, d\mathbf{x}'_2 \, \mathcal{G}^+_{\mathrm{eq}}(\omega; \mathbf{x}_1, \mathbf{x}_2) \, \Sigma^{\gtrless}_{\mathrm{eq}}(\omega; \mathbf{x}_2, \mathbf{x}'_2) \, \mathcal{G}^-_{\mathrm{eq}}(\omega; \mathbf{x}'_2, \mathbf{x}'_1). \tag{2.66}$$

Comparing this result with Eq. (2.61), we immediately find:

$$\Sigma^>_{\sigma,\mathrm{eq}}(\omega; \mathbf{x}_1, \mathbf{x}'_1) = -e^{\beta\omega} \Sigma^<_{\sigma,\mathrm{eq}}(\omega; \mathbf{x}_1, \mathbf{x}'_1), \tag{2.67}$$

and its counterpart in the Wigner representation:

$$\Sigma^>_{\sigma,\text{eq}}(\omega, \mathbf{p}; \mathbf{R}) = -e^{\beta\omega} \Sigma^<_{\sigma,\text{eq}}(\omega, \mathbf{p}; \mathbf{R}). \tag{2.68}$$

The above equation sets the statistical part of the self-energy, c_σ (cf. Eq. 2.32), to the Fermi-Dirac distribution:

$$c_{\sigma,\text{eq}}(\omega, \mathbf{p}; \mathbf{R}) = f_0(\omega) = \frac{1}{e^{\beta\omega} + 1}. \tag{2.69}$$

We immediately see at in equilibrium, the collision integral (cf. Eq. (2.36)) vanishes. The absence of collisions is the statement of detailed balance since $\mathsf{C}_\sigma = G^>_\sigma \Sigma^<_\sigma - G^<_\sigma \Sigma^>_\sigma$. We also easily see that the streaming side of the kinetic equation vanishes at equilibrium. This can be most easily seen in the BM form, Eq. (2.41), using the fact that $\{F, f_0(\omega)\} = 0$ for arbitrary F. The above analysis shows the KMS boundary condition is compatible with the equilibrium solution of the quantum kinetic equations. We refer to the equilibrium state $f_\sigma = c_\sigma = f_0(\omega)$ as the *global* equilibrium state. It is trivial to show that the plugging the Fermi-Dirac distribution in the general expression for the local part of the collision integral (Eq. 2.38) yields a vanishing result. Therefore, $\mathsf{C}^{\text{loc.}}$ and $\delta\mathsf{C}^{\text{mem.}}$ both vanish in the global equilibrium state. In fact, $\mathsf{C}^{\text{loc.}}$ vanishes for a broader class of distributions functions, referred to as the *local* equilibrium states:

$$f_{\text{leq.}}(\omega, \mathbf{p}; T, \mathbf{R}) = \frac{1}{\exp\left(\beta(T, \mathbf{R})\left[\omega + \delta\mu(T, \mathbf{R}) - \mathbf{p} \cdot \mathbf{V}(T, \mathbf{R})\right]\right) + 1}, \tag{2.70}$$

where the local temperature $\beta(T, \mathbf{R})$, local chemical potential correction $\delta\mu(T, \mathbf{R})$ and local macroscopic velocity field $\mathbf{V}(T, \mathbf{R})$ are aribtrary weakly inhomogeneous functions. This can be seen by plugging $f_{\text{leq.}}$ in the general expression for the local collision integral given in Eq. (2.38) and using the properties of the Fermi-Dirac function. A more direct demonstration of this fact results from neglecting gradient corrections in Eq. (2.65) to find the relation between the local Green's function and the local self-energy, which readily gives:

$$\frac{(G^>_\sigma)^{\text{loc.}}}{(G^<_\sigma)^{\text{loc.}}} = \frac{(\Sigma^>_\sigma)^{\text{loc.}}}{(\Sigma^<_\sigma)^{\text{loc.}}} = -\exp\left(\beta(T, \mathbf{R})\left[\omega + \delta\mu(T, \mathbf{R}) - \mathbf{p} \cdot \mathbf{V}(T, \mathbf{R})\right]\right). \tag{2.71}$$

The above equation implies $\mathsf{C}_\sigma^{\text{col.}} = (G_\sigma^>)^{\text{loc.}} (\Sigma_\sigma^<)^{\text{loc.}} - (G_\sigma^<)^{\text{loc.}} (\Sigma_\sigma^>)^{\text{loc.}} = 0.$

We finally note that within the validity limits of first-order gradient expansion, the equilibrium spectral function $\mathsf{A}_{\sigma,\text{eq}}$, the spectral broadening $\Gamma_{\sigma,\text{eq}}$ and their dependent quantities can be calculated within the local density approximation (LDA) provided that the range of interaction r_0 satisfies $r_0 \ll l_{\text{macro}}$:

$$\mathsf{A}_{\sigma,\text{eq}}(\omega, \mathbf{p}; \mathbf{R}) = \mathsf{A}_{\sigma,\text{eq}}^{\text{hom}}(\omega, \mathbf{p})\Big|_{\mu_\sigma \to \mu_\sigma - U_\sigma(\mathbf{R})}, \qquad \Gamma_{\sigma,\text{eq}}(\omega, \mathbf{p}; \mathbf{R}) = \Gamma_{\sigma,\text{eq}}^{\text{hom}}(\omega, \mathbf{p})\Big|_{\mu_\sigma \to \mu_\sigma - U_\sigma(\mathbf{R})}, \tag{2.72}$$

where $\mathsf{A}_{\sigma,\text{eq}}^{\text{hom}}$ and $\Gamma_{\sigma,\text{eq}}^{\text{hom}}$ are the spectral function and spectral broadening of a homogeneous system at equilibrium. This is due to the following facts: (1) the external potential only appears in M_σ and in the combination $\mu_\sigma - U_\sigma(\mathbf{R})$, (2) the self-energies at $\mathbf{R}$ only depend on the Green's functions in a small neighborhood about of size $r_0 \ll l_{\text{macro}}$ about $\mathbf{R}$.

2.4 The ideal hydrodynamical limit

The quantum kinetic equations assume a simple form in the limit where the local collision rate τ_c^{-1} (given by the typical magnitude of the collision integral), is much faster than the macroscopic rate of changes t_{macro}^{-1}. Deviations from $f_{\text{leq.}}$ relax to local equilibrium distributions within a short time scale $\sim \tau_c$. To zeroth order in τ_c/t_{macro}, the distribution function f_σ will be effectively constrained to the class of local equilibrium distributions at all times. As mentioned in the previous section, the local equilibrium distribution functions are completely characterized by three quantities $\beta(T, \mathbf{R})$, $\delta\mu(T, \mathbf{R})$ and $\mathbf{V}(T, \mathbf{R})$. The kinetic equation in this limit reduces to:

$$\left\{ \frac{\mathsf{A}_\sigma^2 \Gamma_\sigma}{2} \left[\{\mathsf{M}_\sigma, f_\sigma\} - \frac{\mathsf{M}_\sigma}{\Gamma_\sigma} \{\Gamma_\sigma, f_\sigma\} \right] - \delta\mathsf{C}_\sigma^{\text{mem.}} \right\}_{f_\sigma \to f_{\text{leq.}}} = 0. \tag{2.73}$$

The dynamical equations for $\beta(T, \mathbf{R})$, $\delta\mu(T, \mathbf{R})$ and $\mathbf{V}(T, \mathbf{R})$ can be obtained by multiplying the sides of Eq. (2.73) by 1, $\mathbf{p}$ and ω and integrating over ω and $\mathbf{p}$. An equally valid approach is to

start from the exact differential forms of the conservation laws for particle number, momentum and energy (Eqs. 1.130, 1.148 and 1.151), make the substitution $f_\sigma \to f_{\text{leq.}}$ and carry out the gradient expansion. The merit of the latter approach is that it directly leads to equations in terms of the thermodynamical quantities such as pressure and energy density. The calculations are straightforward (cf. Ref. [22] for details). We quote the final result here for particles with equal mass $m_\sigma = m$ coupled to the same external field $U_\sigma(T, \mathbf{R}) = U(T, \mathbf{R})$:

$$\partial_T n = -\nabla \cdot (n\mathbf{V}), \tag{2.74a}$$

$$m\,\partial_T [n\,\mathbf{V}] = -n\,\nabla U - \nabla P - m\nabla [n\,\mathbf{VV}], \tag{2.74b}$$

$$\partial_T \left[\mathcal{E}_{\text{tot.}} + \frac{1}{2} nmV^2 \right] = -\nabla \cdot \left[\left(\frac{1}{2} nmV^2 + P + \mathcal{E}_{\text{tot.}} \right) \mathbf{V} \right] - n\mathbf{V} \cdot \nabla U. \tag{2.74c}$$

The above equations correspond to usual ideal hydrodynamic equations: the number density continuity equation, Euler's equation and the energy transfer equation, in order. The quantities appearing in the above hydrodynamic equations are calculated from the local equilibrium spectral function in the co-moving frame $\mathbf{V} \to 0$ as follows:

$$n(T, \mathbf{R}) = \sum_\sigma \int \frac{\mathrm{d}\omega}{2\pi} \frac{\mathrm{d}^d \mathbf{p}}{(2\pi)^d} \left[A_{\sigma,\text{leq.}}(\omega, \mathbf{p}; T, \mathbf{R}) f_{\text{leq.}}(\omega, \mathbf{p}; T, \mathbf{R}) \right]_{\mathbf{V} \to 0}, \tag{2.75a}$$

$$P(T, \mathbf{R}) = \frac{2}{d} \sum_\sigma \int \frac{\mathrm{d}\omega}{2\pi} \frac{\mathrm{d}^d \mathbf{p}}{(2\pi)^d} \frac{p^2}{2m} \left[A_{\sigma,\text{leq.}}(\omega, \mathbf{p}; T, \mathbf{R}) f_{\text{leq.}}(\omega, \mathbf{p}; T, \mathbf{R}) \right]_{\mathbf{V} \to 0} + \mathcal{E}_{\text{int.}}(T, \mathbf{R}), \tag{2.75b}$$

$$\mathcal{E}_{\text{int.}}(T, \mathbf{R}) = \sum_\sigma \int \frac{\mathrm{d}\omega}{2\pi} \frac{\mathrm{d}^d \mathbf{p}}{(2\pi)^d} \frac{1}{2} \left(\omega + \mu_\sigma - \frac{p^2}{2m} \right) \left[A_{\sigma,\text{leq.}}(\omega, \mathbf{p}; T, \mathbf{R}) f_{\text{leq.}}(\omega, \mathbf{p}; T, \mathbf{R}) \right]_{\mathbf{V} \to 0}, \tag{2.75c}$$

$$\mathcal{E}_{\text{tot.}}(T, \mathbf{R}) = \sum_\sigma \int \frac{\mathrm{d}\omega}{2\pi} \frac{\mathrm{d}^d \mathbf{p}}{(2\pi)^d} \omega \left[A_{\sigma,\text{leq.}}(\omega, \mathbf{p}; T, \mathbf{R}) f_{\text{leq.}}(\omega, \mathbf{p}; T, \mathbf{R}) \right]_{\mathbf{V} \to 0} - \mathcal{E}_{\text{int.}}. \tag{2.75d}$$

The expression for the interaction energy density $\mathcal{E}_{\text{int.}}$ and total energy density $\mathcal{E}_{\text{tot.}}$ shown above are easily obtained from Eq. (1.147) and the Dyson's equation (cf. Ref. [66] for details). All of the quantities appearing in Eqs. (2.74a)-(2.74c) are functions of $\beta(T, \mathbf{R})$ and $\delta\mu(T, \mathbf{R})$. In physical systems, the collision rate is finite and the above equations only approximately describe the

dynamics. A systematic expansion of the kinetic equations about this ideal limit is known as the Chapman-Enskog expansion [67] and yields the equations of viscous hydrodynamics [68].

An important consequence of the ideal hydrodynamical description is the emergence of the so-called *surface modes* in the collective dynamics of systems in isotropic harmonic traps. The surface modes have universal frequencies, unaffected by the equation of state. A general proof for the existence of the surface modes is provided in Appendix. B.1. The universality of the frequency of surface modes is often taken as evidence for hydrodynamical behavior in experiments with ultracold atoms [11].

2.5   Linear response theory of weakly inhomogeneous systems

One of most useful aspects of the kinetic description of weakly inhomogeneous systems is the facilitation of calculating the linear response to weakly inhomogeneous fields in a spatially inhomogeneous equilibrium state. In principle, the linear response may also be obtained directing using the Kubo formula, which amounts to solving the Bethe-Salpeter (BS) equation, Eq. (1.99), for the connected 4-point Green's function $\mathcal{G}_2^{(2c)}$. The micro- and macro- separation of scales, however, is not evident in the resulting BS equation. While the gradient expansion may still be implemented at the level of the BS equation, it is clearly much simpler to do it at level of the 2-point functions, so that the resulting BS equations already acknowledges the scale separation; and this is exactly the program of the quantum kinetic formalism.

Our goal in this section is to derive the equivalent of the BS equation starting from the kinetic equation. We restrict our analysis to the case that the system is initially in the thermal equilibrium, possibly in the presence of a static external potential $U(\mathbf{R})$ (e.g. the optical potential in case of cold atoms, the vacuum interface potential for metallic electrons, etc). We also assume U to be a weakly inhomogeneous potential. The equilibrium state is perturbed by an additional weakly

inhomogeneous external field $\delta U(T, \mathbf{R})$ at $T = 0$. We only consider responses to scalar fields here. The response to vector potentials may also be calculated in the same fashion, however, this requires a gauge invariant formulation of the kinetic equations as mentioned before and is beyond the scope of this work.

2.5.1 The general case

According to the discussion of the previous section, $f_\sigma = c_\sigma \equiv f_0(\omega)$ at equilibrium and both the streaming and collision side of the kinetic equation vanish. Perturbing the external field $U_\sigma(T, \mathbf{R}) \to U_\sigma(\mathbf{R}) + \delta U_\sigma(T, \mathbf{R})$, the thermal equilibrium will be perturbed and the system undergoes a slow dynamics. As a first step, we determine the first-order change in the statistical and spectral functions, δf_σ and $\delta \mathsf{A}_\sigma$, using which the evolution of the local observables of the system (such as density, current, energy and entropy) can be calculated. We denote the equilibrium quantities with a 0 index, and their non-equilibrium deviations with a δ prefix, e.g. $\mathsf{A} \to \mathsf{A}_0 + \delta \mathsf{A}$. Keeping the first-order changes in the kinetic equation in the BM form, we obtain:

$$\frac{\mathsf{A}_{\sigma,0}^2 \, \Gamma_{\sigma,0}}{2} \left[\{-\delta U_\sigma - \Re[\delta \Sigma_\sigma^+], f_0\} + \{\mathsf{M}_{\sigma,0}, \delta f_\sigma\} - \frac{\mathsf{M}_{\sigma,0}}{\Gamma_{\sigma,0}} \Big[\{\delta \Gamma_{\sigma,0}, f_0\} + \{\Gamma_{\sigma,0}, \delta f_\sigma\} \Big] \right] =$$
$$- \Gamma_{\sigma,0} \mathsf{A}_{\sigma,0} (\delta f_\sigma - \delta c_\sigma) + \mathcal{O}(\delta U^2). \quad (2.76)$$

It is convenient to parametrize δf_σ as follows:

$$\delta f_\sigma(\omega, \mathbf{p}; T, \mathbf{R}) \equiv \partial_\omega f_0(\omega) \, \Psi_\sigma(\omega, \mathbf{p}; T, \mathbf{R}), \quad (2.77)$$

using which Eq. (2.76) can be written as:

$$\frac{\mathsf{A}_{\sigma,0}^2 \, \Gamma_{\sigma,0}}{2} \, \partial_\omega f_0 \left[\{\mathsf{M}_{\sigma,0}, \Psi_\sigma\} - \frac{\mathsf{M}_{\sigma,0}}{\Gamma_{\sigma,0}} \{\Gamma_{\sigma,0}, \Psi_\sigma\} + \partial_T \, \delta U_\sigma + \partial_T \left(\Re[\delta \Sigma_\sigma^+] + \frac{\mathsf{M}_{\sigma,0}}{\Gamma_{\sigma,0}} \delta \Gamma_{\sigma,0} \right) \right] =$$
$$\delta \mathsf{C}_\sigma[\Psi] + \mathcal{O}(\delta U^2), \quad (2.78)$$

where we have defined the $\delta\mathsf{C}_\sigma[\Psi]$ as:

$$\delta\mathsf{C}_\sigma[\Psi] \equiv -\Gamma_{\sigma,0}\mathsf{A}_{\sigma,0}\left(\partial_\omega f_0\,\Psi_\sigma - \delta c_\sigma\right). \tag{2.79}$$

Note that δc_σ, $\delta\Sigma_\sigma^+$ and $\delta\Gamma_\sigma$ can be expressed as linear functionals of Ψ if the self-energy is given as a functional of the Green's function, as it is the case for Φ-derivable approximations. Consider a spin-independent external perturbing field like:

$$\delta U(T,\mathbf{R}) = \zeta(T)\,u(\mathbf{R}), \tag{2.80}$$

where $\zeta(T)$ is an arbitrary time envelope. If the linear response to an impulse $\zeta(T) = \delta(T)$ envelope function is known, the response to an arbitrary $\zeta(T)$ can be found by convolving the impulse response with $\zeta(T)$:

$$\Psi(\omega,\mathbf{p};T,\mathbf{R};\zeta) = \int_0^\infty \mathrm{d}T'\,\zeta(T')\,\Psi_{\mathrm{imp}}(\omega,\mathbf{p};T-T',\mathbf{R}), \tag{2.81}$$

where $\Psi_{\mathrm{imp}}(\omega,\mathbf{p};T,\mathbf{R})$ is the impulse response. The impulse response can calculated easily using Laplace (one-sided Fourier) transforms, defined as:

$$\tilde{\Psi}_{\sigma,\mathrm{imp}}(\omega,\mathbf{p};\Omega,\mathbf{R}) = \int_{0^+}^\infty e^{i\Omega T}\,\Psi_{\sigma,\mathrm{imp}}(\omega,\mathbf{p};T,\mathbf{R}). \tag{2.82}$$

Note that we have set the lower bound of the integration to $T = 0^+$, i.e. right after the impulse. Expanding the Poisson brackets and taking a Laplace transform of Eq. (2.78), we find:

$$\frac{\mathsf{A}_{\sigma,0}^2\,\Gamma_{\sigma,0}}{2}\,\partial_\omega f_0\left[-i\Omega\,\gamma_{\omega,\sigma}\tilde{\Psi}_{\sigma,\mathrm{imp}} + \gamma_{\mathbf{p},\sigma}\cdot\partial_{\mathbf{R}}\tilde{\Psi}_{\sigma,\mathrm{imp}} - \gamma_{\mathbf{R},\sigma}\cdot\partial_{\mathbf{p}}\tilde{\Psi}_{\sigma,\mathrm{imp}} - i\Omega\mathsf{F}_\sigma[\tilde{\Psi}_{\mathrm{imp}}] - \delta\mathsf{C}_\sigma[\tilde{\Psi}_{\mathrm{imp}}] = \right.$$

$$\frac{\mathsf{A}_{\sigma,0}^2\,\Gamma_{\sigma,0}}{2}\,\partial_\omega f_0\left[\gamma_{\omega,\sigma}\Psi_{\sigma,\mathrm{imp}}(0^+) + \mathsf{F}\left[\Psi_{\sigma,\mathrm{imp}}(0^+)\right]\right], \tag{2.83}$$

where we have defined the shorthand notation:

$$\gamma_{\omega,\sigma}(\omega, \mathbf{p}; \mathbf{R}) \equiv 1 - \partial_\omega \Re[\Sigma_{\sigma,0}^+] - \frac{\mathsf{M}_{\sigma,0}}{\Gamma_{\sigma,0}} \partial_\omega \Gamma_{\sigma,0},$$

$$\gamma_{\mathbf{p},\sigma}(\omega, \mathbf{p}; \mathbf{R}) \equiv \frac{\mathbf{p}}{m} + \partial_\mathbf{p} \Re[\Sigma_{\sigma,0}^+] + \frac{\mathsf{M}_{\sigma,0}}{\Gamma_{\sigma,0}} \partial_\mathbf{p} \Gamma_{\sigma,0},$$

$$\gamma_{\mathbf{R},\sigma}(\omega, \mathbf{p}; \mathbf{R}) \equiv \partial_\mathbf{R} U(\mathbf{R}) + \partial_\mathbf{R} \Re[\Sigma_{\sigma,0}^+] + \frac{\mathsf{M}_{\sigma,0}}{\Gamma_{\sigma,0}} \partial_\mathbf{R} \Gamma_{\sigma,0},$$

$$\mathsf{F}_\sigma[\tilde\Psi](\omega, \mathbf{p}; \Omega, \mathbf{R}) \equiv \Re\left[\delta\Sigma_\sigma^+[\tilde\Psi]\right] + \frac{\mathsf{M}_{\sigma,0}}{\Gamma_{\sigma,0}} \delta\Gamma_{\sigma,0}[\tilde\Psi]. \tag{2.84}$$

Since the lower bound of the Laplace transform is set to time right after the impulse, the impulse external field does not appear in Eq. (2.83). Instead, the equation relies on the knowledge of the initial disturbance caused by the impulse, $\Psi_{\mathrm{imp}}(0^+)$. We study this sub-problem in detail later in Sec. 4.6, where we show that for particles with equal masses, the right hand side of Eq. (2.83) assumes the simple form:

$$\text{r.h.s. of Eq. (2.83):} \quad \frac{\mathsf{A}_{\sigma,0}^2 \Gamma_{\sigma,0}}{2} \partial_\omega f_0 \gamma_{\mathbf{p},\sigma} \cdot \partial_\mathbf{R} u(\mathbf{R}). \tag{2.85}$$

The above result only relies on the underlying local Galilean invariance of the system. Eq. (2.83) combined with Eq. (2.85) pose a integro-differential equation for $\tilde\Psi_{\sigma,\mathrm{imp}}(\omega, \mathbf{p}; \Omega, \mathbf{R})$. We will discuss an effective method for solving such equations using a generalization of the method of moments, originally proposed by Grad [69] to solve the classical Boltzmann equation. We delegate the details of this discussion to Chapter 4, where we investigate the dynamics of attractive Fermi gases in confined geometries. Once $\tilde\Psi_{\sigma,\mathrm{imp}}$ is calculated, the linear response functions can be found easily. For example, the change in the number density can be expressed as:

$$\delta\tilde{n}_{\sigma,\mathrm{imp}}(\Omega, \mathbf{R}) \equiv -i \int_{0^+}^\infty \mathrm{d}T\, e^{i\Omega T} \int \frac{\mathrm{d}\omega}{2\pi} \frac{\mathrm{d}^d\mathbf{p}}{(2\pi)^d} \delta G_{\sigma,\mathrm{imp}}^<(\omega, \mathbf{p}; T, \mathbf{R})$$

$$= \int \frac{\mathrm{d}\omega}{2\pi} \frac{\mathrm{d}^d\mathbf{p}}{(2\pi)^d} \left[\delta\mathsf{A}_{\sigma,\mathrm{imp}}(\omega, \mathbf{p}; \Omega, \mathbf{R}) f_0(\omega) + \mathsf{A}_{\sigma,0}(\omega, \mathbf{p}; \mathbf{R}) \partial_\omega f_0(\omega) \tilde\Psi_{\sigma,\mathrm{imp}}(\omega, \mathbf{p}; \Omega, \mathbf{R})\right].$$

$$\tag{2.86}$$

In the linear regime, the variations in the density has two sources as it is evident in the second line: the change in the spectral function and the change in the spectral function. In principle, δA_σ can be expressed as a linear functional of $\tilde{\Psi}$. The expectation value of various observables, relevant to experiments with trapped ultracold gases, can be directly obtained from $\delta \tilde{n}_{\sigma,\mathrm{imp}}(\Omega, \mathbf{R})$ (cf. Sec. 4.6.4).

2.5.2 The quasiparticle approximation

We investigated the linearized dynamics of systems described by the general quantum kinetic equation in the previous section. In this section, we consider the simpler situations where the quasiparticle approximation is admissible. Since the particles obey the mass shell relation in the quasiparticle limit, the analysis can be carried out just in terms of the quasiparticle distribution function $n_\sigma(\mathbf{p}; T, \mathbf{R})$, and the intricacies due to off-mass-shell processes will be absent. We parametrize the linear change in the quasiparticle distribution δn_σ as:

$$\delta n_\sigma(\mathbf{p}; T, \mathbf{R}) = \Delta_{\sigma,0}(\mathbf{p}; \mathbf{R})\, \Psi_\sigma(\mathbf{p}; T, \mathbf{R}), \tag{2.87}$$

where:

$$\Delta_{\sigma,0}(\mathbf{p}; \mathbf{R}) \equiv -\partial_\omega f_0(\omega)\big|_{\omega = E_{\sigma,0}(\mathbf{p};\mathbf{R})} = \beta\left[f_0(\omega)[1 - f_0(\omega)]\right]_{\omega = E_{\sigma,0}(\mathbf{p};\mathbf{R})}. \tag{2.88}$$

Linearizing the CBV equation (Eq 2.59), we find:

$$\Delta_{\sigma,0}\, \partial_T \Psi_\sigma + \{\Delta_{\sigma,0}\, \Psi_\sigma, E_{\sigma,0}\} + \{n_{\sigma,0}, \delta E_\sigma[\Psi]\} = \delta I_\sigma[\Psi], \tag{2.89}$$

where:

$$n_{\sigma,0}(\mathbf{p}; \mathbf{R}) = f_0(E_{\sigma,0}), \tag{2.90}$$

is the equilibrium quasiparticle distribution, and $\delta E_\sigma[\Psi]$ is the change in the quasiparticle energy and is given by:

$$\delta E_\sigma[\Psi](\mathbf{p}; T, \mathbf{R}) = \delta U_\sigma(T, \mathbf{R}) + \Re[\delta \Sigma_\sigma^+(\omega, \mathbf{p}; T, \mathbf{R})]\big|_{\omega = E_\sigma(\mathbf{p};T,\mathbf{R})}. \tag{2.91}$$

For weak interaction, the quasiparticle energy can be calculated at the HF level to leading order, so that:

$$\delta E_\sigma[\Psi](\mathbf{p}; T, \mathbf{R}) = \delta U_\sigma(\mathbf{p}; T, \mathbf{R}) + \sum_{\sigma'} \int \mathrm{d}^d\mathbf{R}'\, \mathrm{d}^d\mathbf{p}'\, V(\mathbf{R} - \mathbf{R}')\, \Delta_{\sigma',0}(\mathbf{p}'; \mathbf{R})\, \Psi_{\sigma'}(\mathbf{p}'; T, \mathbf{R}')$$

$$- \int \mathrm{d}^d\mathbf{p}_1\, \mathcal{V}(\mathbf{p} - \mathbf{p}_1)\, \Delta_{\sigma,0}(\mathbf{p}_1; \mathbf{R})\, \Psi_\sigma(\mathbf{p}_1; T, \mathbf{R}). \quad (2.92)$$

Eq. (2.89) may also be simplified using the properties of the Poisson brackets:

$$\Delta_{\sigma,0}\left[\partial_T \Psi_\sigma + \{\Psi_\sigma + \delta E_\sigma[\Psi], E_{\sigma,0}\}\right] = \delta I_\sigma[\Psi]. \quad (2.93)$$

Finally, $\delta I_\sigma[\Psi]$ can be generally expressed as follows using Eq. (2.58):

$$\delta I_\sigma[\Psi] = -\beta \sum_{\sigma_1, \sigma', \sigma_1'} \int \frac{\mathrm{d}^d\mathbf{p}_1}{(2\pi)^d} \frac{\mathrm{d}^d\mathbf{p}'}{(2\pi)^d} \frac{\mathrm{d}^d\mathbf{p}_1'}{(2\pi)^d} (2\pi)^{d+1} \delta^d(\mathbf{p} + \mathbf{p}_1 - \mathbf{p}' - \mathbf{p}_1')$$

$$\times \delta\left(E_{\sigma,0} + E_{\sigma_1,0} - E_{\sigma',0} - E_{\sigma_1',0}\right) W(\mathbf{p}, \sigma; \mathbf{p}_1, \sigma_1 \to \mathbf{p}', \sigma'; \mathbf{p}_1', \sigma_1') \mathrm{S}[\Psi_\sigma]$$

$$\times n_{\sigma,0}\, n_{\sigma_1,0}\, (1 - n_{\sigma',0})(1 - n_{\sigma_1',0}), \quad (2.94)$$

where we have defined the shorthands $\mathrm{S}[\Psi] = \Psi(\mathbf{p}; T, \mathbf{R}) + \Psi(\mathbf{p}_1; T, \mathbf{R}) - \Psi(\mathbf{p}'; T, \mathbf{R}) - \Psi(\mathbf{p}_1'; T, \mathbf{R})$, $E_{\sigma,0} = E_{\sigma,0}(\mathbf{p}; T, \mathbf{R})$, $n_{\sigma,0} = n_{\sigma,0}(\mathbf{p}; T, \mathbf{R})$, $E_{\sigma_1,0} = E_{\sigma_1,0}(\mathbf{p}_1; T, \mathbf{R})$, $n_{\sigma_1,0} = n_{\sigma_1,0}(\mathbf{p}_1; T, \mathbf{R})$, etc. Similar to the general case studied in the previous section, the quasiparticle kinetic equation may also be put in a more useful form by taking a Laplace transform. This time, however, we do not need to study the initial disturbance separately and we define the Laplace transform as:

$$\tilde{\Psi}_\sigma(\mathbf{p}; \Omega, \mathbf{R}) \equiv \int_{0^-}^\infty \mathrm{d}T\, e^{i\Omega T}\, \Psi_\sigma(\mathbf{p}; T, \mathbf{R}). \quad (2.95)$$

Note that 0^- denotes to the time right before the external perturbing field so that $\Psi_\sigma(\mathbf{p}; 0^-, \mathbf{R}) = 0$. Taking a Laplace transform of the sides of Eq. (2.93), we find:

$$\Delta_{\sigma,0}\left[-i\Omega\tilde{\Psi}_\sigma + \{\tilde{\Psi}_\sigma + \Sigma_\sigma[\tilde{\Psi}], E_{\sigma,0}\}\right] - \delta I_\sigma[\tilde{\Psi}] = -\{n_{\sigma,0}, \delta\tilde{U}_\sigma(\Omega, \mathbf{R})\}, \quad (2.96)$$

where $\Sigma_\sigma[\tilde{\Psi}]$ denotes the HF self-energy functional (the last two terms in Eq. 2.92). In the case of an impulse external disturbance $\delta U_\sigma(T, \mathbf{R}) = \delta(T)\, u_\sigma(\mathbf{R})$, we readily find $\delta \tilde{U}_\sigma(\Omega, \mathbf{R}) = u_\sigma(\mathbf{R})$. Eq. (2.96) along with Eqs.(2.94) and (2.92) pose an integro-differential equation for $\tilde{\Psi}_{\sigma,\mathrm{imp.}}$. The change in the number density can be readily expressed in terms of $\tilde{\Psi}_\sigma$:

$$\delta \tilde{n}_{\sigma,\mathrm{imp.}}(\Omega, \mathbf{R}) = \int \mathrm{d}^d \mathbf{p}\, \delta \tilde{n}_{\sigma,\mathrm{imp.}}(\mathbf{p}; T, \mathbf{R}) = \int \mathrm{d}^d \mathbf{p}\, \Delta_{\sigma,0}(\mathbf{p}; \mathbf{R})\, \tilde{\Psi}_{\sigma,\mathrm{imp.}}(\mathbf{p}; \Omega, \mathbf{R}), \qquad (2.97)$$

using which the impulse response functions can be calculated. We discuss the numerical solution of the linearized CBV equation next chapter, where we study the dynamics of trapped dipolar fermions.

3

Collective dynamics of quasi-two-dimensional dipolar fermions

Dipolar quantum gases have been the subject of much interest and significant experimental and theoretical investigations in the recent years. The long-range anisotropic dipole-dipole interaction gives rise to novel phenomena in these systems (see Ref. [14] and the references therein). Dipolar Bose-Einstein condensates (BECs) with magnetic dipole-dipole interactions have been exhaustively studied both theoretically and experimentally [70]. The most recent experimental achievements

along this line are the realization of BEC of rare earth atoms such as ^{164}Dy [71] and ^{168}Er [72] with large magnetic dipole moments of $10\,\mu_B$ and $7\,\mu_B$ respectively. The many-body effects of dipolar interactions are much easier to observe in dipolar BECs compared to dipolar Fermi gases. Pauli exclusion sets a large energy scale set for fermions and stronger dipolar interactions are required for the interaction effects to become appreciable.

Since electric dipole-dipole interactions are typically stronger than magnetic ones, much of the recent experimental efforts have been focused on the realization of ultracold heternucleus bi-alkali molecules which have large permanent electric dipole moments. An important experimental achievement in this direction was the realization of a nearly quantum degenerate gas of fermionic KRb molecules at JILA [15, 16, 17]. The experiments with other bi-alkali fermionic polar molecules such as LiCs [73, 74] are also making significant progress.

More recently, the group at Stanford have realized a quantum degenerate gas of fermionic ^{161}Dy through sympathetic cooling with the bosonic species ^{162}Dy [75]. Having a large permanent magnetic dipole moment of $10\,\mu_B$ and being free of the complication of ultracold chemistry, these species have opened a new window of opportunity toward the experimental observation of many-body physics of dipolar fermions.

An important experimental probe for the many-body physics of ultracold gases is the measurement of collective oscillations of trapped gases in response to perturbations of the trap potential. These oscillations constitute the low-lying collective excitations of these systems. The measurement of the frequency and damping of these oscillations can be utilized to understand the properties of the ground state and to extract important information such as the character of self-energy corrections, the equilibrium equation of state, and the kinetic coefficients. Moreover, the possibility of carrying out extremely precise measurements of these quantities allows us to put our theoretical understanding of the system to the test. For instance, by measuring the frequency

of the radial breathing mode for a two-component Fermi gas near the BEC-BCS crossover with a 10^{-3} accuracy level, the Innsbruck group could clearly verify the Quantum Monte-Carlo result for the unitary gas and invalidate the predictions of the BCS theory [76]. Another remarkable example is the recent measurement of the universal quantum viscosity of the unitary gas [77] that confirmed the theoretical $T^{3/2}$ scaling and also provided evidence for a conjecture on the lower bound for the viscosity/entropy ratio obtained using string theory methods [78]. At the moment, the collective oscillations of trapped BECs [79] and two-component atomic gases with s-wave interactions in three dimensions [80] are both understood fairly well. Recently, the experimental and theoretical studies of the 2D Fermi gas interacting via s-wave Feshbach resonances have also shown a remarkable progress [18, 81, 82, 83, 84].

In this chapter, we study the collective modes of quasi-two-dimensional (quasi-2D) dipolar fermionic gases prepared in a single hyperfine state and loaded into an isotropic harmonic trap. Experimentally, this configuration may be realized using a highly anisotropic optical potentials such that $\omega_z \gg \omega_x = \omega_y$, where ω_i is the trap frequency along ith axis. Stronger transverse confinements (larger ω_z) can be achieved using an optical lattice to slice the trapped gas into thin "pancakes" [15, 16, 17]. In that case, we confine our attention to a single pancake here. We assume that the dipoles are aligned perpendicular to the confining plane (see Fig. 3.1). In this setting, the effective dipole-dipole interactions have a repulsive long-range character and give rise to a normal Fermi liquid state. This particular configuration is also necessary in order to suppress inelastic dipolar collisions and also to reduce the rate of chemical reactions in experiments with reactive bi-alkali polar molecules.

In highly quantum degenerate Fermi liquids ($T \ll T_F$, where T_F is the Fermi temperature), the elastic collisions are suppressed due to Pauli exclusion and collisional effects may be ignored

as a first approximation in the study of collective excitations. In this so-called collisionless (CL) limit, the collective modes are undamped and no energy dissipation occurs. As the temperature is increased, the collision rate rapidly grows and the collisional effects may no longer be ignored. In this regime, the dynamics is dissipative and the collective modes are damped. However, if the collision rate surpasses than the typical frequency of collective oscillations (whose scale is set by the trap frequency), the gas will remain "locally" in a thermal equilibrium and a hydrodynamical (HD) description emerges [22]. This ideal HD limit is again dissipationless and the quasi-equilibrium dynamics is simply described by differential conservation laws of mass, momentum and energy currents [85, 22]. A realistic system, however, typically lies in the dissipative crossover regime between these two ideal limits[1]. An important aspect of understanding a many-body system is to determine where it lies within the CL-HD spectrum, both qualitatively and quantitatively.

The theoretical investigation of collective modes of trapped dipolar fermions has started more than a decade ago. Góral *et al.* have studied the stability condition [86] and hydrodynamic excitations in traps with different degrees of of anisotropy [87] at zero temperature. Lima *et al.* have studied the same problems in more detail [88, 89], while Sogo *et al.* have studied the the collisionless limit [90]. More recently, Abad *et al.* have compared the predictions of collisionless and hydrodynamic formulations at zero temperature for vertically aligned and tilted dipoles [91].

In light of the recent experimental progress with dipolar fermions and the possibility of carrying out precise measurement of the collective modes, it is worthwhile to carry out a more detailed and quantitatively reliable theoretical treatment of this problem. The issue of finite temperature has not been addressed in any of the above works and once the thermal effects are taken into account, all of the previously used formulations become unreliable. The applicability of ideal hydrodynamic formulation at zero temperature is questionable since collisions are absent. Also, the collisionless

---

[1] There are exceptional cases where certain dynamical symmetries forbid collisions altogether, see Ref. [18] for example.

approximation is only relevant to extremely quantum degenerate conditions which is not within the reach of the experiments yet. Most importantly, the crossover regime, which is most relevant to current experiments, has not been studied so far.

Here, we make no prior assumption about where the system lies in the CL-HD spectrum. We use the framework of quantum kinetic equations (in particular, the collisional Boltzmann-Vlasov limit) which in principle allows us to study the dynamics in the whole spectrum in a unified way. The CL and HD limits emergence naturally when the right physical conditions are met. We evaluate the linear response of the gas to monopole and quadrupole perturbations of the trap potential and study the oscillation frequency and damping of the generated excitations. We restrict our analysis to situations where collisions lie well within the near-threshold scattering regime so that Born approximation is applicable [92, 93]. This condition is satisfied well in the current experiments.

We carry out the calculations in two stages. First, we neglect the self-energy corrections to quasiparticle dispersions (the Boltzmann limit) and utilize the widely used linearized scaling ansatz approximation [94, 95, 96, 97] to obtain a simple semi-analytic picture. In the second stage, we include the self-energy corrections to quasiparticle dispersions and also extend the scaling ansatz by including higher order moments (up to the eighth order). We find that both of these refinements result in significant quantitative corrections. Furthermore, inclusion of higher moments allows us to study higher order modes in addition to the nodeless modes described by the scaling ansatz.

Before delving into the formalism and details, we find it useful to briefly summarize our main results, some of which are novel features of dipolar fermions in 2D. Without self-energy corrections, the scaling ansatz analysis predicts the well-known undamped monopole oscillations at a fixed frequency of $2\omega_0$, independent of the interaction strength and temperature [98, 99]. Here, $\omega_0 \equiv \omega_x = \omega_y$ is the in-plane trap frequency. Taking self-energy corrections into account, we find that the oscillation frequency of the nodeless monopole mode increase from $2\omega_0$ due to the

repulsive interactions while it also assumes a small damping (see Fig. 3.5). While collisions have a small influence on the dynamics of the scaling mode, we find that higher order monopole modes are strongly influenced by collisions: they go through a dissipative crossover regime as the interaction strength is increased and finally approach the HD regime (see Fig. 4.18). The quadrupole modes, including the lowest lying nodeless mode, exhibit the same CL to HD transition. In particular, the oscillation frequency of the nodeless quadrupole mode approaches $\sqrt{2}\omega_0$ in the collision dominated regime, which is the universal frequency of the quadrupole "surface" mode [100] (see Fig. 3.8). The appearance of surface modes is an indication for the emergence of the HD limit.

We find simple analytic results in the Boltzmann limit using the linearized scaling ansatz approximation. In particular, we find that the frequency and damping of the quadrupole oscillations are controlled by a single parameter, the quadrupole collision rate ν_c (Ref. to Sec. 3.4.2). Small and large values of ν_c correspond to collisionless and hydrodynamic behavior respectively. For small T/T_F, we obtain $\nu_c \sim T^2$ which is due to Pauli blocking. For large T/T_F, the behavior of ν_c depends on the degree of quasi-two-dimensinality (quantified by η, see Eq. 3.21). In the strictly 2D limit, we show that ν_c reaches a plateau for $T \gtrsim T_F$. The existence of this plateau is a unique feature of 2D dipolar fermions and results from the balance between rarefaction of the gas at higher temperatures and the growth of the dipolar scattering cross section. The high temperature cut-off for this plateau behavior is $T_{\text{dip}} \equiv \hbar^2/(ma_d^2 k_B)$, where $a_d \equiv mD^2/\hbar^2$ is the "dipolar length". Here, m and D denote the mass and the dipole moment of a single particle. For $T \gtrsim T_{\text{dip}}$, the scattering energies become semi-classical and we find $\nu_c \sim T^{-3/4}$.

We look into the effect of mean-field correction to quasiparticle dispersions and show that it has a significant effect in the quantum degenerate regime. This is again in contrast to the case of s-wave fermions where self-energy correction is found to have a small effect on the frequency of collective modes [101]. Finally, going beyond the scaling ansatz by satisfying higher order moments of the CBV equation, we show that the simple scaling ansatz overestimates the

collision rates in agreement with the findings of Ref. [102]. We also show that refinements to the predictions for the lowest lying monopole and quadrupole modes become negligible beyond forth order moments. Finally, we discuss the observability of our predictions in the experiments with ^{40}K^{87}Rb and ^{161}Dy and show that although the HD regime is not currently achievable, a significant collisional damping and the plateau in the collision rates are both expected to be observable.

This chapter is organized as follows. We review the atomic physics of polar molecules in external electric fields, and the effective low-energy Hamiltonian for a many-particle system of such polarized molecules in the Sec. 3.1. The formalism of quantum kinetic equations was discussed at length in the previous chapter. Here, we briefly discuss the validity condition of the quasiparticle approximation in the context of experiments with dipolar quantum gases. The equilibrium state of the trapped gas in discussed in Sec. 3.3. The linear response theory of the CBV equation is described in Sec. 3.4 and the variational calculation of the response functions using the method of moments is discussed. The linearized scaling ansatz analysis in given in Sec. 3.4.2, followed by the its extension to higher order moments and inclusion of self-energy corrections in Sec. 3.4.3. Finally, we discuss the experimental outlook of this work in Sec. 3.5 and conclude this chapter with further discussions in Sec. 3.6. Most of the technical details and tedious calculations are left to the Appendices.

3.1   Polar molecules in optical traps

The purpose of this section, which forms the basis of discussion in the following sections, is to review the physics of polar molecules in dc electric fields and the effective low-energy Hamiltonian for a many-particle system of polarized molecules in optical traps. We are interested in the rotational excitations of cold $\nu^{2S+1}\Lambda(v)$ spinless ($S = 0$) polar molecules in their electronic ($\nu = 0$) and vibrational ($v = 0$) ground state, with zero projection ($\Lambda = 0$) of the total angular momentum on

the internuclear axis. The spectroscopic notation for the electronic-vibrational ground state of these molecules is $X^1\Sigma(0)$. The application of external fields will serve as a key element to engineer effective interaction potentials between the molecules [8]. As a first step, we derive a low-energy effective Hamiltonian for the center-of-mass motion of a single molecule in its electronic-vibrational ground state. A single polar molecule can be described with the following Hamiltonian:

$$H_{\mathrm{mol.}} = \frac{\mathbf{p}^2}{2m} + H_{\mathrm{rot}} + H_{\mathrm{dc}}, \tag{3.1}$$

where $\mathbf{p}^2/2m$ is the kinetic energy for the center-of-mass motion of a molecule of mass m, H_{rot} accounts for the rotational degrees of freedom, and H_{dc} denote the interaction with a dc electric field and the optical trapping of the molecule in the ground electronic-vibrational manifold. We consider polar molecules with Σ in their electronic-vibrational ground state. The low-energy internal excitations correspond to the rotation of the internuclear axis of the molecules with total internal angular momentum $\mathbf{J}$. The corresponding Hamiltonian H_{rot} is the one of rigid spherical rotor:

$$H_{\mathrm{rot}} = B\mathbf{J}^2. \tag{3.2}$$

Here, B is the rotational constant for the electronic-vibrational ground state, which is of the order of $B \sim h \times 10$ GHz. We denote the energy of the eigenstates of H_{rot} by $|J, M\rangle$, where J J is the quantum number associated with the total internal angular momentum and M is the quantum number associated with its projection onto a space-fixed quantization axis. The excitation spectrum is $E_J = BJ(J + 1)$. Each J level is $(2J + 1)$-fold degenerate. A polar molecule has an electric dipole moment D which couples its internal rotational levels. This dipole moment gives rise to the dipole-dipole interaction between two molecules. For Σ molecules the dipole operator is along the internuclear axis $\mathbf{e}_{ab}$, i.e., $\mathbf{D} = D\mathbf{e}_{ab}$. Here, D is the "permanent" dipole moment of a molecule in its electronic-vibrational ground state.

The spherical components of the dipole operator on a space-fixed spherical basis $\{\mathbf{e}_{-1}, \mathbf{e}_0, \mathbf{e}_1\}$, with $\mathbf{e}_{q=0} \equiv \mathbf{e}_z$ and $\mathbf{e}_{\pm 1} = \mp(\mathbf{e}_x \pm i\mathbf{e}_y)/\sqrt{2}$, are given by are given by $D_q = \mathbf{e}_q \cdot \mathbf{D} = DC_q^{(1)}(\theta, \phi)$,

where $C_q^{(k)}(\theta, \phi)$ are the unnormalized spherical harmonics and $\theta(\phi)$ is the polar (azimuthal) angle for the orientation of the molecule in the space-fixed frame, respectively. We note that for a spherically symmetric system, e.g., in the absence of external fields, the eigenstates of the rotor have no net dipole moment, $\langle J, M | \mathbf{D} | J, M \rangle = 0$. On the other hand, the component D_q couples the rotational states $|J, M\rangle$ and $|J \pm 1, M + q\rangle$:

$$\langle J\pm 1, M+q|D_q|J, M\rangle = D\,(J, M; 1, q|J\pm 1, M+q)\,(J, 0; 1, 0|J\pm 1, 0)\sqrt{\frac{2J+1}{2(J\pm 1)+1}}, \quad (3.3)$$

where $(J_1, M_1; K, M_2|J, M)$ are Clebsch-Gordan coefficients. We are interested in the interaction of the molecules with an external dc electric field along $\mathbf{e}_z$, i.e., $\mathbf{E}_{\mathrm{dc}} = E_{\mathrm{dc}}\mathbf{e}_0$. These dc field couples to a molecule via the electric dipole interaction,

$$H_{\mathrm{dc}} = -\mathbf{D} \cdot \mathbf{E}_{\mathrm{dc}} = -D_0 E_{\mathrm{dc}}, \quad (3.4)$$

which try to align the molecule along the field, while competing with its rotation, as $[\mathbf{J}^2, D_q] \neq 0$. The effects of a dc electric field $\mathbf{E}_{\mathrm{dc}}$ on a single polar molecule are (a) to split the $(2J + 1)$-fold degeneracy in the rotor spectrum, and (b) to align the molecule along the direction of the field, which amounts to inducing a finite dipole moment in each rotational state. We choose the direction of the dc field as the quantization axis, $\mathbf{E}_{\mathrm{dc}} \equiv E_{\mathrm{dc}}\mathbf{e}_0$. Then, the internal Hamiltonian is that of a rigid spherical pendulum,

$$H_{\mathrm{mol.}} = H_{\mathrm{rot}} + H_{\mathrm{dc}} = B\mathbf{J}^2 - D_0 E_{\mathrm{dc}}, \quad (3.5)$$

which conserves the projection of the angular momentum J on the quantization axis, i.e., M is a good quantum number. The energy eigenvalues and the eigenstates of Eq. (3.5), are labeled as $E_{J,M}$ and $|\phi_{J,M}\rangle$, respectively. We are interested in weak fields, $E_{\mathrm{dc}} \ll B/D$, where the effects of the electric field are a quadratic dc Stark shift of the rotational energy levels and a finite induced dipole moment along the axis of the field in each rotational state. For a typical rotational constant $B \sim h \times 10\,\mathrm{GHz}$ and a dipole moment $D \sim 9\,\mathrm{Debye}$, this corresponds to considering dc fields

(much) weaker than $B/D \sim 2$ kV/cm. To lowest order in $\tilde{E} \equiv dE_{\text{dc}}/B$, the energy eigenvalues and eigenstates are:

$$E_{J,M}/B = J(J+1) + \frac{\tilde{E}^2}{2}\frac{1 - 3M^2/J(J+1)}{(2J-1)(2J+3)},$$

$$|\phi_{J,M}\rangle = |J,M\rangle - \frac{\tilde{E}}{2J}\frac{J^2 - M^2}{4J^2 - 1}|J-1,M\rangle + \frac{\tilde{E}}{2(J+1)}\sqrt{\frac{(J+1)^2 - M^2}{4(J+1)^2 - 1}}|J+1,M\rangle. \quad (3.6)$$

Thus, the ground-state energy is shifted downward by $E_{0,0} = -B\tilde{E}^2/6$, while the energies of the lowest excited states are split by:

$$\hbar\delta \equiv E_{1,0} - E_{1,\pm 1} = 3B\tilde{E}^2/20. \quad (3.7)$$

The induced dipole moments to lowest order in $\tilde{E}$ are:

$$\langle\phi_{J,M}|\mathbf{D}|\phi_{J,M}\rangle = D\tilde{E}\frac{3M^2/J(J+1) - 1}{(2J-1)(2J+3)}\mathbf{e}_0. \quad (3.8)$$

This equation shows that the ground state acquires a finite dipole moment $D_{\text{eff}} \equiv \langle\phi_{0,0}|D_0|\phi_{0,0}\rangle = D\tilde{E}/3$ along the field axis. We simply refer to D_{eff} as D for brevity hereafter.

With this brief introduction about the physics of cold polar molecules in a dc polarizing field, we move on to the many-particle ensembles of polar molecules. The low-energy effective Hamiltonian is obtained by adding (1) center-of-mass kinetic energy of the molecules, (2) coupling to the trap laser field, and (3) the dipole-dipole interaction between the molecules with partially aligned dipolar moments:

$$H_{\text{3D}} = \int d^3\mathbf{r}\,\psi^\dagger(\mathbf{r})\left(-\frac{\nabla^2}{2m} + U_{\text{trap}}^{\text{3D}}(\mathbf{r})\right)\psi(\mathbf{r}) + \int d^3\mathbf{r}\,d^3\mathbf{r}'\,\mathcal{V}_{\text{dip}}^{\text{3D}}(\mathbf{r}-\mathbf{r}')\,\psi^\dagger(\mathbf{r})\,\psi^\dagger(\mathbf{r}')\,\psi(\mathbf{r}')\,\psi(\mathbf{r}).$$
$$(3.9)$$

The trap potential is modeled with a harmonic potential with different transverse and in-plane frequencies:

$$U_{\text{trap}}^{\text{3D}}(\mathbf{r}) = \frac{1}{2}m\omega_z^2 z^2 + \frac{1}{2}m\omega_0^2(x^2 + y^2), \quad (3.10)$$
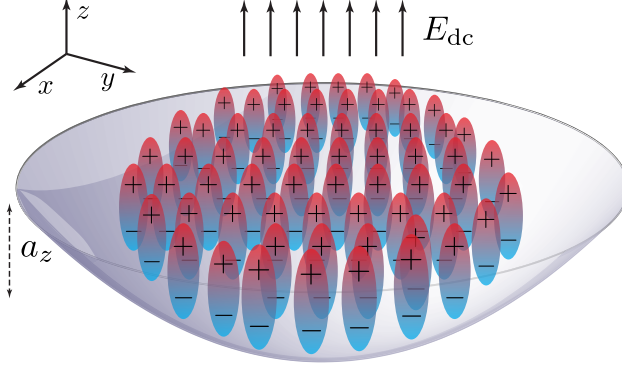
Figure 3.1: A schematic picture of quasi-2D dipolar fermions in an isotropic in-plane trap. A strong dc field aligns the dipoles along the vertical axis (z). The quasi-2D limit is achieved when $a_z \equiv [\hbar/(m\omega_z)]^{1/2}$ is much smaller than both the inter-particle separation $n_{\mathrm{2D}}^{-1/2}$ and the thermal de Broglie wavelength $\lambda_T \equiv h/(2\pi m k_B T)^{1/2}$ (equivalently, when $\omega_z \gg \max\{\epsilon_F, k_B T\}$).

and:

$$\mathcal{V}_{\mathrm{dip}}^{\mathrm{3D}}(\mathbf{r}) = \frac{D^2}{|\mathbf{r}|^5}\left(|\mathbf{r}|^2 - 3z^2\right), \tag{3.11}$$

is the dipole-dipole interaction. We set $\hbar = 1$ throughout unless it appears explicitly. A schematic picture of the system is shown in Fig. 3.1. Here, $\psi^{(\dagger)}(\mathbf{r})$ is the fermion annihilation (creation) operator in 3D space. In the limit $\omega_z \gg \omega_0, \epsilon_F, k_B T$ (where ϵ_F and T denote the Fermi energy and the temperature), the particles occupy only the lowest band of the transverse trap potential, allowing us to reduce the above 3D Hamiltonian to an effective 2D model:

$$H_{\mathrm{2D}} = \int \mathrm{d}^2\mathbf{r}\, \psi_0^\dagger(\mathbf{r}) \left(-\frac{\nabla^2}{2m} + U_{\mathrm{trap}}^{\mathrm{2D}}(\mathbf{r})\right)\psi_0(\mathbf{r})$$
$$+ \int \mathrm{d}^2\mathbf{r}\, \mathrm{d}^2\mathbf{r}'\, \mathcal{V}_{\mathrm{dip}}^{\mathrm{2D}}(\mathbf{r}-\mathbf{r}')\,\psi_0^\dagger(\mathbf{r})\,\psi_0^\dagger(\mathbf{r}')\,\psi_0(\mathbf{r}')\,\psi_0(\mathbf{r}). \tag{3.12}$$

Here, $\mathbf{r} = (x, y)$ denote the in-plane 2D coordinates and $\psi_0^{(\dagger)}(\mathbf{r})$ denotes the fermion annihilation (creation) in the lowest transverse band. We have neglected the constant zero point energy $\hbar\omega_z/2$. $U_{\mathrm{trap}}^{\mathrm{2D}}(\mathbf{r}) = m\omega_0^2(x^2 + y^2)/2$ is the in-plane part of the original trap potential and $\mathcal{V}_{\mathrm{dip}}^{\mathrm{2D}}(\mathbf{r})$ is the

effective dipole-dipole interaction in the lowest band given by:

$$\mathcal{V}_{\mathrm{dip}}^{\mathrm{2D}}(\mathbf{r}) = \int \mathrm{d}z \, \mathrm{d}z' \, |\phi_0(z)|^2 \, |\phi_0(z')|^2 \, \mathcal{V}_{\mathrm{dip}}^{\mathrm{3D}}(\mathbf{r}, z - z'), \tag{3.13}$$

where $\phi_0(z) = e^{-z^2/(2a_z^2)}/(\sqrt{\pi} \, a_z)^{\frac{1}{2}}$ is the transverse wavefunction of particles in the lowest band and $a_z \equiv (m\omega_z)^{-1/2}$ is the transverse oscillator length. The above integral can be calculated analytically and we find:

$$\mathcal{V}_{\mathrm{dip}}^{\mathrm{2D}}(r) = \frac{1}{\sqrt{2\pi}} \frac{D^2}{2a_z^3} e^{r^2/(4a_z^2)} \left[\left(2 + \frac{r^2}{a_z^2} \right) K_0 \left(\frac{r^2}{4a_z^2} \right) - \frac{r^2}{a_z^2} K_1 \left(\frac{r^2}{4a_z^2} \right) \right], \tag{3.14}$$

where $\{K_n(x)\}$ denote the modified Bessel functions of the second kind. In the momentum space, we get:

$$\tilde{\mathcal{V}}_{\mathrm{dip}}^{\mathrm{2D}}(q) = \frac{2\pi D^2}{a_z} \left[\sqrt{\frac{2}{\pi}} - q a_z e^{q^2 a_z^2/2} \mathrm{Erfc} \left(\frac{q a_z}{\sqrt{2}} \right) \right]. \tag{3.15}$$

The effective interaction is purely repulsive regardless of the choice for a_z, however, its strength decreases as a_z is increased. We denote $\mathcal{V}_{\mathrm{dip}}^{\mathrm{2D}} \equiv \mathcal{V}$, $\tilde{\mathcal{V}}_{\mathrm{dip}}^{\mathrm{2D}} \equiv \tilde{\mathcal{V}}$ and $U_{\mathrm{dip}}^{\mathrm{2D}} \equiv U$ in the remainder of this paper for brevity. It is worthwhile to study the behavior of the effective 2D interaction in various limits. For $q a_z \ll 1$, we find:

$$\tilde{\mathcal{V}}(q) \simeq \frac{4\sqrt{2\pi} D^2}{3a_z} - 2\pi D^2 q + \mathcal{O}(q^2), \tag{3.16}$$

whereas for $q a_z \gg 1$, we get:

$$\tilde{\mathcal{V}}(q) \simeq -\frac{2D^2 \sqrt{2\pi}}{3a_z} \left(1 - \frac{3}{q^2 a_z^2} + \mathcal{O}(q^{-4} a_z^{-4}) \right). \tag{3.17}$$

Apart from the constant term in Eq. (3.16), which only contributes to interactions in the s-wave channel and is immaterial here, we find a linear dependence on q. This linear behavior eventually reaches a plateau once $q \sim 1/a_z$. We shall see later that this linear dependence has interesting consequences on the temperature dependence of low lying collective excitations. In real space, for small r/a_z, we find a behavior similar to the 2D Coulomb gas:

$$\mathcal{V}(r) \approx \frac{D^2}{\sqrt{2\pi} a_z^3} \left\{ -2 - \gamma - \ln[r^2/(8a_z^2)] + \mathcal{O}(r^2 \ln r) \right\}, \tag{3.18}$$

where γ is the Euler's constant. For large r/a_z, the r^{-3} dipole-dipole interaction is recovered:

$$\mathcal{V}(r) \approx D^2/r^3 + \mathcal{O}(a_z^2/r^5).$$

(3.19)

It is useful to define a "dipolar length":

$$a_d \equiv \frac{mD^2}{\hbar^2},$$

(3.20)

which is a quantum length scale associated to dipolar interactions. We also define the following useful dimensionless parameters:

$$\lambda_d \equiv \frac{mD^2}{\hbar^2} \left(\frac{m\omega_0}{\hbar}\right)^{\frac{1}{2}} (2N)^{\frac{1}{4}} \equiv \left(\frac{a_d}{a_0}\right) (2N)^{\frac{1}{4}}, \qquad \eta \equiv (2N)^{\frac{1}{4}} \left(\frac{\omega_0}{\omega_z}\right)^{\frac{1}{2}},$$

(3.21)

where $a_0 \equiv [\hbar/(m\omega_0)]^{\frac{1}{2}}$ is the in-plane oscillator length and N is the number of trapped particles. λ_d is a measure of dipolar interaction strength and is of the order of the typical value of interaction energy over the kinetic energy in the quantum degenerate regime. η is a measure of "quasi-two-dimensionality" and is of the order of the transverse oscillator length a_z divided by the inter-particle separation. The strict 2D limit $\omega_z \to \infty$ corresponds to $\eta = 0$.

3.2   Linear response functions and collective modes of trapped dipoles

A typical experiment for measuring the collective excitations of trapped particles is the following: the gas is prepared in a thermal equilibrium state at $t < 0^-$. For $t > 0^-$, the system is subjected to a perturbation such as a kick or modulation of the trap potential and a certain observable is monitored. If the frequency and amplitude of the perturbing potential is small compared to the macroscopic scales, such an experiment can be theoretically investigated within the linear response theory. Let us denote the perturbing potential and the observable as $\delta U(\mathbf{r}, t)$ and $O(\mathbf{r})$ respectively, and their corresponding second quantized operators are $\delta \hat{U} \equiv \int \mathrm{d}^2\mathbf{r}\, \psi_0^\dagger(\mathbf{r})\, \delta U(\mathbf{r}, t)\, \psi_0(\mathbf{r})$

and $\hat{O} \equiv \int d^2\mathbf{r}\, \psi_0^\dagger(\mathbf{r})\, O(\mathbf{r})\, \psi_0(\mathbf{r})$. The usual linear response theory then yields:

$$\langle \hat{O} \rangle_t = \int_{0-}^{t} dt' \int d^2\mathbf{r}\, d^2\mathbf{r}'\, \chi_{dd}^+(\mathbf{r}, \mathbf{r}'; t - t')\, O(\mathbf{r})\, \delta U(\mathbf{r}', t'), \qquad (3.22)$$

where $\chi_{dd}^+(\mathbf{r}, \mathbf{r}'; t - t')$ is the retarded density-density response function:

$$\chi_{dd}^+(\mathbf{r}, \mathbf{r}'; t - t') \equiv -i\theta(t - t') \mathrm{Tr}\{\hat{\rho}_0[\hat{n}(\mathbf{r}, t), \hat{n}(\mathbf{r}', t)]\}, \qquad (3.23)$$

where $\hat{n}(\mathbf{r}, t) = \psi_0^\dagger(\mathbf{r}, t)\psi_0(\mathbf{r}, t)$ is the density operator and $\hat{\rho}_0$ is the initial density matrix. At this stage, one may choose a proper many-body approximation scheme and attempt to evaluate the response function using the diagram technique. However, the lack of translational symmetry due to the presence of the trap potential makes this approach complicated. In practice, one will have to make assumptions about separation of microscopic and macroscopic time and length scales in order to make the calculations tractable. It is, however, much more transparent to acknowledge the existence of such a separation of scales from the outset and reduce the complicated evolution equations of the non-equilibrium Green's functions to quantum kinetic equations. One may then evaluate the linear response functions directly using the quantum kinetic equations. This procedure was described in detailed in the previous Chapter.

It is useful to define the response functions relevant to monopole and quadrupole oscillation experiments. The monopole oscillations can be excited by choosing $\delta U(\mathbf{r}, t) \equiv \delta U_m(\mathbf{r}, t) \equiv \mathcal{A}(t)\, m\omega_0^2 r^2$, where $\mathcal{A}(t)$ is the temporal shape of the perturbation (e.g. a δ-function, a finite pulse or a periodic modulation). We choose $\mathcal{A}(t) \equiv \mathcal{A}_0\, \omega_0^{-1}\delta(t)$ for concreteness. The linear response to any other pulse shape can be determined from the impulse response. Note that we have "defined" the monopole oscillations as the response of the trapped gas to $\sim r^2$ perturbation. One may choose any other isotropic trap perturbation (such as r^4, etc). Such choices, however, excite higher order modes to a greater degree which may not be desirable. Here, the observable is the variation in the size of the cloud, $\hat{r}^2 - \langle \hat{r}^2 \rangle_0$. We define the "monopole response function" as:

$$\chi_{x^2+y^2}(t) = \mathcal{A}_0^{-1} m\omega_0\, \theta(t) \left(\langle \hat{r}^2 \rangle_t - \langle \hat{r}^2 \rangle_0 \right). \qquad (3.24)$$

Likewise, we define the quadrupole oscillations as the response of the trapped gas to $\delta U(\mathbf{r}, t) \equiv$ $\delta U_q(\mathbf{r}, t) \equiv \mathcal{A}(t)\, m\omega_0^2(x^2 - y^2)$ and define the "quadrupole response function" as:

$$\chi_{x^2 - y^2}(t) = \mathcal{A}_0^{-1} m\omega_0\, \theta(t)\, \langle \hat{x}^2 - \hat{y}^2 \rangle_t. \qquad (3.25)$$

Note that $\langle \hat{x}^2 - \hat{y}^2 \rangle_0 = 0$ due to the isotropy of the trap.

We calculate the response functions using the quantum kinetic formalism described in the previous Chapter. We confine our analysis to weakly interacting systems $\lambda_d \lesssim 1$ so that the quasiparticle approximation is admissible. In this limit, the quantum kinetic equations reduce to the collisional Boltzmann-Vlasov (CBV) equation (cf. Eq. 2.56), which we quote here[2]:

$$\left[\partial_t + \partial_{\mathbf{p}} \left(\frac{|\mathbf{p}|^2}{2m} + \Sigma^+[n](\mathbf{p}; \mathbf{r}, t) \right) \cdot \partial_{\mathbf{r}} - \partial_{\mathbf{r}} \left(U(\mathbf{r}, t) + \Sigma^+[n](\mathbf{p}; \mathbf{r}, t) \right) \cdot \partial_{\mathbf{p}} \right] n(\mathbf{p}; T, \mathbf{R}) = I_c[n],$$

$$(3.26)$$

where $n(\mathbf{p}; \mathbf{r}, t)$ is the quasiparticle distribution function, $U(\mathbf{r}, t)$ is the external potential (including the static trap potential and its time-dependent perturbation). The Luttinger-Ward functional in the weakly interacting limit can be obtained from the loop expansion. The simplest approximation that describes collisions is 3-loop expansion, i.e. the Born approximation discussed in Sec. 2.2.1. Retardation effect can be neglected to leading order in λ_d within the validity limit of the quasiparticle approximation, so that the retarded self-energy is simply given by the 2-loop (Hartree-Fock) diagram:

$$\Sigma^+[n](\mathbf{p}; \mathbf{r}, t) = \int d^2 \mathbf{r}'\, \frac{d^2 \mathbf{p}'}{(2\pi)^2} \left[\mathcal{V}(\mathbf{r} - \mathbf{r}') - \delta^2(\mathbf{r} - \mathbf{r}') \tilde{\mathcal{V}}(\mathbf{p} - \mathbf{p}') \right] n(\mathbf{p}'; \mathbf{r}', t), \qquad (3.27)$$

where $\mathcal{V}(\mathbf{r})$ and $\tilde{\mathcal{V}}(\mathbf{p})$ are the two-body interactions in the real and momentum space. The Hartree term in the self-energy describes the non-local dipole-dipole interaction between between the spatially separated segments of the gas in the trap. However, we will shortly show that non-local

---

[2]We depart from the notation introduced in the previous chapter and refer to the macroscopic coordinates as $(t, \mathbf{r})$ instead of $(T, \mathbf{R})$ in order to avoid confusion with the temperature T. We also refer to the number density as ρ (instead of n) in order to avoid confusion with the quasiparticle distribution function.

contributions are negligible in the case of dipole-dipole interactions. Also, note that since Σ^+ has no ω-dependence, the quasiparticle residue is 1. The quasiparticle collision integral in the Born approximation is given by Eq. 2.58, which we copy here:

$$I_c[n] = \int \frac{\mathrm{d}^2 \mathbf{p}_1}{(2\pi)^2} \frac{\mathrm{d}^2 \mathbf{p}'}{(2\pi)^2} \frac{\mathrm{d}^2 \mathbf{p}'_1}{(2\pi)^2} (2\pi)^2 \delta^2(\Delta \mathbf{P})(2\pi)\delta(\Delta E)$$

$$\times \frac{1}{2} |\mathcal{M}|^2 \Big[(1-n)(1-n_1)n'n'_1 - nn_1(1-n')(1-n'_1)\Big], \quad (3.28)$$

where $\mathcal{M} = \tilde{\mathcal{V}}(\mathbf{p} - \mathbf{p}') - \tilde{\mathcal{V}}(\mathbf{p} - \mathbf{p}'_1)$ is the Born scattering amplitude, $\Delta \mathbf{P} = \mathbf{p} + \mathbf{p}_1 - \mathbf{p}' - \mathbf{p}'_1$ and $\Delta E = E_\mathbf{p} + E_{\mathbf{p}_1} - E_{\mathbf{p}'} - E_{\mathbf{p}'_1}$. Note that $E_\mathbf{p} = p^2/(2m) + U(\mathbf{r}, t) + \Sigma^+[n](\mathbf{p}; \mathbf{r}, t)$. We have also used the shorthand $n \equiv n(\mathbf{p}; \mathbf{r}, t)$, $n_1 \equiv n(\mathbf{p}_1; \mathbf{r}, t)$, etc. in the above equation.

3.2.1 Validity of the CBV equation and the Born approximation

Since we have described the interactions using the lowest order processes, the predictions are quantitatively reliable only as long as the system is in the weakly interacting regime, i.e. $\lambda_d \ll 1$ (see Eq. 3.21). For dipolar interactions, this condition is equivalent to diluteness $\sqrt{\rho}a_d \ll 1$, where ρ is the 2D density and a_d is the dipolar length defined earlier (Eq. 3.20). Since the Fermi liquid state is expected to be stable for a wide range of interaction strengths (up to the crystallization point), we do not expect the higher order many-body corrections to lead to qualitatively different physics. Therefore, although our approximations are only controlled in the dilute limit, we allow ourselves to extend our analysis to $\lambda_d \sim \mathcal{O}(1)$ as well. Apart from the many-body physics, the validity of Born approximation in describing two-body scatterings and the negligence of multiple scatterings must also be assessed. The Born approximation is valid when $\hbar v \gg \mathcal{V}a$, where v is the typical velocity of the scattering pairs in the center of mass frame and a is range of interactions. Identifying a with a_d and $v \sim [m \max(k_B T, k_B T_F)]^{\frac{1}{2}}$, this condition implies:

$$\max(k_B T, k_B T_F) \ll k_B T_{\mathrm{dip}} \equiv \frac{\hbar^2}{ma_d^2}, \quad (3.29)$$

where we have defined a "dipolar temperature" T_{dip}. This is precisely the condition for near-threshold scatterings. The dipolar scatterings in 2D is studied in detail in Ref. [92] and it is shown that the Born approximation is quantitatively reliable provided that $mva_d/\hbar \lesssim 0.1$. Inclusion of multiple scatterings, however, results in significant quantitative corrections as one approaches the semi-classical regime and the Born approximation consistently found to over-estimate the cross section. In this paper, we confine our analysis to near-threshold scatterings. Therefore, the quantitative validity of our results crucially relies on Eq. (3.29). Here, we assume that the following scale separation:

$$T_F \ll T_{\text{dip}} \quad \Leftrightarrow \quad \frac{a_0}{a_d} \gg N^{\frac{1}{4}}, \tag{3.30}$$

so that we can allow ourselves to investigate both the quantum degenerate regime ($T/T_F \ll 1$) and the thermal regime ($T/T_F \gg 1$) up to $T \sim T_{\text{dip}}$. We note that this condition is satisfied well in the current experiments with both polar molecules and rare earth atoms (see Sec. 3.5).

3.3 The equilibrium state of dipolar fermions in isotropic traps

The first step in the linear response analysis using the kinetic equations is to determine the equilibrium distribution about which the perturbation analysis is carried out. We assume that the system has reached a thermal equilibrium state in the external potential $U(\mathbf{r}) = m\omega_0^2 r^2/2$ before the perturbation is introduced. At equilibrium, the energy distribution function is the Fermi-Dirac function $f_0(\omega)$ and yields the following quasiparticle distribution function:

$$n_0(p; r) = \left\{ \exp\left[\beta\left(\frac{p^2}{2m} + \Sigma_0(p; r) + \frac{1}{2}m\omega_0^2 r^2 - \mu \right) \right] + 1 \right\}^{-1}, \tag{3.31}$$

where we have introduced the shorthand $\Sigma_0 \equiv \Sigma^+[n_0]$. The above equation has to be solved self-consistenty along with the expression for the self-energy, Eq. (3.27). It is easily verified that the above solution satisfies $I_c[n_0] = 0$ and at the same time, it solves the left hand side of the CBV

equation. The global chemical potential μ has to be found such that the equilibrium distribution function yields the correct number of trapped particles:

$$\int d\Gamma \, n_0(\mathbf{p};\mathbf{r}) = N, \tag{3.32}$$

where we have defined the phase-space volume differential as $d\Gamma \equiv d^2\mathbf{r}\, d^2\mathbf{p}/(2\pi)^2$. In the case of harmonic traps, it is useful to define the following scaled coordinates:

$$\bar{\mathbf{r}} \equiv \frac{\mathbf{r}}{r_0}, \qquad r_0 \equiv [2N/(m\omega_0)^2]^{1/4},$$

$$\bar{\mathbf{p}} \equiv \frac{\mathbf{p}}{p_0}, \qquad p_0 \equiv [2N(m\omega_0)^2]^{1/4}. \tag{3.33}$$

In the scaled coordinates, the equation for the particle number is $\int d\bar{\Gamma}\, n_0(\bar{\mathbf{p}};\bar{\mathbf{r}}) = 1/2$, where $d\bar{\Gamma} \equiv d^2\bar{\mathbf{r}}\, d^2\bar{\mathbf{p}}/(2\pi)^2 = d\Gamma/(2N)$. The equilibrium distribution function also reads as:

$$n_0(\bar{\mathbf{p}};\bar{\mathbf{r}}) = \left\{ \exp\left[\bar{\beta}\left(\frac{\bar{p}^2 + \bar{r}^2}{2} + \bar{\Sigma}_0(\bar{r};\bar{p}) - \bar{\mu} \right) \right] + 1 \right\}^{-1}, \tag{3.34}$$

where $\bar{\beta} = T_F/T$ and:

$$T_F = (2N)^{\frac{1}{2}} \frac{\hbar\omega_0}{k_B}, \tag{3.35}$$

is the (in-trap) Fermi temperature, $\bar{\mu} = \mu/(k_B T_F)$ is the dimensionless chemical potential and:

$$\bar{\Sigma}^+[n](\bar{\mathbf{p}};\bar{\mathbf{r}},t) = \omega_0^{-1} \int d\bar{\Gamma}' \left[\sqrt{2N}\, \mathcal{V}[r_0(\bar{\mathbf{r}}-\bar{\mathbf{r}}')] - m\omega_0 \delta^2(\bar{\mathbf{r}}-\bar{\mathbf{r}}')\tilde{\mathcal{V}}[p_0(\bar{\mathbf{p}}-\bar{\mathbf{p}}')] \right] n(\bar{\mathbf{p}}';\bar{\mathbf{r}}',t), \tag{3.36}$$

is the dimensionless self-energy functional. Also, $\bar{\Sigma}_0 \equiv \bar{\Sigma}^+[n_0]$. The motivation for using scaled coordinates becomes clear upon investigating the equilibrium state of the non-interacting problem. In this case, the (dimensionless) equilibrium density $\bar{\rho}_0^{(0)}(\bar{r})$ can be found analytically:

$$\bar{\rho}_0^{(0)}(\bar{r}) \equiv \int \frac{d^2\bar{\mathbf{p}}}{(2\pi)^2} \, \bar{n}_0(\bar{p};\bar{r}) = \log\left[1 + e^{\bar{\beta}(\bar{\mu}-\bar{r}^2/2)} \right] /(2\pi\bar{\beta}), \tag{3.37}$$

using which we obtain an equation for the chemical potential of the non-interacting trapped gas:

$$\bar{\mu}^2 + \frac{\pi^2}{3}\bar{T}^2 + 2\bar{T}^2 \, \mathrm{Li}_2[-\exp(-\bar{\mu}/\bar{T})] = 1, \tag{3.38}$$

where $\bar{T} = T/T_F$. At low temperatures, the above equation admits the solution $\bar{\mu} = 1 - \pi^2 \bar{T}^2/6 + \mathcal{O}(\bar{\beta}^{-2} e^{-\bar{\beta}})$. The zero-temperature Thomas-Fermi radius of the cloud is easily obtained from Eq. (3.37), yielding $R_{\mathrm{TF}}^{(0)} = [2\sqrt{2N}/(m\omega_0)]^{1/2} \equiv \sqrt{2}\, r_0$. Also, the Fermi momentum at the center of the trap is given by $p_F^{(0)} = [2\sqrt{2N}(m\omega_0)]^{1/2} \equiv \sqrt{2}\, p_0$. We note that N does not appear explicitly in the expressions written in terms of the scaled coordinates. Moreover, at low temperatures, the equilibrium distribution function is only appreciably larger than zero in a region of size $\mathcal{O}(1)$ in the scaled phase-space coordinates. Once the interactions are taken into account, analytical solutions can no longer be obtained and the equilibrium distribution function has to found numerically. It is, however, useful to investigate the effect of non-local Hartree self-energy term first: the forthcoming calculations will be significantly simplified if the non-local effects can be neglected. Carrying out the trivial momentum integration in the first term of Eq. (3.36), the Hartree self-energy can be expressed as a linear functional of just the density:

$$\bar{\Sigma}_H^+[\bar{\rho}](\bar{\mathbf{r}}, t) = \omega_0^{-1} \int \mathrm{d}^2 \bar{\mathbf{r}}'\, \sqrt{2N}\, \mathcal{V}(r_0 \bar{\mathbf{r}}')\, \bar{\rho}(\bar{\mathbf{r}} - \bar{\mathbf{r}}', t). \tag{3.39}$$

Observing that the density is only appreciable in a region of size $\mathcal{O}(1)$ in the scaled coordinates and the appearance of $r_0 \sim N^{1/4}$ in the argument of interaction potential, the above integral is expected to only depend of the values of the density within a small region of size $\sim N^{-1/4}$ about $\bar{\mathbf{r}}$. Assuming that the density variation is smooth, we may expand $\bar{\rho}$ to quadratic order about $\bar{\mathbf{r}}$ to get:

$$\bar{\Sigma}_H^+[\bar{\rho}](\bar{\mathbf{r}}, t) \approx \omega_0^{-1} \int \mathrm{d}^2 \bar{\mathbf{r}}'\, \sqrt{2N}\, \mathcal{V}(r_0 \bar{\mathbf{r}}') \left[\bar{\rho}(\bar{\mathbf{r}}, t) - \bar{\mathbf{r}}' \cdot \nabla \bar{\rho}(\bar{\mathbf{r}}, t) + \bar{r}'_\alpha \bar{r}'_\beta \partial_\alpha \partial_\beta \bar{\rho}(\bar{\mathbf{r}}, t)/2 \right]. \tag{3.40}$$

The first contribution is the usual local density approximation (LDA):

$$\bar{\Sigma}_{H,\mathrm{LDA}}^+[\bar{\rho}](\bar{\mathbf{r}}, t) \equiv \sqrt{2N}\omega_0^{-1} \bar{\rho}(\bar{\mathbf{r}}, t) \int \mathrm{d}^2 \bar{\mathbf{r}}'\, \mathcal{V}(r_0 \bar{\mathbf{r}}')$$

$$= m\, \tilde{\mathcal{V}}(0)\, \bar{\rho}(\bar{\mathbf{r}}, t). \tag{3.41}$$

The gradient term vanishes due to the isotropy of $\mathcal{V}(\mathbf{r})$. The quadratic term is dominated by the long-range behavior of $\mathcal{V}(\mathbf{r})$ assuming that the short-range part of $\mathcal{V}(\mathbf{r})$ is integrable (which is the
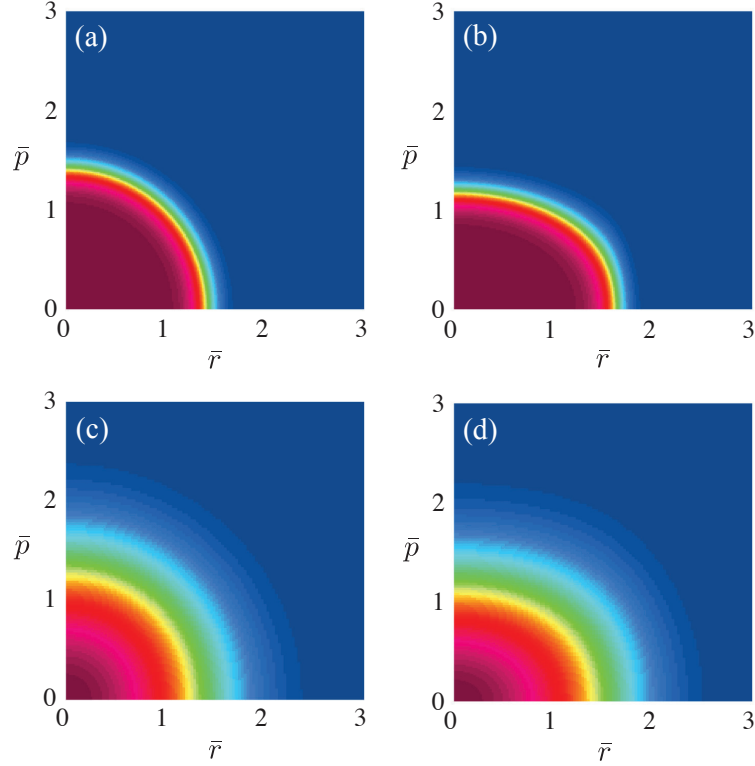
Figure 3.2: Equilibrium quasiparticle distribution function of quasi-2D dipolar fermions for different temperatures and interactions strengths ($\omega_z = 2\pi \times 23\,\text{kHz}$, $\omega_0 = 2\pi \times 36\,\text{Hz}$, $N = 2200$ in all cases). (a) $T/T_F = 0.1$, $\lambda_d = 0$, (b) $T/T_F = 0.1$, $\lambda_d = 1$, (c) $T/T_F = 0.5$, $\lambda_d = 0$, (d) $T/T_F = 0.5$, $\lambda_d = 1$. Red and blue regions (near to and far from the origin, respectively) correspond to occupied and empty states.

case for dipolar interactions, see Eq. 3.18). Observing that the Hessian matrix of the density is also

$\mathcal{O}(1)$ in the scaled coordinates, we easily find that the quadratic term yields a correction that scales

like $N^{1/2-\alpha/4}$ for a potential with power-law tail $\mathcal{V}(\mathbf{r}) \sim r^{-\alpha}$. For dipolar interactions, $\alpha = 3$

and we find that the leading corrections to LDA scale like $N^{-1/4}$ and can be neglected for large

N. Note that if we were dealing with an electron gas ($\alpha = 1$), such corrections would grow larger

with N and the non-local Hartree functional had to be kept untouched. A direct result of this simple

analysis is that the Landau damping, which is driven by non-local direct interactions, is expected to

be absent in a dipolar fermi gas in the thermodynamic limit. In the remainder of this paper, we treat

the Hartree potential in the LDA approximation and use the following local self-energy functional:

$$\bar{\Sigma}^+_{\text{LDA}}[n](\bar{\mathbf{p}}; \bar{\mathbf{r}}, t) = m \int \frac{\mathrm{d}^2\bar{\mathbf{p}}'}{(2\pi)^2} \Big[\tilde{\mathcal{V}}(0) - \tilde{\mathcal{V}}[p_0(\bar{\mathbf{p}} - \bar{\mathbf{p}}')] \Big] n(\bar{\mathbf{p}}'; \bar{\mathbf{r}}', t)$$

$$= \lambda_d \int \frac{\mathrm{d}^2\bar{\mathbf{p}}'}{(2\pi)^2} \, u(|\bar{\mathbf{p}} - \bar{\mathbf{p}}'|, \eta) \, n(\bar{\mathbf{p}}'; \bar{\mathbf{r}}', t), \tag{3.42}$$

where we have used Eq. (3.15) in the second line and have defined:

$$u(x, \eta) = 2\pi x \operatorname{Erfcx}\left(\frac{x\eta}{\sqrt{2}}\right), \tag{3.43}$$

where $\operatorname{Erfcx}(x) \equiv e^{x^2}\operatorname{Erfc}(x)$. The dimensionless parameters λ_d and η were defined earlier (Eq. 3.21) Note that the dependence on N enters the equations only through these two dimensionless parameters.

We obtain the equilibrium distribution function using a simple iterative method. At the initial step, we set $\bar{\Sigma}_0 = 0$ and define the function $n_0(\bar{\mu}) \equiv n[\bar{\Sigma}_0, \bar{\mu}]$, i.e. the distribution function obtained using the self-energy $\bar{\Sigma}_0 = 0$ and chemical potential $\bar{\mu}$. We find μ_0 such that $\int \mathrm{d}\bar{\Gamma}\, n_0(\mu_0) = 1/2$. To proceed from i'th step to $(i+1)$'th step, we set $\bar{\Sigma}_{i+1} = \bar{\Sigma}^+[n_i]$, define $n_{i+1}(\bar{\mu}) \equiv n[\bar{\Sigma}_{i+1}, \bar{\mu}]$ and find $\bar{\mu}_{i+1}$ such that $\int \mathrm{d}\Gamma'\, n_{i+1}(\bar{\mu}_{i+1}) = 1/2$. At the end of this step, we set $n_{i+1} \to (1-\delta)n_i + \delta\, n_{i+1}$, where $0 < \delta < 1$. The last step is to stabilize the iterative procedure and to damp possible oscillations that prevent convergence. With an arbitrary choice $\delta = 0.75$, we found the this iterative procedure converges to a fixed point in less than ten steps within a relative error tolerance of 10^{-8}. It is trivial to show that the fixed point is indeed the solution.

Fig. 3.2 shows the equilibrium quasiparticle distribution function as a function of $\bar{p}$ and $\bar{r}$ for several values of $\bar{T}$ and λ_d. As one expects, the presence of interactions results in the expansion of the gas in the trap (compare panels a and b) and thermal fluctuations smear the Fermi surface (compare panels a and c). The equilibrium density is shown in Fig. 4.12a. The nearly Gaussian distribution around the edge of the trap at finite temperatures, and the reduction of the density at the center of the trap at low temperatures due to repulsive interactions can be clearly seen. We
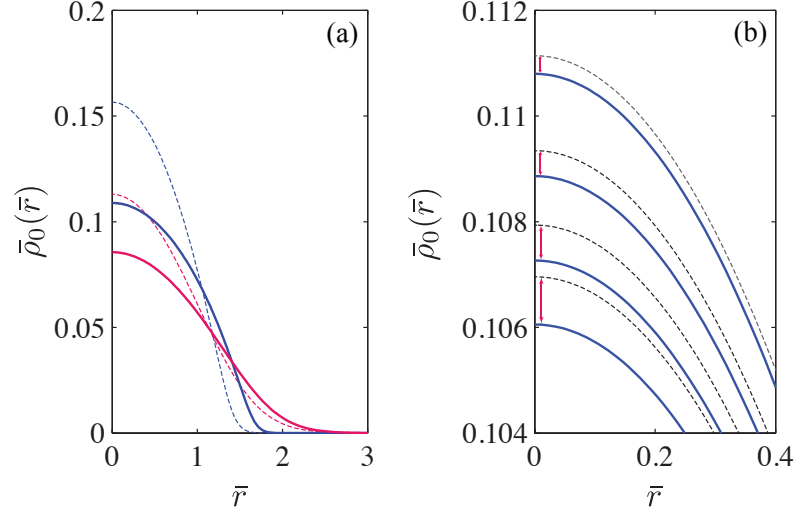
Figure 3.3: Equilibrium density of a quasi-2D dipolar Fermi gas as a function of the distance from the center of the trap ($\omega_z = 2\pi \times 23\,\mathrm{kHz}$, $\omega_0 = 2\pi \times 36\,\mathrm{Hz}$). (a) dashed and solid lines correspond to the non-interacting ($\lambda_d = 0$) and interacting ($\lambda_d = 1$), blue (top) and red (bottom) lines correspond to $T/T_F = 0.1$ and 0.5 respectively. In all cases, $N = 2200$. (b) A comparison between the equilibrium densities obtained from LDA (solid lines) and non-local (dashed lines) Hartree self-energy functionals. From bottom to top, $N = 500$, 1000, 2200, and 5000. $\lambda_d = 1$ and $T/T_F = 0.1$ in all cases. The non-local corrections are clearly negligible and become smaller as N is increased.

also compare the LDA and full non-local Hartree self-energy functionals in Fig. 4.12b for various number of particles in the trap. The relative correction to the LDA predictions is of the order of 10^{-3} for realistic number of trapped particles and as argued earlier, becomes smaller for larger system sizes.

Having found the equilibrium state, we can move on to the investigation of the low lying collective excitations. To this end, we discuss the linear response theory of the CBV equation in the next section as a first step.

3.4   Analysis of the collective modes

The linear response can be conveniently evaluated using kinetic equations by introducing a perturbation to the external potential, linearizing the resulting equation about deviations from the

global equilibrium state, $\delta n(\bar{\mathbf{p}}; \bar{\mathbf{r}}, t) \equiv n(\bar{\mathbf{p}}; \bar{\mathbf{r}}, t) - n_0(\bar{p}; \bar{r})$ and solving the resulting linear integro-differential equation. The benefit of this fomulation compared to the diagram technique is the possibility of obtaining approximate solutions using well-known variational methods. Since we are mostly concerned with low temperatures here, it is beneficial to introduce the following ansatz for δn:

$$\delta n(\bar{\mathbf{p}}; \bar{\mathbf{r}}, t) \equiv \theta(t)\, \Delta_0(\bar{p}; \bar{r})\, \Psi(\bar{\mathbf{p}}; \bar{\mathbf{r}}, t), \tag{3.44}$$

where $\Delta_0 \equiv \partial n_0 / \partial \bar{\mu} = \bar{\beta} n_0 (1 - n_0)$. The above ansatz is not restrictive for $T > 0$ since $\Delta_0 > 0$ everywhere on the phase-space. The only exception is $T = 0$ where Δ_0 restricts the deviations to the local Fermi surface. This is in fact a favorable feature since the low lying collective modes are formed from the particle-hole excitations about the Fermi surface at $T = 0$. Also, at finite T, Δ_0 is sharply peaked about the local Fermi surface and allows the solution of the linearized CBV equation to be representable with a smooth choice of Ψ [85]. As we shall see, this feature allows us to construct decent approximate solutions by choosing a linear combination of smooth functions as a variational ansatz for Ψ.

3.4.1 The linear response theory of the CBV equation

The linear response theory of the CBV equation was outlined in Sec. 2.5.2. We discuss this problem in more detail in this section, in particular, the practical methods for solving the resulting equations. As a first step, we plug the ansatz given in Eq. (3.44) into the CBV equation, expand to first order in Ψ and take a Fourier transform in time. The final result is the following linear integral equation for $\Psi(\bar{\mathbf{p}}; \bar{\mathbf{r}}, \omega)$:

$$-i\,\bar{\omega}\,\Delta_0 \Psi + \mathscr{D}[\Psi] - \mathscr{I}[\Psi] = -(2N)^{-\frac{1}{2}}\{n_0, \delta U(r_0\bar{\mathbf{r}}, \omega)\}, \tag{3.45}$$

where $\{\Psi, \Phi\} \equiv \nabla_{\bar{\mathbf{r}}}\Psi \cdot \nabla_{\bar{\mathbf{p}}}\Phi - \nabla_{\bar{\mathbf{p}}}\Psi \cdot \nabla_{\bar{\mathbf{r}}}\Phi$ is the Poisson bracket with respect to the scaled phase-space coordinates, and $\bar{\omega} \equiv \omega/\omega_0$. $\mathscr{D}[\Psi]$ describes the collisionless self-consistent mean-field

116

dynamics of quasiparticles:

$$\mathscr{D}[\Psi] = \Delta_0\{\Psi, \bar{\mathcal{H}}_0\} + \{n_0, \bar{\Sigma}[\Delta_0\Psi]\} = \Delta_0\{\Psi + \bar{\Sigma}[\Delta_0\Psi], \bar{\mathcal{H}}_0\}, \tag{3.46}$$

where $\bar{\mathcal{H}}_0 = (\bar{p}^2 + \bar{r}^2)/2 + \bar{\Sigma}_0$. To get the second line, we have used the identity $\{n_0, \mathcal{A}\} \equiv -\Delta_0\{\bar{\mathcal{H}}_0, \mathcal{A}\}$ which can be easily proved by direct calculation and is valid for arbitrary $\mathcal{A}$. The first term in the first line of Eq. (3.46) describes the evolution of quasiparticles in the equilibrium mean-field whereas the second term describes their dynamics in the self-consistently generated residual mean-field $\bar{\Sigma}[\Delta_0\Psi]$. $\mathscr{I}[\Psi]$ describes the collisional dynamics and can be written as:

$$\mathscr{I}[\Psi] = -\frac{\bar{\beta}(2N)^{\frac{1}{2}}}{2} \int \frac{\mathrm{d}^2\bar{\mathbf{p}}_1}{(2\pi)^2} \frac{\mathrm{d}^2\bar{\mathbf{p}}'}{(2\pi)^2} \frac{\mathrm{d}^2\bar{\mathbf{p}}'_1}{(2\pi)^2} (2\pi)^2 \delta^2(\Delta\bar{\mathbf{P}})$$

$$\times (2\pi)\delta(\Delta\bar{E}) |\bar{\mathcal{M}}|^2 \, \mathrm{S}\{\Psi\} \, n_0 n_{0,1}(1 - n'_0)(1 - n'_{0,1}), \quad (3.47)$$

where $\Delta\bar{E} \equiv \bar{\mathcal{H}}_0(\bar{\mathbf{p}}, \bar{\mathbf{r}}) + \bar{\mathcal{H}}_0(\bar{\mathbf{p}}_1, \bar{\mathbf{r}}) - \bar{\mathcal{H}}_0(\bar{\mathbf{p}}', \bar{\mathbf{r}}) - \bar{\mathcal{H}}_0(\bar{\mathbf{p}}'_1, \bar{\mathbf{r}})$, $\Delta\bar{\mathbf{P}} \equiv \bar{\mathbf{p}} + \bar{\mathbf{p}}_1 - \bar{\mathbf{p}}' - \bar{\mathbf{p}}'_1$, $\bar{\mathcal{M}} = m(\tilde{\mathcal{V}}[p_0(\bar{\mathbf{p}} - \bar{\mathbf{p}}')] - \tilde{\mathcal{V}}[p_0(\bar{\mathbf{p}} - \bar{\mathbf{p}}'_1)])$, and $\mathrm{S}[\Psi] \equiv \Psi(\bar{\mathbf{p}}; \bar{\mathbf{r}}, \omega) + \Psi(\bar{\mathbf{p}}_1; \bar{\mathbf{r}}, \omega) - \Psi(\bar{\mathbf{p}}'; \bar{\mathbf{r}}, \omega) - \Psi(\bar{\mathbf{p}}'_1; \bar{\mathbf{r}}, \omega)$. Note that the dressed quasiparticle dispersions have been used in the collision integrals. Specializing to the case of dipole-dipole interactions, we get:

$$|\bar{\mathcal{M}}|^2 = \lambda_d^2 \left[u(|\bar{\mathbf{p}} - \bar{\mathbf{p}}'|, \eta) - u(|\bar{\mathbf{p}} - \bar{\mathbf{p}}'_1|, \eta) \right]^2. \tag{3.48}$$

Formally, the solution of Eq. (3.45) can be written as:

$$\Psi = - \left(-i\bar{\omega}\Delta_0 + \mathscr{D} - \mathscr{I} \right)^{-1} \frac{\{n_0, \delta U(r_0\bar{\mathbf{r}}, \omega)\}}{(2N)^{\frac{1}{2}}}, \tag{3.49}$$

and the linear response can be determined using Eq. (3.44):

$$\langle O \rangle_t = \int \mathrm{d}\Gamma \int \frac{\mathrm{d}\omega}{2\pi} e^{-i\omega t} \Delta_0(\bar{p}; \bar{r}) \, \Psi(\bar{\mathbf{p}}; \bar{\mathbf{r}}, \omega^+) \, O(\mathbf{p}; \mathbf{r}). \tag{3.50}$$

The difficulty is in inverting the operator appearing in the parenthesis in Eq. (3.49). Decent approximate solutions, however, can be found using a variational technique known as the method of moments. To this end, we restrict the solution space of Eq. (3.45) to a subspace spanned by a set of

basis functions of the phase-space variables $\{\phi_\alpha(\bar{\mathbf{p}}; \bar{\mathbf{r}})\}$ (the "moments") and expand Ψ and δU in this basis:

$$\Psi(\bar{\mathbf{p}}; \bar{\mathbf{r}}, \omega) = \sum_\alpha \Psi_\alpha(\omega)\, \phi_\alpha(\bar{\mathbf{p}}; \bar{\mathbf{r}}),$$

$$(2N)^{-\frac{1}{2}} \delta U(r_0 \bar{\mathbf{r}}, \omega) = \sum_\alpha \delta U_\alpha(\omega)\, \phi_\alpha(\bar{\mathbf{p}}; \bar{\mathbf{r}}). \tag{3.51}$$

Plugging this ansatz into Eq. (3.45) and evaluating the moments of the resulting equation with respect to each of the basis functions, i.e. multiplying the sides of the CBV equation by each of the basis functions and integrating over the phase-space variables, we find a closed set of linear equations for the coefficients $\{\Psi_\alpha\}$:

$$-i\bar{\omega} \langle\!\langle \phi_\beta \phi_\alpha \rangle\!\rangle \Psi_\alpha(\omega) + \langle\!\langle \phi_\beta \{\phi_\alpha, \bar{\mathcal{H}}_0\} \rangle\!\rangle \left[\delta U_\alpha(\omega) + \Psi_\alpha(\omega) \right]$$

$$+ \langle\!\langle \phi_\beta \{ \bar{\Sigma}[\Delta_0 \phi_\alpha], \bar{\mathcal{H}}_0 \} \rangle\!\rangle \phi_\alpha(\omega) - \mathscr{I}_{\beta\alpha} \Psi_\alpha(\omega) = 0, \tag{3.52}$$

where we have defined the "Δ_0-average" as:

$$\langle\!\langle \mathcal{A}(\bar{\mathbf{p}}; \bar{\mathbf{r}}) \rangle\!\rangle \equiv \int d\bar{\Gamma}\, \Delta_0(\bar{\mathbf{p}}; \bar{\mathbf{r}}) \mathcal{A}(\bar{\mathbf{p}}; \bar{\mathbf{r}}). \tag{3.53}$$

Summation over repeated indices is implied in Eq. (3.52). The matrix elements of the collision integral, $\mathscr{I}_{\alpha\beta} \equiv \int d\bar{\Gamma}\, \Psi_\alpha \mathscr{I}[\Psi_\beta]$ can be put in the following symmetric form using the symmetry properties of the collision integral kernel:

$$\mathscr{I}_{\alpha\beta} = -\frac{\bar{\beta}(2N)^{\frac{1}{2}}}{8} \int d^2\bar{\mathbf{r}} \int \frac{d^2\bar{\mathbf{p}}}{(2\pi)^2} \frac{d^2\bar{\mathbf{p}}_1}{(2\pi)^2} \frac{d^2\bar{\mathbf{p}}'}{(2\pi)^2} \frac{d^2\bar{\mathbf{p}}'_1}{(2\pi)^2} (2\pi)\delta(\Delta\bar{E})\, (2\pi)^2 \delta^2(\Delta\bar{\mathbf{P}})\, |\bar{\mathcal{M}}|^2$$

$$\times \mathrm{S}[\phi_\alpha]\, \mathrm{S}[\phi_\beta]\, n_0 n_{0,1}(1 - n'_0)(1 - n'_{0,1}). \tag{3.54}$$

The first term on the second line of Eq. (3.52) can be put in a more useful form using the identity $\phi_\beta \{ \bar{\Sigma}[\Delta_0 \phi_\alpha], \bar{\mathcal{H}}_0 \} = \{ \phi_\beta \bar{\Sigma}[\Delta_0 \phi_\alpha], \bar{\mathcal{H}}_0 \} - \bar{\Sigma}[\Delta_0 \phi_\alpha]\{ \phi_\beta, \bar{\mathcal{H}}_0 \}$. Taking the Δ_0-average of both sides on this identity, the first term on the left hand side vanishes. To see this, note that $\langle\!\langle \{\phi, \bar{\mathcal{H}}_0\} \rangle\!\rangle = \int d\bar{\Gamma}\, \Delta_0\{\phi, \bar{\mathcal{H}}_0\} = \int d\bar{\Gamma}\, \{\Delta_0 \phi, \bar{\mathcal{H}}_0\}$ for arbitrary ϕ. The last equality holds since $\{\Delta_0, \bar{\mathcal{H}}_0\} =$

0. Since $\Delta_0 \to 0$ exponentially fast for large $\bar{\mathbf{r}}$ or $\bar{\mathbf{p}}$, the Stokes' theorem implies that the last integral vanishes as long as ϕ is exponentially bounded. Here, $\phi = \phi_\beta \bar{\Sigma}[\Delta_0 \phi_\alpha]$ which is in fact exponentially bounded. Finally, Eq. (3.52) can be put in the following matrix form:

$$(-i\bar{\omega}\mathsf{M} + \mathsf{H}_0 - \Sigma - \mathsf{I}_c)\boldsymbol{\Psi}(\omega) = -\mathsf{H}_0\,\delta\mathbf{U}(\omega), \tag{3.55}$$

where:

$$(\mathsf{M})_{\alpha\beta} = \langle\!\langle \phi_\alpha \phi_\beta \rangle\!\rangle,$$

$$(\mathsf{H}_0)_{\alpha\beta} = \langle\!\langle \phi_\alpha \{\phi_\beta, \bar{\mathcal{H}}_0\} \rangle\!\rangle,$$

$$(\Sigma)_{\alpha\beta} = \langle\!\langle \bar{\Sigma}[\Delta_0 \phi_\beta]\{\phi_\alpha, \bar{\mathcal{H}}_0\} \rangle\!\rangle,$$

$$(\mathsf{I}_c)_{\alpha\beta} = \mathscr{I}_{\alpha\beta}, \tag{3.56}$$

and $\boldsymbol{\Psi}(\omega)$ and $\delta\mathbf{U}(\omega)$ are the vectors with entries $\Psi_\alpha(\omega)$ and $\delta U_\alpha(\omega)$ respectively. If the observable $O(\bar{\mathbf{p}}; \bar{\mathbf{r}})$ is also expressible in terms of the basis functions, $O(\bar{\mathbf{p}}; \bar{\mathbf{r}}) = \sum_\alpha O_\alpha \phi_\alpha(\bar{\mathbf{p}}; \bar{\mathbf{r}})$, then the linear response can be conveniently written as:

$$\langle O \rangle_\omega = \int d\bar{\Gamma}\, O_\beta \phi_\beta\, \Delta_0 \Psi_\alpha(\omega^+)\phi_\alpha = \mathbf{O}^T \mathsf{M}\, \boldsymbol{\Psi}(\omega^+). \tag{3.57}$$

Eqs. (3.55)-(3.57) are similar to the analysis of Ref. [102]. Here, however, we have an additional matrix Σ that accounts for the residual mean-field due to self-consistency. It is useful to define an "evolution matrix" and express it in its diagonal basis:

$$\mathsf{E} \equiv \mathsf{M}^{-1}(\mathsf{H}_0 - \Sigma - \mathsf{I}_c) = i\,\mathsf{V}\Omega\mathsf{V}^{-1}, \tag{3.58}$$

where Ω is the diagonal matrix of eigenvalues and V is the matrix of eigenvectors. Note that in general, E is a not a Hermitian matrix and may have complex eigenvalues. Moreover, it is a non-normal matrix and therefore, its eigenvectors are not orthogonal [3]. Using diagonal form of the

---

[3] The non-normality of the linearized Boltzmann-Vlasov equation is the key to Landau damping [see N. G. van Kampen, Physica **21** (1955)]. However, as we argued earlier, dipole-dipole interactions are not long-ranged enough to give rise to this phenomenon.

evolution matrix, Eq. (3.55) can be expressed as:

$$\mathbf{\Psi}(\omega) = -i\mathsf{V}\,\frac{1}{\omega - \Omega}\,\mathsf{V}^{-1}\mathsf{M}^{-1}\mathsf{H}_0\,\delta\mathbf{U}(\omega). \tag{3.59}$$

The real and imaginary parts of Ω determine the oscillation frequency and damping of the eigenmodes. Clearly, not all of the eigenmodes are expected to contribute to the linear response to a given perturbation. This becomes particularly important when one is dealing with a large variational basis set. In such cases, as we will see later, the evolution matrix will have poles which are very close to each other on the complex frequency plane and it is not a priori clear which one(s) and in what proportion contribute to the response of the system. Using the linear response formalism described here, however, this question does not need to be dealt separately. Using Eqs. (3.57) and (3.59), we get:

$$\langle O \rangle_\omega = \sum_\alpha \frac{r_\alpha(\omega)}{\omega - \Omega_\alpha},$$

$$r_\alpha(\omega) = -i[\mathsf{V}^T\mathsf{M}\mathbf{O}]_\alpha[\mathsf{V}^{-1}\mathsf{M}^{-1}\mathsf{H}_0\,\delta\mathbf{U}(\omega)]_\alpha, \tag{3.60}$$

i.e. the residues r_α can be expressed in terms of the known matrices. Note that in case of Dirac delta perturbations, $\delta\mathbf{U}(\omega)$ is independent of ω and so are the residues.

Before we attempt to obtain accurate solutions obtained using large variational basis sets, we find it useful to make simple analytical predictions using a small basis set as the first step. We use the scaling ansatz approach to find such a basis set and neglect self-energy corrections to simplify the calculations at first. We extend the basis set and include self-energy corrections later and discuss the nature and importance of the corrections that follow.

3.4.2   The scaling ansatz approximation

The scaling ansatz provides a simple and intuitive picture of the collective excitations of confined gases. This method has been applied to various systems in both isotropic and anisotropic traps,

including Bose gases below and above the critical temperature, s-wave and dipolar fermions in the collisionless and hydrodynamics regimes [94, 95, 96, 97, 86, 87, 88, 89, 90, 91]. Here, we apply the method to the CBV equation which as we shall see, allows us to study both CL and HD limits as well as transition from one regime to the other.

In this method, one assumes that the non-equilibrium quasiparticle distribution function can be approximately described as a scaled copy of the equilibrium distribution:

$$n_{\mathrm{SA}}(\bar{\mathbf{p}}; \bar{\mathbf{r}}, t) \equiv \frac{1}{\prod_i (b_i c_i)} \, n_0 \big[c_i^{-1}(\bar{p}_i - \dot{b}_i \bar{r}_i / b_i); \bar{r}_i / b_i \big], \tag{3.61}$$

where b_i and c_i ($i = x, y$) are time-dependent scale factors of positions and momenta. The prefactor is to ensure conservation of particle number. The equilibrium solution corresponds to the choice $b_x = b_y = c_x = c_y = 1$. Introducing the following reparametrization of the scaling variables:

$$b_x(t) = 1 + \bar{\lambda}(t) + \lambda(t), \quad b_y(t) = 1 + \bar{\lambda}(t) - \lambda(t),$$

$$c_x(t) = 1 + \bar{\nu}(t) + \nu(t), \quad c_y(t) = 1 + \bar{\nu}(t) - \nu(t), \tag{3.62}$$

and expanding Eq. (3.61) to first order in λ, $\bar{\lambda}$, ν and $\bar{\nu}$, we get:

$$\delta n_{\mathrm{SA}} \approx -2(\bar{\lambda} + \bar{\nu}) n_0 + \Delta_0 \big[\dot{\bar{\lambda}} \, \bar{\mathbf{r}} \cdot \bar{\mathbf{p}} + \bar{\nu} \, \bar{p}^2 + \bar{\lambda} \, \bar{r}^2 \big] + \Delta_0 \big[\dot{\lambda} \, (\bar{x} \bar{p}_x - \bar{y} \bar{p}_y) + \nu \, (\bar{p}_x^2 - \bar{p}_y^2) + \lambda \, (\bar{x}^2 - \bar{y}^2) \big],$$

$$\tag{3.63}$$

where $\delta n_{\mathrm{SA}} \equiv n_{\mathrm{SA}} - n_0$. We have neglected self-energy corrections to simplify the analysis and explicitly used the non-interacting equilibrium solution. Also, $\Delta_0 = \partial n_0 / \partial \bar{\mu} = \bar{\beta} n_0 (1 - n_0)$ as before. Here, $(\bar{\lambda}, \bar{\nu})$ and (λ, ν) control the isotropic (monopole) and anisotropic (quadrupole) scalings. Comparing the last equation to Eq. (3.44), we can recognize the first and second set of terms in the brackets as Ψ_{mon} and Ψ_{quad}, i.e. the variational basis set that the scaling ansatz provides for monopole and quadrupole modes respectively.

The first term in Eq. (3.63), which is a consequence of the normalization prefactor of the scaling ansatz requires further discussion. First of all, we note that this term may only be non-vanishing in

the monopole case. Since quadrupole oscillations are purely anisotropic, none of the terms appearing in Ψ_{quad} violate the conservation of mass in the linear regime and therefore no normalization is necessary. The monopole oscillations as described by Ψ_{mon}, however, may violate the conservation of mass and the ansatz must be fixed with a counter term. The scaling ansatz fixes this defect with a uniform scaling of the distribution, leading to the first term in Eq. (3.63). Unless one restricts the ansatz by setting $c_i^{-1} = b_i$ (so that $\bar{\lambda} + \bar{\nu} = 0$), the ansatz may lead to unphysical conclusions once collisions are taken into account. It is generally understood that the non-equilibrium dynamics of degenerate Fermi gases are governed by excitations near the Fermi surface while the fermions deep inside the Fermi sea remain in place due to their large excitation energy gap. A global rescaling of the quasiparticle distribution, i.e. a uniform rescaling of quasiparticle occupations irrespective of their energy gap implies mobilization of all particles with the same likelihood, including those which are deep inside the Fermi sea. This is clearly an unphysical picture and may lead to unrealistically large collision rates.

To address this issue, we remove the global normalization factor and allow the chemical potential to vary instead. This amounts to adding a term $\sim \delta\bar{\mu}(t)\,\partial n_0/\partial\bar{\mu} = \Delta_0\,\delta\mu(t)$ to the ansatz, i.e. adding $\phi = 1$ to the monopole basis set. The phase-space moment equation that os associated to this trivial moment function is exactly the statement of conservation of mass. In summary, we obtain:

$$\Psi_{\text{mon}} = \delta\mu(t) + c_1(t)\,\bar{\mathbf{r}}\cdot\bar{\mathbf{p}} + c_2(t)\,\bar{r}^2 + c_3(t)\,\bar{p}^2, \tag{3.64}$$

and:

$$\Psi_{\text{quad}} = d_1(t)\,(\bar{x}\bar{p}_x - \bar{y}\bar{p}_y) + d_2(t)(\bar{x}^2 - \bar{y}^2) + d_3(t)(\bar{p}_x^2 - \bar{p}_y^2), \tag{3.65}$$

where $\delta\mu(t)$, $c_i(t)$ and $d_i(t)$ are time-dependent functions to be determined. The determination of these unknown functions is usually done by plugging the ansatz into the kinetic equation, multiplying the resulting equation by each of the basis functions and integrating over the phase-space variables to obtain a close set of differential equations. This is equivalent to the formalism described

in Sec. 3.4 and we prefer to do it in our matrix notation as a warm-up for the later sections where we extend the basis set and include self-energy corrections. We remark that the role of various terms appearing in Eqs. (3.64) and (3.65) can be understood intuitively. In particular, $\bar{\mathbf{r}} \cdot \bar{\mathbf{p}}$ and $\bar{x}\bar{p}_x - \bar{y}\bar{p}_y$ in Ψ_{mon} and Ψ_{quad} correspond to isotropic and anisotropic scaling velocity fields, $\mathbf{v}_{\text{mon}} \propto \bar{\mathbf{r}}$ and $\mathbf{v}_{\text{quad}} \propto \bar{x}\mathbf{e}_x - \bar{y}\mathbf{e}_y$.

Monopole oscillations from the scaling ansatz:

Neglecting self-energy corrections, we get $\Sigma = 0$, and $\bar{\mathcal{H}}_0 = (\bar{r}^2 + \bar{p}^2)/2$ using which we can easily calculate M and H_0.

$$
\text{M}_{\text{SA}}^{\text{mon}} =
\begin{pmatrix}
\langle\!\langle 1 \rangle\!\rangle & 0 & \langle\!\langle \bar{r}^2 \rangle\!\rangle & \langle\!\langle \bar{p}^2 \rangle\!\rangle \\
0 & \langle\!\langle (\bar{\mathbf{r}} \cdot \bar{\mathbf{p}})^2 \rangle\!\rangle & 0 & 0 \\
\langle\!\langle \bar{r}^2 \rangle\!\rangle & 0 & \langle\!\langle \bar{r}^4 \rangle\!\rangle & \langle\!\langle \bar{r}^2 \bar{p}^2 \rangle\!\rangle \\
\langle\!\langle \bar{p}^2 \rangle\!\rangle & 0 & \langle\!\langle \bar{r}^2 \bar{p}^2 \rangle\!\rangle & \langle\!\langle \bar{p}^4 \rangle\!\rangle
\end{pmatrix},
\tag{3.66}
$$

and:

$$
\text{H}_{0,\text{SA}}^{\text{mon}} =
\begin{pmatrix}
0 & 0 & 0 & 0 \\
0 & 0 & 2\langle\!\langle (\bar{\mathbf{r}} \cdot \bar{\mathbf{p}})^2 \rangle\!\rangle & -2\langle\!\langle (\bar{\mathbf{r}} \cdot \bar{\mathbf{p}})^2 \rangle\!\rangle \\
0 & \langle\!\langle \bar{r}^2 \bar{p}^2 - \bar{r}^4 \rangle\!\rangle & 0 & 0 \\
0 & \langle\!\langle \bar{p}^4 - \bar{r}^2 \bar{p}^2 \rangle\!\rangle & 0 & 0
\end{pmatrix},
\tag{3.67}
$$

The collision matrix elements identically vanish due to conservation of energy and momentum (see Eq. 3.54, and notice that $\text{S}[1] = \text{S}[\bar{r}^2] = 0$, $\text{S}[\bar{p}^2] = 2\Delta\bar{E}$ and $\text{S}[\bar{\mathbf{r}} \cdot \bar{\mathbf{p}}] = \bar{\mathbf{r}} \cdot \Delta\bar{\mathbf{P}}$). While it is possible to find analytic expressions for the Δ_0-averages appearing in M and H_0, we find that they all factor out from the evolution matrix using the relations $\langle\!\langle \bar{r}^2 \rangle\!\rangle = \langle\!\langle \bar{p}^2 \rangle\!\rangle$ and $\langle\!\langle \bar{r}^4 \rangle\!\rangle = \langle\!\langle \bar{p}^4 \rangle\!\rangle$ we have

here. The evolution matrix evaluates to the following simple form:

$$
\mathsf{E}^{\mathrm{mon}}_{\mathrm{SA}} = \begin{pmatrix} 0 & 0 & 0 & 0 \\ 0 & 0 & 2 & -2 \\ 0 & -1 & 0 & 0 \\ 0 & 1 & 0 & 0 \end{pmatrix}, \tag{3.68}
$$

and is independent of temperature. In the above equation, the matrix elements appear in the same order as the basis functions in Eq. (3.64). The monopole excitation operator is r^2, which gives the "excitation vector" $\delta \mathbf{U} = (0, 0, 1, 0)^T$ in the scaling ansatz basis (see the definition of $\delta \mathbf{U}$ after Eq. 3.56). Using Eq. (3.59), we finally find:

$$
\Psi_{\mathrm{mon}}(\bar{\mathbf{p}}; \bar{\mathbf{r}}, \omega) = \left[-2i\bar{\omega}(\bar{\mathbf{r}} \cdot \bar{\mathbf{p}}) + 2\bar{r}^2 - 2\bar{p}^2 \right] / (\bar{\omega}^2 - 4). \tag{3.69}
$$

The frequency of oscillations is given by the poles of the denominator, $\bar{\omega}_{\mathrm{mon}} = \pm 2$, which is a well-known result [99]. We state it without proof that extending the monopole basis has no effect on this result as long as self-energy corrections are neglected. In fact, it is a well-known fact that the full nonlinear Boltzmann equation (including collisions) admits an exact monopole solution with frequency $2\omega_0$ [99], corresponding to a nodeless scaling velocity field $\propto \mathbf{r}$. The existence of this undamped solution is deeply related to the fact that the trap potential is harmonic and the particles are assumed to have quadratic dispersions. Using dressed quasiparticle dispersions or adding an anharmoniticity to the trap potential both lead to the violation of this exact result.

We remark that besides the $\bar{\omega} = \pm 2$, the above evolution matrix admits two zero eigenvalues that correspond to eigenvector $\Psi \sim 1$ and $\Psi \sim \bar{r}^2 + \bar{p}^2$. Both of these eigenvectors correspond to unphysical excitations since they violate conservation of mass. However, it is easy to see that both lie in the null space of $\mathsf{H}^{\mathrm{mon}}_{0,\mathrm{SA}}$. Therefore, using of Eq. (3.59), we see that these unphysical modes will never be excited regardless of one's choice of excitation vector $\delta \mathbf{U}$. The number of such unphysical modes increases as one extends the variational basis set.

Quadrupole oscillations from the scaling ansatz:
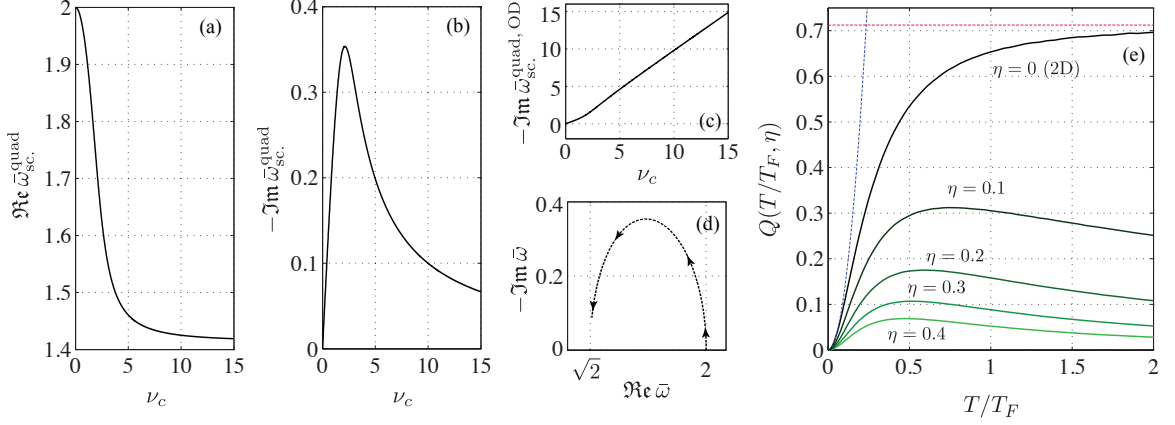
Figure 3.4: Frequency and damping of quadrupole oscillations of quasi-2D dipolar fermions in isotropic harmonic traps from the scaling ansatz analysis. (a) and (b): the frequency and damping of oscillations vs. ν_c respectively. (c) the damping rate of the overdamped component vs. ν_c. (d) the evolution of the damped oscillatory pole on the complex plane upon increasing ν_c in the range $[0, 15]$. (e) $Q(T/T_F, \eta)$ as a function of T/T_F for different values of $\eta \equiv (2N)^{\frac{1}{4}}(\omega_0/\omega_z)^{\frac{1}{2}}$. Q is related to the quadrupole collision rate as $\nu_c = N(a_d/a_0)^2 Q(T/T_F, \eta)$. The low temperature and high temperature asymptotes in the 2D limit are shown as blue and red (horizontal) dashed lines respectively.

We find the following forms for M and H_0 in the quadrupole basis:

$$
\mathsf{M}_{\mathrm{SA}}^{\mathrm{quad}} = \frac{1}{2}
\begin{pmatrix}
\langle\!\langle \bar{r}^2 \bar{p}^2 \rangle\!\rangle & 0 & 0 \\
0 & \langle\!\langle \bar{r}^4 \rangle\!\rangle & 0 \\
0 & 0 & \langle\!\langle \bar{p}^4 \rangle\!\rangle
\end{pmatrix},
\tag{3.70}
$$

and:

$$
\mathsf{H}_{0,\mathrm{SA}}^{\mathrm{quad}} = \frac{1}{2}
\begin{pmatrix}
0 & 2\langle\!\langle \bar{r}^2 \bar{p}^2 \rangle\!\rangle & -2\langle\!\langle \bar{r}^2 \bar{p}^2 \rangle\!\rangle \\
-\langle\!\langle \bar{r}^4 \rangle\!\rangle & 0 & 0 \\
-\langle\!\langle \bar{p}^4 \rangle\!\rangle & 0 & 0
\end{pmatrix}.
\tag{3.71}
$$

The order of basis functions is the same as it appears in Eq. (3.65). The only non-zero collision matrix element is $\mathscr{I}_{33}$, the rest of which vanish again due to conservation laws (see Eq. 3.54, and note that $\mathrm{S}[\bar{x}^2 - \bar{y}^2] = 0$ and $\mathrm{S}[\bar{x}\bar{p}_x - \bar{y}\bar{p}_y] = (\bar{x}\mathbf{e}_x - \bar{y}\mathbf{e}_y) \cdot \Delta\bar{\mathbf{P}})$. The collision integral can be

125

expressed as follows using the results of Appendices C.3 and C.4 (in particular, see Eq. C.33):

$$
\mathscr{I}_{33}^{\text{quad}} = - 64\pi(2N)^{\frac{1}{2}}\lambda_d^2\,\bar{T}^5 \int_0^\infty \rho^5\,\mathrm{d}\rho \int_0^{2\pi} \frac{\mathrm{d}\phi}{2\pi} \int_0^{2\pi} \frac{\mathrm{d}\phi'}{2\pi} \int_0^{\frac{\pi}{2}} \mathrm{d}\xi\;\sin^7\xi\,\cos\xi \int_0^{\frac{\pi}{2}} \mathrm{d}\nu\,\sin^5\nu\,\cos\nu
$$

$$
\times \sin^2(\phi - \phi') \left[\chi_1\,\mathrm{Erfcx}\left(2\eta\chi_1\sqrt{\bar{T}}\rho\right) - \chi_2\,\mathrm{Erfcx}\left(2\eta\chi_2\sqrt{\bar{T}}\rho\right) \right]^2
$$

$$
\times \left[\frac{1}{\cosh(\rho - \bar{\mu}/\bar{T}) + \cosh(\rho\,\sin^2\xi\,\sin 2\nu\,\cos\phi)} \; \frac{1}{\cosh(\rho - \bar{\mu}/\bar{T}) + \cosh(\rho\,\sin^2\xi\,\sin 2\nu\,\cos\phi')} \right],
$$

$$(3.72)$$

where $\chi_1 = \sin\xi\,\sin\nu\,|\sin[(\phi-\phi')/2]|$ and $\chi_2 = \sin\xi\,\sin\nu\,|\cos[(\phi-\phi')/2]|$. The above integration can not be carried out analytically in general and requires a numerical treatment. The analytical low T and high T asymptotic results are given in Appendix C.2. Note that the (dimensionless) non-interacting chemical potential $\bar{\mu}$ is given implicitly by Eq. (3.38) and only depends on the dimensionless temperature $\bar{T}$. Therefore, except for the pre-factor, the above integral is a universal function of $\bar{T}$ and η. We define the dimensionless "quadrupole collision rate" ν_c as:

$$
\nu_c \equiv -\frac{2\mathscr{I}_{33}^{\text{quad}}}{\langle\!\langle\bar{p}^4\rangle\!\rangle} \equiv N\left(\frac{a_d}{a_0}\right)^2 Q(\bar{T},\eta). \tag{3.73}
$$

The last equation also serves as the definition of the universal function $Q(\bar{T},\eta)$. The quadrupole excitation operator is $x^2 - y^2$ which yields $\delta\mathbf{U} = (0,1,0)^T$ in this basis and finally, a simple calculation similar to the monopole case yields:

$$
\Psi_{\text{quad}}(\bar{\mathbf{p}};\bar{\mathbf{r}},\omega) = \left[2\bar{\omega}(\nu_c - i\bar{\omega})(\bar{x}\bar{p}_x - \bar{y}\bar{p}_y) + 2i(\nu_c - i\bar{\omega})(\bar{x}^2 - \bar{y}^2) + 2\bar{\omega}(\bar{p}_x^2 - \bar{p}_y^2)\right]/\mathfrak{D}_{\text{quad}}(\bar{\omega},\nu_c),
$$

$$(3.74)$$

where $\mathfrak{D}_{\text{quad}}(\bar{\omega},\nu_c)$ is the quadrupole characteristic equation and is given by:

$$
\mathfrak{D}_{\text{quad}}(\bar{\omega},\nu_c) = \bar{\omega}(\bar{\omega}^2 - 4) + i\nu_c(\bar{\omega}^2 - 2). \tag{3.75}
$$

The roots of $\mathfrak{D}_{\text{quad}}(\bar{\omega},\nu_c)$ determine the frequency and damping of quadrupole oscillations. We note that Eq. (3.74), along with the characteristic equation given above, are "generic" results in the sense that one obtains the same expression for quadrupole oscillations independent of the specific

form of interactions. For instance, Refs. [98] and [103] obtain the same characteristic equation for s-wave fermions and a classical gas respectively. The model-specific details are encoded in the collision rate ν_c. Therefore, it is worthwhile to review the generic features of the quadrupole oscillations from Eq. (3.74) in terms of ν_c as a first step. We return to the analysis of ν_c afterwards.

Two important limits can be recognized for quadrupole oscillations. The collisionless limit is achieved for $\nu_c \to 0$:

$$\lim_{\nu_c \to 0} \Psi_{\text{quad}}(\bar{\mathbf{p}}; \bar{\mathbf{r}}, \omega) \equiv \Psi_{\text{quad}}^{\text{CL}}(\bar{\mathbf{p}}; \bar{\mathbf{r}}, \omega) = \left[-2i\bar{\omega}(\bar{x}\bar{p}_x - \bar{y}\bar{p}_y) + 2(\bar{x}^2 - \bar{y}^2) - 2(\bar{p}_x^2 - \bar{p}_y^2) \right]/(\bar{\omega}^2 - 4).$$

$$(3.76)$$

Notice the formal similarity to the monopole case. In this limit, we obtain undamped oscillations at $\omega_{\text{quad}}^{\text{CL}} = 2\omega_0$ which correspond to the free motion of particles in the trap. In the limit of very fast collisions, $\nu_c \to \infty$, we find:

$$\lim_{\nu_c \to \infty} \Psi_{\text{quad}}(\bar{\mathbf{p}}; \bar{\mathbf{r}}, \omega) \equiv \Psi_{\text{quad}}^{\text{HD}}(\bar{\mathbf{p}}; \bar{\mathbf{r}}, \omega) = \left[-2i\bar{\omega}(\bar{x}\bar{p}_x - \bar{y}\bar{p}_y) + 2(\bar{x}^2 - \bar{y}^2) \right]/(\bar{\omega}^2 - 2), \quad (3.77)$$

which describes undamped oscillations at a frequency $\omega_{\text{quad}}^{\text{HD}} = \sqrt{2}\omega_0$. This is the well-known quadrupole "surface" mode which is also obtained by solving ideal hydrodynamics equations for harmonically trapped gases [100]. Although we have neglected self-energy corrections here, it can be shown that the frequencies of these hydrodynamical modes are universal since they do not change the density in the bulk, are confined to the surface, and are entirely driven by the trap restoring force [100]. We will observe this universality in later sections, where we include self-energy corrections and still obtain the same oscillation frequency in the HD limit.

Except for the two ideal limits discussed so far, quadrupole oscillations are otherwise damped for any finite value of ν_c. For large nu_c (near HD), this is due to the fact that the collisions are not fast enough to maintain the local equilibrium and thus lead to dissipation. For small ν_c (near CL), collisions result in a friction between the otherwise freely moving particles and again lead to

dissipation. In general, the oscillation frequency and damping rate can be found by analyzing the roots $\mathfrak{D}_{\text{quad}}(\bar{\omega}, \nu_c)$. Fig. 3.4a-c show the real and imaginary parts of the poles as a function of ν_c. In the limit $\nu_c \ll 1$, the three poles are approximately located at:

$$\pm \left(2 - \frac{5\nu_c^2}{64} \right) - \frac{i\nu_c}{4} + \mathcal{O}(\nu_c^5), \quad -\frac{i\nu_c}{2} + i\mathcal{O}(\nu_c^3). \tag{3.78}$$

The first two poles describe a damped oscillatory mode at a frequency slightly lower than $2\omega_0$ and a damping rate of $\sim \nu_c \omega_0/2$. The third pole corresponds to an over-damped component. In the other limit $\nu_c \gg 1$, we get:

$$\pm \left(\sqrt{2} + \frac{3}{2\sqrt{2}\nu_c^2} \right) - \frac{i}{\nu_c} + \mathcal{O}(\nu_c^{-3}), \quad -i\nu_c + i\mathcal{O}(\nu_c^{-1}). \tag{3.79}$$

Again, the first two poles describe a damped oscillatory mode at a frequency slightly higher than $\sqrt{2}\omega_0$ and a damping rate of $\sim \nu_c^{-1}\omega_0$, accompanied by a (highly) over-damped component with a damping rate of $\omega_0 \nu_c$. Studying the residues of the over-damped poles, we find that the contribution of the this component is $\propto \nu_c^2$ and $\propto \nu_c^{-2}$ to leading order in the CL and HD limits respectively and has its maximum contribution in the CL-HD crossover regime. We associate the presence of such an over-damped component to the initial high energy excitations. Fig. 3.4d shows the evolution of the first pole on the complex frequency plane upon increasing ν_c: it starts off on $2\omega_0$, moves to the lower half plane and finally returns to the real axis at the hydrodynamic frequency $\sqrt{2}\omega_0$.

We finally turn to the analysis of $Q(\bar{T}, \eta)$, the universal function that controls the quadrupole collision rate ν_c for dipole-dipole interactions (Eq. 3.73). ν_c can be identified with different quantities in different regimes. In the collision dominated regime (i.e. $\nu_c \gg 1$) where a viscous hydrodynamic description is admissible, the shear viscosity sum rule yields ν_c as $\omega_0 \langle P/\eta_s \rangle_{\text{trap}}$, where P, η_s and ω_0 are the local pressure, shear viscosity and the trap frequency respectively [81]. By $\langle \ldots \rangle_{\text{trap}}$, we imply averaging over the trap. In the classical regime ($T \gg T_F$), one finds $\nu_c \sim \tau_c^{-1}$ where τ_c is the typical time between two single-particle collisions [98]. This can be established by replacing

the Fermi-Dirac with Boltzmann-Maxwell distribution and evaluating the collision integral in the saddle-point approximation.

We have calculated Q for several values of η as a function of $\bar{T}$ by evaluating the five dimensional integral appearing in Eq. (3.72) numerically. The results are shown in Fig. 3.4e. The asymptotic behavior of Q can be found analytically in the low and high temperature regimes and is given in Appendix C.2 in the 2D limit ($\eta = 0$). They appear on the same figure as red and blue dashed lines. We find that $Q \sim \bar{T}^2$ for small T while it saturates to a constant value for large $\bar{T}$. The low temperature T^2 scaling is related to Pauli blocking, however, it is different from the case of 2D s-wave fermions (and 2D paramagnetic electron gas), where one finds $\nu_c \sim T^2 \log(T/T_F)^{-2}$ [81, 104]. This difference can be traced back to the fact that the system investigated here is spin polarized and the s-wave scattering channel is blocked. The logarithmic enhancement of the shear viscosity (i.e. attenuation of ν_c) originates from the logarithmic divergence of the s-wave scattering length in the near-threshold regime in 2D. We remark that the near-threshold cross section of all other scattering channels remains bounded [93], leading to a bounded Born cross section.

The high temperature plateau is a unique feature of near-threshold dipole-dipole scatterings in the 2D limit and its existence can be understood in terms of the interplay between the temperature dependence of the scattering cross section and rarefaction of the gas. Provided that $T_F \ll T \ll T_{\mathrm{dip}}$, we can estimate the relaxation rate using the aforementioned identification $\nu_c \sim \tau_c^{-1}$. The Born 2D scattering cross section scales like $\sigma_{\mathrm{B}} \sim q^{-1}|\tilde{\mathcal{V}}(q)|^2 \sim qa_d^2 \mathrm{Erfcx}^2(qa_z)$, where q is the typical momentum of scattering particles and is $\sim (mk_BT)^{1/2}$ in the high temperature regime. The collision frequency is $\tau_c^{-1} \sim \hbar q l_{\mathrm{mfp}}^{-1} \equiv \hbar qn\sigma$, where $l_{\mathrm{mfp}} = (n\sigma)^{-1}$ is the mean free path. The density at the center of the trap is $n_0 = m\omega_0^2 N/(2\pi T)$ and decreases as $1/T$. Combining these results, the collision rate amounts to:

$$\nu_c \sim N \left(\frac{a_d}{a_0}\right)^2 \mathrm{Erfcx}^2\left[\left(\frac{k_BT}{\hbar\omega_z}\right)^{\frac{1}{2}}\right], \quad (T_F \ll T \ll T_{\mathrm{dip}}) \tag{3.80}$$

In the $2D$ limit, $\omega_z \to \infty$ and we find $\nu_c = \text{const}$ (note that $\text{Erfcx}(0) = 1$). In other words, the growth of scattering cross section counteracts rarefaction of the gas to yield a constant collision rate. For finite ω_z, the scattering cross section starts to decrease once $k_B T \gtrsim \hbar \omega_z$ and consequently, ν_c decays like $\sim 1/T$ (note that $\text{Erfcx}(x) \sim 1/x$ for large x). We remark that the single band picture adopted here is no longer valid in the quasi-2D regime for $k_B T \gtrsim \hbar \omega_z$ and one must take into account the higher bands as well. We have shown in a previous paper [105] that all inter-band interaction matrix elements have the same long wavelength behavior and therefore, we expect this scaling result to remain unaffected. The plateau reached in the 2D limit relies crucially on the applicability of Born approximation. As mentioned earlier, the scatterings enter the semi-classical regime for $T \gtrsim T_{\text{dip}}$ (see Eq. 3.29) and Born approximation breaks down. In this regime, the total scattering cross section can be estimated using the Eikonal approximation [92] and one finds $\sigma_{\text{SC}} \sim (a_d/q)^{1/2}$. Repeating the same analysis with the semi-classical cross section, we find:

$$\nu_c \sim N \left(\frac{a_d}{a_0} \right)^{\frac{1}{2}} \left(\frac{\hbar \omega_0}{k_B T} \right)^{\frac{3}{4}}, \qquad (T \gtrsim T_{\text{dip}}). \tag{3.81}$$

The qualitative behavior of ν_c for the full range of temperatures was shown earlier in Fig. 4.18b1.

So far, we have neglected self-energy corrections in the description of the collective modes. We have also restricted our analysis to a variational calculation within a small basis set. In the next section, we extend our analysis to address both of these shortcomings.

3.4.3 Extended basis analysis: the effect of higher order moments and self-energy corrections

The general formalism described in Sec. 3.4 allows one to include self-energy corrections and to obtain a more accurate calculation of the response functions by extending the variational basis set in a controlled way. Using simple symmetry considerations, we introduce extensible polynomial-like

variational basis sets relevant for describing monopole and quadrupole dynamics. Finite truncations of these basis sets allows one to satisfy all phase-space moments of the CBV equation up to the truncation order. Since we are dealing with large basis sets and self-energy corrections at finite temperatures, resorting to numerical methods is inevitable at this stage and no simple analytic results are expected to be found.

Our goal here is to evaluate the linear responses accurately within the approximations made so far. In practice, the reliability of the approximate linear response functions obtained using the method of moments depends on one's choice of the basis functions. This choice can be motivated by the symmetries of the perturbing potential and the equilibrium state. Here, the trap potential is assumed to be isotropic and it is easy to see that $[\mathscr{D}, L_z] = [\mathscr{I}, L_z] = 0$, where $L_z \equiv L_z^{(r)} + L_z^{(p)}$, and $L_z^{(r)} = i(x\partial_y - y\partial_x)$ and $L_z^{(p)} = i(p_x\partial_{p_y} - p_y\partial_{p_x})$ are the rotation operators in the coordinate and momentum space respectively. Therefore, if δU lies in a certain eigenspace of L_z, so will the solution of the linearized equation Ψ and one may choose the basis functions from the same eigenspace. Another symmetry which is preserved by the CBV equation is the reflection symmetry. Defining the x-reflection operator as $R_x\Psi(p_x, p_y; x, y) = \Psi(-p_x, p_y; -x, y)$, it is easy to show that the linearized evolution operator commutes with R_x as well. We will utilize these observations to define appropriate (and extensible) basis sets for monopole and quadrupole dynamics in the next two sections.

Variational basis set for monopole oscillations:

The generator of monopole oscillations, $\delta U_m \sim r^2$, belong to the zero angular momentum representation of L_z. An arbitrary function of such type can be expressed as $f(p, r)[(x + iy)(p_x - ip_y)]^n$ for $n \in \mathbb{Z}$ and arbitrary $f(p, r)$. Any smooth function of this type can be written as a power series expansion in r^2, p^2, $\mathbf{r} \cdot \mathbf{p}$ and $\xi \equiv yp_x - xp_y$. Observing that $\xi^2 = r^2p^2 - (\mathbf{r} \cdot \mathbf{p})^2$, the most

general basis for such functions can be constructed from the following two classes:

$$\phi_\alpha^+ \equiv \phi_{(m_\alpha, n_\alpha, k_\alpha)} = r^{2m_\alpha}\, p^{2n_\alpha} (\mathbf{r} \cdot \mathbf{p})^{k_\alpha},$$

$$\phi_\alpha^- \equiv \phi_{(m_\alpha, n_\alpha, k_\alpha)} = \xi\, r^{2m_\alpha}\, p^{2n_\alpha} (\mathbf{r} \cdot \mathbf{p})^{k_\alpha}. \tag{3.82}$$

Observing that $R_x \phi_\alpha^\pm = \pm \phi_\alpha^\pm$ and the fact that the equilibrium state and the perturbations are reflection symmetric, we discard $\{\phi_\alpha^-\}$. We define $\{\phi_\alpha^+\}$ as the "extended monopole basis" and drop the $+$ superscript for brevity. To truncate the basis set, we keep all basis functions satisfying $m + n + k \leq M$, where M is a positive integer which we call the order of the basis set. A first order basis set contains four elements, $\{1, \mathbf{r} \cdot \mathbf{p}, p^2, r^2\}$ and is equivalent to the linearized scaling ansatz discussed earlier. In general, a basis set of order M has $(M + 1)(M + 2)(M + 3)/6$ elements. Expressions useful for numerical evaluation of the matrix elements of M, H$_0$, Σ and I$_c$ in the monopole basis are given in Appendix C.3.

Variational basis set for quadrupole oscillations:

By definition, a quadrupole (d-wave) function in two dimensions changes sign upon a simultaneous $\pi/2$ rotation of both $\mathbf{r}$ and $\mathbf{p}$. Such functions belong to the $m_z = \pm 2$ representation of L_z which can be expressed as $f(p, r)\, e^{iM\phi_r}\, e^{iN\phi_p}$, where M and N are two integers such that $M - N = \pm 2$, ϕ_r and ϕ_p are the angles $\mathbf{r}$ and $\mathbf{p}$ make with a fixed axis (we arbitrarily choose the x-axis) and $f(p, r)$ is an arbitrary scalar function of $\mathbf{p}$ and $\mathbf{r}$. One can identify 12 classes of functions with such symmetry. Apart from the arbitrary scalar function $f(p, r)$, the accompanying multipliers can be:

$$\xi_1^+ \equiv x^2 - y^2, \quad \xi_2^+ \equiv p_x^2 - p_y^2, \quad \xi_3^+ \equiv xp_x - yp_y,$$

$$\eta_1^+ \equiv xy(yp_x - xp_y), \quad \eta_2^+ \equiv p_x p_y(yp_x - xp_y),$$

$$\eta_3^+ \equiv (yp_x + xp_y)(yp_x - xp_y),$$

and:

$$\xi_1^- \equiv xy, \quad \xi_2^- \equiv p_x p_y, \quad \xi_3^- \equiv yp_x + xp_y,$$

$$\eta_1^- \equiv (yp_x - xp_y)(x^2 - y^2), \quad \eta_2^- \equiv (yp_x - xp_y)(p_x^2 - p_y^2),$$

$$\eta_3^- \equiv (yp_x - xp_y)(xp_x - yp_y).$$

The functions with $+$ and $-$ superscript are even and odd eigenfunctions of the reflection operator R_x, respectively. Like before, we drop the second class. Also, we find the following relations between these pre-factors:

$$2\eta_1^+ = r^2 \xi_3^+ - (\mathbf{r} \cdot \mathbf{p})\,\xi_1^+,$$

$$2\eta_2^+ = (\mathbf{r} \cdot \mathbf{p})\,\xi_2^+ - p^2\,\xi_3^+,$$

$$2\eta_3^+ = r^2\,\xi_2^+ - p^2\,\xi_1^+, \tag{3.83}$$

using which we can drop the class of functions $f(p, r)\,\eta_i^+$ from the basis set. Since $f(p, r)$ is assumed to be a smooth scalar function of $\mathbf{p}$ and $\mathbf{r}$, in can be expanded in the monopole basis. Thus, in summary, we find that any smooth reflection symmetric quadrupolar function can be expanded in terms of $\{\xi_i^+ \phi_\alpha^+\}$ for $i = 1, 2, 3$ and $\alpha = (m, n, k)$, where m, n and k are non-negative integers and ϕ_α^+ are the previously introduced monopole basis functions. We denote this basis set as the "extended quadrupole basis". We also remark that this basis set can be reduced further in light of the relation $2(\mathbf{r} \cdot \mathbf{p})\,\xi_2^+ = p^2 \xi_1^+ + r^2 \xi_3^+$, so that the basis functions of the type $\xi_2^+\,r^{2m} p^{2n}(\mathbf{r} \cdot \mathbf{p})^{k+1}$ can be written as a linear combination of $\xi_1^+\,r^{2m} p^{2n+2}(\mathbf{r} \cdot \mathbf{p})^k$ and $\xi_3^+\,r^{2m+2} p^{2n}(\mathbf{r} \cdot \mathbf{p})^k$. Like before, we drop the $+$ superscript for brevity in the remainder of the paper. An order-M truncation of the quadrupole basis set is the finite set that comprises all quadrupole basis functions satisfying $k + m + n \leq M - 1$. The first order basis set contains three elements, $\{x^2 - y^2, p_x^2 - p_y^2, xp_x - yp_y\}$ and is equivalent to the linearized scaling ansatz discussed earlier. In general, a quadrupole basis set of order M contains $M(M + 1)(2M + 7)/6$ elements. Again, expressions useful for numerical calculation of the matrix elements of M, H_0, Σ and I_c in the quadrupole basis are given in Appendix C.4.

Numerical implementation:

In this section, we present the numerical results obtained by calculating the linear responses to monopole and quadrupole perturbations using the extended basis set approach. We varied λ_d and T/T_F in the range $(0, 2)$ at fixed $N = 2200$. We studied the 2D limit $\omega_z = \infty$ as well as a quasi-2D case corresponding to the current experiments with KRb ($\omega_0 = 2\pi \times 36\,\text{Hz}$, $\omega_z = 2\pi \times 23\,\text{kHz}$ [15, 16, 17]). This choice of parameters yields $\eta \simeq 0.322$ in the quasi-2D case.

For each configuration, we performed the calculations within a forth order basis set comprising 35 and 50 basis functions for the monopole and quadrupole cases respectively, and satisfying all phase-space moments of the CBV equation up to the eighth order. The matrix elements of M, H_0 and Σ can be calculated with little computational effort using the expressions provided in Appendices C.3 and C.4 and the previously obtained equilibrium solutions. The most computationally demanding part is the evaluation of the collision matrix elements. Although a considerable number of them vanish either due to symmetries or conservation laws, a forth order basis set still requires calculation of 118 (monopole) and 307 (quadrupole) unique collision matrix elements, each of which is a five-dimensional integral that has to be evaluated for each choice of λ_d, η and T/T_F. Such a task clearly requires considerably more computational effort compared to the simple scaling ansatz analysis we presented earlier, where only a single collision matrix element had to be dealt with.

We calculated the collision matrix elements using the Monte-Carlo integration method with 5×10^8 integration points yielding a relative statistical error of less than 10^{-3}. We incorporated the dressed quasiparticle dispersions into the collision integral within a local effective mass approximation (see Appendix C.3) which we found to be an excellent approximation in all cases. However, in order to assess the accuracy of this approximation and the consistency of the obtained results, we (1) we performed exact calculation of the collision integrals for a few representative cases using an extrapolation technique (see Appendix C.5), and (2) checked the satisfaction of conservation laws. We will discuss both of these consistency checks later.

For the monopole case, we calculated the dimensionless spectral function $A_{x^2+y^2}(\omega)$ defined as:

$$A_{x^2+y^2}(\omega) \equiv -(2N)^{-\frac{1}{2}} \mathfrak{Im}[\chi_{x^2+y^2}(\omega)], \qquad (3.84)$$

This quantity can be found using Eqs. (3.57) and (3.59) by choosing the excitation and observation vectors as $\delta U_\alpha = O_\alpha = \delta_{m\alpha}$, where m is the index that corresponds to the basis function $\phi = r^2$. For the quadrupole case, we calculated the spectral function $A_{x^2-y^2}(\omega)$ defined as:

$$A_{x^2-y^2}(\omega) \equiv -(2N)^{-\frac{1}{2}} \mathfrak{Im}[\chi_{x^2-y^2}(\omega)]. \qquad (3.85)$$

Likewise, this quantity can be evaluated by choosing the excitation and observation vectors as $\delta U_\alpha = O_\alpha = \delta_{q\alpha}$, where q is the index that corresponds to the basis function $\phi = \xi_1 = x^2 - y^2$. These spectral functions can be directly measured in the experiments in different ways (Ref. to Sec. 3.5).

Although the evolution matrix has a large number of eigenmodes, some of which are isolated in the complex plane and some may belong to branch lines, only a few of them get excited and contribute to the response. Many of the modes lie inside the null space of H_0, are unphysical and do not get excited (see the discussion at the end of Sec. 3.4.2). In all cases, we found that the spectral functions can be reproduced accurately by a fit function with two simple poles in the lower half plane:

$$A_{\text{fit}}(\omega) = \mathfrak{Im}\left[\frac{\mathcal{A}}{\omega - \Omega - i\Gamma} - \frac{\mathcal{A}^*}{\omega + \Omega - i\Gamma} + \frac{i\mathcal{B}}{\omega - i\Gamma'} \right], \qquad (3.86)$$

corresponding to damped oscillations with a frequency and damping rate of Ω and Γ respectively, and a possibly overdamped component with a decay rate of Γ'. The overdamped component is only present in the quadrupole response. The above model extracts the most important features of the numerically obtained spectral functions and also allows us to present the obtained results in a concise way. Although we kept up to eight moments (and in some cases, up to twelve moments) of the CBV equation, we found the inclusion of sixth order moments (and above) to result in relative
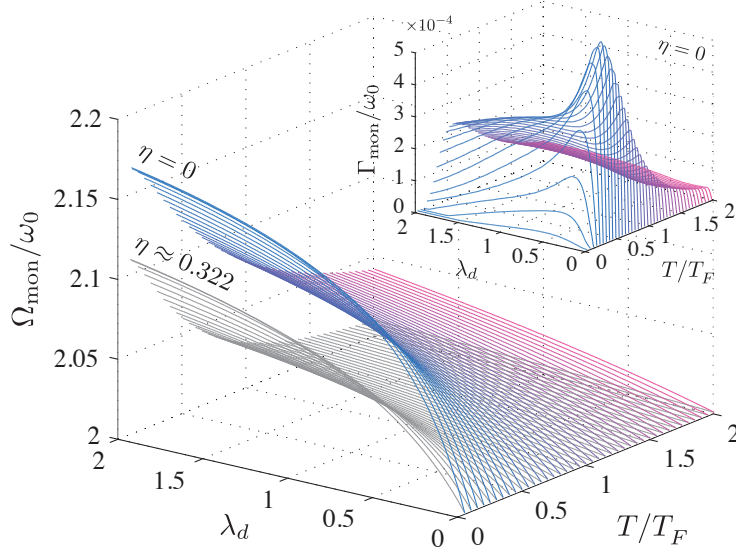
Figure 3.5: The oscillation frequency and the damping (inset) of the monopole excitations extracted from the numerically obtained spectral functions using a forth order basis set (including self-energy corrections). The colored and grayscale (upper and lower) graphs correspond to an ideal 2D system ($\eta = 0$) and a quasi-2D system ($\eta \simeq 0.322$) respectively. Blue and red line colors correspond to low and high temperatures respectively. In all cases, $N = 2200$. The inset plot shows the damping rate in the 2D case ($\eta = 0$).

refinements to the frequency of the first and second excited modes which are smaller than 10^{-3} and 10^{-2} respectively in all cases.

Monopole oscillations:

As mentioned earlier in Sec. 3.4.2, without self-energy corrections, the CBV equation for harmonically trapped gases admits an exact solution corresponding to a scaling velocity field $\mathbf{v} \sim \mathbf{r}$ which has a fixed oscillation frequency of $2\omega_0$ with no damping, independent of the interaction strength and temperature. This is due to fact that the Boltzmann equation admits a rigorously closed set of equations for the phase-space averages of r^2, p^2 and $\mathbf{r} \cdot \mathbf{p}$, all of which are unaffected by collisions due to conservation laws. Taking self-energy corrections into account, the quasiparticle dispersions no longer remain quadratic and one finds that this simple chain of moment equations can not be closed anymore. In particular, contributions from higher order moments, many of which
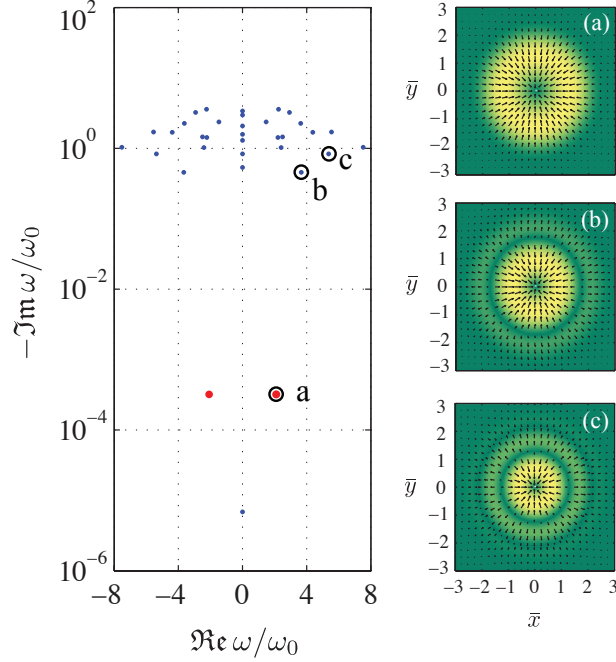
Figure 3.6: (left) A typical picture of the poles of the evolution matrix ($T/T_F = 0.45$, $\lambda_d = 2$, $N = 2200$ and $\eta = 0$). (right) the mass currents associated to the indicated poles. Yellow (bright) and green (dark) background colors indicate large and small current magnitudes, respectively. The three indicated poles (a, b, and c) have the largest residues in the monopole response function and are also the lowest lying modes that survive in the collision dominated regime.

are strongly influenced by the collisions, become important. Therefore, we expect the monopole oscillations to be damped to a certain degree.

Fig. 3.5 shows the frequency and damping of the monopole oscillations extracted from the numerically obtained spectral functions. The colored and grayscale (top and bottom) plots correspond to the 2D limit ($\eta = 0$) and a quasi-2D sample ($\eta \simeq 0.322$). The repulsive dipole-dipole interactions clearly result in a significant increase in the oscillation frequency. Also, as one expects, finite transverse confinement leads to a weaker effective repulsive effective interaction and thus, a smaller increase in the frequency of collective modes.

Fig. 3.6 shows a typical plot of the poles of the evolution matrix as well as the mass currents associated to the three lowest lying modes that get excited by the monopole perturbation. The lowest

Figure 3.7: The evolution of the two lowest lying monopole modes upon increasing T at fixed $\lambda_d = 1$ and $N = 2200$. The temperature is uniformly increased from $T/T_F = 0.05$ to 2 with 0.05 increments. $\omega^{(n)}$ and $\gamma^{(n)}$ denote the real and imaginary parts of the complex eigenvalue. The arrows indicates the direction of increasing T. (a) and (b) correspond to the $n = 0$ and $n = 1$ modes respectively for a 2D system ($\eta = 0$). (c) and (d) show the same quantities for a sample quasi-2D system ($\eta \approx 0.322$). While the 2D system reaches a plateau for $T \gg T_F$ (indicated by P), the quasi-2D system eventually becomes collisionless, i.e. $\gamma_{\text{mon}}^{(i)} \to 0$, $\omega_{\text{mon}}^{(n)} \to 2(n+1)\,\omega_0$. The dashed lines show this expected behavior qualitatively.

lying mode (indicated by "a" and having a nodeless mass current) makes the most contribution. In fact, the relative spectral weight of all other modes are generally found to be less than $\sim 10^{-3}$ in all cases. We label the monopole modes according to the number of nodes in their mass current, i.e. (a), (b) and (c) correspond to $n = 0$, 1 and 2 respectively.

The most intriguing finding is that the nodeless mode exhibits a negligible damping in all of the studied cases despite the presence of remarkably large self-energy corrections ($\Gamma_{\text{mon}} < 10^{-3}\omega_0$, see the inset plot of Fig. 3.5). This is, however, not the case for the higher order modes. Fig. 3.7 shows the evolution of $n = 0$ and $n = 1$ modes upon increasing T at fixed λ_d for a 2D (a and b) and a quasi-2D system (c and d). The behavior of the $n = 0$ mode is similar in 2D and quasi-2D: the
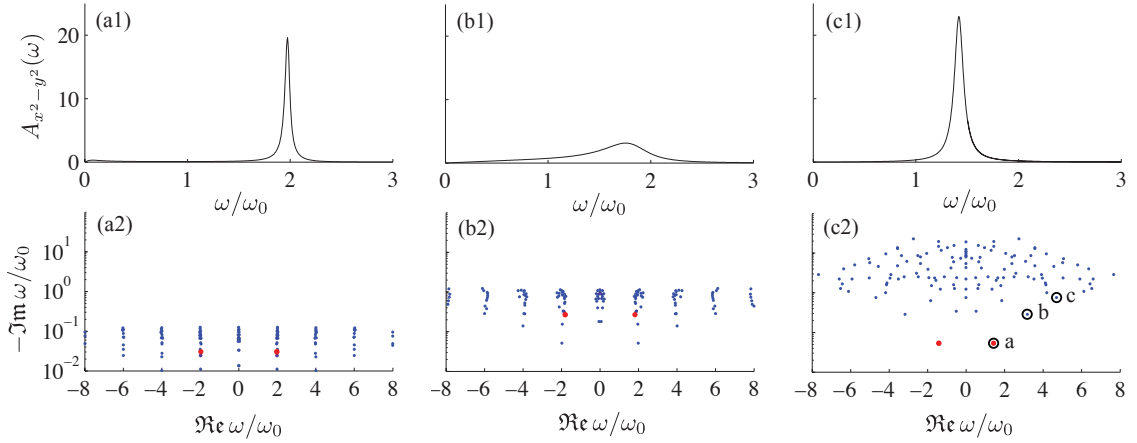
Figure 3.8: Evolution of the quadrupole oscillations from collisionless (CL) to hydrodynamic (HD) regime upon increasing the interaction strength (left to right). In all cases, $T/T_F = 0.45$ and $\eta = 0$ ($\omega_z = \infty$). The top row shows the quadrupole spectral function and the bottom row shows the location of the poles of the evolution matrix on the complex plane. The pole shown as red is the pole that makes the dominant contribution to the response. (a1) and (a2): $\lambda_d = 0.1$, (b1) and (b2): $\lambda_d = 0.4$, (c1) and (c2): $\lambda_d = 2$. See Fig. 3.9 for a plot of the mass currents associated to the encircled poles. Refer to Sec. 3.5 for a discussion on the experimental methods of measuring the spectral functions.

rise in temperature reduces the self-energy effects and the frequency approaches its non-interacting value of $2\omega_0$. The damping remains small $\sim 10^{-4}\omega_0$ and exhibits a peak around $T \sim T_F$. While the mode eventually becomes collisionless in quasi-2D (for $T \gg \hbar\omega_z$), on the contrary, it reaches a plateau in 2D. The difference between 2D and quasi-2D systems is more striking for $n = 1$ and higher order modes: upon increasing T, while the frequency of oscillations monotonically decreases in 2D until it reaches the plateau, it has a non-monotonic behavior in quasi-2D. Initially, it decreases due to enhanced collisions and reduced self-energy effects. Once $T \sim \hbar\omega_z$, the collision rate starts to decrease and the mode eventually becomes collisionless. A qualitative account of this behavior was given in Sec. 3.4.2. Finally, we note that the character of the plateau in 2D is determined by λ_d and N, and the modes in the plateau may lie anywhere in the CL-HD spectrum.

In summary, we find that the monopole response is governed predominantly by the lowest lying (nodeless) mode, with the higher order modes capturing a relative spectral weight of less than 10^{-3}.
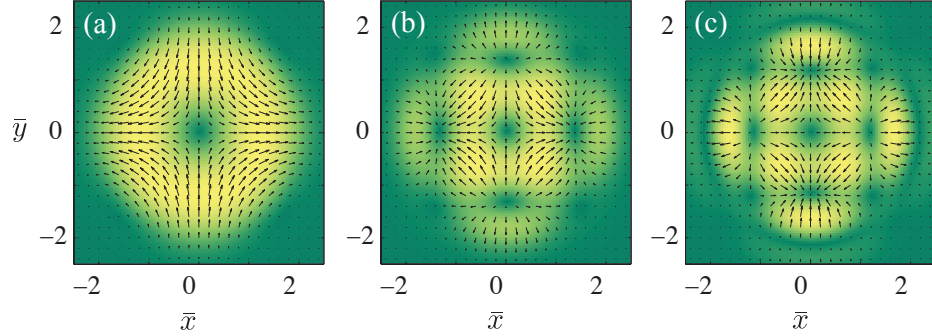
Figure 3.9: The mass current associated to the three modes marked in Fig. 3.8c2. Yellow (bright) and green (dark) shades indicate large and small current magnitudes, respectively. (a) is the lowest lying mode, known as the surface mode, characterized by the velocity field $\mathbf{v} \sim x\mathbf{e}_x - y\mathbf{e}_y$. (b) and (c) are the next two modes. The nodal structure of the mass current is clearly noticeable.

The collisional effects play a little role in defining the character of this dominant mode. In contrast, the higher order modes are found to be significantly affected by collisions. They undergo a transition from the collisionless to the hydrodynamic regime.

Quadrupole oscillations:

In the previous section, we found that the nodeless monopole mode is essentially immune to collisions. This is not the case for the nodeless quadrupole mode. The scaling ansatz analysis presented earlier already shows that this mode is in fact strongly affected by collisions. Similar to the monopole case, we find that quadrupole perturbations of the trap potential primarily excite the lowest lying quadrupole mode and the relative spectral weight of higher order modes are generally less than 10^{-3}. In this case, however, we find a small but significant contribution from a few overdamped modes, specially in the crossover regime. This is in agreement with the scaling ansatz analysis.

A typical scenario for the quadrupole response is shown in Fig. 3.8. The top and bottom rows show the quadrupole spectral function and the location of the poles on the complex frequency plane respectively. For weak interactions ($\lambda_d \ll 1$, Fig. 3.8a1-2), the spectral function is sharply peak
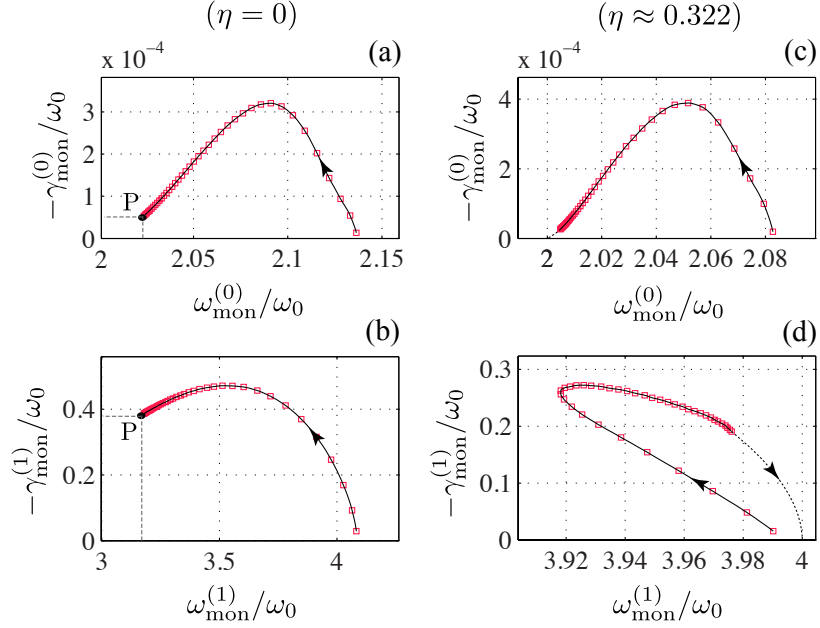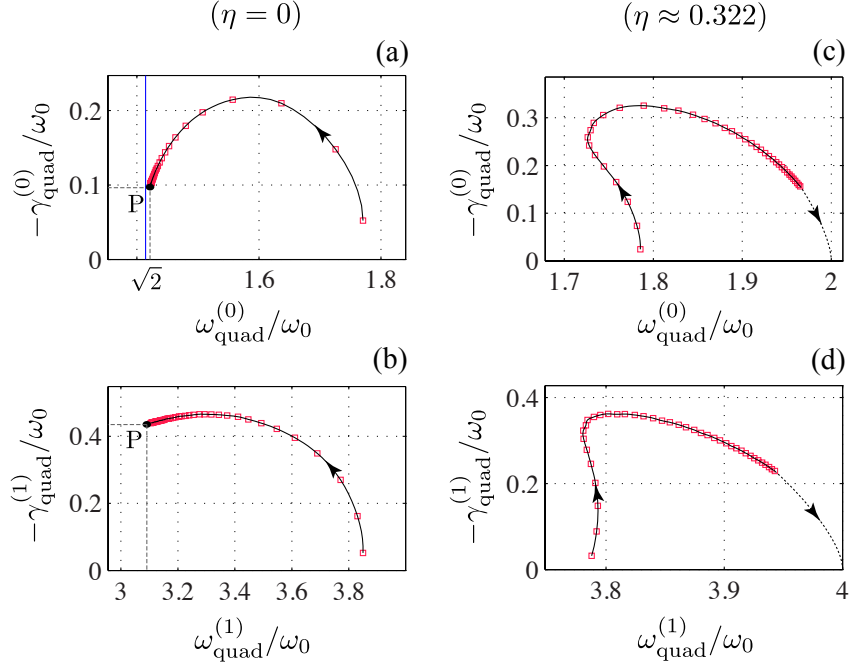
Figure 3.10: The evolution of the two lowest lying quadrupole modes upon increasing T for fixed $\lambda_d = 1$ and $N = 2200$. See the caption of Fig. 3.7 for the description of various panels. The blue line in (a) denotes $\sqrt{2}\omega_0$, the frequency of quadrupole surface mode.

around $2\omega_0$ and the poles of the evolution matrix lie very close to the real axis about their colli-sionless frequencies. Upon increasing the interactions, the poles spread to the lower half complex frequency plane, indicating entrance to the dissipative CL-HD crossover regime. The spectral func-tion is significantly broadened (see Fig. 3.8b1) in this regime. For stronger interactions, the local equilibrium picture starts to emerge, indicated by a reduction in damping. Fig. 3.8c2 clearly shows a sharply peaked spectral function near $\sqrt{2}\omega_0$ in the strongly interacting regime. This is exactly the universal frequency of the hydrodynamic quadrupole surface mode discussed earlier.

Fig. 3.9 shows the mass currents associated to the three lowest lying modes marked in Fig. 3.8c2. The axially averaged mass currents have $n = 0$, 1 and 2 nodes respectively. Fig. 3.10 shows the evolution of the first two upon increasing the temperature for a 2D and a quasi-2D case. Both modes are strongly influenced by collisions and their qualitative behavior is similar to the $n = 1$ monopole mode discussed in the previous section. While these modes eventually become collisionless in
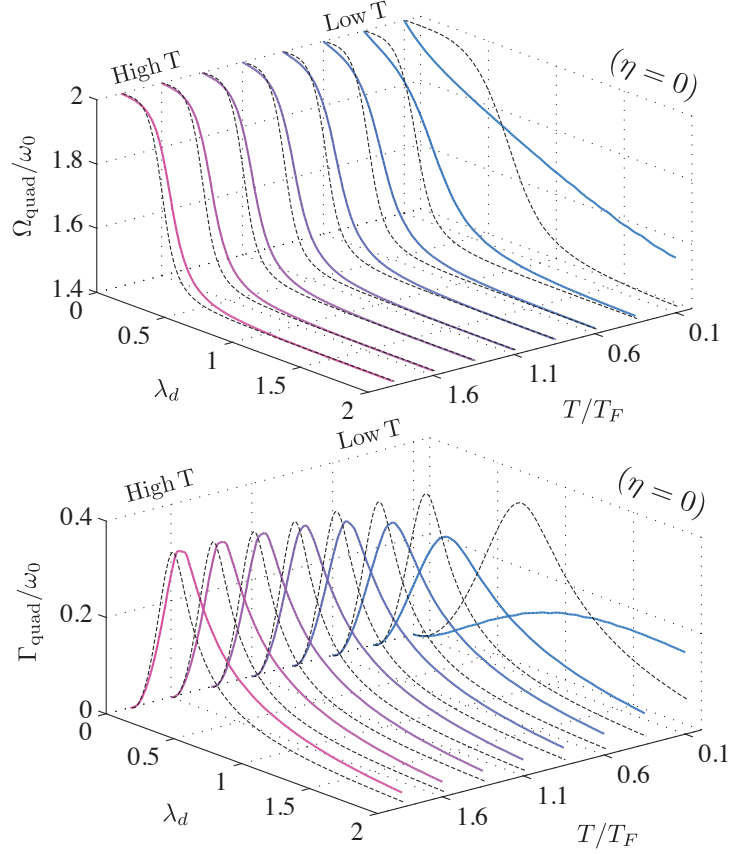
Figure 3.11: Frequency and damping (top and bottom graphs respectively) of quadrupole oscillations in a 2D system ($\eta = 0$) with $N = 2200$ particles. The solid colored lines are the numerical results obtained using a forth order basis set, including self-energy corrections. The red and blue line colors denote high and low temperatures respectively. The dashed black lines correspond to the analytic scaling ansatz analysis presented earlier (Sec. 3.4.2).

quasi-2D for $T \gg \hbar\omega_z$, they reach a plateau for $T \gg T_F$ in 2D [marked with P in (a) and (b)].

Figs. 3.11 and 3.12 show the frequency and damping rate of the quadrupole oscillations obtained from the fit to the quadrupole spectral function, in 2D and quasi-2D respectively. The result from the previous scaling ansatz analysis without self-energy corrections is also shown as dashed black lines for reference. Since the quadrupole spectral function is virtually exhausted by the nodeless mode, these plots essentially show the interaction- and temperature-dependence of the nodeless mode.

The refinements arising from inclusion of both self-energy corrections and higher order moments are significant. In the low temperature regime, self-energy corrections are dominant and yield a
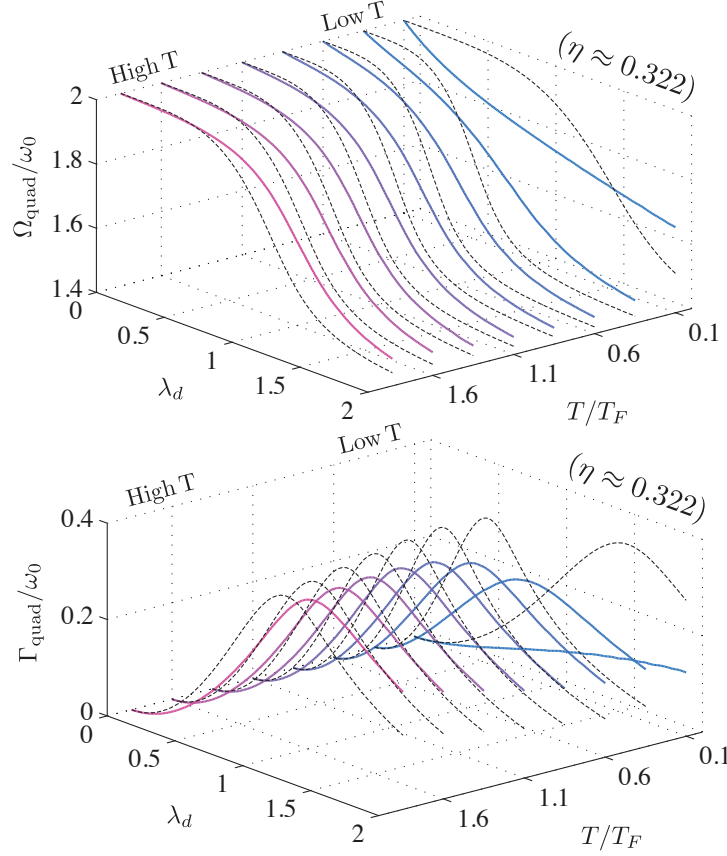
Figure 3.12: Frequency and damping of quadrupole oscillations for a quasi-2D system corresponding to $\eta \simeq 0.322$ (refer to the caption of Fig. 3.11 for details)

$\propto \lambda_d$ shift of the frequencies (see the rightmost plot on the top panel of Fig. 3.11). The collisional corrections are only $\propto \lambda_d^4$ in the weakly interacting regime (see Eq. 3.78 and note that $\nu_c \propto \lambda_d^2$). The corrections resulting from the inclusion of higher order moments can also be seen in the high temperature curves appearing in the same figure. For $T > T_F$, self-energy corrections become negligible and the refinement is predominantly due to inclusion of higher order moments.

In summary, we find that all quadrupole modes are strongly influenced by collisions and exhibit the transition from the CL to HD regime. There is a notably large mean-field shift in the oscillation frequency at low temperatures. Similar to the monopole case, the quadrupole spectral function is essentially exhausted by the lowest lying (nodeless) mode, with a small contribution from overdamped

modes in the crossover regime. Upon increasing the temperature, the frequency and damping of all modes reach a plateau for a strictly 2D system. A qualitative account of this behavior was given in Sec. 3.4.2. In a quasi-2D system, however, the CL regime appears again for $T \gtrsim \hbar\omega_z$.

3.5 Experimental outlook

The collective modes can be probed experimentally in various ways. As described earlier, one common method is to perturb the trap potential with a short pulse and monitor the evolution of the cloud using either in-situ or absorption imaging techniques (for example, see Ref. [76]). The relevant observables are the radius and anisotropy of the cloud in case of monopole and quadrupole perturbations respectively. The frequency and damping of the collective modes are found by fitting the measured time evolution of the observable $O_{\mathrm{exp}}(t)$ to a function of the form $O_{\mathrm{fit}}(t) = Ae^{-\gamma t}\sin(\omega t + \Psi_0) + Be^{-\gamma_{\mathrm{OD}}t}$, where ω is the frequency of oscillations, and γ and γ_{OD} are damping rate of the oscillatory and overdamped components. If required, the spectral function can be subsequently found by taking a Fourier transform of the measured impulse response signal $O_{\mathrm{exp}}(t)$. Another approach which may yield more accurate results is the direct measurement of spectral functions via trap modulation spectroscopy. In this method, one introduces a low-amplitude periodic modulation at a fixed frequency Ω to the trap potential for a duration $\tau \gg \omega_0^{-1}, \Omega^{-1}$ and measures the absorbed energy. For a finite trap modulation pulse such as $\delta U \sim e^{-|t|/\tau}\cos(\Omega t)\,v(\mathbf{r})$, a simple linear response analysis yields [106]:

$$\Delta E_{\mathrm{abs}} \sim -\tau\,\Omega\,\mathfrak{Im}[\chi_{v(\mathbf{r})}(\Omega + i/\tau)], \qquad (3.87)$$

where ΔE_{abs} is the absorbed energy, $v(\mathbf{r})$ is the shape of the trap perturbation (i.e. $x^2 + y^2$ and $x^2 - y^2$ for monopole and quadrupole modes respectively), and $\chi_{v(\mathbf{r})}$ is the retarded response function of $v(\mathbf{r})$. Eq. (3.87) implies that the absorbed energy in a modulation experiment provides a direct measurement of the spectral function. The absorbed energy can be measured in various ways.

One method is to let the system rethermalize after the modulation pulse, followed by mapping it to a non-interacting system by switching off the interactions adiabatically and finally measuring the temperature rise of the non-interacting gas through a time of flight expansion experiment. The location of the peak in the measured spectral function and its width yield the frequency and damping of the collective mode. According to the results presented in the previous section, quadratic perturbations in the trap potential predominantly excite the lowest lying mode. If required, the spectral weight of higher order modes can be increased using quartic perturbations, e.g. $(x^2 + y^2)^2$ and $x^4 - y^4$ for monopole and quadrupole symmetries.

At the time this paper is written, the dipolar interaction strengths in the experiments are not strong enough to drive the system to the HD regime. In the experiments with fermionic ^{40}K^{87}Rb at JILA [15, 16, 17], the transverse and in-plane trap frequencies are $\omega_z = (2\pi) \times 23$ kHz and $\omega_0 = (2\pi) \times 36$ Hz respectively. The central layer has 2200 molecules, the temperature is $T = 500$ nK and dipole moment is $D = 0.158$ Debye, using which we find $T/T_F \approx 4.36$, $\eta \approx 0.322$ and $\lambda_d \approx 0.252$. The dipolar temperature is $T_{\rm dip} \sim 1.8$ μK and $T_F/T_{\rm dip} \approx 6.4 \times 10^{-2}$. Therefore, the near-threshold scattering condition can be satisfied well for quantum degenerate temperatures. However, the current temperature is above quantum degeneracy and we find $T/T_{\rm dip} \approx 0.28$. The scattering energies lie in the crossover between the threshold and semiclassical energies and we estimate the Born approximation to overestimate the cross section by a factor of 3 using the results of Ref. [92]. Since the temperature is high, mean-field corrections are small and the change in the monopole oscillation frequency is negligible. For quadrupole oscillations, we obtain $\Omega_{\rm quad} \approx 1.9990\,\omega_0$ and $\Gamma_{\rm quad} \approx 0.007\,\omega_0 = 1.7$ Hz. Including corrections to the Born approximation, we estimate $\Gamma_{\rm quad} \approx 0.6$ Hz which might be difficult to observe due to the presence of a two-body loss rate of ~ 4 Hz. We remark that the collision rates can be dramatically increased by making the transverse confinement stronger. For example, in the strictly 2D limit $\omega_z \to \infty$, we get $\Omega_{\rm quad}^{\rm 2D} \approx 1.8\,\omega_0$ and $\Gamma_{\rm quad}^{\rm 2D} \approx 0.3\,\omega_0 \approx 71$ Hz at the same temperature and phase-space density.

At this time, the recent experiments with ^{161}Dy [75] at Stanford seem to be more promising candidate toward the observation of the predictions of this paper. With $N = 6000$ atoms at a temperature $T/T_F = 0.21$ and a large magnetic dipole moment of $10\,\mu_B$, one is able to study both quantum degenerate and thermal regimes. Once the atoms are loaded into an optical lattice, we believe it will be possible to trap at least $N = 2000$ atoms at the Fermi temperature in the central pancake, with $\omega_z = (2\pi) \times 20\,\mathrm{kHz}$ and $\omega_0 = (2\pi) \times 100\,\mathrm{Hz}$. For this configuration, we find $T_F/T_\mathrm{dip} \approx 0.04$, $\lambda_d \approx 0.21$ and $\eta \approx 0.56$. The near-threshold condition is satisfied well and we reliably obtain $\Omega_\mathrm{quad} \approx 1.992\,\omega_0$ and $\Gamma_\mathrm{quad} \approx 0.0085\,\omega_0 \approx 5.3\,\mathrm{Hz}$. That damping is expected to be easily observable due to the long time stability of the gas. The mean-field shifts of the frequencies may also be observed at lower temperatures. With $N = 1000$ atoms in the central pancake and at $T/T_F = 0.2$ with the same trap frequencies, we obtain $\Omega_\mathrm{quad} \approx 1.95\,\omega_0$ and $\Gamma_\mathrm{quad} \approx 0.0065\,\omega_0 \approx 4.8\,\mathrm{Hz}$, and $\Omega_\mathrm{mon} - 2\omega_0 = 0.015\,\omega_0 \approx 9.3\,\mathrm{Hz}$, all of which are expected to be observable. Another intriguing possibility is the observation of the predicted plateau of the collision rate, which is also a direct consequence of universal near-threshold dipolar scatterings. This can be simply done by heating the gas and probing the collective modes at temperatures above T_F.

3.6   Discussions

Most of the relevant discussions were already given in the main text. Here, we give a brief summary of the main results along with several complementary comments. We started our analysis by investigating the equilibrium state of quasi-2D dipolar fermions in isotropic traps. In order to study the collective modes of the system, we solved the collisional Boltzmann-Vlasov equation for small perturbations of the trap potential with monopole and quadrupole symmetries. The self-energy

corrections to quasiparticle dispersions and collisions were taken into account via the self-consistent Hartree-Fock and Born approximations respectively. The validity of these approximations were assessed at the end of Sec. 3.2.1. In particular, the usage of Born approximation restricts the validity domain of our results to near-threshold scattering energies (see Eq. 3.29). We confined our attention to the regime where $T_F \ll T_{\mathrm{dip}}$, so that the scatterings remain in the near-threshold regime even in the thermal regime $T \gg T_F$. We showed that this condition is satisfied well in the current experiments. We emphasize that once the conditions for the applicability of our approximations are met, the formalism of collisional Boltzmann-Vlasov equation is universally applicable to both collisionless and collision-dominated (hydrodynamical) regimes, as well as the crossover between the two.

We carried out the analysis of collective modes in two stages: as a first approximation, we studied the problem in the Boltzmann limit by only keeping the collisional effects and using bare dispersions. We calculated the response functions using the simple picture of scaling ansatz. This analysis implied the generic result that monopole oscillations occur at a fixed frequency of $2\omega_0$, are undamped, and are independent of temperature and interaction strength. In case of quadrupole oscillations, however, we found a transition from the CL limit to the HD limit. We calculated the quadrupole collision rate, ν_c, for various temperatures and transverse trap frequencies. We found that in the 2D limit ($\eta = 0$), ν_c is a monotonically increasing function of temperature and reaches a plateau for large T/T_F. This plateau persists up to $T \simeq T_{\mathrm{dip}}$ beyond which the scattering energies enter the semiclassical regime and the cross section starts to decrease upon increasing the temperature further. The existence of this plateau, which is a novel feature arising from universal dipolar scatterings implies that (1) the character of trap excitations of a polarized 2D dipolar gas becomes essentially temperature-independent in the regime $T_F \lesssim T \lesssim T_{\mathrm{dip}}$, and (2) collisional effects persists in the thermal regime despite the fact that gas becomes very dilute. This behavior differentiates 2D dipolar fermionic gases from s-wave fermions where rarefaction of the gas at high

temperatures carries the system back to the collisionless regime for $T \gtrsim T_F$. Also, the temperature window for collisional behavior is universal for s-wave fermions and is not amenable to tuning, whereas for quasi-2D dipolar fermions, one can expand this window by (1) making the transverse confinement stronger to approach the 2D limit, and (2) either increase T_{dip} by using weaker dipoles or decrease T_F by decreasing the density.

The existence of the plateau is guaranteed as long as the scale separation $T_F \ll T_{\mathrm{dip}}$ is met. Combining Eqs. (3.29) and (3.73), one can find the condition for the plateau to lie in the collision dominated (hydrodynamic) regime as well:

$$N^{\frac{1}{4}} \ll \frac{a_0}{a_d} \ll N^{\frac{1}{2}}. \qquad \text{(HD plateau)} \qquad (3.88)$$

The left and right hand sides of this inequality are equivalent to $T_F \ll T_{\mathrm{dip}}$ and $N(a_d/a_0)^2 \gg 1$ respectively, where the latter condition implies $\nu_c \gg 1$. The above inequality may be used as a simple experimental guideline to observe hydrodynamical behavior with dipolar fermions.

In the second stage of calculations, we extended the analysis by (1) including self-energy corrections and (2) going beyond the scaling ansatz by satisfying higher moments of the CBV equation. Chiacchiera *et al.* [102] and Pantel *et al.* [107] have carried out a similar extended moments analysis of the Boltzmann equation for s-wave fermions and have shown that corrections of this type significantly improves the matching between the theory and the experiments.

We evaluated all of the matrix elements of the CBV equation numerically exactly with the exception of the collision integral matrix elements where we incorporated the dressed quasiparticle dispersions via a local effective mass approximation (LEMA) for practical reasons. Nevertheless, we found this scheme to be an excellent approximation. We will show later in this section that the conservation laws are satisfied well. Moreover, we evaluated the exact collision matrix elements in a few cases using an extrapolation technique (albeit at the costs of a significantly increased computation time; see Appendix. C.5) and found the corrections beyond LEMA to be negligible indeed.

The extension of the scaling ansatz analysis allowed us to (1) study the effects of self-energy corrections on the frequency and damping of various modes, and (2) investigate the higher order (nodal) monopole and quadrupole modes which are beyond the scope of the scaling ansatz, and (3) study the speculated damping of the nodeless monopole mode, which is a direct consequence of self-energy corrections. We found that despite the fact that inclusion of higher order moments results in the appearance of numerous new normal modes, the responses to the monopole and quadrupole perturbations ($\sim r^2$ and $x^2 - y^2$ respectively) are predominantly governed by the lowest lying (nodeless) mode. We remark that the frequency and damping of the mode, however, is significantly modified by both self-energy corrections and inclusion of higher order moments.

We argued that the self-energy corrections are expected to result in the damping of the nodeless monopole mode, a feature which is absent in the simple Boltzmann equation. We found that although this expectation is met, the damping remains very small ($< 10^{-3}\omega_0$) even in the strongly interacting regime. The frequency of oscillations, however, is significantly increased from its non-interacting value of $2\omega_0$. This mean-field frequency shift was found to be most significant at low temperatures where self-energy effects are large.

By investigating the velocity field of nodeless monopole mode, we found that it retains its scaling character to an good approximation (i.e. $\mathbf{v} \sim \mathbf{r}$), as well as its isothermal character. It is known from the hydrodynamic theory of non-ideal fluids that for a true isotropic and isothermal scaling flow, no dissipation results from shear viscosity or thermal conduction and the only source of dissipation is the bulk viscosity (for instance, see Ref. [68], §49). In this situation, one finds $\mathrm{d}S/\mathrm{d}t = \int \mathrm{d}^2\mathbf{r}\, n_0^{-1} T^{-1} \zeta (\nabla \cdot \mathbf{v})^2$ where S is the total entropy and ζ is the bulk viscosity. Note that the dissipation rate is second order in $\mathbf{v}$ and is therefore small.

At this point, we can not rule out the possibility that a more accurate description of the strongly correlated regime would change this finding. In particular, going beyond the quasiparticle ansatz in the kinetic equation and taking the collisional broadening of the single particle spectrum into

account may yield a larger damping of the nodeless monopole mode. We will investigate this possibility in the future works.

The analysis of higher order monopole modes ($n \geq 1$) and all quadrupole modes yields the same qualitative picture that the scaling ansatz analysis of the nodeless quadrupole mode provides, i.e. existence of a plateau in 2D upon increasing the temperature and reappearance of the CL regime in quasi-2D. We find, however, significant quantitative corrections. At low temperatures, self-energy corrections result in a shift of the frequencies proportional to λ_d. We also found that the scaling ansatz overestimates the collision rates in general. This defect is mostly noticeable in the high temperature regime where the gas is extended in the trap and higher order moments are required to accurately account for the density variations.

We included up to eight moments in the extended analysis (and up to twelve moments in pilot studies). We generally found that the most important corrections to the scaling ansatz stems from the forth order moments, beyond which the corrections become increasingly smaller. In practice, a second order basis set is sufficient to obtain the frequencies of the nodeless modes within a 0.1% tolerance of the exact solution. The accurate description of higher order modes naturally require inclusion of higher order moments.

Finally, we investigate the satisfaction of conservation laws as a consistency check for our numerical calculations. The CBV equation conserves the particle number, momentum and energy, both in the differential form and the integral form (see Appendix C.1). The quadrupole oscillations trivially satisfy these conservation laws due to the axial symmetry of the equilibrium state. This is not trivial for monopole oscillations as they have same symmetry as the equilibrium state. Fig. 3.13 shows the maximum relative deviations of the particle number and energy in monopole oscillations as a function of moment satisfaction order for a sample case. We find that the particle number is conserved within a relative error of $\sim 10^{-6}$ even in a first order basis set (this is because one of the moment equations is in fact a statement of mass conservation). On the other hand, we find that
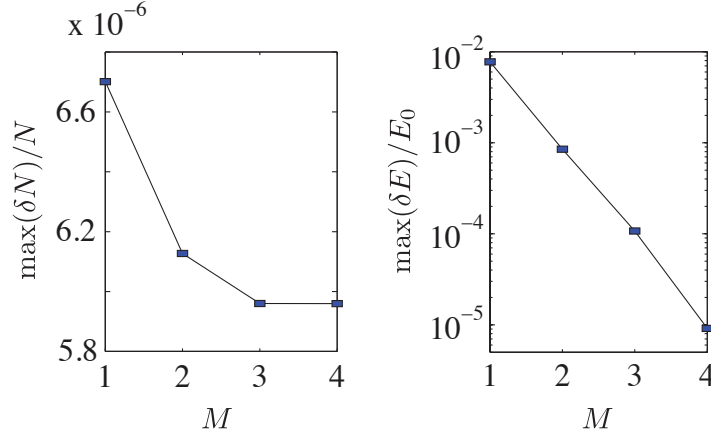
Figure 3.13: Maximum relative deviations of the particle number (left) and energy (right) for monopole oscillations in a sample configuration ($T/T_F = 0.1$, $\lambda_d = 0.5$, $\eta = 0$ and $N = 2200$). M is the truncation order of the basis set.

conservation of energy improves substantially upon extending the basis set. For the forth order basis set, the relative error in the conservation of energy is $\sim 10^{-5}$.

Some of the possible extensions of this work are (1) going beyond the Born approximation and including multiple scatterings in order to rigorously extend this study to semiclassical scattering energies ($T > T_{\mathrm{dip}}$), (2) going beyond the quasiparticle approximation and taking into account the collisional broadening of the single-particle spectrum toward quantitatively reliable predictions in the strongly interacting regime, and (3) inclusion of higher transverse bands to account for $T \gtrsim \hbar\omega_z$ in quasi-2D systems.

4

Non-equilibrium dynamics of attractive

two-component Fermi gases

4.1 Introduction

The two-component Fermi gas with short-range attractive interactions is one of the simplest yet richest models in condensed-matter physics. It is directly applicable to a wide range of naturally occurring physical systems ranging from atomic nuclei and superconductors to primordial matter

(quark-gluon plasma), white dwarfs and neutron stars. The Hamiltonian for such a system in d spatial dimensions may be written as:

$$H = \sum_{\sigma=\uparrow,\downarrow} \int \mathrm{d}^d\mathbf{x}\, \Psi_\sigma^\dagger(\mathbf{x}) \left[-\frac{\nabla^2}{2m} - \mu \right] \Psi_\sigma(\mathbf{x}) + \lambda \int \mathrm{d}^d\mathbf{x}\, \Psi_\uparrow^\dagger(\mathbf{x})\, \Psi_\downarrow^\dagger(\mathbf{x})\, \Psi_\downarrow(\mathbf{x})\, \Psi_\uparrow(\mathbf{x}), \quad (4.1)$$

where $\sigma = \uparrow, \downarrow$ is the component index and depending on the system, it corresponds to either the spin (electrons, atomic nuclei), color (quark-gluon plasma) or the hyperfine state (ultracold atoms); m and μ denote the mass and the chemical potential of particles, and $\lambda < 0$ is the strength of the contact attractive interaction. The contact interaction leads to a UV divergence which can be regulated either by imposing a physical UV cutoff Λ or by trading λ with renormalized quantities such as binding energy ϵ_b or the s-wave scattering length a_s. We refer to the above model as the *attractive Fermi gas* (AFG) for brevity.

This model was used by Bardeen, Cooper and Schrieffer (BCS) [108, 109] in 1957 toward constructing a microscopic theory of superconductivity. The weak phonon-mediated attraction between the electrons near the Fermi surface was approximated with a contact interaction with a UV cutoff Λ of the order of the Debye frequency ω_D [108]. The effective electron-phonon mediated attraction is typically very weak (several orders of magnitude smaller than the Fermi energy ϵ_F) and the electrons do not form bound pairs in a three dimensional vacuum. This scenario, however, is significantly different in a many-body system. At temperatures below a critical temperature T_c, the Fermi surface becomes sharp enough so that the phase space available to quasiparticles near the Fermi surface is effectively reduced to two spatial dimensions due to the Pauli blocking of $k < k_F$ momentum states (k_F is the Fermi momentum). Therefore, even the presence of a weak attraction leads to formation of bound pairs of the quasiparticles near the Fermi surface, known as the Cooper pairs [108]. The Bose condensation of Cooper pairs is the basis of the celebrated BCS theory of superconductivity.

The BCS theory was phenomenally successful in describing superconductors. Soon after the

th!
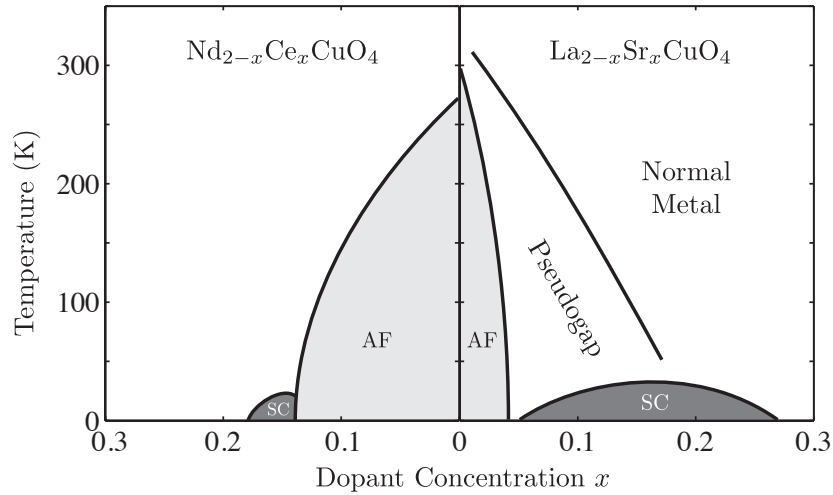
Figure 4.1: The schematic phase diagram of high-T_c superconductors showing hole-doping (p-type) on the right side, and electron-doping (n-type) on the left side (reproduced from Ref. [112])

publication of the BCS paper, several theorists proposed that a similar phenomenon could occur in fluids made up of fermions other than electrons, such as ^{3}He atoms. These speculations were confirmed in 1971, when experiments performed by Osheroff [110, 111] showed that ^{3}He becomes a superfluid below 2.5 mK. Although the interaction between ^{3}He atoms is not purely attractive, it was soon verified that the superfluidity of ^{3}He arises from a BCS-like mechanism as well.

High-T_c compounds and strong-coupling superconductivity:

The discovery of high-temperature superconductivity (HTSC) in cuprates by Bednorz and Mueller in 1986 [113] and the rapid raising of the transition temperature to well above the melting point of nitrogen started a new era of great excitement for the condensed-matter physics community. The fact that HTSC was discovered in an unexpected material, i.e. a transition metal oxide compound (Ba-La-Cu-O), made it clear that a novel mechanism must be at work. The unusual properties of high-T_c compounds revealed new problems in solid state physics in general, and challenged the phenomenally successful BCS theory of superconductivity in particular.

While hundreds of high-T_c cuprate compounds have been produced since their first discovery, they all share a layered structure made up of one or more copper-oxygen planes. They all fit into a *universal* phase diagram shown in Fig. 4.1. One starts with the so-called *parent compound*, such as La$_2$CuO$_4$. There is a general agreement that the parent compound is a Mott insulator with long-range antiferromagnetic (AF) order. The parent compound can be doped by substituting some of the trivalent La by divalent Sr. The result is that x holes are added to the Cu-O plane in La$_{2-x}$Sr$_x$CuO$_4$ (hole doping). In the compound Nd$_{2-x}$Ce$_x$CuO$_4$, the reverse scenario must be carried out, i.e. x electrons are added to the Cu-O plane (electron doping). As we can see from Fig. 4.1, on the hole doping side the AF order is rapidly suppressed and once the hole concentration exceeds 3 to 5 percents. Almost immediately after the suppression of AF, superconductivity appears, ranging from $x = 6\%$ to 25%.

The density of the itinerant carries introduced by hole- or electron-doping is not as large as it the carrier density in ordinary metals, so that the mean distance between them proves to be comparable with the pair size ξ_{pair}. This scenario is significantly different from the conventional BCS theory where ξ_{pair} greatly exceeds the mean distance between the carries. Experimentally, the dimensionless value $k_F \xi_{\mathrm{pair}}$, which describes the ratio of the pair size and the distance between carriers is about $5 \sim 20$ for HTSC while for low-temperature superconductors it is about $10^3 \sim 10^4$. This observation rekindled the interest in the *strong-coupling* superconductivity, in particular, in the theoretical description of the crossover from condensation of weakly-bound Cooper pairs (BCS) to the condensation of the deeply-bound singlet pairs (BEC).

The metallic state above T_c exhibits many unusual properties not encountered before in any other metal. This region of the phase diagram has been called the *pseudogap* phase and corresponds to the depletion of the single-particle spectral weight around the Fermi level. The earliest experiments to reveal such gap-like behavior were the NMR measurements of the Knight shift [4], where a gap-like behavior was found in the the spin susceptibility below a temperature $T^* > T_c$. This manifestation

of the pseudogap phenomenon was thus called a *spin-gap*. Subsequently, the optical conductivity [6], specific heat measurements and finally the direct measurement of the spectral function using angle-resolved photo-emission spectroscopy (ARPES) showed in addition a gapping of the charge degrees of freedom below T^*. The existence of the pseudogap, i.e. a wide region in the phase diagram between T^* and T_c with gap-like features but without superconductivity, is one of the most striking differences between the BCS scenario of superconductivity of the behavior of cuprates. The Fermi surface in the pseudogap phase is nearly destroyed and the elementary excitations do not have a particle-like nature. Both ARPES and tunneling experiments suggest that the pseudogap evolves smoothly into the superconducting gap as the temperature is lowered from T^* to T_c.

A combination of factors, including unusual magnetic and electronic properties, lowered dimensionality, proximity to the metal-insulator transition, relatively low carries densities, the d-wave symmetry and the competition between spin density waves (SDW), charge density waves (CDW) and pairing makes the construction of an appropriate theory for high-T_c both difficult and far from being fully resolved. Different authors have pursued different paths with different degrees of faithfulness to the phenomenology of high-T_c compounds. The converging point of a large body of such theoretical is the Hubbard model and its simplified relative, the t-J model, describing the hopping of electrons on the Cu-O layer. A general discussion of the theoretical developments directly related to the phenomenology of high-T_c cuprates is beyond the scope of this work and we refer the reader to Ref. [114] for an excellent review.

One line of thought, in the tradition of Occam's razor, is to proceed by *isolation* and *simplification* of the high-T_c phenomenology by focusing on only a small subset of the involved physical processes. This approach will inevitably diverge from the reality of high-T_c physics and will lead to models which are only marginally relevant to high-T_c compounds. On the bright side, the simplicity of such models allows us to explore and understand their physics on much deeper levels. Focusing on the physics of strong-coupling superconductivity in its simplest and purest form is one of such

endeavors.

The interaction between the itinerant carriers in high-T_c cuprates is believed to be mediated by the exchange of softened magnons to a great extent, as suggested by Scalapino, Miyake, Emery and their collaborators [115, 116, 117, 118, 119, 120][1] The proximity to the parent AF Mott insulator suggests that the effective interaction has a strong d-wave character. The carrier density is generally very low (about 0.2 holes per Cu-O$_4$) and the lattice structure is unresolved by the itinerant carriers. The above considerations suggest that the AFG Hamiltonian in two spatial dimensions (Eq. 4.1) may be used as a caricature for the physics of mobile carriers on the Cu-O layers. Committing to this model, one neglects the d-wave character of interactions, the tunneling of carriers between the adjacent Cu-O layers and the lattice effects altogether, all of which are believed to be important ingredients in the physics of cuprate superconductors. Nevertheless, the theoretical investigations of the AFG model has served to illuminate important aspects of the pairing physics, in particular, the need to depart from the mean-field BCS theory, strong-coupling effects such as Bose condensation of the pre-formed di-electronic pairs, and the non-Fermi liquid aspects of the pairing pseudogap phase.

The advent of ultracold atoms:

The rapid advancement of the experimental techniques of cooling and optical/magnetic trapping of dilute atomic gases in the late 90's and early 2000's dramatically changed the status of the AFG model. Instead of being a caricature for electronic superconductors or a model describing dense and nearly inaccessible states of matter such as the quark-gluon plasma and neutron stars, the AFG model achieved the status of arguably one of the most realistic models in the history of condensed-matter physics for a system realizable on a table-top setup and amenable to extensive experimental

---

[1]The idea of magnon exchange dates back to the works of Berk and Schrieffer [121], and Anderson and Brinkman [122] in the context of the effect of magnetic correlations in BCS-type superfluids, and the anisotropic pairing in ^{3}He.

scrutiny. The creation of a strongly interacting atomic Fermi gas was first reported in 2002 by the group at Duke University [5] and ENS Paris [123] using an ultracold gas of ^{6}Li atoms.

Having simple hydrogen-like atomic structures, the internal state of alkali atoms can be easily manipulated and controlled and are therefore the elements of choice for such experiments. A typical gas of ultracold alkali atoms consists of about $10^5 \sim 10^9$ atoms in their ground state and has a density of $10^{12} \sim 10^{15}$ cm^{-3}. While this is many orders of magnitude less dense than air, the gas can be cooled down to such low temperatures that it reaches the quantum degenerate regime where the thermal de Broglie wavelength $\lambda_T \equiv (2\pi\hbar^2/mk_BT)^{1/2}$ is of the same order of the average interatomic distance $n^{-1/3}$. The quantum degeneracy requires $T \approx 1 \sim 100$ nK range for the densities mentioned above and this is achieved using a combination of sympathetic, laser and evaporative cooling methods [9]. The thermal energy of atoms in the nK range is several orders of magnitude smaller than the hyperfine splitting (which is in the mK range), so that the spin structure of the atoms will remain undisturbed during collisions. Therefore, the ultracold atoms behave as composite particles with well-defined bosonic or fermionic statistics depending on their total hyperfine number.

The interatomic potential is well approximated by a zero-range contact interaction in dilute alkali gases. The range of the Van der Waals interatomic potential $r_0 \sim 50a_0$ is negligible compared to the de Broglie wavelength λ_T and the mean interparticle distance $n^{-1/3} \sim 10^4 a_0$ (here, $a_0 \approx 0.53$ Å is the Bohr radius). Furthermore, the binary collisions in the nK temperature regime is dominated by the s-wave ($l = 0$) scattering channel since the atoms can not overcome the centrifugal barrier for non-zero angular momentum scattering. The properties of the system is universal is this regime, i.e. independent of the details of the interatomic potentials, and the interactions are parametrized using

the s-wave scattering length a_s defined as:

$$a_s \equiv - \lim_{k \to 0^+} \delta_0(k)/k, \tag{4.2}$$

where $\delta_0(k)$ is s-wave scattering phase shift. By regarding the two different hyperfine states of fermionic atoms as $\uparrow$ and $\downarrow$ states, the atomic gas will be accurately described by the AFG Hamiltonian. We will discuss the renormalization of the bare interactions appearing in Eq. (4.1) in terms of a_s in the next section.

An important factor in achieving nK temperatures is isolating the gas from the material walls using optical or magnetic trapping. Because of their complete isolation these ultracold gases are, unlike solid-state systems, very clean in the sense that there are essentially no impurities unless deliberately added. The physical basis of the magnetic trapping is the Zeeman coupling of the electronic and nuclear spins to a spatially varying magnetic field. Magnetic trapping is usually used only during the laser cooling phase in experiments with fermionic atoms, after which the atoms are transferred to an optical trap [9].

The physical origin of the optical confinement of atoms is the dipole force $\mathbf{F}_{\text{dip}} = \alpha(\omega_L)/2 \, \nabla[|\mathbf{E}(\mathbf{r})|^2]$ due to a spatially varying ac Stark shift the atoms experience in an off-resonant light field [124]. The direction of the force depends on the sign of the polarizability $\alpha(\omega_L)$, where ω_L is the laser frequency. In the vicinity of an atomic resonance from the ground state $|g\rangle$ to an excited state $|e\rangle$ at frequency ω_0, the polarizibility has the form $|\langle e|\hat{d}_{\mathbf{E}}|g\rangle|^2/[\hbar(\omega_0 - \omega_L)]$, with $\hat{d}_{\mathbf{E}}$ being the dipolar operator along the direction of the electric field. Atoms are thus attracted to the nodes or the anti-nodes of the laser intensity for blue- ($\omega_L > \omega_0$) or red-detuned ($\omega_L < \omega_0$) laser light, respectively. A spatially varying laser intensity profile $I(\mathbf{r})$, therefore, creates a trapping potential for the neutral atoms. Provided that the detuning $\Delta = \omega_L - \omega_0$ is small compared to the transition frequency ω_0 and large compared to Γ the decay rate of the excited state, the time-
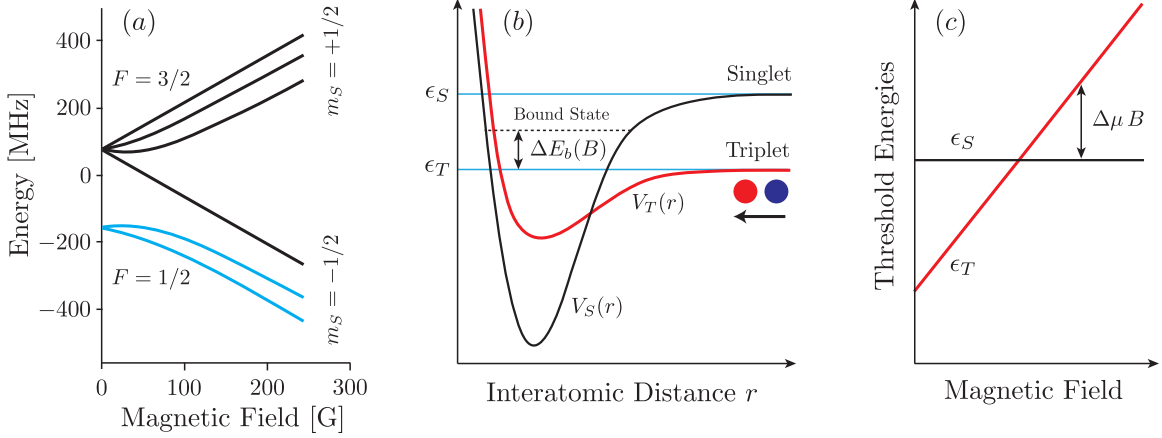
Figure 4.2: (a) The energy splitting of ^{6}Li in a magnetic field. The lowest two hyperfine states $|F, m_f\rangle = |1/2, \pm 1/2\rangle$ are used as $|\uparrow\rangle$ and $|\downarrow\rangle$ states. The projection of the electronic spin in both states is mainly along the $m_S = -1/2$ state for large magnetic fields. (b) A schematic plot of the Born-Oppenheimer potentials in the triplet (V_T) and singlet (V_S) channels. The scattering pairs enter primarily in the triplet (open) channel for large magnetic fields. The hyperfine splitting introduces a small coupling to the singlet (closed) channel. The existence of a bound state in the closed channel will modify the scattering properties of the particles in the open channel. (c) The magnetic moment of scattering pairs in the triplet and singlet channel differs by an amount $\Delta\mu$. Changing the magnetic field shifts the threshold energies of the triplet (ϵ_T) and singlet (ϵ_S) channels and consequently, the energy difference of the closed channel bound state $\Delta E_b(B)$ with respect to the triplet threshold energy. The Feshbach resonance occurs at the field strength B_0 where $\Delta E_b(B_0) = 0$.

averaged optical potential can be written as $V(\mathbf{r}) = (3\pi c^2 \Gamma)/(2\omega_0^3 \Delta) \, I(\mathbf{r})$ [124]. The shape of the laser intensity $I(\mathbf{r})$ can be engineered by combining several laser beams. Expanding $I(\mathbf{r})$ about its minimum for a red-detuned laser field, one obtains an approximately harmonic optical potential:

$$V(\mathbf{r}) = V_0 + \frac{1}{2} m \left(\omega_x^2 \, x^2 + \omega_y^2 \, y^2 + \omega_z^2 \, z^2 \right). \tag{4.3}$$

The above equation defines the trap frequencies $(\omega_x, \omega_y, \omega_z)$ along the three axes. In practice, the accessible trap frequencies lie in the range $1 \sim 100$ Hz in experiments with ^{6}Li and ^{40}K atoms.

Unlike the electronic systems, ultracold atomic gases have a remarkable feature that the strength of attraction between the fermions can be tuned arbitrarily using magnetic field induced *Feshbach resonances*. The principal idea behind the Feshbach resonance is explained in Fig. 4.2. In brief,

the hyperfine splitting couples the "incoming" (open) scattering channel, i.e. the spin configuration that is adiabatically connected to the internal state of a well-separated scattering pair, to *closed* scattering channels, i.e. the spin configurations that have higher asymptotic energies and inelastic decay of the incoming particles into them is energetically forbidden. The presence of a bound state in a closed scattering channel will modify the s-wave scattering length in the open channel (cf. the caption of Fig. 4.2 for details). The dependence of the open channel a_s on the magnetic field B near a Feshbach resonance can be generally written as:

$$a_s = a_{\mathrm{bg}} \left(1 - \frac{\Delta B}{B - B_0} \right),\tag{4.4}$$

where a_{bg} is the so-called background s-wave scattering length and is the scattering length in the open channel in the absence of the Feshbach resonance, and ΔB is the width of the resonance[2]. By sweeping the magnetic field across a Feshbach resonance at B_0, a_s can be in principle tuned to any value between $-\infty$ and ∞. Positive scattering lengths are obtained when the detuning of the energy of the close channel bound state $\Delta E_b(B)$ is negative and result in the emergence of a real bound state with energy $\epsilon_b = 1/(ma_s^2)$ in the open channel.

In 2003, the JILA group demonstrated the formation of stable diatomic molecules of an ultracold Fermi gas of ^{40}K [125] in their ground state, followed by three groups working with ^{6}Li [126, 127, 128]. Later that year, three groups reported the achievement of BEC of such ultracold molecules [129, 130, 131]. The radio-frequency (rf) spectroscopy of fermionic pairing was done along the BCS-BEC crossover [132] in 2005. After several pieces of experimental evidence provided by different groups, the final proof of superfluidity in strongly interacting Fermi gases was provided by the MIT group in 2005 [133], where vortices and vortex arrays was observed in a

---

[2]There generally exists several Feshbach resonances corresponding to the crossing of different closed channel bound states. The Feshbach resonances are generally categorized into *wide* and *narrow* resonances depending on whether the effective range of the induced resonance is small or comparable to the interparticle spacing, respectively. Clearly, the universal physics depends on the zero-range limit of interactions and therefore, wide Feshbach resonances. An ultracold gas of ^{6}Li atoms composed of $|F, m_f\rangle = |1/2, -1/2\rangle$ and $|1/2, 1/2\rangle$ hyperfine states has a wide Feshbach resonance at $B = 834.15$ G and a narrow resonance at $B = 543$ G.

strongly interacting Fermi gas in various interaction regimes.

The BCS-BEC crossover in $d = 3$
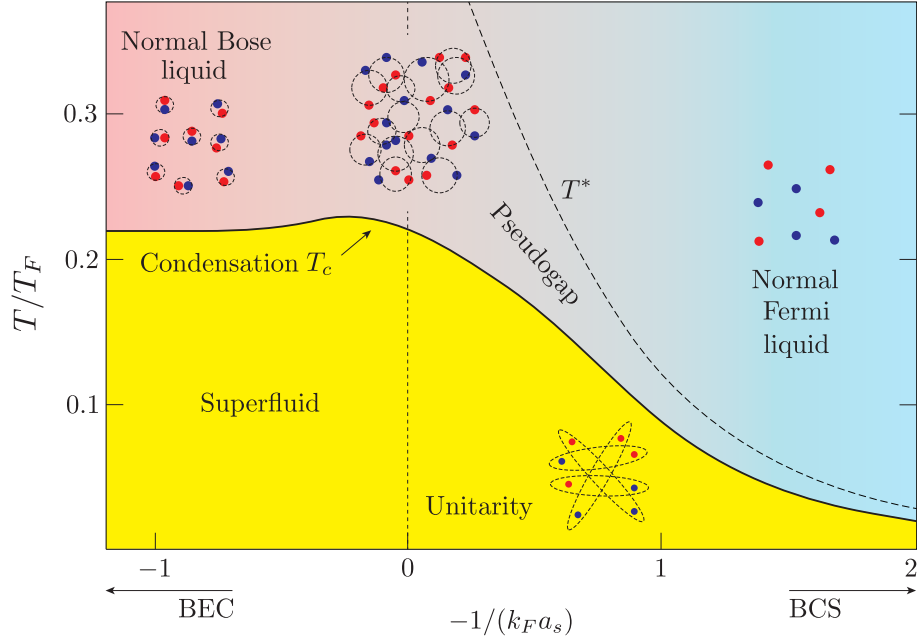
Figure 4.3: The global phase diagram of the attractive Fermi gas in $d = 3$ as a function of temperature and inverse scattering length. $T_F = (3\pi^2 n)^{2/3}/(2mk_B)$ is the Fermi temperature and $k_F = (3\pi^2 n)^{1/3}$ is the Fermi momentum. The figure is based on the non-self-consistent T-matrix analysis of Ref. [134]. The QMC analysis can be found in Refs. [135, 136].

A prominent aspect of ultracold atoms is the unprecedentedly precise experimental probing techniques that were developed along the way within the past decade, including the various time-of-flight imaging techniques [9], in-situ imaging with single atom resolution [10], measurement of transport properties via collective modes in traps [11], measurement of the equation of state, and the momentum-resolved radio-frequency (rf) spectroscopy of the single-particle spectral function [137]. The combination of extensive experimental data along with extensive analytical and numerical analyses has culminated in an exhaustive understanding of the physics of the AFG model in $d = 3$.

The global phase diagram of AFG in $d = 3$ is shown in Fig. 4.3. The qualitative understanding of the phase diagram is provided by picture of a BCS-BEC crossover [138]. When the attraction

between fermions is weak (BCS limit: $a_s < 0$, and $|k_F a_s| \ll 1$), the system is a weakly interacting Fermi gas. Its ground state is superfluid by the BCS mechanism, i.e. a condensate of weakly bound Cooper pairs. On the other hand, when the attraction is strong (BEC limit: $a_s > 0$, $k_F a_s \ll 1$), the fermions form real bound states (molecules) and the system becomes a weakly interacting Bose gas of such molecules. Its ground state again exhibits superfluidity, but by the condensation of the tightly bound molecules. These two regimes are smoothly connected without phase transitions, which implies that the ground state of the system is a superfluid at all couplings. Both BCS and BEC limits can be understood quantitatively by using the standard perturbative expansion in terms of the small parameter $|k_F a_s| \ll 1$. In contrast, a strongly interacting regime exists in the middle of the BCS-BEC crossover, where the scattering length is comparable to or exceeds the mean interparticle distance, $|k_F a_s| \sim 1$. In particular, the limit of infinite scattering length, which is often called the *unitarity* limit, has attracted intense attention by experimentalists and theorists. The ground state properties of the unitary Fermi gas is solely determined by its density, and therefore, the system becomes scale- and conformal-invariant in this limit [139] and is amenable to novel non-perturbative field theoretical treatments [140].

Another interesting property of the AFG is the presence of a pairing pseudogap regime below a crossover temperature T^* and above T_c, where the spectral function exhibits gap-like features, resembling the pseudogap regime of the high-T_c compounds. The lack of phase coherence of the pre-formed pairs in this regime due to thermal fluctuations results in the absence of a condensate. The existence of the pseudogap has been experimentally confirmed using momentum-resolved rf spectroscopy [137]. The pseudogap in the spectral function evolves continuously to the superconducting gap as the temperature is lowered to below the condensation temperature T_c. The characteristic temperature of the pseudogap asymptotically merges to T_c on the BCS side, whereas T^* grows unboundedly like the binding energy $\epsilon_b = 1/(m a_s^2)$ on the BEC side. Deep in the BEC side and in the temperature window $T_c < T < T^*$, the

system is described as a weakly interacting composite Bose liquid made of fermionic pairs. On the other hand, the system is described as a normal Fermi liquid for $T > T_c \sim T^*$ deep in the BCS side.

The measurement of transport properties within the BCS-BEC crossover has played an instrumental role in revealing the nature of the system in various regimes. Collective modes have been studied very early in atomic BEC research, both in experiments [102, 103] and in theory [104]. Measurements on collective oscillations have proven powerful tools for the investigation of various phenomena in atomic BECs [105, 106, 107, 108, 109]. Building on this rich experience, collective modes attracted immediate attention to study strongly interacting Fermi gases [110, 33, 34] as soon as these systems became experimentally available. In fact, the first experimental evidence for the presence of strong resonant interactions in ^{6}Li was provided by showing hydrodynamic behavior in the time-of-flight expansion of the trapped gap [5].

To understand collective modes in a Fermi gas, it is useful to distinguish between two different dynamical regimes:

- The *collisionless* (CL) regime: this regime is achieved in two distinct limits. (1) in a weakly interacting degenerate Fermi gas (BCS side, $T > T_c$), the elastic collisions are effectively suppressed due to the Pauli blocking of the final scattering states. The typical oscillation frequency of elementary excitations of the trapped gas is set by the trap frequency ω_{trap}. Provided that $\omega_{\text{trap}} \gg \tau_c$ (where τ_c is the average time between two collisions), the system will undergo several coherent oscillations before being appreciably affected by collisional damping. (2) deep in the BEC side ($a_s > 0$, $k_F a_s \ll 1$) and for $T > T_c$, the system is described as a weakly interacting Bose liquid. The scattering cross section is $\sigma \propto a_s^2$ and is negligible for large binding energies $\epsilon_b = 1/(m a_s^2)$. In both cases, the elementary particle-like excitations (free fermions, or deeply bound composite bosons) perform independent oscillations in the trapping potential and the ensemble shows decoupled oscillations along the different degrees

of freedom with frequencies that are twice the respective trap frequencies, save for small corrections due to weak residual interactions. In the ideal collisionless limit, no heat is generated and the collective oscillations are dissipationless.

- The *hydrodynamic* (HD) regime: this regime is also achieved via two distinct mechanisms. (1) A superfluid is formed for $T < T_c$. For sufficiently low temperatures ($T \ll T_c$), the non-condensed fraction is small and the evolution of the condensate is described by the Gross-Pitaevskii (GP) equation [141]. The latter bears the character of ideal hydrodynamics. (2) the presence of fast collisions $\tau_c^{-1} \gg \omega_0$ in the strongly interacting normal state ($|k_F a_s| \lesssim 1$, $T > T_c$) results in the local equilibration of each segment of the gas in the trap. The evolution of the local thermodynamical quantities (temperature, particle and energy density) is governed by viscous hydrodynamic equations as mentioned in Sec. 2.4. In the hypothetical extreme limits, $T = 0$ in case of superfluidity and $\tau_c^{-1} = \infty$ in case of collision-induced hydrodynamics, the viscosity identically vanishes and the oscillations are undamped and dissipationless. An interesting consequence of harmonic traps is the emergence of the so-called *hydrodynamical surface modes* which have universal frequencies independent of the equation of state of the gas [100]. A general demonstration of this fact is given in Appendix. B.1. The universal frequency of such modes is often used as the experimental indication for the hydrodynamic regime.

Except for the above extreme limits, the collective oscillations are generally affected by collisions, which lead to dissipation and damping. The dissipation is the largest within the transition windows between the collisionless and hydrodynamic regimes.

The various collective oscillation modalities of an ultracold gas in an anisotropic optical trap may be classified according to their symmetry. Much of the experiments on the AFG in $d = 3$ are done in cigar-shaped optical traps $V(\mathbf{r}) = (m/2)[\omega_z^2 z^2 + \omega_\perp^2 (x^2 + y^2)]$ [11, 9]. The low-lying

oscillation modalities in a long cigar-shaped trap are the *axial mode* (monopole oscillations along the z-axis), the *radial breathing mode* (monopole oscillations in the xy-plane), the *radial quadrupole mode* (quadrupole oscillations in the xy-plane), and the *scissors mode* (oscillation about an axis in the xy-plane). The mode of one's choice is easily excited by perturbing the trap potential momentarily according to the symmetry of the mode. The ensuing oscillations of the trapped gas can be measured with remarkable accuracy (with relative errors as low as 10^{-3} [76]) by absorption imaging. The measurement of the frequency and damping of different collective oscillation modes and subsequently fitting the data to the predictions of the viscous hydrodynamic equations can be used to extract important kinetic coefficients such as bulk viscosity ζ, shear viscosity η and thermal conduction κ. The possibility of carrying out such precision measurements makes such experiments ideal for testing the predictions of the many-body approximations.
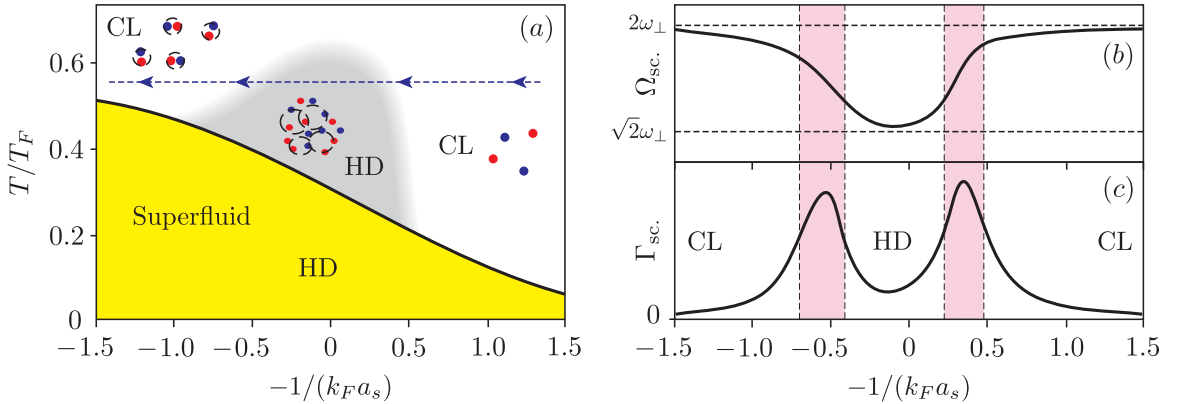
Figure 4.4: (a) A schematic diagram of the dynamical regimes of the scissors mode of the trapped attractive Fermi gas. The white regions denote collisionless (CL) dynamics whereas the grey region corresponds to the strongly interacting normal gas and is hydrodynamical (HD). The normal-superfluid transition of the trapped gas is based on Ref. [142]. The grey region is based on the measurement of the scissors mode given in Ref. [143] about the $B = 834$ G Feshbach resonance of ^{6}Li. (b) The schematic behavior of the frequency $\Omega_{\rm sc.}$ and (c) the damping $\Gamma_{\rm sc.}$ of the scissors mode upon sweeping the scattering length across the Feshbach resonance in the normal state along the dashed line shown in (a). The red regions correspond to the CL-HD transitions within which the dissipation is most appreciable.

Fig. 4.4 shows a schematic plot of the dynamical regime of the scissors mode in a typical experiment (ref. to the caption for more details). Upon sweeping the magnetic field across the Feshbach resonance at a constant temperature above T_c, the gas passes through various regimes: from the collisionless (CL) Fermi gas to the strongly interacting hydrodynamical (HD) pseudogap regime and finally to the collisionless normal Bose gas. The oscillation frequency in the CL and HD regimes are $\approx 2\omega_0$ and $\approx \sqrt{2}\omega_\perp$ (e.g. cf. Refs. [144, 145]). During the sweep, the system experiences two CL-HD crossovers and hence, two peaks in the damping rate $\Gamma_{\text{sc.}}$ as shown in panel (c). The oscillation frequency is shown in panel (b). We note that the same behavior is expected for all other modes that induce a shear flow and hence, measure the sheer viscosity η, such as the radial quadrupole mode. The behavior of radial breathing mode, which is mainly affected by the bulk viscosity ζ, is different due to the scale invariance of the gas at unitarity and the associated vanishing of η [139, 146].

Ultracold quantum gases in reduced dimensions

A salient feature of experiments with ultracold gases is the possibility of a clean realization of low-dimensional quantum gases. The principal idea is to *slice* the trapped gas using an *optical lattice*. An optical lattice is created either using a single mirror-reflected laser beam or two counter-propagating laser beams to generate a standing wave. The spatially-varying intensity of the standing light field results in an oscillating ac Stark shift potential and traps the atoms into a stack of thin *pancakes* as shown in Fig. 4.5. The total optical potential is the sum of the standing laser potential and the optical trap potential:

$$V(\mathbf{r}) = \frac{1}{2}m\omega_z^2 z^2 + \frac{1}{2}\omega_\perp^2(x^2 + y^2), \tag{4.5}$$

where it is assumed that the optical lattice is along the z-axis and the optical trap is isotropic. Large transverse trap frequencies ω_z of the order of $2\pi \times 100$ kHz can be generated using μm wavelength lasers such that $\omega_z \gg \max\{\epsilon_F, \mu, k_B T\}$. In this limit, only the lowest transverse band of each
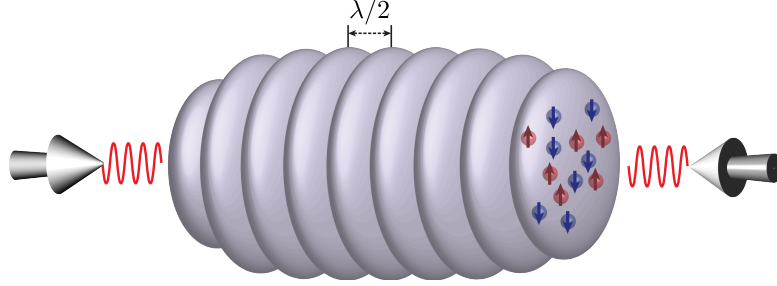
Figure 4.5: Slicing a trapped gas into pancakes using two counter-propagating laser beams. The separation between the pancakes is half the wavelength of the lasers. The laser used in the University of Cambridge experiments with ^{40}K has a wavelength of $\lambda = 1064$ nm focused to a waist of 140 μm [13, 18]. This setup yields approximately 30 pancakes each with about 5×10^3 atoms. $\omega_z = 2\pi \times 78.2$ kHz and $\omega_\perp = 2\pi \times 127$ Hz. The Fermi energy of the central pancakes is $\sim 2\pi \times 10$ kHz and is about an order of magnitude smaller than ω_z.

pancake is occupied. In other words, the mechanical motion of particles is frozen perpendicular to the pancakes and the sliced gas can be thought of as a collection of genuinely two-dimensional systems. The pancakes can be isolated from one another by suppressing the inter-layer tunneling by increasing the intensity of the optical lattice. The same principle has been used to create one-dimensional gases by slicing the pancakes into *tubes* using a second optical lattice and has led to a clean physical realization of theoretical 1D models such as the Tonks-Girardeau gas [147].

The 2D attractive Fermi gas has been recently realized using the above technique with ^{6}Li atoms in 2010 by the group in the Institute of Applied Physics, Russian Academy of Sciences (Nizhniy Novgorod) [148] and with ^{40}K atoms by the group in the University of Cambridge [13, 18]. In $d = 2$, the interactions are parametrized with the binding energy ϵ_b between the $|\uparrow\rangle$ and $|\downarrow\rangle$ states. The relation between the the two-dimensional binding energy ϵ_b and the s-wave scattering length is found by solving the two-body problem in a 2D harmonic potential [149, 150, 151, 152] and is given by the solution of the following transcendental equation:

$$\frac{l_z}{a_s} = \int_0^\infty \frac{\mathrm{d}x}{\sqrt{4\pi x^3}} \left(1 - \frac{\exp(-\epsilon_b x/(\hbar\omega_z))}{\sqrt{(1 - \exp(-2x))/(2x)}} \right), \tag{4.6}$$

where $l_z = [\hbar/(m\omega_z)]^{1/2}$ is the oscillator length along the z-axis. It is customary to parametrize

the interaction strength using the dimensionless quantity:

$$\eta \equiv \ln(k_F a_2) = \frac{1}{2}\ln(2\epsilon_F/\epsilon_b), \qquad \epsilon_F = \sqrt{2\pi n}, \quad a_2 = 1/\sqrt{m\epsilon_b}. \tag{4.7}$$

Large positive and negative η corresponds to the weak-coupling $\epsilon_b \ll \epsilon_F$ and $\epsilon_b \gg \epsilon_F$ regimes, respectively. The global phase diagram of the homogeneous and trapped AFG in $d = 2$ has been theoretically investigated in Refs. [153, 154, 155] using the non-self-consistent T-matrix approximation and the findings are qualitatively similar to the phase diagram of the $d = 3$ AFG shown discussed earlier (cf. Fig. 4.3). At zero-temperature, the QMC analysis has been carried out in Ref. [156]. The major differences between $d = 3$ and $d = 2$ are the shift of the superfluid transition to lower temperatures due to stronger thermal and quantum fluctuations in $d = 2$, and the change of the universality class of superfluid transition to the Berezinskii-Kosterlitz-Thouless (BKT). We will discuss these nuances in detail in the forthcoming sections.

The existence of the pairing pseudogap in near $\eta \approx 0$ has been experimentally demonstrated by the group in the University of Cambridge [13] using momentum-resolved rf spectroscopy technique. Experiments on the collective oscillation of the trapped has been carried by the same group [18, 157]. In particular, the quadrupole oscillations is found to exhibit the behavior shown in Fig. 4.4.

The theoretical literature on collective oscillations of trapped Fermi gases is vast, in particular, in three dimensional. These contributions can be categorized into two main classes, the studies focusing on the HD regime [158, 159, 160, 161, 162, 163, 164], and the studies based on the quasiparticle Boltzmann equation. Refs. [165, 98, 166, 167, 168, 144, 145, 169, 170, 171, 102, 107, 172] have addressed this problem in $d = 3$ and more recently, Refs. [83, 81, 84, 157] has repeated similar analyses for the $d = 2$ case.

Both of these approaches, i.e. the quasiparticle Boltzmann equation and the ideal HD equations,

have limited domain of applicability and neither provide a globally valid description of the collective dynamics. The ideal HD limit is only relevant to low-temperature $(T \ll T_c)$ superfluids, and approximately to the strongly interacting normal state. Even in these limits, the rarefied gas near the edge of the trap is in a normal weakly interacting state and can not be treated as being hydrodynamical. On the other hand, the studies based on the quasiparticle Boltzmann equation are only valid when well-defined fermionic quasiparticles exist and constitute the elementary excitation of the system. While this approach qualitatively explains the CL-HD transition from the weak-coupling side, it breaks down upon entrance to the strong-coupling regime where the Fermi surface is destroyed and the bosonic degrees of freedom emerge.

Our main goal in this chapter to present a systematic derivation of the quantum kinetic equations of the AFG in $d = 2$ and $d = 3$ within the self-consistent T-matrix approximation (SCTMA). The kinetic equations to be derived surpass the quasiparticle approximation and constitute an exact kinetic expansion of the Kadanoff-Baym equations within the SCTMA. We will show that the obtained equations provide a globally valid description of the transport of the AFG model: they reduce to the collisionless Boltzmann-like equation of fermionic quasiparticles in the weak-coupling limit, the hydrodynamical equations in the strongly interacting regime, and back again to the collisionless Boltzmann-like equation describing the dynamics of free composite bosons (bound fermions) in the strong-coupling limit.

This chapter is organized as follows. We start with a brief review of the physics of pairing fluctuations from the perspective of Ginzburg-Landau and Nozières-Schmitt-Rink (NSR) theories in Sec. 4.2. We discuss the generalization of the self-consistent T-matrix approximation to non-equilibrium states and the regularization of the contact interaction in Sec. 4.3. The linear response theory of the AFG within the T-matrix approximation is discussed from a diagrammatic perspective in Sec. 4.4. We derive the quantum kinetic equations corresponding to the T-matrix approximation

in Sec. 4.5 and discuss the numerical technique for solving the obtained equations in confined geometries. The numerical results and comparison to the existing literature is discussed in Sec. 4.6.6. Conserving approximations beyond the SCTMA are discussed in Sec. 4.7. We finally summarize the results and discuss the outlook of our analysis in Sec. 4.8.

4.2 The many-body theories of pairing flucations

The qualitative behavior of the AFG and the problem of the BCS-BEC crossover was briefly discussed in the introductory remarks. In this section, we give a more detailed account of the prominent theoretical approaches to this problem with emphasis on the new features of $d = 2$. The covered topics include the BCS theory, the Ginzburg-Landau approach and the Nozières-Schmitt-Rink (NSR) theory.

4.2.1 Preliminaries

The Hamiltonian given in Eq. (4.1) with a proper UV regularization constitutes the microscopic model for a two-component attractive Fermi gases in the vicinity of a broad s-wave Feshbach resonance. As it stands, the contact interaction in Eq. (4.1) leads to UV divergences in particle-particle loops in spatial dimensions $d \geq 2$. The the divergences can be regulated by imposing a UV cutoff Λ. The cutoff-dependent microscopic coupling constant λ must be subsequently traded with the renormalized quantities a_s in $d = 3$ or ϵ_b in $d = 2$ while taking the zero-range limit $\Lambda \to \infty$.[3]

In this section, we define the regulated AFG Hamiltonian. The discussion of renormalization is postponed until Sec. 4.3 where the T-matrix approximation is discussed. In order to keep the discussion general, we allow the different spin states to have different masses and define the following

---

[3]This task can be streamlined using the zero-range Fermi-Huang pesudopotential [173, 174]. Here, we adopt the more transparent method of momentum-space regularization.

auxiliary quantities:

$$m_{\rm red} \equiv (m_\uparrow \, m_\downarrow)/(m_\uparrow + m_\downarrow), \qquad m_{\rm tot} \equiv m_\uparrow + m_\downarrow,$$

$$\eta_\uparrow \equiv m_\uparrow/(m_\uparrow + m_\downarrow), \qquad\qquad \eta_\downarrow \equiv m_\downarrow/(m_\uparrow + m_\downarrow). \qquad (4.8)$$

If a scattering pair has a total center-of-mass momentum of $\mathbf{q}$ and a relative momentum of $2\mathbf{k}$ in the center-of-mass frame, their momenta in the lab frame can be expressed as $\mathbf{p}_\uparrow = \eta_\uparrow \mathbf{q} + \mathbf{k}$ and $\mathbf{p}_\downarrow = \eta_\downarrow \mathbf{q} - \mathbf{k}$. Quite generally, an arbitrary two-body interaction term in the Hamiltonian can be written as:

$$H_{\rm int} = \int \frac{{\rm d}^d \mathbf{q}}{(2\pi)^d} \frac{{\rm d}^d \mathbf{k}}{(2\pi)^d} \frac{{\rm d}^d \mathbf{k}'}{(2\pi)^d} \, W(\mathbf{q}; \mathbf{k}, \mathbf{k}') \, \Psi_\uparrow^\dagger(\eta_\uparrow \mathbf{q} + \mathbf{k}) \, \Psi_\downarrow^\dagger(\eta_\downarrow \mathbf{q} - \mathbf{k}) \, \Psi_\downarrow(\eta_\downarrow \mathbf{q} - \mathbf{k}') \, \Psi_\uparrow(\eta_\uparrow \mathbf{q} + \mathbf{k}'),$$

$$(4.9)$$

where $\mathbf{q}$ is the center-of-mass momentum of the interacting pairs, and $\mathbf{k}$ and $\mathbf{k}'$ denote the relative momentum of outgoing and incoming pairs. Galilean invariance requires W to be independent of $\mathbf{q}$. A short-range interaction can be modeled conveniently using the following separable choice for $W(\mathbf{q}; \mathbf{k}, \mathbf{k}')$ [138, 175, 176]:

$$W(\mathbf{q}; \mathbf{k}, \mathbf{k}') = \lambda_\Lambda \, \tilde{w}_\Lambda(\mathbf{k}) \, \tilde{w}_\Lambda(\mathbf{k}'), \qquad (4.10)$$

where λ_Λ is the coupling constant and $\tilde{w}_\Lambda(\mathbf{k})$ is a soft and isotropic regulator function with a real-space range of $\sim 1/\Lambda$. The Hamiltonian in the real space reads as:

$$H = \sum_{\sigma=\uparrow,\downarrow} \int {\rm d}^d \mathbf{x} \, \Psi_\sigma^\dagger(\mathbf{x}) \left[-\frac{\nabla^2}{2m_\sigma} - \mu_\sigma - U_\sigma(t, \mathbf{x}) \right] \Psi_\sigma(\mathbf{x}) + \lambda_\Lambda \int {\rm d}^d \mathbf{R} \int {\rm d}^d \mathbf{x} \int {\rm d}^d \mathbf{x}' \, w_\Lambda(\mathbf{x})$$

$$\times w_\Lambda(\mathbf{x}') \, \Psi_\uparrow^\dagger \left(\mathbf{R} + \eta_\downarrow \mathbf{x} \right) \Psi_\downarrow^\dagger \left(\mathbf{R} - \eta_\uparrow \mathbf{x} \right) \Psi_\downarrow \left(\mathbf{R} - \eta_\uparrow \mathbf{x}' \right) \Psi_\uparrow \left(\mathbf{R} + \eta_\downarrow \mathbf{x}' \right), \quad (4.11)$$

where:

$$w_\Lambda(\mathbf{x}) \equiv \int \frac{{\rm d}^d \mathbf{k}}{(2\pi)^d} \, \tilde{w}_\Lambda(\mathbf{k}) \, e^{i\mathbf{k}\cdot\mathbf{x}}. \qquad (4.12)$$

Setting $\tilde{w}_\Lambda(\mathbf{k}) = 1$ takes us back to the Hamiltonian in Eq. (4.1). We will show later that the above model Hamiltonian is free of UV divergences provided that $|\tilde{w}_\Lambda(\mathbf{k})|$ falls faster than $k^{1-d/2}$ for large k.

The cut-off dependent microscopic interaction strength λ_Λ has to be chosen such that the resulting low-energy effective theory of the model matches that a gas with zero-range interactions. In $d = 3$, this amounts to requiring that the low-energy expansion of the on-shell T-matrix in vacuum assumes the following s-wave form:

$$(d = 3): \qquad T(E) = \frac{2\pi}{m_{\mathrm{red}}} \left[\frac{1}{a_s} + i\sqrt{2m_{\mathrm{red}}E} + \mathcal{O}(E) \right]^{-1}, \qquad (4.13)$$

where E is the energy of the scattering pair in the center-of-mass frame. In $d = 2$, the low-energy T-matrix is characterized by the the binding energy ϵ_b and is given by the following expression [150]:

$$(d = 2): \qquad T(E) = \frac{2\pi}{m_{\mathrm{red}}} \left[\ln(-\epsilon_b/E^+) + \mathcal{O}(E) \right]^{-1}. \qquad (4.14)$$

This discussion will be continued in Sec. 4.3 where the self-consistent T-matrix approximation is introduced.

4.2.2 The zero-temperature analysis: the BCS wave function

The BCS theory provides a simple and intuitive model of the attractive Fermi gas at zero temperature. At $T = 0$, complications due to thermal fluctuations are absent and the mean-field theory yields a physically appealing picture of the evolution of the system from the weak- to the strong-coupling limit.

Let us first consider the strong-coupling limit first, i.e. when the binding energy ϵ_b is much larger than $\epsilon_F \propto n^{d/2}$. In this limit, all of the fermions are paired into singlet bound states. The energy dispersion of the bound-state is given by $\omega_{\mathbf{q}} = -\epsilon_b + q^2/(2m_{\mathrm{tot}})$ and the corresponding creation operator of this composite bosonic particle is:

$$b_{\mathbf{q}}^\dagger \equiv \sum_{\mathbf{k}} \phi_{\mathbf{k}} \, c_{\mathbf{k}+\mathbf{q}/2,\uparrow}^\dagger \, c_{-\mathbf{k}+\mathbf{q}/2,\downarrow}^\dagger, \qquad (4.15)$$

where $\phi_{\mathbf{k}}$ is the internal wavefunction of the bound state, extending over a characteristic length $\xi_{\mathrm{pair}} \sim \epsilon_b^{-1/2}$. If two bound pairs have only a small overlap, i.e. $n^{1/d}\xi_{\mathrm{pair}} \ll 1$, the bound pairs

can be treated as a free gas of point-like bosons whose internal orbital structure is irrelevant. One expects the system to undergo a Bose-Einstein condensation into a single quantum state with total momentum $\mathbf{q} = 0$ when the pair chemical potential, $\mu_{\text{pair}} \equiv 2\mu$, reaches the bottom of the bound state band, i.e. for $\mu_{\text{pair}} = -\epsilon_b$. Neglecting the overlap between the pairs, the ground state is simply:

$$|\Psi_{\text{SC}}\rangle = \exp\left(\sqrt{N/2}\, b_{\mathbf{q}=0}^\dagger\right)|0\rangle. \tag{4.16}$$

Here, N is the total number of fermions and $|0\rangle$ is the zero-particle vacuum state. The occupancy of the fermion state at momentum $\mathbf{k}$ is $n_{\mathbf{k}} = (N/2)|\phi_{\mathbf{k}}|^2$. As long as $n^{1/d}\xi_{\text{pair}} \ll 1$, $|\phi_{\mathbf{k}}| \ll 1$ and consequently $n_{\mathbf{k}} \ll 1$, so that the fermion exchange corrections are immaterial.

This picture changes dramatically when $n^{1/d}\xi_{\text{pair}} \geq 1$. The bound pairs overlap and fermion exchange becomes an important ingredient of the picture. Since the Pauli exclusion principle imposes $n_{\mathbf{k}} < 1$, $n_{\mathbf{k}}$ saturates and the internal wave function extends further out in the momentum space in order to accommodate the large number of particles. In this weak-coupling limit, the suitable wave function is that of a free Fermi gas:

$$|\Psi_{\text{WC}}\rangle = \prod_{\mathbf{k}} c_{\mathbf{k},\uparrow}^\dagger c_{-\mathbf{k},\downarrow}^\dagger |0\rangle. \tag{4.17}$$

In $d \leq 2$, the attractive potential always admits a real two-body bound state in the singlet $l = 0$ (s-wave) channel. For $d = 3$, a real bound state is only present when the interactions are strong, as indicated by a positive s-wave scattering length. The celebrated BCS theory [109] shows that even in $d = 3$, the weak attraction in the weak-coupling limit gives rise to a superconducting instability due to Pauli blocking of the $k < k_F$ states. The ground state is described well by the usual mean-field BCS wave function:

$$|\Psi_{\text{BCS}}\rangle = \prod_{\mathbf{k}}(u_{\mathbf{k}} + v_{\mathbf{k}} c_{\mathbf{k},\uparrow}^\dagger c_{-\mathbf{k},\downarrow}^\dagger)|0\rangle. \tag{4.18}$$

Here, $n_{\mathbf{k}} = |v_{\mathbf{k}}|^2 = 1 - |u_{\mathbf{k}}|^2$ is slightly smeared near the Fermi level. Superconductivity may be viewed as Bose condensation of weakly bound Cooper pairs. Indeed, the wave function of the

BEC of composite bosons in the strong-coupling limit may be thought of as a BCS state with the choice [138]:

$$v_{\mathbf{k}} = \frac{\sqrt{N/2}\,\phi_{\mathbf{k}}}{(1 + (N/2)\,|\phi_{\mathbf{k}}|^2)^{1/2}}.$$ (4.19)

The ground state goes smoothly from one limit to the other. In the strong-coupling limit, $v_{\mathbf{k}} \approx \sqrt{N/2}\,\phi_{\mathbf{k}} \ll 1$ reflects the internal structure of the pairs. In the weak-coupling limit, binding is a cooperative phenomenon in the vicinity of the Fermi surface (the Cooper pair radius is much larger than the inter-particle spacing), but the structure of the wave function is the same, characteristic of Bose condensation. We note that this point is crucial in treating pairing correlations: it is only because all pairs have the same momentum $\mathbf{q} = 0$ that we can describe them in terms of the mean-field order parameter $\langle c^{\dagger}_{\mathbf{k},\uparrow} c^{\dagger}_{-\mathbf{k},\downarrow} \rangle$. Such a simplifying feature no longer holds at finite temperature.

Let us explore the implications of the BCS wavefunction for intermediate couplings. Let $\xi_{\mathbf{k}} \equiv k^2/(2m) - \mu$ be the dispersion of free fermions measured from the chemical potential. The superconducting gap $\Delta_{\mathbf{k}} = \sum_{\mathbf{k}'} W(\mathbf{k}, \mathbf{k}') \langle c^{\dagger}_{\mathbf{k},\uparrow} c^{\dagger}_{-\mathbf{k},\downarrow} \rangle$ obeys the BCS gap equation:

$$\Delta_{\mathbf{k}} = \sum_{\mathbf{k}'} W(\mathbf{k}, \mathbf{k}') \frac{\Delta_{\mathbf{k}'}}{2\xi_{\mathbf{k}'}} (1 - n_{\mathbf{k}'}),$$ (4.20)

where $n_{\mathbf{k}}$ is the fermion distribution in the ground state:

$$n_{\mathbf{k}} = \frac{1}{2} \left[1 - \frac{\xi_{\mathbf{k}}}{(\xi_{\mathbf{k}}^2 + \Delta_{\mathbf{k}}^2)^{1/2}} \right].$$ (4.21)

The chemical potential is fixed by requiring:

$$\sum_{\mathbf{k}} n_{\mathbf{k}} = N.$$ (4.22)

Introducing the function $\tilde{\phi}_{\mathbf{k}} = \Delta_{\mathbf{k}}/(\xi_{\mathbf{k}}^2 + \Delta_{\mathbf{k}}^2)^{1/2}$, we can write the gap and number equations as:

$$\left(\frac{k^2}{2m_{\text{red}}} - 2\mu \right) \phi_{\mathbf{k}} = (1 - 2n_{\mathbf{k}}) \sum_{\mathbf{k}'} W(\mathbf{k}, \mathbf{k}')\,\tilde{\phi}_{\mathbf{k}'}, \qquad n_{\mathbf{k}} = \frac{1}{2} \left[1 - \sqrt{1 - |\tilde{\phi}_{\mathbf{k}}|^2}\,\text{sign}(\xi_{\mathbf{k}}) \right].$$ (4.23)

In the strong-coupling limit, the above equation reduces in the leading order to:

$$(k^2/m - 2\mu)\,\tilde{\phi}_{\mathbf{k}} = \sum_{\mathbf{k}'} W(\mathbf{k}, \mathbf{k}')\,\tilde{\phi}_{\mathbf{k}'}, \tag{4.24}$$

which is just the Schrödinger equation for a single bound pair. The 2μ plays the role of the eigenvalue; hence, to leading order, $\mu = -\epsilon_b/2$. Also, to leading order, $N = (1/2)\sum_{\mathbf{k}}|\tilde{\phi}_{\mathbf{k}}|^2$, so that $\tilde{\phi}_{\mathbf{k}} = 2\sqrt{N/2}\,\phi_{\mathbf{k}}$ as expected. In summary, we find that mean-field theory correctly describes Bose condensation of strongly bound composite pairs and provides a simple interpolation scheme between a non-interacting Fermi gas to a BEC of composite bosons at $T = 0$.

4.2.3 The Ginzburg-Landau approach

The simple BCS mean-field theory, while efficient and economical, does not satisfactorily extend to finite temperatures in the strong coupling limit. In fact, as briefly mentioned above, the only reason the BCS theory applies to the strong-coupling limit at $T = 0$ is that the bound states occupy the same $\mathbf{q} = 0$ state while finite momentum bosonic states are left unoccupied. At finite temperatures, collective excitations, in particular motional degrees of freedom of the bound pairs, becomes important. In fact, upon heating the system in the strong-coupling regime, the superfluidity is destroyed due to the proliferation of thermal excitation of collective modes (in contrast to the weak-coupling regime, where the normal state is recovered by pair breaking). Collective excitations are beyond the grasp of a BCS-like mean-field theory and a successful description of the system requires taking pairing correlations into account. There exists a vast literature on the physics of pairing fluctuations and a complete review is beyond the scope of our work. In this section, we give a brief account of the simplest theories to the extent that is required for the forthcoming developments. We momentarily switch to the Matsubara formalism to make contact with the existing literature, the vast majority of which only address systems in thermal equilibrium. We will also consider a δ-interaction (i.e. $\tilde{w}_\Lambda(\mathbf{k}) = 1$) for simpler discussion and

regularize the divergent loop integrals by imposing a UV momentum cutoff.

The simplest and most clear account of the physics of pairing fluctuations is obtained using functional methods, which provide us with the Ginzburg-Landau (GL) functional for the system using which phase transitions can be investigated, while a first flavor of the dynamics may also be tasted. We loosely follow Refs. [153, 175] in this section. Consider the partition function of the system in thermal equilibrium:

$$Z = \int \mathcal{D}[\psi, \bar{\psi}]\, e^{-\beta S[\psi, \bar{\psi}]},$$

$$S[\psi, \bar{\psi}] = \sum_{\alpha = \uparrow, \downarrow} \int_0^\beta \int d^d\mathbf{x}\, \bar{\psi}_\alpha(\mathbf{x}, \tau) \left(\partial_\tau - \frac{\nabla^2}{2m} - \mu \right) \psi_\alpha(\mathbf{x}, \tau)$$

$$+ \lambda_\Lambda \int_0^\beta \int d^d\mathbf{x}\, \bar{\psi}_\uparrow(\mathbf{x}, \tau) \bar{\psi}_\downarrow(\mathbf{x}, \tau)\, \psi_\downarrow(\mathbf{x}, \tau)\, \psi_\uparrow(\mathbf{x}, \tau). \tag{4.25}$$

The interaction term can be decoupled by introducing a Hubbard-Stratonovich pairing field $\Delta(\mathbf{x}, \tau) \sim \lambda_\Lambda \psi_\downarrow(\mathbf{x}, \tau) \psi_\uparrow(\mathbf{x}, \tau)$. The fermions can be integrated out in the resulting quadratic theory leading to the following fully bosonic partition function:

$$Z = \int \mathcal{D}[\Delta, \Delta^*]\, \exp\left[\frac{1}{\lambda_\Lambda} \int_0^\beta d\tau \int \frac{d^d\mathbf{q}}{(2\pi)^d} |\Delta(\mathbf{q}, \tau)|^2 \right] \mathsf{L}[\Delta],$$

$$\mathsf{L}[\Delta] = \mathrm{Tr}\, \exp\left[-\int_0^\beta d\tau \left(\sum_{\mathbf{k}, \sigma} \xi_\mathbf{k}\, \bar{c}_\sigma(\mathbf{k}, \tau)\, c_\sigma(\mathbf{k}, \tau) + \sum_\mathbf{q} [\Delta(\mathbf{q}, \tau) B^*(\mathbf{q}, \tau) + \mathrm{h.c.}] \right) \right], \tag{4.26}$$

where $c_\sigma(\mathbf{k}, \tau)$ and $\Delta(\mathbf{q}, \tau)$ are Fourier transforms of $\psi_\sigma(\mathbf{x}, \tau)$ and $\Delta(\mathbf{x}, \tau)$, respectively, and $B(\mathbf{q}, \tau) = \sum_\mathbf{k} c_\uparrow(-\mathbf{k}, \tau) c_\downarrow(\mathbf{k} + \mathbf{q}, \tau)$. Expanding the $\mathsf{L}[\Delta]$ up to fourth-order in Δ, we find $Z = Z_0 \int \mathcal{D} \exp(-\beta S_{\mathrm{GL}}[\Delta])$, where $Z_0 = \exp(-\beta \Omega_0)$ is the partition function for free Fermions and S_{GL} is the GL functional:

$$S_{\mathrm{GL}}[\Delta] = -\sum_{i\nu_n} \int \frac{d^d\mathbf{q}}{(2\pi)^d} T_{\mathrm{MB},0}(\mathbf{q}, i\nu_n) |\Delta(\mathbf{q}, i\nu_n)|^2 + \frac{b}{2} \sum_{1,2,3} \Delta(1)\, \Delta^*(2) \Delta(3) \Delta^*(1 - 2 + 3), \tag{4.27}$$

where the integer indices stand for both momentum and Matsubara frequency, and b is given by:

$$b = \frac{1}{\beta} \int \frac{\mathrm{d}^d \mathbf{k}}{(2\pi)^d} \left[G_0(\mathbf{k}, i\omega_n) \, G_0(\mathbf{k}, -i\omega_n) \right]^2 . \tag{4.28}$$

Since we are interested in the low-energy behavior of the system, we have set the external momentum and frequency of the effective four-boson interaction vertex b to zero. The ordering transitions of the system in various regimes can be investigated by expanding $T_{\mathrm{MB},0}(\mathbf{q}, i\nu_n)$ for small frequency and momentum:

$$T_{\mathrm{MB},0}(\mathbf{q}, i\nu_n)^{-1} = \frac{1}{\lambda_\Lambda} - \int \frac{\mathrm{d}^d \mathbf{k}}{(2\pi)^d} \frac{1 - f(\xi_{\mathbf{q}/2+\mathbf{k}}) - f(\xi_{\mathbf{q}/2-\mathbf{k}})}{i\nu_n - \xi_{\mathbf{q}/2+\mathbf{k}} - \xi_{\mathbf{q}/2-\mathbf{k}}}$$

$$= c_0 - c_1 \frac{q^2}{2m} + c_2 i\nu_n + \dots \tag{4.29}$$

For concreteness, with consider the $d = 2$ case which is of central interest for us. The unrenormalized coupling λ_Λ can be traded with ϵ_b, the binding energy of two particles in the singlet state. The relation between ϵ_b, λ_Λ and the UV cutoff Λ can be found by calculating the retarded two-body T-matrix in the center-of-mass frame:

$$T_{2\mathrm{B}}(\omega)^{-1} = \frac{1}{\lambda_\Lambda} - \int^\Lambda \frac{\mathrm{d}^d \mathbf{k}}{(2\pi)^2} \frac{1}{\omega - |\mathbf{k}|^2/m + i0^+} = \frac{1}{\lambda_\Lambda} + \frac{N(0)}{2} \ln\left(1 - \frac{2\Lambda}{\omega}\right), \tag{4.30}$$

where $N(0) = m/(2\pi)$ is the 2D density of states (per spin). The inverse T-matrix vanishes at the binding energy and we get:

$$\frac{1}{\lambda_\Lambda} = -\frac{N(0)}{2} \ln\left(1 + \frac{2\Lambda}{\epsilon_b}\right). \tag{4.31}$$

The coefficients (c_0, c_1, c_2, d) can be calculated analytically in 2D by expanding the integral in Eq. (4.29) for small ν_n and $\mathbf{q}$ while using the regularization equation Eq. (4.31). Such analytic expressions are given in the Appendix D.1.

The weak-coupling limit $\epsilon_b \ll \epsilon_F$**:**

Let us first consider the weak-coupling $\epsilon_b/\epsilon_F \ll 1$, where $\mu \simeq \epsilon_F = \pi n/m$. Taking the weak-coupling limit and assuming $\beta\mu \gg 1$, T-matrix assumes the following form:

$$T_{\mathrm{MB},0}^{-1}(\mathbf{q}, i\nu_n; \epsilon_b/\epsilon_F \ll 1) = -N(0)\ln\left(\frac{T}{T_c}\right) - N(0)\frac{7\zeta(3)\epsilon_F}{8\pi^2 T^2}\frac{q^2}{2m} + N(0)\left(\frac{1}{4\epsilon_F} + i\frac{\pi}{8T}\right)i\nu_n.$$

(4.32)

We also find $b = N(0)7\zeta(3)\beta^2/(8\pi^2)$. In the above expression, $T_c \equiv (e^\gamma/\pi)\sqrt{2\epsilon_F\epsilon_b}$ (γ is the Euler's constant), is the usual BCS critical temperature. The weak-coupling GL function can be written directly using the above results:

$$S_{\mathrm{GL,WC}}[\Psi] = \frac{1}{\beta}\int_0^\beta \int d^2\mathbf{x}\left[\Psi^*(\mathbf{x}, \tau)\left(d_{\mathrm{WC}}\,\partial_\tau - \frac{\nabla^2}{4m} + a_{\mathrm{WC}}\right)\Psi(\mathbf{x}, \tau) + \frac{b_{\mathrm{WC}}}{2}|\Psi(\mathbf{x}, \tau)|^4\right],$$

(4.33)

where $\Psi \equiv \sqrt{7\zeta(3)n/(8\pi^2 T_c^2)}\,\Delta$ so that the kinetic term resembles that of a particle with mass $2m$. The weak-coupling coefficients appearing above are given by:

$$a_{\mathrm{WC}} = \frac{4\pi^2}{7\zeta(3)}\frac{T_c^2}{\epsilon_F}\ln\frac{T}{T_c}, \quad b_{\mathrm{WC}} = \frac{4\pi^2}{7\zeta(3)}\frac{T_c^2}{n\epsilon_F}, \quad d_{\mathrm{WC}} = \frac{4\pi^2}{7\zeta(3)}\frac{T_c^2}{\epsilon_F}\left(\frac{1}{4\epsilon_F} + \frac{i\pi}{8T}\right). \quad (4.34)$$

Without that τ derivative term, the above functional is the result given by Gor'kov [33]. a_{WC} changes sign at $T = T_c$ and the GL energy is minimized by the symmetry broken phase $\langle\Delta\rangle = |\Delta_0|e^{i\phi_0}$ for T below T_c. Here, $|\Delta_0|$ is the value the minimizes the static part of the GL functional and ϕ_0 is arbitrary. Considering fluctuations around the mean-field solution, i.e. by taking the ansatz $\Delta = (|\Delta_0| + \delta\rho)\exp(i\phi_0 + \delta\phi)$, we find that the phase fluctuations are given by a Gaussian term $\propto |\nabla\delta\phi|^2$ in the GL functional. In $d = 2$ and at finite T, such thermal phase fluctuations are divergent in the infrared regime due to the celebrated Mermin-Wagner-Hohenberg theorem [177, 178, 179], and in fact, we find that the long-range order is destroyed. Nevertheless, by considering topological vortex-antivortex fluctuations in the phase of the order parameter, one finds that the exponential decay of correlations gives way to a slower algebraic decay at a temperature T_{BKT},

known as the Berezinskii-Kosterlitz-Thouless (BKT) transition temperature. For $T > T_{\mathrm{BKT}}$, the superfluid density $n_s = |\Psi|^2$ is renormalized to zero due to the proliferation of unbound vortex and antivortex pairs, while for $T < T_{\mathrm{BKT}}$, the vortex-antivortex excitations will be bound and one finds a finite $n_s(T_{\mathrm{BKT}}) = (2/\pi)T_{\mathrm{BKT}}$ in the superfluid stiffness, known as the universal Nelson-Kosterlitz jump [180]. In the weakly interacting regime $T_c \ll \epsilon_F$, we find $T_{\mathrm{BKT}} \simeq T_c(1 - 4T_c/\epsilon_F)$, which asymptotically merges with the mean-field T_c [181].

The most important feature of the weak-coupling limit for our current purpose is the presence of an imaginary part in d_{WC}. Continuing the GL functional to real times, neglecting the forth-order term and assuming $T > T_c$, we find a diffusion equation, $\partial_t \Psi = D_{\mathrm{WC}} \nabla^2 \Psi$ for the order parameter, where:

$$D_{\mathrm{WC}} = \frac{T}{\epsilon_b} \frac{\hbar}{m} \frac{7\zeta(3)}{4e^{2\gamma}}. \tag{4.35}$$

The above results indicates that in the normal state and in the weak-coupling regime, the dynamics of the composite bosons is *diffusive*. In other words, bosonic fluctuations are short-lived and quickly decay.

The strong-coupling limit $\epsilon_b \gg \epsilon_F$:

Let us consider the strong-coupling (SC) limit, where $\epsilon_b/\epsilon_F \gg 1$. In this limit, the condition $c_0 = 0$ implies $\mu = -\epsilon_b/2$ to leading order. In general, we assume $\mu_{\mathrm{SC}} = -\epsilon_b/2 + \mu_B/2$, where μ_B is a sub-leading correction to be determined. The many-body T-matrix assumes the form:

$$T_{\mathrm{MB},0}^{-1}(\mathbf{q}, i\nu_n; \epsilon_b/\epsilon_F \gg 1) = \frac{m}{4\pi\epsilon_b}\left(i\nu_n + \mu_B - \frac{q^2}{4m}\right), \tag{4.36}$$

to leading order in ϵ_F/ϵ_b. Defining $\Psi_B \equiv \sqrt{m/(4\pi\epsilon_b)}\,\Delta$, the strong-coupling GL functional reads:

$$S_{\mathrm{GL,SC}}[\Psi_B] = \frac{1}{\beta}\int_0^\beta \int \mathrm{d}^2\mathbf{x} \left[\Psi_B^*(\mathbf{x},\tau)\left(\partial_\tau - \frac{\nabla^2}{4m} + \mu_B\right)\Psi_B(\mathbf{x},\tau) + \frac{g}{2}|\Psi_B(\mathbf{x},\tau)|^4\right], \tag{4.37}$$

where $g = b/c_2^2 = 1/N(0)$ in the strong-coupling limit. Neglecting interaction term for the moment, the GL functional describes free bosons at the chemical potential μ_B. Therefore, we imme-

diately identify $\mu_B \approx \mu_{B,0}$, where $\mu_{B,0}$ is chemical potential of free 2D Bose gas with a number density $n/2$. We note that this strong-coupling behavior is in a striking contrast to the weak-coupling behavior, where the bosonic fluctuations were found to have diffusive dynamics. The ideal Bose gas undergoes a Bose-Einstein condensation (BEC) at $T_{\text{BEC}} = 4\pi n^{2/d} \left[\zeta(d/2)\right]^{-2/d}$ in d dimensions and develops a long-range order. The BEC temperature is finite for $d > 2$ and the interaction effects only lead to sub-leading corrections. The elementary excitations in the BEC regime are described well by the Bogoliubov theory [182]: the dispersion is phonon-like for $k \lesssim 2|\mu_B|^{1/2}$ and free-particle-like for $k \gtrsim 2|\mu_B|^{1/2}$. Approaching $d = 2$ from above, $T_{\text{BEC}} \sim 2\pi(d-2)n^{d/2}$ and tends to zero, which is consistent with the absence of long-range-order at finite T in $d = 2$ due to the Mermin-Wagner-Hohenberg theorem [177, 178, 179]. The inclusion of interactions, however, leads to a finite superfluid density in $d = 2$ below the BKT transition temperature, along with the formation of a *quasi*-condensate with *quasi*-long-range order. We note that $\langle \Psi_B \rangle$ is still strictly zero at finite temperatures due to thermal phase fluctuations.

The problem of quasi-condensation of dilute Bose gas in $d = 2$ has been first studied at length by Popov [183]. Fisher and Hohenberg [182] re-derived Popov's diagrammatic results using a renormalization group (RG) approach and have argued that this analysis is only valid in ultra-dilute regime $\ln \ln(1/\gamma_0) \gg 1$, where $\gamma_0 \equiv n_B r_0^2$ with r_0 being the range of the boson-boson interactions. A quantitative estimate of T_{BKT} with a less stringent diluteness condition has been obtained more recently using QMC [184, 185, 186] and functional RG [187] techniques, culminating in the following expression for the BKT transition temperature:

$$T_{\text{BKT}} = \frac{2\pi n_B}{m_B \left[\ln(\xi/4\pi) + \ln\ln(1/\gamma_0)\right]}, \tag{4.38}$$

where $\xi = 380 \pm 3$ [184]. The above expression is valid in the dilute regime $\ln(1/\gamma_0) \gg 1$ and reduces to the Popov result in the ultra-dilute regime. A simple and accurate account of the BKT transition in the strong-coupling limit of the AFG can be obtained using the above expression by

identifying $m_B = 2m$, $n_B = n/2$ and $\gamma_0 = \epsilon_F/\epsilon_b$ (the exact numerical factor in γ_0 is not important due to the double logarithm). This problem has been studied earlier in Refs. [153, 188, 154, 189] albeit in a crude manner by neglecting the renormalization of the superfluid density which leads to a constant BKT transition temperature, independent of γ_0.

Keeping the quartic term into account, the GL functional describes non-relativistic bosons with a contact interaction. The appearance of the contact interaction is in fact due to our careless treatment of the boson-boson interaction term by approximately setting the external momenta to zero in Eq. 4.28. The exact boson-boson interaction vertex is expected to be cut off at a UV momentum scale determined by the size of the bound state wave function $\Lambda_B \sim \xi_B^{-1} \sim (m\epsilon_b)^{1/2}$ (cf. Sec. 4.4). Quantum fluctuations dramatically modify the effective interaction between the low-energy bosons. This is most easily seen using a momentum-shell RG analysis. The RG flow equations are found using the standard momentum-shell integration procedure. In d spatial dimensions and for $T = \mu = 0$, the running of g is given by [182]:

$$\frac{\mathrm{d}g}{\mathrm{d}l} = (2 - d)g - 4m_B\Lambda_B^{d-2} 2^{-d}\pi^{-d/2}\,\Gamma(d/2)\,g^2 + \mathcal{O}(g^3), \tag{4.39}$$

where l is the RG scale factor related to the physical length scale as $R = \Lambda_B^{-1}e^l$. The first term is the tree-level contribution whereas the second term is the one- particle-particle loop contribution [182]. In $d = 2$, the tree-level contribution vanishes and the the contact interaction is marginal. Integrating the flow equation down to an energy scale $E \sim (\Lambda_B^2/m)e^{-2l}$, we find:

$$g(E) = \frac{g}{1 + (m_B/2\pi)\,g\,\ln[\Lambda_B^2/(m_B E)]}. \tag{4.40}$$

In the strong-coupling limit, $\Lambda_B \to \infty$ and consequently, $g(E) \to 0$ provided that $E \ll \epsilon_b$. In other words, the bosons are asymptotically free in the infra-red regime in $d = 2$. The above result can be obtained using diagrammatic methods as well by summing the ladder diagrams in the particle-particle channel. We will discuss this alternative approach in Sec. 4.4.

Had it not been for strong quantum fluctuations in $d = 2$, $g = 1/N(0) = 2\pi/m$ even for tightly bound bosonic molecules deep in the strong-coupling regime. The IR asymptotic freedom therefore poses a useful merit test for many-body approximations of the AFG model in $d = 2$.

Intermediate couplings $\epsilon_b \sim \epsilon_F \sim T$:

So far, we only studied the GL functional in the weak-coupling and strong-coupling limits. An important concept, widely discussed in the context of high-T_c superconductors, is the existence of a pairing pseudogap regime in the intermediate coupling regime. The conventional picture, based on mean-field ideas, is that in the weak-coupling regime, pairing and phase coherence happen at the same temperature whereas in the strong-coupling regime, the pairing temperature T^* is set by the binding energy $\epsilon_b \gg \epsilon_F$ while phase coherence (quasi-long-range order in $d = 2$) may occur at a much lower temperature. In the latter case, the Fermi surface is destroyed well before superfluidity occurs. In the intermediate-coupling regime, however, it is possible to retain aspects of both the Fermi surface of weak-coupling and the preformed-pair ideas of strong coupling. In other words, one expects to find an intermediate-coupling regime $\epsilon_b \sim \epsilon_F$ in which the superconducting gap is not fully developed, in the sense there are long-lived pairs whose phase coherence is destroyed by thermal and quantum fluctuations.

The spectral weight of fermions in the vicinity of the Fermi surface, while still finite, is significantly reduced due to pairing fluctuations. The physics in the pairing pseudogap regime has a strong flavor of both fermionic and bosonic degrees of freedom. Microscopically, the pairing pseudogap is the regime in which the expectation value of the modulus of the order parameter, $\langle|\Delta|\rangle$, is finite yet its phase is fluctuating and delocalized. Since $\langle|\Delta|\rangle$ is not directly observable quantity, there exists a certain extent of ambiguity in the exact criterion of pseudogap in the literature. In practice, one must resort to observable manifestations of the pseudogap such as thte reduced spectral weight and density of states of fermions.

With this brief review of the GL approach and the general physical picture of the AFG in $d = 2$, we turn to to the description of the system in a purely fermionic language using Green's functions. The latter approach provides us with important observable quantities, such the fermionic spectral function, using which the physics of weak-coupling to pseudogap to strong-coupling can be studied. In the next section, we review the simplest of such theories proposed by The Nozières and Schmitt-Rink [138].

4.2.4 The Nozières-Schmitt-Rink (NSR) theory

The simplest theory that successfully describes the crossover from the weak-coupling fermionic regime to the strong-coupling bosonic regime in the normal state was given by The Nozières and Schmitt-Rink (NSR) [138]. While it was originally proposed for AFG in $d = 3$, it was later generalized to two dimensions [190, 153]. The NSR theory is reminiscent of the self-consistent paramagnon exchange theories in metals. The basic idea is that the effect of pairing fluctuations in the normal state can be captured by considering the interaction of quasiparticles with a particle-particle fluctuations (often referred to as the Cooperon, or the many-body T-matrix). The fundamental NSR equations are:

$$G(\mathbf{q}, i\omega_n) = G_0(\mathbf{k}, i\omega_n) + G_0(\mathbf{k}, i\omega_n)\Sigma_{\text{NSR}}(\mathbf{k}, i\omega_n)\, G_0(\mathbf{k}, i\omega_n), \tag{4.41a}$$

where:

$$\Sigma_{\text{NSR}}(\mathbf{k}, i\omega_n) = \frac{1}{\beta}\sum_{i\nu_n}\int\frac{\mathrm{d}^d\mathbf{q}}{(2\pi)^d}\, T_{\text{MB},0}(\mathbf{q}, i\nu_n)\, G_0(\mathbf{q} - \mathbf{k}, i\nu_n - i\omega_n) \tag{4.41b}$$

and:

$$T_{\mathrm{MB},0}(\mathbf{q}, i\nu_n) = \left[\lambda_\Lambda^{-1} + \frac{1}{\beta} \sum_{i\omega_n} \int^\Lambda \frac{\mathrm{d}^d\mathbf{k}}{(2\pi)^d} G_0(\mathbf{k}, i\omega_n) G_0(\mathbf{q} - \mathbf{k}, i\nu_n - i\omega_n) \right]^{-1}. \tag{4.41c}$$

In the above equations, $G_0(\mathbf{k}, i\omega_n) = 1/(i\omega_n - \xi_{\mathbf{k}})$ is the non-interacting Matsubara Green's function, where $\xi_{\mathbf{k}} = |\mathbf{k}|^2/(2m) - \mu$, μ is the chemical potential, and $\nu_n = 2\pi n/\beta$ and $\omega_n = \pi(2n+1)/\beta$ denote the bosonic and fermionic Matsubara frequencies, respectively. We have assumed that $\uparrow$ and $\downarrow$ states have the same mass and chemical potential. Therefore, the spin indices have been dropped from the Green's functions for brevity. In the diagrams, thin and thick lines denote G_0 and G, respectively, the double-line denotes the T-matrix, and the dotted line is the bare interaction. The chemical potential is determined by fixing the number density of the gas n:

$$n = \frac{1}{\beta} \sum_{i\omega_n} \int \frac{\mathrm{d}^d\mathbf{k}}{(2\pi)^d} G(\mathbf{k}, i\omega_n). \tag{4.42}$$

The thermodynamic potential $\Omega = -\beta^{-1} \ln Z$ can be easily found from Eq. (4.41a) using the coupling-constant integration technique [33] and one finds $\Omega_{\mathrm{NSR}} = \Omega_0 + \Omega_{\mathrm{fluc.}}$ [138], where Ω_0 is the thermodynamic potential of a free Fermi gas at chemical potential μ and temperature β^{-1}, and:

$$\Omega_{\mathrm{fluc.}} = \frac{V}{\beta} \sum_{i\nu_n} \int^\Lambda \frac{\mathrm{d}^d\mathbf{q}}{(2\pi)^d} \ln\left[1 - \lambda_\Lambda \chi_0(\mathbf{q}, i\nu_n)\right]. \tag{4.43}$$

Here, V is the volume of the gas and χ_0 is the bare two-particle propagator (i.e. the last term in Eq. 4.41c). The diagrammatic representation is given in Fig. 4.7. Comparing the Ω_{NSR} with the GL functional derived earlier, Eq. (4.27), we immediate identity the NSR theory as keeping only the quadratic term in S_{GL}. In other words, only Gaussian fluctuations are considered and the interaction between the bosonic fluctuations is ignored.

The various limits of the T-matrix was studied in the previous section. In the weak-coupling limit, we have shown earlier that $N(0) T_{\mathrm{MB},0} \sim 2/\ln(\epsilon_F/\epsilon_b) \ll 1$ for typical energies and mo-

menta (cf. Eq. 4.32). The weak fluctuations were also shown to have a diffusive character. Thus, fluctuation effects can be neglected altogether in this limit and the free Fermi gas picture is recovered, i.e. $\mu \simeq \mu_F(T)$, the chemical potential of a free 2D Fermi gas with number density n. In the strong-coupling limit, however, the T-matrix assumes the polar form given in Eq. (4.36), valid as long as $|\omega|$, $|\mathbf{q}|^2/(2m) \ll \epsilon_b$, and describes the propagation of long-lived pairs. Let us investigate fermion Green's function in this limit. As a first step, we calculate *spectral broadening*, $\Gamma(\omega, \mathbf{p}) \equiv -2\Im\left[\Sigma_{\mathrm{NSR}}(\mathbf{p}, i\omega_n \to \omega + i0^+)\right]$. The calculation in elementary and we find:

$$\Gamma(\omega, \mathbf{p}) = \int \frac{d\omega_B}{2\pi} \frac{d^2\mathbf{q}}{(2\pi)^2} \, A_0(\omega_B - \omega, \mathbf{q} - \mathbf{p}) \, B_0(\omega_B, \mathbf{q}) \left[f_0(\omega_B - \omega) + b_0(\omega_B)\right], \quad (4.44)$$

where $f_0(x) = (e^{\beta x} + 1)^{-1}$ and $b_0(x) = (e^{\beta x} - 1)^{-1}$ denote the Fermi-Dirac and Bose-Einstein distribution functions, and:

$$A_0(\omega, \mathbf{k}) = -2\Im\left[G_0(\mathbf{k}, i\omega_n \to \omega + i0^+)\right] = 2\pi\delta(\omega - \xi_\mathbf{k}),$$

$$B_0(\omega, \mathbf{q}) = -2\Im\left[T_{\mathrm{MB},0}(\mathbf{q}, i\omega_n \to \omega + i0^+)\right] = \frac{8\pi^2\epsilon_b}{m}\,\delta(\omega + \mu_B - |\mathbf{q}|^2/(4m)), \quad (4.45)$$

denote the bare fermionic and bosonic spectral functions. Like before, we have expressed the chemical potential as $\mu = -\epsilon_b/2 + \mu_B/2$. Plugging the above expressions into Eq. (4.44), we find after some simplifications:

$$\Gamma(\omega, p) = 8\pi\epsilon_b\,\theta[\Omega(\omega, p)] \int_0^{2\pi} \frac{d\phi}{2\pi}\, b_0\left(\Omega(\omega, p) + \frac{p^2}{m} - \mu_B + \frac{p\sqrt{4m\Omega(\omega, p)}}{m}\cos\phi\right),$$

$$\Omega(\omega, p) = \frac{p^2}{2m} - \omega + \omega_{\mathrm{th}}, \qquad \omega_{\mathrm{th}} = -(\epsilon_b + \mu_B)/2. \quad (4.46)$$

The angular integration becomes trivial for $p = 0$ and give the following simple analytic result:

$$\Gamma(\omega, 0) = 8\pi\epsilon_b\,\theta(\omega_{\mathrm{th}} - \omega)\, b_0\left[(\omega_{\mathrm{th}} - \omega - \mu_B)\right]. \quad (4.47)$$

The real self-energy is obtained through a Kramers-Kronig transform:

$$\Re[\Sigma^+(\omega, p)] = -\int_{\omega^-(p)}^{\infty} \frac{d\omega'}{2\pi} \frac{\Gamma(-\omega', p)}{\omega' - \omega}, \qquad \omega^-(p) \equiv -\omega_{\mathrm{th}} - p^2/(2m). \quad (4.48)$$
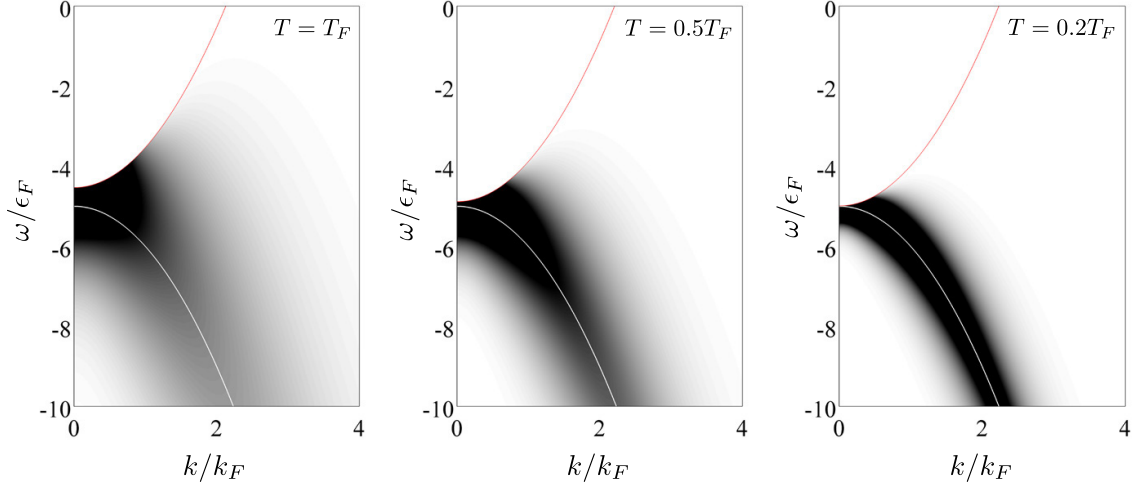
Figure 4.6: The spectral broadening $\Gamma(\omega, p)$ from the NSR theory in the strong-coupling limit $\epsilon_b/\epsilon_F = 10$. The red line indicates the threshold $\omega_{\text{th}}(p) \equiv p^2/(2m) + \omega_{\text{th}}$ for the hole branch. The white line shows $-\epsilon_b/2 - p^2/2m$, the low-temperature coherent limit of the hole branch. Note that the coherence of the hole branch is increased as the temperature is decreased and starts to resemble the lower Bogoliubov quasihole branch as in the BCS theory.

The spectral function is obtained using $\mathsf{A}_{\text{NSR}}(\omega, p) \equiv -2\Im\left[G_{\text{NSR}}(p, i\omega_n \to \omega + i0^+)\right]$, which takes the following form in the strong-coupling regime:

$$\mathsf{A}_{\text{NSR}}(\omega, p) = 2\pi\,\delta(\omega - \xi_p) + \frac{\Gamma(\omega, p)}{(\omega - \xi_p)^2}. \tag{4.49}$$

The first term results from G_0 in Eq. (4.41a) and is the contribution from unpaired fermions. The second term is the contribution from bound fermions.

We immediately observe several important features by investigating the above expressions:

(1) The spectral function has two branches: the upper (particle) branch and a lower (hole) branch. The physical interpretation of these two branches can be understood in analogy to the BCS state. By definition, the fermion spectral function is the probability of creating and subsequently annihilating a particle in the state $(\omega, \mathbf{p})$. The injected particle may either remain free, or may form a bound state. In the former case, the particle obeys the mass-shell relation

$\omega = \xi_{\mathbf{p}}$ and gives the upper branch. In the second case, the injected particle forms a bound state with momentum $\mathbf{p} + \mathbf{q}$ and subsequently, a particle with momentum $\mathbf{q}$ is annihilated. Conservation of energy requires $\omega = |\mathbf{p} + \mathbf{q}|^2/(4m) - \epsilon_b - 2\mu - (|\mathbf{q}|^2/(2m) - \mu)$. At finite temperatures, conservation of energy can be satisfied for a range of different $\mathbf{q}$. The angular integration in Eq. (4.46) weighted by the Bose-Einstein distribution is a manifestation of such different possibilities. Therefore, the hole branch is broad and incoherent. This behavior shows an important difference between the NSR and the mean-field BCS theories: in the latter, only zero momentum bosonic states are allowed, so that $\mathbf{q} = -\mathbf{p}$ the hole branch is also coherent. Fig. 4.6 shows Γ for different temperatures. The increased coherence of the lower branch at lower temperature is clearly noticeable.

(2) The presence of the Bose-Einstein distribution in Γ and in turn in A is a first indication of the importance of a proper treatment of the fermion spectral function in the strong coupling regime. The statistics of composite bosons is *encoded* in the spectral function of fermions. Therefore, the dynamics of bosons will also be manifest in the dynamics of the fermion spectral function. We note that this observation is not limited to the NSR approximation. Let us consider an arbitrary derived quantity of the Green's function:

$$\langle Q \rangle = \left(\int_{-\infty}^{-\epsilon^*} + \int_{-\epsilon^*}^{\epsilon^*} + \int_{\epsilon^*}^{\infty} \right) \frac{d\omega}{2\pi} \int \frac{d^d \mathbf{p}}{(2\pi)^d} \, Q(\omega, \mathbf{p}) \, A(\omega, \mathbf{p}) \, f(\omega, \mathbf{p}), \qquad (4.50)$$

where $Q(\omega, \mathbf{p})$ is an arbitrary function. We have broken the frequency integral into three segments by defining ϵ^* such that $T \ll \epsilon^* \ll \epsilon_b$. The presence of the pseudogap in the spectrum implies that the middle integral is of the order of the spectral weight of the pseudogap and is therefore vanishingly small in the strong coupling limit. The last integral, corresponding to the number density of unpaired fermions, is also exponentially suppressed due to the Fermi-Dirac distribution (see Eq. 4.52). Therefore, the derived quantities from the fermion Green's functions are predominantly given by the first integral corresponding to the hole branch, in

which we may also set $f_0(\omega) \to 1$ up to exponentially small corrections. This conclusion remains valid in application to non-equilibrium problems as well, provided that that the energy of the disturbances is much smaller than the gap $\sim \epsilon_b$.

(3) The NSR approximation violates the sum rule, $\int \mathrm{d}\omega/(2\pi)\, \mathsf{A}(\omega, \mathbf{k}) = 1$. Moreover, the density of states may become negative in the intermediate-coupling regime [191]. These artefacts are related to the truncation of the Dyson's series at the lowest order. A simple variant of the NSR theory, known as the $G_0 G_0$ theory, is free of such unphysical issues.

(4) The spectral weight of the hole branch at any given momentum is small in the strong-coupling regime:

$$\rho_{\text{hole}}(p) \equiv \int \mathrm{d}\omega\, \frac{\Gamma(\omega, p)}{(\omega - \xi_p)^2} = \mathcal{O}\left(\frac{T}{\epsilon_b}\right). \tag{4.51}$$

Yet, $\int \mathrm{d}^d \mathbf{p}\, \rho_{\text{hole}}(p) \sim n$ and is finite. The smallness of the spectral weight of the hole branch implies that the particle branch is extremely sharp, with a quasiparticle residue $Z = 1 - \mathcal{O}(T/\epsilon_b)$.

Let us show that μ_B is indeed given by the chemical potential of free 2D bosons in the limit $\beta \epsilon_b \gg 1$. According to Eq. (4.41a), the density has contributions both from unpaired and unpaired fermions. The former is given by:

$$
\begin{aligned}
n_F &= 2 \int \frac{\mathrm{d}\omega}{2\pi} \frac{\mathrm{d}^2 \mathbf{p}}{(2\pi)^2}\, \mathsf{A}_0(\omega, \mathbf{p})\, f_0(\omega) \\
&= \frac{2N(0)}{\beta} \int_{-\beta\mu}^{\infty} \frac{\mathrm{d}\xi}{e^\xi + 1} = \frac{2N(0)}{\beta} \ln\left(1 + e^{\beta\mu}\right).
\end{aligned} \tag{4.52}
$$

In the limit $\beta \epsilon_b \gg 1$, $n_F \sim N(0)T\, e^{-\beta\epsilon_b/2}$ and is exponentially small. The fluctuation contribution

Nozières-Schmitt-Rink ($G_0 G_0$)   Kadanoff-Martin ($G G_0$)   Self-consistent (GG, SCTMA)

$$\sum_n \frac{1}{n}$$ $$\sum_n \frac{1}{n}$$ $$\sum_n \frac{1}{n}$$
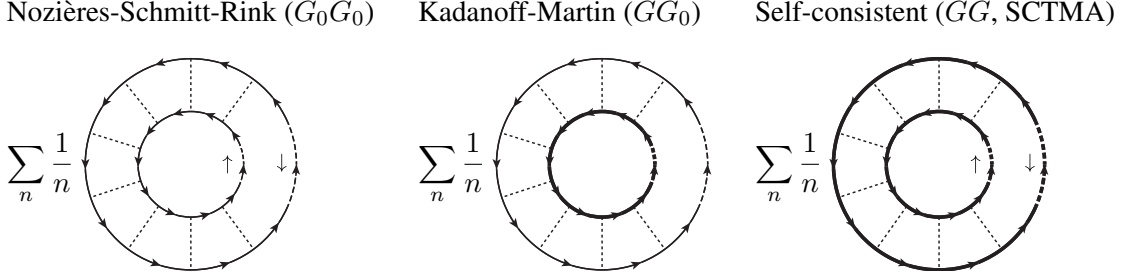
Figure 4.7: The thermodynamical potential Ω of NSR-like theories. Ω coincides with the Luttinger-Ward functional $\Phi[\mathcal{G}]$ in the fully self-consistent (GG) approximation.

can be calculated using Eqs. (4.44) and (4.49):

$$
\begin{aligned}
n_{\text{fluc.}} &= 2 \int \frac{\mathrm{d}\omega}{2\pi} \frac{\mathrm{d}^2 \mathbf{p}}{(2\pi)^2} \frac{\Gamma(\omega, p)}{(\omega - \xi_p)^2} f_0(\omega) \\
&= \frac{8\pi\epsilon_b}{m} \int \frac{\mathrm{d}^2 \mathbf{p}}{(2\pi)^2} \frac{\mathrm{d}^2 \mathbf{q}}{(2\pi)^2} \frac{b_0(\epsilon_{\mathbf{q}}/2 - \mu_B)}{(\epsilon_{\mathbf{q}}/2 - \epsilon_{\mathbf{q}-\mathbf{p}} - \epsilon_{\mathbf{p}} - \epsilon_b)^2} = 2 \int \frac{\mathrm{d}^2 \mathbf{q}}{(2\pi)^2} b_0(\epsilon_{\mathbf{q}}/2 - \mu_B) \\
&= -\frac{2N(0)}{\beta} \ln\left(1 - e^{\beta\mu_B}\right).
\end{aligned}
\tag{4.53}
$$

We find that $n_{\text{fluc.}} = 2n_B(\beta, \mu_B)$, as promised. We have neglected exponentially small corrections from the Fermi-Dirac distribution in the second line. We identify μ_B as the chemical potential of a free Bose gas with density $n/2$.

4.2.5 The class of T-matrix-like theories and their limitations

The NSR theory is the simplest pairing fluctuation-exchange approximation and can be improved in several ways. Instead of truncating the Dyson's equation at the lowest order, the 1PI self-energy diagrams can be resummed to all orders by solving the Dyson's equation exactly, i.e. $G = \left[G_0^{-1} - \Sigma_{\text{NSR}}\right]^{-1}$. The resulting approximation, known as the $G_0 G_0$ T-matrix approximation, while sharing many features with the original NSR theory, fixes the spectral function sum rule violation. The $G_0 G_0$ approximation in $d = 3$ has been explored to a great extent is Refs. [192, 193, 191] (and the references therein). It is known that this simple approximation compares favorably with the experimental measurement of the spectral function [12, 194]. More recently, the $G_0 G_0$ theory has

also been applied to $d = 2$ toward studying the Fermi polaron problem [152] and the population-balanced AFG [155].

The next refinement of the NSR theory is obtained by promoting one of the bare Green's functions appearing in the T-matrix to a full Green's function, while solving the Dyson's equation self-consistently. The resulting approximation is known as the Kadanoff-Martin (KM) theory, also referred to as the GG_0 approximation. While the KM theory strikes as a heuristic improvement of NSR at the first glance, in fact it is the description one obtains by truncating the Martin-Schwinger hierarchy at the 3-particle level [195]. The thermodynamic potential of the KM theory is shown in Fig. 4.7. Provided that the two spin states have equal population and masses, the GG_0 approximation is conserving at the lowest level of expectation values [195]. The predictions of the GG_0 theory in $d = 3$ has been discussed in Refs. [196], where it is found to give a better description at low temperatures compared to G_0G_0 and the NSR approximations.

The ultimate refinement of the NSR theory is obtained by promoting all Green's functions appearing in Σ_{NSR} to full Green's function, and solving the Dyson's equation self-consistently. The resulting approximation is the self-consistent T-matrix approximation (SCTMA), also referred to as the GG approximation. The thermodynamic potential of SCTMA is shown in Fig. 4.7. Being a self-consistent (Φ-derivable) approximation, SCTMA is fully conserving and satisfies the complete 2PI-WTH (cf. Sec. 1.4). The complete phase diagram of the the attractive Fermi gas in $d = 3$ within this approximation, including the superfluid regime, has been studied by Haussmann *et al.* [197, 198]. This scheme yields the best estimates to the thermodynamic quantities of the AFG in $d = 3$ [198] compared to the benchmark Quantum Monte-Carlo results [136, 135] and the rest of the NSR family. Nevertheless, the SCTMA is far from being exact and has known shortcomings: comparing its spectral functions with those obtained by ARPES experiments with ultracold atoms shows that SCTMA fails to exhibit the pseudogap behavior at unitarity [199], a feature present in G_0G_0, GG_0, QMC and experiments. At the moment, the SCTMA results are not available in

$d = 2$. More extensive discussion regarding the comparison of these approximations can be found in Ref. [200].

The studies based on the T-matrix-like schemes have so far been focused to systems in thermal equilibrium. There exists strong experimental indications that the predictions of the T-matrix theory in equilibrium is very satisfactory. In applications to the dynamics of ultracold gases and non-equilibrium superconductivity, it is desirable to obtain an extension of the T-matrix theory to non-equilibrium states. The only Φ-derivable scheme in the family of T-matrix-like approximations is the SCTMA. In the next few sections, we utilize the results of chapter 2 and extend SCTMA to non-equilibrium situations using the real-time Schwinger-Keldysh formalism. In particular, we derive a set of quantum kinetic equations that describe the dynamics of unpaired and paired fermions on an equal footing and rigorously respect the conservation laws. We will utilize the obtained formalism later to analyze the quantum dynamics of the AFG in optical traps.

4.3 The non-equilibrium T-matrix theory

This section is devoted to a detailed and general discussion on the extension of SCTMA to non-equilibrium states in the non-superfluid regime. The extension to non-equilibrium state is done using the 2PI-EA formalism on the Schwinger-Keldysh contour as discussed in chapter 1. We also continue discussion of the renormalization of contact interactions and provide expressions that are manifestly divergence-free both in equilibrium and non-equilibrium settings.

As mentioned in Sec. 1.3.2, SCTMA can alternatively be obtained by truncating the Luttinger-Ward functional of the $Sp(N)$-symmetric extension of the AFG model at the next-to-leading-order (NLO) level in the large-N limit. The self-energy is readily obtained by opening a fermion line in

$\Phi[\mathcal{G}]$ shown in Fig. 4.7:

$$\Sigma_\sigma(1, 1') = -i \int d2\, d2'\, \mathcal{G}_{\bar\sigma}(2', 2^+)\, \mathcal{T}(1, 2; 1', 2') = \quad \tag{4.54}$$

where the contour T-matrix $\mathcal{T}$ is given by the following self-consistent equation:

$$\mathcal{T}(1, 2; 1', 2') = v_\Lambda(1, 2; 1', 2') + i \int d3\, d4\, d3'\, d4'\, v_\Lambda(1, 2; 3, 4)\, \mathcal{G}_\uparrow(3, 3')\, \mathcal{G}_\downarrow(4, 4')\, \mathcal{T}(3', 4'; 1', 2').$$
$$\tag{4.55}$$

We have used the notation $\bar\uparrow = \downarrow$ and $\bar\downarrow = \uparrow$. In the above equations and in the forthcoming equations, the integer indices is a shorthand notation for the bundle of contour times and the space coordinates, i.e. $1 \equiv (\tau_1, \mathbf{x}_1)$, etc. We use the UV regulated expression for interaction vertex v_Λ discussed earlier (cf. Eq. 4.11):

$$v_\Lambda(1, 2; 1', 2') \equiv \delta_{\mathcal{C}}(\tau_1, \tau_1')\, \delta_{\mathcal{C}}(\tau_2, \tau_2')\, \delta_{\mathcal{C}}(\tau_1, \tau_2)\, \delta^d(\eta_\uparrow \mathbf{x}_1 + \eta_\downarrow \mathbf{x}_2 - \eta_\uparrow \mathbf{x}_1' - \eta_\downarrow \mathbf{x}_2')$$
$$\times \lambda_\Lambda\, w_\Lambda(\mathbf{x}_1 - \mathbf{x}_2)\, w_\Lambda(\mathbf{x}_1' - \mathbf{x}_2').$$

As a direct consequence of the conservation of the momentum at the bare vertex, and the instantaneity of the bare interaction, we find that the following ansatz solves Eq. (4.55):

$$\mathcal{T}(1, 2; 1', 2') = \delta_C(\tau_1, \tau_2)\, \delta_C(\tau_1', \tau_2')\, w_\Lambda(\mathbf{x}_1 - \mathbf{x}_2)\, w_\Lambda(\mathbf{x}_1' - \mathbf{x}_2')$$
$$\times \mathsf{T}\big[\tau_1, \tau_1'; (\eta_\uparrow \mathbf{x}_1 + \eta_\downarrow \mathbf{x}_2), (\eta_\uparrow \mathbf{x}_1' + \eta_\downarrow \mathbf{x}_2')\big]. \tag{4.56}$$

Plugging the above ansatz into Eq. (4.55), we find the following integral equation for the *reduced* T-matrix, T:

$$\mathsf{T}(\tau_1, \tau_1'; \mathbf{R}_1, \mathbf{R}_1') = \lambda_\Lambda\, \delta_{\mathcal{C}}(\tau_1, \tau_1')\, \delta^d(\mathbf{R}_1 - \mathbf{R}_1')$$
$$+ i\lambda_\Lambda \int_{\mathcal{C}} d\tau_2 \int d^d\mathbf{R}_2\, \chi(\tau_1, \tau_2; \mathbf{R}_1, \mathbf{R}_2)\, \mathsf{T}(\tau_2, \tau_1'; \mathbf{R}_2, \mathbf{R}_1'), \tag{4.57}$$

where:

$$\chi(\tau_1, \tau_2; \mathbf{R}_1, \mathbf{R}_2) = \int d^d \mathbf{y}_1 \int d^d \mathbf{y}_2 \, w_\Lambda(\mathbf{y}_1) \, w_\Lambda(\mathbf{y}_2)$$

$$\times \, \mathcal{G}_\uparrow(\tau_1, \mathbf{R}_1 + \eta_\downarrow \mathbf{y}_1; \tau_2, \mathbf{R}_2 + \eta_\downarrow \mathbf{y}_2) \, \mathcal{G}_\downarrow(\tau_1, \mathbf{R}_1 - \eta_\uparrow \mathbf{y}_1; \tau_2, \mathbf{R}_2 - \eta_\uparrow \mathbf{y}_2). \quad (4.58)$$

Before we embark on renormalizing the reduced T-matrix, we derive formal expressions for the explicit-time components of the self-energy for future use in terms of T. Pluging Eq. (4.56) into Eq. (4.54) and using the $\delta_{\mathcal{C}}$-functions to evaluate the contour time integrals, the greater/lesser components can be easily expressed as:

$$\Sigma_{\bar{\sigma}}^{\gtrless}(1, 1') = -i \int d\mathbf{x}_2 \int d\mathbf{x}_2' \, w_\Lambda(\mathbf{x}_1 - \mathbf{x}_2) \, w_\Lambda(\mathbf{x}_1' - \mathbf{x}_2') \, G_{\bar{\sigma}}^{\lessgtr}(t_1', \mathbf{x}_2'; t_1, \mathbf{x}_2)$$

$$\times \, \mathsf{T}^{\gtrless}[t_1, t_1'; (\eta_\uparrow \mathbf{x}_1 + \eta_\downarrow \mathbf{x}_2), (\eta_\uparrow \mathbf{x}_1' + \eta_\downarrow \mathbf{x}_2')]. \quad (4.59)$$

The retarded/advanced is the the sum of the collisional contribution obtained from Eq. (4.59), and the instantaneous Hartree term arising from the first term on the right hand side of Eq. (4.57), and :

$$\Sigma_{\bar{\sigma}}^{\pm}(1, 1') = \pm\theta(\pm t_1 \mp t_1') \left(\Sigma_{\bar{\sigma}}^{>}(1, 1') - \Sigma_{\bar{\sigma}}^{<}(1, 1') \right)$$

$$- i\lambda_\Lambda \, \delta(t_1 - t_1') \int d\mathbf{x}_2 \int d\mathbf{x}_2' \, w_\Lambda(\mathbf{x}_1 - \mathbf{x}_2) \, w_\Lambda(\mathbf{x}_1' - \mathbf{x}_2')$$

$$\times \, G_{\bar{\sigma}}^{<}(t_1, \mathbf{x}_2'; t_1, \mathbf{x}_2) \, \delta^d(\eta_\uparrow \mathbf{x}_1 + \eta_\downarrow \mathbf{x}_2 - \eta_\uparrow \mathbf{x}_1' - \eta_\downarrow \mathbf{x}_2'). \quad (4.60)$$

In order to obtain expressions for the explicit-time components of T, we apply the Langreth rules to Eq. (4.57):

$$\mathsf{T}^{\gtrless}(t_1, t_1'; \mathbf{R}_1, \mathbf{R}_1') = i\lambda_\Lambda \left(\chi^+ \star \mathsf{T}^{\gtrless} \right)(t_1, t_1'; \mathbf{R}_1, \mathbf{R}_1') + i\lambda_\Lambda \left(\chi^{\gtrless} \star \mathsf{T}^- \right)(t_1, t_1'; \mathbf{R}_1, \mathbf{R}_1'),$$

$$(4.61a)$$

$$\mathsf{T}^{\pm}(t_1, t_1'; \mathbf{R}_1, \mathbf{R}_1') = \lambda_\Lambda \, \delta(t_1 - t_1') \, \delta^d(\mathbf{R}_1 - \mathbf{R}_1') + i\lambda_\Lambda \left(\chi^{\pm} \star \mathsf{T}^{\pm} \right)(t_1, t_1'; \mathbf{R}_1, \mathbf{R}_1'). \quad (4.61b)$$

Combining the last two equations, we obtain:

$$\mathsf{T}^{\gtrless}(t_1, t_1'; \mathbf{R}_1, \mathbf{R}_1') = (\mathsf{T}^+ \star \chi^{\gtrless} \star \mathsf{T}^-)(t_1, t_1'; \mathbf{R}_1, \mathbf{R}_1'). \quad (4.62)$$

4.3.1 Renormalization of the T-matrix in vacuum

In order to make connection between the parameters of the microscopic model, $\{\lambda_\Lambda, w_\Lambda(\mathbf{x})\}$, and experimentally observable quantities (a_s in $d = 3$, ϵ_b in $d = 2$), we calculate the T-matrix in vacuum using the expressions given in the previous section. This is done by simply using vacuum fermion propagators in the expressions derived in the previous section. We affix the superscript 0 to quantities evaluated in vacuum. Clearly, $\chi_0^\pm(t_1, t_1'; \mathbf{R}_1, \mathbf{R}_1')$ and $\mathsf{T}_0^\pm(t_1, t_1'; \mathbf{R}_1, \mathbf{R}_1')$ are just functions of $t_1 - t_1'$ and $\mathbf{R}_1 - \mathbf{R}_1$. Therefore, Eq. (4.143) becomes a simple algebraic equation in the Fourier space as follows:

$$\mathsf{T}_0^\pm(\omega; \mathbf{q}) = \lambda_\Lambda + i\lambda_\Lambda \chi_0^\pm(\omega; \mathbf{q}) \mathsf{T}_0^\pm(\omega; \mathbf{q}). \tag{4.63}$$

The retarded two-particle propagator in vacuum, $\chi_0^\pm(\omega; \mathbf{q})$, can be calculated from Eq. (4.58) and by noting that $G_{0,\sigma}^<(1, 1') = i\langle 0|\Psi_\sigma^\dagger(1')\Psi_\sigma(1)|0\rangle = 0$, and:

$$G_{0,\sigma}^>(1, 1') = -i \int \frac{d\omega}{2\pi} \frac{d^d\mathbf{k}}{(2\pi)^d} \mathsf{A}_{0,\sigma}(\omega, \mathbf{k}) e^{i\omega(t_1 - t_1')} e^{-i\mathbf{k}\cdot(\mathbf{x}_1 - \mathbf{x}_1')}, \tag{4.64}$$

where $\mathsf{A}_{0,\sigma}(\omega, \mathbf{k}) = 2\pi \delta(\omega - |\mathbf{k}|^2/(2m_\sigma))$ is the non-interacting spectral function for the σ component. A straightforward calculation yields:

$$\begin{aligned} \chi_0^\pm(\omega; \mathbf{q}) &= -i \int \frac{d\omega_1}{2\pi} \frac{d\omega_2}{2\pi} \frac{d^d\mathbf{k}}{(2\pi)^d} \frac{|\tilde{w}_\Lambda(\mathbf{k})|^2}{\omega^\pm - \omega_1 - \omega_2} \mathsf{A}_{0,\uparrow}(\omega_1, \eta_\uparrow \mathbf{q} + \mathbf{k}) \mathsf{A}_{0,\downarrow}(\omega_2, \eta_\downarrow \mathbf{q} - \mathbf{k}) \\ &= -i \int \frac{d^d\mathbf{k}}{(2\pi)^d} \frac{|\tilde{w}_\Lambda(\mathbf{k})|^2}{\omega^\pm - |\mathbf{k}|^2/(2m_{\text{red}}) - |\mathbf{q}|^2/(2m_{\text{tot}})}. \end{aligned} \tag{4.65}$$

The above integral is convergent provided that $|\tilde{w}_\Lambda(\mathbf{k})|$ falls faster than $k^{1-d/2}$ for large k. Plugging this result into Eq. (4.63), we get:

$$\left[\mathsf{T}_0^\pm(\omega; \mathbf{q})\right]^{-1} = \frac{1}{\lambda_\Lambda} - \int \frac{d^d\mathbf{k}}{(2\pi)^d} \frac{|\tilde{w}_\Lambda(\mathbf{k})|^2}{\omega^\pm - |\mathbf{k}|^2/(2m_{\text{red}}) - |\mathbf{q}|^2/(2m_{\text{tot}})}. \tag{4.66}$$

Fixing the value of the on-shell T-matrix at an energy scale E_0, we find the renormalization equation in d dimensions:

$$\frac{1}{\lambda_\Lambda} = [\mathsf{T}_0(E_0)]^{-1} + \int \frac{d^d\mathbf{k}}{(2\pi)^d} \frac{|\tilde{w}_\Lambda(\mathbf{k})|^2}{E_0^+ - |\mathbf{k}|^2/(2m_{\text{red}})}. \tag{4.67}$$

Regularization in $d = 3$:

Eq. (4.67) provides the sought-after connection between the microscopic and renormalized parameters. In $d = 3$, we match the zero energy T-matrix, whose value can be determined from Eq. (4.13) in terms of the s-wave scattering length. Eq. (4.67) then gives:

$$\frac{1}{\lambda_\Lambda} = \frac{m_{\text{red}}}{2\pi a_s} - \int \frac{\mathrm{d}^3 \mathbf{k}}{(2\pi)^3} \frac{|\tilde{w}_\Lambda(\mathbf{k})|^2}{|\mathbf{k}|^2/(2m_{\text{red}})}. \tag{4.68}$$

Once λ is determined from the above equation, the zero-range limit $\Lambda \to \infty$ can be taken. Regardless of one's choice of w_Λ, this procedure yields:

$$\mathsf{T}_0^\pm(\omega; \mathbf{q}) = \frac{2\pi}{m_{\text{red}}} \left[\frac{1}{a_s} + i\sqrt{2m_{\text{red}} \left[\omega^\pm - |\mathbf{q}|^2/(2m_{\text{tot}}) \right]} \right]^{-1}. \tag{4.69}$$

Note that the branch cut is taken along the negative real axis. For concreteness, the renormalization equation for the choice $\tilde{w}_\Lambda(\mathbf{k}) = \theta(\Lambda - |\mathbf{k}|)$ is given by:

$$\frac{1}{\lambda_\Lambda} = \frac{m_{\text{red}}}{2\pi a_s} - \frac{m_{\text{red}}\Lambda}{\pi^2}. \tag{4.70}$$

Note that $\lim_{\Lambda \to \infty} \lambda_\Lambda = 0$. This result implies that only diagrams involving formally divergent loop integrals yield non-zero contributions to the renormalized theory.

Regularization in $d = 2$:

In $d = 2$, the renormalization equation can be found by requiring $\mathsf{T}_0^+(E)$ to have a pole at $E = -\epsilon_b$. Using Eq. (4.66), we immediately find:

$$\frac{1}{\lambda_\Lambda} = -\int \frac{\mathrm{d}^2 \mathbf{k}}{(2\pi)^2} \frac{|\tilde{w}_\Lambda(\mathbf{k})|^2}{\epsilon_b + |\mathbf{k}|^2/(2m_{\text{red}})}. \tag{4.71}$$

Using the above prescription for λ and taking the zero-range limit $\Lambda \to \infty$ of the T-matrix, we find (independent of the choice of w_Λ):

$$\mathsf{T}_0^\pm(\omega; \mathbf{q}) = \frac{2\pi/m_{\text{red}}}{\ln\left[-\epsilon_b/(\omega^\pm - |\mathbf{q}|^2/(2m_{\text{tot}}))\right]}, \tag{4.72}$$

where the branch cut is again taken along the negative real axis. The renormalization equation for the choice $\tilde{w}_\Lambda(\mathbf{k}) = \theta(\Lambda - |\mathbf{k}|)$ is given by:

$$\frac{1}{\lambda_\Lambda} = -\frac{m_{\text{red}}}{2\pi} \ln\left(1 + \frac{2\Lambda}{\epsilon_b}\right). \tag{4.73}$$

Again, we find $\lim_{\Lambda \to \infty} \lambda_\Lambda = 0$.

4.3.2   Renormalization of the in-medium T-matrix

A procedure for taking the zero-range limit and renormalizing the in-medium T-matrix can be easily devised as follows: since the in-medium and vacuum Green's functions asymptotically match in the high energy limit, $\lim_{\Lambda \to \infty}(\chi^\pm - \chi_0^\pm)$ exists since the UV divergences $\chi^\pm$ and $\chi_0^\pm$ cancel each other. Inverting Eq. (4.57) for T, we obtain $(\mathsf{T}^\pm)^{-1} = \lambda_\Lambda^{-1} - i\chi^\pm$, which in turn can be decomposed like:

$$\left(\mathsf{T}^\pm\right)^{-1} = \left(\frac{1}{\lambda_\Lambda} - i\chi_0^\pm\right) - i\left(\chi^\pm - \chi_0^\pm\right). \tag{4.74}$$

Taking the zero-range limit of the right hand side and using the renormalization condition of λ_Λ derived in the previous section, we find that each bundle of terms has a well-defined limit. In particular, the first term parenthesis is simply the vacuum T-matrix. Thus, we formally obtain:

$$\lim_{\Lambda \to \infty} \left(\mathsf{T}^\pm\right)^{-1} = \left(\mathsf{T}_0^\pm\right)^{-1} - i \lim_{\Lambda \to \infty} \left(\chi^\pm - \chi_0^\pm\right). \tag{4.75}$$

Note that only renormalized quantities appear in the above equation. At this stage, we may also take the zero-range limit of the expressions we derived for the self-energy, Eq. (4.59) and Eq. (4.60). The w-functions become δ-functions in this limit and simplify the analysis further. The details of this procedure may be carried out most transparently in the Wigner representation, which is the subject of the next section.

4.3.3   The T-matrix approximation in the Wigner representation

In this section, we obtain analogous expressions to those derived in Sec. 4.3 in the Wigner representation. We also take the zero-range limit, which is ultimately the limit in which we wish to carry out the rest of the analysis. As a first step, we take the zero-range limit of Eq. (4.59) and Eq. (4.60). As mentioned above, the w-functions simply become δ-functions resulting in the following simple expressions:

$$\lim_{\Lambda \to \infty} \Sigma_{\sigma}^{\gtrless}(1, 1') = -iG_{\bar{\sigma}}^{\lessgtr}(t_1', \mathbf{x}_2'; t_1, \mathbf{x}_2) \left[\lim_{\Lambda \to \infty} \mathsf{T}^{\gtrless}(t_1, t_1'; \mathbf{x}_1, \mathbf{x}_1') \right],$$

$$\lim_{\Lambda \to \infty} \Sigma_{\sigma}^{\pm}(1, 1') = \pm \theta(\pm t_1 \mp t_1') \left(\lim_{\Lambda \to \infty} \Sigma_{\sigma}^{>}(1, 1') - \lim_{\Lambda \to \infty} \Sigma_{\sigma}^{<}(1, 1') \right)$$

$$+ \lim_{\Lambda \to \infty} \lambda_{\Lambda} \, \delta(t_1 - t_1') \, \delta(\mathbf{x}_1 - \mathbf{x}_1') \left[-iG_{\bar{\sigma}}^{<}(t_1, \mathbf{x}_1; t_1, \mathbf{x}_1) \right]. \qquad (4.76)$$

The instantaneous Hartree term (the last line) vanishes since $\lim_{\Lambda \to \infty} \lambda_{\Lambda} = 0$ (cf. Sec. 4.3.1). The zero-range limit is to be assumed everywhere hereafter and we drop the $\lim_{\Lambda \to \infty}$ for brevity.

The reduced T-matrix, T, is a two-time contour function. Furthermore, it can be easily shown to satisfy the criteria for a Keldysh function. To see this, one first establishes that the bare two-particle propagator, χ (cf. Eq. 4.58) satisfies the relations in Eq. (1.6) independent of one's choice of w_{Λ}. These properties are then trivially inherited by $\mathsf{T}^{-1} = \lambda_{\Lambda}^{-1} - i\chi$ and in turn by T. We will see shortly that T satisfies the bosonic KMS boundary conditions at equilibrium. This is expected since T assumes the form of a free bosonic propagator in the strong-coupling and describes the propagation of long-lived composite bosons. These observations suggest treating T like $\mathcal{G}$. We introduce the Wigner transform of T in the following natural way:

$$\mathsf{T}^{\diamond}(\omega, \mathbf{p}; T, \mathbf{R}) \equiv \int \mathrm{d}^d \mathbf{x} \, \mathrm{d}t \, e^{i\omega t} \, e^{-i\mathbf{p} \cdot \mathbf{x}} \, \mathsf{T}^{\diamond} \left(T + \frac{t}{2}, T - \frac{t}{2}; \mathbf{R} + \frac{\mathbf{x}}{2}, \mathbf{R} - \frac{\mathbf{x}}{2} \right), \qquad (4.77)$$

where the $\diamond$ superscript stands for either $\gtrless$ or $\pm$. Plugging the above definition into Eq. (4.76) and

Wigner transforming both sides, we obtain:

$$\Sigma_\sigma^{\gtrless}(\tilde{1}; T, \mathbf{R}) = -i \int d\tilde{2}\, d\tilde{3}\, \delta(\tilde{1} + \tilde{2} - \tilde{3})\, G_{\bar\sigma}^{\lessgtr}(\tilde{2}; T, \mathbf{R})\, \mathsf{T}^{\gtrless}(\tilde{3}; T, \mathbf{R}),$$

$$\Sigma_\sigma^{\pm}(\tilde{1}; T, \mathbf{R}) = -i \int d\tilde{2}\, d\tilde{3}\, \frac{i}{\omega_1^\pm + \omega_2 - \omega_3}\, (2\pi)^d\, \delta^d(\mathbf{p}_1 + \mathbf{p}_2 - \mathbf{p}_3)$$

$$\times \left[G_{\bar\sigma}^{<}(\tilde{2}; T, \mathbf{R})\, \mathsf{T}^{>}(\tilde{3}; T, \mathbf{R}) - G_{\bar\sigma}^{>}(\tilde{2}; T, \mathbf{R})\, \mathsf{T}^{<}(\tilde{3}; T, \mathbf{R}) \right], \qquad (4.78)$$

where we have introduced the useful shorthand notations:

$$\tilde{1} \equiv (\omega_1, \mathbf{p}_1), \quad d\tilde{1} \equiv \frac{d\omega_1}{(2\pi)} \frac{d^d\mathbf{p}_1}{(2\pi)^d}, \quad \delta(\tilde{1}) \equiv (2\pi)^{d+1}\, \delta(\omega_1)\, \delta^d(\mathbf{p}_1). \qquad (4.79)$$

The arithmetic is also naturally defined like $\tilde{1} + \tilde{2} \equiv (\omega_1 + \omega_2, \mathbf{p}_1 + \mathbf{p}_2)$, etc. At this stage, it is also useful to switch to the spectral/statistical representation for G, Σ and T. The former two were defined earlier (Eq. 2.32; also copied here):

$$G_\sigma^{<} \equiv i\mathsf{A}_\sigma f_\sigma, \qquad G_\sigma^{>} \equiv -i\mathsf{A}_\sigma(1 - f_\sigma),$$

$$\Sigma_\sigma^{<} \equiv i\Gamma_\sigma c_\sigma, \qquad \Sigma_\sigma^{>} \equiv -i\Gamma_\sigma(1 - c_\sigma),$$

$$\mathsf{T}^{<} \equiv -i\mathsf{B}b, \qquad \mathsf{T}^{>} \equiv -i\mathsf{B}(1 + b). \qquad (4.80)$$

We have introduced a bosonic parametrization for the T-matrix, a choice whose merits will shortly become clear. The spectral parts $\{\mathsf{A}_\sigma, \Gamma_\sigma, \mathsf{B}\}$ are related to the retarded functions through the exact relations that exist between the greater/lesser and retarded/advanced components:

$$\mathsf{A}_\sigma = -2\Im[G_\sigma^+], \qquad \Gamma_\sigma = -2\Im[\Sigma_\sigma^+], \qquad \mathsf{B}_\sigma = -2\Im[\mathsf{T}_\sigma^+]. \qquad (4.81)$$

The expressions for the self-energies can be written conveniently in terms of the spectral/statistical functions:

$$\Sigma_\sigma^{<}(\tilde{1}) = i \int d\tilde{2}\, d\tilde{3}\, \delta(\tilde{1} + \tilde{2} - \tilde{3})\, \mathsf{A}_{\bar\sigma}(\tilde{2})\, \mathsf{B}(\tilde{3})\, [1 - f_{\bar\sigma}(\tilde{2})]\, b(\tilde{3}), \qquad (4.82a)$$

$$\Sigma_\sigma^{>}(\tilde{1}) = -i \int d\tilde{2}\, d\tilde{3}\, \delta(\tilde{1} + \tilde{2} - \tilde{3})\, \mathsf{A}_{\bar\sigma}(\tilde{2})\, \mathsf{B}(\tilde{3})\, f_{\bar\sigma}(\tilde{2})\, [1 + b(\tilde{3})], \qquad (4.82b)$$

$$\Sigma_\sigma^{\pm}(\tilde{1}) = \int d\tilde{2}\, d\tilde{3}\, \frac{1}{\omega_1^\pm + \omega_2 - \omega_3}\, (2\pi)^d\, \delta^d(\mathbf{p}_1 + \mathbf{p}_2 - \mathbf{p}_3)\, \mathsf{A}_{\bar\sigma}(\tilde{2})\, \mathsf{B}(\tilde{3})\, [f_{\bar\sigma}(\tilde{2}) + b(\tilde{3})]. \quad (4.82c)$$

4.3.4 Renormalized in-medium T-matrix in the Wigner representation

In this section, we provide explicit expressions for the renormalized in-medium T-matrix in terms of the fermionic spectral functions. Such expressions, along with Eq. (4.82), constitute a complete prescription for calculating the self-energy of fermions and brings us one step closer to setting up the quantum kinetic equations.

The in-medium T-matrix in the zero-range limit can be conveniently renormalized using the procedure outlined in Sec. 4.3.2. To reiterate, the procedure relies on the premise that the propagation of high-energy particles is unaffected by the medium provided that $E \gg \max\{\epsilon_F, k_B T\}$. The diverging UV behavior can therefore be tamed by subtracting the vacuum T-matrix from the in-medium T-matrix, and the remainder will be regular and the zero-range limit can be taken. This procedure can be most conveniently implemented by observing that Eq. (4.57) can be solved in two steps by introducing an auxiliary T-matrix, $\tilde{\mathsf{T}}_0$, as follows:

$$\tilde{\mathsf{T}}_0 \equiv \lambda_\Lambda \, \mathbb{I} + i\lambda_\Lambda \, \tilde{\chi}_0 \star \tilde{\mathsf{T}}_0, \tag{4.83a}$$

$$\mathsf{T} = \tilde{\mathsf{T}}_0 + i\tilde{\mathsf{T}}_0 \star (\chi - \tilde{\chi}_0) \star \mathsf{T}, \tag{4.83b}$$

where $\mathbb{I}(\tau_1, \tau_1'; \mathbf{R}_1, \mathbf{R}_1') \equiv \delta_\mathcal{C}(\tau_1, \tau_1') \, \delta^d(\mathbf{R}_1 - \mathbf{R}_1')$ is the identity operator. The above decomposition is valid as long as $\tilde{\mathsf{T}}_0$ exists, irrespective of one's choice of $\tilde{\chi}_0$. Choosing $\tilde{\chi}_0$ to be the vacuum two-particle propagator, $\tilde{\mathsf{T}}_0$ will coincide with the vacuum T-matrix found earlier. Here, we use a slightly different choice for future convenience. Instead of using the vacuum Green's function $\mathcal{G}_{0,\sigma}$, we define $\tilde{\mathcal{G}}_{0,\sigma}$ as:

$$\tilde{G}_{0,\sigma}^< \equiv 0, \quad \tilde{G}_{0,\sigma}^> \equiv -i\tilde{\mathsf{A}}_{0,\sigma}, \tag{4.84}$$

where:

$$\tilde{\mathsf{A}}_{0,\sigma}(\omega, \mathbf{p}; T, \mathbf{R}) \equiv (2\pi) \, \delta\Big[\omega - |\mathbf{p}|^2/(2m_\sigma) + \mu_\sigma - U_\sigma(T, \mathbf{R})\Big]. \tag{4.85}$$

We note that $\tilde{\mathcal{G}}_{0,\sigma}$ can be thought of as the single-particle Green's function evaluated in vacuum, however, with energies shifted to the local value of the chemical potential of the interacting system. As a first step, we formally solve Eq. (4.83a) for $\tilde{\mathsf{T}}_0^{-1}$ and Eq. (4.83b) for $\tilde{\mathsf{T}}^{-1}$:

$$\tilde{\mathsf{T}}_0^{-1} = \lambda_\Lambda^{-1} \mathbb{I} - i\tilde{\chi}_0, \tag{4.86a}$$

$$\mathsf{T}^{-1} = \tilde{\mathsf{T}}_0^{-1} - i(\chi - \tilde{\chi}_0). \tag{4.86b}$$

Our goal is to calculate a renormalized equation for T^{-1} in the Wigner representation, which may then be inverted to give T. To this end, we need to write the above two equations in the Wigner representation. We define the Wigner transform of χ and $\tilde{\chi}_0$ according to Eq. (4.77). A straightforward calculation using Eq. (4.58) yields:

$$\chi^{\gtrless}(\omega, \mathbf{p}; T, \mathbf{R}) = \int \frac{d^d \mathbf{k}}{(2\pi)^d} \frac{d\omega_\uparrow}{2\pi} \frac{d\omega_\downarrow}{2\pi} (2\pi)\,\delta(\omega - \omega_\uparrow - \omega_\downarrow)$$
$$\times \tilde{w}_\Lambda(\mathbf{k}) \left[G_\uparrow^{\gtrless}\left(\omega_\uparrow, \eta_\uparrow \mathbf{p} + \mathbf{k}; T, \mathbf{R} - \frac{i\eta_\downarrow}{2}(\overleftarrow{\partial_\mathbf{k}^w} - \overrightarrow{\partial_\mathbf{k}^{\tilde{w}}})\right) \right.$$
$$\left. \times G_\downarrow^{\gtrless}\left(\omega_\downarrow, \eta_\downarrow \mathbf{p} - \mathbf{k}; T, \mathbf{R} + \frac{i\eta_\uparrow}{2}(\overleftarrow{\partial_\mathbf{k}^w} - \overrightarrow{\partial_\mathbf{k}^{\tilde{w}}})\right) \right] \tilde{w}_\Lambda(-\mathbf{k}), \tag{4.87}$$

where $\overleftarrow{\partial_\mathbf{k}^w}$ and $\overrightarrow{\partial_\mathbf{k}^{\tilde{w}}}$ only act on the left and right $\tilde{w}_\Lambda$ functions. The non-locality which is introduced in the form of the derivatives is due to the fact that the microscopic interaction has a finite range for a finite value of Λ. In the zero-range limit, $\tilde{w}_\Lambda(\mathbf{k})$ is constant and the $\mathbf{k}$-derivatives are ineffective. $\tilde{\chi}_0^\pm$ can be calculated with the help of the above expression, Eqs. (2.10), (2.11) and definition of $\tilde{\mathcal{G}}_{0,\sigma}$. The final result is:

$$\tilde{\chi}_0^\pm(\omega, \mathbf{p}; T, \mathbf{R}) = \int \frac{d^d \mathbf{k}}{(2\pi)^d}$$
$$\times \tilde{w}_\Lambda(\mathbf{k}) \frac{-i}{\omega^\pm - \xi_{\mathrm{CM}}^0(\mathbf{p}) - |\mathbf{k}|^2/(2m_{\mathrm{red}}) - U_\uparrow(T, \mathbf{R} + \eta_\downarrow \mathcal{D}_\mathbf{k}) - U_\downarrow(T, \mathbf{R} - \eta_\uparrow \mathcal{D}_\mathbf{k})} \tilde{w}_\Lambda(-\mathbf{k}),$$
$$\tag{4.88}$$

where we have introduced the shorthand notations $\mathcal{D}_\mathbf{k} \equiv -i(\overleftarrow{\partial_\mathbf{k}^w} - \overrightarrow{\partial_\mathbf{k}^{\tilde{w}}})/2$, and $\xi_{\mathrm{CM}}^0(\mathbf{p}) \equiv |\mathbf{p}|^2/(2m_{\mathrm{tot}}) - \mu_\uparrow - \mu_\downarrow$. If $w_\Lambda(\mathbf{x})$ is a function of range $\sim 1/\Lambda$, then $\tilde{w}_\Lambda(\mathbf{k})\mathcal{D}_\mathbf{k}\tilde{w}_\Lambda(-\mathbf{k}) \sim 1/\Lambda$

and we can expand the spatial arguments of the potential terms, $U_\uparrow$ and $U_\downarrow$, about $\mathbf{R}$:

$$\tilde{\chi}_0^\pm(\omega, \mathbf{p}; T, \mathbf{R}) = \int \frac{\mathrm{d}^d \mathbf{k}}{(2\pi)^d} \frac{-i \, |\tilde{w}_\Lambda(\mathbf{k})|^2}{\omega^\pm - \xi_{\mathrm{CM}}^0(\mathbf{p}) - |\mathbf{k}|^2/(2m_{\mathrm{red}}) - U_\uparrow(T, \mathbf{R}) - U_\downarrow(T, \mathbf{R})}$$
$$+ \int \frac{\mathrm{d}^d \mathbf{k}}{(2\pi)^d} \frac{-i \, [\eta_\downarrow \partial_\mathbf{R} U_\uparrow(T, \mathbf{R}) - \eta_\uparrow \partial_\mathbf{R} U_\downarrow(T, \mathbf{R})] \cdot [\tilde{w}_\Lambda(\mathbf{k}) \mathcal{D}_\mathbf{k} \tilde{w}_\Lambda(-\mathbf{k})]}{\left[\omega^\pm - \xi_{\mathrm{CM}}^0(\mathbf{p}) - |\mathbf{k}|^2/(2m_{\mathrm{red}}) - U_\uparrow(T, \mathbf{R}) - U_\downarrow(T, \mathbf{R})\right]^2} + \mathcal{O}(\mathcal{D}_\mathbf{k}^2). \quad (4.89)$$

Since $\tilde{w}_\Lambda(\mathbf{k})$ was assumed to fall faster than $k^{1-d/2}$, the integrand of the second term in the above expansion falls faster than k^{-4} and the UV part of the integral is therefore bounded by Λ^{-3}. The IR contribution can also be made as small as possible with a choice of $\tilde{w}_\Lambda(\mathbf{k})$ which is nearly constant for $|\mathbf{k}| \lesssim \Lambda$. As a result, we can neglect the $\mathcal{D}_\mathbf{k}$ terms in the denominator while sending Λ to infinity. Finally, using the renormalization condition, Eq. (4.67), and Eqs. (4.86a) and (4.88) and the above considerations, we find:

$$\lim_{\Lambda \to \infty} \left(\tilde{\mathsf{T}}_0^{-1}\right)^\pm (\omega, \mathbf{p}; T, \mathbf{R}) = \frac{1}{\mathsf{T}_0(E_0)} + \lim_{\Lambda \to \infty} \left[\int \frac{\mathrm{d}^d \mathbf{k}}{(2\pi)^d} \frac{|\tilde{w}_\Lambda(\mathbf{k})|^2}{E_0^+ - |\mathbf{k}|^2/(2m_{\mathrm{red}})} \right.$$
$$\left. - \frac{|\tilde{w}_\Lambda(\mathbf{k})|^2}{\omega^\pm + \xi_{\mathrm{CM}}(\mathbf{p}) - |\mathbf{k}|^2/(2m_{\mathrm{red}}) - U_\uparrow(T, \mathbf{R}) - U_\downarrow(T, \mathbf{R})} \right]. \quad (4.90)$$

The last integral is regular and we can set $\tilde{w}_\Lambda(\mathbf{k}) = 1$. The above expression, however, can be simply expressed as the retarded/advanced vacuum T-matrix with energies shifted to the local chemical potential:

$$\lim_{\Lambda \to \infty} \left(\tilde{\mathsf{T}}_0^{-1}\right)^\pm (\omega, \mathbf{p}; T, \mathbf{R}) = \left(\mathsf{T}_0^{-1}\right)^\pm \left(\omega + \mu_\uparrow + \mu_\downarrow - U_\uparrow(T, \mathbf{R}) - U_\downarrow(T, \mathbf{R}), \mathbf{p}\right). \quad (4.91a)$$

The lesser/greater components of $\tilde{\mathsf{T}}_0^{-1}$ can be evaluated either directly from the definition, Eq. (4.86a). A shortcut trick is to notice that the lesser component is zero, since $\left[\tilde{\mathsf{T}}_0^{-1}\right]^< = -i\tilde{\chi}_0^< = 0$, and using the relation between the Keldysh components (Eq. 2.10) and Eq. (4.91a). The final result is:

$$\lim_{\Lambda \to \infty} \left[\tilde{\mathsf{T}}_0^{-1}\right]^< = 0,$$
$$\lim_{\Lambda \to \infty} \left[\tilde{\mathsf{T}}_0^{-1}\right]^> = 2i\Im \left[\tilde{\mathsf{T}}_0^{-1}\right]^+ = \frac{iS_d \, m_{\mathrm{red}}}{(2\pi)^{d-1}} \theta(E_{\mathrm{th}}) \, (2m_{\mathrm{red}} E_{\mathrm{th}})^{d/2-1}, \quad (4.91b)$$

where S_d is the surface area of a d-sphere, and:

$$E_{\text{th}}(\omega, \mathbf{p}; T, \mathbf{R}) \equiv \omega + \mu_\uparrow + \mu_\downarrow - U_\uparrow(T, \mathbf{R}) - U_\downarrow(T, \mathbf{R}) - \frac{|\mathbf{p}|^2}{2m_{\text{tot}}}, \tag{4.92}$$

is the threshold energy for having a physical two-particle state in vacuum, and shifted to the local value of the chemical potential.

Equipped with a fully renormalized solution for $\tilde{\mathsf{T}}_0^{-1}$, we proceed to the second step which is finding a renormalized equation for T^{-1}. We define:

$$\mathcal{Q} \equiv \lim_{\Lambda \to \infty} i(\chi - \tilde{\chi}_0) = \text{} . \tag{4.93}$$

The dashed lines denotes $\tilde{G}_0$ Green's functions. The limit exists since the UV divergence of χ and $\tilde{\chi}_0$ cancel each other. In fact, $\tilde{\chi}_0$ coincides with the usual counter-term in minimal-subtraction regularization procedure. Using Eq. (4.87) and the spectral/statistical representation for $\mathcal{G}_\sigma$ and $\tilde{\mathcal{G}}_{0,\sigma}$, we find:

$$Q^<(\tilde{1}) = -i \int d\tilde{2}\, d\tilde{3}\, \delta(\tilde{1} - \tilde{2} - \tilde{3})\, \mathsf{A}_\uparrow(\tilde{2})\, \mathsf{A}_\downarrow(\tilde{3})\, f_\uparrow(\tilde{2})\, f_\downarrow(\tilde{3}), \tag{4.94a}$$

$$Q^>(\tilde{1}) = -i \int d\tilde{2}\, d\tilde{3}\, \delta(\tilde{1} - \tilde{2} - \tilde{3}) \left\{ \mathsf{A}_\uparrow(\tilde{2})\, \mathsf{A}_\downarrow(\tilde{3}) \left[1 - f_\uparrow(\tilde{2})\right] \left[1 - f_\downarrow(\tilde{3})\right] - \tilde{\mathsf{A}}_{0,\uparrow}(\tilde{2})\, \tilde{\mathsf{A}}_{0,\downarrow}(\tilde{3}) \right\}, \tag{4.94b}$$

$$\Im\left[Q^+(\tilde{1})\right] = -\frac{1}{2} \int d\tilde{2}\, d\tilde{3}\, \delta(\tilde{1} - \tilde{2} - \tilde{3}) \left\{ \mathsf{A}_\uparrow(\tilde{2})\, \mathsf{A}_\downarrow(\tilde{3}) \left[1 - f_\uparrow(\tilde{2}) - f_\downarrow(\tilde{3})\right] - \tilde{\mathsf{A}}_{0,\uparrow}(\tilde{2})\, \tilde{\mathsf{A}}_{0,\downarrow}(\tilde{3}) \right\}. \tag{4.94c}$$

Note that we have again dropped the common macroscopic coordinate $(T, \mathbf{R})$ argument from all functions and used the shorthand notation of Sec. 4.3.3. As usual, $\Re[Q^+]$ is found by Kramers-Kronig transform of $\Im[Q^+]$, and $Q^- = (Q^+)^*$.

The above expressions are manifestly free of UV divergences provided that f_σ is exponentially bounded for large ω and $\mathbf{k}$. This condition is naturally satisfied in realistic situations. The only possibility for a UV divergence is therefore in $\Re[Q^+]$, i.e. in the Kramers-Kronig transform. However,

the matching asymptotic behavior of A_σ and $\tilde{\mathsf{A}}_{0,\sigma}$ implies that the Kramers-Kronig integral kernel falls like k^{-4} for large k. Therefore, the integral is UV-proper provided if $d < 4$. We can finally rewrite Eq. (4.86b) in terms of renormalized quantities:

$$\mathsf{T}^{-1} = \tilde{\mathsf{T}}_0^{-1} - \mathcal{Q}. \tag{4.95}$$

The above equation has a similar structure to the Dyson equation for Green's functions, with $\tilde{\mathsf{T}}_0$ and $\mathcal{Q}$ playing the roles of the bare Green's function and the proper self-energy, respectively. Like the usual non-equilibrium Dyson equation, the above equation may also be transformed into a Kadaoff-Baym equation and subsequently into a quantum kinetic equation. We will see the usefulness of such an auxiliary kinetic equation in the forthcoming discussions.

As mentioned earlier (cf. Sec. 1.1.5), the thermal equilibrium Green's function are constrained by the KMS boundary condition. The KMS condition constrains the derived quantities at equilibrium as well. In particular, the equilibrium T-matrix will be constrained by the bosonic KMS condition:

$$\mathsf{T}^>(\omega; \mathbf{R}_1, \mathbf{R}_1') = e^{\beta\omega} \mathsf{T}^<(\omega; \mathbf{R}_1, \mathbf{R}_1'). \tag{4.96}$$

The above equation can be established by first observing $\chi^>(\omega; \mathbf{R}_1, \mathbf{R}_1') = e^{\beta\omega} \chi^<(\omega; \mathbf{R}_1, \mathbf{R}_1')$, which is a direct consequence of Eq. (2.61) (cf. Eq. 4.58 for the definition of χ). The KMS condition on χ, combined with Eq. (4.62), yields the desired result. The bosonic KMS condition on T sets the statistical part of T to the Bose-Einstein distribution function $b_0(\omega)$:

$$b_{\mathrm{eq}}(\omega, \mathbf{p}; \mathbf{R}) = b_0(\omega) \equiv \frac{1}{e^{\beta\omega} - 1}. \tag{4.97}$$

4.3.5 The weak-coupling and strong-coupling limits

The weak-coupling and strong-coupling limits of the NSR theory in equilibrium was discussed in Sec. 4.2.4 in $d = 2$. We repeat the same analysis for the SCTMA in this section in $d = 2$ and

3. Due to the self-consistent nature of the SCTMA, no analytical results is expected to be found for intermediate couplings $T \sim \epsilon_F \sim \epsilon_b$, and is not attempted.

By definition, the weak-coupling regime in $d = 2$ corresponds to $\epsilon_b/\epsilon_F \ll 1$. Restriction to the normal state further restricts the temperature to be greater than the binding energy, $\beta\epsilon_b \lesssim 1$. In $d = 3$, the weak-coupling regime corresponds to $a_s < 0, k_F|a_s| \ll 1$. In both cases, the renormalized retarded T-matrix $\mathsf{T}^+(\omega, \mathbf{p})$ is small in magnitude: $\mathsf{T}^+(d = 3) \sim 4\pi a_s/m$, and $\mathsf{T}^+(d = 2) \sim 1/m \ln(\epsilon_b/\epsilon_F)$. To the zeroth order in ϵ_b/ϵ_F, the fermion spectral function assumes its non-interacting form $\mathsf{A}(\omega, \mathbf{p}) = 2\pi\delta(\omega - \xi_{\mathbf{p}})$ and we recover the free Fermi gas with $\mu = \epsilon_F$.

The analysis is more involved in the strong coupling limit since the effects of self-consistency is not immediately clear. Again, we assume $\mu = -\epsilon_b/2 + \mu_B$, where μ_B is a correction to be determined. We remind that the NSR approximation identifies μ_B as the chemical potential of a free Bose gas with density $n_B = n/2$ (cf. Eq. 4.53). Our strategy is to improve the NSR approximation iteratively. We calculate the T-matrix with bare Green's functions at first, followed by calculating the resulting correction to the Green's functions using the obtained T-matrix. We finally consider the feedback on the T-matrix. In case the feedback effect is small and bounded, the NSR picture of the free Bose gas will be justified *a posteriori*. Otherwise, the scenario of a free Bose gas picture will be invalidated. In that case, no simple analytical results can be obtained using the iterative scheme and a numerical analysis seems unavoidable.

The zeroth-order bosonic self-energy Q_0^+ (as obtained using bare Green's functions) can be found from Eq. (4.94c) by replacing A with A_0:

$$\Im[Q_0^+(\omega, \mathbf{p})] = \frac{1}{2} \int \frac{\mathrm{d}^d \mathbf{q}}{(2\pi)^d} \, (2\pi) \, \delta\left(\omega - \xi_{\mathbf{p}/2+\mathbf{q}} - \xi_{\mathbf{p}/2-\mathbf{q}}\right) \left(f_0(\xi_{\mathbf{p}/2+\mathbf{q}}) + f_0(\xi_{\mathbf{p}/2-\mathbf{q}})\right),$$

$$\Re[Q_0^+(\omega, \mathbf{p})] = -\text{P.V.} \int \frac{\mathrm{d}^d \mathbf{q}}{(2\pi)^d} \frac{1}{\omega - \xi_{\mathbf{p}/2+\mathbf{q}} - \xi_{\mathbf{p}/2-\mathbf{q}}} \left(f_0(\xi_{\mathbf{p}/2+\mathbf{q}}) + f_0(\xi_{\mathbf{p}/2-\mathbf{q}})\right). \quad (4.98)$$

Both contributions are $\propto e^{-\beta\epsilon_b/2}$ as long as $E \equiv \omega + \mu_B - |\mathbf{p}|^2/(4m) \ll \epsilon_b$. Therefore, as a first approximation, we may neglect self-energy corrections to the T-matrix and set T^+ to the shifted

vacuum T-matrix, $\tilde{\mathsf{T}}_0^+$, as given by Eq. (4.91a). We find in $d = 2, 3$:

$$
\begin{aligned}
(d = 2) : \mathsf{T}^+(\omega, \mathbf{p}) &\to \frac{4\pi}{m} \frac{1}{\ln\left[-\epsilon_b/(\omega - |\mathbf{p}|^2/(4m) + 2\mu)\right]} \\
&= \frac{4\pi\epsilon_b}{m} \frac{1}{\omega + \mu_B - |\mathbf{p}|^2/(4m)} + \mathcal{O}(E/\epsilon_b), \\
(d = 3) : \mathsf{T}^+(\omega, \mathbf{p}) &\to \frac{4\pi}{m} \frac{1}{a_s^{-1} - i\sqrt{m(\omega + 2\mu - |\mathbf{p}|^2/(4m)}} \\
&= \frac{8\pi\sqrt{m\epsilon_b}}{m^2} \frac{1}{\omega + \mu_B - |\mathbf{p}|^2/(4m)} + \mathcal{O}(E/\epsilon_b).
\end{aligned}
\tag{4.99}
$$

The residues of the bound-state pole in d dimensions, λ_d, can be read from the above equations:

$$
\lambda_2 \equiv 4\pi\epsilon_b/m, \qquad \lambda_3 \equiv 8\pi\sqrt{m\epsilon_b}/m^2.
\tag{4.100}
$$

Note the different functional dependence of λ_d on ϵ_b in $d = 2$ and 3. Note that by expanding the T-matrix about the bound-state pole, we are effectively neglecting the scattering states. However, there is a large energetic separation between the scattering states and the bound state of the order of ϵ_b. Therefore, neglecting the scattering states is allowed to leading order in E/ϵ_b. The bosonic spectral function is given by:

$$
\mathsf{B}(\omega, \mathbf{p}) = 2\pi\lambda_d \, \delta(\omega + \mu_B - |\mathbf{p}|^2/(4m)).
\tag{4.101}
$$

We proceed and calculate the self-energy of fermions using Eq. (4.82):

$$
\Sigma^+(\omega, \mathbf{p}) = \lambda_d \int \frac{d^d\mathbf{q}}{(2\pi)^d} \frac{f_0(\xi_{\mathbf{q}-\mathbf{p}}) + b_0(\xi_{\mathbf{q}}^B)}{\omega + \xi_{\mathbf{q}-\mathbf{p}} - \xi_{\mathbf{q}}^B + i0^+}, \qquad \xi_{\mathbf{q}}^B \equiv |\mathbf{q}|^2/(4m) - \mu_B.
\tag{4.102}
$$

The above expression coincides with the NSR self-energy mentioned earlier. The rest of the analysis, however, differs from NSR since the 1PI self-energy diagrams are summed to all orders in the GG approximation:

$$
G^+ = G_0^+ + G_0^+\Sigma^+G_0^+ + G_0^+\Sigma^+G_0^+\Sigma^+G_0^+ + \ldots.
\tag{4.103}
$$

The reason for expanding the Dyson's series will become clear shortly. According to Eq. (4.102), $\Im[\Sigma^+]$ vanishes unless $\omega < \omega_{\text{th}} \equiv -(\epsilon_b + \mu_B)/2$, which is the threshold energy for the hole branch.

On the other hand, $G_0^+ = 1/(\omega - \xi_{\mathbf{p}})$ is purely real in this regime. Therefore, we find:

$$\mathsf{A}(\omega, \mathbf{p}; \omega > \omega_{\text{th}}) = 2\pi\delta(\omega - \xi_{\mathbf{p}}),$$

$$\mathsf{A}(\omega, \mathbf{p}; \omega < \omega_{\text{th}}) = \frac{\Gamma(\omega, \mathbf{p})}{(\omega - \xi_{\mathbf{p}})^2} - \frac{2}{(\omega - \xi_{\mathbf{p}})^3}\Im\left[(\Sigma^+)^2\right] - \frac{2}{(\omega - \xi_{\mathbf{p}})^4}\Im\left[(\Sigma^+)^3\right] + \dots. \quad (4.104)$$

μ_B is determined by fixing the number density. The particle branch $\omega > \omega_{\text{th}}$ gives an exponentially small density and the major contribution comes from the hole branch:

$$n = 2\int \frac{\mathrm{d}\omega}{2\pi}\frac{\mathrm{d}^d\mathbf{p}}{(2\pi)^d}\,\mathsf{A}(\omega, \mathbf{p})\,f_0(\omega)$$

$$= 2\int_{-\infty}^{\omega_{\text{th}}} \frac{\mathrm{d}\omega}{2\pi}\int \frac{\mathrm{d}^d\mathbf{p}}{(2\pi)^d}\left[\frac{\Gamma(\omega, \mathbf{p})}{(\omega - \xi_{\mathbf{p}})^2} - \frac{2}{(\omega - \xi_{\mathbf{p}})^3}\Im\left[(\Sigma^+)^2\right] + \dots\right]. \quad (4.105)$$

Similar to the analysis presented for $d = 2$ earlier, the first term can be calculated analytically again and gives $2n_B(\beta, \mu)$. For our current purpose, we do not need to calculate the rest of the integrals explicitly and an order of magnitude estimate is sufficient. A straightforward analysis shows that the contribution of j'th term in the series to the density, Δn_j, is of the other of:

$$\Delta n_j \sim \lambda_d^j\, b_0(-\mu_B)^j\, T^{j(d/2-1)+1}\int_0^\infty \frac{p^{d-1}\,\mathrm{d}p}{\left[p^2/(2m) + \epsilon_b\right]^{j+1}}, \quad (4.106)$$

up to a numerical factor. In $d = 3$, we find $\Delta n_{j+1}/\Delta n_j \sim b_0(-\mu_B)\sqrt{T/\epsilon_b}$. This can be traced back to the fact that $\lambda_3 \sim \sqrt{\epsilon_b}$. Therefore, we immediately see that the series can be truncated after the first term, so that both SCTMA and NSR describe non-interacting bosons in the strong-coupling limit. This result is valid both in quantum ($\beta\epsilon_F \sim 1$) and thermal ($\beta\epsilon_F \ll 1$) regimes.

In $d = 2$, the situation is different since $\Delta n_{j+1}/\Delta n_j \sim b_0(-\mu_B)$. In the quantum regime $\beta\epsilon_F \sim 1$, $b_0(-\mu_B)$ is not small and all terms in the series must be retained. This results a departure from the free Bose gas relation between μ_B and n and brings us to the conclusion that *the composite bosons as described by the fermionic T-matrix theory in $d = 2$ do not exhibit the physically expected low-energy asymptotic freedom, even in the $\epsilon_b = \infty$ limit.* We will show later that this unphysical result is due to the absence of multiple collisions between the composite bosons. The role of quantum

fluctuations is much more pronounced in $d = 2$ compared to $d = 3$, and the IR asymptotic freedom of composite bosons is bound to the inclusion of multiple scatterings in the bosonic particle-particle channel.

In the high-temperature limit $\beta\epsilon_F \ll 1$, the composite bosons will be in the thermal regime and $e^{\beta\mu_B} \sim \beta\epsilon_F \ll 1$, which implies $b_0(-\mu_B) \ll 1$. Furthermore, the composite bosons will be stable provided that $\beta\epsilon_b \gg 1$. In this limit, which we refer to as the *thermal composite Bose gas limit*, the Dyson series may again be truncated at the lowest order as in the $d = 3$ case.

We delegate the detailed discussion of the feedback on the T-matrix self-energy to Sec. 4.5.3 in order to avoid repetition. We just quote the final result here: in $d = 3$, the feedback results in a chemical potential shift $\delta\mu_B \sim a_s n/m$, which vanishes in the limit $\epsilon_b \to \infty$ and justifies the iterative procedure. In $d = 2$ and in the thermal composite Bose gas regime, we find $\delta\mu_B \sim n/m$, which does not depend on the binding energy. Nevertheless, $\delta\mu_B/|\mu_B| \ll 1$ in this regime and the iterative scheme coincides with the usual high-temperature (Virial) expansion, and is controlled. In summary, we find:

(1) ($d = 3$): The strong-coupling limit of SCTMA matches the NSR theory up to corrections of the order of $\mathcal{O}(1/\beta\epsilon_b)$. Furnishing the Green's functions with more than one self-energy insertion is sub-leading in this limit. The GG approximation describes free composite bosons in the strong-coupling limit both in the thermal and quantum regimes.

(1) ($d = 2$): The SCTMA does not describe the expected low-energy asymptotic freedom of composite bosons in the quantum regime and departs from the simpler NSR approximation. A high-temperature expansion of the Dyson equation is feasible in the thermal composite Bose gas regime. Furnishing the Green's functions with more than one self-energy insertion is again sub-leading in this limit. The SCTMA approximation reduces to the description of free thermal composite bosons.

4.3.6 Numerical results: the equilibrium spectral functions

Except for the very weak- and strong-coupling limits, the Green's functions can not be calculated analytically and may only reliably be found using numerical methods. We present such numerically obtained equilibrium spectral functions in this section in $d = 2$. The obtained results will be used later to study the dynamics of confined attractive Fermi gases in the weak- to moderate coupling regimes.

The homogeneous equilibrium state:

The KMS boundary conditions were discussed earlier and were found to give $f \to f_0(\omega)$ and $b \to b_0(\omega)$ for equilibrium quantities. This immediately implies that the lesser and greater functions are related to the retarded functions via the fluctuation-dissipation relation. The fermionic and bosonic spectral functions, A_σ and B, are to be found self-consistently such that they solve their respective Dyson's equations. We first consider the case of homogeneous systems. The spectral broadening Γ_σ is found using Eqs. (4.81) and 4.82 by replacing the statistical functions with their equilibrium values:

$$\Gamma_\sigma(\omega_1, \mathbf{p}_1) = \int d\tilde{2}\, d\tilde{3}\, \delta(\tilde{1} + \tilde{2} - \tilde{3})\, \mathsf{A}_{\bar{\sigma}}(\tilde{2})\, \mathsf{B}(\tilde{3})\left[f_0(\omega_2) + b_0(\omega_3)\right]. \tag{4.107a}$$

The fermionic spectral function is given by the Dyson's equation $G_\sigma^{+,-1} = G_{\sigma,0}^{+,-1} - \Sigma_\sigma^+$ with the following explicit expression:

$$\mathsf{A}_\sigma(\omega_1, \mathbf{p}_1) = \frac{\Gamma_\sigma(\omega_1, \mathbf{p}_1)}{\left(\omega + \mu_\sigma - \dfrac{|\mathbf{p}|^2}{2m_\sigma} + \dfrac{1}{2}\mathfrak{K}\mathfrak{K}[\Gamma_\sigma](\omega_1, \mathbf{p}_1)\right)^2 + \dfrac{1}{4}\Gamma_\sigma(\omega_1, \mathbf{p}_1)^2}. \tag{4.107b}$$

Note that the real part of the retarded self-energy is obtained from a Kramers-Kronig transform of $-\Gamma_\sigma/2$ as usual. The bosonic counterparts of the above equations are obtained from the results of

Sec. 4.3.4. As first step, we calculate the bosonic (T-matrix) spectral broadening $\Gamma_b \equiv -2\Im[Q^+]$:

$$\Gamma_b(\omega_1, \mathbf{p}_1) = \int d\tilde{2}\, d\tilde{3}\, \delta(\tilde{1} - \tilde{2} - \tilde{3}) \left\{ \mathsf{A}_\uparrow(\tilde{2})\, \mathsf{A}_\downarrow(\tilde{3}) \left[1 - f_0(\omega_2) - f_0(\omega_3)\right] - \tilde{\mathsf{A}}_{0,\uparrow}(\tilde{2})\, \tilde{\mathsf{A}}_{0,\downarrow}(\tilde{3}) \right\}.$$

(4.107c)

In the above equation, $\tilde{\mathsf{A}}_{0,\sigma}(\omega, \mathbf{p}) = 2\pi\, \delta(\omega + \mu_\sigma - |\mathbf{p}|^2/(2m))$ corresponds to the bare fermionic spectral function. The bosonic spectral function $\mathsf{B} = -2i\Im[\mathsf{T}^+]$ is then found from the T-matrix Dyson's equation, Eq. (4.95):

$$\mathsf{B}(\omega_1, \mathbf{p}_1) = \frac{\Gamma_b(\omega_1, \mathbf{p}_1) - 2\Im[Y(\omega_1, \mathbf{p}_1)]}{\left(\Re[Y(\omega_1, \mathbf{p}_1)] + \frac{1}{2}\mathfrak{K}\mathfrak{K}[\Gamma_b](\omega_1, \mathbf{p}_1)\right)^2 + \frac{1}{4}\left(\Gamma_b(\omega_1, \mathbf{p}_1) - 2\Im[Y(\omega_1, \mathbf{p}_1)]\right)^2},$$

(4.107d)

where $1/Y(\omega_1, \mathbf{p}_1) = \mathsf{T}_0^+\left(\omega_1 + \mu_\uparrow + \mu_\downarrow - |\mathbf{p}_1|^2/(4m)\right)$. The expressions for the renormalized retarded T-matrix in vacuum, T_0^+, are given in Sec. 4.3.1. In $d = 2$, we find:

$$(d = 2):\qquad Y(\omega_1, \mathbf{p}_1) = \frac{m_{\mathrm{red}}}{2\pi}\left[i\pi + \ln\left(\frac{\omega_1 + \mu_\uparrow + \mu_\downarrow - |\mathbf{p}_1|^2/(4m)}{\epsilon_b}\right)\right].$$

(4.107e)

If required, the chemical potentials μ_σ must finally be traded for the number densities n_σ using the number equation:

$$n_\sigma = \int d\tilde{1}\, \mathsf{A}_\sigma(\tilde{1})\, f_0(\omega_1).$$

(4.107f)

The above expressions constitute the complete set of equations required for characterizing the equilibrium state. The only practical strategy toward solving nonlinear equations as such is by iterations. A simple implementation is done using two self-consistency loops as described below. The main loops is the *spectral self-consistency loop*, where the spectral functions and the number densities are calculated at fixed chemical potentials $(\mu_\uparrow, \mu_\downarrow)$ to a desired degree of accuracy:

Require: physical parameters $(\beta, \mu_\uparrow, \mu_\downarrow, \epsilon_b)$, error tolerance δ

$j \Leftarrow 0$

$\mathsf{A}_\sigma^{(0)}(\omega, \mathbf{p}) \Leftarrow 2\pi\, \delta(\omega + \mu_\sigma - |\mathbf{p}|^2/(2m_\sigma))$

calculate $n_\sigma^{(0)}$ from Eq. (4.107f) using $\mathsf{A}_\sigma^{(0)}$

while $err > \delta$ **do**

    calculate $\Gamma_b^{(j)}$ from Eq. (4.107c) using $\mathsf{A}_\sigma^{(j)}$

    calculate the Kramers-Kronig transform of $\Gamma_b^{(j)}$

    calculate $\mathsf{B}^{(j)}$ from Eq. (4.107d)

    calculate $\Gamma_\sigma^{(j+1)}$ from Eq. (4.107a)

    calculate the Kramers-Kronig transform of $\Gamma_\sigma^{(j+1)}$

    calculate $\mathsf{A}_\sigma^{(j+1)}$ from Eq. (4.107b)

    calculate $n_\sigma^{(j+1)}$ from Eq. (4.107f)

    $err \Leftarrow |n_\uparrow^{(j+1)} - n_\uparrow^{(j)}| + |n_\downarrow^{(j+1)} - n_\downarrow^{(j)}|$

    $j \Leftarrow j+1$

end while

The second loop adjusts the chemical potentials so that that the desired number densities are obtained. This is simply done by finding lower and upper bounds on the chemical potential and proceeding by bisection. The most expensive part of the calculation is the spectral self-consistency loop. Truncating this iteration loop at the level of $\mathsf{A}^{(1)}$ yields the previously mentioned $G_0 G_0$ approximation, with is an improvement of NSR approximation by including the sum of all 1PI self-energy diagrams. According to the discussions of earlier sections, the $G_0 G_0$ approximation already captures the gist of the physics and interpolates between the weak fermionic to the strong-coupling bosonic regimes.

At the moment, the numerical results available to us are done at the level of $G_0 G_0$ approximation. The full self-consistent solution is left for future works. The $G_0 G_0$ calculations has been appeared earlier in Ref. [152]. We consider the spin-symmetric case $\mu_\uparrow = \mu_\downarrow = \mu$, $m_\uparrow = m_\downarrow = m$. We refer to the total number density as $n \equiv n_\uparrow + n_\downarrow$. As usual, the Fermi energy is defined as

the chemical potential of a non-interacting system with the same density, $\epsilon_F \equiv \pi n/m$. The Fermi temperature is $T_F = \epsilon_F$ (the Boltzmann constant is set to 1 throughout). The Fermi momentum is given by $k_F = \sqrt{2m\epsilon_F} = \sqrt{2\pi n}$. The strength of attractive interactions is parametrized using dimensionless interaction parameter $\eta = \ln(k_F a_2)$ (cf. Eq. 4.7). The interaction parameter varies in the range $(-\infty, +\infty)$. Large positive and negative values correspond to weak and strong coupling, respectively. The density of states per spin is defined as:

$$N(\omega) \equiv 2\pi \int \frac{\mathrm{d}^2\mathbf{k}}{(2\pi)^2} \, \mathsf{A}(\omega, \mathbf{k}). \qquad (4.108)$$

Since we are only concerned with the normal state here, we have made no attempt toward calculating the critical superfluidity temperature T_c numerically. As stressed before, the T-matrix approximation does not give a proper account of BKT superfluidity in $d = 2$ and must be generally avoided at very low temperatures. Nevertheless, it is legitimate theoretical question to ask for the prediction of the T-matrix theory for T_c in $d = 2$. T_c is most easily found from the Thouless criterion [201] stating that pairing susceptibility diverges at $\omega = \mathbf{q} = 0$ at T_c, signaling the emergence of a gapless Goldstone mode. The pairing susceptibility coincides with the many-body T-matrix here. T_c has been found at the level of NSR approximation in Refs. [190, 202]. Once the chemical potential renormalization is properly taken into account, one finds $T_c = 0$, regardless of the interaction parameter η. It is an interesting fact that the finite BCS mean-field T_c is *not* recovered by the NSR approximation even in the weak-coupling limit. This is due to the large renormalization of μ due to the scattering states of the T-matrix [202].

We start discussing the results by first investigating a typical plot of the chemical potential vs. $\ln(k_F a_2)$ as shown in Fig. 4.3.6. For comparison, we have also included the chemical potential of a free Fermi gas at the same temperature $\mu_F(T)$ (green dashed lines), as well as the that of free composite bosons $-\epsilon_b/2 + \mu_B(T)$, where $\mu_B(T)$ is the chemical potential of free bosons with

number density $n/2$ at temperature T. As expected, we find that the attractive Fermi gas smoothly interpolates between these two regime.
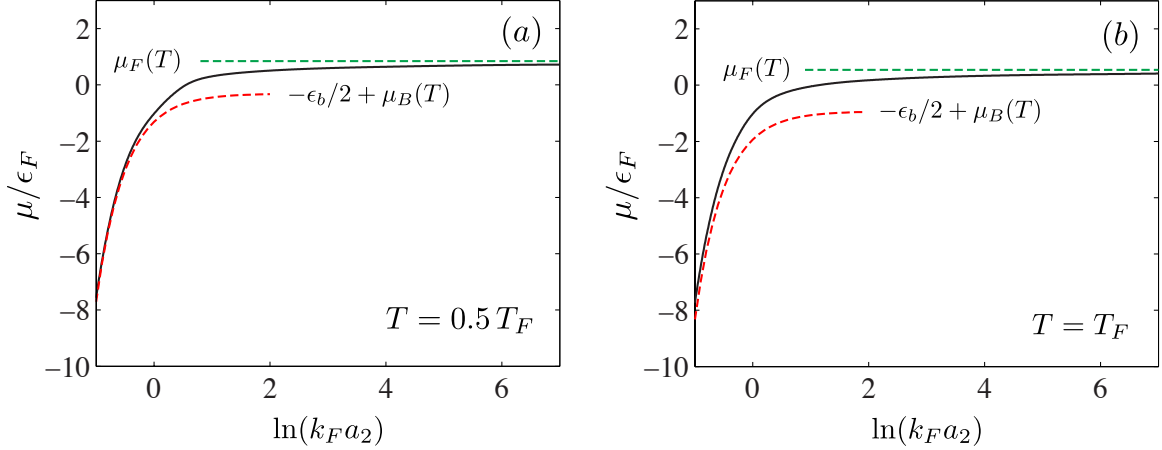
Figure 4.8: The chemical potential of the homogeneous attractive Fermi gas at fixed density as a function of the interaction parameter $\ln(k_F a_2)$ at (a) $T/T_F = 0.5$ and (b) $T/T_F = 1$. The dashed green and red lines show the weak-coupling (free fermions) and strong-coupling (free bosons) limits, respectively. The chemical potential smoothly interpolates between the two limits.

The spectral functions are shown in Figs. 4.9 and 4.10 at two different temperatures $T/T_F = 0.5,\ 1$ and several interaction parameters $\ln(k_F a_2) = 7,\ 1,\ 0.5,\ -0.5$ along with the density of states. In the weak-coupling example $\ln(k_F a_2) = 7$, the spectral function has a strong resemblance to the free Fermi gas. The density of states $N(\omega)$ is zero for $\omega < -\mu$ and sharply reaches the flat non-interacting value $m/\hbar^2$ for $\omega > -\mu$. For larger binding energies, a dip smoothly develops in the spectral function starting at $\omega = 0$, $k \approx k_F$, which eventually cuts the spectral weight into the particle and hole branches. The temperature at which a dip appears in the spectral function referred to as T^{**}, which is larger than T^*, the temperature at which the dip also appears in the density of states (see Fig. 4.10(c2)). The missing spectral weight at the chemical potential level is taken as an indication of the pairing pseudogap. For $\ln(k_F a_2) \lesssim 0$, the system smoothly reaches to the strong-coupling regime where the separation between the particle and hole branches increases and a large

gap of size $\sim \epsilon_b$ develops in the density of states at the chemical potential level. The incoherent hole branch is narrower at lower temperatures as thermal population of higher energy bosonic states are suppressing, hence, the spectral function resembles a BCS state (in which only the single $\mathbf{q} = 0$ bosonic state is occupied).
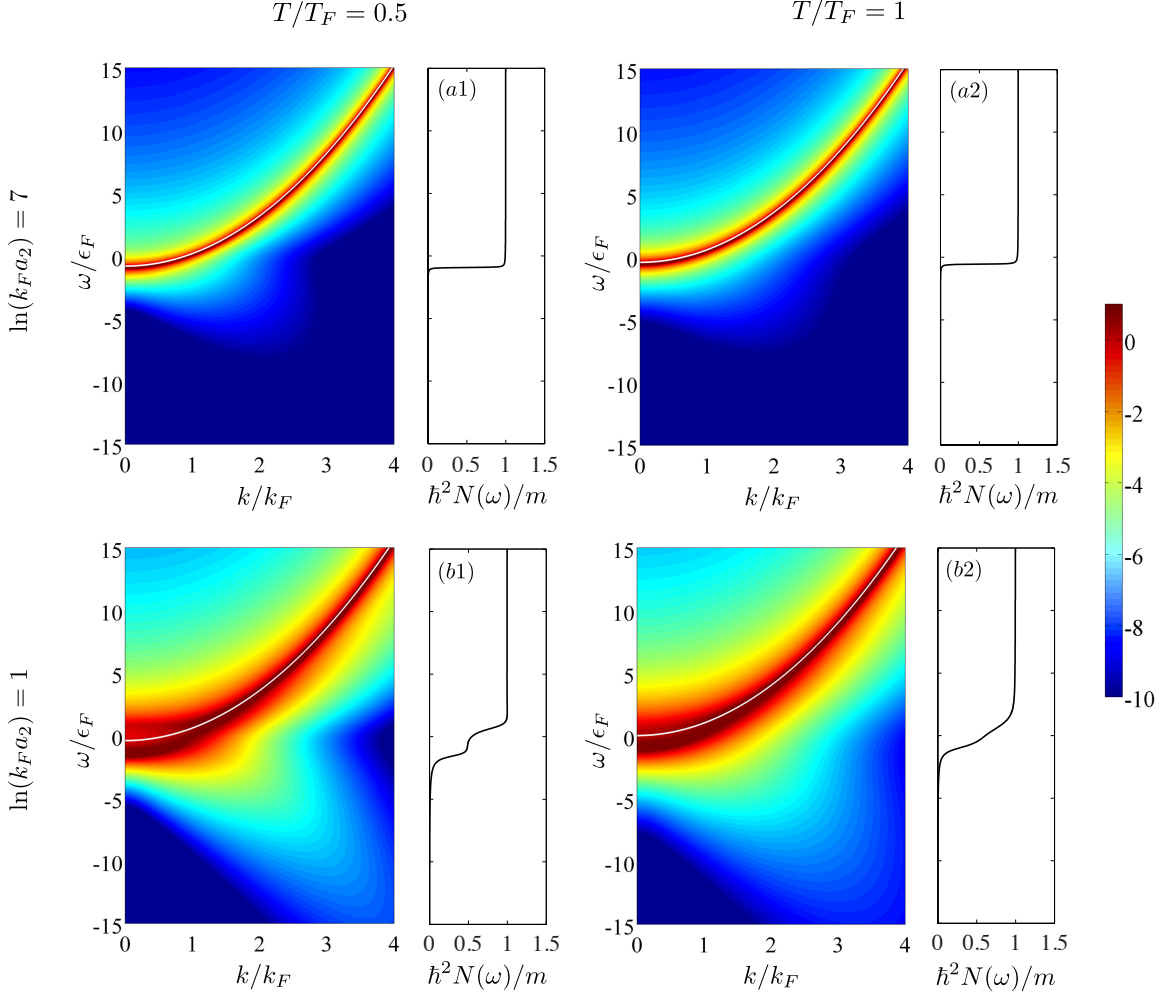
Figure 4.9: The $G_0 G_0$ spectral function $A(\omega, \mathbf{k})$ and density of states $N(\omega)$ at fixed density. The left and right columns show the results for $T/T_F = 0.5$ and $T/T_F = 1$, respectively. The rows correspond to $\ln(k_F a_2) = 7, \ 1, \ 0.5, \ -0.5$ from top to bottom, respectively. The coloring of the spectral function plots is done using a logarithmic mapping, $\ln(A/\epsilon_F)$. Red and blue regions indicate high and low spectral weights, respectively (the colorbar is shown on the right). The white lines show the free particle dispersion $\omega = |\mathbf{p}|^2/(2m) - \mu$.
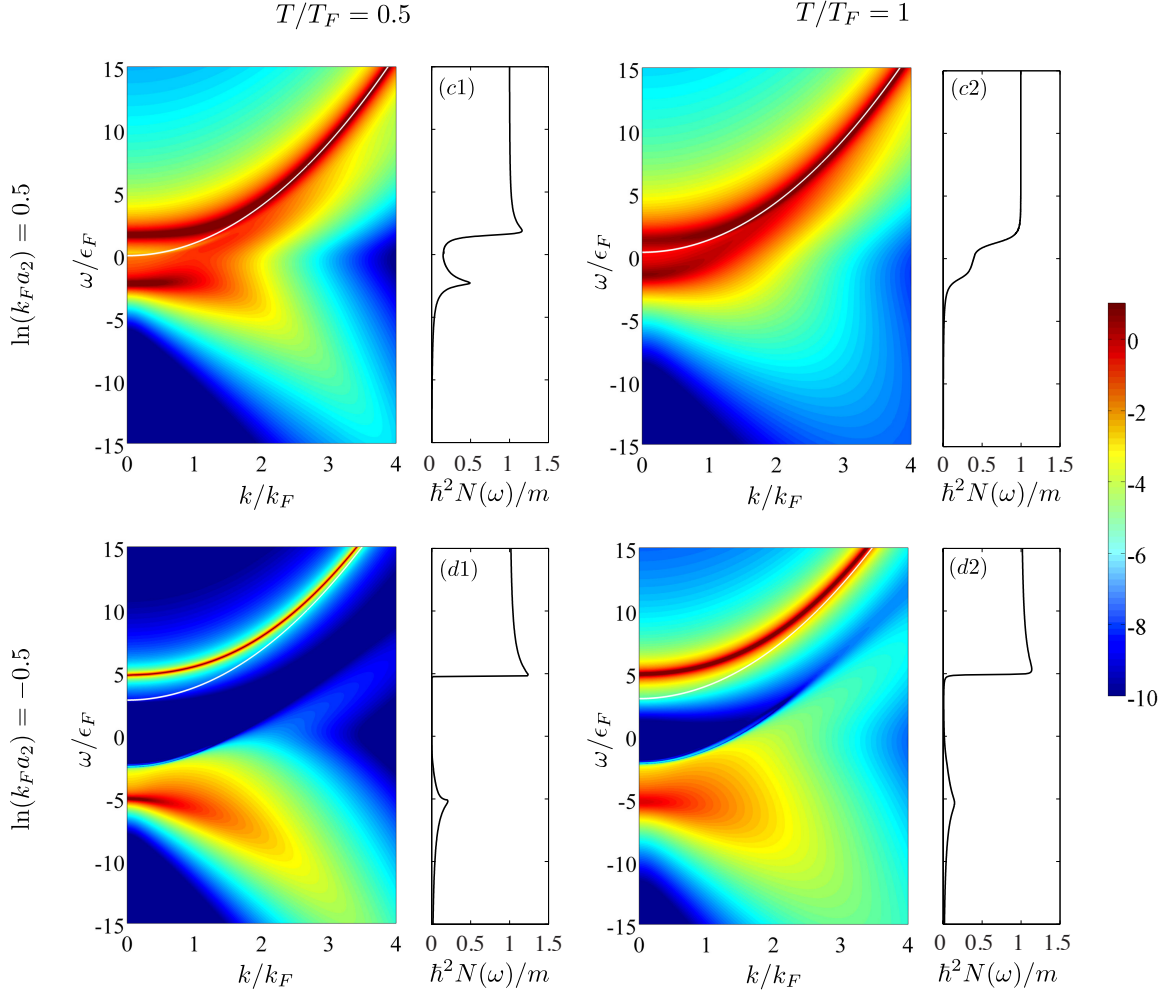
Figure 4.10: (continued from Fig. 4.9; refer to the caption of Fig. 4.9) for details.

The gas in a harmonic confining potential:

The equilibrium state of the homogeneous system was discussed in the previous section. Here, we present the result for a gas confined in an static harmonic potential:

$$U(\mathbf{R}) = \frac{1}{2}m\omega_0^2(X^2 + Y^2). \tag{4.109}$$

Provided that $\omega_0 \ll \epsilon_F$, $U(\mathbf{R})$ varies on a scale much larger than the inter-particle separation and the equilibrium state of the inhomogeneous system can be obtained using the local density approx-
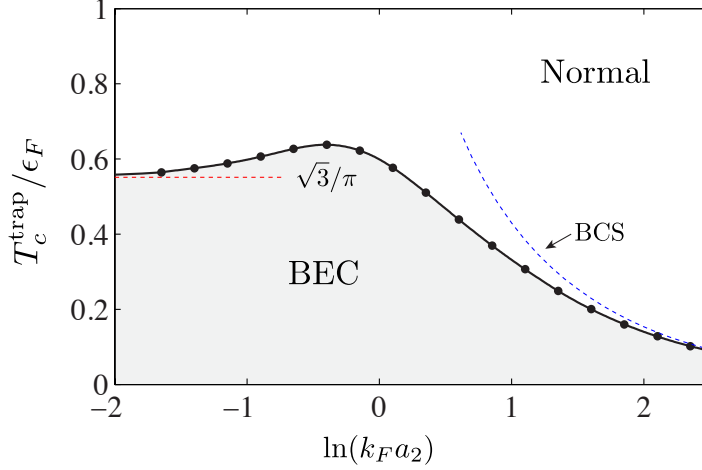
Figure 4.11: The phase diagram of the attractive 2D Fermi gas in a harmonic trap as described by the $G_0 G_0$ approximation. The lack of interaction between the composite bosons results in the formation of a BEC at finite temperatures. The dashed blue and red lines correspond to the prediction of the BCS theory and condensation temperature of free 2D bosons (calculated in the text), respectively.

imation (LDA) by simply replacing the chemical potentials of the solution of the homogeneous system with its local value $\mu(\mathbf{R}) \to \mu_0 - \mu(\mathbf{R})$. The local spectral function and the local density of states are given by:

$$\mathsf{A}(\omega, \mathbf{p}; \mathbf{R}) = \mathsf{A}(\omega, \mathbf{p})\Big|_{\mu \to \mu(\mathbf{R})}, \qquad N(\omega, \mathbf{R}) \equiv N\left(\omega; \mu \to \mu_0 - U(\mathbf{R})\right). \tag{4.110}$$

The chemical potential at the center of the trap $\mu(\mathbf{0}) = \mu_0$ is determined by fixing the total number of trapped particles:

$$N_{\text{tot.}} = 2 \int_0^\infty (2\pi R)\, \mathrm{d}R \int \mathrm{d}\omega\, N\left(\omega; \mu \to \mu_0 - U(\mathbf{R})\right) f_0(\omega). \tag{4.111}$$

The natural units of length and energy for the trapped gas is given by the radius and the chemical potential of a non-interacting trapped Fermi gas at zero temperature, referred to as the *Thomas-Fermi radius* R_{TF} and the *trap Fermi energy* ϵ_F, respectively. These quantities are easily calculated from the above formula and read as:

$$\epsilon_F = \sqrt{N_{\text{tot.}}}\omega_0, \qquad R_{\text{TF}} = (4N_{\text{tot.}})^{1/4}\, (m\omega_0)^{-1/2}. \tag{4.112}$$

216

A nuisance of the $G_0 G_0$ approximation is that it spuriously leads to a BEC at a finite T_c in the presence of the confining potential. This behavior can be traced back to the fact that the composite bosons are described as free at the $G_0 G_0$ level. It is known that free bosons in $d = 2$ condense at a finite temperature [203, 204, 205]. The BEC, however, is unphysical since the density at the center of the trap diverges. This is most easily shown in the extreme strong-coupling limit where $G_0 G_0$ describes the system as a gas of free composite bosons of mass $2m$. The LDA density in this limit is given by:

$$n(\mathbf{R}) = -\frac{2(2m)}{2\pi\beta} \ln\left[1 - e^{\beta(\mu_B - 2U(\mathbf{R}))}\right], \tag{4.113}$$

where $\mu_B = 2\mu_0 + \epsilon_b$ is the bosonic chemical potential at the center of the trap. The total number of particles is found by integration over $\mathbf{R}$:

$$N_{\text{tot.}} = \frac{\epsilon_F^2}{\omega_0^2} = \frac{2}{\beta^2 \omega_0^2} \text{Li}_2\left(e^{\beta\mu_B}\right). \tag{4.114}$$

The poly-logarithm function evaluates to the finite value $\pi^2/6$ in the limit $\mu_B \to 0$ and implies a finite BEC temperature:

$$\lim_{\epsilon_b \to \infty} T_c^{\text{trap}} = \frac{\sqrt{3}}{\pi}. \tag{4.115}$$

However, $n(\mathbf{R}) \sim -\ln(R)$ for $\mu_B = 0$ and diverges at $R = 0$. Once the repulsion between the composite bosons is taken into account at the mean-field level, the finite-temperature BEC will disappear and T_c will be pushed down to 0 [206]. This scenario is still incomplete as the physics associated to the BKT transition is not described by the mean-field description. In fact, a more careful analysis reveals that the BEC transition is replaced by the BKT transition at $T_{\text{BKT}}^{\text{trap}}$. In the dilute limit $\ln^{-1}(1/na_B^2) \ll 1$ (a_B is the effective range of the boson-boson interaction), $T_{\text{BKT}}^{\text{trap}} \sim T_c^{\text{trap}} + \mathcal{O}(\ln^{-1}(1/na_B^2))$ [204]. It will be shown in the next section that the SCTMA gives rise to a mean-field repulsion between the composite bosons. Therefore, while it does not describe the BKT transition, it is free from the spurious BEC transition with diverging densities.

The numerically obtained phase diagram of the trapped Fermi gas in the $G_0 G_0$ approximation is

shown in Fig. 4.11 along with the weak-coupling and strong-coupling asymptotes. The same result

has also been reported in Ref. [155]. The BEC disappears for $T_{c,\text{max}}^{\text{trap}}/T_F \gtrsim 0.63$. Fig. 4.12 shows
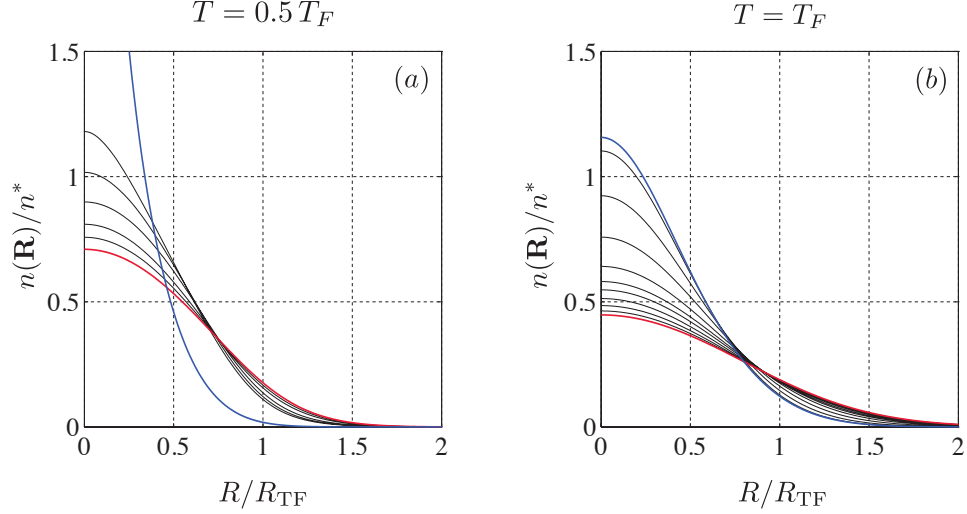
Figure 4.12: The density profile of the attractive Fermi gas in an isotropic trap obtained within the $G_0 G_0$ approximation. Here, $n^* \equiv m\epsilon_F/\pi = (m\omega_0/\pi)(N_{\text{tot.}})^{1/2}$ and $R_{\text{TF}} = (4N_{\text{tot.}})^{1/4} (m\omega_0)^{-1/2}$. The blue and red dashed lines lines show the free Fermi gas and free Bose gas limits. (a) $T/T_F = 0.5$, The black lines denote $\ln(k_F a_2) = 5$, 2, 0.75, 0.5, 0.4 from from the bottom to the top. The density diverges at the center of the trap at $\ln(k_F a_2) \simeq 0.39$ (cf. Fig. 4.11). (b) $T/T_F = 1$, The black lines denote $\ln(k_F a_2) = 5$, 2, 1, 0.5, 0.25, 0, -0.25, -0.5, -1 from from the bottom to the top.

the density profile of the trapped gas at $T/T_F = 0.5$ and 1 for different interaction parameters. The

blue and red lines show the free Fermi gas and free Bose gas limits. The density profile smoothly

connects these two asymptotes as the binding energy is increased.

4.4 Linear response theory: crossover from free fermions to composite bosons

The response of a physical system to small external perturbations provides invaluable informa-

tions about the underlying microscopic mechanisms involved in the emergent bulk properties. In

fact, the first, and the most important test for the validity of a microscopic theory is comparing its

linear response predictions (and related derived quantities) against the experimental observations. In this section, we study the linear response of the attractive Fermi gas in the normal state to an external field formally using diagrammatic methods. This analysis, as we shall see, sheds light on the processes involved in transport in such systems. We only consider density-density response functions here. The current-current response functions may be simply found by affixing current bare vertices to the bubble diagrams.

As mentioned in Sec. 1.4, a an important feature of Φ-derivable approximations is that they provide a prescription for calculating n-point correlation functions in a symmetry preserving way. The irreducible vertex corrections are given by the 2PI vertices. The general procedure was described in Sec. 1.2.4. The $\Phi^{(2)}$ vertex for T-matrix theory can be obtained either by opening two lines in Φ, or equivalently opening one more line in Σ. Either way, we find the following two class of contributions:

$$\tag{4.116}$$

These processes were discovered in 1968, in the papers of Aslamazov and Larkin [207], Maki [208] and bit later Thompson [209] in the context of microscopic theory of pairing fluctuations in the normal phase of superconductors. The integral equation for the particle-hole vertex is given in Eq. (1.106). The contributing diagrams can be found by iterating the integral equation order by order and gives an infinite number of diagrams with different number of insertions of irreducible

MT and AL vertices. Some of the first few diagrams are:

$$(4.117)$$
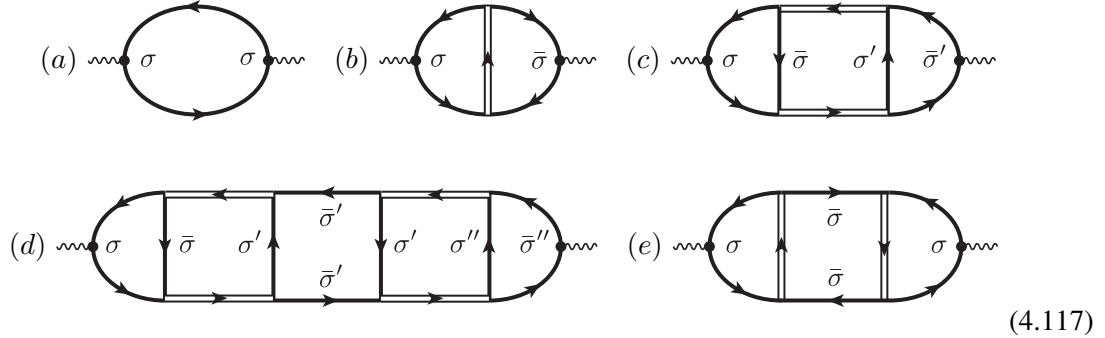
We have used a more compact diagrammatic notation of double lines instead of T-matrices. We note that the two different AL processes shown in Eq. (4.116) have the same appearance in the double line diagrammatic notation. (a) is obtained from the bare vertex, (b) is a single MT, (c) is a single AL, (d) is a double AL and finally (e) is a double MT process. Higher order diagrams include further AL and MT vertex corrections is arbitrary order. The fermion and boson lines appearing in the diagram are fully dressed.

MT and AL diagrams describe different mechanisms of transport and consequently, their degree of importance varies from one regime to the other. The physical process invoked is in fact very clear in the diagrams: the MT process is reminiscent of the Andreev reflection in superconducting states, where a particle scatters from a Cooper pair and is exchanged with a hole. The only difference in the normal state is that the Cooper pair is replaced by a pairing fluctuation. The AL process describes transport via bound pairs as it is evident from diagram (c): the external field makes a *bosonic* particle-hole excitation by boosting a bound pair; the pair propagates to the observation point and gives back the excess energy and momentum. Accordingly, we expect the AL diagrams to make the most important contributions in the strong-coupling regime.

In the weak-coupling regime and to zeroth order in ϵ_b/ϵ_F, the bosonic fluctuations can be neglected and only (a) survives, which in turn yields the Lindhard function, i.e. the density-density

response of a free Fermi gas. The sub-leading fluctuation corrections has been examined at length in the context of fluctuation conductivity of superconducting materials (cf. Ref. [210] for an excellent review).

We denote the outgoing energy and momentum of the the linear response diagrams as Ω and $\mathbf{Q}$ respectively. We are interested to investigate low-energy excitations with energies not exceeding the binding energy in the strong-coupling limit. Therefore, we assume $E = \max\{|\Omega|, Q^2/(4m)\} \ll \epsilon_b$. This analysis has been partially carried out earlier in Ref. [211] for the lowest order diagrams in $d = 3$. According to the discussion given in the previous section, we may use the NSR strong-coupling Green's functions in $d = 3$ to leading order in ϵ_F/ϵ_b. In $d = 2$, we further require the high-temperature condition $\beta\epsilon_F \ll 1$. Diagram (a) yields:

$$\chi_{\mathrm{dd}}^{(a)}(\Omega, \mathbf{Q}) = 2 \int \frac{d\omega_1}{2\pi} \frac{d\omega_2}{2\pi} \frac{d^d\mathbf{k}}{(2\pi)^d} \, A(\omega_1, \mathbf{k} + \mathbf{Q}) \, A(\omega_2, \mathbf{k}) \frac{f_0(\omega_1) - f_0(\omega_2)}{\Omega - \omega_1 + \omega_2 + i0^+}. \qquad (4.118)$$

Due to the gap in the spectrum, one line must be in the particle branch and the other in the hole branch. The diagram is often referred to as the density of states (DOS) diagram in the context of pairing fluctuations [210]:

$$\chi_{\mathrm{dd}}^{(a)}(\Omega, \mathbf{Q}) \simeq 2 \sum_\sigma \quad \overset{\sigma \qquad \sigma}{\bigcirc} \quad = -4 \int \frac{d\omega_1}{2\pi} \frac{d^d\mathbf{k}}{(2\pi)^d} \frac{\Gamma(\omega_1, \mathbf{k} + \mathbf{Q})}{(\Omega - \omega_1 + \xi_\mathbf{k})(\omega_1 - \xi_{\mathbf{k}+\mathbf{Q}})^2} \sim -\frac{n}{\epsilon_b}.$$
$$(4.119)$$

The leading contribution from the MT diagram results from using all bare lines. The result is most easily obtained in the Matsubara formalism. There are five poles contributing to the double Matsubara sum (for from Green's function and one from the boson propagator). The calculation is lengthy but straightforward. The final result is:

$$\chi_{\mathrm{dd}}^{(b)}(\Omega, \mathbf{Q}) = \int \frac{d^d\mathbf{k}}{(2\pi)^d} \frac{d^d\mathbf{p}}{(2\pi)^d} \frac{-2f_0(\xi_\mathbf{k})f_0(\xi_\mathbf{p}) + 2b_0(\xi_{\mathbf{k}+\mathbf{p}}^B)[1 - f_0(\xi_\mathbf{k}) - f_0(\xi_\mathbf{p})]}{(\xi_\mathbf{k} + \xi_\mathbf{p} - \xi_{\mathbf{k}+\mathbf{p}}^B)^3 - (\xi_\mathbf{k} + \xi_\mathbf{p} - \xi_{\mathbf{k}+\mathbf{p}}^B)\Omega^2} + \mathcal{O}(E/\epsilon_b).$$
$$(4.120)$$

All Fermi-Dirac distributions can be set to zero and we find $\chi_{\mathrm{dd}}^{(b)}(\Omega, \mathbf{Q}) \sim -n/\epsilon_b$. In fact, we find that the MT and DOS contributions are exactly equal in the strong-coupling limit, and both

are negligibly small. A similar analysis shows that all diagrams containing a MT insertion can be neglected in the strong-coupling regime and this brings us to AL diagrams.

The AL diagrams, i.e. (c), (d) and the rest, can generally be expressed as two triangular CAP diagrams at the beginning and the end. The interaction between bosonic particle-hole pairs is given by a BOX diagram. Comparing these diagrams with the RPA response functions, we immediately find that in the strong-coupling limit, the SCTMA reduces to the Hartree theory for composite bosons, with an effective interaction given by BOX. This is a result already pointed out in Ref. [212] and later in Ref. [213] in $d = 3$.

As a first step, we calculate the strong-coupling limit of the cap and box diagrams. To the leading order, we may set the external momenta to zero and use bare Green's functions. The low-energy cap diagram per spin state evaluates to:

$$\mathsf{CAP}(Q, q) = \,\, {}^{Q}\!\!\!\overset{q}{\diagram} \,\, = -\int \frac{\mathrm{d}^d \mathbf{k}}{(2\pi)^d} \frac{1}{4\xi_{\mathbf{k}}^2} + \mathcal{O}(E/\epsilon_b) = -\frac{1}{\lambda_d}. \tag{4.121}$$

We remind that λ_d is the pre-factor that the bosonic propagators carry and is defined in Eq. (4.99). We evaluate the box diagram (per spin) with finite incoming momentum and in the static limit:

$$\mathsf{BOX}(k, k') = \,\, \overset{k \qquad k'}{\underset{-k' \qquad -k}{\diagram}} \,\, = \frac{1}{\beta} \sum_{i\omega_n} \int \frac{\mathrm{d}^d \mathbf{q}}{(2\pi)^d} G_0(q) G_0(k-q) G_0(k'-q) G_0(q-k-k'). \tag{4.122}$$

The analysis is done in Appendix. In particular, we find $\mathsf{BOX}(0,0) = m/(4\pi\epsilon_b^2)$ in $d = 2$ and $\mathsf{BOX}(0,0) = m^3/(16\pi(m\epsilon_b)^{3/2})$ in $d = 3$. For $k \gg \sqrt{m\epsilon_b}$, BOX decays like $1/k^4$ in $d = 2$ and $1/k^3$ in $d = 3$. The plots of $\mathsf{BOX}(k, k)$ is shown in Fig. 4.13 for both $d = 2$ and $d = 3$. Let us consider the $d = 3$ case. An AL diagram with n AL insertions gives:

$$2^{n+1} \mathsf{CAP}(0)^2 \mathsf{BOX}(0,0)^{n-1} \lambda_d^{2n} \left[\chi_{\mathrm{dd}}^{\mathrm{BB}}(\Omega, \mathbf{Q}) \right]^n =$$

$$2^{n+1} \left[\frac{8\pi\sqrt{m\epsilon_b}}{m^2} \right]^{2n-2} \left[\frac{m^3}{16\pi(m\epsilon_b)^{3/2}} \right]^{n-1} \left[\chi_{\mathrm{dd}}^{\mathrm{BB}}(\Omega, \mathbf{Q}) \right]^n, \tag{4.123}$$
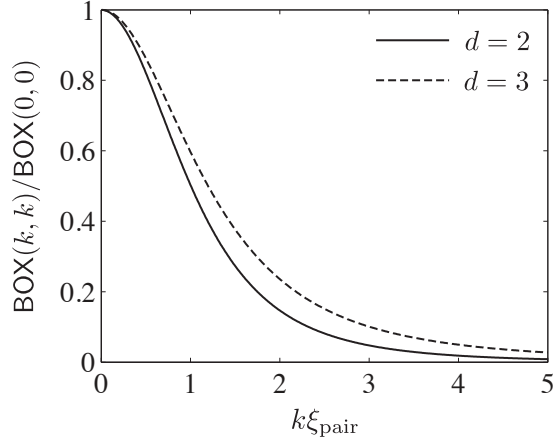
Figure 4.13: Plot of the static BOX diagram as function of external momentum k in $d = 2$ and $d = 3$. The BOX diagram describes a potential with a range $\sim 1/\xi_{\text{pair}}$ in the real space.

where $\chi_{\text{dd}}^{\text{BB}}(\Omega, \mathbf{Q})$ is the bosonic particle-hole propagator:

$$\chi_{\text{dd}}^{\text{BB}}(\Omega, \mathbf{Q}) = \int \frac{\mathrm{d}^d \mathbf{k}}{(2\pi)^d} \frac{b_0(\xi_{\mathbf{k}}^B) - b_0(\xi_{\mathbf{k}+\mathbf{Q}}^B)}{\Omega - \xi_{\mathbf{k}+\mathbf{Q}}^B + \xi_{\mathbf{k}}^B + i0^+}. \tag{4.124}$$

Eq. (4.123) imply that the n'th diagram is $\propto 1/\epsilon_b^{(n-1)/2}$. Therefore, only the $n = 1$ diagram is relevant in the strong-coupling limit and we immediately get:

$$(d = 3): \qquad \lim_{\epsilon_b/\epsilon_F \to \infty} \chi_{\text{dd}}(\Omega, \mathbf{Q}) = 4\chi_{\text{dd}}^{\text{BB}}(\Omega, \mathbf{Q}), \tag{4.125}$$

as we expected. For large but finite ϵ_b, we find the effective interaction boson-boson interaction:

$$(d = 3): \qquad U_{\text{BB}} \simeq 2\,\text{BOX}(0,0)\,\lambda_d^2 = 2\,\frac{4\pi(2a_s)}{2m}. \tag{4.126}$$

The factor of 2 is for the spin sum the in BOX diagram and λ_d^{-2} is due to the extra two bosonic propagators. Comparing the above result with bosons with mass $2m$ with short-range interaction $U = 4\pi a_B/(2m)$ in the Born approximation, we recover the known result $a_B = 2a_s$ [212, 213]. The interaction is repulsive and is a consequence of the Pauli exchange interaction between the constituent fermions.

The situation in $d = 2$ is different, as it could be anticipated from the discussion of the previous section. Indeed Eq. (4.123) shows that all n'th order diagrams are of the same order. However, we remember that the strong-coupling forms for the T-matrix and the Green's function we have used here is only warranted in the thermal regime $\beta \epsilon_F \ll 1$. For concreteness, let us consider the static limit $\Omega = 0$. Each $\chi_{\rm dd}^{\rm BB}$ carry a factor of $z = e^{-\beta|\mu_B|}$ which is small in the thermal regime. Therefore, the higher order AL diagrams must be neglected to be consistent, and we recover the free Bose gas response in the thermal regime. The effective interaction between the composite bosons can be calculated like before:

$$(d = 2): \qquad U_{\rm BB} \simeq 2\, {\rm BOX}(0,0)\, \lambda_d^2 = \frac{8\pi}{m}. \qquad (4.127)$$

The above results can be obtained from a more direct calculation. A simple analysis of the composite boson-boson interaction by retaining only the processes described by the BOX diagram yields the following expression:

$$U_{\rm BB}(\Omega, \mathbf{K} = 0) = 2 \int \frac{{\rm d}^d \mathbf{k}}{(2\pi)^d} \, |\tilde{\phi}_0(\mathbf{k})|^4 \left[-\Omega + 4\left(\mathbf{k}^2/(2m) + \epsilon_b/2 \right) \right], \qquad (4.128)$$

where Ω and $\mathbf{K}$ denote the center-of-mass energy and momentum of the boson-boson complex and $\tilde{\phi}_0(\mathbf{k})$ is the Fourier transformed normalized bound-state wave function (cf. Eq. A15 in Ref. [212] for a concise derivation of the above result). The normalized orbital wave function of the s-wave bound-state in $d = 2$ and $d = 3$ are given by:

$$(d = 2): \qquad \phi_0(\mathbf{r}) = [\sqrt{\pi a_2^2}]^{-1} K_0(r/a_2), \quad \tilde{\phi}_0(\mathbf{k}) = \sqrt{4\pi a_2^2} \left(1 + a_2^2 k^2 \right)^{-1},$$

$$(d = 3): \qquad \phi_0(\mathbf{r}) = [\sqrt{2\pi a_s}\, r]^{-1} \exp(-r/a_s), \quad \tilde{\phi}_0(\mathbf{k}) = \sqrt{8\pi a_s^3} \left(1 + a_s^2 k^2 \right)^{-1}. \qquad (4.129)$$

In $d = 2$, we find $\phi_0(\mathbf{r}) \sim -\log(r/a_2)$ for $r \ll a_2$ and $\phi_0(\mathbf{r}) \sim e^{-r/a_2}/\sqrt{r}$ for $r \gg a_2$. Plugging the above wave functions into Eq. (4.128) yields the results we found here using the diagrammatic method.

We argued earlier that an accurate treatment of 2D bosons must lead to the IR asymptotic freedom. Nevertheless, even in the thermal regime, the SCTMA yields a constant effective interaction. This is a good time to investigate the predictions of a more complicated theory than SCTMA, which only addresses the effect of boson-boson interactions at the mean-field level.

The BOX diagram is the simplest irreducible boson-boson interaction diagram and according to the explicit calculations given in Appendix D.2, it is localized in momentum space (see Fig. 4.13) and has a a range of the order of ξ_{pair} in the real space. This is indeed the expected behavior since BOX originates from the exchange repulsion between the constituent fermions and is expected to have a range of the order the size of the bound pairs, $\xi_{\mathrm{pair}} \sim 1/\sqrt{m\epsilon_b}$. A controlled expansion of the boson-boson interaction is feasible in the dilute limit $n\xi_{\mathrm{pair}}^2 \ll 1$. To $\mathcal{O}(n_B\xi_{\mathrm{pair}}^2)$, this is given by the bosonic ladder diagrams in the particle-particle channel:

$$
\mathsf{T}_{\mathrm{BB}} = U_{\mathrm{BB}}^{\mathrm{irr.}} + U_{\mathrm{BB}}^{\mathrm{irr.}} \; \mathsf{T}_{\mathrm{BB}} \;,
$$

$$
U_{\mathrm{BB}}^{\mathrm{irr.}} = \;\; + \ldots \tag{4.130}
$$

Interactions in the particle-hole channel and generally diagrams with more cycles introduce additional factors of density. In the above equation, $U_{\mathrm{BB}}^{\mathrm{irr.}}$ correspond to the sum of all 2-boson irreducible diagrams. The full classification of such diagrams in given in Ref. [214]. As shown above, the simplest of such diagrams is the twisted BOX diagram. In principle, $U_{\mathrm{BB}}^{\mathrm{irr.}}$ is given as a functional of G and T. The exact calculation of T_{BB} is beyond the scope of our current work. Nevertheless, we expect the real-space range of $U_{\mathrm{BB}}^{\mathrm{irr.}}$ to be given by the size of the bound pair $\sim 1/\xi_{\mathrm{pair}}$. Here, we are only interested in the low-energy behavior of T_{BB} and the very details of $U_{\mathrm{BB}}^{\mathrm{irr.}}$ are immaterial to us. The most important features can be seen simply using the following pseudo-potential instead of

the exact $U_{\mathrm{BB}}^{\mathrm{irr.}}$:

$$U_{\mathrm{BB}}^{\mathrm{irr.}}(k, k') \to u_0 \, \theta(k - k_0) \, \theta(k' - k_0), \tag{4.131}$$

where $u_0 \equiv c_0 m/(4\pi\epsilon_b^2)$ with c_0 being a $\mathcal{O}(1)$ numerical constant and k_0 is a UV cutoff $\sim 1/\xi_{\mathrm{pair}}$.

Substituting the above pseudo-potential in Eq. (4.130) yields an integral equation for T_{BB}. The calculation is analogous to what presented earlier for the fermion T-matrix (cf. Sec. 4.3.1). We define the reduced bosonic T-matrix $\mathsf{T}_{\mathrm{BB}}^+(\Omega, \mathbf{Q})$ via the ansatz:

$$T_{\mathrm{BB}}^+(k, k'; \Omega, \mathbf{Q}) = \theta(k - k_0) \, \theta(k' - k_0) \, \mathsf{T}_{\mathrm{BB}}^+(\Omega, \mathbf{Q}), \tag{4.132}$$

and subsequently find the following equation for $\mathsf{T}_{\mathrm{BB}}^+(\Omega, \mathbf{Q})$:

$$\mathsf{T}_{\mathrm{BB}}^+(\Omega, \mathbf{Q}) = u_0 + i u_0 \, \chi_{0,\mathrm{BB}}^+(\Omega, \mathbf{Q}) \, \mathsf{T}_{\mathrm{BB}}^+(\Omega, \mathbf{Q}). \tag{4.133}$$

Here, $\chi_{0,\mathrm{BB}}^+(\Omega, \mathbf{Q})$ is the bare 2-boson propagator given by:

$$
\begin{aligned}
i\chi_{0,\mathrm{BB}}^+(\Omega, \mathbf{Q}) &= \lambda_2^2 \int \frac{\mathrm{d}^2\mathbf{k}}{(2\pi)^2} \frac{\theta(k - k_0)}{\Omega - \xi_{\mathbf{Q}/2+\mathbf{k}}^B - \xi_{\mathbf{Q}/2-\mathbf{k}}^B + i0^+} \\
&= \left(\frac{4\pi\epsilon_b}{m}\right)^2 \frac{m_B}{4\pi} \ln\left[1 - \frac{k_0^2/m_B}{\Omega + 2\mu_B - Q^4/(4m_B) + i0^+}\right],
\end{aligned} \tag{4.134}
$$

where $m_B = 2m$. Put together, the above equations give:

$$T_{\mathrm{BB}}^+(k, k'; \Omega, \mathbf{Q}) = \frac{m}{4\pi\epsilon_b^2} \frac{\theta(k - k_0)\,\theta(k' - k_0)}{i\pi + \ln\left[\dfrac{\Omega + 2\mu_B - Q^4/(4m_B)}{\exp(c_0)\,k_0^2/m}\right]}. \tag{4.135}$$

The above result exhibit the sought-after IR asymptotic freedom of bosons in $d = 2$ and agrees with the RG analysis presented earlier (cf. Eq. 4.40). For small center of mass energy of the two-boson complex $\Omega + 2\mu_B - Q^4/(4m_B)$ compared to ϵ_b, the denominator diverges logarithmically and $T_{\mathrm{BB}} \to 0$.

Returning back to the discussion of the AL diagrams, we expect that whenever a Φ-derivable theory is powerful enough to describe boson-boson interactions at the level of ladder diagrams, the BOX diagrams will be naturally replaced with T_{BB}. The center of mass momentum of the scattering

bosonic pairs is small as long as low-energy energy processes are concerned, and each additional AL insertion is accompanied by a logarithmically small factor $\sim 1/\ln(mE/k_0^2)$. Therefore, only the simplest AL diagram survives for low energies even in the quantum regime. The same IR freedom will be also present at the level of fermionic Green's functions and bosonic propagators, justifying the usage of strong-coupling NSR Green's functions in the quantum regime. We will discuss such a "powerful enough" Φ-derivable approximations in Sec. 4.7.

Setting aside the intricacies of 2D physics discussed in this section, a glimpse at the linear response diagrams of the SCTMA shows that practical diagrammatic calculations of the linear response can be a quite challenging task. The number of articles written on superconducting fluctuations in the past four decades is of the order of ten thousands. A large number of these contributions deal with calculating the lowest order MT, AL and DOS diagrams and their correction to transport coefficients and thermodynamical quantities [210]. Application to systems with broken translational symmetry only makes the analysis more formidable. In the next section, we develop a quantum kinetic formalism based on the SCTMA that allows us to do realistic calculations and even obtain exact numerical results that are quite formidable using standard diagrammatic methods.

4.5 Quantum kinetic equations in the self-consistent T-matrix approximation

We discussed the general theory of quantum kinetic equations in chapter 2 at length. We also formulated the self-consistent T-matrix theory for general non-equilibrium states in the previous section and discussed its content in the weak and strong coupling regimes. In this section, we use the results of the previous sections and formulate a quantum kinetic description based on the self-consistent T-matrix approximation.

4.5.1 Phenomenological kinetic equations

Before we carry out the formal development starting from microscopic equations, it is worthwhile discussing the general phenomenology of many-particle systems with *attractive* interactions. An important consequence of attractive interactions is the possibility of formation of meta-stable two-body (generally few-body) complexes with long lifetimes $\tau_{\text{comp.}} \sim \tau_{\text{c}} \epsilon_b / (k_B T)$. Here, τ_{c} is the time between collisions and ϵ_b is the binding energy of the complex. In dilute systems with large binding energy, $\tau_{\text{comp.}}$ may become comparable or even exceed the macroscopic time scale of transport t_{macro}. Denoting the local momentum distribution of the free particles and complexes as $n_f(\mathbf{p}; T, \mathbf{R})$ and $n_c(\mathbf{p}; T, \mathbf{R})$, respectively, we may then write the following phenomenological Boltzmann equations:

$$\partial_T n_f + \frac{\mathbf{p}}{m} \cdot \partial_{\mathbf{R}} n_f - \partial_{\mathbf{R}} \left(U_{\text{ext},f}(T, \mathbf{R}) + U_{\text{eff},f}[n_f, n_c] \right) \cdot \partial_{\mathbf{p}} n_f = \mathsf{C}_{ff}[n_f, n_f] + \mathsf{C}_{cf}[n_f, n_c],$$

$$(4.136\text{a})$$

$$\partial_T n_c + \frac{\mathbf{p}}{m_c} \cdot \partial_{\mathbf{R}} n_c - \partial_{\mathbf{R}} \left(U_{\text{ext},c}(T, \mathbf{R}) + U_{\text{eff},c}[n_f, n_c] \right) \cdot \partial_{\mathbf{p}} n_c = \mathsf{C}_{cc}[n_c, n_c] + \mathsf{C}_{fc}[n_f, n_c].$$

$$(4.136\text{b})$$

In the above equations, m is the mass of a free particle, m_c is the mass of the complex and $U_{\text{ext},f(c)}$ denote external potentials. The right hand side terms describe collisional physics: C_{ff} denotes the collisional rate of change of the phase space density due to free-free collisions, C_{cf} denotes the net complex $\to$ free dissociation rate:

$$\mathsf{C}_{ff}(\mathbf{p}; T, \mathbf{R}) = \int \frac{\mathrm{d}^d \mathbf{p}_1}{(2\pi)^d} \frac{\mathrm{d}^d \mathbf{p}'}{(2\pi)^d} \frac{\mathrm{d}^d \mathbf{p}'_1}{(2\pi)^d} (2\pi)^{d+1} \delta(\mathbf{p} + \mathbf{p}_1 - \mathbf{p}' - \mathbf{p}'_1) \delta(E_{\mathbf{p}} + E_{\mathbf{p}_1} - E_{\mathbf{p}'} - E_{\mathbf{p}'_1})$$

$$\times W_{ff}(\mathbf{p}, \mathbf{p}_1 \to \mathbf{p}', \mathbf{p}'_1) \left[n_f(\mathbf{p}'; T, \mathbf{R}) n_f(\mathbf{p}'_1; T, \mathbf{R}) - n_f(\mathbf{p}; T, \mathbf{R}) n_f(\mathbf{p}_1; T, \mathbf{R}) \right],$$

$$\mathsf{C}_{cf}(\mathbf{p}; T, \mathbf{R}) = \int \frac{\mathrm{d}^d \mathbf{p}_1}{(2\pi)^d} \frac{\mathrm{d}^d \mathbf{p}_c}{(2\pi)^d} (2\pi)^{d+1} \delta(\mathbf{p} + \mathbf{p}_1 - \mathbf{p}_c) \delta(E_{\mathbf{p}} + E_{\mathbf{p}'} - E_{\mathbf{p}_c}^c)$$

$$\times W_{fc}(\mathbf{p}, \mathbf{p}_1 \to \mathbf{p}_c) \left[n_c(\mathbf{p}_c; T, \mathbf{R}) n_f(\mathbf{p}_1; T, \mathbf{R}) - n_c(\mathbf{p}_c; T, \mathbf{R}) n_f(\mathbf{p}; T, \mathbf{R}) \right].$$

$$(4.137)$$

Similar expressions can be written for C_{cc} and C_{fc}. The total mass density at a given macroscopic point is:

$$\rho(T, \mathbf{R}) = \int \frac{\mathrm{d}^d \mathbf{p}}{(2\pi)^d} \left[m \, n_f(\mathbf{p}; T, \mathbf{R}) + m_c \, n_c(\mathbf{p}; T, \mathbf{R}) \right]. \tag{4.138}$$

In the weak-coupling limit ($\epsilon_b \ll k_B T$), the majority of particles are in free form, whereas this scenario is reversed in the strong-coupling ($\epsilon_b \gg k_B T$) limit.

The quantum effects have been left out in the above phenomenology and it was assumed that complexes and free particles are distinguishable entities. In a general quantum mechanical setting, this implies that the spatial extent of the wave function of the complex $\lambda_c \sim \hbar/\sqrt{m\epsilon_b}$ is much smaller than the relevant quantum wavelength $\lambda_q = \min\{h/\sqrt{2\pi m k_B T}, k_F\}$. Otherwise, the uncertainty principle does not allow a well-defined distinction between free particles and complexes. In particular, in the regime $\lambda_c \sim \lambda_q$, the free particles and complexes *melt* into each other due to quantum fluctuations, resembling the pairing pseudogap regime.

Even in such cases, we may still write similar kinetic equations in terms of the energy distribution of particles, f, and the statistics of *pairing fluctuations*, b, both of which remain well-defined in a fully quantum mechanical setting. In the weak-coupling limit, pairing fluctuations are small, we recover Eq. (4.136a) (with quantum mechanical corrections if $\lambda_q \sim n^{1/d}$). In the strong-coupling limit, pairing fluctuations describe stable complexes $b \to n_c$, $n_f \to 0$, we recover Eq. (4.136a). Furthermore, $\rho \simeq m\rho_f$ and $\rho \simeq m_c\rho_c$ in the weak- and strong-coupling limits, respectively.

Memory effects play a central role in the dynamics of many-particle systems that allow formation of long-lived bound states. This is in particular important in the strong-coupling limit, where 2-particle correlations G_2 develop off-diagonal long-time order due to stable complexes. A physically faithful closure of the BBGKY hierarchy at the level of 2-point functions will inevitably have strong retardation effects, i.e. will be non-Markovian. Therefore, a Markovian approximation at the level of 2-point functions is guaranteed to fail in the strong-coupling limit.

4.5.2 Microscopic derivation of the kinetic equations

In this section, we show that a consistent pursuit of the gradient expansion program for the SCTMA indeed yields the sought-after phenomenological coupled kinetic equations described in the previous section in a natural way.

Derivation of kinetic equations based on the T-matrix approximation has a long history indeed, going back to Kadanoff and Baym's seminal contribution in 1962 [22]. They discussed the T-matrix approximation for particles with short-range *repulsive* interactions. In their analysis, as well as subsequent developments [23, 24], gradient terms in the T-matrix were not acknowledged and or were tacitly ignored. In any event, the neglect of memory effects in collisions is a reasonable approximation for repulsive interactions as the lifetime of binary collisions is of the order of $\tau_{\text{comp.}} \sim r_0/v_{\text{rms}}$, where r_0 is the range of interactions and v_{rms} is the r.m.s. velocity. On the other hand, $\tau_{\text{comp.}} \sim \tau_c \epsilon_b/(k_B T)$ can become very large for attractive interactions and memory effects become increasingly more important. Inclusion of retardation effects in kinetic equations for systems with bound states and strong retardation have been discussed in Refs. [215, 216, 217, 218] and more recently in Refs. [219, 220, 221, 222, 223, 224, 225]. These developments are along the line of reconstructing retardation effects from the time-diagonal Green's functions, the so-called generalized Kadanoff-Baym ansatz [218], or by calculating non-Markovian corrections to the Boltzmann equation [224]. Earlier works are based on heuristic closure of the BBGKY hierarchies and approximate inclusion of retardation effects. There is no guarantee that conservation laws will be satisfied in approximate treatment of memory effects.

Recently, Ivanov, Knoll and Voskresensky have recently shown that a fully consistent gradient expansion of the KB equations is guaranteed to respect the exact conservation laws [25, 61, 62]. This is the line of thought that we pursue in this section. Starting from the KB equations for the fermionic Green's functions, we write the exact quantum kinetic equations for $f_\sigma(\omega, \mathbf{p}; T, \mathbf{R})$. The resulting equation, however, is incomplete without the knowledge of $b(\omega, \mathbf{p}; T, \mathbf{R})$ and

$\mathsf{B}(\omega, \mathbf{p}; T, \mathbf{R})$, the statistical and spectral parts of the T-matrix. The memory effects of the bosonic degrees of freedom reside in $b(\omega, \mathbf{p}; T, \mathbf{R})$, and consequently in the fermionic self-energies (cf. Eq. 4.82). We depart from the earlier works at this stage: instead of attempting to reconstruct the memory effects in $b(\omega, \mathbf{p}; T, \mathbf{R})$ approximately and obtaining a non-Markovian kinetic equation, we carry out the gradient expansion program for the renormalized non-equilibrium Dyson's equation for the T-matrix, Eq. (4.95). The result is a quantum kinetic equation for $b(\omega, \mathbf{p}; T, \mathbf{R})$. Together with the kinetic equation for $f_\sigma(\omega, \mathbf{p}; T, \mathbf{R})$, these two equations constitute the equations provisioned from phenomenological arguments. Furthermore, the gradient corrections are accounted form in a fully consistent manner, conservation laws are guaranteed to be respected [62].

In order to avoid fragmentation of the discussion, we copy some of the results obtained earlier when necessary. Our starting point in the generalized kinetic equation for $\mathcal{G}_\sigma$ in the Boterman-Malfliet (BM) form (cf. Eq. 2.41):

$$\frac{\mathsf{A}_\sigma^2 \, \Gamma_\sigma}{2} \left[\{\mathsf{M}_\sigma, f_\sigma\} - \frac{\mathsf{M}_\sigma}{\Gamma_\sigma} \{\Gamma_\sigma, f_\sigma\} \right] = \mathsf{C}_\sigma + \mathcal{O}(\partial_X^2). \tag{4.139a}$$

The various quantities appearing in the above equations (spectral broadening Γ_σ, spectral function A_σ, mass-shell M_σ, and the collision integral C_σ) were given in the Sec. 4.3. We copy the results here:

$$\mathsf{A}_\sigma(\tilde{1}) = -2\Im[G_\sigma^+(\tilde{1})] = \frac{\Gamma_\sigma(\tilde{1})}{\mathsf{M}_\sigma(\tilde{1})^2 + \Gamma_\sigma(\tilde{1})^2/4} + \mathcal{O}(\partial_X)^2, \tag{4.139b}$$

$$\Gamma_\sigma(\tilde{1}) = -2\Im[\Sigma_\sigma^+(\tilde{1})] = \int \mathrm{d}\tilde{2}\, \mathrm{d}\tilde{3}\, \delta(\tilde{1} + \tilde{2} - \tilde{3})\, \mathsf{A}_{\bar{\sigma}}(\tilde{2})\, \mathsf{B}(\tilde{3}) \left[f_{\bar{\sigma}}(\tilde{2}) + b(\tilde{3}) \right], \tag{4.139c}$$

$$\mathsf{M}_\sigma(\tilde{1}) = \omega_1 + \mu_\sigma - \frac{|\mathbf{p}_1|^2}{2m_\sigma} - U_\sigma(T, \mathbf{R}) - \Re[\Sigma_\sigma^+(\tilde{1})]. \tag{4.139d}$$

We remind that the shorthand $\mathrm{d}\tilde{1}$ stands for $(2\pi)^{-d-1}\, \mathrm{d}\omega_1\, \mathrm{d}^d\, \mathbf{p}_1$. All of the functions carry a label of $(T, \mathbf{R})$ corresponding to the macroscopic time and space coordinates. We remember that B and

b denote the spectral and statistical parts of the T-matrix:

$$\mathsf{T}^> = -i\mathsf{B}(b+1), \qquad \mathsf{T}^< = -i\mathsf{B}b. \tag{4.139e}$$

The real part of the fermionic self-energy $\Re[\Sigma_\sigma^+]$ is given by the Kramers-Kronig transform of $\Im[\Sigma_\sigma^+] = -\Gamma_\sigma/2$:

$$\Re[\Sigma_\sigma^+(\tilde{1})] = -\frac{1}{2}\,\mathfrak{K}\mathfrak{K}[\Gamma_\sigma(\tilde{1})]. \tag{4.139f}$$

The fermionic collision integral is:

$$\mathsf{C}_\sigma(\tilde{1}) = G_\sigma^>(\tilde{1})\Sigma_\sigma^<(\tilde{1}) - \Sigma_\sigma^>(\tilde{1})G_\sigma^<(\tilde{1})$$

$$= \int \mathrm{d}\tilde{2}\,\mathrm{d}\tilde{3}\,\delta(\tilde{1}+\tilde{2}-\tilde{3})\,\mathsf{A}_\sigma(\tilde{1})\,\mathsf{A}_{\bar{\sigma}}(\tilde{2})\,\mathsf{B}(\tilde{3})$$

$$\times \left\{ \left[1 - f_\sigma(\tilde{1})\right]\left[1 - f_{\bar{\sigma}}(\tilde{2})\right]b(\tilde{3}) - f_\sigma(\tilde{1})\,f_{\bar{\sigma}}(\tilde{2})\left[1 + b(\tilde{3})\right] \right\}$$

$$= \int \mathrm{d}\tilde{2}\,\mathrm{d}\tilde{3}\,\delta(\tilde{1}+\tilde{2}-\tilde{3}) \left[\text{(diagram)} - \text{(diagram)} \right] \tag{4.139g}$$

The quantity $\mathsf{C}_\sigma(\omega, \mathbf{p}; T, \mathbf{R})$ has the simple intuitive interpretation of the net rate of change of f_σ due to annihilation and creation of bosonic fluctuations, resolved by the energy and momentum $(\omega, \mathbf{p})$ of a fermion with spin σ. We will show later that neglecting memory effects in the T-matrix and a local approximation gives the result obtained earlier by Kadanoff and Baym [22] and Danielewicz [23].

The non-equilibrium Dyson's equation for the T-matrix, Eq. (4.95), is precisely what we need to proceed with our development:

$$\mathsf{T}(1, 1')^{-1} = \tilde{\mathsf{T}}_0^{-1}(1, 1') - \mathcal{Q}(1, 1')$$

$$\mathcal{Q}(1, 1') = i\chi(1, 1') - i\tilde{\chi}_0(1, 1') = \text{(diagram)} - \text{(diagram)}. \tag{4.140}$$

Identifying the renormalized vacuum T-matrix $\tilde{\mathsf{T}}_0^{-1}$ and $\mathcal{Q}$ as the free bosonic Green's function and bosonic self-energy, respectively, we can take all of the steps we took earlier to derive the kinetic

equation for $\mathcal{G}$ to derive a kinetic equation for T. The only difference is that $\tilde{\mathsf{T}}_0^{-1}$ has a somewhat more complex structure and has a non-vanishing *greater* component (cf. Eq. 4.91b). As a first step, we convert the Dyson's equation to a KB equation for T. The explicit-time functions are found using Langreth rules. The resulting KB equations and their adjoints in the Wigner representation (analogous to Eq. 2.22) read as:

$$\left[\tilde{\mathsf{T}}_0^{-1}\right]^+ \star_{\mathrm{GM}} \mathsf{T}^{\gtrless} + \left[\tilde{\mathsf{T}}_0^{-1}\right]^{\gtrless} \star_{\mathrm{GM}} \mathsf{T}^- = Q^+ \star_{\mathrm{GM}} \mathsf{T}^{\gtrless} + Q^{\gtrless} \star_{\mathrm{GM}} \mathsf{T}^-, \tag{4.141a}$$

$$\left[\tilde{\mathsf{T}}_0^{-1}\right]^{\pm} \star_{\mathrm{GM}} T^{\pm} = 1 + Q^{\pm} \star_{\mathrm{GM}} \mathsf{T}^{\pm}, \tag{4.141b}$$

$$\mathsf{T}^+ \star_{\mathrm{GM}} \left[\tilde{\mathsf{T}}_0^{-1}\right]^{\gtrless} + \mathsf{T}^{\gtrless} \star_{\mathrm{GM}} \left[\tilde{\mathsf{T}}_0^{-1}\right]^- = \mathsf{T}^+ \star_{\mathrm{GM}} Q^{\gtrless} + \mathsf{T}^{\gtrless} \star_{\mathrm{GM}} Q^-, \tag{4.141c}$$

$$\mathsf{T}^{\pm} \star_{\mathrm{GM}} \left[\tilde{\mathsf{T}}_0^{-1}\right]^{\pm} = 1 + \mathsf{T}^{\pm} \star_{\mathrm{GM}} Q^{\pm}. \tag{4.141d}$$

The operator $\star_{\mathrm{GM}}$ is the Groenewold-Moyal product defined earlier (cf. Eq. 2.12). The first-order gradient expansion of the equation for the $\pm$ component and its adjoint give:

$$\left(\left[\tilde{\mathsf{T}}_0^{-1}\right]^{\pm} - Q^{\pm}\right) \mathsf{T}^{\pm} + \frac{i}{2}\left\{\left[\tilde{\mathsf{T}}_0^{-1}\right]^{\pm} - Q^{\pm}, \mathsf{T}^{\pm}\right\} = 1 + \mathcal{O}(\partial_X^2), \tag{4.142a}$$

$$\left(\left[\tilde{\mathsf{T}}_0^{-1}\right]^{\pm} - Q^{\pm}\right) \mathsf{T}^{\pm} + \frac{i}{2}\left\{\mathsf{T}^{\pm}, \left[\tilde{\mathsf{T}}_0^{-1}\right]^{\pm} - Q^{\pm}\right\} = 1 + \mathcal{O}(\partial_X^2). \tag{4.142b}$$

Similar to the situation with $\mathcal{G}$, the above equations have the following simple algebraic solution:

$$\mathsf{T}^{\pm} = \frac{1}{\left[\tilde{\mathsf{T}}_0^{-1}\right]^{\pm} - Q^{\pm}} + \mathcal{O}(\partial_X^2). \tag{4.143}$$

Carrying out the first-order gradient expansion of Eqs. (4.141a) and (4.141c) and subtracting the latter from the former, we find:

$$\left\{\Re\left(\left[\tilde{\mathsf{T}}_0^{-1}\right]^+ - Q^+\right), i\mathsf{T}^{\gtrless}\right\} + \left\{\Re[\mathsf{T}^+], i\left(Q^{\gtrless} - \left[\tilde{\mathsf{T}}_0^{-1}\right]^{\gtrless}\right)\right\} =$$
$$\mathsf{T}^{<}\left(Q^{>} - \left[\tilde{\mathsf{T}}_0^{-1}\right]^{>}\right) - \mathsf{T}^{>}\left(Q^{<} - \left[\tilde{\mathsf{T}}_0^{-1}\right]^{<}\right) + \mathcal{O}(\partial_X^2), \tag{4.144}$$

which is the KB quantum kinetic equation for the T-matrix. The above equation assumes the following simple form in the spectral/statistical representation:

$$\{\mathsf{M}_b, \mathsf{B}\, b\} + \left\{\frac{\mathsf{M}_b}{\mathsf{M}_b^2 + \Gamma_b^2/4}, \Gamma_b c_b\right\} = \mathsf{C}_b + \mathcal{O}(\partial_X^2), \tag{4.145}$$

where we have defined a bosonic spectral/statistical representation for the combination $\mathcal{Q} - \left[\tilde{\mathsf{T}}_0^{-1}\right]$:

$$Q^< - \left[\tilde{\mathsf{T}}_0^{-1}\right]^< \equiv -i\Gamma_b\, c_b, \qquad Q^> - \left[\tilde{\mathsf{T}}_0^{-1}\right]^> \equiv -i\Gamma_b(c_b + 1), \tag{4.146}$$

the bosonic mass-shell function M_b as:

$$\mathsf{M}_b \equiv \Re\left(\left[\tilde{\mathsf{T}}_0^{-1}\right]^+ - Q^+\right), \tag{4.147}$$

and the bosonic collision integral C_b as:

$$\mathsf{C}_b \equiv -\mathsf{B}\Gamma_b(b - c_b). \tag{4.148}$$

Using Eq. (4.143), the real and imaginary parts of T^+ can be written as:

$$\Re[\mathsf{T}^+] = \frac{\mathsf{M}_b}{\mathsf{M}_b^2 + \Gamma_b^2/4}, \qquad \Im[\mathsf{T}^+] = \frac{-\Gamma_b/2}{\mathsf{M}_b^2 + \Gamma_b^2/4}. \tag{4.149}$$

Observing that $b - c_b \sim \mathcal{O}(\partial_X)$, we can replace c_b with b inside the second Poisson bracket on the left hand side of Eq. (4.145) to find the BM form after some elementary rearrangements:

$$\frac{\mathsf{B}^2\,\Gamma_b}{2}\left[\{\mathsf{M}_b, b\} - \frac{\mathsf{M}_b}{\Gamma_b}\{\Gamma_b, b\}\right] = \mathsf{C}_b + \mathcal{O}(\partial_X^2), \tag{4.150a}$$

We summarize the explicit expressions for the quantities that appear inside the T-matrix kinetic equation:

$$\mathsf{B}(\tilde{1}) = -2\Im[\mathsf{T}^+(\tilde{1})] = \frac{\Gamma_b(\tilde{1})}{\mathsf{M}_b(\tilde{1})^2 + \Gamma_b(\tilde{1})^2/4} + \mathcal{O}(\partial_X^2), \tag{4.150b}$$

$$\Gamma_b(\tilde{1}) = -2\Im\left(Q^+(\tilde{1}) - \left[\tilde{\mathsf{T}}_0^{-1}(\tilde{1})\right]^+\right)$$

$$= \int d\tilde{2}\, d\tilde{3}\, \delta(\tilde{1} - \tilde{2} - \tilde{3})\, \mathsf{A}_\uparrow(\tilde{2})\, \mathsf{A}_\downarrow(\tilde{3})\, [1 - f_\uparrow(\tilde{2}) - f_\downarrow(\tilde{3})], \tag{4.150c}$$

$$c_b(\tilde{1}) = \Gamma_b(\tilde{1})^{-1}\int d\tilde{2}\, d\tilde{3}\, \delta(\tilde{1} - \tilde{2} - \tilde{3})\, \mathsf{A}_\uparrow(\tilde{2})\, \mathsf{A}_\downarrow(\tilde{3})\, f_\uparrow(\tilde{2})\, f_\downarrow(\tilde{3}), \tag{4.150d}$$

$$\mathsf{M}_b(\tilde{1}) = \Re\left(\left[\tilde{\mathsf{T}}_0^{-1}\right]^+ - Q^+\right)$$

$$= \Re\left[\left(\mathsf{T}_0^{-1}\right)^+\left(\omega_1 + \mu_\uparrow + \mu_\downarrow - U_\uparrow - U_\downarrow, \mathbf{p}_1\right)\right] - \mathfrak{K}\mathfrak{K}\left[\Im\left[Q^+(\tilde{1})\right]\right], \tag{4.150e}$$

$$\Im\left[Q^+(\tilde{1})\right] = -\frac{1}{2}\int d\tilde{2}\, d\tilde{3}\, \delta(\tilde{1}-\tilde{2}-\tilde{3})\left\{A_\uparrow(\tilde{2})\,A_\downarrow(\tilde{3})\left[1-f_\uparrow(\tilde{2})-f_\downarrow(\tilde{3})\right]-\tilde{A}_{0,\uparrow}(\tilde{2})\,\tilde{A}_{0,\downarrow}(\tilde{3})\right\}.$$

$$(4.150\text{f})$$

Finally, the bosonic collision integral $C_b(\omega,\mathbf{p};T,\mathbf{R})$ is:

$$C_b(\tilde{1}) = T^<\left(Q^> - \left[\tilde{T}_0^{-1}\right]^>\right) - T^>\left(Q^< - \left[\tilde{T}_0^{-1}\right]^<\right)$$

$$= \int d\tilde{2}\, d\tilde{3}\, \delta(\tilde{1}-\tilde{2}-\tilde{3})\, B(\tilde{1})\, A_\uparrow(\tilde{2})\, A_\downarrow(\tilde{3})\left\{\left[1+b(\tilde{1})\right]f_\uparrow(\tilde{2})\,f_\downarrow(\tilde{3})\right.$$

$$\left. - b(\tilde{1})\left[1-f_\uparrow(\tilde{2})\right]\left[1-f_\downarrow(\tilde{3})\right]\right\}$$

$$= \int d\tilde{2}\, d\tilde{3}\, \delta(\tilde{1}-\tilde{2}-\tilde{3})\left[\,\vcenter{\hbox{}}\,\right],\qquad (4.150\text{g})$$

The quantity $C_b(\omega,\mathbf{p};T,\mathbf{R})$ has the simple intuitive interpretation of the net rate of change of $b(\omega,\mathbf{p};T,\mathbf{R})$ due to formation and dissociation of a bosonic fluctuations with energy and momentum $(\omega,\mathbf{p})$. It is easy to see that the fermionic and bosonic collision integrals satisfy the following exact relation:

$$\int d\tilde{1}\, p^\mu(\tilde{1})\left[C_\uparrow(\tilde{1})+C_\downarrow(\tilde{1})+C_b(\tilde{1})\right]=0,\qquad (4.151)$$

where $p^\mu(\tilde{1})\equiv(\omega_1,\mathbf{p}_1)$. The above relation follows directly from Eqs. (4.139g) and (4.150g) and imply that the energy and momentum is conserving in the formation and dissociation of a bosonic fluctuation.

We have obtained a complete set of equations that determine the evolution of (f_σ, b) in the kinetic limit. Our treatment has two important features: (1) The Groenewold-Moyal products are expanded consistently to first order in all evolution equations, so that the conservation laws are guaranteed to be respected [62]; (2) the coupled equations have a simple Markovian structure in the extended state space (f_σ, b): the spectral functions, mass-shell functions, spectral broadenings and collision integrals are all local in $(T,\mathbf{R})$. The Markovian structure comes at the cost of an

extended state space $f_\sigma \to (f_\sigma, b)$. This added expense is however to our benefit: we will show later that b indeed describes the statistics of bound states in the strong-coupling limit. (3) The quantum kinetic equations obtained here from the microscopic theory resemble those provisioned from phenomenological arguments.

The methodology used here can be applied to other fluctuation-exchange Φ-derivable approximations. Whenever the self-energy is expressible in terms of one or more sub-diagrams, each admit a Dyson's equation (e.g. the Cooperon, magnon, change density wave, etc.). The state space may be augmented by introducing additional bosonic statistical functions $(b_1, \ldots, b_N)$, each satisfying a Markovian kinetic equation. The coupled system of equations are guaranteed to conserve the symmetries of the microscopic theory.

4.5.3 The weak-coupling and strong-coupling limits

The coupled kinetic equations describing fermionic and bosonic degrees of freedom are expected to assume simple forms in the weak-coupling and strong-coupling limits. In the weak-coupling limit, the dynamics of the bosonic fluctuations is highly diffusive (cf. Sec. 4.2.3), so that the bosonic excitations are short-lived (memoryless) in the first approximation. Therefore, the statistics of bosonic excitations b is expected to be determined *instantaneously* by the non-equilibrium configuration of the fermionic degree of freedom. In this limit, the weak collisions are predominantly governed by the Maki-Thompson processes, i.e. Andreev reflection from the short-lived bosonic excitations. During the passage to the strong-coupling limit, the bosonic degree of freedom smoothly changes its character from local short-lived fluctuations to propagating long-lived bound pairs of fermions. The population of free fermions is suppressed by an exponentially small factor $\sim e^{-\beta\epsilon_b/2}$ and only appear as short-lived excitations during the collision of bosonic pairs. The transport is described by the Aslamazov-Larkin process as mentioned earlier. We make these ideas rigorous in the remainder of this section.

The weak-coupling limit ($\epsilon_b/\epsilon_F \ll 1$, $\beta\epsilon_b \ll 1$):

We assume that both spin states have equal mass and chemical potential for simplicity, and that $U_\uparrow = U_\downarrow = U$. The diffusive character of bosonic fluctuations can be seen by investigating the T-matrix kinetic equation, Eq. (4.150a). In this limit, self-consistency is immaterial due to weak interactions and we may use the equilibrium form of the retarded many-body T-matrix. The latter is most easily obtained by analytically continuing the Matsubara T-matrix given in Eq. (4.29) by the substitution $i\nu_n \rightarrow \omega - 2U(T, \mathbf{R}) + i0^+$:

$$\mathsf{T}^+(\omega, \mathbf{q}; T, \mathbf{R}) \approx \frac{1}{(\gamma_1 + i\gamma_2)(\omega - 2U(T, \mathbf{R})) - c_1|\mathbf{q}|^2/(2m) - c_0}, \tag{4.152}$$

where $c_0 = -N(0)\ln(\beta T_c)$, $c_1 = N(0)7\beta^2\zeta(3)\epsilon_F/(8\pi^2)$, $\gamma_1 = N(0)/(4\epsilon_F)$ and $\gamma_2 = N(0)\beta\pi/8$ according to Eq. (4.32). We remember that $T_c \sim \sqrt{\epsilon_b\epsilon_F}$ so that $c(0)/N(0) \sim -\ln(\beta\epsilon_b) \gg 1$. The above expression yields $\mathsf{M}_b \approx c_0 - c_1|\mathbf{q}|^2/(2m) + \gamma_1(\omega - 2U(T, \mathbf{R}))$ and $\Gamma_b \approx 2\gamma_2(\omega - 2U(T, \mathbf{R}))$. Plugging these expressions into Eq. (4.150a), we find:

$$\frac{\gamma_2[\omega - 2U(T, \mathbf{R})]}{c_0^2}\left(\gamma_1\partial_T b + \frac{c_1}{m}\mathbf{q}\cdot\partial_{\mathbf{R}}b - 2\gamma_1\partial_{\mathbf{R}}U\cdot\partial_{\mathbf{p}}b\right) + \frac{\gamma_2}{c_0}(\partial_T b - 2\partial_{\mathbf{R}}U\cdot\partial_{\mathbf{p}}b) = c_b - b. \tag{4.153}$$

The first term on the left hand side is sub-leading to the second term due to an extra factor of c_0 in the denominator and can be neglected. The resulting equation can be written as:

$$\partial_T b - 2\partial_{\mathbf{R}}U\cdot\partial_{\mathbf{p}}b \approx -\frac{b - c_b}{\tau_b}, \tag{4.154}$$

where $\tau_b \equiv \gamma_2/c_0$, is a relaxation time. The above equation implies that deviations of the bosonic statistical function b from c_b relax to c_b within a short time $\tau_b \sim \beta/\ln(\beta T_c)$. We remember that c_b is exactly the instantaneous distribution of bosonic fluctuations for a given configuration of fermions. According to Eq. (4.150d), c_b can be thought of as the rate at which two fermions meet (with a given center of mass energy and momentum), multiplied by the lifetime of bosonic fluctuation Γ_b. The above result may also be obtained from a different perspective. Combining Eqs. (4.141a)-(4.141d),

we find the following exact equation[4] for $\mathsf{T}^{\gtrless}$:

$$-i\mathsf{T}^{\gtrless} = \mathsf{T}^{+} \star_{\mathrm{GM}} \chi^{\gtrless} \star_{\mathrm{GM}} \mathsf{T}^{-}. \tag{4.155}$$

Expanding the GM product to linear order, we find:

$$-i\mathsf{T}^{\gtrless} = |\mathsf{T}^{+}|^{2}\chi^{\gtrless} + \frac{i}{2}\left[\{\mathsf{T}^{+}, \chi^{\gtrless}\}\mathsf{T}^{-} + \mathsf{T}^{+}\{\chi^{\gtrless}, \mathsf{T}^{-}\} + \chi^{\gtrless}\{\mathsf{T}^{+}, \mathsf{T}^{-}\}\right] + \mathcal{O}(\partial_{X}^{2}). \tag{4.156}$$

Since $N(0)\mathsf{T}^{+} \sim N(0)/c_{0} \ll 1$ and the gradient terms in the kinetic limit introduce additional smallness factors (by definition), the Poisson brackets in the square brackets may therefore be neglected and we obtain:

$$\mathsf{T}^{\gtrless} = i|\mathsf{T}^{+}|^{2}\chi^{\gtrless} + \mathcal{O}(\partial_{X}/\ln^{2}\beta\epsilon_{b}). \tag{4.157}$$

Keeping only the product term directly gives $c_{b} = b$. However, neglecting the gradient terms involving the T-matrix is simply the statement of neglecting memory effects of bosonic degrees of freedom. In summary, we find:

$$b = c_{b} + \mathcal{O}(1/\ln\beta\epsilon_{b}). \tag{4.158}$$

To leading order in $1/\ln\beta\epsilon_{b}$, the fermionic kinetic equation (Eq. 4.139a) is self-sufficient. Replacing b with c_{b} in Eq. (4.139c) yields Γ_{σ} just in terms of A_{σ} and f_{σ}. In fact, Γ_{σ} and C_{σ} are already $\mathcal{O}(1/\ln^{2}\beta\epsilon_{b})$ due to the factor $\mathsf{B} \sim 1/\ln^{2}\beta\epsilon_{b}$. Therefore, the error introduced by replacing b with c_{b} is only $\mathcal{O}(1/\ln^{3}\beta\epsilon_{b})$ and the approximation is quite accurate in the weak-coupling limit. The weak-coupling fermionic collision integral (Eq. 4.139g) assumes the following form following the

---

[4]The most general equation of this type includes a term involving the initial conditions (e.g. see Eq. (3.13) in Ref. [23]). Here, we have assumed that the system is in equilibrium at $t = -\infty$. The KMS boundary condition is automatically satisfied by Eq. (4.155).

replacement $b \to c_b$:

$$\mathsf{C}_\sigma(\tilde{1}) = \int d\tilde{2}\, d\tilde{3}\, d\tilde{4}\, \delta(\tilde{1} + \tilde{2} - \tilde{3} - \tilde{4})\, \mathsf{A}_\sigma(\tilde{1})\, \mathsf{A}_{\bar{\sigma}}(\tilde{2})\, \mathsf{A}_\uparrow(\tilde{3})\, \mathsf{A}_\downarrow(\tilde{4})\, \left| \mathsf{T}^+(\tilde{3} + \tilde{4}) \right|^2$$

$$\times \left\{ [1 - f_\sigma(\tilde{1})]\,[1 - f_{\bar{\sigma}}(\tilde{2})]\, f_\uparrow(\tilde{3}) f_\downarrow(\tilde{4}) - f_\sigma(\tilde{1})\, f_{\bar{\sigma}}(\tilde{2})\,[1 - f_\uparrow(\tilde{3})]\,[1 - f_\downarrow(\tilde{4})] \right\}$$

$$= \int d\tilde{2}\, d\tilde{3}\, d\tilde{4}\, \delta(\tilde{1} + \tilde{2} - \tilde{3} - \tilde{4})\, \begin{bmatrix} \vcenter{\hbox{\includegraphics{diagram}}} \end{bmatrix} + \mathcal{O}(1/\ln^3 \beta \epsilon_b).$$

(4.159)

The above collision integral is the local (memoryless) part of the collision terms and formally resembles the result obtained earlier for the Born approximation (Eq. 2.47c). The symmetry of the collision integral kernel implies local conservation of particle number, energy and momentum:

$$\sum_\sigma \int d1\, \mathsf{C}_\sigma(\tilde{1}) = 0, \qquad \sum_\sigma \int d1\, p^\mu(\tilde{1})\, \mathsf{C}_\sigma(\tilde{1}) = 0, \tag{4.160}$$

where $p^\mu(\tilde{1}) \equiv (\omega_1, \mathbf{p}_1)$. Eq. (4.159) has been obtained earlier by Kadanoff and Baym [22] and Danielewics [23] in the context of hard-core repulsive fermionic matter in the T-matrix approximation (Bruckner theory). These works, however, have not acknowledged the existence of independent bosonic degrees of freedom to begin with, and have assumed Eq. (4.157) as an exact fact from the outset. Nevertheless, their analyses are expected to remain valid up to moderately large interactions in light of the fact that repulsively interacting fermions do not form bound states and the bosonic excitations always have a diffusive character. The diffusion time of bosonic fluctuations can still become large in the strong-coupling limit, leading to the breakdown of the memoryless approximation (and the Fermi surface).

We conclude this discussion by mentioning that the Fermi surface is sharp in the weak-coupling limit, so that we may also use the quasiparticle approximation. The spectral broadening of fermions, Γ_σ, is $\mathcal{O}(1/\ln^2 \beta \epsilon_b)$ and can be set to zero in the extremely weak-coupling limit. In this limit, the

fermion spectral function assumes the non-interacting $\sim \delta(\omega - \xi_{\mathbf{p}})$ form. The quasi-equilibrium dynamics of the gas is essentially described by the changes in the statistics of free fermions.

The strong-coupling limit ($\epsilon_b/\epsilon_F \gg 1$, $\beta\epsilon_b \gg 1$):

According to the previous discussions, the equilibrium chemical potential in this limit can be written as $\mu = -\epsilon_b/2 + \mu_B/2$, where μ_B the bosonic correction. The number of unpaired fermions is suppressed by an exponentially small factor $e^{-\beta\epsilon_b/2}$ and the system is described as a gas of weakly interacting composite bosons. A large gap of the order of ϵ_b about $\omega = 0$ separates the sharp particle branch of the spectral function, $\omega \approx \xi_{\mathbf{p}}$, from the incoherent hole branch. The threshold energy for the hole branch is $\omega_{\text{th}} \simeq -\epsilon_b/2$. As a first step, we show that the bosonic excitations have a sharp particle-like nature. Using Eq. (4.150c), we obtain the estimate:

$$
\begin{aligned}
\Gamma_b(\omega = 0, \mathbf{p} = \mathbf{0}) &= \int \frac{d\omega'}{(2\pi)} \frac{d^d\mathbf{p}'}{(2\pi)^d} A_\uparrow(\omega', \mathbf{p}') A_\downarrow(-\omega', -\mathbf{p}') \left[1 - f_\uparrow(\omega', \mathbf{p}') - f_\downarrow(-\omega', \mathbf{p}')\right] \\
&\simeq 2 \int \frac{d\omega'}{(2\pi)} \frac{d^d\mathbf{p}'}{(2\pi)^d} (2\pi) Z_{\mathbf{p}'} \, \delta(\omega' - \xi'_{\mathbf{p}}) \frac{\Gamma_\uparrow(-\omega', -\mathbf{p}')}{(-\omega' - \xi_{-\mathbf{p}})^2} \\
&= \mathcal{O}(\epsilon_F/(\beta\epsilon_b)).
\end{aligned}
\tag{4.161}
$$

The second line follows from the fact that the non-zero integral kernel requires one particle to be in the hole branch while the other being in the particle branch. The quasiparticle residue of the particle particle is $Z_{\mathbf{p}} \sim 1 - \mathcal{O}(1/(\beta\epsilon_b))$ as mentioned earlier and can be safely set to unity here. The last line finally follows from the fact that the incoherent branch is exponentially suppressed at the thermal energy scale (cf. Eq. 4.46). The above result immediately implies that the bosonic kinetic equation assumes a Boltzmann structure.

As a next step, we calculate the bosonic mass-shell function M_b. According to Eq. (4.150e), there are two types of contributions to the mass-shell function: a part coming from the bare T-

matrix, $M_{b,0}$, and a self-energy part $M_{b,Q}$. The first contribution in $d = 2$ and 3 is:

$$(d = 2): \qquad M_{b,0}(\omega, \mathbf{p}; T, \mathbf{R}) = \frac{m}{4\pi} \ln\left[-\epsilon_b/(\omega - 2U(T, \mathbf{R}) - |\mathbf{p}|^2/(4m)\right]$$

$$= \frac{m}{4\pi\epsilon_b}\left(\omega + \mu_B - 2U(T, \mathbf{R}) - |\mathbf{p}|^2/(4m)\right) + \mathcal{O}(E/\epsilon_b),$$

$$(d = 3): \qquad M_{b,0}(\omega, \mathbf{p}; T, \mathbf{R}) = \frac{m}{4\pi}\left[\frac{1}{a_s} - i\sqrt{m(\omega - 2U(T, \mathbf{R}) - |\mathbf{p}|^2/(4m)}\right]$$

$$= \frac{m^2}{8\pi\sqrt{m\epsilon_b}}\left(\omega + \mu_B - 2U(T, \mathbf{R}) - |\mathbf{p}|^2/(4m)\right) + \mathcal{O}(E/\epsilon_b).$$

$$(4.162)$$

We have expanded the inverse retarded T-matrix in small $E \equiv \max\{|\omega|, |U|, |p^2/(2m)\}$ in the second line. Note that $\epsilon_b = 1/(ma_s^2)$ in the $d = 3$. The T-matrix contribution, as expected, assumes a polar structure which describe the center of mass motion of bound pairs. The self-energy contribution to the mass-shell is:

$$M_{b,Q}(\omega, \mathbf{p}_1; T, \mathbf{R}) \equiv -\mathfrak{K}\mathfrak{K}\left[\Im\left[Q^+\right]\right](\omega, \mathbf{p}_1; T, \mathbf{R}) = \text{P.V.}\int \frac{d\omega_1}{2\pi} \frac{1}{\omega_1 - \omega}\int d\tilde{2}\, d\tilde{3}\,\delta(\tilde{1} - \tilde{2} - \tilde{3})$$

$$\times \left\{A_\uparrow(\tilde{2})\, A_\downarrow(\tilde{3})\left[1 - f_\uparrow(\tilde{2}) - f_\downarrow(\tilde{3})\right] - \tilde{A}_{0,\uparrow}(\tilde{2})\,\tilde{A}_{0,\downarrow}(\tilde{3})\right\}. \quad (4.163)$$

The self-energy corrections can be evaluated at $\omega = \mathbf{p} = 0$ to leading order in the energy of bosonic excitations (this will be justified *a posteriori*). Combining Eqs. (4.161),(4.162), and (4.163), we general find in d-dimensions:

$$B(\omega, \mathbf{p}; T, \mathbf{R}) = 2\pi\lambda_d\,\delta\left(\omega + \mu_B - 2U(T, \mathbf{R}) - |\mathbf{p}|^2/(4m) - \Sigma_{\text{BB}}(T, \mathbf{R})\right) + \mathcal{O}(E/\epsilon_b, 1/\beta\epsilon_b)$$

$$(4.164)$$

where the residue of the bound-state pole λ_d was defined in Eq. (4.100), and:

$$\Sigma_{\text{BB}}(T, \mathbf{R}) \equiv -\lambda_d\, M_{b,Q}(0, \mathbf{0}; T, \mathbf{R}). \qquad (4.165)$$

Σ_{BB} can be interpreted as the effective boson-boson self-energy functional. $M_{b,Q}$ must be found self-consistently from Eqs. (4.163), (4.164), (4.139b), (4.139d) and(4.139c). The calculated of $M_{b,Q}$

is facilitated using its diagrammatic interpretation:

$$M_{b,Q}(\omega, \mathbf{p}_1; T, \mathbf{R}) = \Re \left[\quad - \quad \right]^{+}$$

$$= \Re \left[\quad + \quad + \quad \right.$$

$$\left. + \quad - \quad \right]^{+}. \tag{4.166}$$

The second equality is obtained by using Dyson's expansion of the dressed Green's function, $G = G_0 + G_0 \Sigma G$. The $+$ signs indicate the retarded component. The external frequency and momentum is ω and $\mathbf{p}_1$, respectively.

- $M_{b,Q}$ *in* $d = 2$:

In $d = 2$, each loop, fermionic propagator and bosonic propagator result in a factor of ϵ_b, $1/\epsilon_b$ and ϵ_b, respectively. The combination of the first diagram $\sim G_0 G_0$ (thin lines) and last counter-term diagram $\sim \tilde{G}_0 \tilde{G}_0$ (dashed lines) give a small contribution $\sim \mathcal{O}(e^{-\beta \epsilon_F})$ and can be neglected. However, we immediately see that all diagrams the remaining diagrams are of the order $\sim m/\epsilon_b$, so that $(4\pi \epsilon_b / m) M_{b,Q} \sim \mathcal{O}(1)$. We recover the same pathological result we found from the linear response analysis: in the T-matrix approximation, the composite bosons do not become free even in the extreme strong coupling limit $\epsilon_b \to \infty$.

Nevertheless, we may ask for the prediction of this theory. In general, $M_{b,Q}$ can not be found by perturbation in $d = 2$. The only tractable case is the classical regime ($\beta |\mu_B| \gg 1$, $|\mu_B| \ll \epsilon_b$), where the bound states are still thermally stable, yet, $|\mu_B|/\epsilon_b \gg 1$. This allows us to write a Virial series for $M_{b,Q}$ in the powers of $\beta \epsilon_F$. In this limit, the power of fugacity $z = e^{-\beta |\mu_B|}$ is given by the number of bosonic lines. The leading-order contributions are the diagrams with a single

bosonic line, i.e. the second and third diagrams in Eq. (4.166) with all Green's functions replaced by bare lines. The leading contribution results from the bosonic pole. A lengthy but straightforward calculation gives:

$$\mathsf{M}_{b,Q}(\omega, \mathbf{p}; T, \mathbf{R}) = -2\,v(\omega, \mathbf{p})\,n_B(T, \mathbf{R}) + \text{(diagrams with more than one bosonic line)}. \quad (4.167)$$

In the above equation,

$$n_B(T, \mathbf{R}) \equiv \frac{1}{\lambda_d} \int \frac{\mathrm{d}\Omega}{2\pi} \frac{\mathrm{d}^d \mathbf{Q}}{(2\pi)^d}\, \mathsf{B}(\Omega, \mathbf{Q}; T, \mathbf{R})\, b(\Omega, \mathbf{Q}; T, \mathbf{R}), \quad (4.168)$$

and:

$$v(\omega, \mathbf{p}) \equiv \lambda_d \,\mathrm{P.V.} \int \frac{\mathrm{d}\omega'}{2\pi} \frac{\mathrm{d}^d \mathbf{k}}{(2\pi)^d} \frac{1}{(\omega + \omega' - \xi_{\mathbf{p}+\mathbf{p}'})^2 (-\omega' - \xi_{-\mathbf{p}'})(-\omega - \omega' - \xi_{-\mathbf{p}'-\mathbf{p}})}$$
$$+ \mathcal{O}\left(e^{-\beta\epsilon_b}, (\epsilon_F/\epsilon_b)^2\right). \quad (4.169)$$

The result is valid for arbitrary d. The contribution of the fermion statistical function f is confined to either very large or very small energies, $|\omega| > \epsilon_b$. Within the confines of the kinetic theory, f is undisturbed in these high energy regimes and we have allowed ourselves to replace $f(\omega, \mathbf{p}; T, \mathbf{R})$ with its zero temperature limit $\theta(-\omega)$ in light of $\beta\epsilon_b \gg 1$. In $d = 2$, we find:

$$v(\omega, \mathbf{p}) = \frac{1}{\epsilon_b} + \mathcal{O}(E/\epsilon_b^2), \quad (4.170)$$

where $E = \max\{\omega, |\mathbf{p}|^2/(2m)\}$. The last result justifies the restriction to $\omega = \mathbf{p} = 0$ in Eq. (4.164). In summary, we find:

$$\Sigma_{\mathrm{BB}}(T, \mathbf{R}) \simeq \frac{8\pi}{m}\, n_B(T, \mathbf{R}). \quad (4.171)$$

The effective interaction is simply the Hartree mean-field energy of bosons with a δ potential, a result obtained earlier from the linear response analysis. We again remark that this conclusion is in fact an artifact of the T-matrix theory in $d = 2$, which treats the composite bosons at the mean-field level. Once multiple scatterings between the bosons are taken into account, they become

asymptotically free in the low-energy $\omega/\epsilon_b \ll 1$ limit.

• $\mathsf{M}_{b,Q}$ *in* $d = 3$:

In $d = 3$, the bosonic propagators give a factor of $\lambda_3 \sim \sqrt{\epsilon_b}$ instead of ϵ_b. This immediately permits a controlled expansion of $\mathsf{M}_{b,Q}$ in the powers of ϵ_F/ϵ_b both in quantum and thermal regimes. A simple power counting shows that the second, third and forth diagrams appearing in the second and third lines of Eq. (4.166) are $\mathcal{O}(\epsilon_b^{-3/2})$, $\mathcal{O}(\epsilon_b^{-3/2})$ and $\mathcal{O}(\epsilon_b^{-4})$, respectively. The leading contribution is the same as Eq. (4.167) and we find:

$$v(\omega, \mathbf{p}) = \frac{1}{2\epsilon_b} + \mathcal{O}(E/\epsilon_b), \tag{4.172}$$

and consequently:

$$\Sigma_{\mathrm{BB}}(T, \mathbf{R}) = 2 \, \frac{4\pi(2a_s)}{2m} \, n_B(T, \mathbf{R}) + \mathcal{O}(a_s^2). \tag{4.173}$$

The above result is again interpreted as the Hartree self-energy for bosons with an effective s-wave scattering length $a_B \equiv 2a_s$ [226]. Considering multiple scatterings between the bosons (and inclusion of more complicated irreducible boson-boson interaction vertices) yield a numerical correction $a_B^{\mathrm{exact}} \simeq 0.6 \, a_s$ [227, 228]. In any event, the effective boson-boson interaction vanishes in the limit $\epsilon_b \to \infty$, yielding a gas of free composite bosons.

We return to the discussion of the bosonic kinetic equation in light of the above results. Since $\Gamma_b \sim 1/\beta\epsilon_b$, we may use the identity:

$$\lim_{\Gamma_b \to 0} \frac{\mathsf{B}^2 \, \Gamma_b}{2} = (2\pi) \, \lambda_d \, \delta(\mathsf{M}_b), \tag{4.174}$$

Eq. (4.150a) can be written as:

$$(2\pi) \, \delta(\mathsf{M}_b) \left[\{\mathsf{M}_b, b\} + \Gamma_b(b - c_b) \right] = 0. \tag{4.175}$$

The collision term is smaller than the streaming term by a factor of $1/(\beta\epsilon_b)$ and can be neglected.

We obtain the sought-after bosonic Boltzmann equation upon integrating over the frequency:

$$\partial_T\, n_B(\mathbf{p}; T, \mathbf{R}) + \frac{\mathbf{p}}{m_B} \cdot \partial_\mathbf{R}\, n_B(\mathbf{p}; T, \mathbf{R}) - \partial_\mathbf{R}\left[2U(T, \mathbf{R}) + \Sigma_{\mathrm{BB}}(T, \mathbf{R})\right] \cdot \partial_\mathbf{p} n_B(\mathbf{p}; T, \mathbf{R}) = 0,$$

(4.176)

where $m_B = 2m$. Finally, let us show that the non-equilibrium density is indeed given by $2n_B(T, \mathbf{R})$ in this limit. We have by definition:

$$n(T, \mathbf{R}) = \sum_\sigma \int \frac{d\omega}{2\pi} \frac{d^d\mathbf{p}}{(2\pi)^d}\, A_\sigma(\omega, \mathbf{p}; T, \mathbf{R}) f(\omega, \mathbf{p}; T, \mathbf{R})$$

$$= \sum_\sigma \left[\, \text{⟜}\bigcirc \,\right]$$

$$= \sum_\sigma \left[\, \text{⟜}\bigcirc + \text{⟜}\bigcirc\!\!\!\bigcirc \,\right].$$

(4.177)

The outgoing frequency/momentum of the tadpole is to be set to zero. We have used Dyson's equation to get the third line. The bare tadpole gives the number of unpaired fermions, n_1:

$$n_1(T, \mathbf{R}) = \sum_\sigma \int \frac{d\omega}{2\pi} \frac{d^d\mathbf{p}}{(2\pi)^d}\, 2\pi\, \delta(\omega - \xi_\mathbf{p})\, f(\omega, \mathbf{p}; T, \mathbf{R}) \simeq \frac{2}{\beta} \int_{-\beta\mu}^{\infty} \frac{d\xi\, N_d(\xi)}{e^\xi + 1} \sim \mathcal{O}(e^{-\beta\epsilon_b/2}).$$

(4.178)

Here, $N_d(\xi)$ is the density of states per spin for a free Fermi gas. Note that we have replaced the non-equilibrium fermion statistics with $f_0(\omega)$ in the integral since $\omega \gg \epsilon_b$. The analytic result for this contribution is given in Eq. (4.52) for $d = 2$. The second tadpole accounts for the composite bosons. According to the above discussions, this diagram can be expanded in the number of bosonic lines in the strong-coupling limit. To leading order, the thick lines can be replaced with thin lines and using the strong-coupling bosonic spectral function (Eq. 4.164), we find:

$$n_2(T, \mathbf{R}) = 2\lambda_d \int \frac{d^d\mathbf{p}}{(2\pi)^d} \frac{d^d\mathbf{q}}{(2\pi)^d} \frac{f(\xi_{\mathbf{q}-\mathbf{p}}, \mathbf{q} - \mathbf{p}; T, \mathbf{R}) + b(\xi_{B,\mathbf{q}}, \mathbf{q}; T, \mathbf{R})}{(|\mathbf{p}|^2/m + \epsilon_b - \Sigma_{\mathrm{BB}})^2}$$

$$= 2 \int \frac{d^d\mathbf{q}}{(2\pi)^d}\, b(\xi_{B,\mathbf{q}}, \mathbf{q}; T, \mathbf{R}) + \mathcal{O}\left(\Sigma_{\mathrm{BB}}/\epsilon_b, e^{-\beta\epsilon_b}\right)$$

$$\simeq 2\, n_B(T, \mathbf{R}).$$

(4.179)

We have defined the shorthand $\xi_{B,\mathbf{q}} \equiv |\mathbf{q}|^2/(4m) + \mu_B - \Sigma_{\mathrm{BB}}(T, \mathbf{R})$. The factor λ_d is exactly cancelled by the result of the $\mathbf{p}$ momentum integral. The last line becomes exact in the limit $\beta\epsilon_b \to \infty$ in $d = 3$. This result is expected to remain valid in $d = 2$ in general. However, as discussed before, SCTMA suffers from the artifact that does not decouple the bosons in the quantum regime. Therefore, the above result only holds in the thermal composite Bose gas regime and is valid as long as $\beta\epsilon_F, \beta\epsilon_b \gg 1$.

4.5.4   On the emergence of bosonic degrees of freedom

We discussed and the weak- and strong-coupling limits of the kinetic equations in the previous section. Of particular interest was the different interpretation of b in different regimes: in the weak-coupling limit, $b \simeq c_b$ and describes the energy distribution of short-lived fluctuations during the collision of fermions. In the strong-coupling limit, on the other hand, b describes the energy distribution of stable bound pairs. In this limit, b is governed by a Boltzmann equation for nearly free bosonic particles of mass $2m$. Here, we give a perspective for interpreting the emergence of such bosonic degrees of freedom. In fact, the steps we were naturally led to take for a consistent derivation of the kinetic equations can be understood in a more transparent and general way by combining ideas from Hubbard-Stratonovich transformations and the 2PI effective action (2PI-EA) formalism.

Generally speaking, Φ-derivable approximations that include infinite resummation of a certain class of vacuum diagrams may often be equivalently obtained by introducing one or more auxiliary bosonic Hubbard-Stratonovich (HS) fields to mediate the exchange of fluctuations. The original Φ-derivable approximation may then be obtained identically by keeping a certain class of vacuum diagrams (often finite and much simpler; see below), composed of both fermionic and bosonic Green's functions. To this end, we simply follow the procedure of obtaining the 2PI-EA as before. The new 2PI-EA, however, is defined in the extended Hilbert space this time and is a functional of

both the fermionic and the bosonic Green's functions.

We start the discussion by assuming that the interaction term in the microscopic fermionic action has been decoupled in a convenient way upon introducing n HS bosonic fields $(\Delta_1, \ldots, \Delta_n)$. We consider only the case of normal systems for the clarity of the discussion[5]. We define the generating functional of the $2n$-point Green's functions by introducing a 2-point source field K coupling to $\bar{\psi}_\sigma \psi_\sigma$, and n additional 2-point source fields $(K'_1, \ldots, K'_n)$ coupling to $(\Delta_1^* \Delta_1, \ldots, \Delta_n^* \Delta_n)$ as follows:

$$Z[K, K'_1, \ldots, K'_n] \equiv \int \mathcal{D}[\psi, \bar{\psi}] \, \mathcal{D}[\Delta_1, \Delta_1^*] \, \ldots \, \mathcal{D}[\Delta_n, \Delta_n^*]$$

$$\times \exp\left(iS_{\text{HSd}} + iS_2 + iS_{2,1} + \ldots + iS_{2,n}\right), \quad (4.180)$$

where $S_{\text{HSd}}[\psi, \bar{\psi}; \Delta_i, \Delta_i^*]$ is the HS-decoupled microscopic action, and:

$$S_2[\psi, \bar{\psi}; K] \equiv -\int_\mathcal{C} d\tau_1 \, d\tau_1' \, d^d\mathbf{x}_1 \, d^d\mathbf{x}_1' \, \bar{\psi}_\sigma(\tau_1, \mathbf{x}_1) \, K(\tau_1, \mathbf{x}_1; \tau_1', \mathbf{x}_1') \, \psi_\sigma(\tau_1', \mathbf{x}_1'),$$

$$S_{2,j}[\Delta_j, \Delta_j^*; K'_j] \equiv -\int_\mathcal{C} d\tau_1 \, d\tau_1' \, d^d\mathbf{x}_1 \, d^d\mathbf{x}_1' \, \Delta_j^*(\tau_1, \mathbf{x}_1) \, K'_j(\tau_1, \mathbf{x}_1; \tau_1', \mathbf{x}_1') \, \Delta_j(\tau_1', \mathbf{x}_1'). \quad (4.181)$$

The above action is in every way similar to a physical Fermi-Bose model, save for the fact that the HS fields do not directly couple to external fields, and do not have *intrinsic* dynamics. We may proceed and find the 2PI-EA of such a model by following the standard steps of trading the source fields with Green's functions, which we outline here. The generating functional of the 2-connected vacuum diagrams is given by the linked-cluster theorem, $W = \ln Z$. The vacuum diagrams are constructed from the cubic (and possibly quartic) terms of the HS-decoupled action S_{HSd}. The Green's functions are given by:

$$\mathcal{G}(1, 1'; K) = \frac{\delta W}{\delta K(1', 1)}, \qquad \mathcal{B}_j(1, 1'; K) = \frac{\delta W}{\delta K'_j(1', 1)}, \qquad (4.182)$$

---

[5]The generalization to superconducting states is immediate by adding a charge index to the fermion operators and using the super Green's function formalism discussed in Sec. 1.2.1

where $\mathcal{G}$ is the usual fermionic Green's function, and $\{\mathcal{B}\}$ correspond to the auxiliary bosonic Green's functions. The 2PI effective action $\Gamma[\mathcal{G}, \mathcal{B}_1, \ldots, \mathcal{B}_n]$ is obtained through a Legendre transform of W as usual:

$$\Gamma[\mathcal{G}, \{\mathcal{B}\}] \equiv W - \int d1\, d1' \left[\frac{\delta W}{\delta K(1, 1')} \mathcal{G}(1, 1') + \sum_j \frac{\delta W}{\delta K'_j(1, 1')} \mathcal{B}_j(1, 1') \right]$$

$$= \operatorname{Tr} \ln \mathcal{G}^{-1} + \operatorname{Tr} \left(\tilde{\mathcal{G}}_0^{-1} \tilde{\mathcal{G}} \right) + \sum_j \left[\operatorname{Tr} \ln \mathcal{B}_j^{-1} + \operatorname{Tr} \left(\mathcal{B}_{j,0}^{-1} \mathcal{B}_j \right) \right] + \tilde{\Phi}[\mathcal{G}, \{\mathcal{B}\}]. \quad (4.183)$$

We have separated the 1-loop contributions from the rest in the second line. $\tilde{\Phi}$ is the Luttinger-Ward functional and is formally the sum of all 2PI vacuum diagrams of S_{HSd}. The stationarity condition on $\Gamma[\mathcal{G}, \{\mathcal{B}\}]$ for vanishing source fields (cf. Sec. 1.2.3) yields the non-equilibrium Dyson's equation for $\mathcal{G}$ and $\mathcal{B}_j$:

$$\mathcal{G}(1, 1')^{-1} = \mathcal{G}_0^{-1}(1, 1') - \Sigma_{\mathcal{G}}[\mathcal{G}, \{\mathcal{B}\}](1, 1'),$$

$$\mathcal{B}_j(1, 1')^{-1} = \mathcal{B}_{j,0}^{-1}(1, 1') - \Sigma_{\mathcal{B}_j}[\mathcal{G}, \{\mathcal{B}\}](1, 1'), \quad (4.184)$$

where:

$$\Sigma_{\mathcal{G}}[\mathcal{G}, \{\mathcal{B}\}](1, 1') \equiv -\frac{\delta \tilde{\Phi}}{\delta \mathcal{G}(1', 1)}, \qquad \Sigma_{\mathcal{B}_j}[\mathcal{G}, \{\mathcal{B}\}](1, 1') \equiv -\frac{\delta \tilde{\Phi}}{\delta \mathcal{B}_j(1', 1)}. \quad (4.185)$$

Since the Bose-Fermi action is obtained from a HS decoupling, the bare bosonic inverse propagators $\mathcal{B}_{j,0}^{-1}$ are static. The self-energy $\Sigma_{\mathcal{B}_j}$ can however generate the dynamics for the HS fields. We also notice the analogy between Eq. (4.189), and the coupled Dyson's equation we obtained for $\mathcal{G}$ and T earlier.
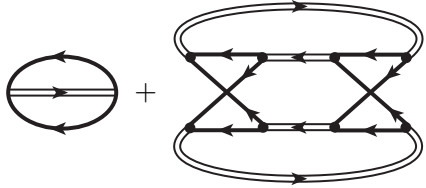
The above procedure offers a more transparent and economic way of obtaining the T-matrix kinetic equations derived in the previous section. As an example, we carry out the procedure outlined above starting from the microscopic action of the attractive Fermi gas:

$$S[\psi, \bar{\psi}] = \int_{\mathcal{C}} d\tau \int d^d\mathbf{x} \left[\bar{\psi}_\sigma \left(i\partial_\tau + \nabla^2/(2m) + \mu - U \right) \bar{\psi} - \lambda_\Lambda \bar{\psi}_\uparrow \bar{\psi}_\downarrow \psi_\downarrow \psi_\uparrow \right], \quad (4.186)$$

248

where $\lambda_\Lambda < 0$ is a short-range attractive interaction. The HS decoupling in the Cooper channel yields:

$$S_{\text{HSd}}[\psi, \bar\psi; \Delta, \Delta^*] = \int_{\mathcal{C}} \mathrm{d}\tau \int \mathrm{d}^d \mathbf{x} \Big[\bar\psi_\sigma \left(i\partial_\tau + \nabla^2/(2m) + \mu - U \right) \bar\psi_\sigma(\tau, \mathbf{x})$$

$$+ \lambda_\Lambda^{-1} \Delta^* \Delta - \Delta^* \psi_\downarrow \psi_\uparrow - \Delta \bar\psi_\downarrow \bar\psi_\uparrow \Big]. \quad (4.187)$$

We immediately read $\mathcal{B}_0^{-1}(1,1') \equiv \lambda_\Lambda^{-1} \delta_{\mathcal{C}}(1,1')$ from S_{HSd}. The 2PI vacuum diagrams of S_{HSd} are given by Eq. (1.85) using the cubic term in S_{HSd} as S_{int}:

$$\tilde\Phi[\mathcal{G}, \mathsf{T}] = \left[\ln \int \mathcal{D}[\psi, \bar\psi] \, \mathcal{D}[\Delta, \Delta^*] \, \exp \left(i S_{\text{HFd}}^{(\text{cubic})}[\psi, \bar\psi; \Delta, \Delta^*] \right) \right]_{2\text{PI}, \, \mathcal{G}_0 \to \mathcal{G}, \mathsf{T}_0 \to \mathsf{T}}$$

$$= \quad + \quad + \ldots \quad (4.188)$$

In the above diagrams, the single and double lines correspond to $\mathcal{G}$ and $\mathcal{B}$, respectively. The fermionic T-matrix approximation is simply obtained by keeping the first vacuum diagram. The resulting Dyson's equations are:

$$\mathcal{G}_\sigma(1,1')^{-1} = \mathcal{G}_{\sigma,0}^{-1}(1,1') + i\mathcal{B}(1,1')\mathcal{G}_{\bar\sigma}(1',1),$$

$$\mathcal{B}(1,1')^{-1} = \lambda_\Lambda^{-1} - i\mathcal{G}_\uparrow(1,1')\mathcal{G}_\downarrow(1,1'). \quad (4.189)$$

We immediately see that $\mathsf{B} \equiv \mathsf{T}$, and the above Bose-Fermi Φ-derivable approximation coincides with the fermionic T-matrix approximation. The rest of the development parallels the previous analysis: the T-matrix is regularized using vacuum Green's functions:

$$\mathcal{B}(1,1')^{-1} = \underbrace{\lambda_\Lambda^{-1} - i\tilde{\mathcal{G}}_{0,\uparrow}(1,1')\tilde{\mathcal{G}}_{0,\downarrow}(1,1')}_{\tilde{\mathsf{T}}_0^{-1}(1,1')} - \underbrace{i\left[\mathcal{G}_\uparrow(1,1')\mathcal{G}_\downarrow(1,1') - \tilde{\mathcal{G}}_{0,\uparrow}(1,1')\tilde{\mathcal{G}}_{0,\downarrow}(1,1') \right]}_{\mathcal{Q}(1,1')}.$$

$$(4.190)$$

In the strong-coupling limit, we find $\tilde{\mathsf{T}}_0^{-1}(1,1') \to \lambda_d^{-1}\big[i\partial_{t_1} + (2\mu - \epsilon_b) - \nabla^2/(4m) - 2U(1)\big]\delta_{\mathcal{C}}(1,1')$ while $Q(1,1')$ acts as a small self-energy correction. The dynamical generation

of the derivative terms in the Dyson's equation for T following the regularization of the UV divergence is a manifestation of the bound state, without which T would retain its diffusive character.

From this new perspective, what we achieved in the previous section using a purely fermionic language is virtually identical to the introduction of a HS field, i.e. the T-matrix. The T-matrix acts like a *local memory storage* for fermions, and permits a Markovian formulation of transport equation, albeit in an extended state space $(\mathcal{G}, \mathsf{T})$.

4.6 Collective oscillations in confined geometries

In this section, we use the transport formalism developed in the previous section to investigate the collective dynamics of attractive 2D Fermi gases in an external confining potential. We consider the case where the system is in equilibrium for $t < 0$, and is perturbed by a short-time external impulse. Our goal is to calculate the expectation value an arbitrary observable $O(\mathbf{p}, \mathbf{R})$ in the times after the impulse. This scenario closely resembles the experimental situation for exciting trap collective modes as discussed in the introduction. The initial disturbance is assumed to be weak, so that a linear response analysis is admissible.

Strictly speaking, the evolution system during the short period of the external impulse is beyond the limits of the kinetic theory since the duration of the impulse is assumed to be much shorter than $t_{\mathrm{mac}} \sim 1/\omega_0$, where ω_0 is the trap frequency. We find it easiest to separate the dynamics into two regimes: (1) the initial evolution in the presence of the external field, $T \in [0, t_{\mathrm{imp.}}]$, (2) the slow evolution of the disturbed state as described by the kinetic equations, $T \in [t_{\mathrm{imp.}}, \infty]$. This scenario is depicted in Fig. 4.14. We address the first phase of the evolution in the next section and we find that the effect of the external field is interchangeable with a space-varying Galilean boost. The ensuing kinetic evolution is discussed afterwards.
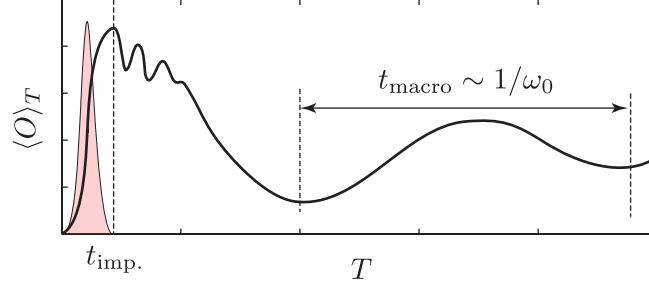
Figure 4.14: A schematic plot of the evolution of an observable O vs. the macroscopic time T in a typical impulse response experiment. The black curve depicts $\langle O \rangle_T$. The red curve denotes the time envelope of the impulse $\mathcal{A}(T)$. The transient oscillations right after the impulse are due to the excitement of high energy modes and are usually overdamped.

4.6.1 Short-time response to an external impulse

We consider the initial disturbance caused by an external field:

$$\delta U(T, \mathbf{R}) = u(\mathbf{R}) \, \mathcal{A}(T), \tag{4.191}$$

on a system initially in a thermal equilibrium state. Here, $\mathcal{A}(T)$ is the pulse envelope function and $u(\mathbf{R})$ is the spatial profile of the external perturbing field. We assume that $\mathcal{A}(T)$ is only non-vanishing during $0 < T < t_{\text{imp}}$, and that $t_{\text{imp}} \ll t_{\text{macro}}$. Furthermore, $u(\mathbf{R})$ is assumed to vary on a large length scale of the order of l_{macro}.

The external field exerts a space-time varying force $\mathbf{F}(T, \mathbf{R}) = \nabla u(\mathbf{R}) \, \mathcal{A}(T)$ on the particles, resulting in a space-time varying Galilean boost. Had $u(\mathbf{R})$ been just a field gradient (i.e. a constant force) and the initial state been homogeneous, the equilibrium state would remain undisturbed in the frame of reference of a moving observer with the time-dependent velocity $\mathbf{V}(T) = (\mathbf{F}/m) \int_0^T \mathcal{A}(t) \, \mathrm{d}t$. This scenario is expected to remain *locally* applicable, provided that $u(\mathbf{R})$ and $U(\mathbf{R})$ vary on a scale much larger than the distance the particles can travel during impulse, $v_{\delta U} t_{\text{imp.}}$. Here, $v_{\delta U}$ is the typical velocity boost. We note that this framework is only valid if all particles experience the same Galilean boost. In application to systems comprising particles with different masses (or different coupling to the external field),

there is no single moving frame in which the equilibrium state remains undisturbed. We assume $m_\sigma = m$ and $u_\sigma = u$ hereafter (different spin spaces may still have different chemical potentials). In the remainder of this section, we lay the above arguments on rigorous grounds. As we shall see, establishing this innocuous scenario demands the usage of a considerable amount of formalism.

We start with the KB equations for the non-equilibrium Green's functions. We drop the discrete indices in this section for simpler notation (as long as the external fields are globally diagonal in the space of discrete indices, the same set of discrete indices carries through every step of the derivation and can be put back at will). Let $\delta U(t, \mathbf{x})$ be a general one-body external field acting on the system. The KB equation for the lesser/greater Green's function reads:

$$\left(i\partial_{t_1} + \mu - U(\mathbf{x}_1) + \frac{\partial_{\mathbf{x}_1}^2}{2m} - \delta U(1) \right) G^{\gtrless}(1, 1') = (\Sigma \star \mathcal{G})^{\gtrless}(1, 1'). \tag{4.192}$$

The boundary condition is such that for $t_1, t_1' < 0$, $G^{\gtrless}(1, 1')$ is the analytically continued thermal Green's function, i.e. it only depends on $t_1 - t_1'$ and satisfies the KMS boundary conditions. As a first step, we trade the potential δU with a force using a local $U(1)$ gauge transformation $\psi(1) \rightarrow e^{i\Lambda(1)}\bar{\psi}(1)$. The original Green's function $\mathcal{G}$ and its gauge transformed counterpart $\bar{\mathcal{G}}$ are related to each other as:

$$\mathcal{G}(1, 1') = e^{i\Lambda(1)} \bar{\mathcal{G}}(1, 1') e^{-i\Lambda(1')}. \tag{4.193}$$

The equation of motion for $\bar{G}^{\gtrless}$ can be easily found from the equation of motion for $G^{\gtrless}$:

$$\left(i\partial_{t_1} + \mu - U(\mathbf{x}_1) - \frac{1}{2m} [-i\partial_{\mathbf{x}_1} + \partial_{\mathbf{x}_1}\Lambda(1)]^2 + \delta U(1) + \partial_{t_1}\Lambda(1) \right) \bar{G}^{\gtrless}(1, 1') =$$

$$e^{-i\Lambda(1)} (\Sigma \star_{\mathcal{C}} \mathcal{G})^{\gtrless}(1, 1') e^{i\Lambda(1')} = \left(\bar{\Sigma} \star_{\mathcal{C}} \bar{\mathcal{G}} \right)^{\gtrless}(1, 1'). \tag{4.194}$$

The last equality only holds for the exact and Φ-derivable self-energies which satisfy:

$$\bar{\Sigma}(1, 1') \equiv \Sigma[\bar{\mathcal{G}}](1, 1') = e^{i\Lambda(1)} \Sigma[\mathcal{G}] e^{-i\Lambda(1')}. \tag{4.195}$$

The above transformation property is a direct result of the local $U(1)$ gauge invariance of S_{int} which is also inherited by Φ-derivable approximations. The scalar field δU can be traded for a vector potential with the gauge choice:

$$\Lambda(t_1, \mathbf{x}_1) = -\int_{-\infty}^{t_1} dt' \, \delta U(t', \mathbf{x}_1). \tag{4.196}$$

We refer to this gauge as the *Weyl gauge* in analogy to the electromagnetism. We define:

$$\Xi(t_1, \mathbf{x}_1) \equiv -\frac{1}{m} \int_{-\infty}^{t_1} dt' \, \partial_{\mathbf{x}_1} \Lambda(t', \mathbf{x}_1) = \frac{1}{m} \int_{-\infty}^{t_1} dt' \int_{-\infty}^{t'} dt'' \, \partial_{\mathbf{x}_1} \delta U(t'', \mathbf{x}_1), \tag{4.197}$$

using which Eq. (4.194) can be written as:

$$\left(i\partial_{t_1} + \mu - U(\mathbf{x}_1) + \frac{\partial_{\mathbf{x}_1}^2}{2m} - i\partial_{t_1}\Xi(1) \cdot \partial_{\mathbf{x}_1} \right) \bar{G}^{\gtrless}(1, 1') = \left(\bar{\Sigma} \star_{\mathcal{C}} \bar{\mathcal{G}} \right)^{\gtrless}(1, 1'). \tag{4.198}$$

to first order in δU. The above equation has the simple interpretation of being the equations of motion as seen by an observer that views the space-time point $[t, \mathbf{x}]$ at $[t, \mathbf{x} + \Xi(t, \mathbf{x})]$. The typical value of Ξ is $\sim v_{\delta \text{U}} T$, where T is the macroscopic time and $v_{\delta \text{U}} \sim m^{-1} \int dt \, \partial_{\mathbf{x}} \, \delta U$ is the typical velocity boost brought about by δU. A natural small parameter in this problem is $v_{\delta U} T / l_{\text{macro}}$, where l_{macro} is the length scale of the spatial inhomogeneity of the external potential U (and δU). We wish to find a solution for $\mathcal{G}$ in the presence of δU using our knowledge of the equilibrium solution. To this end, we propose the following ansatz:

$$\bar{G}^{\gtrless}(1, 1') = \tilde{G}^{\gtrless}\left(t_1, \mathbf{x}_1 + \Xi(1); t_1', \mathbf{x}_1' + \Xi(1') \right), \tag{4.199}$$

as a step toward the picture suggested in the introduction. Plugging this ansatz into the left hand side of Eq. (4.198) and changing variables to $\mathbf{X}_1 \equiv \mathbf{x}_1 + \Xi(t_1, \mathbf{x}_1)$ and $\mathbf{X}_1' \equiv \mathbf{x}_1' + \Xi(t_1', \mathbf{x}_1')$ (i.e. going to a moving frame), the left hand side becomes:

$$\left[i\partial_{t_1} + \mu - [1 + \mathcal{O}(v_{\delta U} T / l_{\text{macro}})] \left(-U(\mathbf{X}_1) + \frac{\partial_{\mathbf{X}_1}^2}{2m} \right) \right] \tilde{G}^{\gtrless}(t_1, \mathbf{X}_1; t_1', \mathbf{X}_1'). \tag{4.200}$$

There are two (bounded) sources of error in the above equation, in approximating (1) $U(\mathbf{x}_1) \approx U(\mathbf{X}_1)$, and (2) $\partial_{\mathbf{x}_1}^2 \approx \partial_{\mathbf{X}_1}^2$. Both of these errors are due to the weak breaking of translation

invariance due to the spatially inhomogeneous external fields and are bounded for short times as indicated above. The right hand side also assumes the following simple form:

$$\bar{\Sigma}(1, 1') = \Sigma[\bar{\mathcal{G}}] = \Sigma[\tilde{\mathcal{G}}] \left(t_1, \mathbf{x}_1 + \Xi(1); t_1', \mathbf{x}_1' + \Xi(1')\right) \left[1 + \mathcal{O}(v_{\delta U} T / l_{\mathrm{macro}})\right]. \qquad (4.201)$$

Let us elaborate on the last result. To this end, we consider a typical self-energy diagram such as the Born diagram. The self-energy expression for this diagram is:

$$\Sigma_{\mathrm{Born}}(1, 1') \sim \int \mathrm{d}2 \, \mathrm{d}2' \, \mathcal{G}(1, 1') \, \mathcal{G}(1', 1) \, \mathcal{G}(2, 2') \, \mathcal{G}(2', 2) \, v(1, 2) \, v(1', 2'). \qquad (4.202)$$

We plug $\bar{\mathcal{G}}$ in terms of $\tilde{\mathcal{G}}$ using Eq. (4.199) and change variables to $\mathbf{x}_i \to \mathbf{X}_i = \mathbf{x}_i + \Xi(t_i, \mathbf{x}_i)$ for both internal and external vertices. This results in formally the same expression for the self-energy[6], however, with $\tilde{\mathcal{G}}$ in place of $\mathcal{G}$. The Jacobian of this transformation is:

$$J = 1 + \sum_{j \in \mathrm{internal}} \partial_i \Xi_i(t_j, \mathbf{X}_j) + \mathcal{O}(\Xi^2) \sim 1 + v_{\delta U} T / l_{\mathrm{macro}}. \qquad (4.203)$$

In terms of the new variables, an arbitrary interaction term can be written as:

$$v(\mathbf{x}_i - \mathbf{x}_j) \, \delta(t_i - t_j) = v\left(\mathbf{X}_i - \mathbf{X}_j - \Xi(t_i, \mathbf{X}_i) + \Xi(t_i, \mathbf{X}_j)\right) \, \delta(t_i - t_j)$$

$$= v(\mathbf{X}_i - \mathbf{X}_j) \, \delta(t_i - t_j) \left(1 + (\mathbf{X}_i - \mathbf{X}_j)_\alpha \frac{\partial_\beta v}{v} \, \partial_\alpha \Xi_\beta\right). \qquad (4.204)$$

The last parenthesis again is of the order of $1 + \mathcal{O}(v_{\delta U} T / l_{\mathrm{macro}})$. Eq. (4.201) follows by combining these observations. The correction terms are solely due to the non-uniform nature of the transformation between $\mathcal{G}$ and $\tilde{\mathcal{G}}$ which breaks the Galilean invariance. Clearly, if δU is a linear function of $\mathbf{x}$ and $U = \mathrm{const.}$, the resulting transformation will be uniform and Eq. (4.201) will be exact. Combining the Eqs. (4.198), (4.200) and (4.201), we finally reach:

$$\left(i\partial_{t_1} + \mu - U(\mathbf{X}_1) + \frac{\partial_{\mathbf{X}_1}^2}{2m}\right) \tilde{G}^{\gtrless}(t_1, \mathbf{X}_1; t_1', \mathbf{X}_1') =$$

---

[6]If we had particles of different masses, the *observer position* Ξ would be different for each type of $\tilde{\mathcal{G}}$ and we could no longer obtain the self-energy in terms of $\tilde{\mathcal{G}}$ by a simple change of variables.

$$\left(\tilde{\Sigma} \star_\mathcal{C} \tilde{\mathcal{G}}\right)^{\gtrless} (t_1, \mathbf{X}_1; t_1', \mathbf{X}_1') + \mathcal{O}(v_{\delta U} T / l_{\mathrm{macro}}), \quad (4.205)$$

which is identical for the equation of motion for $G^{\gtrless}$, however, with $\tilde{\mathcal{G}}$ in place of $\mathcal{G}$. Since $\delta U = 0$ and $\mathbf{X}_i = \mathbf{x}_i$ for $t < 0$, $\tilde{\mathcal{G}} = \mathcal{G}$ for $t_1, t_1' < 0$. Moreover, since they have the same evolution equation up to corrections bounded in time, they match within a bounded error for $t_1, t_1' > 0$. More explicitly, we find:

$$\mathcal{G}(1, 1'; \delta U) = e^{i\Lambda(1)} \mathcal{G}\left(t_1, \mathbf{x}_1 + \Xi(1); t_1', \mathbf{x}_1' + \Xi(1'); \delta U = 0\right) e^{-i\Lambda(1')} \left[1 + \mathcal{O}(v_{\delta U} T / l_{\mathrm{macro}})\right].$$

$$(4.206)$$

The above result is very useful. Provided that $\nabla u(\mathbf{x}) = \mathrm{const.}$, it describes the *exact* evolution of a system which is initially in a homogeneous equilibrium. For inhomogeneous external fields and initial states, its error is bounded linearly in time.

We use Eq. (4.206) to describe the initial disturbance caused by an external field like Eq. (4.191). For simplicity, we choose $\mathcal{A}(t) = \delta(t)$, although the final results are identically valid as long as the pulse duration is much smaller than t_{macro}. For the δ-impulse, Λ and Ξ are:

$$\Lambda(t, \mathbf{x}) = -\theta(t) u(\mathbf{x}), \qquad \Xi(t, \mathbf{x}) = \frac{1}{m} \partial_{\mathbf{x}} u(\mathbf{x}) \theta(t) t. \qquad (4.207)$$

We define the local velocity boost field corresponding to the external impulse as $\mathbf{V}(\mathbf{x}) \equiv -\partial_{\mathbf{x}} u(\mathbf{x})/m$. We would like to express the Wigner transform of $\mathcal{G}(1, 1'; \delta U)$ in terms of the the Wigner transform of the equilibrium Green's functions. A direct application of Eq. (4.206) yields:

$$G^{\gtrless}(\omega, \mathbf{p}; T, \mathbf{R}; \delta U) =$$

$$\int \mathrm{d}t \, \mathrm{d}^d \mathbf{x} \, \frac{\mathrm{d}\omega_1}{2\pi} \frac{\mathrm{d}^d \mathbf{p}_1}{(2\pi)^d} G^{\gtrless}\left(\omega_1, \mathbf{p}_1; T, \mathbf{R} - \left[\mathbf{V}(\mathbf{x}_1) \theta(t_1) t_1 + \mathbf{V}(\mathbf{x}_2) \theta(t_2) t_2\right]/2\right)$$

$$\times e^{i\omega t} e^{-i\mathbf{p}\cdot\mathbf{x}} e^{-i\omega_1 t} e^{i\mathbf{p}_1 \cdot [\mathbf{x} - \mathbf{V}(\mathbf{x}_1) \theta(t_1) t_1 + \mathbf{V}(\mathbf{x}_2) \theta(t_2) t_2]} e^{-i[\theta(t_1) u(\mathbf{x}_1) - \theta(t_2) u(\mathbf{x}_2)]}$$

$$= \int \mathrm{d}t \, \mathrm{d}^d \mathbf{x} \, \frac{\mathrm{d}\omega_1}{2\pi} \frac{\mathrm{d}^d \mathbf{p}_1}{(2\pi)^d} G^{\gtrless}\left(\omega_1, \mathbf{p}_1; T, \mathbf{R} - \mathbf{V}(\mathbf{R}) T\right)$$

$$\times e^{i\omega t} e^{-i\mathbf{p}\cdot\mathbf{x}} e^{-i\omega_1 t} e^{i\mathbf{p}_1 \cdot [\mathbf{x} - \mathbf{V}(\mathbf{R}) t]} e^{im\mathbf{V}(\mathbf{R})\cdot\mathbf{x}} + \mathcal{O}(\partial_X^2)$$

$$= G^{\gtrless}\left(\omega - \mathbf{p} \cdot \mathbf{V}(\mathbf{R}), \mathbf{p} - m\mathbf{V}(\mathbf{R}); T, \mathbf{R}\right) \left[1 + \mathcal{O}(VT / l_{\mathrm{macro}})\right]. \qquad (4.208)$$

255

To get the second equality, we have neglected the θ-functions, which is allowed if $T \gg t_{\mathrm{micro}}$ [7]. The above result is very natural: a short-time spatially varying external field results in a spatially weakly inhomogeneous force that boosts each element of the system according to the local impact it exerts on the system. The Galilean invariance then identifies the value of an observable at $(\omega, \mathbf{p})$ after the boost to its value at $(\omega - \mathbf{V} \cdot \mathbf{p}, \mathbf{p} - m\mathbf{V})$ before the boost. A corollary of Eq. (4.208) is that the spectral/statistical functions following the impulse is related to the equilibrium spectral/statistical functions as:

$$\mathsf{A}_\sigma(\omega, \mathbf{p}; T, \mathbf{R}; \delta U) = \mathsf{A}_{\mathrm{eq},\sigma}(\omega - \mathbf{p} \cdot \mathbf{V}(\mathbf{R}), \mathbf{p} - m\mathbf{V}(\mathbf{R})) \left[1 + \mathcal{O}(VT/l_{\mathrm{macro}})\right],$$

$$f_\sigma(\omega, \mathbf{p}; T, \mathbf{R}; \delta U) = f_0(\omega - \mathbf{p} \cdot \mathbf{V}(\mathbf{R})) \left[1 + \mathcal{O}(VT/l_{\mathrm{macro}})\right], \tag{4.209}$$

where $\mathbf{V}(\mathbf{x}) \equiv -\partial_{\mathbf{x}} u(\mathbf{x}) \int_0^{t_{\mathrm{imp.}}} \mathcal{A}(t) \, \mathrm{d}t/m$ in general.

The short-time dynamics of the quantities derived from the Green's function may also be determined using the same approach. Let us consider the case of the T-matrix. First, we observe that the renormalized auxiliary quantity, $\left[\tilde{\mathsf{T}}_0^{-1}\right](\omega, \mathbf{p}; T, \mathbf{R})$ depends on the microscopic variables only in the combination $\omega - |\mathbf{p}|^2/(4m)$. This can be seen from Eq. (4.91a) and the explicit formulas for the renormalized vacuum T-matrix given at the end of Sec. 4.3.1 (note that we have assumed $m_\uparrow = m_\downarrow = m$ here). The combination, $\omega - |\mathbf{p}|^2/(4m)$, is invariant under the Galilean boost $\omega \to \omega - \mathbf{p} \cdot \mathbf{V}$ and $\mathbf{p} \to \mathbf{p} - 2m\mathbf{V}$ up to $\mathcal{O}(V)$. Therefore,

$$\left[\tilde{\mathsf{T}}_0^{-1}\right]^\pm (\omega, \mathbf{p}; T, \mathbf{R}) = \left[\tilde{\mathsf{T}}_0^{-1}\right]^\pm (\omega - \mathbf{p} \cdot \mathbf{V}(\mathbf{R}), \mathbf{p} - 2m\mathbf{V}(\mathbf{R})) + \mathcal{O}(V^2). \tag{4.210}$$

Plugging in A_σ and f_σ from Eq. (4.209) into Eq. (4.94c), a simple investigation shows $\Im\left[Q^+(\omega, \mathbf{p}; T, \mathbf{R}; \delta U)\right] = \Im\left[Q_{\mathrm{eq}}^+(\omega - \mathbf{p} \cdot \mathbf{V}(\mathbf{R}), \mathbf{p} - 2m\mathbf{V}(\mathbf{R}); \mathbf{R})\right] \left[1 + \mathcal{O}(VT/l_{\mathrm{macro}})\right]$. The

---

[7]Assuming $\omega \sim 1/t_{\mathrm{micro}}$, the most important region of integration over the microscopic time t is $|t| \lesssim t_{\mathrm{micro}}$. Assuming that $T \gg t_{\mathrm{micro}}$, neglecting the θ-functions only modifies the contribution of the integral for $|t| \gg t_{\mathrm{micro}}$, which is expected to be unimportant.

Kramers-Kroning transform gives the same result for the real part. The advanced component follows by complex conjugation. The same result can be established for $Q^{\gtrless}$ as well. These observations combined with Eq. (4.143) yields:

$$\mathsf{T}^{\pm}(\omega, \mathbf{p}; T, \mathbf{R}; \delta U) = \mathsf{T}^{\pm}_{\text{eq}}\left(\omega - \mathbf{p} \cdot \mathbf{V}(\mathbf{R}), \mathbf{p} - 2m\mathbf{V}(\mathbf{R}); \mathbf{R}\right)\left[1 + \mathcal{O}(VT/l_{\text{macro}})\right]. \quad (4.211)$$

Now, we notice that combining Eqs. (4.141a) and (4.141b), we find the following exact identity, $\mathsf{T}^{\gtrless} = \mathsf{T}^{+} \star_{\text{GM}} Q^{\gtrless} \star_{\text{GM}} \mathsf{T}^{-}$, which in combination with the above short-time expressions for $\mathsf{T}^{\pm}$ and $Q^{\gtrless}$ yields:

$$\mathsf{T}^{\gtrless}(\omega, \mathbf{p}; T, \mathbf{R}; \delta U) = \mathsf{T}^{\gtrless}_{\text{eq}}\left(\omega - \mathbf{p} \cdot \mathbf{V}(\mathbf{R}), \mathbf{p} - 2m\mathbf{V}(\mathbf{R}); \mathbf{R}\right)\left[1 + \mathcal{O}(VT/l_{\text{macro}})\right]. \quad (4.212)$$

Eqs. (4.211) and (4.212) finally yield the short-time dynamics of the spectral/statistical function of T:

$$\mathsf{B}(\omega, \mathbf{p}; T, \mathbf{R}; \delta U) = \mathsf{B}_{\text{eq}}\left(\omega - \mathbf{p} \cdot \mathbf{V}(\mathbf{R}), \mathbf{p} - 2m\mathbf{V}(\mathbf{R})\right)\left[1 + \mathcal{O}(VT/l_{\text{macro}})\right],$$

$$b(\omega, \mathbf{p}; T, \mathbf{R}; \delta U) = b_0\left(\omega - \mathbf{p} \cdot \mathbf{V}(\mathbf{R})\right)\left[1 + \mathcal{O}(VT/l_{\text{macro}})\right]. \quad (4.213)$$

This result is again very natural: following the short pulse, the equilibrium T-matrix is locally Galilean boosted. The appearance of $2m$ instead of m is simply because the mass of the composite bosons is $2m$ and experience twice the momentum boost of a single fermion.

4.6.2 The linear response theory of T-matrix kinetic equations

We study the kinetic phase of the evolution $T > t_{\text{imp.}}$ in this section (cf. Fig. 4.14), where Eqs. (4.209) and (4.213) serve as the initial seed for the linearized non-equilibrium kinetic evolution. We restrict the analysis to the case of particles with equal mass ($m_{\uparrow} = m_{\downarrow} \equiv m$) in a population-balanced equilibrium initial state, $U_{\uparrow} \equiv U_{\downarrow} = U$ and $\mu_{\uparrow} = \mu_{\downarrow} \equiv \mu$ for simplicity. The disturbing external field is also assumed to be spin-symmetric, i.e. $u_{\uparrow} = u_{\downarrow} \equiv u$. This symmetry is preserved by the $SU(2)$ symmetry of the action at all times. Therefore, we drop the spin indices throughout

the analysis and use the letter f to label the fermionic quantities. We treat the general case and the weak-coupling limit (cf. Sec. 4.5.3) separately.

General case:

The strategy for calculating the linear response within the kinetic theory was outlined in Sec. 2.5. As a first step, we define a convenient parametrization $\delta f(\omega, \mathbf{p}; T, \mathbf{R}) \equiv f(\omega, \mathbf{p}; T, \mathbf{R}) - f_0(\omega)$ and $\delta b(\omega, \mathbf{p}; T, \mathbf{R}) \equiv b(\omega, \mathbf{p}; T, \mathbf{R}) - b_0(\omega)$ as:

$$\delta f(\omega, \mathbf{p}; T, \mathbf{R}) \equiv \partial_\omega f_0(\omega)\, \Psi(\omega, \mathbf{p}; T, \mathbf{R}),$$

$$\delta b(\omega, \mathbf{p}; T, \mathbf{R}) \equiv \partial_\omega b_0(\omega)\, \Theta(\omega, \mathbf{p}; T, \mathbf{R}). \tag{4.214}$$

We assume $T > t_{\text{imp.}}$, so that $\delta U(T, \mathbf{R}) = 0$. The linearized kinetic equations read:

$$\frac{\mathsf{A}_0^2\, \Gamma_{f,0}}{2}\, \partial_\omega f_0 \left[\{\mathsf{M}_{f,0}, \Psi\} - \frac{\mathsf{M}_{f,0}}{\Gamma_{f,0}} \{\Gamma_{f,0}, \Psi\} + \partial_T \left(\Re[\delta\Sigma_f^+] + \frac{\mathsf{M}_{f,0}}{\Gamma_{f,0}} \delta\Gamma_f \right) \right] = \delta\mathsf{C}_f[\Psi, \Theta], \tag{4.215a}$$

$$\frac{\mathsf{B}_0^2\, \Gamma_{b,0}}{2}\, \partial_\omega b_0 \left[\{\mathsf{M}_{b,0}, \Theta\} - \frac{\mathsf{M}_{b,0}}{\Gamma_{b,0}} \{\Gamma_{b,0}, \Theta\} + \partial_T \left(\Re[\delta Q^+] + \frac{\mathsf{M}_{b,0}}{\Gamma_{b,0}} \delta\Gamma_b \right) \right] = \delta\mathsf{C}_b[\Psi, \Theta]. \tag{4.215b}$$

The linearized collision integrals are given by:

$$\delta\mathsf{C}_f[\Psi, \Theta](\tilde{1}) = \beta \int \mathrm{d}\tilde{2}\, \mathrm{d}\tilde{3}\, \delta(\tilde{1} + \tilde{2} - \tilde{3})\, \mathsf{A}_0(\tilde{1})\, \mathsf{A}_0(\tilde{2})\, \mathsf{B}_0(\tilde{3})$$

$$\times \left[1 - f_0(\tilde{1}) \right] \left[1 - f_0(\tilde{2}) \right] b_0(\tilde{3}) \left[\Psi(\tilde{1}) + \Psi(\tilde{2}) - \Theta(\tilde{3}) \right], \tag{4.216a}$$

$$\delta\mathsf{C}_b[\Psi, \Theta](\tilde{1}) = \beta \int \mathrm{d}\tilde{2}\, \mathrm{d}\tilde{3}\, \delta(\tilde{1} - \tilde{2} - \tilde{3})\, \mathsf{B}_0(\tilde{1})\, \mathsf{A}_0(\tilde{2})\, \mathsf{A}_0(\tilde{3})$$

$$\times b_0(\tilde{1}) \left[1 - f_0(\tilde{2}) \right] \left[1 - f_0(\tilde{3}) \right] \left[\Theta(\tilde{1}) - \Psi(\tilde{2}) - \Psi(\tilde{3}) \right]. \tag{4.216b}$$

The quantities labelled with a 0 index are the equilibrium values. For future reference, we provide the expanded form of the Poisson brackets appearing in Eq. (4.215):

$$\{\mathsf{M}_{f,0}, \Psi\} = \left(1 - \partial_\omega \Re[\Sigma_{f,0}^+]\right) \partial_T \Psi + \left(\frac{\mathbf{p}}{m} + \partial_{\mathbf{p}} \Re[\Sigma_{f,0}^+]\right) \cdot \partial_{\mathbf{R}} \Psi$$

$$- \partial_{\mathbf{R}} \left(U(\mathbf{R}) + \Re[\Sigma_{f,0}^+]\right) \cdot \partial_{\mathbf{p}} \Psi,$$

$$\{\Gamma_{f,0}, \Psi\} = \partial_\omega \Gamma_{f,0} \, \partial_T \Psi - \partial_{\mathbf{p}} \Gamma_{f,0} \cdot \partial_{\mathbf{R}} \Psi + \partial_{\mathbf{R}} \Gamma_{f,0} \cdot \partial_{\mathbf{p}} \Psi,$$

$$\{\mathsf{M}_{b,0}, \Theta\} = \left(Y(\omega - \xi_b) - \partial_\omega \Re[Q_0^+]\right) \partial_T \Theta + \left(Y(\omega - \xi_b) \frac{\mathbf{p}}{2m} + \partial_{\mathbf{p}} \Re[Q_0^+]\right) \cdot \partial_{\mathbf{R}} \Theta$$

$$- \left(2 \, Y(\omega - \xi_b) \, \partial_{\mathbf{R}} U(\mathbf{R}) + \partial_{\mathbf{R}} \Re[Q_0^+]\right) \cdot \partial_{\mathbf{p}} \Theta,$$

$$\{\Gamma_{b,0}, \Theta\} = \partial_\omega \Gamma_{b,0} \, \partial_T \Theta - \partial_{\mathbf{p}} \Gamma_{b,0} \cdot \partial_{\mathbf{R}} \Theta + \partial_{\mathbf{R}} \Gamma_{b,0} \cdot \partial_{\mathbf{p}} \Theta, \tag{4.217}$$

where $\xi_b \equiv |\mathbf{p}|^2/(4m) - 2\mu + 2U(\mathbf{R})$ and $Y(\omega) \equiv \partial_\omega \Re\left[1/\mathsf{T}_0^+(\omega)\right]$.

At equilibrium, the $\mathbf{R}$-dependence of the equilibrium self-energies and spectral functions is fully induced by the static external potential $U(\mathbf{R})$. This can be seen by noticing that (1) these functions have a local $\mathbf{R}$-dependence on one another (cf. Eqs. 4.139 and 4.150), (2) f_0 and b_0 are independent of $\mathbf{R}$, and (3) the $\mathbf{R}$-dependence in only present in $\mathsf{M}_{\uparrow(\downarrow)}$ (Eq. 4.139d) and M_b (Eq. 4.150e) and appears in the combination $\mu_\uparrow - U_\uparrow(\mathbf{R})$, $\mu_\downarrow - U_\downarrow(\mathbf{R})$, or $\mu_\uparrow + \mu_\downarrow - U_\uparrow(\mathbf{R}) - U_\downarrow(\mathbf{R})$. The assumed $SU(2)$ symmetry further implies that the $\mathbf{R}$-dependence appears merely in the combination $\mu - U(\mathbf{R})$, (4) μ only appears in the expressions in conjunction with $U(\mathbf{R})$. Thus, an arbitrary $\mathbf{R}$-dependent equilibrium quantity, K_0, has the following structure:

$$K_0(\omega, \mathbf{p}; \mathbf{R}) \equiv K_0\left(\omega, \mathbf{p}; U = 0\right)\Big|_{\mu \to \mu - U(\mathbf{R})}. \tag{4.218}$$

The above result is simply the statement of the local density approximation (LDA). In other words, LDA is compatible with the first-order gradient expansion in this case[8]. As a corollary

---

[8]Quite generally, the LDA assumption is compatible with the first-order gradient expansion provided that the range of interactions is smaller or comparable to the microscopic length-scale l_{micro}.

of Eq. (4.218), we find:

$$\partial_{\mathbf{R}} K_0(\omega, \mathbf{p}; \mathbf{R}) = -\partial_{\mathbf{R}} U(\mathbf{R}) \, \partial_\mu K_0(\omega, \mathbf{p}; U = 0)\Big|_{\mu \to \mu - U(\mathbf{R})}. \tag{4.219}$$

The $\mathbf{R}$-derivatives of the equilibrium quantities appearing in Eq. 4.217 can be calculated using the above formula.

One of the major difficulties in solving the linearized kinetic equations is calculating the explicit functional dependence of the terms appearing in parentheses in Eqs. (4.215a-b). These terms describe the deviation of the non-equilibrium retarded self-energies from their equilibrium value. As usual, $\Re[\delta \Sigma_f^+]$ and $\Re[\delta Q^+]$ are related to $\delta \Gamma_b$ and $\delta \Gamma_f$ by a Kramers-Kronig transform (cf. Eqs. 4.139f and 4.150):

$$\Re[\delta \Sigma_f^+] = -\frac{1}{2} \mathfrak{K}\mathfrak{K}[\delta \Gamma_f], \qquad \Re[\delta Q^+] = -\frac{1}{2} \mathfrak{K}\mathfrak{K}[\delta \Gamma_b]. \tag{4.220}$$

The two independent quantities, $\delta \Gamma_f$ and $\delta \Gamma_b$, satisfy the following coupled Fredholm integral equations of the second kind:

$$\delta \Gamma_f(\tilde{1}) = \int d\tilde{2} \, d\tilde{3} \, \delta(\tilde{1} + \tilde{2} - \tilde{3}) \left(\mathsf{A}_0(\tilde{2}) \, \mathsf{B}_0(\tilde{3}) \left[\partial_{\omega_2} f_0(\omega_2) \, \Psi(\tilde{2}) + \partial_{\omega_3} b_0(\omega_3) \, \Theta(\tilde{3}) \right] \right.$$
$$\left. + \left[\delta \mathsf{A}(\tilde{2}) \, \mathsf{B}_0(\tilde{3}) + \mathsf{A}_0(\tilde{2}) \, \delta \mathsf{B}(\tilde{3}) \right] \left[f_0(\omega_2) + b_0(\omega_3) \right] \right), \tag{4.221a}$$

$$\delta \Gamma_b(\tilde{1}) = \int d\tilde{2} \, d\tilde{3} \, \delta(\tilde{1} - \tilde{2} - \tilde{3}) \left(\mathsf{A}_0(\tilde{2}) \, \mathsf{A}_0(\tilde{3}) \left[-\partial_{\omega_2} f_0(\omega_2) \, \Psi(\tilde{2}) - \partial_{\omega_3} f_0(\omega_3) \, \Psi(\tilde{3}) \right] \right.$$
$$\left. + \left[\delta \mathsf{A}(\tilde{2}) \, \mathsf{A}_0(\tilde{3}) + \mathsf{A}_0(\tilde{2}) \, \delta \mathsf{A}(\tilde{3}) \right] \left[1 - f_0(\omega_2) - f_0(\omega_3) \right] \right), \tag{4.221b}$$

$$\delta \mathsf{A} = \frac{\left(\mathsf{M}_{f,0}^2 - \Gamma_{f,0}^2/4 \right)}{\left(\mathsf{M}_{f,0}^2 + \Gamma_{f,0}^2/4 \right)^2} \delta \Gamma_f - \frac{\mathsf{M}_{f,0} \, \Gamma_{f,0}}{\left(\mathsf{M}_{f,0}^2 + \Gamma_{f,0}^2/4 \right)^2} \, \mathfrak{K}\mathfrak{K}[\delta \Gamma_f], \tag{4.221c}$$

$$\delta \mathsf{B} = \frac{\left(\mathsf{M}_{b,0}^2 - \Gamma_{b,0}^2/4 \right)}{\left(\mathsf{M}_{b,0}^2 + \Gamma_{b,0}^2/4 \right)^2} \delta \Gamma_b - \frac{\mathsf{M}_{b,0} \, \Gamma_{b,0}}{\left(\mathsf{M}_{b,0}^2 + \Gamma_{b,0}^2/4 \right)^2} \, \mathfrak{K}\mathfrak{K}[\delta \Gamma_b]. \tag{4.221d}$$

The above equations are obtained directly from Eqs. (4.139) and (4.150). In principle, these equations have to be solved numerically, although perturbative treatments are possible in the weak- and

strong-coupling limits. For the sake of the argument, let us define a general ansatz for the terms appearing in curly parentheses in Eqs. (4.215a-b):

$$
\left(\Re[\delta\Sigma_f^+(\tilde{1})] + \frac{\mathsf{M}_{f,0}(\tilde{1})}{\Gamma_{f,0}(\tilde{1})} \, \delta\Gamma_f(\tilde{1}) \right) \equiv \mathsf{F}_{ff}[\Psi] + \mathsf{F}_{fb}[\Theta],
$$

$$
\left(\Re[\delta\Sigma_b^+(\tilde{1})] + \frac{\mathsf{M}_{b,0}(\tilde{1})}{\Gamma_{b,0}(\tilde{1})} \, \delta\Gamma_b(\tilde{1}) \right) \equiv \mathsf{F}_{bf}[\Psi] + \mathsf{F}_{bb}[\Theta], \tag{4.222}
$$

where $\{\mathsf{F}\}$ are linear functionals of their arguments due to the linearity and homogeneity of Eqs. (4.221) in Ψ and Θ. The time derivatives appearing in Eqs. (4.215) can be made algebraic by taking a Laplace transform in T. We define[9]:

$$
\tilde{\Psi}(\omega, \mathbf{p}; \Omega, \mathbf{R}) \equiv \int_{0^+}^{\infty} e^{i\Omega T} \, \Psi(\omega, \mathbf{p}; T, \mathbf{R}). \tag{4.223}
$$

We define $\tilde{\Theta}$ similarly. Here, $0^+ \equiv t_{\text{imp.}} + \epsilon$ denotes the time just after the external impulse. Taking a Laplace transform of both sides of Eqs. (4.215) and expanding the Poisson brackets, we obtain:

$$
\mathsf{G}_f \left[-i\Omega\gamma_{f,\omega}\tilde{\Psi} + \gamma_{f,p}\frac{\mathbf{p}}{m} \cdot \partial_{\mathbf{R}}\tilde{\Psi} - \gamma_{f,\mu}\,\partial_{\mathbf{R}}U(\mathbf{R}) \cdot \partial_{\mathbf{p}}\tilde{\Psi} - i\Omega\left(\mathsf{F}_{ff}[\tilde{\Psi}] + \mathsf{F}_{fb}[\tilde{\Theta}]\right) \right] - \delta\mathsf{C}_f[\tilde{\Psi}, \tilde{\Theta}]
$$

$$
= \mathsf{G}_f \left[\gamma_{f,\omega}\Psi(0^+) + \left(\mathsf{F}_{ff}[\Psi(0^+)] + \mathsf{F}_{fb}[\Theta(0^+)]\right) \right], \tag{4.224a}
$$

$$
\mathsf{G}_b \left[-i\Omega\gamma_{b,\omega}\tilde{\Theta} + \gamma_{b,p}\frac{\mathbf{p}}{2m} \cdot \partial_{\mathbf{R}}\tilde{\Theta} - 2\,\gamma_{b,\mu}\,\partial_{\mathbf{R}}U(\mathbf{R}) \cdot \partial_{\mathbf{p}}\tilde{\Theta} - i\Omega\left(\mathsf{F}_{bf}[\tilde{\Psi}] + \mathsf{F}_{bb}[\tilde{\Theta}]\right) \right] - \delta\mathsf{C}_b[\tilde{\Psi}, \tilde{\Theta}]
$$

$$
= \mathsf{G}_b \left[\gamma_{b,\omega}\Theta(0^+) + \left(\mathsf{F}_{bf}[\Psi(0^+)] + \mathsf{F}_{bb}[\Theta(0^+)]\right) \right], \tag{4.224b}
$$

---

[9]It is customary in to denote the frequency variable in the Laplace domain with s. Here, we make the substitution $s \to -i\Omega$ in order to obtain expressions that formally resemble Fourier transformed quantities.

where the auxiliary quantities $\{\mathsf{G}_{f(b)}, \gamma_{f(b),\omega}, \gamma_{f(b),p}, \gamma_{f(b),\mu}\}$ are defined as:

$$\mathsf{G}_f \equiv \frac{\mathsf{A}_0^2 \, \Gamma_{f,0}}{2} \, \partial_\omega f_0,$$

$$\gamma_{f,\omega} \equiv 1 - \partial_\omega \Re[\Sigma_{f,0}^+] - \frac{\mathsf{M}_{f,0}}{\Gamma_{f,0}} \, \partial_\omega \Gamma_{f,0},$$

$$\gamma_{f,p} \equiv 1 + \frac{m}{|\mathbf{p}|^2} \, \mathbf{p} \cdot \left(\partial_{\mathbf{p}} \Re[\Sigma_{f,0}^+] + \frac{\mathsf{M}_{f,0}}{\Gamma_{f,0}} \, \partial_{\mathbf{p}} \Gamma_{f,0} \right),$$

$$\gamma_{f,\mu} \equiv 1 - \partial_\mu \Re[\Sigma_{f,0}^+] - \frac{\mathsf{M}_{f,0}}{\Gamma_{f,0}} \, \partial_\mu \Gamma_{f,0},$$

$$\mathsf{G}_b \equiv \frac{\mathsf{B}_0^2 \, \Gamma_{b,0}}{2} \, \partial_\omega b_0,$$

$$\gamma_{b,\omega} \equiv Y(\omega - \xi_b) - \partial_\omega \Re[Q_0^+] - \frac{\mathsf{M}_{b,0}}{\Gamma_{b,0}} \, \partial_\omega \Gamma_{b,0},$$

$$\gamma_{b,p} \equiv Y(\omega - \xi_b) + \frac{2m}{|\mathbf{p}|^2} \, \mathbf{p} \cdot \left(\partial_{\mathbf{p}} \Re[Q_0^+] + \frac{\mathsf{M}_{b,0}}{\Gamma_{b,0}} \, \partial_{\mathbf{p}} \Gamma_{b,0} \right),$$

$$\gamma_{b,\mu} \equiv Y(\omega - \xi_b) - \frac{1}{2} \, \partial_\mu \Re[Q_0^+] - \frac{1}{2} \frac{\mathsf{M}_{b,0}}{\Gamma_{b,0}} \, \partial_\mu \Gamma_{b,0}. \tag{4.225}$$

We have used Eq. (4.219) to express the spatial derivatives of the equilibrium quantities in terms of chemical potential derivatives. The functions $\gamma_{f(b),\omega}$ and $\gamma_{f(b),p}$ are related to the scalar and vector vertex functions, respectively [229], and describe the effective charge and mass of the particle-like resonances. The appearance of the real and imaginary parts of the retarded self-energy describe in the vertex functions is responsible for the *drag-flow* and the *back-flow*, respectively [61].

The initial value terms are easily determined using the expressions given at the end of Sec. 4.6.1. Using Eqs. (4.209) and (4.213), we find:

$$\Psi(0^+) = \Theta(0^+) = -\mathbf{p} \cdot \mathbf{V}(\mathbf{R}), \qquad \mathbf{V}(\mathbf{R}) = -\frac{1}{m} \partial_{\mathbf{R}} u(\mathbf{R}) \int_0^{t_{\text{imp.}}} \mathcal{A}(t) \, \mathrm{d}t. \tag{4.226}$$

The same results also allow an exact calculation of the initial value terms that involve F functionals without needing to calculate them. Using the fact that the initial disturbance is a local Galilean

boost, we easily obtain:

$$\mathsf{F}_{ff}\big[\Psi(0^+)\big] + \mathsf{F}_{fb}\big[\Theta(0^+)\big] \to \mathcal{B}(m,\mathbf{V})\,\Re[\Sigma_{f,0}^+] + \frac{\mathsf{M}_{f,0}}{\Gamma_{f,0}}\,\mathcal{B}(m,\mathbf{V})\,\Gamma_f,$$

$$\mathsf{F}_{bf}\big[\Psi(0^+)\big] + \mathsf{F}_{bb}\big[\Theta(0^+)\big] \to \mathcal{B}(2m,\mathbf{V})\,\tilde{\Re}[Q_0^+] + \frac{\mathsf{M}_{b,0}}{\Gamma_{b,0}}\,\mathcal{B}(2m,\mathbf{V})\,\Gamma_b, \qquad (4.227)$$

where we have defined the infinitesimal Galilean boost operator for particles of mass M (in the Wigner representation) as $\mathcal{B}(M,\mathbf{V}) \equiv -\mathbf{p}\cdot\mathbf{V}(\mathbf{R})\,\partial_\omega - M\mathbf{V}(\mathbf{R})\cdot\partial_\mathbf{p}$. Combining the above equation with Eqs. (4.224a-b), the right hand sides (initial seeds) of the fermionic and bosonic equations become:

$$\text{r.h.s. of Eq. (4.224a)} \to -\mathsf{G}_f\gamma_{f,p}\mathbf{p}\cdot\mathbf{V}(\mathbf{R}), \qquad \text{r.h.s. of Eq. (4.224b)} \to -\mathsf{G}_b\gamma_{b,p}\,\mathbf{p}\cdot\mathbf{V}(\mathbf{R}).$$

$$(4.228)$$

The disappearance of the scalar vertex function $\gamma_{f(b),\omega}$ from the initial value terms, and the explicit appearance of the vector vector function $\gamma_{f(b),p}$ appeals to intuition: if $\delta U(T,\mathbf{R})$ has no $\mathbf{R}$-dependence, it couples to the total number of particles which is a conserved quantity. Therefore, it can be gauged out from the evolution equations and has no physical effect. This redundancy can be removed in the Weyl gauge (cf. Eq. 4.198) in which the field gradient $\partial_\mathbf{R} U(T,\mathbf{R})$ couples to the (non-conserved) local current operator $\mathbf{j}$. Therefore, the appearance of the vector vertex function $\gamma_{f(b),\omega}$ as the pre-factor to the initial value term is quite natural. Had it not been for the self-consistent self-energy corrections (the $\{\mathsf{F}\}$ functionals), this result would not follow.

For a given Ω, the coupled integro-differential equations given in Eqs. (4.224a) and (4.224b) must be solved for $\tilde{\Psi}$ and $\tilde{\Theta}$, using which the linear response functions can be readily obtained. The Laplace-transformed change in the number density, $\delta\tilde{n}_\sigma(\Omega,\mathbf{R})$, in response to the external impulse

$\delta U(T, \mathbf{R}) = \delta(T)\, u(\mathbf{R})$ is given by:

$$
\begin{aligned}
\delta \tilde{n}_\sigma(\Omega, \mathbf{R}) &= -i \int_{0^+}^\infty \mathrm{d}T\, e^{i\Omega T} \int \frac{\mathrm{d}\omega}{2\pi} \frac{\mathrm{d}^d\mathbf{p}}{(2\pi)^d}\, \delta G_\sigma^<(\omega, \mathbf{p}; T, \mathbf{R}) \\
&= \int \frac{\mathrm{d}\omega}{2\pi} \frac{\mathrm{d}^d\mathbf{p}}{(2\pi)^d}\, \Big[\delta\mathsf{A}_\sigma(\omega, \mathbf{p}; \Omega, \mathbf{R})\, f_0(\omega) + \mathsf{A}_{\sigma,0}(\omega, \mathbf{p}; \mathbf{R})\, \partial_\omega f_0(\omega)\, \tilde{\Psi}(\omega, \mathbf{p}; \Omega, \mathbf{R}) \Big],
\end{aligned}
$$

$$(4.229)$$

where $\delta\mathsf{A}_\sigma(\omega, \mathbf{p}; \Omega, \mathbf{R})$ is to be expressed in terms of $\tilde{\Psi}$ and $\tilde{\Phi}$ using Eq. (4.221). We will discussion practical numerical methods for solving the linear response equations in coming sections.

The weak-coupling approximation:

The linear response analysis is simplified in the weak-coupling approximation and is obtained by making the replacement $b \to c_b$ (cf. Sec. 4.5.3). The result is a single fermionic kinetic equation, Eq. (4.215a), with the collision integral describing a local 4-fermion scattering process (cf. Eq. (4.159). Once linearized, the local collision integral operator reads as:

$$
\begin{aligned}
\delta\mathsf{C}_f(\tilde{1}) = \beta \int \mathrm{d}\tilde{2}\,\mathrm{d}\tilde{3}\,\mathrm{d}\tilde{4}\, \delta(\tilde{1}+\tilde{2}-\tilde{3}-\tilde{4})\, \mathsf{A}_0(\tilde{1})\, \mathsf{A}_0(\tilde{2})\, \mathsf{A}_0(\tilde{3})\, \mathsf{A}_0(\tilde{4})\, \left| \mathsf{T}^+(\tilde{3}+\tilde{4}) \right|^2 \\
\times \left[1 - f_0(\tilde{1}) \right]\left[1 - f_0(\tilde{2}) \right] f(\tilde{3}) f(\tilde{4}) \left[\Psi(\tilde{1}) + \Psi(\tilde{2}) - \Psi(\tilde{3}) - \Psi(\tilde{4}) \right]. \quad (4.230)
\end{aligned}
$$

We denote the terms appearing in curly brackets in Eq. (4.215a) by $\mathsf{F}[\Psi]$. This functional is determined by Eq. (4.221) by making the replacement:

$$
\delta b(\tilde{1}) \equiv \partial_{\omega_1} b_0(\omega_1)\, \Theta(\tilde{1}) \to \delta c_b(\tilde{1}) = -\frac{\delta\Gamma_b(\tilde{1})}{\Gamma_{b,0}(\tilde{1})}\, b_0(\omega_1) + \frac{1}{\Gamma_{b,0}(\tilde{1})} \int \mathrm{d}\tilde{2}\,\mathrm{d}\tilde{3}\, \delta(\tilde{1}-\tilde{2}-\tilde{3})
$$

$$
\times \Bigg\{ \left[\delta\mathsf{A}(\tilde{2})\, \mathsf{A}_0(\tilde{3}) + \mathsf{A}(\tilde{2})\, \delta\mathsf{A}_0(\tilde{3}) \right] f_0(\omega_2) f_0(\omega_3) + \mathsf{A}_0(\tilde{2})\, \mathsf{A}_0(\tilde{3})\, \partial_{\omega_2} f_0(\omega_2)\, \Psi(\tilde{2})\, \partial_{\omega_3} f_0(\omega_3)\, \Psi(\tilde{3}) \Bigg\}.
$$

$$(4.231)$$

The term proportional to $\delta\Gamma_b$ and the integral term describe the change in the lifetime of fluctuations and the collision rate of fermions, respectively. The remaining of the analysis is similar to the above general case.

The BGK approximation for the quantum collision integrals:

Calculating the collision integral is often the most demanding part of the numerical implementation of the kinetic formalism. Within the quasiparticle approximation, the collision integral is often replaced by an effective relaxation time term according to the Bhatnagar-Gross-Krook (BGK) theory [230]. In the most general case, this procedure yields:

$$\mathsf{C}^{\mathrm{BGK}}(\mathbf{p}; T, \mathbf{R}) \to -\frac{n(\mathbf{p}; T, \mathbf{R}) - n_{\mathrm{leq.}}(\mathbf{p}; T, \mathbf{R})}{\tau_{\mathrm{rel.}}(\mathbf{p}; T, \mathbf{R})}, \tag{4.232}$$

where $\tau_{\mathrm{rel.}}(\mathbf{p}; T, \mathbf{R})$ is a relaxation time to be determined, and $n_{\mathrm{leq.}}(\mathbf{p}; T, \mathbf{R})$ is a local equilibrium distribution function parametrized such that the particle number, energy and momentum is conserved in collisions. An important property of the local collision integral operators (as in Eq. 4.159) is that it satisfies the detailed balance condition for general *local equilibrium* states:

$$f_{\mathrm{leq.}}(\omega, \mathbf{p}; T, \mathbf{R}) = \frac{1}{\exp\left(\beta(T, \mathbf{R})\left[\omega + \delta\mu(T, \mathbf{R}) - \mathbf{p} \cdot \mathbf{V}(T, \mathbf{R})\right]\right) + 1}, \tag{4.233}$$

regardless of the values of $\beta(T, \mathbf{R})$, $\delta\mu(T, \mathbf{R})$ and $\mathbf{V}(T, \mathbf{R})$. This important property is crucial for the correct description of the hydrodynamic regime [231]. Here, in the spirit of the the BGK collision operator, we would like to propose an approximate form for $\delta\mathsf{C}_f$ such that it (1) respects the local conservation laws, (2) vanishes for local equilibrium distributions, and (3) does not rely on the existence of quasiparticles. Starting with Eq. (2.36) and linearizing about the thermal equilibrium state, we find:

$$\delta\mathsf{C}_f = -\delta[\mathsf{A}\Gamma_f(f - c)] = -\mathsf{A}_0\Gamma_{f,0}(\delta f - \delta c), \tag{4.234}$$

where c is the statistical part of the self-energy (cf. Eq. 2.32) and is a known functional of f and A (as given by the Φ-derived self-energy functional). We have used the fact $f(\omega, \mathbf{p}; T, \mathbf{R}) = c(\omega, \mathbf{p}; T, \mathbf{R}) = f_0(\omega)$ at equilibrium to get the right hand side. The local collision integral, Eq. (4.230), is obtained by neglecting the gradient terms in c. In the linear regime, δc may be

expanded in powers of ω and $\mathbf{p}$:

$$\delta c(\omega, \mathbf{p}; T, \mathbf{R}) = \partial_\omega f_0(\omega) \left[\delta\mu_\Sigma(T, \mathbf{R}) + \omega\,\chi_\Sigma(T, \mathbf{R}) - \mathbf{p} \cdot \mathbf{V}_\Sigma(T, \mathbf{R}) + \Psi_\Sigma^{\mathrm{nHD}}(\omega, \mathbf{p}; T, \mathbf{R}) \right],$$
(4.235)

where $\Psi_\Sigma^{\mathrm{nHD}}(\omega, \mathbf{p}; T, \mathbf{R})$ corresponds to terms at least second order in ω and $\mathbf{p}$, and parametrize the non-hydrodynamical fluctuations in the self-energy. Plugging the above ansatz in Eq. (4.234) and using the previously defined parametrization for δf (cf. Eq. 4.214), we find:

$$\mathsf{C}_f[\Psi] = -\mathsf{A}_0 \Gamma_{f,0} \partial_\omega f_0(\omega) \Big[\Psi(\omega, \mathbf{p}; T, \mathbf{R}) - \delta\mu_\Sigma(T, \mathbf{R}) - \omega\,\chi_\Sigma(T, \mathbf{R})$$
$$+ \mathbf{p} \cdot \mathbf{V}_\Sigma(T, \mathbf{R}) - \Psi_\Sigma^{\mathrm{nHD}}(\omega, \mathbf{p}; T, \mathbf{R}) \Big]. \quad (4.236)$$

Comparing the above ansatz for $\delta \mathsf{C}$ with the BGK ansatz, we notice that a similar result is obtained by neglecting non-hydrodynamical corrections to the self-energy. We continue the development by neglecting $\Phi_\Sigma^{\mathrm{nHD}}$ for the moment. The repercussions of this approximation will be be discussed afterwards. The as of yet unknown functions $\{\delta\mu_\Sigma(T, \mathbf{R}), \chi_\Sigma(T, \mathbf{R}), \mathbf{V}_\Sigma(T, \mathbf{R})\}$ can be determined by imposing the local conservation laws (cf. Eq. 4.160). We define the shorthand notation:

$$I[X](T, \mathbf{R}) \equiv \int \mathrm{d}\tilde{1}\, \Gamma_{f,0}(\tilde{1}; T, \mathbf{R})\, \mathsf{A}_0(\tilde{1}; T, \mathbf{R})\, \partial_{\omega_1} f_0(\omega_1)\, X(\tilde{1}; T, \mathbf{R}). \quad (4.237)$$

The conservation laws imply the following constraints:

$$I[\Psi] = \delta\mu_\Sigma\, I[1] + \chi_\Sigma\, I[\omega] - \mathbf{V}_\Sigma \cdot I[\mathbf{p}],$$

$$I[\omega\Psi] = \delta\mu_\Sigma\, I[\omega] + \chi_\Sigma\, I[\omega^2] - \mathbf{V}_\Sigma \cdot I[\omega\mathbf{p}],$$

$$I[p_j\Psi] = \delta\mu_\Sigma\, I[p_j] + \chi_\Sigma\, I[\omega p_j] - V_{\Sigma,i} I[p_i p_j]. \quad (4.238)$$

The solution is simplified for isotropic equilibrium states for which $I[p_j] = 0$ and $I[p_i p_j] = (1/d)\, I[p^2]$. The final result is:

$$\delta \mathsf{C}_f^{\omega\mathrm{BGK}}[\Psi] = -\mathsf{A}_0 \Gamma_{f,0} \partial_\omega f_0(\omega) \Big[\Psi(\omega, \mathbf{p}; T, \mathbf{R}) - D^{-1}(T, \mathbf{R}) \left(I[\Psi] I[\omega^2] - I[\omega] I[\omega\Psi] \right)$$

$$- D^{-1}(T, \mathbf{R})\, (I[1] I[\omega\Psi] - I[\omega] I[\Psi]) - d\, I[p^2]^{-1}\, \mathbf{p} \cdot I[\mathbf{p}\,\Psi] \Big],$$

$$D(T, \mathbf{R}) = I[1] I[\omega^2] - I[\omega]^2. \tag{4.239}$$

We refer to the above approximation of the collision integral of the quantum kinetic equation as the ωBGK scheme. It is easily verified that $\delta\mathsf{C}_f^{\omega\mathrm{BGK}}$ vanishes if Ψ corresponds to hydrodynamical fluctuations, as required.

The ωBGK scheme offers a much more tractable expression for the collision integral since it does not involve nested energy-momentum integrals. Unfortunately, the key approximation that leads to ωBGK, i.e. neglecting non-hydrodynamical fluctuations in the self-energy has an *ad hoc* status. For instance, the relaxation rate that appears in the ωBGK approximation is $\Gamma_{f,0}$, which describes the quasiparticle relaxation rate in equilibrium (in the quasiparticle limit). The relaxation rate for non-equilibrium processes generally differ from $\Gamma_{f,0}$ by $\mathcal{O}(1)$ numerical factors. Nevertheless, Γ_f is a reasonable representative of all relaxation rates associated to low-lying Fermi surface deformations. For concreteness, we compare the result from the ωBGK scheme and the exact collision integral operator for a quadrupolar deformation $\Psi \sim p_x^2 - p_y^2$. The exact collision matrix element $\langle \Psi | \delta \mathsf{C}_f | \Psi \rangle$ is found using Eq. (4.230):

$$\langle \Psi | \delta \mathsf{C}_f | \Psi \rangle = \beta \int \mathrm{d}\tilde{1}\, \mathrm{d}\tilde{2}\, \mathrm{d}\tilde{3}\, \mathrm{d}\tilde{4}\, \delta(\tilde{1} + \tilde{2} - \tilde{3} - \tilde{4})\, \mathsf{A}_0(\tilde{1})\, \mathsf{A}_0(\tilde{2})\, \mathsf{A}_0(\tilde{3})\, \mathsf{A}_0(\tilde{4})\, \left| \mathsf{T}^+(\tilde{3} + \tilde{4}) \right|^2$$

$$\times \left[1 - f_0(\tilde{1}) \right] \left[1 - f_0(\tilde{2}) \right] f(\tilde{3}) f(\tilde{4})\, \Psi(\tilde{1}) \left[\Psi(\tilde{1}) + \Psi(\tilde{2}) - \Psi(\tilde{3}) - \Psi(\tilde{4}) \right]. \tag{4.240}$$

In an isotropic equilibrium state, $I[p_x^2 - p_y^2] = I[\omega(p_x^2 - p_y^2)] = I[\mathbf{p}(p_x^2 - p_y)^2] = 0$. Plugging the

explicit expression for $\Gamma_{f,0}$ in $\delta C_f^{\omega\text{BGK}}$, we easily find:

$$\langle\Psi|\delta C_f^{\omega\text{BGK}}|\Psi\rangle = \beta \int d\tilde{1}\, d\tilde{2}\, d\tilde{3}\, d\tilde{4}\, \delta(\tilde{1} + \tilde{2} - \tilde{3} - \tilde{4})\, A_0(\tilde{1})\, A_0(\tilde{2})\, A_0(\tilde{3})\, A_0(\tilde{4})\, \left|T^+(\tilde{3} + \tilde{4})\right|^2$$

$$\times [1 - f_0(\tilde{1})]\,[1 - f_0(\tilde{2})]\, f(\tilde{3}) f(\tilde{4})\, \Psi(\tilde{1})^2.$$

Comparing the above expressions, we find that $\langle\Psi|\delta C_f^{\omega\text{BGK}}|\Psi\rangle$ can be obtained from $\langle\Psi|\delta C_f|\Psi\rangle$ by setting $\Psi(\tilde{2}) = \Psi(\tilde{3}) = \Psi(\tilde{4}) = 0$ in the integrand of Eq. (4.230). The appearance of extra Ψ factors with momentum labels $\tilde{2}$, $\tilde{3}$ and $\tilde{4}$ in Eq. (4.230) is a natural consequence of self-consistency since the same non-equilibrium distribution function is ascribed to all particles. Neglecting non-hydrodynamical corrections to the self-energy amounts to keeping three of the particles $\{\tilde{2}, \tilde{3}, \tilde{4}\}$ in a local equilibrium. Clearly, $\langle\Psi|\delta C_f^{\omega\text{BGK}}|\Psi$ and $\langle\Psi|\delta C_f|\Psi\rangle$ differ in value, however, they are expected to be of the same order and behave similarly. It is best to avoid such approximate schemes when adequate computation resources are available. Nevertheless, ωBGK may serve as a reasonable starting point for obtaining preliminary results.

4.6.3   Application of the method of moments to the linearized quantum transport

In this section, we discuss a numerical strategy for solving the linearized kinetic equations obtained in the previous section. We introduce a generalization of the Grad's method of moments [69] widely used for solving the classical Bolzmann equation to quantum kinetic equations. The main difference between classical and quantum transport is the absence of the notion of quasiparticles (violation of the mass-shell condition) in the latter, so that the distribution functions depend on the microscopic momentum $\mathbf{p}$ and energy ω on an equal footing.

The linearized quantum transport equations in the Laplace domain (Eqs. 4.224a-b) formally pose an inhomogeneous boundary value problem $\mathcal{L}[f] = f_0(x)$, where $f \equiv \{\tilde{\Psi}, \tilde{\Theta}\}$ and $x \equiv (\omega, \mathbf{p}; \Omega, \mathbf{R})$. The boundary condition imposed on f is the regularity of the solutions (discussed below). $\mathcal{L}$ is the linear integro-differential operator appearing on the left hand sides of Eqs. (4.224a-

b). A practical strategy for solving such boundary value problems is to solve its *weak form*. The latter is obtained by expanding f in the basis functions of a separable Hilbert space, i.e. $f(x) = \sum_{\alpha \in \mathbb{N}} f_\alpha \phi_\alpha(x)$, where $\{\phi_\alpha\}$ is a complete basis. One further demands $\langle \phi_\alpha | \mathcal{L} | f \rangle = \langle \phi_\alpha | f_0 \rangle$, for all α. This procedure yields:

$$\sum_\beta \langle \phi_\alpha | \mathcal{L} | \phi_\beta \rangle f_\beta = \sum_\beta \langle \phi_\alpha | \phi_\beta \rangle f_{0,\beta}, \tag{4.241}$$

where $f_{0,\beta}$ are the coefficients of the expansion of $f_0(x)$. We have not assumed that $\{\phi\}$ are orthonormal, although this may always be achieved using the Gram-Schmidt orthonormalization procedure. In practice, the basis states are truncated by keeping the first n basis functions in a certain order. We denote this truncated basis set by $B_n \equiv \mathrm{span}\{\phi_1, \ldots, \phi_n\}$. The weak solution restricted to B_n is obtained by solving the linear system of equation given in Eq. (4.241) with summations going from 1 to n. We denote this solution by $f^{(n)}$. Provided that $f^{(w)} \equiv \lim_{n \to \infty} f^{(n)}$ exists, $f^{(w)}$ is the (unique) solution of the weak form of the integral equation. The solution of the weak form further coincides with the solution of the strong form with certain smoothness conditions on $\mathcal{L}$.

The Grad's method of moments using in the kinetic theory of classical gases is a special case of the above general procedure, where the basis functions are chosen as polynomials of the momentum $\{p^n\}$ with the inner product measure $d\mu \equiv n_0(p)\, dp$, where $n_0(p)$ is the Maxwell-Boltzmann distribution so that $||p^n||^2 < \infty$. The weak form of the Boltzmann equation in the momentum polynomial basis yields a infinite hierarchy of conditions on the momentum moments of the non-equilibrium distribution function. Truncating this hierarchy at the level of n moments gives an approximate weak solution that satisfies the first n moment conditions, justifying the nomenclature. In practice, this procedure converges rapidly and yields accurate results with just the first few moments. The quantum transport equation may also be solved in a similar fashion. The new feature is that the basis functions explicitly depend on the microscopic energy ω. As a first step, we formally expand

the solution $\{\Psi, \Theta\}$ in a complete basis:

$$\tilde{\Psi}(\omega, \mathbf{p}; \Omega, \mathbf{R}) = \sum_\alpha \tilde{\Psi}_\alpha(\Omega)\, \Psi_\alpha(\omega, \mathbf{p}; \mathbf{R}),$$

$$\tilde{\Theta}(\omega, \mathbf{p}; \Omega, \mathbf{R}) = \sum_\alpha \tilde{\Theta}_\alpha(\Omega)\, \Theta_\alpha(\omega, \mathbf{p}; \mathbf{R}), \tag{4.242}$$

where $\{\Psi_\alpha : \alpha \in \mathbb{N}\}$ and $\{\Theta_\alpha : \alpha \in \mathbb{N}\}$ correspond to two sets of complete basis functions (to be explicitly defined later). Plugging these expansions into Eqs. (4.224a) and (4.224b), multiplying the by each basis function and integrating over ω, $\mathbf{p}$ and $\mathbf{R}$, we obtain:

$$-i\Omega \left(\left\langle \Psi_\alpha \middle| \gamma_{f,\omega} \middle| \Psi_\beta \right\rangle_{\mathsf{G}_\mathsf{f}} \tilde{\Psi}_\beta + \left\langle \Psi_\alpha \middle| \mathsf{F}_{ff}[\Psi_\beta] \right\rangle_{\mathsf{G}_\mathsf{f}} \tilde{\Psi}_\beta + \left\langle \Psi_\alpha \middle| \mathsf{F}_{fb}[\Theta_\beta] \right\rangle_{\mathsf{G}_\mathsf{f}} \tilde{\Theta}_\beta \right)$$

$$+ \left\langle \Psi_\alpha \middle| \gamma_{f,p} \middle| \frac{\mathbf{p}}{m} \cdot \partial_\mathbf{R} \Psi_\beta \right\rangle_{\mathsf{G}_\mathsf{f}} \tilde{\Psi}_\beta - \left\langle \Psi_\alpha \middle| \gamma_{f,\mu} \partial_\mathbf{R} U(\mathbf{R}) \cdot \partial_\mathbf{p} \Psi_\beta \right\rangle_{\mathsf{G}_\mathsf{f}} \tilde{\Psi}_\beta$$

$$- \int \frac{\mathrm{d}\omega}{2\pi} \frac{\mathrm{d}^d \mathbf{p}}{(2\pi)^d} \, \mathrm{d}^d \mathbf{R} \, \Psi_\alpha \, \delta\mathsf{C}_f[\Psi_\beta, \Theta_\gamma] \, \tilde{\Psi}_\beta \tilde{\Theta}_\gamma = - \left\langle \Psi_\alpha \middle| \gamma_{f,p} \middle| \Psi_\beta \right\rangle_{\mathsf{G}_\mathsf{f}} \tilde{\Psi}_\beta^{(0)}, \tag{4.243a}$$

and:

$$-i\Omega \left(\left\langle \Theta_\alpha \middle| \gamma_{b,\omega} \middle| \Theta_\beta \right\rangle_{\mathsf{G}_\mathsf{b}} \tilde{\Theta}_\beta + \left\langle \Theta_\alpha \middle| \mathsf{F}_{bf}[\Psi_\beta] \right\rangle_{\mathsf{G}_\mathsf{b}} \tilde{\Psi}_\beta + \left\langle \Theta_\alpha \middle| \mathsf{F}_{bb}[\Theta_\beta] \right\rangle_{\mathsf{G}_\mathsf{b}} \tilde{\Theta}_\beta \right)$$

$$+ \left\langle \Theta_\alpha \middle| \gamma_{b,p} \middle| \frac{\mathbf{p}}{2m} \cdot \partial_\mathbf{R} \Theta_\beta \right\rangle_{\mathsf{G}_\mathsf{b}} \tilde{\Theta}_\beta - \left\langle \Theta_\alpha \middle| 2\gamma_{b,\mu} \partial_\mathbf{R} U(\mathbf{R}) \cdot \partial_\mathbf{p} \Theta_\beta \right\rangle_{\mathsf{G}_\mathsf{b}} \tilde{\Theta}_\beta$$

$$- \int \frac{\mathrm{d}\omega}{2\pi} \frac{\mathrm{d}^d \mathbf{p}}{(2\pi)^d} \, \mathrm{d}^d \mathbf{R} \, \Theta_\alpha \, \delta\mathsf{C}_b[\Psi_\beta, \Theta_\gamma] \, \tilde{\Psi}_\beta \tilde{\Theta}_\gamma = - \left\langle \Theta_\alpha \middle| \gamma_{b,p} \middle| \Theta_\beta \right\rangle_{\mathsf{G}_\mathsf{b}} \tilde{\Theta}_\beta^{(0)}. \tag{4.243b}$$

Summation over the repeated indices is implied in the above matrix equations. We have also defined $\tilde{\Psi}_\alpha^{(0)}$ and $\tilde{\Theta}_\alpha^{(0)}$ such that:

$$\sum_\alpha \tilde{\Psi}_\alpha^{(0)} \Psi_\alpha = \sum_\alpha \tilde{\Theta}_\alpha^{(0)} \Theta_\alpha = \mathbf{p} \cdot \mathbf{V}(\mathbf{R}). \tag{4.244}$$

The linear products are also defined as:

$$\langle \mathcal{A} | \mathcal{B} \rangle_{\mathsf{G}_{f(b)}} \equiv \int \frac{\mathrm{d}\omega}{2\pi} \frac{\mathrm{d}^d \mathbf{p}}{(2\pi)^d} \, \mathrm{d}^d \mathbf{R} \, \mathsf{G}_{f(b)}(\omega, \mathbf{p}; \mathbf{R}) \, \mathcal{A}(\omega, \mathbf{p}; \mathbf{R}) \, \mathcal{B}(\omega, \mathbf{p}; \mathbf{R}). \tag{4.245}$$

The matrix elements appearing in Eqs. (4.243a) and (4.243b) can be calculated using the equilibrium solution and the expressions given in the previous section for any given set of basis functions. The

resulting system of linear equations can be solved for $\{\tilde{\Psi}_\alpha, \tilde{\Theta}_\alpha\}$ yielding an approximate solution to the weak form of the linearized quantum kinetic equations. In practice, the angular integrations appearing in the matrix elements can be done analytically similar to the expressions given in Appendix C.3 and C.4 for the quasiparticle kinetic equations of the dipolar Fermi gas. The integrations over ω, p and R, however, may only be done numerically except for trivial extreme weak-coupling and strong-coupling limits where approximate analytical expressions are known for the equilibrium quantities. In the next subsections, we provide simple basis functions appropriate to monopole and quadrupole oscillations of particles initially in an isotropic confining potential in $d = 2$.

Basis functions for particles in isotropic confining potentials:

We denote the linear operator appearing on the left hand sides of Eqs. (4.224a) and (4.224b) by $\mathcal{L}_f$ and $\mathcal{L}_b$, respectively. An important feature of the linearized dynamical equations is that the expansion coefficients, $\{\tilde{\Psi}_\alpha, \tilde{\Theta}_\alpha\}$, may be constrained by *selection rules* provided that the (1) the evolution operators $\{\mathcal{L}_f, \mathcal{L}_b\}$ are invariant under the transformations of a continuous group G, (2) the basis functions $\{\Psi_\alpha, \Theta_\alpha\}$ and the initial condition terms both belong to the representations of G. For instance, provided that the static scalar potential $U(\mathbf{R})$ is a scalar function of $\mathbf{R}$, it is straightforward to show that $[\hat{S}, \mathcal{L}_f] = [\hat{S}, \mathcal{L}_b] = 0$, where $\hat{S}$ is a generator of $SO(d)$ acting simultaneously on $\mathbf{R}$ and $\mathbf{p}$ in $\mathcal{F}_\Psi \otimes \mathcal{F}_\Theta$. In $d = 2$, $SO(2)$ has a single generator which represented in $\mathcal{F}_\Psi \otimes \mathcal{F}_\Theta$ as $\hat{S}_z = \hat{S}_z^\Psi + \hat{S}_z^\Theta$, where:

$$i\hat{S}_z \equiv X\partial_Y - Y\partial_X + p_x\partial_{p_y} - p_y\partial_{p_x}. \tag{4.246}$$

The representations of $\hat{S}_z$ are functions with a well-defined angular momentum m. The basis functions may also be chosen from representations of S_z without loss of generality. Provided that the initial condition term can be written as a linear combination of finite number of functions with well-defined angular momenta $\{m_1, \ldots, m_N\}$, this property is also inherited by the solution of

the boundary value problem[10]. Therefore, the basis functions for Ψ and Θ can be restricted to $\{m_1, \ldots, m_N\}$ representations of S_z from the outset, significantly reducing the redundancy in the numerical calculations. Here, we consider the two important cases of monopole ($m = 0$) and quadrupole ($m = 2$) external perturbations for a system initially in an isotropic confining potential in two spatial dimensions. The monopole mode is excited by perturbing the external potential with an external impulse with an isotropic spatial profile. The velocity field following the impulse $\mathbf{V}(\mathbf{R}) = -\partial_{\mathbf{R}} u(\mathbf{R})/m$ can be generally written as:

$$\mathbf{V}_{\mathrm{m}}(\mathbf{R}) = \tilde{V}_{\mathrm{m}}(R^2)\, \mathbf{R}, \tag{4.247}$$

for some scalar function $\tilde{V}_{\mathrm{m}}(R^2)$. This implies that the monopole drive term, $\mathbf{p} \cdot \mathbf{V}_{\mathrm{m}}(\mathbf{R}) = (\mathbf{p} \cdot \mathbf{R})\tilde{V}_{\mathrm{m}}(R^2)$, lies in the $m = 0$ representation of $\hat{S}_z$, i.e. $\hat{S}_z[\mathbf{p} \cdot \mathbf{V}_{\mathrm{m}}(\mathbf{R})] = 0$. This symmetry is preserved by $\mathcal{L}_{f(b)}$, so that $\tilde{\Psi}_\alpha = 0$ unless Ψ_α is also a $m = 0$ representation. Therefore, we may choose Ψ_α from the the $m = 0$ subspace of $\mathcal{F}_\Psi$ (similarly for Θ). A simple complete basis for smooth functions in the $m = 0$ representation is:

$$\Psi_\alpha = \Theta_\alpha = \omega^{l_\alpha}\, R^{2m_\alpha}\, p^{2n_\alpha}\, (\mathbf{p} \cdot \mathbf{R})^{k_\alpha}, \qquad l_\alpha, k_\alpha, n_\alpha, k_\alpha = 0,\, 1,\, \ldots \tag{4.248}$$

In practice, we truncate the monopole basis at order M by keeping all basis functions such that $k + m + n \le M$, and $l \le L$, resulting in a basis set of size $(L+1)(M+1)(M+2)(M+3)/6$.

The quadrupole mode is excited by an external perturbation with a profile $u(\mathbf{R}) \sim X^2 - Y^2$, so that $\mathbf{V}(\mathbf{R})$ can be generally written as:

$$\mathbf{V}_q(\mathbf{R}) = \tilde{V}_q(R^2)\, (X\hat{x} - Y\hat{y}). \tag{4.249}$$

The quadrupole drive term $\mathbf{p} \cdot \mathbf{V}_q(\mathbf{R})$ is then proportional to $Xp_x - Yp_y$ and belongs to the $m = 2$ representation of $\hat{S}_z$. Again, the selection rule implies that we may choose Ψ_α and Θ_α from $m = 2$

---

[10]We assume that the homogeneous problem (i.e. the problem with vanishing initial term) only has the trivial $\Psi = \Theta = 0$ solution. In other words, the ground state is non-degenerate.

representations. A complete basis for such functions is given by:

$$\Psi_\alpha = \Theta_\alpha = \omega^{l_\alpha}\,\xi_{i_\alpha}\,R^{2m_\alpha}\,p^{2n_\alpha}\,(\mathbf{p}\cdot\mathbf{R})^{k_\alpha}, \qquad i_\alpha = 1,\,2,\,3, \qquad l_\alpha, k_\alpha, n_\alpha, k_\alpha = 0,\,1,\,\dots$$

(4.250)

where:

$$\xi_1 \equiv X^2 - Y^2, \qquad \xi_2 \equiv X p_x - Y p_y, \quad \xi_3 \equiv p_x^2 - p_y^2. \tag{4.251}$$

This set of basis functions may be further reduced in light of the relation $2(\mathbf{R}\cdot\mathbf{p})\xi_2 = p^2\xi_1 + R^2\xi_3$. Again, we truncate the basis functions at order M by requiring $k+m+n \le M-1$, and $l \le L$. The size of the basis set (excluding the redundant ones mentioned above) is $(L+1)M(M+1)(2M+7)/6$.

We note that the above basis functions are L^2 with respect to the inner product given in Eq. (4.245) due to the exponentially bounded measure of the inner product.

4.6.4 Trap response functions

We discussed the method of moments for solving the T-matrix kinetic equations for systems in isotropic traps. Once $\tilde{\Psi}$ and $\tilde{\Theta}$ are calculated, the linear change in the number density $\delta\tilde{n}_\sigma(\Omega, \mathbf{R})$ can be readily evaluated using Eq. (4.229). The impulse response of an observable $O(\mathbf{R})$ in the Laplace domain is given by:

$$\chi_O(\Omega) \equiv \int_{0+}^{\infty} dT\, e^{i\Omega T}\,\langle O\rangle_T = \sum_\sigma \int d^d\mathbf{R}\, O(\mathbf{R})\,\delta\tilde{n}_\sigma(\Omega, \mathbf{R}). \tag{4.252}$$

Two useful quantities often measured in experiments with trapped gases is the spread of the gas in the trap, $O(\mathbf{R}) = X^2 + Y^2$, and the anisotropy of the gas $O(\mathbf{R}) = X^2 - Y^2$. The former observable is useful for monitoring the dynamics following an isotropic (monopole) trap perturbation, while the latter is useful for anisotropic (quadrupole) perturbations. We define the trap *monopole* and *quadrupole* response functions as:

$$\text{monopole}: \quad \chi_{x^2+y^2}(\Omega) = \frac{1}{u_0}\sum_\sigma \int d^d\mathbf{R}\,\left(X^2 + Y^2\right)\delta\tilde{n}_\sigma(\Omega, \mathbf{R})\Big|_{u(\mathbf{R})=u_0(X^2+Y^2)}, \tag{4.253a}$$

$$\text{quadrupole}: \quad \chi_{x^2-y^2}(\Omega) = \frac{1}{u_0} \sum_\sigma \int \mathrm{d}^d\mathbf{R} \left(X^2 - Y^2 \right) \delta\tilde{n}_\sigma(\Omega, \mathbf{R}) \Big|_{u(\mathbf{R})=u_0(X^2-Y^2)}. \quad (4.253b)$$

Both of these response functions may be expressed in terms of the retarded density-density response function:

$$\chi_{x^2\pm y^2}(\Omega) = \int_0^\infty \mathrm{d}t \, e^{i\Omega t} \int \mathrm{d}^d\mathbf{R} \, \mathrm{d}^d\mathbf{R}' \, \mathrm{d}t' \left(X^2 \pm Y^2 \right) \chi^+_{dd}(\mathbf{R}, \mathbf{R}'; t-t') \left(X'^2 \pm Y'^2 \right) \delta(t')$$

$$= \int \mathrm{d}^d\mathbf{R} \, \mathrm{d}^d\mathbf{R}' \left(X^2 \pm Y^2 \right) \chi^+_{dd}(\mathbf{R}, \mathbf{R}'; \Omega) \left(X'^2 \pm Y'^2 \right). \quad (4.254)$$

The imaginary part of the trap response function at a frequency Ω has the usual interpretation of the energy absorption rate at that frequency [106].

4.6.5   The longitudinal f-sum rule for trap response functions

As mentioned in Sec. 1.4, conservation laws associated to gauge invariances impose sum rules on equilibrium response functions. In particular, the $U(1)$ gauge invariance and the associated conservation of particle number imposes the well-known *longitudinal f-sum rule* on the retarded density-density response function, which can be written in its most general form as:

$$\int_{-\infty}^{\infty} \mathrm{d}\omega \, \omega \, \chi^+_{dd}(\mathbf{r}_1, \mathbf{r}_2; \omega) = -\frac{i\pi}{m} \nabla_{\mathbf{r}_1} \cdot \nabla_{\mathbf{r}_2} \left[n_0(\mathbf{r}_2) \, \delta^d(\mathbf{r}_1 - \mathbf{r}_2) \right], \quad (4.255)$$

where $n_0(\mathbf{r})$ is the equilibrium density. The f-sum rule can be utilized to find sum rules associated to the trap response functions. To this end, we multiply the sides of Eq. (4.254) by Ω and integrate:

$$\int_{-\infty}^{\infty} \mathrm{d}\Omega \, \Omega \, \chi_{x^2\pm y^2}(\Omega) = -\frac{i\pi}{m} \int \mathrm{d}^d\mathbf{R} \, n_0(\mathbf{R}) \left| \nabla(X^2 \pm Y^2) \right|^2, \quad (4.256)$$

where the right hand side is written using Eq. (4.255). The above sum rule can be further simplified to:

$$-\int_0^\infty \mathrm{d}\Omega \, \Omega \, \Im[\chi_{x^2\pm y^2}(\Omega)] = \frac{2\pi}{m} \int \mathrm{d}^d\mathbf{R} \, n_0(\mathbf{R}) \left(X^2 + Y^2 \right). \quad (4.257)$$

If the confining potential is a spin-independent harmonic potential, i.e. $U_\sigma(\mathbf{R}) = m\omega_0^2(X^2+Y^2)/2$, the right hand side is simply $4\pi\langle U_0\rangle/(m\omega_0^2)$. The above sum rule simply states that the the sum of

absorbed energy for all frequencies is proportional to the initial potential energy of the particles in the trap. The sum rules are surprisingly the same for both monopole and quadrupole trap response functions. We will utilize this sum rule later as a consistency check for the approximations and the numerical calculations.

4.6.6   Numerical results

The quantum kinetic formalism is the ideal platform for studying the quantum dynamics of weakly inhomogeneous systems. The separation of microscopic and macroscopic scales is incorporated into the formalism from the outset, leaving no room for further simplification of the evolution equations without breaking the fundamental conservation laws. Solving the quantum kinetic equations for realistic Φ-derivable approximations, however, can still be a challenging task. The difficulty is two-fold for complicated approximations such as SCTMA: on the one hand, calculating the equilibrium state requires the self-consistent solution of the coupled Dyson's equation for the Green's function and the T-matrix. On the other hand, the quantum transport equations do not obey the mass-shell condition and demand treating the microscopic energy and momentum on a equal footing. The added dimension significantly increase the complexity of the numerical routines.

In this section, we give a preliminary account of the numerical solution of the T-matrix quantum kinetic equations toward studying the collective modes of attractive Fermi gases in isotropic traps. At the moment, a fully self-consistent calculation is not available to us. We have used a number of the approximations discussed in the previous sections to obtain the first proof-of-the-concept results. We leave the full self-consistent calculations to future works. Some of the utilized approximations inevitably break the conservation laws. The severity of these violations can be assessed by checking the sum rules. We will show that the obtained approximate results, nevertheless, are in excellent agreement with the experiments of Ref. [18].

We restrict our analysis to the weak- to intermediate-coupling regime $\epsilon_b/\epsilon_F \lesssim 1$ where the fermionic formulation of the quantum transport equations can be utilized reliably (cf. Sec. 4.5.3). We further introduce additional approximations in the spirit of the weak-coupling limit: (1) we use the equilibrium spectral functions obtained within the $G_0 G_0$ approximation, (2) since non-self-consistent equilibrium spectral functions are utilized, the self-consistently generated self-energy terms in the linearized kinetic equation must also be neglected. The collision integral may also be treated within the ωBGK scheme, which is obtained by neglecting the non-hydrodynamical corrections to the self-energy. In fact, maintaining self-consistency in calculating self-energies is immaterial in the weak-coupling regime and the above assumptions are reasonable to leading order in the strength of interactions. However, they clearly become questionable as the couplings grow larger. To summarize, the kinetic equation we solve here reads as:

$$
\mathsf{G}_f \left[-i\Omega\gamma_{f,\omega}\tilde{\Psi} + \gamma_{f,p}\frac{\mathbf{p}}{m}\cdot\partial_{\mathbf{R}}\tilde{\Psi} - \gamma_{f,\mu}\,\partial_{\mathbf{R}}U(\mathbf{R})\cdot\partial_{\mathbf{p}}\tilde{\Psi} \right] - \delta\mathsf{C}_f^{\omega\mathrm{BGK}}[\tilde{\Psi}] = -\mathsf{G}_f\,\gamma_{f,p},\mathbf{p}\cdot\mathbf{V}(\mathbf{R}).
$$

(4.258)

Despite the approximations built into the above equation, it improves the Boltzmann equation in several important ways. First of all, the above equation does not rely on the existence of quasi-particles and can describe the non-Fermi-liquid aspects of the intermediate-coupling regime. The above equation reduces to the Boltzmann equation in the limit $\epsilon_b/\epsilon_F \to 0$. We focus on quadrupole oscillations excited by a disturbance $u(\mathbf{R}) \sim X^2 - Y^2$ and solve the kinetic equation using the generalized method of moments proposed in the previous section. The quadrupole basis functions are truncated by keeping the first joint 6 moments of p and R, and up to 5 moments of ω. We found that the solutions rapidly converge within a 2% tolerance by including as few as 4 joint moments of p and R and just the first two moments of ω.

Fig. 4.15 shows the obtained quadrupole response functions at two different temperatures $T/T_F = 0.5$ and $T/T_F = 1$. In both cases, we have set $N_{\mathrm{tot.}} = 3600$. The satisfaction of the trap f-sum rule is assessed in Fig. 4.16. The horizontal dashed line in Fig. 4.15 indicates the largest bind-
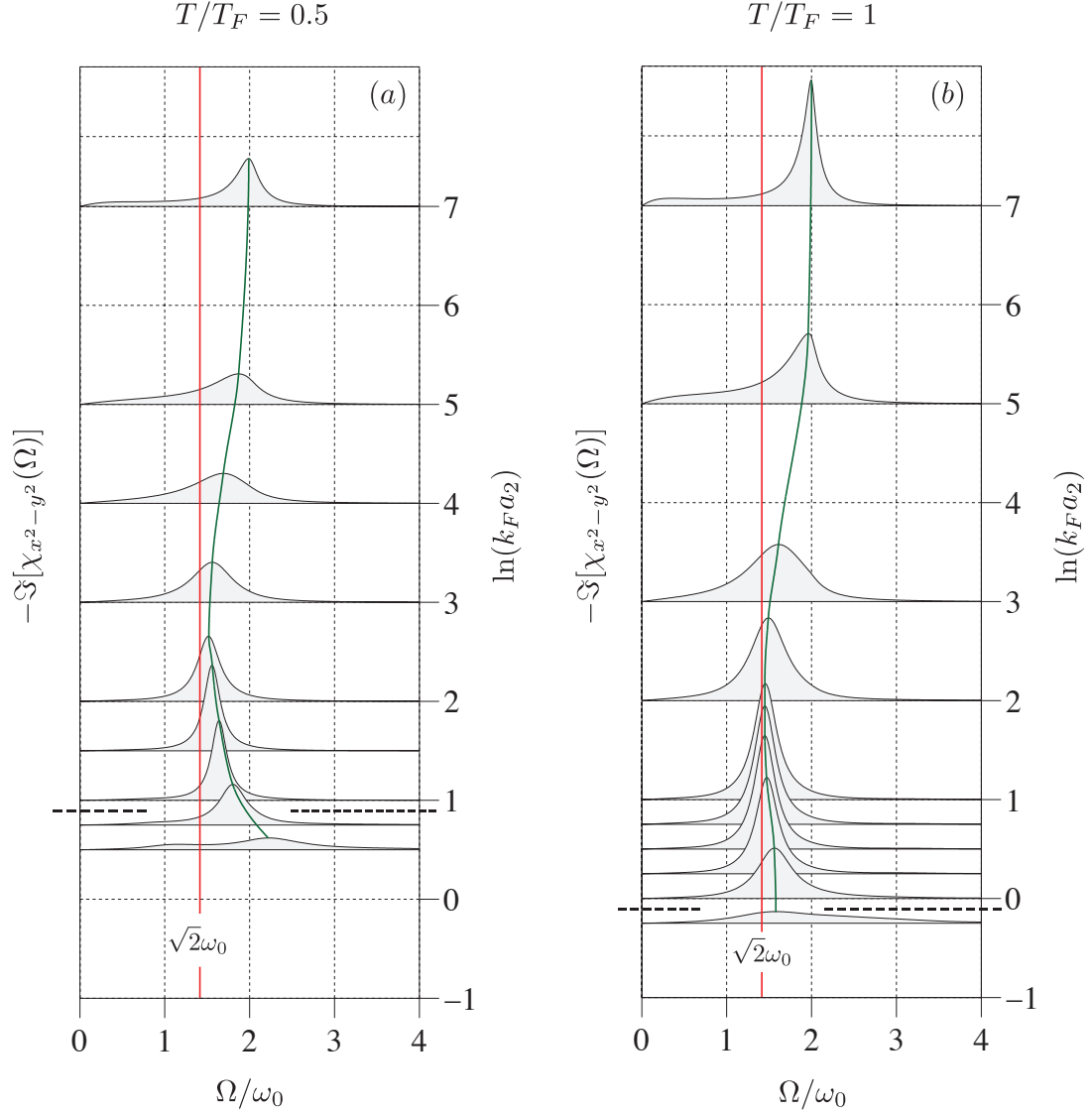
Figure 4.15: The imaginary part of the quadrupole trap response function at (a) $T/T_F = 0.5$ and (b) $T/T_F = 1$. $N_{\text{tot.}} = 3600$ in both cases. The vertical axis shows the value of the interaction parameter $\ln(k_F a_2)$. The units of the response function is arbitrary and the same in all plots. The red line shows the hydrodynamical limit of the oscillation frequency $\Omega_{\text{HD}} = \sqrt{2}\omega_0$. The green line traces the peak of the response functions. The dashed lines indicate the approximate point below which the violation of the f-sum rule exceeds an arbitrary 10% tolerance.

ing energy above which the violation of the f-sum rule exceeds an arbitrary 10% tolerance. Despite

the drastic approximations built into Eq. (4.258), the f-sum rule is found to be satisfied well for most

of the numerical data points. The violation of the sum rule is most likely associated to neglecting

self-consistent self-energy corrections as we argue below. We note that the spurious Bose conden-

sation as predicted by the $G_0 G_0$ approximation is also associated to the lack of self-consistency.

The obtained results exhibit the expected behavior. For weak interactions, the response function is
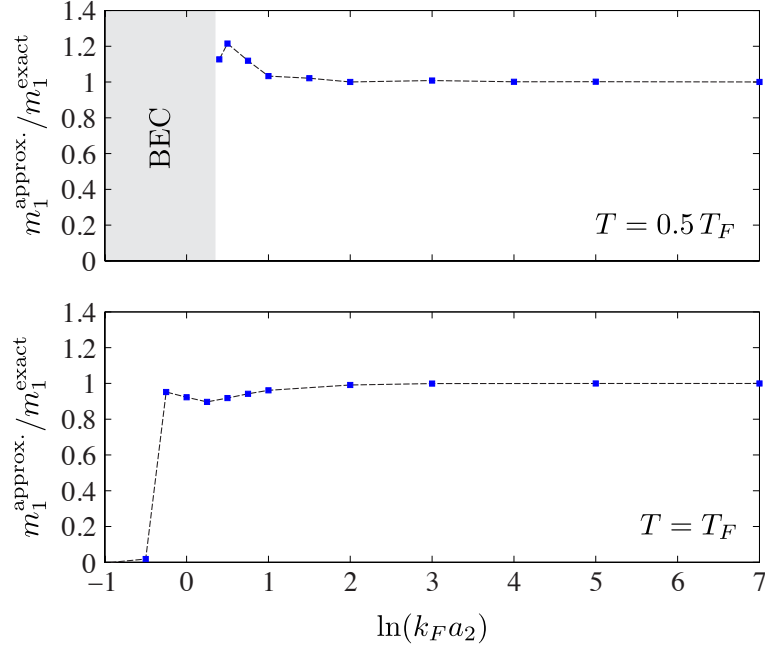

Figure 4.16: The degree of satisfaction of the trap longitudinal f-sum rule vs. the interaction param-
eter $\ln(k_F a_2)$ at $T/T_F = 0.5$ and 1. m_1^{approx} is the first moment of the quadrupole trap response
function directly calculated from the numerically obtained quadrupole response function (left hand
side of Eq. (4.257)) while m_1^{approx} is the value provided by the f-sum rule. The f-sum rule is sat-
isfied within a 10% tolerance up to $\ln(k_F a_2) \simeq 1$ at $T/T_F = 0.5$ and up to $\ln(k_F a_2) \simeq -0.25$ at
$T/T_F = 1$. The gray area in the top plot, $\ln(k_F a_2) \lesssim 0.39$, corresponds to the regime where $G_0 G_0$
approximation (spuriously) indicates transition to a BEC state (cf. Fig. 4.11).

peaked in the frequency at $\Omega \simeq 2\omega_0$, the quadrupole oscillation frequency of a non-interacting gas

in a harmonic potential. The response functions broaden upon increasing the binding energy while

the peak frequency shifts to lower values, a behavior associated to the transition from collisionless

(CL) to the hydrodynamic (HD) regime. During the transition, the collision rate is not fast enough to

maintain the local equilibrium and leads to dissipation of the collective oscillations. Upon increas-

ing the binding energy further, the response functions become sharp again around $\ln(k_F a_2) \simeq 2$

with a peak near $\Omega_{\text{HD}} = \sqrt{2}\omega_0$. In this regime, the collision rate exceeds the frequency of collec-

tive oscillations and maintain the local equilibrium condition and the dynamics is described well by the ideal HD equations. The mode with $\sqrt{2}\omega_0$ is the universal oscillation frequency of the HD quadrupole surface mode (cf. Sec. B.1). Upon increasing the binding energy further, we observe a setback from the HD regime, signaled by the broadening of the response function and the increase in the peak frequency.
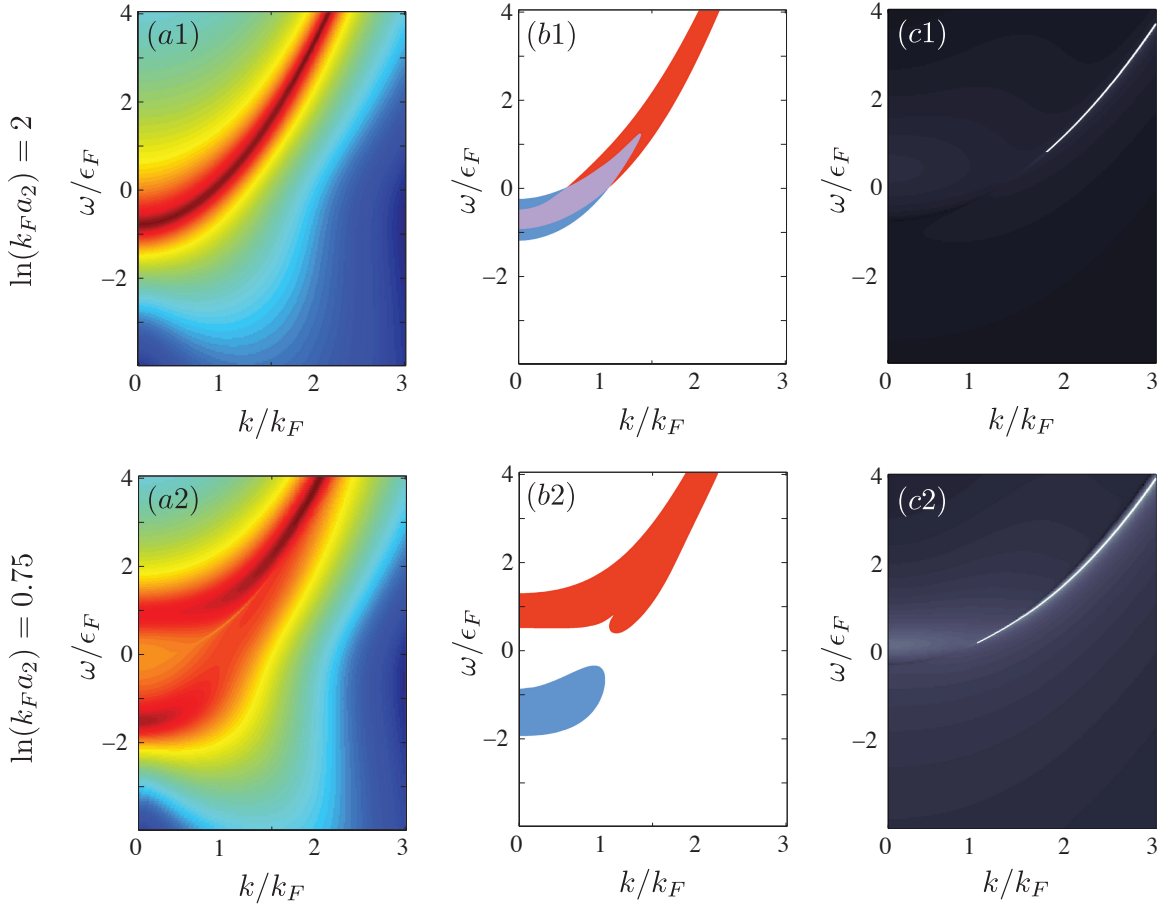

Figure 4.17: The fermionic spectral function $A(\omega, \mathbf{p})$ (a1, a2), the high probability regions for particle (blue) and hole (red) states (b1, b2) and amplitude of the retarded many-body T-matrix $|T^+|^2$ (c1, c2) for $\ln(k_F a_2) = 2$ (top) and 1 (bottom). The shown quantities are calculated at the center of a trap with $N_{\text{tot.}} = 3600$ particles and at a temperature $T = 0.5\,T_F$. The white lines in (c1) and (c2) show the location of the bound state. The blue and red regions in (b1, b2) are obtained from the conditions $\epsilon_F^{-1} A f_0 > 1$ and $\epsilon_F^{-1} A(1 - f_0) > 1$, respectively.

As discussed in the introduction, the re-entrance to the collisionless regime in the strong-

coupling regime can be explained on the basis of emergence of the propagating bound pairs and the weak interaction between them. The approximations used to obtain Eq. (4.258), however, are only justified in the weak-coupling regime. In particular, Eq. (4.258) does not account for the propagation of bosonic fluctuations. However, according to Fig. 4.15, the setback from the HD regime at $T/T_F = 0.5$ occurs as soon as $\ln(k_F a_2) \lesssim 2$. The validity of the weak-coupling approach can be assessed by calculating the decay rate of bosonic fluctuations from Eq. (4.154), which implies $\tau_b^{-1} = c_0/\gamma_2 = -(8T/\pi)/\ln(T_c/T)$, where $T_c = (e^\gamma/\pi)\sqrt{2\epsilon_b\epsilon_F(\mathbf{R})}$ and $\epsilon_F(\mathbf{R}) = \sqrt{2\pi n(\mathbf{R})}$ is the local Fermi energy. The decay rate is largest at the center of the trap and using the results shown in Fig. 4.12, we find $\epsilon_F(0) \sim 0.8\epsilon_F$ in the window $1 \lesssim \ln(k_F a_d) \lesssim 2$. This gives a maximum decay rate τ_b^{-1} ranging from $\sim 1.5\,\epsilon_F$ to $\sim 0.4\,\epsilon_F$. This rate is still much higher than the frequency of the trap collective modes set by $\omega_0 = \epsilon_F/\sqrt{N_{\text{tot.}}} \sim 0.02\,\epsilon_F$, indicating that the bosonic fluctuations are highly diffusive. The diffusive dynamics of bosons is described well by the weak-coupling fermionic kinetic equation used here. On the other hand, Fig. 4.16 shows that the f-sum rule is satisfied within a 5% tolerance in the window $1 \lesssim \ln(k_F a_d) \lesssim 2$, which is another indication for the soundness of the used approximations. Therefore, the setback from HD regime may in fact be described without resorting to the picture of propagating bosons. In fact, our analysis suggests that the setback may occur well *before* the bosonic fluctuations become long-lived and propagating.

To shed some light into this matter, we have plotted the spectral function, the retarded (many-body) T-matrix and the regions with high probability of particle and hole excitations in Fig. 4.17 for two different interaction parameters $\ln(k_F a_2) = 2$ and 0.75, corresponding to the peak of the HD regime and the setback regime, respectively. These quantities are calculated at the center of the trap as a representative point.

Fig. 4.17(a1) shows that the Fermi surface is virtually intact in the regime that is most hydro-dynamical, $\ln(k_F a_2) = 2$, save for the thermal and collisional smearing. There is a large overlap between particle and hole states near $\omega \approx 0$ and for k ranging from 0 to $\sim 2k_F$ (see Fig. 4.17b1).

The large overlap between the particle and hole states results in a large energy-momentum phase space density for scatterings at the energy-momentum pairs where $|T^+|^2$ is large. We note that both the bound state and the scattering states contribute to $|T^+|^2$. The effective Pauli blocking of low-momentum states, however, destroys the bound state with small center of mass momentum and the bound state appears above a momentum threshold $k \gtrsim 2k_F$ (see Fig. 4.17c1).

Upon increasing the binding energy, the scattering amplitude $|T^+|^2$ generally grows larger. Furthermore, the increased binding energy reduces the energy-momentum threshold for the existence of the bound state. This scenario, however, has a feedback on fermions and results in a significant modification of the fermionic spectral function. The emergence of the low-energy bound-state reduces the spectral weight of low-energy fermionic states, resulting in a separation between the particle and hole branches (see Fig. 4.17a2 and b2). This is precisely the pairing pseudogap discussed earlier. Despite the increased scattering amplitude, the weak overlap between the available particle and hole states in the pseudogap regime will reduce the available phase space density for scattering events (compare to the BCS state). The reduced phase space density may overshadow the increase in the scattering amplitude, resulting in an overall decrease in the collision rate. While the above argument shows the plausibility of the setback from the HD regime due to the appearance of the pairing pseudogap, the final verdict of the competition between the reduced scattering phase space and the stronger scattering amplitude generally depends sensitively on the used approximations. In particular, the size of the pseudogap significantly varies from one many-body approximation to the other [200]. Therefore, at the moment, we can not confidently obviate the possibility of a change in this behavior upon promoting the current calculations to a fully self-consistent calculation.

We conclude this section by finally comparing the predictions of the present calculations with results of the recent experiments done by M. Köhl's group at the University of Cambridge [18]. We
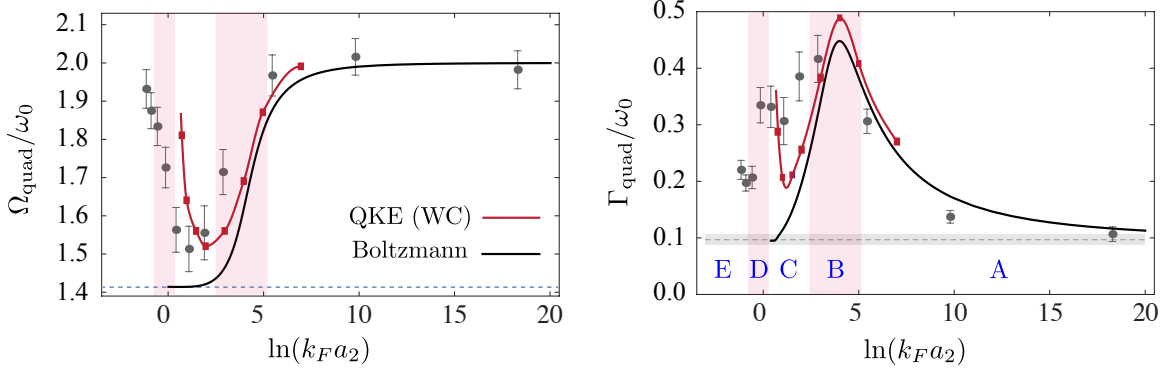
Figure 4.18: The comparison of the oscillation frequency and damping of the quadrupole mode between the theory and the experiment. The dots correspond to the experimental measurements reported in Ref. [18, 157] using a 50/50 mixture of the two hyperfine states $|F = 9/2, m = -9/2\rangle$ and $|F = 9/2, m = -7/2\rangle$ of ^{40}K atoms. The interaction parameter is calculated from Eq. (4.6) using the s-wave scattering length a_s and the transverse trap frequency ω_z. The black lines corresponds to the prediction of the quasiparticle Boltzmann equation within the T-matrix approximation from Ref. [157]. The red line shows the present calculations based on the weak-coupling limit of the quantum kinetic equations. The various dynamical regimes are indicated on the plots (A, B, C, D, and E). A: collisionless transport of single fermions, B: highly dissipative dynamics as a matter of crossover from collisionless single fermion transport to the hydrodynamical regime, C: (nearly ideal) hydrodynamical regime, D: highly dissipative crossover from the hydrodynamical regime to the collisionless transport of bound pairs, E: collisionless transport of bound pairs (cf. the text and Fig. 4.4b for further explanations).

extract the peak frequency and damping of the quadrupole oscillations from the results shown in

Fig. 4.15(a) by fitting the calculated response functions to a two-mode Lorenzian:

$$\chi_{X^2-Y^2}(\Omega) = \frac{\mathcal{A}}{\Omega - \Omega_{\text{quad}} - i\Gamma_{\text{quad}}} - \frac{\mathcal{A}^*}{\Omega + \Omega_{\text{quad}} - i\Gamma_{\text{quad}}} + \frac{i\mathcal{B}}{\Omega - i\Gamma'_{\text{quad}}}, \qquad (4.259)$$

corresponding to a damped oscillatory mode with frequency $\Omega_{\text{quad}} + i\Gamma_{\text{quad}}$ and an over-damped

component with a damping rate Γ'_{quad}. The above model function was found to give excellent fits

to the numerical results. We extract the experimental data points from Ref. [157]. The experimental

estimates for $N_{\text{tot.}}$ and T/T_F are $\sim 4000\pm400$ and $\sim 0.47\pm0.04$, respectively, closely matching the

parameters used here for low-temperature numerical data series ($N_{\text{tot.}} = 3600$ and $T/T_F = 0.5$).

Fig. 4.18 shows the experimental data (dots) and results from the present theory (red squares

and lines) along with the prediction of the quasiparticle Boltzmann equation with the many-body

T-matrix (black lines). We find that the present theory is an excellent agreement with the experimental results, correctly reproducing the crossover from collisionless to the HD regime followed by the setback from the HD regime. As argued earlier, the setback form the HD regime is a novel feature of the system in the pseudogap regime, and may only be described using genuinely quantum kinetic equations which can account for broad off-shell particle resonances. The Boltzmann limit is achieved when long-lived quasiparticles exists.

We finally note that extrapolation of the results to the strong-coupling limit requires a fully self-consistent treatment of the kinetic equations, including the memory effects associated to the long-lived bosonic fluctuations. As shown in Sec. 4.5.3, the derived kinetic equations reduce to the Boltzmann equation for long-lived composite bosons in the strong-coupling limit in principle, implying that $\Omega_{\mathrm{quad}} \to 2\omega_0$ and $\Gamma_{\mathrm{quad}} \to 0$ in the limit $\ln(k_F a_2) \to -\infty$. We already see indications of this behavior in the experimental data shown in Fig. 4.18.

4.7   Beyond the self-consistent T-matrix approximation

The SCTMA provides a simple and intuitively appealing account of the physics of the two-component attractive Fermi gas. In fact, the spectrum of physical phenomena described by the SCTMA is remarkably rich for an approximation that only takes the simplest fluctuation exchange diagram into account. This degree of simplicity, however, comes with inevitable shortcomings, the most important of which is the poor description of the interaction between the composite bosons.

As discussed in Sec. 4.4, the strong-coupling limit of the SCTMA reduces to a mean-field theory for composite bosons in the strong-coupling limit, with an effective interaction described by the BOX diagram. In $d = 3$, this implies a short-range boson-boson interaction $U_{\mathrm{BB}} = 4\pi(2a_s)/(2m)$ (in the momentum space), corresponding to an effective scattering length $a_B = 2a_s$ between the bosons, a previously known result [212, 213]. This picture is physically reasonable since $U_{\mathrm{BB}} \to 0$

in the limit $\epsilon_b = 1/(ma_s^2) \to \infty$. In $d = 2$, on the other hand, we found $U_{\mathrm{BB}} = 8\pi/m$, independent of the binding energy. There is no physical basis to this result and it is in fact an artifact of the mean-field description of the boson-boson interaction.

The difference between $d = 2$ and $d = 3$ can be traced back to the larger residue at the bound-state pole of the T-matrix in $d = 2$ compared to $d = 3$ (cf. Eq. 4.99; the weight of the bound state is $\propto \epsilon_b$ and $\epsilon_b^{1/2}$ in $d = 2$ and $d = 3$, respectively; this is in turn associated to the fact that the bound state wave function decays like $e^{-r/a_2}/\sqrt{r}$ for large r in $d = 2$ compared to $e^{-r/a_s}/r$ in $d = 3$).

In this section, we continue the line of thought initiated in Sec. 4.4 and propose a Φ-derivable approximation that resolves this unphysical behavior of the SCTMA in $d = 2$ while it is powerful enough to describe the BKT physics. Our approach is to add a class of *missing* diagrams to SCTMA so that the resulting approximation reduces the *exact* composite boson-boson interaction in the few-body limit where the vacuum includes only two composite bosons (four fermions). In $d = 3$, a careful analysis of the composite boson-boson interaction in vacuum gives $a_B^{\mathrm{exact}} = 0.6a_s$ [227, 228], a result which is only a numerical improvement over the SCTMA prediction of $a_B = 2a_s$. Therefore, the we do not expect the improvements we propose here to be consequential to the physics of AFG in $d = 3$, which is already described well by the SCTMA.

The situation is different in $d = 2$, where the SCTMA has an pathological behavior and must be fixed. Earlier in Sec. 4.2.3, we presented a simple 1-loop RG analysis showing that the repulsive short-range interaction in $d = 2$ between the bosons is marginal and their IR asymptotic freedom requires quantum corrections. We further showed in Sec. 4.4 that the 1-loop RG result can be reproduced by simply including the scattering between the bosons in the particle-particle channel to all orders. Therefore, a required ingredient of a correct Φ-derivable approximation is the inclusion of such processes.

The problem of composite boson-boson interaction in vacuum has been solved exactly by Brodsky *et al.* [214] using a diagrammatic interpretation of the Faddeev-Yakubovsky equations. Such a diagrammatic analysis can be easily adapted to the many-body problem. Let us briefly review the diagrammatic analysis of Brodsky *et al.*. As a first step, the fermion-boson scattering vertex, T_3, is constructed according to the equation:

$$\tag{4.260}$$

The first diagram is the twisted BOX diagram and constitutes the elementary fermion-boson interaction vertex. In the analysis of Brodsky *et al.*, the fermion and boson lines correspond to the vacuum fermion propagator and the vacuum T-matrix, respectively. The elementary boson-boson interaction vertex is calculated using T_3 as follows:

$$\tag{4.261}$$

where the summation is over the diagrams within the class shown in the square brackets. The full boson-boson vertex is finally found by summing the ladder diagrams built from U_{BB} similar to the analysis provided in Sec. 4.4.

The above diagrammatic formalism can be directly adapted to the many-body problem by simply promoting the vacuum fermion propagators to fully dressed Green's functions, and the vacuum T-matrix to the many-body T-matrix. By doing so, it is guaranteed that the resulting approximation becomes exact in the limit of two composite bosons in vacuum (in the same way that SCTMA is exact for two fermions in vacuum). We propose the following Luttinger-Ward functional based on the above considerations:

$$\tag{4.262}$$

We refer to the above approximation as the *4-particle self-consistent* (4PSC) approximation. Here, we have used the auxiliary field formalism of Sec. 4.5.4. The purely fermionic Luttinger-Ward functional can be found by replacing the boson propagators (double lines) with the expanded T-matrix diagrams. The first vacuum diagram coincides with the SCTMA. The higher order diagrams describe the T-matrix for bosons constructed by taking U_{BB} as the irreducible interaction vertex. The symmetry factor affixed to a boson-boson vacuum diagram with n U_{BB} insertions is $1/(2n)$ and is due to the $\mathbb{Z}_n$ rotation degeneracy of such a diagram. All of the above diagrams are 2PI, except for the diagram with a single U_{BB} insertion of the twisted BOX type, which must be removed from $\tilde{\Phi}_{\mathrm{4PSC}}[\mathcal{G}, \mathsf{T}]$.

The 4PSC scheme is a powerful, yet complicated approximation. As discussed in Sec. 4.4, the unphysical behavior of the SCTMA is lifted even if we replace U_{BB} with the elementary boson-boson interaction vertex, i.e. the twisted BOX diagram. The resulting approximation, however, does not reduce to the exact Faddeev-Yakubovsky equation in the 4-particle limit.

Finally, we remark that Stoof *et al.* have shown that the T-matrix approximation for bosons describes the BKT transition accurately in the dilute limit $\ln(1/na_2^2) \gg 1$ [232]. By construction, the 4PSC approximation reduces to the T-matrix approximation for the composite bosons in the strong-coupling limit and therefore, it will also provide an accurate description of the BKT physics. We leave the study of the 4PSC approximation to future works.

4.8   Summary and outlook

We started with a brief review of the physics of attractive Fermi gases using the paradigmatic BCS, Landau-Ginzburg and NSR calculations in Sec. 4.2. In Sec. 4.3, we discussed the adaptation of the self-consistent T-matrix approximation (SCTMA) in the normal state to non-equilibrium states using the Schwinger-Keldysh real-time formalism. We paid particular attention to the renor-

malization of the non-equilibrium T-matrix.

As a first step, we studied the weak- and strong-coupling limits of SCTMA at equilibrium ($\epsilon_b/\epsilon_F \to \infty$ and $\epsilon_b/\epsilon_F \to 0$, respectively), in particular, from the vantage point of linear response diagrams in Sec. 4.4. We pointed out a major difference between $d = 2$ and $d = 3$ cases in the strong-coupling limit. In $d = 3$, SCTMA reduces to the description of a non-interacting Bose gas as long as $T > T_{\mathrm{BEC}}^{\mathrm{3D}} = 4\pi(n/2)^{2/3}[\zeta(3/2)]^{-2/3}$, as also previously shown in Refs. [212, 211]. The strong-coupling analysis was found to dramatically differ in $d = 2$ since the repulsion between the composite bosons, as described by the SCTMA, becomes independent of ϵ_b and the bosons are not described as free even in the limit $\epsilon_b \to \infty$. We ascribed this unphysical behavior to the absence of multiple scatterings between the composite bosons within SCTMA, and demonstrated how their inclusion resolves the issue (cf. Sec. 4.4).

The novel contribution of this chapter is the derivation of the exact quantum kinetic equations based on the SCTMA in Sec. 4.5. By emphasizing on the important role of memory effects, we departed from the conventional methods of incorporating the memory effects (generalized Kadanoff-Baym ansatz, non-Markovian correction terms). Instead, we promoted the Dyson equation for the T-matrix to a separate quantum kinetic equation and introduced a bosonic distribution function $b(\omega, \mathbf{p}; T, \mathbf{R})$ using the spectral/statistical decomposition of the T-matrix. Our formalism resulted in two kinetic equations which describe the fermionic and bosonic degrees of freedom on an equal footing, and rigorously respect the conservation laws. In the weak-coupling limit, we showed that b describes local (memoryless) bosonic fluctuations and is determined by the instantaneous distribution of fermions. In this limit, we recover the conventional Markovian single kinetic equation for the fermion distribution function $f(\omega, \mathbf{p}; T, \mathbf{R})$. The character of b smoothly changes as the binding energy is increased. Eventually, all of the fermions pair up into long-lived singlet bound states and b describes the energy distribution of such long-lived composite bosons. The kinetic equations reduces to a quasiparticle-like Boltzmann equation for b and describe the dynamics of nearly-free

composite bosons. For intermediate couplings $\epsilon_b \sim \epsilon_F \sim T$, the kinetic equations for f and b are coupled to each other, describing the inter-relation between the paired and unpaired fermions whose lifetimes are comparable to each other.

We described a general strategy for solving the linearized quantum kinetic equations in Sec. 4.6, in particular, in the context of experiments with ultracold atoms in optical traps. The analysis was carried out in two stages, i.e. the short-time preparation of the non-equilibrium state from an initial thermal state, followed by the long-time kinetic evolution of the disturbed quantum gas. A generalization of the method of moments was proposed in Sec. 4.6.3 as a practical numerical method for solving the linearized quantum kinetic equations in confined geometries.

We presented a preliminary account of the numerical solution of the linearized quantum kinetic equation in Sec. 4.6.6 by introducing certain simplifying approximations. We analyzed the quadrupole oscillations of the attractive Fermi gas in 2D harmonic traps and compared our findings with the recent experiments done at the University of Cambridge [18]. We found that the results of the present theory are in excellent agreement with the experiment, exhibiting the transition from collisionless to hydrodynamical regime upon increasing the binding energy, followed by a setback from the hydrodynamical regime upon increasing the binding energy further. We argued that the the last feature may only be described using quantum kinetic equations and are beyond the reach of the widely used quasiparticle-like Boltzmann equation.

We finally proposed a Φ-derivable approximation based on the Faddeev-Yakubovsky equation that fixes the unphysical behavior of SCTMA in $d = 2$ and gives the exact result in the 4-particle limit.

We would like to view the analysis presented in this chapter as the first step of a long journey. The immediate next step is obtaining a fully self-consistent solution of the equilibrium state within the SCTMA in $d = 2$. Although we argued that the SCTMA lacks the processes required for a physically valid description of the system in the strong-coupling regime, it is still important to

know its prediction in this regime as the simplest theory that is known to work surprisingly well in $d = 3$. Once the self-consistent solution is obtained, we would like to revisit the preliminary numerical analysis of the quantum kinetic equations provided here, extrapolate the results to the strong-coupling limit and investigate the dynamics in the pseudogap regime further.

The present work can be extended in various directions. In particular, the introduced core ideas may find applications in other areas of condensed-matter physics. The technique we used to handle the bosonic memory effects is directly adaptable to other types of fluctuation-exchange Φ-derivable approximations such as the FLEX and Parquet approximations. While the bosonic degrees of freedom in the current work is self-consistently generated by fermions (via pairing), similar kinetic equations can be obtained for phenomenological microscopic models that include *physical* bosonic fields coupled to the fermions, such as the electron-phonon system and the two-channel model of the Feshbach resonance.

As a continuation of our work on the attractive Fermi gas, we would like to surpass the SCTMA in $d = 2$ and take steps toward implementing the 4-particle self-consistent (4PSC) approximation proposed in the previous section. Such an analysis allows us to investigate the complicated problem of transport in the BKT phase. We would like to extend the non-equilibrium SCTMA formalism to superconducting states and take steps toward a first-principle derivation of the two-fluid quantum kinetic equations. Last but not the least, extension to disordered systems can be useful toward achieving a better understanding of transport in dirty strongly-correlated superconducting systems.

A

Appendix to Chapter 1

A.1 The Noether's theorem

In this appendix, we provide the exact statement and the proof of the Noether's theorem for completeness.

Theorem: *(Noether's theorem) consider a Lagrangian density $\mathcal{L}(\phi_a, \partial_\mu \phi_a, x^\mu)$ and the classical action given by $\int_\Omega \mathrm{d}^{d+1}x\, \mathcal{L}(\phi_a, \partial_\mu \phi_a, x^\mu)$, where Ω is a given region in the spacetime. Consider*

the following transformation:

$$x^\mu \to \xi^\mu = x^\mu + \epsilon^a X_a^\mu(x),$$

$$\phi_a(x) \to \psi_a(\xi) = \phi_a(x) + \epsilon^b \Phi_{ab}(x),$$

where $X_a^\mu(x)$ and $\Phi_{ab}(x)$ are given fields. Provided that the classical action is invariant under such a transformation to first order in ϵ in the sense $\Delta A(\Omega) = \int_\Omega d^{d+1}x\, \mathcal{L}(\phi_a, \partial_\mu\phi_a, x^\mu) - \int_{\Omega'} d^{d+1}\xi\, \mathcal{L}(\psi_a, \partial_\mu\psi_a, \xi^\mu) = \mathcal{O}(\epsilon^2)$, where Ω' is the image of Ω, then the following currents are conserved, $\partial_\mu j_a^\mu(x) = 0$:

$$j_a^\mu(x) \equiv \frac{\partial \mathcal{L}}{\partial(\partial_\mu\phi_b)}\Phi_{ba}(x) - \left[\frac{\partial \mathcal{L}}{\partial(\partial_\mu\phi_b)}\mathbb{L}_{X_a}\phi_b(x) - X_a^\mu \mathcal{L} \right],$$

where $\mathbb{L}_{X_a}\phi_b(\xi) \equiv X_a^\mu(\xi)\,\partial_\mu\phi_b(\xi)$ is the *Lie derivative* of $\phi_b(x)$ along the vector field $X_b(x)$.

(proof) The proof is elementary. As a first step, we consider the effect of the transformation on the spacetime boundary:

$$\int_{\Omega'} d^{d+1}\xi\, \mathcal{L}(\psi_a, \partial_\mu\psi_a, \xi^\mu) = \int_\Omega d^{d+1}\xi\, \mathcal{L}(\psi_a, \partial_\mu\psi_a, \xi^\mu)$$
$$+ \int_{\partial\Omega} d\sigma_\mu\, \epsilon^a X_a^\mu(x)\, \mathcal{L}(\psi_a, \partial_\mu\psi_a, \xi^\mu) + \mathcal{O}(\epsilon^2), \quad \text{(A.1)}$$

where $d\sigma_\mu$ is the surface differential on $\partial\Omega$, i.e. the boundary of Ω. Changing the dummy integration variable on the integrals from x to ξ and converting the surface integral to a volume integral using the Stokes theorem, the change in the action upon the transformation can be written as:

$$\Delta A(\Omega) = \int_\Omega d^{d+1}x \left[\mathcal{L}(\psi, \partial_\mu\psi, x^\mu) - \mathcal{L}(\phi, \partial_\mu\phi, x^\mu) + \partial_\mu\left(\epsilon^a X_a^\mu(x)\,\mathcal{L}(\psi_a, \partial_\mu\psi_a, \xi^\mu)\right) \right]. \quad \text{(A.2)}$$

We need to be careful with respect to the definition of the field transformation: in the statement of the theorem, the transformed field $\psi(\xi)$ is defined at ξ, however, it is given in terms of fields at x, the pre-image of ξ. It is easy to state the transformation law in terms of the functions of the transformed

coordinates. To find order in ϵ, we find:

$$\psi_a(\xi^\mu) = \phi_a(x^\mu) + \epsilon^b \Phi_{ab}(x^\mu)$$

$$= \phi_a\left(\xi^\mu - \epsilon^b X_b^\mu(\xi)\right) + \epsilon^b \Phi_{ab}(\xi^\mu) + \mathcal{O}(\epsilon^2)$$

$$= \phi_a(\xi^\mu) + \epsilon^b \left[\Phi_{ab}(\xi^\mu) - \mathbb{L}_{X_b}\phi_a(\xi^\mu)\right], \tag{A.3}$$

The Lie derivative $\mathbb{L}_{X_b}$ was defined in the theorem statement. Changing the dummy index ξ^μ to x^μ in the above expression, the difference of the Lagrangian densities in the square brackets in Eq. (A.2) can be written as:

$$\mathcal{L}(\psi, \partial_\mu\psi, x^\mu) - \mathcal{L}(\phi, \partial_\mu\phi, x^\mu) = \frac{\partial\mathcal{L}(\phi, \partial_\mu\phi, x^\mu)}{\partial\phi_a(x)}\Delta\phi_a(x) + \frac{\partial\mathcal{L}(\phi, \partial_\mu\phi, x^\mu)}{\partial(\partial_\mu\phi_a(x))}\partial_\mu(\Delta\phi_a(x))$$

$$= \partial_\mu\left[\frac{\partial\mathcal{L}(\phi, \partial_\mu\phi, x^\mu)}{\partial(\partial_\mu\phi_a(x))}\Delta\phi_a(x)\right] \tag{A.4}$$

where $\Delta\phi_a(x)$ corresponds to the last term in the third line of Eq. (A.3). We have used the Euler-Lagrange equation,

$$\partial_\mu\left[\frac{\partial\mathcal{L}}{\partial(\partial_\mu\phi)}\right] - \frac{\partial\mathcal{L}}{\partial\phi} = 0,$$

to get the second line. Plugging the above result into Eq. (A.2) and assuming that Ω is arbitrary, we reach the sought after conserved current:

$$\partial_\mu j_a^\mu(x) = 0, \qquad j_a^\mu(x) \equiv \frac{\partial\mathcal{L}}{\partial(\partial_\mu\phi_b)}\Phi_{ba}(x) - \left[\frac{\partial\mathcal{L}}{\partial(\partial_\mu\phi_b)}\mathbb{L}_{X_a}\phi_b(x) - X_a^\mu\mathcal{L}\right]. \tag{A.5}$$

Remark: The *energy-momentum tensor* $T_\nu^\mu(x)$ is defined by writing the square bracket in the conserved Noether's current as $T_\nu^\mu X_a^\nu$:

$$T_\nu^\mu(x) \equiv \frac{\partial\mathcal{L}}{\partial(\partial_\mu\phi_b)}\partial_\nu\phi_b(x) - \delta_\nu^\mu\mathcal{L}, \tag{A.6}$$

where δ_ν^μ is the Kronecker's delta. $\qquad\square$

B

Appendix to Chapter 2

B.1 Hydrodynamical surface modes in isotropic harmonic traps: a general proof

A useful experimental signature for the entrance of a quantum fluid to the hydrodynamical regime is the emergence of the so-called *surface modes* in isotropic harmonic traps [100]. The surface modes have universal oscillations frequencies set by the frequency of the harmonic trap. The surface modes correspond to volume-conserving (divergence-less) flows and are driven by the

trap restoring force. As a result, their frequency remains unaffected by the equation of state of the fluid. The existence of the surface modes is shown in Ref. [100] for the non-interacting Bose gas.

Here, we give a general proof valid for all hydrodynamical fluids in $d = 2, 3$ with arbitrary equations of state. Our starting point is the ideal hydrodynamical equations derived in Sec. 2.4:

$$\partial_T n = -\nabla \cdot (n\mathbf{V}), \tag{B.1a}$$

$$M\,\partial_T\,[n\,\mathbf{V}] = -n\,\nabla U - \nabla P - M\nabla\,[n\,\mathbf{V}\mathbf{V}], \tag{B.1b}$$

$$\partial_T\left[\mathcal{E} + \frac{1}{2}nMV^2\right] = -\nabla \cdot \left[\left(\frac{1}{2}nMV^2 + P + \mathcal{E}\right)\mathbf{V}\right] - n\mathbf{V} \cdot \nabla U. \tag{B.1c}$$

In the above equations, n, $\mathbf{V}$, U, P and $\mathcal{E}$ corresponds to the number density, macroscopic velocity, the static trap potential, local pressure and local energy density, respectively. It is assumed that n, $\mathcal{E}$ and P are given as functions of the inverse temperature β and chemical potential μ. It is useful to solve μ for n and using n and β as the independent variables. Therefore, $P \equiv P(n, \beta)$, and $\mathcal{E} \equiv E(n, \beta)$. At equilibrium, $\mathbf{V} = 0$, the temperature $\beta = \beta_0$ is uniform and time derivatives of all quantities vanish. The equilibrium density profile $n_0(\mathbf{R})$ is obtained by setting the right hand side of Eq. (B.1b) to zero:

$$n_0(\mathbf{R})\nabla U(\mathbf{R}) = -\nabla n_0(\mathbf{R})\left(\frac{\partial P}{\partial n}\right)_{n=n_0(\mathbf{R}),\beta=\beta_0}. \tag{B.2}$$

We introduce shorthand notations for the partial derivatives:

$$P_{0,n}(\mathbf{R}) \equiv \left(\frac{\partial P}{\partial n}\right)_{n=n_0(\mathbf{R}),\beta=\beta_0}, \quad P_{0,\beta}(\mathbf{R}) \equiv \left(\frac{\partial P}{\partial \beta}\right)_{n=n_0(\mathbf{R}),\beta=\beta_0},$$

$$\mathcal{E}_{0,n}(\mathbf{R}) \equiv \left(\frac{\partial \mathcal{E}}{\partial n}\right)_{n=n_0(\mathbf{R}),\beta=\beta_0}, \quad \mathcal{E}_{0,\beta}(\mathbf{R}) \equiv \left(\frac{\partial \mathcal{E}}{\partial \beta}\right)_{n=n_0(\mathbf{R}),\beta=\beta_0}. \tag{B.3}$$

As usual, the analysis of the normal modes is done by first linearizing the hydrodynamical equations about the equilibrium state. We define $\delta n \equiv n(T, \mathbf{R}) \equiv n(T, \mathbf{R}) - n_0(\mathbf{R})$, $\delta\beta(T, \mathbf{R}) \equiv \beta(T, \mathbf{R}) - \beta_0$. To linear order in δn, $\delta\beta$ and $\mathbf{V}$, we find:

$$\partial_T \delta n = -\nabla \cdot (n_0\mathbf{V}), \tag{B.4a}$$

$$Mn_0\partial_T\mathbf{V} = -\delta n\,\nabla U - \nabla\left[P_{0,n}\delta n + P_{0,\beta}\delta\beta\right], \tag{B.4b}$$

$$\mathcal{E}_{0,n}\partial_T\delta n + \mathcal{E}_{0,\beta}\partial_T\delta\beta = -(P_{0,n} + \mathcal{E}_{0,n})\nabla n_0\cdot\mathbf{V} - (P_0 + \mathcal{E}_0)\nabla\cdot\mathbf{V} - n_0\mathbf{V}\cdot\nabla U. \tag{B.4c}$$

We omit δn between the three equations and use Eq. (B.2) to simplify the result. A straightforward calculation yields the following two coupled equations for $\mathbf{V}$ and $\delta\beta$:

$$M\partial_T^2\mathbf{V} = -\nabla(\mathbf{V}\cdot\nabla U) + \nabla(P_{0,n}\nabla\cdot\mathbf{V}) - \frac{1}{n_0}\nabla(P_{0,\beta}\,\partial_T\delta\beta), \tag{B.5a}$$

$$\partial_T\delta\beta = -\frac{1}{\mathcal{E}_{0,\beta}}\left(P_0 + \mathcal{E}_0 - n_0\mathcal{E}_{0,n}\right)\nabla\cdot\mathbf{V}. \tag{B.5b}$$

Assuming that $U(\mathbf{R}) = U(R^2)$ is isotropic, the solutions $\mathbf{V}$ will have well-defined quantum numbers associated to the representation of $SO(d)$ on the $(d\text{-}1)$-dimensional sphere. This yields a general ansatz $V_j(\mathbf{R}) = Y_{j,\{l\},\{m\}}(\Omega)V(R)$ where $V(R)$ is the radial part and $Y_{j,\{l\},\{m\}}(\Omega)$ denote the vector spherical harmonic of $SO(d)$. We study the cases $d = 2$ and $d = 3$ here. In $d = 3$, we assume the following ansatz for $\mathbf{V}(\mathbf{R})$:

$$(d = 3): \qquad \mathbf{V}(\mathbf{R}) = V_1(R)\,\hat{\mathbf{R}}Y_{lm}(\theta,\phi) + V_2(R)\,R\,\nabla Y_{lm}(\theta,\phi) + V_3(R)\,\mathbf{R}\times\nabla Y_{lm}(\theta,\phi). \tag{B.6}$$

Note that we immediately find $V_3(R) = 0$ since $\mathbf{V}$ is irrotational as implied by the hydrodynamical equations. The required derivatives are given by:

$$\nabla\cdot\mathbf{V} = \left[V_1'(R) + 2R^{-1}V_1(R) - R^{-1}l(l+1)V_2(R)\right]Y_{lm}(\theta,\phi),$$

$$\nabla(\nabla U\cdot\mathbf{V}) = \frac{\mathrm{d}}{\mathrm{d}R}\left(2U'(R^2)RV_1(R)\right)\hat{\mathbf{R}}\,Y_{lm}(\theta,\phi) + 2U'(R^2)V_1(R)\,R\,\nabla Y_{lm}(\theta,\phi). \tag{B.7}$$

Plugging the above expressions into Eqs. (B.5), we find two coupled ordinary differential equations (ODEs) for $V_1(R)$ and $V_2(R)$. The solution of these equations gives the full normal mode spectrum. Here, we are interested in the solutions for which $\nabla\cdot\mathbf{V} = 0$. In this case, Eq. (B.5b) immediate gives $\partial_T\delta\beta = 0$, i.e. such a mode is isothermal. Furthermore, all state-dependent quantities drop out from Eq. (B.5b) and it reduces to:

$$(\nabla\cdot\mathbf{V} = 0): \qquad m\partial_T^2\mathbf{V} = -\nabla(\mathbf{V}\cdot\nabla U). \tag{B.8}$$

Using Eq. (B.7) and assuming an oscillatory solution with frequency ω, we find:

$$M\omega^2 V_1(R) = \frac{\mathrm{d}}{\mathrm{d}R}(2U'(R^2) R V_1(R)),$$

$$M\omega^2 V_2(R) = 2U'(R^2) V_1(R),$$

$$0 = V_1'(R) + 2R^{-1}V_1(R) - R^{-1}l(l+1)V_2(R). \tag{B.9}$$

The first two equations result from Eq. (B.8) while the third equation is the constraint from $\nabla \cdot \mathbf{V} = 0$. The three equations are compatible only if $U'(R^2) = \mathrm{const}$. Therefore, the divergenceless modes may only exist in harmonic traps. We assume:

$$U(R^2) = \frac{1}{2}M\omega_0^2 R^2. \tag{B.10}$$

The solution $V_1(R) = R^\alpha$ has the general form of a power law. The above equations imply $\omega^2 = \omega_0^2(\alpha + 1)$ and $(\alpha + 1)(\alpha + 2) - l(l+1) = 0$, so that $\alpha = l - 1, -l - 2$. The second solution is irregular at original and we finally find:

$$\omega = \sqrt{l}\,\omega_0. \tag{B.11}$$

The velocity flow and number density for this isothermal and divergence-less mode is:

$$\mathbf{V}(T, \mathbf{R}) = \tilde{V}_0 \cos\left(\sqrt{l}\,\omega_0 T\right) \left[R^{l-1}\,\hat{R}\,Y_{lm}(\theta, \phi) + \frac{R^l}{l}\,\nabla Y_{lm}(\theta, \phi) \right],$$

$$\delta n(T, \mathbf{R}) = \tilde{V}_0 \sin\left(\sqrt{l}\,\omega_0 T\right) \frac{M\omega_0}{\sqrt{l}} \frac{n_0(R)}{P_{0,n}(R)} R^l\, Y_{lm}(\theta, \phi). \tag{B.12}$$

Clearly, the solution is only valid for $l \geq 1$. Finally, we note that general analysis of Eq. (B.5) can be cast into the solution of a second-order self-adjoint ODE using the ideas mentioned above. Since the divergenceless solution is nodeless, the Sturm-Liouville theory of self-adjoint ODEs imply that such a solution has the smallest eigenvalue.

The analysis is similar in $d = 2$, where the general ansatz for $\mathbf{V}(\mathbf{R})$ is:

$$(d = 2): \qquad \mathbf{V}(\mathbf{R}) = V_1(R)\,\hat{\mathbf{R}}\,u_{lm}(\phi) + V_2(R)\,R\,\nabla u_{lm}(\phi), \tag{B.13}$$

where $u_{l1}(\phi) = \sin(l\phi)$ and $u_{l2}(\phi) = \cos(l\phi)$. The required derivatives are given as:

$$\nabla \cdot \mathbf{V} = \left[V_1'(R) + R^{-1}V_1(R) - R^{-1}l^2V_2(R) \right] u_{lm}(\phi),$$

$$\nabla(\nabla U \cdot \mathbf{V}) = \frac{\mathrm{d}}{\mathrm{d}R} \left(2U'(R^2)RV_1(R) \right) \hat{\mathbf{R}} \, u_{lm}(\phi) + 2U'(R^2)V_1(R) \, R \, \nabla u_{lm}(\phi). \tag{B.14}$$

Again, we consider the case of a divergence-less flow. Assuming an oscillatory solution with frequency ω, Eq. (B.8) with the aid of the above derivative formulas read as:

$$M\omega^2 \, V_1(R) = \frac{\mathrm{d}}{\mathrm{d}R}(2U'(R^2) \, R \, V_1(R)),$$

$$M\omega^2 \, V_2(R) = 2U'(R^2) \, V_1(R),$$

$$0 = V_1'(R) + R^{-1}V_1(R) - R^{-1}l^2V_2(R). \tag{B.15}$$

Again, the above equations may only be simultaneously satisfied for a harmonic potential. Assuming the ansatz $V_1(R) = R^\alpha$, we find $\omega^2 = \omega_0^2(\alpha+1)$, $(\alpha+1)^2 = l^2$, with the solutions $\alpha = \pm l - 1$. The negative solution is irregular at the origin and we finally find:

$$\omega = \sqrt{l}\,\omega_0. \tag{B.16}$$

The velocity flow and number density for this isothermal and divergence-less mode is:

$$\mathbf{V}(T,\mathbf{R}) = \tilde{V}_0 \cos\left(\sqrt{l}\,\omega_0 T\right) \left[R^{l-1} \, \hat{R} \, u_{lm}(\phi) + \frac{R^l}{l} \, \nabla u_{lm}(\phi) \right],$$

$$\delta n(T,\mathbf{R}) = \tilde{V}_0 \sin\left(\sqrt{l}\,\omega_0 T\right) \frac{M\omega_0}{\sqrt{l}} \frac{n_0(R)}{P_{0,n}(R)} R^l \, u_{lm}(\phi). \tag{B.17}$$

The $l = 1$ surface mode is the dipole (Kohn) mode associated to the harmonic motion of the center of mass of the fluid in the trap. The $l = 2$ mode is referred to as the quadrupole surface mode. The density modulation of the $l = 2$ surface mode is $\sim (X^2 - Y^2)$ in $d = 2$

C

Appendices to Chapter 3

C.1   Conservation laws of the linearized collisional Boltzmann-Vlasov equation

The CBV equation admits local conservation laws for mass density, mass current and energy, which can be simply established by multiplying the sides of CBV equation by 1, $\mathbf{p}$ and energy density $\mathcal{E}$ respectively and integrating over $\mathbf{p}$ [85]. Here, $\mathcal{E}$ is the energy density. The collision integrals vanish identically in all three cases due to the existence of the same conservation laws in

the level of 2-body scatterings. We state these conservation laws in their integral form here and utilize them later as a consistency check for our numerical calculations. The conservation of mass (or equivalently, particle number) is:

$$\frac{\mathrm{d}}{\mathrm{d}t} \int \mathrm{d}\Gamma \, n(\mathbf{p}; \mathbf{r}, t) = 0. \tag{C.1}$$

The linearized equation using the parametrization given by Eq. (3.44) yields:

$$\frac{\mathrm{d}}{\mathrm{d}t} \int \mathrm{d}\Gamma \, \Delta_0 \, \Psi(\mathbf{p}; \mathbf{r}, t) = 0. \tag{C.2}$$

In the same parametrization, the conservation of momentum reads as:

$$\frac{\mathrm{d}}{\mathrm{d}t} \int \mathrm{d}\Gamma \, \mathbf{p} \, \Delta_0 \, \Psi(\mathbf{p}; \mathbf{r}, t) = 0. \tag{C.3}$$

The energy density is given by $\mathcal{E}_{\mathrm{HF}} = p^2/(2m) + m\omega_0^2 r^2/2 + \Sigma^+[n]/2$ in the Hartree-Fock approximation using which we get the following linearized form of conservation of energy:

$$\frac{\mathrm{d}}{\mathrm{d}t} \int \mathrm{d}\Gamma \, (\delta\mathcal{E} \, n_0 + \mathcal{E}_0 \Delta_0 \, \Psi(\mathbf{p}; \mathbf{r}, t)) = 0, \tag{C.4}$$

where $\mathcal{E}_0 \equiv \mathcal{H}_0$ is the equilibrium energy density and $\delta\mathcal{E} = \Sigma^+[\delta n]/2 = \Sigma^+[\Delta_0 \Psi]/2$. Using the properties of Hartree-Fock self-energy functional, it is easy to show $\int \mathrm{d}\Gamma \delta\mathcal{E} \, n_0 = (1/2) \int \mathrm{d}\Gamma \Sigma^+[\Delta_0 \Psi] \, n_0 \equiv (1/2) \int \mathrm{d}\Gamma \Sigma^+[n_0] \, \Delta_0 \Psi$, using which the two terms in Eq. (C.4) can be combined to yield:

$$\frac{\mathrm{d}}{\mathrm{d}t} \int \mathrm{d}\Gamma \, \mathcal{H}_0 \Delta_0 \Psi(\mathbf{p}; \mathbf{r}, t) = 0. \tag{C.5}$$

C.2 Asymptotic analysis of $Q(\bar{T}, \eta = 0)$

In the 2D limit ($\eta = 0$), the asymptotic behavior of $Q(\bar{T}, \eta)$ can be studied analytically. Setting $\eta = 0$, the Erfcx functions appearing in the collision integral (see Eq. 3.72) evaluate to unity and the expression in the brackets in the second line simply becomes $[\chi_1 - \chi_2]^2 = \sin^2 \xi \, \sin^2 \nu \, [1 - |\sin(\phi - \phi')|]$. This will result in significant simplifications.

C.2.1 Low temperature expansion

In the low temperature regime, $\bar{\mu}/\bar{T} \to \infty$, we may use the following identity:

$$\lim_{\bar{\mu}/\bar{T}\to\infty} (\bar{\mu}/\bar{T})^{-3} \int_0^\infty \rho^5 \, d\rho \left[\frac{1}{\cosh(\rho - \bar{\mu}/\bar{T}) + \cosh(b_1\rho)} \frac{1}{\cosh(\rho - \bar{\mu}/\bar{T}) + \cosh(b_2\rho)} \right] =$$
$$\frac{4\pi^2}{3} \delta(b_1)\,\delta(b_2). \quad \text{(C.6)}$$

The above identity can be established by observing that for large $\bar{\beta}\bar{\mu}$ the integrand is exponentially small unless $\rho \sim \bar{\beta}\bar{\mu}$ and $b_1, b_2 \sim (\bar{\beta}\bar{\mu})^{-1}$. In the limit $\bar{\beta}\bar{\mu} \to \infty$, the right hand side becomes proportional to $\delta(b_1)\,\delta(b_2)$. The proportionality constant can be found by integrating the left hand side over b_1 and b_2, which gives the $4\pi^2/3$ pre-factor. Identifying b_1 and b_2 as $\sin^2\xi \, \sin 2\nu \, \cos\phi$ and $\sin^2\xi \, \sin 2\nu \, \cos\phi'$ respectively, we can carry out the ξ and ν integrations using the δ-functions and we finally get:

$$Q(\bar{T} \to 0, \eta = 0) \approx C \, \frac{(\bar{\mu}/\bar{T})^3}{\langle\!\langle \bar{p}^4 \rangle\!\rangle}, \quad \text{(C.7)}$$

where C is given by:

$$C = \frac{32}{9} \int_0^{2\pi} d\phi \int_0^{2\pi} d\phi' \frac{[1 - |\sin(\phi - \phi')|] \, \sin(\phi - \phi')^2}{\cos^2\phi + \cos^2\phi'}, \quad \text{(C.8)}$$

and is equal to 19.176999 to six digits. $\langle\!\langle \bar{p}^4 \rangle\!\rangle$ can be found analytically with little effort and we get:

$$\langle\!\langle \bar{p}^4 \rangle\!\rangle = -8\bar{T}^3 \, \text{Li}_3(-e^{\bar{\mu}/\bar{T}}). \quad \text{(C.9)}$$

Using the asymptotic expansion of $\text{Li}_3(-x)$ for large x and the low temperature expansion of $\bar{\mu}$ mentioned after Eq. (3.38), the following low temperature expansion follows:

$$-\text{Li}_3(-e^{\bar{\mu}/\bar{T}}) = 1/(6\bar{T}^3) + \pi^2/(12\bar{T}) + \mathcal{O}(\bar{T}). \quad \text{(C.10)}$$

Combining the last four equations, we finally get:

$$Q(\bar{T} \to 0, \eta = 0) \approx \frac{2}{3} C \, \bar{T}^2 \approx 12.784666 \, \bar{T}^2, \quad \text{(C.11)}$$

to leading order. This asymptotic limit is shown in Fig. 3.4e as a blue dashed line and agrees well with the numerical result.

C.2.2   High temperature expansion

The analysis of the classical limit ($\bar{\beta}\bar{\mu} \to 0$) is simpler. First, we rewrite the hyperbolic functions in the denominator as $\cosh(\rho - \ln z) \equiv e^{\rho}/(2z) + (z/2)e^{-\rho}$. Here, $z \equiv \exp(\bar{\mu}/\bar{T})$ is the fugacity and goes to zero in the high temperature limit. Thus, $\cosh(\rho - \ln z) \approx e^{\rho}/(2z)$ to leading order. The denominator of Eq. (3.72) is dominated by the first $\cosh$ term. Neglecting the second $\cosh$ terms, the integrations become elementary and we get:

$$Q(\bar{T} \to 0, \eta = 0) \approx \frac{8(8 - 3\pi)z^2\bar{T}^5}{\langle\!\langle \bar{p}^4 \rangle\!\rangle}. \tag{C.12}$$

The fugacity in the classical limit can be found using Eq. (3.38) and we get $z = 1/(2\bar{T}^2) + \mathcal{O}(\bar{T}^{-4})$. Using the asymptotic expansion $-\mathrm{Li}_3(-z) = z + \mathcal{O}(z^2)$, we finally find:

$$Q(\bar{T} \to \infty, \eta = 0) \approx \frac{1}{2}(3\pi - 8) \approx 0.712389. \tag{C.13}$$

This asymptotic limit is shown in Fig. 3.4e as a red dashed line and is in agreement with the numerical result.

C.3   Matrix elements of the evolution matrix in the monopole basis

The linear response analysis of the CBV equation using extended variational basis sets requires calculation of a large number of matrix elements. This task, however, can be simplified since the angular integrations appearing in expression for the matrix elements of M, Σ and H$_0$ can be carried out analytically using the symmetries of the basis functions and the equilibrium state. The problem reduces to the evaluation of a two-dimensional integral over $\bar{p}$ and $\bar{r}$ for each matrix element which can be done numerically accurately and efficiently. In this appendix, we provide readily computable formulas for the matrix elements in the monopole basis. We define the shorthands $R_\alpha \equiv 2m_\alpha + k_\alpha$, $P_\alpha \equiv 2n_\alpha + k_\alpha$ for given basis function ϕ_α. R_α and P_α count the powers of r and p appearing in ϕ_α respectively.

Matrix elements of M

By definition, we have:

$$
\begin{aligned}
\mathsf{M}_{\alpha\beta} &= \int \mathrm{d}\bar{\Gamma}\,\Delta_0(\bar{p},\bar{r})\,\phi_\alpha\phi_\beta \\
&= \int (2\pi)\,\bar{r}\,\mathrm{d}\bar{r}\,\frac{1}{(2\pi)^2}\,\bar{p}\,\mathrm{d}\bar{p}\,\Delta_0(\bar{p},\bar{r})\,\bar{r}^{R_\alpha+R_\beta}\bar{p}^{P_\alpha+P_\beta}\int_0^{2\pi}\mathrm{d}\phi\,(\cos\phi)^{k_\alpha+k_\beta} \\
&= \frac{E(k_\alpha+k_\beta)(k_\alpha+k_\beta)!}{2^{k_\alpha+k_\beta}\left[\left(\frac{k_\alpha+k_\beta}{2}\right)!\right]^2}\left[\int \bar{r}^{R_\alpha+R_\beta+1}\bar{p}^{P_\alpha+P_\beta+1}\,\Delta_0(\bar{p},\bar{r})\,\mathrm{d}\bar{r}\,\mathrm{d}\bar{p}\right],
\end{aligned}
\tag{C.14}
$$

where $E(n) = 1$ for even n and $E(n) = 0$ for odd n. For future reference, we define:

$$
h(n) = \frac{E(n)\,n!}{2^n\left[(n/2)!\right]^2},
\tag{C.15}
$$

and:

$$
I_n^m[A(\bar{p},\bar{r})] = \int A(\bar{p},\bar{r})\,\bar{r}^{m+1}\,\bar{p}^{n+1}\,\mathrm{d}\bar{r}\,\mathrm{d}\bar{p},
\tag{C.16}
$$

using which we can write $\mathsf{M}_{\alpha\beta} = h(k_\alpha + k_\beta)\,I_{(P_\alpha+P_\beta)}^{(R_\alpha+R_\beta)}[\Delta_0]$.

Matrix elements of H_0

First, we evaluate the Poisson bracket $\{\phi_\beta,\bar{\mathcal{H}}_0\}$:

$$
\begin{aligned}
\{\phi_\beta,\bar{\mathcal{H}}_0\} &= \nabla_{\bar{\mathbf{r}}}\phi_\beta\cdot\nabla_{\bar{\mathbf{p}}}\bar{\mathcal{H}}_0 - \nabla_{\bar{\mathbf{p}}}\phi_\beta\cdot\nabla_{\bar{\mathbf{r}}}\bar{\mathcal{H}}_0 \\
&= \gamma_p\,(\bar{\mathbf{p}}\cdot\nabla_{\bar{\mathbf{r}}})\phi_\beta - \gamma_r\,(\bar{\mathbf{r}}\cdot\nabla_{\bar{\mathbf{p}}})\phi_\beta \\
&= \gamma_p\left[2m_\beta\,\phi_{(m_\beta-1,n_\beta,k_\beta+1)} + k_\beta\,\phi_{(m_\beta,n_\beta+1,k_\beta-1)}\right] \\
&\quad - \gamma_r\left[2n_\beta\,\phi_{(m_\beta,n_\beta-1,k_\beta+1)} - k_\beta\,\phi_{(m_\beta+1,n_\beta,k_\beta-1)}\right],
\end{aligned}
\tag{C.17}
$$

where:

$$
\gamma_r \equiv \bar{r}^{-2}\bar{\mathbf{r}}\cdot\nabla_{\bar{\mathbf{r}}}\bar{\mathcal{H}}_0 = 1 + \bar{r}^{-2}\bar{\mathbf{r}}\cdot\nabla_{\bar{\mathbf{r}}}\bar{\Sigma}_0,
$$

$$
\gamma_p \equiv \bar{p}^{-2}\bar{\mathbf{p}}\cdot\nabla_{\bar{\mathbf{p}}}\bar{\mathcal{H}}_0 = 1 + \bar{p}^{-2}\bar{\mathbf{p}}\cdot\nabla_{\bar{\mathbf{p}}}\bar{\Sigma}_0.
\tag{C.18}
$$

Plugging Eq. (C.17) into the definition of $(\mathsf{H}_0)_{\alpha\beta}$, we get:

$$
\begin{aligned}
(\mathsf{H}_0)_{\alpha\beta} &= \int \mathrm{d}\bar{\Gamma}\, \Delta_0\, \phi_\alpha \{\phi_\beta, \mathcal{H}_0\} \\
&= [2m_\beta\, h(k_\alpha + k_\beta + 1) + k_\beta\, h(k_\alpha + k_\beta - 1)]\, I^{(R_\alpha + R_\beta - 1)}_{(P_\alpha + P_\beta + 1)} [\gamma_p \Delta_0] \\
&\quad - [2n_\beta\, h(k_\alpha + k_\beta + 1) + k_\beta\, h(k_\alpha + k_\beta - 1)]\, I^{(R_\alpha + R_\beta + 1)}_{(P_\alpha + P_\beta - 1)} [\gamma_r \Delta_0].
\end{aligned}
\tag{C.19}
$$

Matrix elements of Σ

By definition,

$$
\bar{\Sigma}[\Delta_0 \phi_\beta] = \lambda_d \int \frac{\mathrm{d}^2 \bar{\mathbf{p}}'}{(2\pi)^2}\, u(|\bar{\mathbf{p}} - \bar{\mathbf{p}}'|, \eta)\, \Delta_0(\bar{p}', \bar{r})\, \phi_\beta(\bar{\mathbf{p}}', \bar{\mathbf{r}}).
\tag{C.20}
$$

It is easy to verify that a simultaneous rotation of $\bar{\mathbf{r}}$ and $\bar{\mathbf{p}}$ leaves $\bar{\Sigma}[\Delta_0 \phi_\beta]$ invariant, so that $\bar{\Sigma}[\Delta_0 \phi_\beta]$ may only depend on $\bar{r}$, $\bar{p}$ and ϕ, the angle between $\bar{\mathbf{r}}$ and $\bar{\mathbf{p}}$. Let $\cos\varphi = (\bar{\mathbf{p}} \cdot \bar{\mathbf{p}}')/(\bar{p}\bar{p}')$ and $\cos\phi = (\bar{\mathbf{r}} \cdot \bar{\mathbf{p}})/(\bar{r}\bar{p})$, so that $\bar{\mathbf{r}} \cdot \bar{\mathbf{p}}' = \bar{r}\bar{p}' \cos(\varphi + \phi)$. Expanding $u(|\bar{\mathbf{p}} - \bar{\mathbf{p}}'|, \eta)$ in a cosine series,

$$
u(|\bar{\mathbf{p}} - \bar{\mathbf{p}}'|, \eta) = \sum_{n=0}^{\infty} u^{(n)}(\bar{p}, \bar{p}'; \eta) \cos(n\varphi),
\tag{C.21}
$$

where:

$$
u^{(n)}(\bar{p}, \bar{p}') = \frac{1}{\pi(\delta_{n,0} + 1)} \int_0^{2\pi} \mathrm{d}\varphi\, u\left(\sqrt{\bar{p}^2 + \bar{p}'^2 - 2\bar{p}\bar{p}' \cos\varphi}, \eta\right) \cos n\varphi,
\tag{C.22}
$$

and plugging into Eq. (C.20), we get:

$$
\begin{aligned}
&\bar{\Sigma}[\Delta_0 \phi_\beta](\bar{p}, \bar{r}, \phi) = \\
&\lambda_d \int \frac{\bar{p}'\, \mathrm{d}\bar{p}'}{2\pi}\, \Delta_0(\bar{p}', \bar{r})\, \bar{p}'^{P_\beta} \bar{r}^{R_\beta} \left(\sum_{n=0}^{\infty} u(\bar{p}, \bar{p}'; \eta) \int_0^{2\pi} \frac{\mathrm{d}\varphi}{2\pi} \cos(n\varphi) \cos(\varphi + \phi)^{k_\beta} \right).
\end{aligned}
\tag{C.23}
$$

The angular integration can be evaluated using contour integral techniques:

$$
\int_0^{2\pi} \frac{\mathrm{d}\varphi}{2\pi} \cos(n\varphi) \cos(\varphi + \phi)^k = \left[\frac{k!}{2^k} \frac{\theta(k - n)\, E(k + n)}{\left[\left(\frac{k-n}{2}\right)!\right]\left[\left(\frac{k+n}{2}\right)!\right]} \right] \cos(n\phi),
\tag{C.24}
$$

where $\theta(n) = 1$ if $n \geq 0$ and $\theta(n) = 0$ otherwise. We denote the numerical prefactor in the brackets of the above equation by $g(n,k)$. Plugging this into Eq. (C.23), we get:

$$\bar{\Sigma}[\Delta_0\phi_\beta](\bar{p},\bar{r},\phi) = \lambda_d \sum_{n=0}^{k_\beta} Q_\beta^{(n)}(\bar{p},\bar{r}) \cos(n\phi), \qquad (C.25)$$

where:

$$Q_\beta^{(n)}(\bar{p},\bar{r}) = -g(n,k_\beta)\,\bar{r}^{R_\beta} \int \frac{\mathrm{d}\bar{p}'}{2\pi}\, \Delta_0(\bar{p}',\bar{r})\, \bar{p}'^{(P_\beta+1)} u^{(n)}(\bar{p},\bar{p}';\eta). \qquad (C.26)$$

The last integral can be easily evaluated numerically. Also, note that we only need $u^{(n)}$ up to $n = k_\beta$ in order to evaluate $\bar{\Sigma}[\Delta_0\phi_\beta]$ exactly. This is due to the fact that $g(n,k_\beta)$ vanishes for $n > k_\beta$. Having evaluated $\bar{\Sigma}[\Delta_0\phi_\beta]$, $\Sigma_{\alpha\beta}$ can be evaluated readily by appealing to its definition:

$$\Sigma_{\alpha\beta} = \lambda_d \sum_{n=0}^{k_\beta} \Big([2m_\alpha\, g(n,k_\alpha+1) + k_\alpha\, g(n,k_\alpha-1)]\, I_{(P_\alpha+1)}^{(R_\alpha-1)}[Q_\beta^{(n)}\Delta_0\gamma_p]$$

$$- [2n_\alpha\, g(n,k_\alpha+1) + k_\alpha\, g(n,k_\alpha-1)]\, I_{(P_\alpha-1)}^{(R_\alpha+1)}[Q_\beta^{(n)}\Delta_0\gamma_r]\Big). \quad (C.27)$$

Matrix elements of I_c

The evaluation of the matrix elements of the linearized collision integral operator is the most computationally expensive part of the calculation. Once Hartree-Fock self-energy corrections are taken into account, deviation of quasiparticle dispersion from the bare quadratic dispersion makes the calculations even more challenging. The collision integrals are commonly evaluated with bare quadratic dispersions. This is justified in the Boltzmann equation limit, where mean-field corrections are neglected altogether. Here, since we have included mean-field effects on the dynamics, we must also use the dressed quasiparticles dispersion in order to satisfy conservation of energy. In order to do this in a numerically tractable way, we have found that the quasiparticle dispersions can be approximated well using a local effective mass approximation (LEMA) within an error of less than 2 percents. To this end, we approximate the dressed quasiparticle energies as:

$$\bar{\mathcal{H}}_0(\bar{p},\bar{r}) \approx \varepsilon_0(\bar{r}) + \frac{\bar{p}^2}{2m^*(r)} + \frac{\bar{r}^2}{2}, \qquad (C.28)$$

where:

$$\varepsilon_0(\bar{r}) = \bar{\Sigma}_0(\bar{r}; 0),$$

$$m^*(\bar{r}) = \left[1 + \partial_{\bar{p}}^2 \bar{\Sigma}_0(\bar{r}; \bar{p})\Big|_{\bar{p}=0}\right]^{-1}. \tag{C.29}$$

As we will see shortly, this approximation allows us to put the collision integral into a simple form suitable for numerical treatments. As a first step, we go to the center of mass frame of the colliding particles and define:

$$\bar{\mathbf{p}} = \frac{\bar{\mathbf{P}}}{2} + \bar{\mathbf{q}}, \qquad \bar{\mathbf{p}}_1 = \frac{\bar{\mathbf{P}}}{2} - \bar{\mathbf{q}},$$

$$\bar{\mathbf{p}}' = \frac{\bar{\mathbf{P}}'}{2} + \bar{\mathbf{q}}', \qquad \bar{\mathbf{p}}'_1 = \frac{\bar{\mathbf{P}}'}{2} - \bar{\mathbf{q}}', \tag{C.30}$$

using which we get:

$$d^2\bar{\mathbf{r}} \frac{d^2\bar{\mathbf{p}}}{(2\pi)^2} \frac{d^2\bar{\mathbf{p}}_1}{(2\pi)^2} \frac{d^2\bar{\mathbf{p}}'}{(2\pi)^2} \frac{d^2\bar{\mathbf{p}}'_1}{(2\pi)^2} (2\pi)\delta(\Delta\bar{E}) (2\pi)^2\delta(\Delta\bar{\mathbf{P}}) \rightarrow \frac{m^*(\bar{r})}{2} \bar{r}\,d\bar{r}\,d\phi \frac{\bar{P}\,d\bar{P}}{2\pi} \frac{\bar{q}\,d\bar{q}}{2\pi} \frac{d\phi}{2\pi} \frac{d\phi'}{2\pi},$$

$$\tag{C.31}$$

where ϕ, ϕ' and ϕ are defined as $\cos\phi = \bar{\mathbf{q}}\cdot\bar{\mathbf{P}}/(\bar{q}\bar{P})$, $\cos\phi' = \bar{\mathbf{q}}'\cdot\bar{\mathbf{P}}/(\bar{q}'\bar{P})$, and $\cos\phi = \bar{\mathbf{r}}\cdot\bar{\mathbf{P}}/(\bar{r}\bar{P})$. Note that $\bar{\mathbf{P}} \equiv \bar{\mathbf{P}}'$ and $\bar{q} \equiv \bar{q}'$ in the rest of the integrand due to conservation of momentum and energy. The scattering amplitude $\bar{\mathcal{M}} = \lambda_d[u(|\bar{\mathbf{p}} - \bar{\mathbf{p}}'|, \eta) - u(|\bar{\mathbf{p}} - \bar{\mathbf{p}}'_1|, \eta)] \rightarrow \lambda_d[u(2\bar{q}|\sin[(\phi - \phi')/2]|, \eta) - u(2\bar{q}|\cos[(\phi - \phi')/2]|, \eta)]$. The product of the equilibrium distribution functions, $n_0\, n_{0,1}(1 - n'_0)(1 - n'_{0,1})$ can be conveniently written as:

$$n_0\, n_{0,1}(1 - n'_0)(1 - n'_{0,1}) \rightarrow \frac{1}{4} \frac{1}{\cosh E + \cosh\gamma} \frac{1}{\cosh E + \cosh\gamma'}, \tag{C.32}$$

where $E = \bar{\beta}(\bar{P}^2/4 + \bar{q}^2)/[2m^*(\bar{r})] + \bar{\beta}\bar{r}^2/2 - \bar{\beta}\bar{\mu}$, $\gamma = \bar{\beta}\bar{P}\bar{q}\cos\phi/[2m^*(\bar{r})]$, $\gamma' = \bar{\beta}\bar{P}\bar{q}\cos\phi'/[2m^*(\bar{r})]$. The angle ϕ is only present in $\mathrm{S}[\phi_\alpha]\mathrm{S}[\phi_\alpha]$. Therefore, the integration over ϕ is immediate and elementary, which we evaluate using Mathematica and define $\mathrm{S}_{\alpha\beta}(\bar{r}, \bar{P}, \bar{q}, \phi, \phi') \equiv \int d\phi\, \mathrm{S}[\phi_\alpha]\mathrm{S}[\phi_\beta]$. The integral can be put in a more useful form using a spherical change of variables, $\bar{P} = (8\rho/\bar{\beta})^{1/2} \sin\xi \cos\nu$, $\bar{q} = (2\rho/\bar{\beta})^{1/2} \sin\xi \sin\nu$ and $\bar{r} = (2\rho/\beta)^{1/2} \cos\xi$, where

$\rho \in [0, \infty)$, $\nu \in [0, \pi/2]$ and $\xi \in [0, \pi/2]$. The final expression is:

$$\mathscr{I}_{\alpha\beta} = -\frac{(2N)^{\frac{1}{2}}\lambda_d^2}{8(2\pi)^2\,\bar{\beta}^{N_\alpha+N_\beta+3}} \int_0^\infty \rho^2\,\mathrm{d}\rho \int_0^{2\pi} \frac{\mathrm{d}\phi}{2\pi} \int_0^{2\pi} \frac{\mathrm{d}\phi'}{2\pi} \int_0^{\frac{\pi}{2}} \mathrm{d}\xi\,\sin^3\xi\,\cos\xi \int_0^{\frac{\pi}{2}} \mathrm{d}\nu\,\sin 2\nu$$

$$\times\, \mathrm{S}_{\alpha\beta}(\sqrt{2\rho}\cos\xi,\,\sqrt{8\rho}\sin\xi\,\cos\nu,\,\sqrt{2\rho}\sin\xi\,\sin\nu,\,\phi,\,\phi')\,m^*(\bar{r})$$

$$\times\left[\sqrt{\bar{\beta}}\,u\left(2\sqrt{2\rho/\bar{\beta}}\,\sin\xi\,\sin\nu\,|\sin[(\phi-\phi')/2]|,\eta\right)\right.$$

$$\left.-\sqrt{\bar{\beta}}\,u\left(2\sqrt{2\rho/\bar{\beta}}\,\sin\xi\,\sin\nu\,|\cos[(\phi-\phi')/2]|,\eta\right)\right]^2$$

$$\times\left\{\left[\cosh\left(\rho\sin^2\xi/m^*(\bar{r}) + \rho\cos^2\xi + \bar{\beta}\varepsilon_0(\bar{r}) - \bar{\beta}\bar{\mu}\right)\right.\right.$$

$$\left.\left.+ \cosh\left(\rho\,\sin^2\xi\,\sin 2\nu\,\cos\phi/m^*(\bar{r})\right)\right] \times (\phi \leftrightarrow \phi')\right\}^{-1},$$

$$\tag{C.33}$$

where $N_{a(b)} = m_{a(b)} + n_{a(b)} + k_{a(b)}$ and $\bar{r} \equiv \sqrt{2\rho/\bar{\beta}}\,\cos\xi$ in $m^*(\bar{r})$ and $\varepsilon(\bar{r})$. We evaluate the above 5-dimensional integral for all pairwise combination of basis functions using a numerical Monte-Carlo integration with 5×10^8 points which we found to yield a relative statistical error of less than 10^{-3} in all cases.

C.4   Matrix elements of the evolution matrix in the quadrupole basis

In this appendix, we provide readily computable expressions for various matrix elements in the quadrupole basis by carrying out the angular integrations analytically. For a given quadrupole basis function $\xi_i\phi_\alpha$, we define the shorthand (μ_i, ν_i) as the number of powers of r and p present in ξ_i respectively, i.e. $(\mu_1, \nu_1) = (2, 0)$, $(\mu_2, \nu_2) = (1, 1)$, and $(\mu_3, \nu_3) = (0, 2)$.

Matrix elements of M

The angular integrations in M can be easily carried out using the parametrization $\cos\phi = \hat{\mathbf{r}} \cdot \hat{x}$ and $\cos\phi = \bar{\mathbf{r}} \cdot \bar{\mathbf{p}}/(\bar{r}\bar{p})$. In this variables, we get $\xi_i = \bar{r}^{\mu_i}\bar{p}^{\nu_i}\cos(2\phi + \nu_j\phi)$. The angular integration

are elementary and we find:

$$\mathsf{M}^{ij}_{\alpha\beta} = \int \mathrm{d}\bar{\Gamma}\,\Delta_0\,\xi_i\,\xi_j\,\phi_\alpha\phi_\beta = \frac{1}{2}\,g(|\nu_i - \nu_j|, k_\alpha + k_\beta)\,I^{(R_\alpha+R_\beta+\mu_i+\mu_j)}_{(P_\alpha+P_\beta+\nu_i+\nu_j)}[\Delta_0]. \tag{C.34}$$

Matrix elements of H

As a first step, we evaluate the Poisson bracket $\{\xi_j\phi_\beta, \bar{\mathcal{H}}_0\} = \xi_j\{\phi_\beta, \bar{\mathcal{H}}_0\} + \phi_\beta\{\xi_j, \bar{\mathcal{H}}_0\}$. The expression for $\{\phi_\beta, \bar{\mathcal{H}}_0\}$ is known from the previous appendix (Eq. C.17). We can write $\{\xi_j, \bar{\mathcal{H}}_0\} = X_{jk}(\bar{p}, \bar{r})\,\xi_k$ (sum over k is implied), where:

$$X_{jk} = \begin{pmatrix} 0 & 2\gamma_p & 0 \\ -\gamma_r & 0 & \gamma_p \\ 0 & -2\gamma_r & 0 \end{pmatrix}. \tag{C.35}$$

Therefore, we get:

$$
\begin{aligned}
(\mathsf{H}_0)^{ij}_{\alpha\beta} &= \int \mathrm{d}\bar{\Gamma}\,\Delta_0\,\xi_i\,\phi_\alpha\{\xi_j\phi_\beta, \bar{\mathcal{H}}_0\} \\
&= \underbrace{\int \mathrm{d}\bar{\Gamma}\,\Delta_0\,\phi_\alpha\{\phi_\beta, \bar{\mathcal{H}}_0\}\,\xi_i\xi_j}_{(\mathsf{H}_0)^{ij}_{\alpha\beta,1}} + \underbrace{\int \mathrm{d}\bar{\Gamma}\,\Delta_0\,\phi_\alpha\phi_\beta\,X_{jk}\,\xi_i\,\xi_k}_{(\mathsf{H}_0)^{ij}_{\alpha\beta,2}}\,.
\end{aligned} \tag{C.36}
$$

The angular integrations in $(\mathsf{H}_0)^{ij}_{\alpha\beta,1}$ can be most easily evaluated using the parametrization defined earlier, $\cos\phi = \hat{\mathbf{r}}\cdot\hat{x}$ and $\cos\phi = \bar{\mathbf{r}}\cdot\bar{\mathbf{p}}/(\bar{r}\bar{p})$. The final result is:

$$
\begin{aligned}
(\mathsf{H}_0)^{ij}_{\alpha\beta,1} &= \frac{1}{2}\Big[2m_\beta\,g(|\nu_i-\nu_j|, k_\alpha+k_\beta+1)+k_\beta\,g(|\nu_i-\nu_j|, k_\alpha+k_\beta-1)\Big]\,I^{(R_\alpha+R_\beta+\mu_i+\mu_j-1)}_{(P_\alpha+P_\beta+\nu_i+\nu_j+1)}[\Delta_0\,\gamma_p] \\
&- \frac{1}{2}\Big[2n_\beta\,g(|\nu_i-\nu_j|, k_\alpha+k_\beta+1)+k_\beta\,g(|\nu_i-\nu_j|, k_\alpha+k_\beta-1)\Big]\,I^{(R_\alpha+R_\beta+\mu_i+\mu_j+1)}_{(P_\alpha+P_\beta+\nu_i+\nu_j-1)}[\Delta_0\,\gamma_r].
\end{aligned}
$$

The angular integrations in $(\mathsf{H}_0)^{ij}_{\alpha\beta,2}$ are similar to those in $(\mathsf{M})^{ij}_{\alpha\beta}$ and the result is:

$$(\mathsf{H}_0)^{ij}_{\alpha\beta,2} = \frac{1}{2}\,g(|\nu_i - \nu_k|, k_\alpha + k_\beta)\,I^{(R_\alpha+R_\beta+\mu_i+\mu_k)}_{(P_\alpha+P_\beta+\nu_i+\nu_k)}[\Delta_0\,X_{jk}]. \tag{C.37}$$

Matrix elements of Σ

Similar to the monopole case, the first step is evaluating $\bar{\Sigma}[\Delta_0 \xi_j \phi_\beta]$:

$$\bar{\Sigma}[\Delta_0 \xi_j \phi_\beta] = \lambda_d \int \frac{\bar{p}' \mathrm{d}\bar{p}'}{2\pi} \sum_{n=0}^{\infty} u^{(n)}(\bar{p}, \bar{p}'; \eta) \, \Delta_0(\bar{p}', \bar{r}) \, \bar{r}^{R_\beta + \mu_j} \, \bar{p}'^{P_\beta + \nu_j}$$

$$\times \int \frac{\mathrm{d}\phi'}{2\pi} \cos^{k_\beta}(\phi + \phi') \, \cos[2\phi + \nu_j(\phi + \phi')] \cos(n\phi'), \quad \text{(C.38)}$$

where we have expressed $u(|\bar{\mathbf{p}} - \bar{\mathbf{p}}'|, \eta)$ as a cosine series like before. The ϕ' integration can be conveniently carried out using the contour integral technique and gives $\tilde{g}(\nu_j, n, k_\beta) \cos(2\phi) \cos(n\phi) - \tilde{h}(\nu_j, n, k_\beta) \sin(2\phi) \sin(n\phi)$, where:

$$\tilde{g}(0, n, k) \equiv g(n, k),$$

$$\tilde{g}(1, n, k) \equiv g(n, k+1),$$

$$\tilde{g}(2, n, k) \equiv 2g(n, k+2) - g(n, k),$$

$$\tilde{h}(\nu, n, k) \equiv \tilde{g}(\nu, n, k) - g(\nu + n, k). \quad \text{(C.39)}$$

Plugging this back into Eq. (C.38), we get:

$$\bar{\Sigma}[\Delta_0 \xi_j \phi_\beta] = \sum_{n=0}^{k_\beta + 2} Q_{\beta,j}^{(n)}(\bar{p}, \bar{r}) \Big[\tilde{g}(\nu_j, n, k_\beta) \cos(2\phi) \cos(n\phi) - \tilde{h}(\nu_j, n, k_\beta) \sin(2\phi) \sin(n\phi) \Big],$$

$$\text{(C.40)}$$

where:

$$Q_{\beta,j}^{(n)}(\bar{p}, \bar{r}) = \lambda_d \int \frac{\mathrm{d}\bar{p}'}{2\pi} \, \bar{r}^{R_\beta + \mu_j} \, \bar{p}'^{P_\beta + \nu_j + 1} u(\bar{p}, \bar{p}'; \eta) \, \Delta_0(\bar{p}', \bar{r}). \quad \text{(C.41)}$$

The last integral can be evaluated easily numerically. The final result can be expressed easily using using last two expressions:

$$\left(\Sigma^F\right)_{\alpha\beta}^{ij} = \sum_{n=0}^{k_\beta + 2} \left[\frac{1}{2} G_{(\nu_j, n, k_\beta)}^{(\nu_k, n, k_\alpha)} I_{(P_\alpha + \nu_k)}^{(R_\alpha + \mu_k)} [\Delta_0 Q_{\beta,j}^{(n)} X_{ik}] + \frac{1}{2} \left(2m_\alpha \, G_{(\nu_j, n, k_\beta)}^{(\nu_i, n, k_\alpha + 1)} + k_\alpha \, G_{(\nu_j, n, k_\beta)}^{(\nu_i, n, k_\alpha - 1)} \right) \right.$$

$$\left. \times I_{(P_\alpha + \nu_i + 1)}^{(R_\alpha + \mu_i - 1)} [\Delta_0 Q_{\beta,j}^{(n)} \gamma_p] + \frac{1}{2} \left(2n_\alpha \, G_{(\nu_j, n, k_\beta)}^{(\nu_i, n, k_\alpha + 1)} + k_\alpha \, G_{(\nu_j, n, k_\beta)}^{(\nu_i, n, k_\alpha - 1)} \right) I_{(P_\alpha + \nu_i - 1)}^{(R_\alpha + \mu_i + 1)} [\Delta_0 Q_{\beta,j}^{(n)} \gamma_r] \right],$$

$$\text{(C.42)}$$

where we have defined the shorthand notation $G^{(\nu_1, n_1, k_1)}_{(\nu_2, n_2, k_2)} = \tilde{g}(\nu_1, n_1, k_1)\, \tilde{g}(\nu_2, n_2, k_2) + \tilde{h}(\nu_1, n_1, k_1)\, \tilde{h}(\nu_2, n_2, k_2)$.

Matrix elements of I_c

The matrix elements of the collision integral in the quadrupole basis is identical in form to those of the monopole basis (Eq. C.33). The only differences are (1) $S_{\alpha\beta}$ must be replaced with:

$$S^{ij}_{\alpha\beta}(\bar{r}, \bar{P}, \bar{q}, \phi, \phi') \equiv \int \frac{d\theta}{2\pi} d\phi\, S[\xi_i \phi_\alpha]\, S[\xi_j \phi_\beta], \tag{C.43}$$

where we introduced an extra angle $\cos\theta = \mathbf{e}_x \cdot \bar{\mathbf{P}}/\bar{P}$, and (2) the pre-factor $\bar{\beta}^{N_\alpha + N_\beta + 3} \rightarrow \bar{\beta}^{N_\alpha + N_\beta + 5}$ in the denominator due to the extra powers of $\bar{\beta}^{-1}$ introduced by ξ_i and ξ_j. The definition of $N_{\alpha(\beta)}$ is the same as before.

C.5 Collision integrals with exact Hartree-Fock quasiparticle dispersions

In Sec. C.3, we simplified the expression for the collision integral matrix elements using the local effective mass approximation (LEMA). Although we found this scheme to be a decent approximation in the weakly interacting regime (the approximate dispersions lie within a few percents of the exact Hartree-Fock dispersions), one may argue that an exact treatment is necessary for stronger interactions. In particular, this may have important consequences when one is looking at the effects that crucially depend on self-energy corrections, such as the damping of the nodeless monopole mode. In this section, we discuss this issue and present numerical justification for the reliability of LEMA.

The major simplification resulting from LEMA is the possibility of an analytic treatment of the δ-function in the collision integral associated to the conservation of energy (see Eq. C.31). In that case, LEMA simply yields $q = q'$, where q and q' are the magnitude of the momenta of the initial
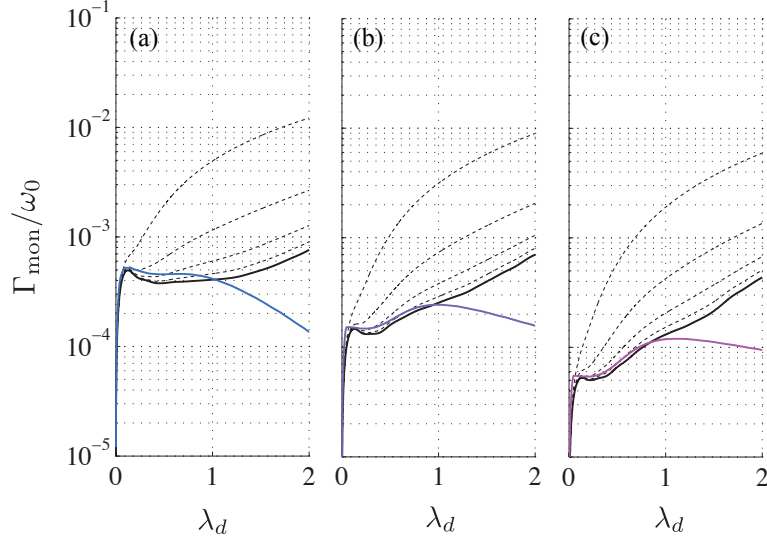
Figure C.1: The damping rate of the monopole oscillations in 2D and with $N = 2200$ particles. (a) $T/T_F = 0.5$, (b) $T/T_F = 1.0$ and (c) $T/T_F = 1.5$. The (light) solid colored lines are the previously discussed result obtained using the local effective mass approximation. The dashed lines denote approximate solutions obtained by relaxing the conservation of energy (from top to bottom, $\sigma = 0.05, 0.02, 0.01$ and 0.005). The solid black line is the extrapolation to $\sigma = 0$ (the exact result).

and final scattering pairs in the center of mass frame. Without a (local) quadratic dispersion, this simple result does not hold anymore and in general, there is no easy way of treating the δ-function analytically since the quasiparticle dispersions are evaluated numerically. Here, we introduce a simple numerical approach to overcome this difficulty. Using a limiting process to to define the delta functions,

$$\delta(\Delta \bar{E}) = \lim_{\sigma \to 0} \frac{1}{\sqrt{2\pi}\sigma} e^{-\Delta \bar{E}^2/(2\sigma^2)}, \tag{C.44}$$

we replace the δ-function with Gaussians and calculate the collision integrals for various values of σ. We find the $\sigma \to 0$ limit by extrapolation. This approach is considerably more computationally demanding than LEMA, however, it yields an accurate calculation of the collision integral matrix elements. The integrals are six dimensional in this case (the variables being $\bar{r}, \bar{P}, \bar{q}, \bar{q}', \phi$ and ϕ') since q and q' may assume different values now.

We implemented the above method for both monopole and quadrupole oscillations within a 2nd

order basis set. The extrapolation is carried out using a polynomial fit. Fig. C.1 shows the damping of monopole oscillations obtained using several choices of σ, the extrapolated result, and the LEMA result for reference. The matching between the effective mass approximation and the exact result is excellent up to $\lambda_d \sim 1$. The LEMA result, however, deviates from the exact result for $\lambda_d \gtrsim 1$. Nonetheless, we find $\gamma_{\text{mon}}^{\text{exact}} < 10^{-3}\omega_0$ and our conclusion about the smallness of the damping of the nodeless monopole mode remains valid. Finally, we note that the beyond-LEMA refinement to the prediction for the frequency of monopole oscillations is much smaller (a relative correction of about 10^{-6}). This is due to the fact that the frequency shift essentially results from the self-energy corrections on the dynamical side of the CBV equation which is already treated exactly.

D

Appendices to Chapter 4

D.1   The expansion of the Ginzburg-Landau functional

We give explicit expressions for the coefficients of the low-energy expansion of the many-body T-matrix, Eq. (4.29). We define the useful shorthand $X \equiv \beta\mu$ and $N(0) = m/(2\pi)$, the 2D density

of states per spin. A straightforward but lengthly calculation yields:

$$c_0 = \frac{N(0)}{2} \left[2\ln\left(\frac{4e^\gamma}{\pi}\right)\theta(X) + \ln\frac{\beta\epsilon_b}{4} + \ln(|X|/2)\tanh(X/2) + \text{sign}(X)\int_{|X|/2}^\infty dx \frac{\ln x}{\cosh^2 x} \right],$$

$$c_1 = \frac{N(0)}{4} \left[\frac{7\zeta(3)}{2\pi^2}\beta X\theta(X) + |\mu|\int_{|\mu|^\infty} d\xi \frac{\tanh(\beta\xi/2)}{\xi^3} \right],$$

$$c_2 = \frac{\beta N(0)}{4X}\tanh(X/2) - i\frac{\beta N(0)\pi}{8}\theta(X),$$

$$b = \frac{N(0)}{4} \left[\frac{7\zeta(3)}{2\pi^2}\beta^2\theta(X) + \frac{1}{\mu^2}\tanh(|X|/2) + \text{sign}(X)\int_{|\mu|}^\infty d\xi \frac{\tanh(\beta\xi/2)}{\xi^3} \right]. \tag{D.1}$$

These expression have also been given in Ref. [153], however, the important imaginary part of c_2 leading to the diffusion equation in the weak-coupling regime was erroneously neglected in Ref. [153]. We note that c_0 and c_1 also have sub-leading imaginary corrections (not shown here).

D.2 The BOX diagram in $d = 2, 3$

In this section, we investigate the analytic behavior of $\text{BOX}(k, k)$ in the strong-coupling limit. We consider the static limit where the incoming/outgoing energy is zero. Our starting point is Eq. (4.122). The Matsubara summation can be done with the usual contour techniques. The result is the contribution of four poles, yielding the intermediate result:

$$\text{BOX}(k, k') = \int \frac{d^d\mathbf{q}}{(2\pi)^d} \frac{\xi_\mathbf{q} + \xi_{\mathbf{k}-\mathbf{q}} + \xi_{\mathbf{k}'-\mathbf{q}} + \xi_{\mathbf{q}-\mathbf{k}-\mathbf{k}'}}{(\xi_\mathbf{q} + \xi_{\mathbf{k}-\mathbf{q}})(\xi_\mathbf{q} + \xi_{\mathbf{k}'-\mathbf{q}})(\xi_{\mathbf{k}-\mathbf{q}} + \xi_{\mathbf{q}-\mathbf{k}-\mathbf{k}'})(\xi_{\mathbf{k}'-\mathbf{q}} + \xi_{\mathbf{q}-\mathbf{k}-\mathbf{k}'})}. \tag{D.2}$$

Note that we have neglected the exponentially small contributions of Fermi-Dirac distributions to the residues. The case $\mathbf{k} = \mathbf{k}'$ can be treated analytically. First we consider the case $d = 2$. A change of variables $\mathbf{q} \to \mathbf{q} + \mathbf{k}$ simplifies the integral kernel, yielding:

$$\text{BOX}(k, k) = \int_0^\infty \frac{q\,dq}{2\pi} \int_0^{2\pi} \frac{d\psi}{2\pi} \frac{16m^3\left(k^2 + 2(\xi_{\text{pair}}^{-2} + q^2)\right)}{\left[\left(k^2 + 2(\xi_{\text{pair}}^{-2} + q^2)\right)^2 - 4k^2q^2\cos^2\psi\right]^2}, \tag{D.3}$$

where $\xi_{\text{pair}} = 1/\sqrt{m\epsilon_b}$. The ψ integration and subsequently the the q integrations can be done using standard contour methods. The final result is:

$$(d = 2): \qquad \mathsf{BOX}(k, k) = \frac{a^4 m^3 \left(2\sqrt{x^2 + 2}\, x + \sqrt{2}\, (x^2 + 4) \tanh^{-1} \left(\frac{x}{\sqrt{2}\sqrt{x^2+2}} \right) \right)}{2\pi x \, (x^2 + 2)^{3/2} \, (x^2 + 4)}, \qquad (\text{D}.4)$$

where $x = ak$. The limiting cases can be found easily:

$$(d = 2): \qquad \mathsf{BOX}(k, k) = \begin{cases} \dfrac{m}{4\pi\epsilon_b^2} \left[1 - 5x^2/6 + \mathcal{O}(x^4) \right] & k \ll 1/\xi_{\text{pair}}, \\[2ex] \mathsf{BOX}(0, 0) \left[6.4929/x^4 + \mathcal{O}(x^{-6}) \right] & k \gg 1/\xi_{\text{pair}}. \end{cases} \qquad (\text{D}.5)$$

The result in $d = 3$ is obtained using similar methods. The integrations are more tedious, yet the final result is simple:

$$(d = 3): \qquad \mathsf{BOX}(k, k) = \begin{cases} \dfrac{m^3}{16\pi(m\epsilon_b)^{3/2}} \left[1 - 5x^2/8 + \mathcal{O}(x^4) \right] & q \ll 1/\xi_{\text{pair}}, \\[2ex] \mathsf{BOX}(0, 0) \left[4/x^3 + \mathcal{O}(x^{-5}) \right] & k \gg 1/\xi_{\text{pair}}. \end{cases} \qquad (\text{D}.6)$$

Bibliography

[1] M. H. Anderson, J. R. Ensher, M. R. Matthews, C. E. Wieman, and E. A. Cornell. Observation of bose-einstein condensation in a dilute atomic vapor. *Science (New York, N.Y.)*, 269(5221):198–201, 1995.

[2] K. Davis, M. Mewes, M. Andrews, N. van Druten, D. Durfee, D. Kurn, and W. Ketterle. Bose-Einstein Condensation in a Gas of Sodium Atoms. *Physical Review Letters*, 75(22):3969–3973, 1995.

[3] M. Greiner, O. Mandel, T. Esslinger, T. W. Hänsch, and I. Bloch. Quantum phase transition from a superfluid to a Mott insulator in a gas of ultracold atoms. *Nature*, 415(6867):39–44, 2002.

[4] M. Köhl, H. Moritz, T. Stöferle, K. Günter, and T. Esslinger. Fermionic Atoms in a Three Dimensional Optical Lattice: Observing Fermi Surfaces, Dynamics, and Interactions. *Physical Review Letters*, 94(8):080403, 2005.

[5] K. M. O'Hara, S. L. Hemmer, M. E. Gehm, S. R. Granade, and J. E. Thomas. Observation of a strongly interacting degenerate Fermi gas of atoms. *Science (New York, N.Y.)*, 298(5601):2179–82, 2002.

[6] J. Dalibard, F. Gerbier, G. Juzelinas, and P. Öhberg. Colloquium: Artificial gauge potentials for neutral atoms. *Reviews of Modern Physics*, 83(4):1523–1543, 2011.

[7] M. Saffman, T. G. Walker, and K. Mø lmer. Quantum information with Rydberg atoms. *Reviews of Modern Physics*, 82(3):2313–2363, 2010.

[8] H. P. Büchler, E. Demler, M. Lukin, A. Micheli, N. Prokofev, G. Pupillo, and P. Zoller. Strongly Correlated 2D Quantum Phases with Cold Polar Molecules: Controlling the Shape of the Interaction Potential. *Physical Review Letters*, 98(6):060404, 2007.

[9] W. Ketterle and M. W. Zwierlein. Making, probing and understanding ultracold Fermi gases. *Nuovo Cimento Rivista Serie*, 31:247–422, 2008.

[10] W. S. Bakr, J. I. Gillen, A. Peng, S. Fölling, and M. Greiner. A quantum gas microscope for detecting single atoms in a Hubbard-regime optical lattice. *Nature*, 462(7269):74–7, 2009.

[11] R. Grimm. Ultracold Fermi gases in the BEC-BCS crossover: a review from the Innsbruck perspective. *arXiv preprint cond-mat/0703091*, 2007.

[12] J. Gaebler, J. Stewart, T. Drake, and D. Jin. Observation of pseudogap behaviour in a strongly interacting Fermi gas. *Nature Physics*, 6(8):569–573, 2010.

[13] M. Feld, B. Fröhlich, E. Vogt, M. Koschorreck, and M. Köhl. Observation of a pairing pseudogap in a two-dimensional Fermi gas. *Nature*, 480(7375):75–8, 2011.

[14] M. Baranov. Theoretical progress in many-body physics with ultracold dipolar gases. *Physics Reports*, 464(3):71–111, 2008.

[15] K.-K. Ni, S. Ospelkaus, M. H. G. de Miranda, A. Pe'er, B. Neyenhuis, J. J. Zirbel, S. Kotochigova, P. S. Julienne, D. S. Jin, and J. Ye. A high phase-space-density gas of polar molecules. *Science (New York, N.Y.)*, 322(5899):231–5, 2008.

[16] K.-K. Ni, S. Ospelkaus, D. Wang, G. Quéméner, B. Neyenhuis, M. H. G. de Miranda, J. L. Bohn, J. Ye, and D. S. Jin. Dipolar collisions of polar molecules in the quantum regime. *Nature*, 464(7293):1324–8, 2010.

[17] M. H. G. de Miranda, A. Chotia, B. Neyenhuis, D. Wang, G. Quéméner, S. Ospelkaus, J. L. Bohn, J. Ye, and D. S. Jin. Controlling the quantum stereodynamics of ultracold bimolecular reactions. *Nature Physics*, 7(6):502–507, 2011.

[18] E. Vogt, M. Feld, B. Fröhlich, D. Pertot, M. Koschorreck, and M. Köhl. Scale Invariance and Viscosity of a Two-Dimensional Fermi Gas. *Physical Review Letters*, 108(7):070404, 2012.

[19] G.-B. Jo, Y.-R. Lee, J.-H. Choi, C. A. Christensen, T. H. Kim, J. H. Thywissen, D. E. Pritchard, and W. Ketterle. Itinerant ferromagnetism in a Fermi gas of ultracold atoms. *Science (New York, N.Y.)*, 325(5947):1521–4, 2009.

[20] C. Sanner, E. J. Su, W. Huang, A. Keshet, J. Gillen, and W. Ketterle. Correlations and Pair Formation in a Repulsively Interacting Fermi Gas. *Physical Review Letters*, 108(24):240404, 2012.

[21] J. Schwinger. Brownian Motion of a Quantum Oscillator. *Journal of Mathematical Physics*, 2(3):407, 1961.

[22] L. P. Kadanoff and G. Baym. *Quantum Statistical Mechanics*. W. A. Benjamin, Inc., New York, 1962.

[23] P. Danielewicz. Quantum theory of nonequilibrium processes, I. *Annals of Physics*, 152(2):239–304, 1984.

[24] W. Botermans and R. Malfliet. Quantum transport theory of nuclear matter. *Physics Reports*, 27(3-4):347–359, 1990.

[25] Y. Ivanov, J. Knoll, and D. Voskresensky. Self-consistent approximations to non-equilibrium many-body theory. *Nuclear Physics A*, 657(4):413–445, 1999.

[26] T. Kita. Introduction to Nonequilibrium Statistical Mechanics with Quantum Field Theory. *Progress of Theoretical Physics*, 123(4):581–658, 2010.

[27] J. Rammer. *Quantum Field Theory of Non-equilibrium States*. Cambridge University Press, 2011.

[28] L. V. Keldysh. Diagram technique for nonequilibrium processes. *Sov. Phys. JETP*, 20(4):1018, 1965.

[29] J. W. Negele and H. Orland. *Quantum Many-particle Systems*. Westview Press (November 27, 1998), 1998.

[30] J. Berges. Introduction to Nonequilibrium Quantum Field Theory. In *AIP Conference Proceedings*, volume 739, pages 3–62. AIP, 2004.

[31] M. Garny and M. Müller. Kadanoff-Baym equations with non-Gaussian initial conditions: The equilibrium limit. *Physical Review D*, 80(8):085011, 2009.

[32] J. Berges, S. Borsányi, and C. Wetterich. Prethermalization. *Physical Review Letters*, 93(14):142002, 2004.

[33] A. L. Fetter and J. D. Walecka. *Quantum Theory of Many-Particle Systems*. Courier Dover Publications, 2003.

[34] P. Martin and J. Schwinger. Theory of many-particle systems. I. *Physical Review*, 139(1958), 1959.

[35] F. Dyson. The S Matrix in Quantum Electrodynamics. *Physical Review*, 75(11):1736–1755, 1949.

[36] J. Schwinger. On the Green's functions of quantized fields. I. *Proceedings of the National Academy of Sciences*, 37(7):452–455, 1951.

[37] C. Cercignani. *The Boltzmann Equation and Its Applications*. Springer-Verlag, New York, 1988.

[38] J. Cornwall, R. Jackiw, and E. Tomboulis. Effective action for composite operators. *Physical Review D*, 10(8):2428–2445, 1974.

[39] G. Baym and L. Kadanoff. Conservation Laws and Correlation Functions. *Physical Review*, 124(2):287–299, 1961.

[40] G. Baym. Self-consistent approximations in many-body systems. *Physical review*, 127(4):1391, 1962.

[41] H. Kleinert. Higher Effective Actions for Bose Systems. *Fortschritte der Physik*, 30(4):187–232, 1982.

[42] J. Berges. n-particle irreducible effective action techniques for gauge theories. *Physical Review D*, 70(10):105010, 2004.

[43] J. Luttinger and J. Ward. Ground-State Energy of a Many-Fermion System. II. *Physical Review*, 118(5):1417–1427, 1960.

[44] C. De Dominicis and P. C. Martin. Stationary Entropy Principle and Renormalization in Normal and Superfluid Systems. II. Diagrammatic Formulation. *Journal of Mathematical Physics*, 5(1):31, 1964.

[45] A. V. Gorshkov, M. Hermele, V. Gurarie, C. Xu, P. S. Julienne, J. Ye, P. Zoller, E. Demler, M. D. Lukin, and A. M. Rey. Two-orbital SU(N) magnetism with ultracold alkaline-earth atoms. *Nature Physics*, 6(4):289–295, 2010.

[46] S. Sachdev and Z. Wang. Pairing in two dimensions: A systematic approach. *Physical Review B*, 43(13):10229–10235, 1991.

[47] M. Veillette, D. Sheehy, and L. Radzihovsky. Large-N expansion for unitary superfluid Fermi gases. *Physical Review A*, 75(4):043614, 2007.

[48] G. Aarts, D. Ahrensmeier, R. Baier, J. Berges, and J. Serreau. Far-from-equilibrium dynamics with broken symmetries from the 1/N expansion of the 2PI effective action. *Physical Review D*, 66(4):045008, 2002.

[49] J. Berges. Controlled nonperturbative dynamics of quantum fields out of equilibrium. *Nuclear Physics A*, 699(3-4):847–886, 2002.

[50] J. Berges, S. Borsányi, and J. Serreau. Thermalization of fermionic quantum fields. *Nuclear Physics B*, 660(1-2):51–80, 2003.

[51] J. Berges and J. Serreau. Parametric Resonance in Quantum Field Theory. *Physical Review Letters*, 91(11):111601, 2003.

[52] M. Kronenwett and T. Gasenzer. Far-from-equilibrium dynamics of an ultracold Fermi gas. *Applied Physics B*, 2011.

[53] H. van Hees and J. Knoll. Renormalization in self-consistent approximation schemes at finite temperature. III. Global symmetries. *Physical Review D*, 66(2):025028, 2002.

[54] U. Reinosa and J. Serreau. Ward Identities for the 2PI effective action in QED. *Journal of High Energy Physics*, 2007(11):097–097, 2007.

[55] S. Engelsberg and J. Schrieffer. Coupled Electron-Phonon System. *Physical Review*, 131(3):993–1008, 1963.

[56] E. Wigner. On the Quantum Correction For Thermodynamic Equilibrium. *Physical Review*, 40(5):749–759, 1932.

[57] M. Hillery, R. O'Connell, M. Scully, and E. Wigner. Distribution functions in physics: Fundamentals. *Physics Reports*, 106(3):121–167, 1984.

[58] R. L. Stratonovich. n/a. *Dokl. Akad. Nauk. SSSR*, 1:72, 1956.

[59] H. Groenewold. On the principles of elementary quantum mechanics. *Physica*, 12(7):405–460, 1946.

[60] J. E. Moyal and M. S. Bartlett. Quantum mechanics as a statistical theory. *Mathematical Proceedings of the Cambridge Philosophical Society*, 45(01):99–124, 1949.

[61] Y. Ivanov, J. Knoll, and D. Voskresensky. Resonance transport and kinetic entropy. *Nuclear Physics A*, 672(1-4):313–356, 2000.

[62] J. Knoll, Y. Ivanov, and D. Voskresensky. Exact Conservation Laws of the Gradient Expanded Kadanoff-Baym Equations. *Annals of Physics*, 293(2):126–146, 2001.

[63] L. D. Landau. Theory of Fermi-liquids. *Sov. Phys. JETP*, 3:920, 1957.

[64] L. D. Landau. Oscillations in a Fermi-liquid. *Sov. Phys. JETP*, 5:101, 1957.

[65] L. D. Landau. On the theory of the Fermi-liquid. *Sov. Phys. JETP*, 8:70, 1959.

[66] D. Voskresensky. Hydrodynamics of resonances. *Nuclear Physics A*, 849(1):120–146, 2011.

[67] S. Chapman and T. G. Cowling. *The mathematical theory of non-uniform gases: an account of the kinetic theory of viscosity, thermal conduction, and diffusion in gases*. Cambridge University Press, 1990.

[68] L. D. Landau and E. M. Lifshitz. *Fluid Mechanics, Course of Theoretical Physics, Vol. 6*. Butterworth-Heinemann, 2 edition, 1987.

[69] H. Grad. On the Kinetic Theory of Rarefied Gases. *Communications on Pure and Applied Mathematics*, 2(4):331–407, 1949.

[70] T. Lahaye, C. Menotti, L. Santos, M. Lewenstein, and T. Pfau. The physics of dipolar bosonic quantum gases. *Reports on Progress in Physics*, 72(12):126401, 2009.

[71] M. Lu, N. Q. Burdick, S. H. Youn, and B. L. Lev. Strongly Dipolar Bose-Einstein Condensate of Dysprosium. *Physical Review Letters*, 107(19):190401, 2011.

[72] K. Aikawa, A. Frisch, M. Mark, S. Baier, A. Rietzler, R. Grimm, and F. Ferlaino. Bose-Einstein Condensation of Erbium. *Physical Review Letters*, 108(21):210401, 2012.

[73] J. Sage, S. Sainis, T. Bergeman, and D. DeMille. Optical Production of Ultracold Polar Molecules. *Physical Review Letters*, 94(20):203001, 2005.

[74] J. Deiglmayr, M. Repp, A. Grochola, O. Dulieu, R. Wester, and M. Weidemüller. Dipolar effects and collisions in an ultracold gas of LiCs molecules. *Journal of Physics: Conference Series*, 264:012014, 2011.

[75] M. Lu, N. Q. Burdick, and B. L. Lev. Quantum Degenerate Dipolar Fermi Gas. *Physical Review Letters*, 108(21):215301, 2012.

[76] A. Altmeyer, S. Riedl, C. Kohstall, M. Wright, R. Geursen, M. Bartenstein, C. Chin, J. Denschlag, and R. Grimm. Precision Measurements of Collective Oscillations in the BEC-BCS Crossover. *Physical Review Letters*, 98(4):040401, 2007.

[77] C. Cao, E. Elliott, J. Joseph, H. Wu, J. Petricka, T. Schäfer, and J. E. Thomas. Universal quantum viscosity in a unitary Fermi gas. *Science (New York, N.Y.)*, 331(6013):58–61, 2011.

[78] P. Kovtun, D. Son, and A. Starinets. Viscosity in Strongly Interacting Quantum Field Theories from Black Hole Physics. *Physical Review Letters*, 94(11):111601, 2005.

[79] F. Dalfovo, S. Giorgini, and S. Stringari. Theory of Bose-Einstein condensation in trapped gases. *Reviews of Modern Physics*, 71(3):463–512, 1999.

[80] R. Grimm. Ultra-cold Fermi Gases. In *Proceedings of the International School of Physics Enrico Fermi*, Amsterdam, 2007. IOS Press.

[81] T. Schäfer. Shear viscosity and damping of collective modes in a two-dimensional Fermi gas. *Physical Review A*, 85(3):033623, 2012.

[82] E. Taylor and M. Randeria. Apparent Low-Energy Scale Invariance in Two-Dimensional Fermi Gases. *Physical Review Letters*, 109(13):135301, 2012.

[83] T. Enss, C. Küppersbusch, and L. Fritz. Shear viscosity and spin diffusion in a two-dimensional Fermi gas. *Physical Review A*, 86(1):013617, 2012.

[84] L. Wu and Y. Zhang. Applicability of the Boltzmann equation for a two-dimensional Fermi gas. *Physical Review A*, 85(4):045601, 2012.

[85] L. P. Pitaevskii and E. M. Lifshitz. *Physical Kinetics, Course of Theoretical Physics, Vol. 10*. Butterworth-Heinemann, 1981.

[86] K. Góral, B.-G. Englert, and K. Rzaewski. Semiclassical theory of trapped fermionic dipoles. *Physical Review A*, 63(3):033606, 2001.

[87] K. Góral, M. Brewczyk, and K. Rzaewski. Hydrodynamic excitations of trapped dipolar fermions. *Physical Review A*, 67(2):025601, 2003.

[88] A. R. P. Lima and A. Pelster. Collective motion of polarized dipolar Fermi gases in the hydrodynamic regime. *Physical Review A*, 81(2):021606, 2010.

[89] A. R. P. Lima and A. Pelster. Dipolar Fermi gases in anisotropic traps. *Physical Review A*, 81(6):063629, 2010.

[90] T. Sogo, L. He, T. Miyakawa, S. Yi, H. Lu, and H. Pu. Dynamical properties of dipolar Fermi gases. *New Journal of Physics*, 11(5):055017, 2009.

[91] M. Abad, A. Recati, and S. Stringari. Quadrupole oscillation in a dipolar Fermi gas: Hydrodynamic versus collisionless regime. *Physical Review A*, 85(3):033639, 2012.

[92] C. Ticknor. Two-dimensional dipolar scattering. *Physical Review A*, 80(5):052702, 2009.

[93] F. Arnecke, H. Friedrich, and P. Raab. Near-threshold scattering, quantum reflection, and quantization in two dimensions. *Physical Review A*, 78(5):052711, 2008.

[94] Y. Castin and R. Dum. Bose-Einstein Condensates in Time Dependent Traps. *Physical Review Letters*, 77(27):5315–5319, 1996.

[95] V. Pérez-García, H. Michinel, J. Cirac, M. Lewenstein, and P. Zoller. Low Energy Excitations of a Bose-Einstein Condensate: A Time-Dependent Variational Analysis. *Physical Review Letters*, 77(27):5320–5323, 1996.

[96] K. Singh and D. Rokhsar. Collective Excitations of a Confined Bose Condensate. *Physical Review Letters*, 77(9):1667–1670, 1996.

[97] F. Dalfovo, C. Minniti, S. Stringari, and L. Pitaevskii. Nonlinear dynamics of a Bose condensed gas. *Physics Letters A*, 227(3-4):259–264, 1997.

[98] L. Vichi. Collisional Damping of the Collective Oscillations of a Trapped Fermi Gas. *Journal of Low Temperature Physics*, 121(3-4):177–197, 2000.

[99] L. Boltzmann and F. Hasenöhrl. *Wissenschaftliche Abhandlungen, Vol. II*. Chelsea Publishing Company, 1968.

[100] A. Griffin, W.-C. Wu, and S. Stringari. Hydrodynamic Modes in a Trapped Bose Gas above the Bose-Einstein Transition. *Physical Review Letters*, 78(10):1838–1841, 1997.

[101] S. Chiacchiera, T. Lepers, D. Davesne, and M. Urban. Collective modes of trapped Fermi gases with in-medium interaction. *Physical Review A*, pages 1–17, 2009.

[102] S. Chiacchiera, T. Lepers, D. Davesne, and M. Urban. Role of fourth-order phase-space moments in collective modes of trapped Fermi gases. *Physical Review A*, 84(4):043634, 2011.

[103] D. Guéry-Odelin, F. Zambelli, J. Dalibard, and S. Stringari. Collective oscillations of a classical gas confined in harmonic traps. *Physical Review A*, 60(6):4851–4856, 1999.

[104] D. S. Novikov. Viscosity of a two-dimensional Fermi liquid. *arXiv:cond-mat/0603184*, 2006.

[105] M. Babadi and E. Demler. Density ordering instabilities of quasi-two-dimensional fermionic polar molecules in single-layer and multilayer configurations: Exact treatment of exchange interactions. *Physical Review B*, 84(23):235124, 2011.

[106] M. Babadi and E. Demler. Collective phenomena in a quasi-two-dimensional system of fermionic polar molecules: Band renormalization and excitons. *Physical Review A*, 84(3):033636, 2011.

[107] P.-A. Pantel, D. Davesne, S. Chiacchiera, and M. Urban. Trap anharmonicity and sloshing mode of a Fermi gas. *Physical Review A*, 86(2):023635, 2012.

[108] L. Cooper. Bound Electron Pairs in a Degenerate Fermi Gas. *Physical Review*, 104(4):1189–1190, 1956.

[109] J. Bardeen, L. N. Cooper, and J. R. Schrieffer. Theory of Superconductivity. *Physical Review*, 108(5):1175–1204, 1957.

[110] D. Osheroff, R. Richardson, and D. Lee. Evidence for a New Phase of Solid He-3. *Physical Review Letters*, 28(14):885–888, 1972.

[111] D. Osheroff, W. Gully, R. Richardson, and D. Lee. New Magnetic Phenomena in Liquid He-3 below 3 mK. *Physical Review Letters*, 29(14):920–923, 1972.

[112] A. Damascelli and Z.-X. Shen. Angle-resolved photoemission studies of the cuprate super-conductors. *Reviews of Modern Physics*, 75(2):473–541, 2003.

[113] J. G. Bednorz and K. A. Müller. Possible high-Tc superconductivity in the Ba-La-Cu-O system. *Zeitschrift für Physik B Condensed Matter*, 64(2):189–193, 1986.

[114] P. A. Lee and X.-G. Wen. Doping a Mott insulator: Physics of high-temperature superconductivity. *Reviews of Modern Physics*, 78(1):17–85, 2006.

[115] D. Scalapino, E. Loh, and J. Hirsch. d-wave pairing near a spin-density-wave instability. *Physical Review B*, 34(11):8190–8192, 1986.

[116] K. Miyake, S. Schmitt-Rink, and C. Varma. Spin-fluctuation-mediated even-parity pairing in heavy-fermion superconductors. *Physical Review B*, 34(9):6554–6556, 1986.

[117] V. Emery. The mechanisms of organic superconductivity. *Synthetic Metals*, 13(1-3):21–27, 1986.

[118] V. Emery. Theory of high-Tc superconductivity in oxides. *Physical Review Letters*, 58(26):2794–2797, 1987.

[119] J. Hirsch, E. Loh, D. Scalapino, and S. Tang. Pairing interaction in CuO clusters. *Physical Review B*, 39(1):243–253, 1989.

[120] P. Monthoux and D. Pines. YBa2Cu3O7: A nearly antiferromagnetic Fermi liquid. *Physical Review B*, 47(10):6069–6081, 1993.

[121] N. Berk and J. Schrieffer. Effect of Ferromagnetic Spin Correlations on Superconductivity. *Physical Review Letters*, 17(8):433–435, 1966.

[122] P. Anderson and W. Brinkman. Anisotropic Superfluidity in He-3: A Possible Interpretation of Its Stability as a Spin-Fluctuation Effect. *Physical Review Letters*, 30(22):1108–1111, 1973.

[123] T. Bourdel, J. Cubizolles, L. Khaykovich, K. M. F. Magalhães, S. J. J. M. F. Kokkelmans, G. V. Shlyapnikov, and C. Salomon. Measurement of the Interaction Energy near a Feshbach Resonance in a Li-6 Fermi Gas. *Physical Review Letters*, 91(2):020402, 2003.

[124] R. Grimm and M. Weidemüller. Optical Dipole Traps for Neutral Atoms. *Advances In Atomic, Molecular, and Optical Physics*, 42:95–170, 2000.

[125] C. A. Regal, C. Ticknor, J. L. Bohn, and D. S. Jin. Creation of ultracold molecules from a Fermi gas of atoms. *Nature*, 424(6944):47–50, 2003.

[126] K. E. Strecker, G. B. Partridge, and R. G. Hulet. Conversion of an Atomic Fermi Gas to a Long-Lived Molecular Bose Gas. *Physical Review Letters*, 91(8):080406, 2003.

[127] J. Cubizolles, T. Bourdel, S. J. J. M. F. Kokkelmans, G. V. Shlyapnikov, and C. Salomon. Production of Long-Lived Ultracold Li2 Molecules from a Fermi Gas. *Physical Review Letters*, 91(24):240401, 2003.

[128] S. Jochim, M. Bartenstein, A. Altmeyer, G. Hendl, C. Chin, J. H. Denschlag, and R. Grimm. Pure Gas of Optically Trapped Molecules Created from Fermionic Atoms. *Physical Review Letters*, 91(24):240402, 2003.

[129] S. Jochim, M. Bartenstein, A. Altmeyer, G. Hendl, S. Riedl, C. Chin, J. Hecker Denschlag, and R. Grimm. Bose-Einstein condensation of molecules. *Science (New York, N.Y.)*, 302(5653):2101–3, 2003.

[130] M. Greiner, C. A. Regal, and D. S. Jin. Emergence of a molecular Bose-Einstein condensate from a Fermi gas. *Nature*, 426(6966):537–40, 2003.

[131] M. Zwierlein, C. Stan, C. Schunck, S. Raupach, S. Gupta, Z. Hadzibabic, and W. Ketterle. Observation of Bose-Einstein Condensation of Molecules. *Physical Review Letters*, 91(25):250401, 2003.

[132] G. B. Partridge, K. E. Strecker, R. I. Kamar, M. W. Jack, and R. G. Hulet. Molecular Probe of Pairing in the BEC-BCS Crossover. *Physical Review Letters*, 95(2):020404, 2005.

[133] M. W. Zwierlein, J. R. Abo-Shaeer, A. Schirotzek, C. H. Schunck, and W. Ketterle. Vortices and superfluidity in a strongly interacting Fermi gas. *Nature*, 435(7045):1047–51, 2005.

[134] C. Sá de Melo, M. Randeria, and J. Engelbrecht. Crossover from BCS to Bose superconductivity: Transition temperature and time-dependent Ginzburg-Landau theory. *Physical Review Letters*, 71(19):3202–3205, 1993.

[135] A. Bulgac, J. Drut, and P. Magierski. Thermodynamics of a Trapped Unitary Fermi Gas. *Physical Review Letters*, 99(12):120401, 2007.

[136] A. Bulgac, J. Drut, and P. Magierski. Quantum Monte Carlo simulations of the BCS-BEC crossover at finite temperature. *Physical Review A*, 78(2):023625, 2008.

[137] J. T. Stewart, J. P. Gaebler, and D. S. Jin. Using photoemission spectroscopy to probe a strongly interacting Fermi gas. *Nature*, 454(7205):744–7, 2008.

[138] P. Nozières and S. Schmitt-Rink. Bose condensation in an attractive fermion gas: From weak to strong coupling superconductivity. *Journal of Low Temperature Physics*, 59(3-4):195–211, 1985.

[139] D. Son and M. Wingate. General coordinate invariance and conformal invariance in nonrelativistic physics: Unitary Fermi gas. *Annals of Physics*, 321(1):197–224, 2006.

[140] Y. Nishida. *Unitary Fermi gas in the epsilon expansion*. PhD thesis, University of Tokyo, 2006.

[141] C. J. Pethick and H. Smith. *Bose-Einstein Condensation in Dilute Gases*. Cambridge University Press, 2 edition, 2008.

[142] A. Perali, P. Pieri, L. Pisani, and G. C. Strinati. BCS-BEC Crossover at Finite Temperature for Superfluid Trapped Fermi Atoms. *Physical Review Letters*, 92(22):220404, 2004.

[143] M. Wright, S. Riedl, A. Altmeyer, C. Kohstall, E. Guajardo, J. Denschlag, and R. Grimm. Finite-Temperature Collective Dynamics of a Fermi Gas in the BEC-BCS Crossover. *Physical Review Letters*, 99(15):150403, 2007.

[144] G. Bruun and H. Smith. Frequency and damping of the scissors mode of a Fermi gas. *Physical Review A*, 76(4):045602, 2007.

[145] M. Urban. Radial quadrupole and scissors modes in trapped Fermi gases across the BCS phase transition. *Physical Review A*, 78(5):053619, 2008.

[146] T. Enss, R. Haussmann, and W. Zwerger. Viscosity and scale invariance in the unitary Fermi gas. *Annals of Physics*, 2011.

[147] I. Bloch and W. Zwerger. Many-body physics with ultracold gases. *Reviews of Modern Physics*, 80(3):885–964, 2008.

[148] K. Martiyanov, V. Makhalov, and A. Turlapov. Observation of a Two-Dimensional Fermi Gas of Atoms. *Physical Review Letters*, 105(3):030404, 2010.

[149] D. S. Petrov, M. Holzmann, and G. V. Shlyapnikov. Bose-Einstein Condensation in Quasi-2D Trapped Gases. *Physical Review Letters*, 84(12):2551–2555, 2000.

[150] D. S. Petrov and G. V. Shlyapnikov. Interatomic collisions in a tightly confined Bose gas. *Physical Review A*, 64(1):012706, 2001.

[151] V. Pietilä, D. Pekker, Y. Nishida, and E. Demler. Pairing instabilities in quasi-two-dimensional Fermi gases. *Physical Review A*, pages 1–6, 2012.

[152] V. Pietilä. Pairing and radio-frequency spectroscopy in two-dimensional Fermi gases. *Physical Review A*, 86(2):023608, 2012.

[153] M. Drechsler and W. Zwerger. Crossover from BCS-superconductivity to Bose-condensation. *Annalen der Physik*, 504(1):15–23, 1992.

[154] S. Botelho and C. Sá de Melo. Vortex-Antivortex Lattice in Ultracold Fermionic Gases. *Physical Review Letters*, 96(4):040404, 2006.

[155] R. Watanabe, S. Tsuchiya, and Y. Ohashi. Two-dimensional pseudogap effects of an ultracold Fermi gas in the BCS-BEC crossover region. *Journal of Low Temperature Physics*, 2012.

[156] G. Bertaina and S. Giorgini. BCS-BEC Crossover in a Two-Dimensional Fermi Gas. *Physical Review Letters*, 106(11):110403, 2011.

[157] S. K. Baur, E. Vogt, M. Köhl, and G. M. Bruun. Collective modes of a two-dimensional spin-1/2 Fermi gas in a harmonic trap. *Physical Review A*, 87(4):043612, 2013.

[158] G. Bruun and C. Clark. Hydrodynamic Excitations of Trapped Fermi Gases. *Physical Review Letters*, 83(26):5415–5418, 1999.

[159] A. Minguzzi and M. Tosi. Scissors mode in a superfluid Fermi gas. *Physical Review A*, 63(2):023609, 2001.

[160] S. Stringari. Collective oscillations of a trapped superfluid Fermi gas near a Feshbach resonance. *Europhysics Letters (EPL)*, 65(6):749–752, 2004.

[161] H. Heiselberg. Collective Modes of Trapped Gases at the BEC-BCS Crossover. *Physical Review Letters*, 93(4):040402, 2004.

[162] A. Bulgac and G. Bertsch. Collective Oscillations of a Trapped Fermi Gas near the Unitary Limit. *Physical Review Letters*, 94(7):070401, 2005.

[163] P. Massignan, G. Bruun, and H. Smith. Viscous relaxation and collective oscillations in a trapped Fermi gas near the unitarity limit. *Physical Review A*, 71(3):033607, 2005.

[164] Y. Kim and A. Zubarev. Collective excitations of strongly interacting Fermi gases of atoms in a harmonic trap. *Physical Review A*, 72(1):011603, 2005.

[165] L. Vichi and S. Stringari. Collective oscillations of an interacting trapped Fermi gas. *Physical Review A*, 60(6):4734–4737, 1999.

[166] E. Taylor and A. Griffin. Two-fluid hydrodynamic modes in a trapped superfluid gas. *Physical Review A*, 72(5):053630, 2005.

[167] M. Urban and P. Schuck. Dynamics of a trapped Fermi gas in the BCS phase. *Physical Review A*, 73(1):013621, 2006.

[168] G. Bruun and H. Smith. Shear viscosity and damping for a Fermi gas in the unitarity limit. *Physical Review A*, 75(4):043612, 2007.

[169] S. Riedl, E. Sánchez Guajardo, C. Kohstall, A. Altmeyer, M. Wright, J. Denschlag, R. Grimm, G. Bruun, and H. Smith. Collective oscillations of a Fermi gas in the unitarity limit: Temperature effects and the role of pair correlations. *Physical Review A*, 78(5):053609, 2008.

[170] S. Chiacchiera, T. Lepers, D. Davesne, and M. Urban. Collective modes of trapped Fermi gases with in-medium interaction. *Physical Review A*, 79(3):033613, 2009.

[171] T. Lepers, D. Davesne, S. Chiacchiera, and M. Urban. Numerical solution of the Boltzmann equation for the collective modes of trapped Fermi gases. *Physical Review A*, 82(2):023609, 2010.

[172] L. Wu and Y. Zhang. Numerical investigation of the radial quadrupole and scissors modes in trapped gases. *Europhysics Letters*, 97(1):16003, 2012.

[173] E. Fermi. n/a. *Ricerca Sci.*, 7(13), 1936.

[174] K. Huang and C. Yang. Quantum-Mechanical Many-Body Problem with Hard-Sphere Interaction. *Physical Review*, 105(3):767–775, 1957.

[175] F. Pistolesi and G. Strinati. Evolution from BCS superconductivity to Bose condensation: Calculation of the zero-temperature phase coherence length. *Physical review. B, Condensed matter*, 53(22):15168–15192, 1996.

[176] S. Beane, T. Cohen, and D. Phillips. The potential of effective field theory in NN scattering. *Nuclear Physics A*, 632(3):445–469, 1998.

[177] N. D. Mermin and H. Wagner. Absence of Ferromagnetism or Antiferromagnetism in One- or Two-Dimensional Isotropic Heisenberg Models. *Physical Review Letters*, 17(22):1133–1136, 1966.

[178] P. Hohenberg. Existence of Long-Range Order in One and Two Dimensions. *Physical Review*, 158(2):383–386, 1967.

[179] S. Coleman. There are no Goldstone bosons in two dimensions. *Communications in Mathematical Physics*, 31(4):259–264, 1973.

[180] D. R. Nelson. Universal Jump in the Superfluid Density of Two-Dimensional Superfluids. *Physical Review Letters*, 39(19):1201–1205, 1977.

[181] V. Loktev, R. Quick, and S. Sharapov. Phase fluctuations and pseudogap phenomena. *Physics Reports*, 349, 2001.

[182] D. Fisher and P. Hohenberg. Dilute Bose gas in two dimensions. *Physical Review B*, 37(10), 1988.

[183] V. N. Popov. On the theory of the superfluidity of two- and one-dimensional bose systems. *Theoretical and Mathematical Physics*, 11(3):565–573, 1972.

[184] N. Prokof'ev, O. Ruebenacker, and B. Svistunov. Critical Point of a Weakly Interacting Two-Dimensional Bose Gas. *Physical Review Letters*, 87(27):270402, 2001.

[185] N. Prokof'ev and B. Svistunov. Two-dimensional weakly interacting Bose gas in the fluctuation region. *Physical Review A*, 66(4):043608, 2002.

[186] S. Pilati, S. Giorgini, and N. Prokofev. Critical Temperature of Interacting Bose Gases in Two and Three Dimensions. *Physical Review Letters*, 100(14):140405, 2008.

[187] S. Floerchinger and C. Wetterich. Superfluid Bose gas in two dimensions. *Physical Review A*, 79(1):013601, 2009.

[188] S. Traven. Superfluidity of a two-dimensional dilute attractive Fermi gas. *Physical review letters*, 73(25):3451–3454, 1994.

[189] S. N. Klimin, J. Tempere, and J. T. Devreese. Pseudogap and preformed pairs in the imbalanced Fermi gas in two dimensions. *New Journal of Physics*, 14(10):103044, 2012.

[190] S. Schmitt-Rink, C. Varma, and A. Ruckenstein. Pairing in Two Dimensions. *Physical review letters*, 63(4):445–448, 1989.

[191] S. Tsuchiya, R. Watanabe, and Y. Ohashi. Single-particle properties and pseudogap effects in the BCS-BEC crossover regime of an ultracold Fermi gas above Tc. *Physical Review A*, pages 1–23, 2009.

[192] A. Perali, P. Pieri, G. Strinati, and C. Castellani. Pseudogap and spectral function from superconducting fluctuations to the bosonic limit. *Physical Review B*, 66(2):024510, 2002.

[193] P. Pieri, L. Pisani, and G. Strinati. BCS-BEC crossover at finite temperature in the broken-symmetry phase. *Physical Review B*, 70(9):094508, 2004.

[194] S. Tsuchiya, R. Watanabe, and Y. Ohashi. Pseudogap temperature and effects of a harmonic trap in the BCS-BEC crossover regime of an ultracold Fermi gas. *Physical Review A*, 84(4):043647, 2011.

[195] L. Kadanoff and P. Martin. Theory of Many-Particle Systems. II. Superconductivity. *Physical Review*, 124(3):670–697, 1961.

[196] Q. Chen, Y. He, C.-C. Chien, and K. Levin. Theory of radio frequency spectroscopy experiments in ultracold Fermi gases and their relation to photoemission in the cuprates. *Reports on Progress in Physics*, 72(12):122501, 2009.

[197] R. Haussmann, W. Rantner, S. Cerrito, and W. Zwerger. Thermodynamics of the BCS-BEC crossover. *Physical Review A*, 75(2):023610, 2007.

[198] R. Haussmann and W. Zwerger. Thermodynamics of a trapped unitary Fermi gas. *Physical Review A*, 78(6):063602, 2008.

[199] R. Haussmann, M. Punk, and W. Zwerger. Spectral functions and rf response of ultracold fermionic atoms. *Physical Review A*, 80(6):063612, 2009.

[200] K. Levin, Q. Chen, C.-C. Chien, and Y. He. Comparison of different pairing fluctuation approaches to BCSBEC crossover. *Annals of Physics*, 325(2):233–264, 2010.

[201] D. J. Thouless. Perturbation theory in statistical mechanics and the theory of superconductivity. *Annals of Physics*, 10(4):553–588, 1960.

[202] A. Tokumitu, K. Miyake, and K. Yamada. Cooper-pair and Bose-Einstein condensations in two dimensions: A critical analysis based on the Nozieres and Schmitt-Rink formalism. *Physical Review B*, 47(18), 1993.

[203] S. I. Shevchenko. n/a. *Sov. J. Low Temp.*, 16(64), 1990.

[204] S. I. Shevchenko. Theory of two-dimensional superfluidity in a nonuniform external field. *Soviet physics, JETP*, 1991.

[205] V. Bagnato and D. Kleppner. Bose-Einstein condensation in low-dimensional traps. *Physical Review A*, 44(11):7439–7441, 1991.

[206] R. K. Bhaduri, S. M. Reimann, S. Viefers, A. G. Choudhury, and M. K. Srivastava. The effect of interactions on Bose-Einstein condensation in a quasi two-dimensional harmonic trap. *Journal of Physics B: Atomic, Molecular and Optical Physics*, 33(19):3895–3903, 2000.

[207] L. G. Aslamazov and A. I. Larkin. Effect of Fluctuations on the Properties of a Superconductor Above the Critical Temperature. *Sov. Phys. Solid State*, 10(4):875–880, 1968.

[208] K. Maki. The Critical Fluctuation of the Order Parameter in Type-II Superconductors. *Progress of Theoretical Physics*, 39(4):897–906, 1968.

[209] R. S. Thompson. Microwave, Flux Flow, and Fluctuation Resistance of Dirty Type-II Superconductors. *Physical Review B*, 1(1):327–333, 1970.

[210] A. I. Larkin and A. A. Varlamov. *Fluctuation Phenomena in High Temperature Superconductors*. Springer Netherlands, 1997.

[211] G. Strinati, P. Pieri, and C. Lucheroni. From superconducting fluctuations to the bosonic limit in the response functions above the critical temperature. *The European Physical Journal B*, 30(2):161–173, 2002.

[212] R. Haussmann. Crossover from BCS superconductivity to Bose-Einstein condensation: A self-consistent theory. *Zeitschrift für Physik B Condensed Matter*, 91(3):291–308, 1993.

[213] P. Pieri and G. Strinati. Strong-coupling limit in the evolution from BCS superconductivity to Bose-Einstein condensation. *Physical Review B*, 61(22):15370–15381, 2000.

[214] I. Brodsky, M. Kagan, A. Klaptsov, R. Combescot, and X. Leyronas. Exact diagrammatic approach for dimer-dimer scattering and bound states of three and four resonantly interacting particles. *Physical Review A*, 73(3):032724, 2006.

[215] S. Peletminskii. Theory of kinetic equations for systems with bound states of particles. *Theoretical and Mathematical Physics*, 6(1):88–101, 1971.

[216] Y. L. Klimontovich and W. Ebeling. Quantum kinetic equations for a nonideal gas and a nonideal plasma. *Soviet Physics-JETP*, 36(3), 1973.

[217] Y. Klimontovich and D. Kremp. Quantum kinetic equations in systems with bound states. *Physica A: Statistical Mechanics and its Applications*, 109(3):517–530, 1981.

[218] P. Lipavský, V. Špička, and B. Velický. Generalized Kadanoff-Baym ansatz for deriving quantum transport equations. *Physical Review B*, 34(10):6933–6942, 1986.

[219] H. Schoeller. A New Transport Equation for Single-Time Greens Functions in an Arbitrary Quantum System. General Formalism. *Annals of Physics*, 229(2):273–319, 1994.

[220] V. Morozov and G. Röpke. Quantum kinetic equation for nonequilibrium dense systems. *Physica A: Statistical Mechanics and its Applications*, 221(4):511–538, 1995.

[221] T. Bornath, D. Kremp, W. Kraeft, and M. Schlanges. Kinetic equations for a nonideal quantum system. *Physical review. E, Statistical physics, plasmas, fluids, and related interdisciplinary topics*, 54(4):3274–3284, 1996.

[222] V. Morozov and G. Röpke. The Mixed Green's Function Approach to Quantum Kinetics with Initial Correlations. *Annals of Physics*, 1999.

[223] D. Kremp, T. Bornath, M. Bonitz, W. D. Kraeft, and M. Schlanges. Quantum kinetic equations for nonideal plasmas: Bound states and ionization kinetics. *Physics of Plasmas*, 7(1):59, 2000.

[224] D. Semkat, D. Kremp, and M. Bonitz. KadanoffBaym equations and non-Markovian Boltzmann equation in generalized T-matrix approximation. *Journal of Mathematical Physics*, 41(11):7458, 2000.

[225] K. Morawetz, P. Lipavský, and V. Špička. Retarded versus time-nonlocal quantum kinetic equations. *Annals of Physics*, 2001.

[226] P. Pieri and G. Strinati. Strong-coupling limit in the evolution from BCS superconductivity to Bose-Einstein condensation. *Physical Review B*, 61(22):15370–15381, 2000.

[227] D. Petrov, C. Salomon, and G. Shlyapnikov. Scattering properties of weakly bound dimers of fermionic atoms. *Physical Review A*, 71(1):012708, 2005.

[228] J. Levinsen and V. Gurarie. Properties of strongly paired fermionic condensates. *Physical Review A*, 80309, 2006.

[229] G. D. Mahan. *Many-Particle Physics*. Springer, third edition, 2010.

[230] P. Bhatnagar, E. Gross, and M. Krook. A Model for Collision Processes in Gases. I. Small Amplitude Processes in Charged and Neutral One-Component Systems. *Physical Review*, 94(3):511–525, 1954.

[231] S. M. Troian and N. D. Mermin. Pitfalls of the relaxation time approximation: Hydrodynamic sound in a multicomponent Fermi liquid. *Journal of Low Temperature Physics*, 59(1-2):115–121, 1985.

[232] H. Stoof and M. Bijlsma. Kosterlitz-Thouless transition in a dilute Bose gas. *Physical Review E*, 47(2), 1993.